

EDITORIAL BOARD

Jiri Cizek (Waterloo, Canada)
David P. Craig (Canberra, Australia)
Raymond Daudel (Paris, France)
Ernst R. Davidson (Bloomington, Indiana)
Inga Fischer-Hjalmars (Stockholm, Sweden)
Kenichi Fukui (Kyoto, Japan)
George G. Hall (Nottingham, England)
Jan Linderberg (Aarhus, Denmark)
Frederick A. Matsen (Austin, Texas)
Roy McWeeney (Pisa, Italy)
William H. Miller (Berkeley, California)
Keiji Morokuma (Okazaki, Japan)
Joseph Paldus (Waterloo, Canada)
Ruben Pauncz (Haifa, Israel)
Siegfried Peyerimhoff (Bonn, Germany)
John A. Pople (Pittsburgh, Pennsylvania)
Alberte Pullman (Paris, France)
Pekka Pyykkö (Helsinki, Finland)
Leo Radom (Canberra, Australia)
Klaus Ruedenberg (Ames, Iowa)
Henry F. Schaefer III (Athens, Georgia)
Isaiah Shavitt (Columbus, Ohio)
Per Siegbahn (Stockholm, Sweden)
Au-Chin Tang (Kirin, Changchun, China)
Rudolf Zahradnik (Prague, Czech Republic)

ADVISORY EDITORIAL BOARD

David M. Bishop (Ottawa, Canada)
Giuseppe del Re (Naples, Italy)
Fritz Grein (Fredericton, Canada)
Mu Shik Jhon (Seoul, Korea)
Mel Levy (New Orleans, Louisiana)
Jens Oddershede (Odense, Denmark)
Mark Ratner (Evanston, Illinois)
Dennis R. Salahub (Montreal, Canada)
Harel Weinstein (New York, New York)
Robert E. Wyatt (Austin, Texas)
Tokio Yamabe (Kyoto, Japan)

ADVANCES IN QUANTUM CHEMISTRY

DENSITY FUNCTIONAL THEORY

EDITOR-IN-CHIEF

PER-OLOV LÖWDIN

PROFESSOR EMERITUS

DEPARTMENT OF QUANTUM CHEMISTRY

UPPSALA UNIVERSITY

UPPSALA, SWEDEN

AND

QUANTUM THEORY PROJECT

UNIVERSITY OF FLORIDA

GAINESVILLE, FLORIDA

EDITORS

**JOHN R. SABIN
MICHAEL C. ZERNER**

QUANTUM THEORY PROJECT

UNIVERSITY OF FLORIDA

GAINESVILLE, FLORIDA

ERKKI BRÄNDAS

DEPARTMENT OF QUANTUM CHEMISTRY

UPPSALA UNIVERSITY

UPPSALA, SWEDEN

GUEST EDITOR

JORGE M. SEMINARIO

DEPARTMENT OF CHEMISTRY

AND BIOCHEMISTRY

UNIVERSITY OF SOUTH CAROLINA

COLUMBIA, SOUTH CAROLINA

VOLUME 33



ACADEMIC PRESS

San Diego

London

Boston


New York

Sydney

Tokyo

Toronto

Academic Press Rapid Manuscript Reproduction

This book is printed on acid-free paper. 

Copyright © 1999 by ACADEMIC PRESS

All Rights Reserved.

No part of this publication may be reproduced or transmitted in any form or by any means, electronic or mechanical, including photocopy, recording, or any information storage and retrieval system, without permission in writing from the Publisher.

The appearance of the code at the bottom of the first page of a chapter in this book indicates the Publisher's consent that copies of the chapter may be made for personal or internal use of specific clients. This consent is given on the condition, however, that the copier pay the stated per copy fee through the Copyright Clearance Center, Inc. (222 Rosewood Drive, Danvers, Massachusetts 01923), for copying beyond that permitted by Sections 107 or 108 of the U.S. Copyright Law. This consent does not extend to other kinds of copying, such as copying for general distribution, for advertising or promotional purposes, for creating new collective works, or for resale. Copy fees for pre-1999 chapters are as shown on the title pages. If no fee code appears on the title page, the copy fee is the same as for current chapters.
0065-3276/99 \$30.00

Academic Press

a division of Harcourt Brace & Company

525 B Street, Suite 1900, San Diego, California 92101-4495, USA

<http://www.apnet.com>

Academic Press

24-28 Oval Road, London NW1 7DX, UK

<http://www.hbuk.co.uk/ap/>

International Standard Book Number: 0-12-034832-2

PRINTED IN THE UNITED STATES OF AMERICA

98 99 00 01 02 03 MM 9 8 7 6 5 4 3 2 1

Contributors

Numbers in parentheses indicate the pages on which the authors' contributions begin.

- J. A. Alonso** (327), Departamento de Física Teórica, Universidad de Valladolid, 47011 Valladolid, Spain
- L. C. Balbás** (327) Departamento de Física Teórica, Universidad de Valladolid, 47011 Valladolid, Spain
- P. Blaha** (209) Institut für Technische Elektrochemie, Technische Universität Wien, A-1060 Vienna, Austria
- Ewa Broclawik** (347) Institute of Catalysis and Surface Chemistry, Polish Academy of Science, Cracow, Poland
- Kieron Burke** (1) Department of Chemistry, Rutgers University, Camden, New Jersey 08102
- D. M. Bylander** (151) Department of Physics, University of Texas, Austin, Texas 78712
- H. Chermette** (105) Laboratoire de Chimie-Physique Théorique, Université Claude Bernard–Lyon1, and Institut Recherches sur la Catalyse, UPR 5401-CNRS 43, F-69622 Villeurbanne Cedex, France
- R. Colle** (49) Dipartimento di Chimica Applicata, Università di Bologna, Bologna, Italy; and Scuola Normale Superiore, Pisa, Italy
- F. De Proft** (301) Eenheid Algemene Chemie, Faculteit Wetenschappen, Vrije Universiteit Brussel, 1050 Brussels, Belgium
- R. M. Dreizler** (209) Institut für Theoretische Physik, Universität Frankfurt, D-60054 Frankfurt/Main, Germany
- Brett. I. Dunlap** (167) Theoretical Chemistry Section, Naval Research Laboratory, Washington, DC 20375
- E. Engel** (209) Institut für Theoretische Physik, Universität Frankfurt, D-60054 Frankfurt/Main, Germany
- Matthias Ernzerhof** (1) Department of Physics and Quantum Theory Group, Tulane University, New Orleans, Louisiana 70118
- W. M. C. Foulkes** (189) The Blackett Laboratory, Imperial College, London SW7 2BZ, United Kingdom

- P. Geerlings** (301) Eenheid Algemene Chemie, Faculteit Wetenschappen, Vrije Universiteit Brussel, 1050 Brussels, Belgium
- A. Gonis** (85) Department of Chemistry and Materials Science, Lawrence Livermore National Laboratory, Livermore, California 94550
- Xavier Gonze** (225) Unité P.C.P.M., Université Catholique de Louvain, 1, B-1348 Louvain-la-Neuve, Belgium
- T. Grabo** (31) Institut für Theoretische Physik, Universität Würzburg, 97074 Würzburg, Germany
- E. K. U. Gross** (31) Institut für Theoretische Physik, Universität Würzburg, 97074 Würzburg, Germany
- J. Hinze** (49) Fakultät für Chemie, Universität Bielefeld, Bielefeld, Germany
- Stanislav Ivanov** (11) Chemistry Department and Quantum Theory Group, Tulane University, New Orleans, Louisiana 70118
- V. Karasiev** (49) Química, Instituto Venezolano de Investigaciones Científicas, Caracas 1020-A, Venezuela
- Leonard Kleinman** (151) Department of Physics, University of Texas, Austin, Texas 78712
- T. Kreibich** (31) Institut für Theoretische Physik, Universität Würzburg, 97074 Würzburg, Germany
- S. Kurth** (31) Department of Physics, University of Antwerpen (RUCA), 2020 Antwerp, Belgium
- Pat Lane** (291) Department of Chemistry, University of New Orleans, Louisiana 70148
- W. Langenaeker** (301) Eenheid Algemene Chemie, Faculteit Wetenschappen, Vrije Universiteit Brussel, 1050 Brussels, Belgium
- A. Lembarki** (105) Laboratoire de Chimie-Physique Théorique, Université Claude Bernard-Lyon1, F-69622 Villeurbanne Cedex, France
- Mel Levy** (11) Chemistry Department and Quantum Theory Group, Tulane University, New Orleans, Louisiana 70118
- M. J. López** (327) Departamento de Física Teórica, Universidad de Valladolid, 47011 Valladolid, Spain
- R. López-Boada** (49) Química, Instituto Venezolano de Investigaciones Científicas, Caracas 1020-A, Venezuela
- E. V. Ludeña** (49) Química, Instituto Venezolano de Investigaciones Científicas, Caracas 1020-A, Venezuela
- J. Maldonado** (49) Química, Instituto Venezolano de Investigaciones Científicas, Caracas 1020-A, Venezuela
- T. Mineva** (273) Institute of Catalysis, Bulgarian Academy of Science, 1113 Sofia, Bulgaria
- L. M. Molina** (327) Departamento de Física Teórica, Universidad de Valladolid, 47011 Valladolid, Spain
- R. J. Needs** (189) TCM Group, Cavendish Laboratory, Madingley Road, Cambridge CB3 0HE, United Kingdom

- Maziar Nekovee** (189) The Blackett Laboratory, Imperial College, London SW7 2BZ, United Kingdom
- R. K. Nesbet** (71) IBM Almaden Research Center, San Jose, California 95120
- N. Neshev** (273) Institute of Catalysis, Bulgarian Academy of Science, 1113 Sofia, Bulgaria
- J. K. Percus** (131) Courant Institute of Mathematical Sciences and Physics Department, New York University, New York, New York
- John P. Perdew** (1) Department of Physics and Quantum Theory Group, Tulane University, New Orleans, Louisiana 70118
- R. Pino** (49) Química, Instituto Venezolano de Investigaciones Científicas, Caracas 1020-A, Venezuela
- Peter Politzer** (291) Department of Chemistry, University of New Orleans, Louisiana 70148
- G. Rajagopal** (189) TCM Group, Cavendish Laboratory, Cambridge CB3 0HE, United Kingdom
- H. Razafinjanahary** (105) Laboratoire de Chimie-Physique Théorique, Université Claude Bernard–Lyon1, F-69622 Villeurbanne Cedex, France
- F. Rogemond** (105) Laboratoire de Chimie-Physique Théorique, Université Claude Bernard–Lyon1, and Institut Recherches sur la Catalyse, UPR 5401-CNRS 43, F-69622 Villeurbanne Cedex, France
- A. Rubio** (327) Departamento de Física Teórica, Universidad de Valladolid, 47011 Valladolid, Spain
- N. Russo** (273) Dipartimento di Chimica, Università della Calabria, I-87030 Arcavacata di Rende (CS), Italy
- Viraht Sahni** (241) Department of Physics, Brooklyn College of the City University of New York, Brooklyn, New York 11210; and The Graduate School and University Center of the City University of New York, New York, New York 10036
- Frank C. Sanders** (367) Department of Physics, Southern Illinois University at Carbondale, Carbondale, Illinois 62901
- R. N. Schmid** (209) Institut für Theoretische Physik, Universität Frankfurt, D-60054 Frankfurt/Main, Germany
- T. C. Schulthess** (85) Metals and Ceramics Division, Oak Ridge National Laboratory, Oak Ridge, Tennessee 37831
- K. Schwarz** (209) Institut für Technische Elektrochemie, Technische Universität Wien, A-1060 Vienna, Austria
- E. Sicilia** (273) Dipartimento di Chimica, Università della Calabria, I-87030 Arcavacata di Rende (CS), Italy
- Alexander Solomatin** (241) Department of Physics, Brooklyn College of the City University of New York, Brooklyn, New York 11210; and The Graduate School and University Center of the City University of New York, New York, New York 10036

- M. Toscano** (273) Dipartimento di Chimica, Università della Calabria, I-87030 Arcavacata di Rende (CS), Italy
- P. E. A. Turchi** (85) Department of Chemistry and Materials Science, Lawrence Livermore National Laboratory, Livermore, California 94550
- E. Valderrama** (49) Química, Instituto Venezolano de Investigaciones Científicas, Caracas 1020-A, Venezuela
- J. van Ek** (85) Department of Physics, Tulane University, New Orleans, Louisiana 70118
- Robert W. Warren** (167) Theoretical Chemistry Section, Naval Research Laboratory, Washington, DC 20375
- A. J. Williamson** (189) TCM Group, Cavendish Laboratory, Cambridge CB3 0HE, United Kingdom
- Aleš Zupan** (1) Department of Physical and Organic Chemistry, Jožef Stefan Institute, 1000 Ljubljana, Slovenia

Preface

As the millennium comes to a close, a striking area of knowledge has emerged as the most promising for explaining the behavior of all known matter. This area is quantum mechanics. As experience teaches us, it is not wise to say that this is the final theory; nevertheless, we are witnessing how the equations of quantum mechanics, which predict the behavior of nature, can be used to design matter according to our needs and goals. Quantum mechanical equations can describe the detailed structure and behavior of matter, from electrons, atoms, and molecules to the whole universe. Quantum mechanics is an area of knowledge that yields the most remarkable precision. This precision is limited only by the computational resources available. For instance, the energy of helium-like atoms can be calculated with a precision of about 15 decimal places. Comparatively speaking, this is equivalent to determining the distance between one point in New York and another in Paris with a tolerance smaller than 10 Å. Such precision is possible when the nonrelativistic Schrödinger equation is sufficiently precise, a condition that covers a large part of chemistry.

Quantum mechanics has become a great tool for chemistry. For this reason, the methods of quantum mechanics used in chemistry have been grouped into a field called quantum chemistry, as in the title of this serial. The techniques of quantum chemistry were developed at a tremendous rate by the combined efforts of pure quantum theorists, application specialists, and scientific programmers, along with feedback from numerous precision experiments. These techniques have become routine in most universities worldwide, and courses on quantum chemistry at all levels are part of their curricula.

Solving the Schrödinger equation for chemical and chemistry-related applications from first principles has been the goal of two communities. Initially working separately, the standard *ab initio* and the density functional theory (DFT) groups had to deal with similar problems. In most cases, applications in chemistry require specific constraints on the methodologies to be used. For instance, it is necessary that methods be size-consistent or size-extensive, i.e., that systems of different size be treated with the same footing. In practical terms, this means that errors, if not zero, should in some way be proportional to the size of the system so that energy differences can take advantage of error cancellations. If a system only needs to be analyzed individually, this requirement may be irrelevant. A parallel and perhaps much more important requirement

for solving the Schrödinger equation is that the chosen method not use ad hoc parameters. This is a very important requirement, of special significance in the design of new materials where experimental information is scarce or difficult to obtain; unfortunately, it is very challenging to fulfill. Sometimes a very small empirical correction can avoid a large computational process. Typical examples of this correction in *ab initio* methods are the high-level correction (HLC) in the G1 and G2 methods and the ~ 0.9 correction to the zero-point vibrational energies. Other common corrections are based on criteria of energy partitions; these include the basis set superposition error correction and the basis set incompleteness corrections. Alternative criteria are given by the need for variational methods, implying that the final energies are always upper bounds of the correct energy. This implies that an improvement in the basis set will always yield an energy closer to the exact one. Finally, in a practical sense, a very good compromise between precision and cost of the calculation is highly desired. Usually the cost of a calculation is determined by the scaling of the CPU time with respect to the size of the calculation and expressed in the form N^m , where N is an indicator of the size of the calculation (number of basis sets, number of electron, atoms, etc.) An N^7 method will require 128 times more CPU resources if the size of the system is doubled. In practice, such a formal scaling is reduced by 1 or 2 units. For instance, the formal scaling for the HF method is N^4 , whereas practical calculations tend to scale close to N^2 .

The standard *ab initio* methods solve the Schrödinger equation in a direct way. They assume a wavefunction, which is expanded on a basis set and able to approach the ultimate solution in several ways. Unfortunately, this has a tremendous cost. These methods can initially use a single reference or a multi-reference wavefunction as a starting point. In the Hartree–Fock approximation, historically called the self-consistent method (SCF), the wavefunction is a Slater determinant composed of molecular orbitals representing the electrons in the molecule. These electrons interact with the mean field of the other electrons and the nuclei. Improvements to this approximation, which recognize that electrons actually do not interact with the mean field of other electrons but with each one individually, are performed with methods such as truncated configuration interaction, quadratic configuration interaction, Møller–Plesset perturbation theory, and coupled cluster theory. All these methods tend to obtain better and better solutions to the Schrödinger equation but simultaneously demand larger and larger basis sets in order to take advantage of the higher degree of treatment of the correlation energy, which is defined as the error of calculation with a single determinant, i.e., with the HF approximation. If a large enough basis set is used, a full configuration interaction method will yield the exact solution to the Schrödinger equation.

Alternatively, the convergence toward the precise solution of the Schrödinger equation can be accelerated by using a multireference approach. There is a corresponding multireference (MR) approach to each of the single reference

approaches; these are named MR-HF or MR-SCF, MR-CI, MR-MP, and MRCC. In general, the degree of complication is a function of the excited determinants used to represent the wavefunction. The inclusion of triple and quadruple excited determinants still constitutes the best alternative in standard *ab initio* quantum chemistry. The methods MP4SDTQ, CCSD(T), and QCISDTQ, for instance, have the same scaling of N^7 , and their precision is approximately similar when basis sets containing f or higher angular momentum functions are used. Calculations with such a high degree of computational resources can obtain accuracies in relative energies approaching 1 kcal/mol. Calculations of this kind are limited for practical reasons to systems containing no more than 10 atoms due to their large use of computational resources. Calculations using more expensive basis sets using g and higher angular momentum functions have been reported with precisions approaching 0.1 kcal/mol. At present, calculations of this degree of precision are limited to systems containing only around 20 electrons.

The alternative method of solving the Schrödinger equation is density functional theory (DFT). This theory was developed simultaneously with the standard *ab initio* methods. However, it took a little longer to gain a very solid footing. The work of Hohenberg, Kohn, Sham, and Levy has contributed enormously to the recognition of DFT as an *ab initio* procedure. The theory and philosophy of DFT do not follow its standard *ab initio* counterparts, which delayed its acceptance as a formal theory. As demonstrated by the Hohenberg–Kohn theorem, the total energy of an electronic system can be expressed by a functional of the electron density. Actually, the implementation of several modern generalized gradient approximation (GGA) functionals attracted the quantum chemistry community to the use of DFT because of the great success of the GGAs in reproducing well-established experimental results that were not possible to obtain with the tools available in standard *ab initio* methods. The *ab initio* nature of GGA functionals such as those of Perdew and Wang, published in 1991, gave confidence to the systematic search for first principles functionals. The improvement of the functionals has been enormous, to the point that present calculations using a standard basis set including d -type functions and modern functionals are more precise than any of those using the sophisticated standard *ab initio* methods, including all those that scale as N^7 and even in several cases where the latter are used with much larger basis sets. Most of the methods in DFT are based on the Kohn–Sham procedure, in which the Schrödinger equation is solved for the exact energy using a wavefunction from an ideal system of non-interacting electrons, bypassing the calculation of the real wavefunction, which is the major difficulty in the standard methods. Since the system of noninteracting electrons is constrained to possess the same electron density as the real interacting system, the quality of the energies is limited only by the functionals used to represent the total energy. The formal scaling of DFT methods is N^3 or N^4 depending on the particular method; however, as happens with the standard *ab initio* methods, in practice this scaling tends to be lower, about N^2 for DFT,

and work to reach even smaller scalings is in progress. The other great advantage of DFT methods lies in the fact that an improvement in the functionals does not imply an increase in the scaling.

At present, it is fair to say that most calculations are done using DFT rather than the standard *ab initio* methods. This is the justification of and motivation for this thematic volume. The papers presented here constitute the latest DFT research of their authors. It is to them that I express my most sincere gratitude for their effort in this work, which surely constitutes one of the most comprehensive summaries currently available for DFT or related areas. My thanks also go to Per-Olov Löwdin for encouraging me to edit this book.

JORGE M. SEMINARIO
COLUMBIA, SOUTH CAROLINA

Why Density-Gradient Corrections Improve Atomization Energies and Barrier Heights

John P. Perdew and Matthias Ernzerhof

Department of Physics and Quantum Theory Group, Tulane University, New Orleans, LA 70118

Aleš Zupan

Department of Physical and Organic Chemistry, Jožef Stefan Institute, Jamova 39, 1000 Ljubljana, Slovenia

Kieron Burke

Department of Chemistry, Rutgers University, Camden, NJ 08102

While the Hartree-Fock (HF) approximation typically underestimates the strength of the chemical bond, the local spin density (LSD) approximation overestimates it. Thus LSD overbinds atoms in molecules, and underestimates the heights of energy barriers when the transition state is more highly bonded than the initial state. Generalized gradient approximations (GGA's), which incorporate density-gradient corrections to LSD, improve the agreement between calculated and measured energetics. This has been previously understood as a consequence of the fact that gradient corrections favor density inhomogeneity, which increases when a bond is stretched or broken. We show that gradient corrections also favor high density, which increases when a bond is compressed or formed, but that the inhomogeneity effect usually prevails. To quantify the discussion, we present a thermodynamic-like inequality which is satisfied when gradient corrections favor a process.

I. ENERGY FUNCTIONALS AND CHEMICAL ENERGETICS

Quantum chemistry is most simply done with single-particle orbitals $\psi_{\alpha,\sigma}$ which are obtained from selfconsistent single-particle equations. The exchange-correlation energy E_{xc} is then constructed from the orbitals, or from the spin densities n_{\uparrow} and n_{\downarrow} . The Hartree-Fock (HF) approximation neglects correlation but treats exchange exactly:

$$E_x^{HF}[\{\psi_{\alpha,\sigma}\}] = -\frac{1}{2} \sum_{\sigma} \int d^3r \int d^3r' |\sum_{\alpha} \psi_{\alpha,\sigma}^*(\mathbf{r}') \psi_{\alpha,\sigma}(\mathbf{r})|^2 / |\mathbf{r}' - \mathbf{r}|. \quad (1)$$

The local spin density (LSD) approximation [1]

$$E_{xc}^{LSD}[n_{\uparrow}, n_{\downarrow}] = \int d^3r n(\mathbf{r}) \epsilon_{xc}(n_{\uparrow}(\mathbf{r}), n_{\downarrow}(\mathbf{r})) \quad (2)$$

invokes $\epsilon_{xc}(n_{\uparrow}, n_{\downarrow})$, the exchange-correlation energy per particle of an electron gas with uniform spin densities n_{\uparrow} and n_{\downarrow} [2]. The generalized gradient approximation (GGA) [3-8]

$$E_{xc}^{GGA}[n_{\uparrow}, n_{\downarrow}] = \int d^3r f(n_{\uparrow}, n_{\downarrow}, \nabla n_{\uparrow}, \nabla n_{\downarrow}) \quad (3)$$

makes use of the local density gradient as well as the local density. (Except where other units are specified, we use atomic units in which $\hbar = m = e^2 = 1$).

The “GGA made simple” [7], which we employ in this work, arises from two different non-empirical derivations [7,8]. All its parameters (other than those in LSD) are fundamental constants.

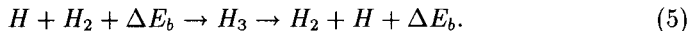
Both LSD and GGA predict realistic geometries and vibrational frequencies for molecules, but GGA gives a better account of atomization energies [9,10] and barrier heights [11-15]. The aim of this article is to explain why, using a density-parameter analysis we have recently developed [16,17], and to provide a pedagogical discussion of these issues. We will show how the chemical effects of gradient corrections follow from the gradient dependence of the functional E_{xc}^{GGA} . For an explanation of the physical origins of this non-locality, see Ref. [18]. For some reasons why LSD and GGA work as well as they do, see Ref. [19]. For methods which incorporate but go beyond GGA, see Refs. [20] and [21].

The atomization energy ΔE_a is the extra energy needed to break up a molecule into separate atoms. For the nitrogen dimer,



For this reaction, as for most others, HF underbinds ($\Delta E_a = 5.0$ eV), LSD overbinds ($\Delta E_a = 11.6$ eV), and GGA gives a more realistic binding energy ($\Delta E_a = 10.5$ eV). The experimental result is $\Delta E_a = 9.9$ eV. All values are taken from Ref. [7]. Other reaction exothermicities or endothermicities [22,23] have also been studied.

The rates of many chemical reactions are limited by an energy barrier ΔE_b which must be surmounted [24]. A well-studied case [14,15,17,25] is the hydrogen abstraction



In the initial state, a hydrogen atom approaches a hydrogen molecule along its bond axis from one side, with energy ΔE_b . The $H \cdots H_2$ distance will be denoted by x . Taking x to be the independent reaction coordinate, we determine y , the H_2 bond length ($y \leq x$), by minimizing the total energy for each x . In the transition state of H_3 , we find $y = x$. When the transition state H_3 fissions, it kicks out a hydrogen atom to the other side. The net effect of this one-dimensional process is a transfer of nuclei. In this reaction [17], as in others where the transition state is more highly bonded than the initial state, the HF barrier is too high ($\Delta E_b = 0.8$ eV), the LSD barrier is too low ($\Delta E_b = -0.1$ eV, making H_3 bound in LSD), and the GGA barrier is more realistic ($\Delta E_b = 0.2$ eV) in comparison with experiment ($\Delta E_b = 0.4$ eV, from Ref. [25]).

Sometimes the transition state has as many bonds as the initial state, e.g., in isomerizations or internal rotations. LSD gives realistic barrier heights

for isomerizations [26], and presumably so does GGA. LSD and GGA predict essentially the same (correct) barriers for internal rotations [27].

The transition state for an atom hopping on a metal surface [28] can have a *lower* coordination number than the initial state, and then GGA barrier heights are lower (and presumably again more correct) than LSD barriers.

II. QUALITATIVE EXPLANATIONS FOR FUNCTIONAL PERFORMANCE

All of the effects described in the preceding section are consistent with one neat statement [11,12]: LSD likes bonds too much, and GGA corrects this bias. Compelling further evidence for this statement can be found in a comparison of LSD and GGA energies for different structures of C_n clusters [29]: The fewer the bonds, the more the gradient corrections lower the total energy. GGA usually weakens and stretches bonds relative to LSD. When bonds stretch or break, the density gradient or inhomogeneity grows, and this lowers the GGA energy relative to LSD. Much can be explained by this statement [30]: GGA favors density inhomogeneity more than LSD does.

However, this cannot be the whole story, because gradient corrections usually and correctly *shrink* the lengths of covalent bonds to hydrogen [14,15,17], counter to expectations based upon the statement at the end of the previous paragraph.

Our current explanation can be summarized qualitatively in this statement [17]: GGA favors both inhomogeneity and high density more than LSD does. These effects usually compete; for example, inhomogeneity increases and density decreases as we stretch or break a bond. The inhomogeneity effect usually prevails but, for the bond length of H_2 , the density effect is large enough to carry the day. The final two sections of this article will quantify and test this statement.

Alternative explanations [10,13] appeal to the selfconsistent effect of gradient corrections on the electron density. For example, gradient corrections shrink the ionic cores of the atoms, producing a stronger screening of the nuclear potential and a more diffuse valence-electron density, hence a longer bond length between most atoms which have cores. We do not disagree with these alternative explanations, but we believe that ours is more robust, because it explains why gradient corrections produce all their characteristic energetic effects, even when applied to the LSD density [13,15].

III. DENSITY PARAMETERS AND THEIR AVERAGES

To quantify the explanation given at the end of the preceding section, let us define the local density parameter $r_s(\mathbf{r})$, the local relative spin polarization

$\zeta(\mathbf{r})$, and the local inhomogeneity parameter or reduced density gradient $s(\mathbf{r})$ by the equations

$$n = n_{\uparrow} + n_{\downarrow}, \quad (6)$$

$$\zeta = (n_{\uparrow} - n_{\downarrow})/n, \quad (7)$$

$$s = |\nabla n|/2(3\pi^2)^{1/3}n^{4/3}. \quad (8)$$

The Seitz radius r_s is the radius of a sphere which on average contains one electron, so $r_s \rightarrow 0$ in the high-density limit; valence electrons typically have $1 \text{ bohr} \leq r_s \leq 6 \text{ bohr}$. The relative spin polarization ζ vanishes for a spin-unpolarized system, and equals $+1$ or -1 where all the electron spins are up or down, respectively. The inhomogeneity parameter s measures how fast the density varies on the scale of the local Fermi wavelength; valence electrons typically have $0 \leq s \leq 3$. Both r_s and s diverge in the low-density tail of an atom or molecule.

In previous work [16,17], we have studied distributions and averages of these parameters in atoms, molecules and solids, and how these change in various processes. Typically, the averages $\langle r_s \rangle$, $\langle |\zeta| \rangle$, and $\langle s \rangle$ all increase when we stretch or break a bond, as shown in Fig. 1 for the fission of the H_3 transition state.

Because the distributions of the density parameters p are broad, their averages must be defined carefully. We want true averages $\langle p \rangle$, which fall between the minimum and maximum values of p present in the system. But we also want averages that will give meaningful estimates of LSD and GGA exchange-correlation energies.

To a good approximation, any GGA can be written as

$$E_{xc}^{GGA} = \int d^3r n \epsilon_x(r_s) F_{xc}(r_s, \zeta, s), \quad (9)$$

where small $\nabla\zeta$ contributions have been neglected. (The barrier height in the reaction of Eq. (5) is 0.15 eV with and 0.21 eV without these contributions.) In Eq. (9),

$$\epsilon_x(r_s) = -\frac{3}{4\pi} \left(\frac{9\pi}{4} \right)^{1/3} \frac{1}{r_s} \quad (10)$$

is the exchange energy per electron of a spin-unpolarized uniform electron gas of density parameter r_s . The enhancement factor over spin-unpolarized local exchange, $F_{xc}(r_s, \zeta, s)$, is displayed in Fig. 1 of Ref. [7]. It can be decomposed into exchange and correlation components:

$$F_{xc}(r_s, \zeta, s) = F_x(\zeta, s) + F_c(r_s, \zeta, s) \quad (11)$$

where $F_c \rightarrow 0$ as $r_s \rightarrow 0$. The s -dependence of Eq. (11) is the nonlocality of GGA, which reduces to LSD when we set $s = 0$:

$$E_{xc}^{LSD} = \int d^3r \, n\epsilon_x(r_s)F_{xc}(r_s, \zeta, 0). \quad (12)$$

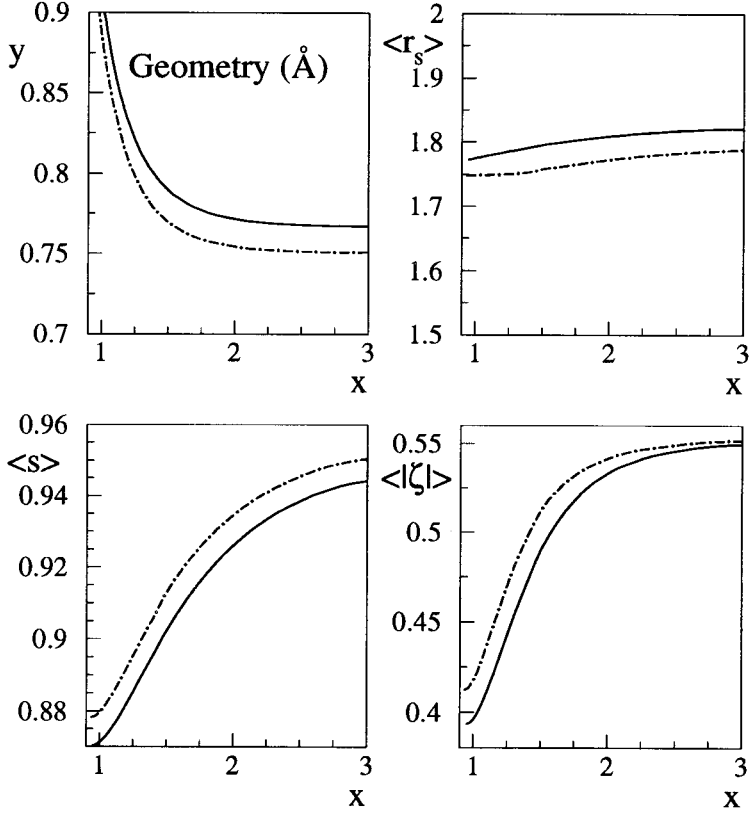


FIG. 1. Geometry and density-parameter averages for the fragmentation of H_3 transition state of Eq. (5). x is the longer of the two bond lengths, and increases from $x = y = 0.95$ Å (LSD) or 0.935 Å (GGA) at the transition state to infinity in the dissociated limit. The averages defined in Eqs. (13)-(15) have been evaluated selfconsistently in LSD (solid curve) and GGA (dashed curves). Note that gradient corrections increase the inhomogeneity parameter $\langle s \rangle$ and reduce $\langle r_s \rangle$, as expected.

To define our density-parameter averages, we use the exchange-only limit:

$$\epsilon_x(\langle r_s \rangle) = \int d^3r \, n\epsilon_x(r_s) / \int d^3r \, n, \quad (13)$$

$$F_x(\langle|\zeta|\rangle, 0) = \int d^3r \, n_{\epsilon_x}(r_s) F_x(\zeta, 0) / \int d^3r \, n_{\epsilon_x}(r_s), \quad (14)$$

$$F_x(0, \langle s \rangle) = \int d^3r \, n_{\epsilon_x}(r_s) F_x(0, s) / \int d^3r \, n_{\epsilon_x}(r_s). \quad (15)$$

The averages $\langle r_s \rangle$, $\langle|\zeta|\rangle$, and $\langle s \rangle$ are found as numerical roots of these equations. If the statement that “gradient corrections favor density inhomogeneity” were the whole story, we would expect that gradient corrections would favor any physical process in which

$$d\langle s \rangle > 0. \quad (16)$$

As we will see in the next section, Eq. (16) is *not* the right condition.

IV. QUANTITATIVE EXPLANATION OF FUNCTIONAL PERFORMANCE

The averages defined in Eqs. (13) - (15) can be used to estimate the GGA and LSD exchange-correlation energies as

$$E_{xc}^{GGA} \approx N \epsilon_x(\langle r_s \rangle) F_{xc}(\langle r_s \rangle, \langle|\zeta|\rangle, \langle s \rangle), \quad (17)$$

$$E_{xc}^{LSD} \approx N \epsilon_x(\langle r_s \rangle) F_{xc}(\langle r_s \rangle, \langle|\zeta|\rangle, 0), \quad (18)$$

where N is the number of electrons. Eqs. (17) and (18) become exact when spin-unpolarized exchange dominates all other effects, or when the distributions of the density variables are very narrow. However, these equations are surprisingly accurate for real atoms, molecules, and solids [17]. For very heavy atoms, one might want to eliminate the core-electron contributions to (17) and (18), but we have not found this to be necessary in our studies for atomic numbers up to 17.

Now the effect of gradient corrections upon the energy per electron is

$$\begin{aligned} \Delta &\equiv (E_{xc}^{GGA} - E_{xc}^{LSD})/N \\ &\approx \epsilon_x(\langle r_s \rangle) [F_{xc}(\langle r_s \rangle, \langle|\zeta|\rangle, \langle s \rangle) - F_{xc}(\langle r_s \rangle, \langle|\zeta|\rangle, 0)]. \end{aligned} \quad (19)$$

The exact evaluation of Δ is simpler and more accurate than evaluation of the last line of Eq. (19), but the latter expression permits us to make a quantitative test of our qualitative explanations.

Consider a physical process in which each density-parameter average $\langle p \rangle$ changes to $\langle p \rangle + d\langle p \rangle$ at fixed N . This process will be favored by gradient corrections if and only if

$$d\Delta < 0 \quad (20)$$

i.e., (for $\partial\Delta/\partial\langle s \rangle < 0$)

$$\frac{d\langle s \rangle}{\langle s \rangle} > P \frac{d\langle r_s \rangle}{2\langle r_s \rangle} + Q d\langle|\zeta|\rangle, \quad (21)$$

where

$$P = -\frac{2\langle r_s \rangle}{\langle s \rangle} \frac{\partial \Delta / \partial \langle r_s \rangle}{\partial \Delta / \partial \langle s \rangle}, \quad (22)$$

$$Q = -\frac{1}{\langle s \rangle} \frac{\partial \Delta / \partial \langle |\zeta| \rangle}{\partial \Delta / \partial \langle s \rangle}. \quad (23)$$

We have tested ([17,18]) the inequality (21) for about 20 atomization processes and a smaller number of bond stretchings and transition - state fragmentations. We find that the inequality (21) holds whenever gradient corrections favor a process.

A simple model in which $P = 1$ and $Q = 0$ is

$$F_{xc}(r_s, \zeta, s) = F_{xc}(r_s, \zeta, 0) + \mu s^2, \quad (24)$$

where μ is any positive constant. Although the true GGA nonlocality is more complicated than Eq. (24), it also yields [17] $P \approx 1$ and $Q \approx 0$. Thus we can simplify Eq. (21) for qualitative purposes to

$$\frac{d\langle s \rangle}{\langle s \rangle} > \frac{d\langle r_s \rangle}{2\langle r_s \rangle}, \quad (25)$$

which clearly differs from the naive condition (16) when $d\langle r_s \rangle \neq 0$. In bond stretching, for example, both the left- and right-hand sides of (25) are typically positive. The left- hand side is usually bigger, but in H_2 and H_3 it is smaller than the right-hand side. Thus gradient corrections stretch most bonds, but contract the H_2 and H_3 bonds, and affect atomization energies and barrier heights as described in the first section of this article.

Our inequalities (21) and (25), which follow from the fact that the GGA enhancement factor $F_{xc}(r_s, \zeta, s)$ increases with s , tell us when a process will be favored by gradient corrections. How strongly it will be favored then depends upon how strongly $F_{xc}(r_s, \zeta, s)$ increases with s . Fig. 1 of Ref. [7] shows that the exchange-only ($r_s = 0$) enhancement factor has an especially strong increase with s , which partly explains why the HF approximation underbinds atoms in molecules. For example, consider the atomization of NH_3 , in which the exchange-correlation energy increases by 8.9 eV. The corresponding increases in the exchange energy are 7.0 (LSD), 5.9 (GGA), and 4.7 (HF) eV [31]. Thus, neglecting the nonlocality of exchange has an effect somewhat like including correlation.

The inequalities (21) and (25) also explain the effects of gradient corrections upon structural transformations in solids [32] and upon surface energies [17].

V. ACKNOWLEDGMENTS

J.P.P. and M.E. acknowledge the support of the National Science Foundation under Grant No. DMR 95-21353. A.Z. acknowledges the support of the Slovenian Ministry for Science and Technology under Grant J1-8665.

VI. REFERENCES

- [1] W. Kohn and L.J. Sham, *Phys. Rev.* 140, A1133 (1965).
- [2] J.P. Perdew and Y. Wang, *Phys. Rev.* B45, 13244 (1992).
- [3] D.C. Langreth and M. J. Mehl, *Phys. Rev.* B28, 1809 (1983).
- [4] J.P. Perdew and Y. Wang, *Phys. Rev.* B33, 8800 (1986); 40, 3399 (E) (1989).
- [5] J.P. Perdew, *Phys. Rev.* B33, 8822 (1986); 34, 7406 (E) (1986).
- [6] A.D. Becke, *Phys. Rev.* A38, 3098 (1988).
- [7] J.P. Perdew, K. Burke, and M. Ernzerhof, *Phys. Rev. Lett.* 77, 3865 (1996); 78, 1396 (E) (1997).
- [8] J.P. Perdew, K. Burke, and Y. Wang, *Phys. Rev. B* 54, 16533 (1996).
- [9] L.A. Curtiss, K. Raghavachari, P.C. Redfern, and J.A. Pople, *J. Chem. Phys.* 106, 1063 (1997), and references therein.
- [10] D.C. Patton, D.V. Porezag, and M. R. Pederson, *Phys. Rev.* B55, 7454 (1997).
- [11] L. Fan and T. Ziegler, *J. Am. Chem. Soc.* 114, 10890 (1992).
- [12] L. Deng, T. Ziegler, and L. Fan, *J. Chem. Phys.* 99, 3823 (1993).
- [13] B. Hammer, K. W. Jacobsen, and J.K. Nørskov, *Phys. Rev. Lett.* 70, 3971 (1993).
- [14] B.G. Johnson, C.A. Gonzales, P.M.W. Gill, and J.A. Pople, *Chem. Phys. Lett.* 221, 100 (1994).
- [15] D. Porezag and M.R. Pederson, *J. Chem. Phys.* 102, 9345 (1995).
- [16] A. Zupan, J.P. Perdew, K. Burke, and M. Causá, *Int. J. Quantum Chem.* 61, 835 (1997).
- [17] A. Zupan, K. Burke, M. Ernzerhof, and J. P. Perdew, *J. Chem. Phys.* 106, 10184 (1997).

- [18] J.P. Perdew, M. Ernzerhof, A. Zupan, and K. Burke, J. Chem. Phys., to appear.
- [19] K. Burke, M. Ernzerhof, and J.P. Perdew, unpublished.
- [20] M. Ernzerhof, Chem. Phys. Lett. 263, 499 (1996); J.P. Perdew, M. Ernzerhof, and K. Burke, J. Chem. Phys. 105, 9982 (1996); K. Burke, M. Ernzerhof, and J.P. Perdew, Chem. Phys. Lett. 265, 115 (1997).
- [21] M. Noland, E.L. Coitiño, and D.G. Truhlar, J. Phys. Chem. A101, 1193 (1997).
- [22] R. Neumann and N.C. Handy, Chem. Phys. Lett. 246, 381 (1995).
- [23] J.M. Martell, J.D. Goddard, and L.A. Eriksson, J. Phys. Chem. A101, 1927 (1997).
- [24] P.J. Feibelman and J. Harris, Nature 372, 135 (1994).
- [25] W.R. Schultz and D.J. LeRoy, J. Chem. Phys. 42, 3869 (1965).
- [26] J.M. Seminario, M. Grodzicki, and P. Politzer, in *Density Functional Methods in Chemistry*, edited by J. Labanowski and J. Andzelm (Springer-Verlag, Berlin, 1990).
- [27] A. Borrmann and R.O. Jones, Chem. Phys. Lett. 252, 1 (1996).
- [28] B.D. Yu and M. Scheffler, Phys. Rev. Lett. 77, 1095 (1996).
- [29] R.O. Jones and G. Seifert, Phys. Rev. Lett. 79, 443 (1997).
- [30] J.P. Perdew, J.A. Chevary, S.H. Vosko, K.A. Jackson, M.R. Pederson, D.J. Singh, and C. Fiolhais, Phys. Rev. B46, 6671 (1992); 48, 4978 (E) (1993).
- [31] M. Ernzerhof, J.P. Perdew, and K. Burke, Int. J. Quantum Chem. 64, 285 (1997).
- [32] A. Zupan, P. Blaha, K. Schwarz, and J.P. Perdew, unpublished.

Second-Order Relations Involving Correlation Energy and its Functional Derivative

Stanislav Ivanov and Mel Levy

Chemistry Department and
Quantum Theory Group, Tulane University
New Orleans, Louisiana 70118

Abstract

For continuing to search for ever-better approximations to the traditional density-functional correlation energy functional, $E_c[n]$, the link between its second-order component, $E_c^{(2)}[n]$, and the known result for the second-order Z^{-1} quantum chemistry correlation energy, $E_c^{QC,(2)}$, is first presented, and numerical results are given. $E_c^{(2)}[n]$, identified as a high-density scaling limit, is the leading term in the expansion for $E_c[n]$. Except when certain degeneracies occur, it is shown that $E_c^{QC,(2)}$ provides an upper bound for $E_c^{(2)}[n]$, with an equality only for two electrons. Moreover, different correlation energy functionals, meant to be employed in hybrid schemes, are also discussed. For these functionals, the second-order Z^{-1} quantum chemistry correlation energy is exactly the same as their high-density limits, for any number of electrons, except when some degeneracies occur. Next, conditions are presented in order to improve approximations to the density functional correlation potential (the functional derivative of the correlation energy). For any spherically symmetric two-electron density, the difference, $2 E_c^{(2)}[n] - \int d\mathbf{r} v_c^{(2)}([n];\mathbf{r}) n(\mathbf{r})$, is written as a functional of the density $n(\mathbf{r})$ only, and the analytical expression is obtained. Approximate functionals that scale to constants, are tested against exact numerical results.

I. Introduction

The problem of finding the ground-state properties of a system consisting of more than one electron is very important in the study of atoms, molecules and solids. In order to obtain the ground-state properties, one has to solve the Schrödinger equation for the system under investigation. Since no exact solution exists to this problem for Coulomb systems, many different approximate methods have been developed for approaching this subject.

Modern density functional theory (DFT) provides an enormous simplification of the many-body problem [1-7]. It enables one to replace the complicated conventional wavefunction approach with the simpler density functional formalism. The ground-state properties of the system under investigation are obtained through a minimization over densities rather than a minimization over wavefunctions. The electron density is especially attractive for calculations involving large systems, because it contains only three dimensions regardless of the size of the system. In addition, even for relatively small systems, it has been found that density-functional methods, for certain situations, often yield results competitive with, or superior to those obtained from various traditional wavefunction approaches.

Correlation energies in DFT must be approximated. For this purpose, knowledge of exact properties is necessary. With this in mind, it is now known that the exact correlation energy for use as part of a full DFT calculation, $E_c[n]$ [1-10], satisfies [10-13] the expansion

$$E_c[n_\lambda] = E_c^{(2)}[n] + \lambda^{-1}E_c^{(3)}[n] + \lambda^{-2}E_c^{(4)}[n] \dots = \sum_{j=2}^{\infty} \lambda^{2-j} E_c^{(j)}[n] , \quad (1)$$

for high-enough λ , where

$$n_\lambda(x, y, z) \equiv \lambda^3 n(\lambda x, \lambda y, \lambda z) . \quad (2)$$

Hence, $E_c[n_\lambda]$ is bounded, and is equal to $E_c^{(2)}[n]$, as $\lambda \rightarrow \infty$.

It is our purpose to briefly review expansion (1) through the adiabatic perturbation theory of Görling and Levy [11], which arrives at the formal expression for the second-order energy, $E_c^{(2)}[n]$, in terms of Kohn-Sham orbitals.

The quantity $2E_c^{(2)}[n]$ is particularly important because it is the initial slope in the adiabatic connection method (coupling-constant formula) for $E_c[n]$ [10,14-18]. In fact, quite good use of the evaluation of $2E_c^{(2)}[n]$ has recently been made by Ernzerhof [19] and by Perdew, Burke, and Ernzerhof [20-23] in their modeling of

the adiabatic connection integrand, not only about zero but all the way to unity, to produce very encouraging results in their hybrid schemes.

It is also believed that $E_c[n]$ is relatively insensitive to coordinate scaling [11], i.e. $\lim_{\lambda \rightarrow \infty} E_c[n_\lambda] \equiv E_c^{(2)}[n] \approx E_c[n]$ for small atoms, where $E_c^{(2)}[n]$, the second-order component of $E_c[n]$, is the leading term in the expansion for $E_c[n]$. As a result, knowledge of the high-density scaling limit, $\lim_{\lambda \rightarrow \infty} E_c[n_\lambda]$, is essential for

arriving at the very best approximations to $E_c[n]$. In a recent work, Liu and Parr [24] have ascertained that $E_c^{(2)}[n]$ accounts for a significant part ($\sim 80\%$) of the total correlation energy.

Numerical bounds for $E_c^{(2)}[n]$, as recently generated by Ivanov and Levy [25], shall be given for hydrogenic densities, corresponding to two, three, nine, ten, and eleven electrons. For two electrons, the bounds become an equality.

Relations shall also be presented involving the correlation energy, ${}^{\text{HF}}E_c[n]$, [11], whose functional derivative is meant to be added to the ordinary Fock potential to produce, upon self-consistency, the exact ground-state energy and density.

We shall reveal very recently derived [26] high-density limit for the correlation energy functional of the Hartree-Fock density, $E_c^{\text{QC}}[n^{\text{HF}}]$ [27,28]. This functional should be used as a “tack-on” functional to the completed Hartree-Fock energy to produce the exact ground-state energy. We shall also emphasize some subtle differences between $E_c[n]$ and $E_c^{\text{QC}}[n^{\text{HF}}]$ in light of the increasing use of DFT functionals as approximations to the correlation energy functional of the Hartree-Fock density.

Most of the present approximations to $E_c[n]$ give relatively good results for $E_c[n]$ but the shapes of the corresponding correlation potentials are not quite satisfactory. With this in mind, for comparison purposes, we introduce the first known closed-form expression connecting a component of the correlation potential to the correlation energy functional from which the potential is obtained by taking a functional derivative [29]. In particular, the closed-form expression connects $E_c^{(2)}[n]$ with its functional derivative, $v_c^{(2)}([n];\mathbf{r})$. We will present our analytical results for spherically symmetric two-electron spin-nonpolarized densities.

Finally, comparisons shall be made, for the mentioned relations involving $E_c[n]$, ${}^{\text{HF}}E_c[n]$, and $E_c^{\text{QC}}[n^{\text{HF}}]$, with the correlation energy functionals of Perdew-Burke-Ernzerhof [30], Lee-Yang-Parr [31], and Wilson-Levy [32].

II. Definitions

In atomic units (a.u. are to be used throughout the paper), let us define the Hamiltonian operator for the system of interest as

$$\hat{H} = \hat{T} + \hat{V}_{ee} + \sum_{i=1}^N v(\mathbf{r}_i) \quad , \quad (3)$$

where \hat{T} is the kinetic energy operator,

$$\hat{T} = \sum_{i=1}^N -\frac{1}{2} \nabla_i^2 \quad , \quad (4)$$

where \hat{V}_{ee} is the operator for the electron-electron repulsion,

$$\hat{V}_{ee} = \sum_{i>j}^{N-1} \sum_{j=1}^N \frac{1}{|\mathbf{r}_i - \mathbf{r}_j|} \quad , \quad (5)$$

and where $v(\mathbf{r})$ is the local spin-independent multiplicative potential of interest.

The ground-state energy of the system under investigation is obtained [1-7] by

$$E^{GS} = \text{Min}_{n(\mathbf{r}) \rightarrow N} \left\{ F[n] + \int v(\mathbf{r}) n(\mathbf{r}) d\mathbf{r} \right\} \quad , \quad (6)$$

where $F[n]$ is the universal Hohenberg-Kohn functional of the density. The constrained-search definition [33] of $F[n]$ is

$$F[n] = \text{Min}_{\Psi \rightarrow n(\mathbf{r})} \langle \Psi | \hat{T} + \hat{V}_{ee} | \Psi \rangle \equiv \langle \Psi[n] | \hat{T} + \hat{V}_{ee} | \Psi[n] \rangle \quad . \quad (7)$$

In other words, $\Psi[n]$ is that antisymmetric wavefunction that minimizes $\langle \hat{T} + \hat{V}_{ee} \rangle$ and yields the density $n(\mathbf{r})$.

For computational purposes $F[n]$ must be approximated and it is commonly

partitioned [3-8] as

$$F[n] = T_s[n] + U[n] + E_x[n] + E_c[n] . \quad (8)$$

In Eq.(8), $T_s[n]$ is the noninteracting kinetic energy

$$T_s[n] = \langle \Phi_o[n] | \hat{T} | \Phi_o[n] \rangle , \quad (9)$$

where $\Phi_o[n]$ is the Kohn-Sham (KS) wavefunction. That is, by definition, $\Phi_o[n]$ is the wavefunction that minimizes just $\langle \hat{T} \rangle$ and yields the same density as $\Psi[n]$. Except for certain degenerate cases, $\Phi_o[n]$ is a single determinant [34]. The Hartree electron-electron repulsion energy $U[n]$ is given by

$$U[n] = \frac{1}{2} \int \int \frac{n(\mathbf{r}_1)n(\mathbf{r}_2)}{|\mathbf{r}_1 - \mathbf{r}_2|} d\mathbf{r}_1 d\mathbf{r}_2 . \quad (10)$$

The exchange energy, $E_x[n]$, defined in terms of the KS single determinant, is

$$E_x[n] = \langle \Phi_o[n] | \hat{V}_{ee} | \Phi_o[n] \rangle - U[n] , \quad (11)$$

and the correlation energy, $E_c[n]$, is defined as

$$E_c[n] = \langle \Psi[n] | \hat{T} + \hat{V}_{ee} | \Psi[n] \rangle - \langle \Phi_o[n] | \hat{T} + \hat{V}_{ee} | \Phi_o[n] \rangle . \quad (12)$$

With these definitions, Eqs.(9)-(12), the following simple scaling occurs with $E_x[n]$, [8]:

$$E_x[n_\lambda] = \lambda E_x[n] . \quad (13)$$

On the other hand, upon uniform scaling of the electron density, Eq.(2), $E_c[n]$ does not scale homogeneously. Instead, $E_c[n]$ satisfies the following high-density relationship [10-13]:

$$\lim_{\lambda \rightarrow \infty} E_c[n_\lambda] = E_c^{(2)}[n] \quad . \quad (14)$$

In other words, $E_d[n_\lambda]$ is bounded, as $\lambda \rightarrow \infty$, and is equal to a second-order energy. It is important to stress here that, in contrast to Eq.(14), the LDA correlation energy diverges as $-\ln\lambda$, as $\lambda \rightarrow \infty$, because of the Gell-Mann and Brueckner contribution to the correlation energy per particle of a uniform electron gas [35].

The link between uniform scaling of the electron density and scaling of the electron-electron interaction has been developed by Görling and Levy in a series of papers [11,36]. The effective potential and the electron-electron interaction along the coupling constant path, which connects a noninteracting and a fully interacting system with the same electron density, have been used by them for a DFT perturbation theory. For a very recent review of the derivation of the Görling-Levy perturbation theory, see Ref.37.

The Hamiltonian along the adiabatic path, as developed by Görling and Levy [11], has the following form

$$\hat{H}_\alpha[n] = \hat{T} + \alpha \hat{V}_{ee} + \sum_{i=1}^N v_\alpha([n]; \mathbf{r}_i) \quad , \quad (15)$$

where

$$v_\alpha([n]; \mathbf{r}) = v_0([n]; \mathbf{r}) - \alpha u([n]; \mathbf{r}) - \alpha v_x([n]; \mathbf{r}) - v_c^\alpha([n]; \mathbf{r}) \quad . \quad (16)$$

For small enough α ,

$$v_c^\alpha([n]; \mathbf{r}) = \alpha^2 v_c^{(2)}([n]; \mathbf{r}) + \alpha^3 v_c^{(3)}([n]; \mathbf{r}) + \dots \quad . \quad (17)$$

In the above equations, $u([n]; \mathbf{r})$, $v_x([n]; \mathbf{r})$, $v_c^{(0)}([n]; \mathbf{r})$ are the functional derivatives of $U[n]$, $E_x[n]$ and $E_c^{(0)}[n]$ with respect to the density.

By using their perturbation theory, Görling and Levy have arrived at the following high-density expression for $E_c^{(2)}[n]$

$$E_c^{(2)}[n] = \sum_{k=1}^{\infty} \frac{|\langle \Phi_k | \hat{V}_{ee} - \sum_{i=1}^N \{u([n]; \mathbf{r}) + v_x([n]; \mathbf{r})\} | \Phi_0 \rangle|^2}{E_0 - E_k^0} \quad , \quad (18)$$

or

$$\lim_{\lambda \rightarrow \infty} E_c[n_\lambda] = E_c^{(2)}[n] = \sum_{k=1}^{\infty} \frac{|\langle \Phi_k | \hat{V}_{ee} - \sum_{i=1}^N \{u([n]; r_i) + v_x([n]; r_i)\} | \Phi_0 \rangle|^2}{E_0 - E_k^0} \quad (18A)$$

In Eq.(18), the KS wavefunction Φ_0 is the ground-state solution to the non-interacting Schrödinger equation

$$\hat{H}_0[n] \Phi_k = E_k \Phi_k ; \quad E_0 < E_1^0 \leq \dots \leq E_k^0 \leq \dots \quad , \quad (19)$$

where we shall assume that E_0 is nondegenerate. The energies E_0 and E_k^0 are the eigenvalues corresponding to Φ_0 and Φ_k respectively.

III. Different Correlation Energy Functionals

Another type of correlation energy functional, ${}^{\text{HF}}E_c[n]$, is defined [10,11,38] by

$${}^{\text{HF}}E_c[n] \equiv \langle \Psi_n | \hat{T} + \hat{V}_{ee} | \Psi_n \rangle - \langle \Phi_n^{\text{HF}} | \hat{T} + \hat{V}_{ee} | \Phi_n^{\text{HF}} \rangle \quad , \quad (20)$$

where Φ_n^{HF} is the single determinant which minimizes the expectation value $\langle \hat{T} + \hat{V}_{ee} \rangle$ and yields the density $n(\mathbf{r})$. The functional derivative of ${}^{\text{HF}}E_c[n]$ is meant to be added to the HF nonlocal potential in order to produce HF-like equations, but whose solution upon self-consistency, in principle, leads to the exact density and to the exact ground-state energy [10,11]. (Without this added functional derivative, the familiar HF density and energy are obtained upon self-consistency.)

For the high-density scaling limit of ${}^{\text{HF}}E_c[n]$, Görling and Levy [11], using their adiabatic perturbation theory, arrived at

$${}^{\text{HF}}E_c[n_\lambda] = {}^{\text{HF}}E_c^{(2)}[n] + \lambda^{-1} {}^{\text{HF}}E_c^{(3)}[n] + \dots = \sum_{j=2}^{\infty} \lambda^{2-j} {}^{\text{HF}}E_c^{(j)}[n], \quad (21)$$

with

$$\lim_{\lambda \rightarrow \infty} {}^{\text{HF}}E_c[n_\lambda] = {}^{\text{HF}}E_c^{(2)}[n] = \sum_{k=1}^{\infty} \frac{|\langle \Phi_k | \hat{V}_{ee} - \sum_{i=1}^N \{u([n]; r_i) + {}^{\text{HF}}\hat{v}_x([\Phi_0]; r_i)\} | \Phi_0 \rangle|^2}{E_0 - E_k^0} \quad (22)$$

In the above formula, ${}^{\text{HF}}\hat{v}_x([\Phi_0];\mathbf{r})$ is the familiar nonlocal Fock exchange operator, but here built from the one-particle Kohn-Sham orbitals of Φ_0 instead of from the Hartree-Fock orbitals.

By separating the infinite summations in Eqs.(19) and (22) into summations over singly excited states and summations over doubly-excited states, Ivanov and Levy [25] have shown that

$$\lim_{\lambda \rightarrow \infty} E_c[n_\lambda] \leq \lim_{\lambda \rightarrow \infty} {}^{\text{HF}}E_c[n_\lambda] . \quad (23)$$

In the above formula, the equality is held only and only for two-electron densities.

Formal extensions of the ${}^{\text{HF}}E_c[n]$ idea, to include generalized Kohn-Sham and hybrid formulations where, say, only a part of the exact exchange energy (expressed in terms of orbitals) and corresponding Fock potentials are employed, have recently been studied in depth [39,40]. Bounds and expressions analogous to Eq.(22) apply in these generalized hybrid formulations [40]. Further work is now in progress along these lines.

Further, for the Hamiltonian \hat{H} , in Eq.(3), we shall define the quantum chemistry correlation energy as a functional of the HF density, $E_c^{\text{QC}}[n^{\text{HF}}]$, [27,28]. Namely

$$E_c^{\text{QC}}[n^{\text{HF}}] \equiv E^{\text{GS}} - E^{\text{HF}} = \langle \Psi_{\text{n}^{\text{GS}}}^{\text{min}} | \hat{H} | \Psi_{\text{n}^{\text{GS}}}^{\text{min}} \rangle - \langle \Phi^{\text{HF}} | \hat{H} | \Phi^{\text{HF}} \rangle . \quad (24)$$

In Eq.(24), which yields $n^{\text{HF}} \Psi_{\text{n}^{\text{GS}}}^{\text{min}}$ is the ground state of \hat{H} , and yields the ground-state density, and Φ^{HF} is the single determinant that minimizes $\langle \hat{H} \rangle$. Note that the density $n^{\text{HF}}(\mathbf{r})$, obtained from Φ^{HF} , is different from $n^{\text{GS}}(\mathbf{r})$. $E_c^{\text{QC}}[n^{\text{HF}}]$ should be used as a "tack-on" functional to the completed Hartree-Fock energy to produce the exact ground-state energy of the system under investigation.

Levy has shown [41] that

$$\lim_{\lambda \rightarrow \infty} E_c^{\text{QC}}[n_\lambda^{\text{HF}}] > -\infty , \quad (25)$$

where

$$n_\lambda^{\text{HF}}(x, y, z) \equiv \lambda^3 n^{\text{HF}}(\lambda x, \lambda y, \lambda z) . \quad (26)$$

IV. Identification of $\lim_{\lambda \rightarrow \infty} E_c^{QC}[n_\lambda^{HF}]$

Ivanov and Levy [26] have very recently studied $E_c^{QC}[n^{HF}]$ by considering a different Hamiltonian operator \hat{H}_α^{QC} , namely

$$\hat{H}_\alpha^{QC} = \hat{T} + \alpha \hat{V}_{ee} + \sum_{i=1}^N \tilde{v}(\mathbf{r}_i) \quad . \quad (27)$$

The above Hamiltonian is a result of a canonical transformation of the coordinate system applied to the Hamiltonian given in Eq.(3), when the external potential is homogeneous. This approach has been first utilized by Linderberg and Shull [42] in the study of the QC correlation energy for high-enough Z , small α , with $\alpha=Z^{-1}$. Notice that \hat{H}_α^{QC} does not keep the density fixed as α changes in contrast to $\hat{H}_\alpha[n]$.

The eigenvalue problem corresponding to \hat{H}_0^{QC} is

$$\hat{H}_0^{QC} \tilde{\Phi}_k = \tilde{E}_k \tilde{\Phi}_k ; \quad \tilde{E}_0 < \tilde{E}_1^0 \leq \tilde{E}_2^0 \leq \dots \leq \tilde{E}_k^0 \leq \dots \quad . \quad (28)$$

Next, we shall assume that $\tilde{v}(\mathbf{r})$ is the Kohn-Sham potential for the density $n(\mathbf{r})$. In other words, $\tilde{v}(\mathbf{r}) = v_0([n]; \mathbf{r})$ and $\hat{H}_0^{QC} = \hat{H}_0[n]$. As a result, the eigenfunctions and eigenvalues in Eqs.(19) and (28) are the same. By using perturbation theory for small enough α , with $Z=\lambda$, Ivanov and Levy [26] have developed an expansion for the HF density, i.e.

$$n_\lambda^{HF}(x,y,z) = \lambda^3 n(\lambda x, \lambda y, \lambda z) + \lambda^2 \delta n(\lambda x, \lambda y, \lambda z) + \lambda \dots \quad . \quad (29)$$

For a similar high- Z expansion for the density obtained from $\Psi_{n_{gs}}^{\min}$ see the recent work of Chakravorty and Davidson [43]. In Eq.(29), density $n(\mathbf{r})$ is obtained from Φ_0 , i.e.

$$n(\mathbf{r}) = \langle \Phi_0 | \hat{\rho} | \Phi_0 \rangle \quad . \quad (30)$$

Also,

$$\delta n(\mathbf{r}) = \langle \Phi_{HF}^{(1)} | \hat{\rho} | \Phi_0 \rangle + \langle \Phi_0 | \hat{\rho} | \Phi_{HF}^{(1)} \rangle \quad , \quad (31)$$

where

$$\Phi_{\text{HF}}^{(1)} = \sum_{k=1}^{\infty} \frac{\langle \Phi_k | \sum_{i=1}^N \{ u([\mathbf{n}]; \mathbf{r}_i) + {}^{\text{HF}}\hat{V}_x([\Phi_o]; \mathbf{r}_i) \} | \Phi_o \rangle}{E_o - E_k^o} \Phi_k. \quad (32)$$

For nondegenerate ground state, Ivanov and Levy [26] have arrived at

$$\lim_{\lambda \rightarrow \infty} E_c^{\text{QC}}[\mathbf{n}_{\lambda}^{\text{HF}}] = E_c^{\text{QC}(2)} = \sum_{k=1}^{\infty} \frac{|\langle \Phi_k | \hat{V}_{ee} | \Phi_o \rangle|^2}{E_o - E_k^o}. \quad (33)$$

In the above equation, D.E. signifies double excitations. In other words, the summation in Eq.(33) goes over those eigenstates Φ_k which are obtained by exciting two electrons from Φ_o . There is no contribution coming from singly-excited states.

Moreover, if $v_o(\mathbf{r})$ in Eq.(27) is a Kohn-Sham potential for some noninteracting system with ground-state density $n(\mathbf{r})$, i.e. $\hat{H}_o^{\text{QC}} = \hat{H}_o$, then

$$\lim_{\lambda \rightarrow \infty} E_c[\mathbf{n}_{\lambda}] \leq \lim_{\lambda \rightarrow \infty} {}^{\text{HF}}E_c[\mathbf{n}_{\lambda}] = \lim_{\lambda \rightarrow \infty} E_c^{\text{QC}}[\mathbf{n}_{\lambda}^{\text{HF}}] = E_c^{\text{QC}(2)}. \quad (34)$$

Also, if one uses the same reference density for ${}^{\text{HF}}E_c[\mathbf{n}]$ and $E_c^{\text{QC}}[\mathbf{n}]$, then

$$\lim_{\lambda \rightarrow \infty} {}^{\text{HF}}E_c[\mathbf{n}_{\lambda}] = \lim_{\lambda \rightarrow \infty} E_c^{\text{QC}}[\mathbf{n}_{\lambda}]. \quad (35)$$

V. Numerical Results

Expressions (34) and (35) enable one to use published numbers for the high- Z asymptotic expansion of QC correlation energy for comparison with approximations to $E_c[\mathbf{n}_{\lambda}]$ and ${}^{\text{HF}}E_c[\mathbf{n}_{\lambda}]$, and $E_c^{\text{QC}}[\mathbf{n}_{\lambda}^{\text{HF}}]$.

To test approximations to $E_c[\mathbf{n}_{\lambda}]$ and ${}^{\text{HF}}E_c[\mathbf{n}_{\lambda}]$, and $E_c^{\text{QC}}[\mathbf{n}_{\lambda}^{\text{HF}}]$ for hydrogenic $n(\mathbf{r})$'s, as $\lambda \rightarrow \infty$, we take the exact values by Ivanova and Safronova [44] and Davidson and co-workers [43,45,46] for the second-order energy $E_c^{\text{QC}(2)}$ for five

different hydrogenic densities. The two- and ten-electron densities are generated from the nondegenerate ground-state wavefunctions of the noninteracting hydrogenic \hat{H}_0^{QC} in Eq.(27) . The ground state of \hat{H}_0^{QC} in Eq.(27) is degenerate for three, nine and eleven electrons. However, Eqs.(34) and (35) still hold because of symmetry [42]. The three-, nine- and eleven-electron densities were obtained from those $\Phi_0[n]$'s that correspond to the configurations $1s^22s$, $1s^22s^22p^5$, $1s^22s^22p^63s$.

We compare, in Table I, the values of $E_c^{QC,(2)}$ with those of $E_c^{APP}[n_\lambda]$, as $\lambda \rightarrow \infty$, where $E_c^{APP}[n_\lambda]$ refers to the one of Lee, Yang, and Parr (LYP), the one of Perdew, Burke, and Ernzerhof (PBE) and the one of Levy and Wilson (WL).

Table I

“Comparison of $E_c^{QC,(2)}$ for \hat{H}_0^{QC} in Eq.(62) with $E_c^{APP}[n_\lambda]$, as $\lambda \rightarrow \infty$, where n is the ground-state density of \hat{H}_0^{QC} ”

DENSITY	$E_c^{QC,(2)}$	$\lim_{\lambda \rightarrow \infty} E_c^{PBE}[n_\lambda]$	$\lim_{\lambda \rightarrow \infty} E_c^{LYP}[n_\lambda]$	$\lim_{\lambda \rightarrow \infty} E_c^{WL}[n_\lambda]$
2-electron	-0.0467*	-0.0479	-0.0565	-0.0480
3-electron	-0.0537*	-0.0584	-0.0991	-0.0568
9-electron	-0.3694*	-0.3856	-0.4648	-0.3826
10-electron	-0.4278*	-0.4577	-0.5275	-0.4504
11-electron	-0.5434**	-0.4753	-0.5868	-0.4718

*From Refs. 43, 44

**From Ref. 43

The second column in the table is the value corresponding to $\lim_{\lambda \rightarrow \infty} {}^{HF}E_c[n_\lambda] = E_c^{QC,(2)}$

when $n(r)$ is the hydrogenic ground-state density of \hat{H}_0^{QC} in Eq.(27). For $E_c[n]$ as

required by Eq.(34) for more than two electrons, the three tested approximations give more negative values than the respective values for $E_c^{QC(2)}$. For a two-electron density the equality $\lim_{\lambda \rightarrow \infty} E_c[n_\lambda] = \lim_{\lambda \rightarrow \infty} {}^{HF}E_c[n_\lambda] = E_c^{QC(2)}$ is desired. If one uses the

same reference density for $E_c^{QC}[n]$ and ${}^{HF}E_c[n]$, then their high-density scaling limits are the same. It can be seen that the use of approximations to $E_c[n]$ as approximations to $E_c^{QC}[n]$ is not well justified as far as the high-density-limit constraint is concerned. Future work for designing approximations specifically to $E_c^{QC}[n]$ is needed. However, the data in the table partially explain the results obtained by Fuentealba and Savin [47]. They have found that the WL functional gives better results than the LYP when used as a “tack-on” functional. In that line, the PBE functional is expected to produce very good results when used as an approximation to $E_c^{QC}[n]$. Other exact numbers for the traditional DFT correlation energy are available from works by Umrigar and Gonze [48,49].

IV. Relationships Involving the High-Density Limit of the Correlation Potential

Recently, Görling and Levy [36] by means of their DFT perturbation theory have derived the following high-density identity connecting $E_c^{(2)}[n]$ and its functional derivative, $v_c^{(2)}([n];\mathbf{r})$:

$$E_c^{(2)}[n] - \sum_{k=2}^N \int d\mathbf{r} v_c^{(2)}([n^k];\mathbf{r}) \varphi_k^*(\mathbf{r}) \varphi_k(\mathbf{r}) = \sum_{k=2}^N \sum_{i=1}^{k-1} \sum_{m=k}^{\infty} \frac{|\langle \varphi_m(\mathbf{r}) | u([n^k];\mathbf{r}) + v_x([n^k];\mathbf{r}) - u([n^{k-1}];\mathbf{r}) - v_x([n^{k-1}];\mathbf{r}) | \varphi_i(\mathbf{r}) \rangle|^2}{\varepsilon_i - \varepsilon_m}. \quad (36)$$

In the above expression, $v_c^{(2)}([n^k];\mathbf{r})$, $u([n^k];\mathbf{r})$ and $v_x([n^k];\mathbf{r})$ are the functional derivatives of $E_c^{(2)}[n^k]$, $U[n^k]$ and $E_x[n^k]$ with respect to the density. The density $n^k(\mathbf{r})$ is obtained through

$$n^k(\mathbf{r}) = \sum_{m=1}^k \varphi_m^*([n];\mathbf{r}) \varphi_m([n];\mathbf{r}) . \quad (37)$$

In Eq.(37), ϵ_m are the orbital energies corresponding to the KS orbitals $\phi_m(\mathbf{r})$. If the summation in formula (37) goes over all occupied $\phi_m(\mathbf{r})$, then $n^N(\mathbf{r})=n(\mathbf{r})$.

Very recently, Ivanov et al. [29] have expressed the right-hand side of Eq.(36) in a closed form. For any diamagnetic two-electron system with a spherical symmetry they have arrived at the following analytical expressions:

$$\begin{aligned} 2 E_c^{(2)}[n] - 4\pi \int r^2 v_c^{(2)}([n];\mathbf{r}) n(\mathbf{r}) d\mathbf{r} = \\ \left(\frac{1}{2}\right) 4\pi \int r^2 f(r) n(r) \left\{ u([n];\mathbf{r}) - 2 \epsilon_1^{(1)} \right\} d\mathbf{r} , \end{aligned} \quad (38)$$

with $f(r)$ being given by

$$f(r) = \int_0^r \frac{dr'}{r'^2 n(r')} \int_0^{r'} r''^2 \left\{ u([n];\mathbf{r}'') - 2 \epsilon_1^{(1)} \right\} n(r'') dr'' , \quad (39)$$

where $\epsilon_1^{(1)}$ is

$$\epsilon_1^{(1)} = \left(\frac{1}{4}\right) 4\pi \int d\mathbf{r} r^2 n(r) u([n];\mathbf{r}) . \quad (40)$$

The Hartree potential $u([n];\mathbf{r})$ is given by

$$u([n];\mathbf{r}) = \int \frac{n(\mathbf{r}')}{|\mathbf{r} - \mathbf{r}'|} d\mathbf{r}' , \quad (41)$$

or, here for spherically symmetric systems

$$u([n];\mathbf{r}) = 4\pi \left\{ \frac{1}{r} \int_0^r r'^2 n(r') dr' + \int_r^\infty r' n(r') dr' \right\} . \quad (41A)$$

Formulas (38)-(41) enable one to arrive at tests for the difference
 $2 E_c^{(2)}[n] - \int d\mathbf{r} v_c^{(2)}([n]; \mathbf{r}) n(\mathbf{r})$, obtained from different approximations to $E_c[n]$.

Further, $E_c^{(2)}[n]$ can be completely eliminated by using a line integration [50,29]. For this purpose, first note that

$$E_c^{(2)}[n] = \int_0^\infty dE_c[n_\lambda] \quad , \quad (42)$$

because [10]

$$\lim_{\lambda \rightarrow 0} E_c[n_\lambda] = 0 \quad . \quad (43)$$

Next, we express Eq.(43) as

$$E_c^{(2)}[n] = \int_0^\infty \frac{\partial E_c[n_\lambda]}{\partial \lambda} d\lambda \quad . \quad (44)$$

By using the chain rule technique, as employed by Ghosh and Parr [51] for a functional that depends on parameter λ , i.e.

$$\frac{\partial E_c[n_\lambda]}{\partial \lambda} = \int \frac{\delta E_c[\rho]}{\delta \rho(\mathbf{r})} \bigg|_{\rho=n_\lambda(\mathbf{r})} \frac{\partial n_\lambda}{\partial \lambda} d\mathbf{r} \quad , \quad (45)$$

where $\rho(\mathbf{r})$ is an arbitrary density, we obtain our desired result

$$E_c^{(2)}[n] = \int_0^\infty \int d\mathbf{r} v_c([n_\lambda]; \mathbf{r}) [3n(\mathbf{r}) + \mathbf{r} \cdot \nabla n(\mathbf{r})] d\mathbf{r} d\lambda \quad . \quad (46)$$

Eqs.(42)-(46) are held for any number of electrons. Eq.(46) is simply a variant of a formula of van Leeuwen and Baerends [50]. For example, for two-electron spherically symmetric densities, the combination of Eqs.(38) and (46) leads to an expression involving the functional derivative of $E_c^{(2)}[n]$ only, namely

$$\begin{aligned}
& 4\pi \int r^2 v_c^{(2)}([n];r) n(r) dr + \\
& \left(\frac{1}{2}\right) 4\pi \int r^2 f(r) n(r) \left\{ u([n];r) - 2 \varepsilon_1^{(1)} \right\} dr = \\
& 8\pi \int_0^\infty \int r^2 v_c([n_\lambda];r) \left[3n(r) + r \frac{\partial}{\partial r} n(r) \right] dr d\lambda .
\end{aligned} \tag{47}$$

Last but not least, we present numerical implementation of formula (38) for a simple exponential density. For density

$$n(r) = \left(\frac{2a^3}{\pi}\right) e^{-2ar} , \tag{48}$$

the right-hand side of formula (38) reads

$$\begin{aligned}
& \left(\frac{1}{2}\right) 4\pi \int r^2 f(r)n(r) \left\{ u([n];r) - 2 \varepsilon_1^{(1)} \right\} dr = \\
& \frac{1}{2} \left\{ \frac{-26 + 243 \ln 3 - 243 \ln 4}{432} \right\} = -0.111003 .
\end{aligned} \tag{49}$$

By making use of the result for two-electron hydrogen-like density from section V, i.e.

$$E_c^{(2)}[n] = -0.046663 , \tag{50}$$

we obtain

$$\int dr v_c^{(2)}([n];r) n(r) = 0.017677 . \tag{51}$$

We have applied conditions (50) and (51) to the Lee-Yang-Parr functional (LYP), to the Wilson-Levy functional (WL), and to Perdew-Burke-Ernzerhof functional (PBE). The results are presented in Table II. As far as the value of $E_c^{(2)}[n]$ is concerned, all three functionals give numbers close to the theoretically-calculated value. Unfortunately, the functionals do not have the correct functional

derivatives as required by condition (51); $\int dr v_c^{(2)}([n];\mathbf{r}) n(\mathbf{r})$ has the wrong sign. The results are not surprising because none of the present approximations has been designed with this condition in mind.

Table II

“Comparison of the exact values for $E_c^{(2)}[n]$ and $\int dr v_c^{(2)}([n];\mathbf{r}) n(\mathbf{r})$ for density $n(\mathbf{r}) = (2 a^3/\pi) e^{-2a r}$, with those obtained from different approximations”

	$E_c^{(2)}[n]$	$\int dr v_c^{(2)}([n];\mathbf{r}) n(\mathbf{r})$
Exact Value	-0.046663	0.017677
$E_c^{PBE}[n]$	-0.047896	-0.073013
$E_c^{LYP}[n]$	-0.056481	-0.108922
$E_c^{WL}[n]$	-0.048030	-0.073415

VI. Closing Remarks

By considering the Hamiltonian in the well-studied $1/Z$ expansion, as $Z \rightarrow \infty$, Eq.(27), and the Hamiltonian featured in the Görling-Levy adiabatic perturbation theory, Eq.(15), we have introduced relationships that connect known results for the second-order quantum chemistry correlation energy, $E_c^{QC,(2)}$, and the unknown $E_c^{(2)}[n]$. Moreover, we have reviewed that $\lim_{\lambda \rightarrow \infty} {}^{HF}E_c[n_\lambda]$ equals $E_c^{QC,(2)}$, where ${}^{HF}E_c[n]$ is defined slightly differently from $E_c[n]$. The functional derivative of ${}^{HF}E_c[n]$ is meant to be added to the Hartree-Fock (HF) nonlocal potential, leading

to Hartree-Fock-like equations, but with the generation of the exact ground-state energy and density.

We have presented an expression providing the high-density scaling limit of the correlation energy functional of the HF density which is to be added to the completed HF energy to produce the exact energy. This functional, $E_c^{QC}[n]$, is of significant interest because it enables one to replace the time consuming conventional methods for calculating the QC correlation energy. We have shown that $\lim_{\lambda \rightarrow \infty} {}^{HF}E_c[n_\lambda] = \lim_{\lambda \rightarrow \infty} E_c^{QC}[n_\lambda]$.

For high-quality Kohn-Sham calculations, approximate correlation potentials with improved properties are especially needed. With this in mind, we have presented exact properties of the unknown correlation potential in the high-density limit. We have introduced a simple numerical test for $\int d\mathbf{r} v_c^{(2)}([n];\mathbf{r}) n(\mathbf{r})$. Numerical results obtained from three widely used approximations have been compared to the exact values for hydrogen-like densities.

Very recently Ivanov, Burke, and Levy [52] have derived a pointwise identity for the high-density limit of the correlation potential $v_c^{(2)}([n];\mathbf{r})$ for two-electron densities.

VII. References

- [1] P. Hohenberg and W. Kohn, Phys. Rev. 136 B864 (1964).
- [2] W. Kohn and L. J. Sham, Phys. Rev. 140 A1133 (1965).
- [3] R. G. Parr and W. Yang, Density Functional Theory of Atoms and Molecules, Oxford University Press, New York, 1989, and references therein.
- [4] R. M. Dreizler and E. K. U. Gross, Density Functional Theory, Springer-Verlag, Berlin-New York, 1990, and references therein.
- [5] R. O. Jones and O. Gunnarsson, Rev. Mod. Physics 61, 689 (1989).
- [6] Recent Developments and Applications of Density Functional Theory, Theoretical and Computational Chemistry, Vol. 4, edited by J. Seminario, Elsevier, Amsterdam, 1996.
- [7] Density Functional Theory of Many-Fermion Systems, Advances in Quantum Chemistry, Vol. 21, edited by S. Trickey, Academic Press, San Diego, 1990.
- [8] M. Levy and J. P. Perdew, Phys. Rev. A 32, 2010 (1985).
- [9] M. Levy, W. Yang, and R. G. Parr, J. Chem. Phys. 83, 2334 (1985).
- [10] M. Levy, Phys. Rev. A 43, 4637 (1991), and references therein.

- [11] A. Görling and M. Levy, Phys. Rev. B 47, 13105 (1993).
- [12] M. Levy, Int. J. Quantum Chem. S 23, 617 (1989).
- [13] A. Görling and M. Levy, Phys. Rev. A 45, 1509 (1992).
- [14] D. C. Langreth and J. P. Perdew, Solid State Commun. 17, 1425 (1975).
- [15] O. Gunnarsson and B. I. Lundqvist, Phys. Rev. B 13, 4274 (1976).
- [16] A. D. Becke, J. Chem. Phys. 98, 1372 (1993).
- [17] A. D. Becke, J. Chem. Phys. 98, 5648 (1993).
- [18] M. Levy, N. A. March, and N. C. Handy, J. Chem. Phys. 104, 1989 (1996).
- [19] M. Ernzerhof, Chem. Phys. Lett. 263, 499 (1996).
- [20] J. P. Perdew, M. Ernzerhof, and K. Burke, J. Chem. Phys. 105, 9982 (1996).
- [21] M. Ernzerhof, K. Burke, and J. P. Perdew, in Recent Developments in Density Functional Theory, edited by J.M. Seminario, Theoretical and Computational Chemistry, Elsevier, Amsterdam, 1996.
- [22] K. Burke, M. Ernzerhof, and J. P. Perdew, Chem. Phys. Lett., to appear.
- [23] M. Ernzerhof, J. P. Perdew, and K. Burke, Int. J. Quantum Chem., to appear.
- [24] S. Liu and R. G. Parr, Phys. Rev. A 53, 2211 (1996).
- [25] S. Ivanov and M. Levy, unpublished.
- [26] S. Ivanov and M. Levy, unpublished.
- [27] R. A. Harris and L. R. Pratt, J. Chem. Phys. 83, 4024 (1985).
- [28] M. Levy, in Density Matrices and Density Functionals, edited by R. Eradahl and V. H. Smith, Jr., Reidel, Boston, 1987.
- [29] S. Ivanov, R. Lopez-Boada, A. Görling, and M. Levy, unpublished.
- [30] J. P. Perdew, K. Burke, and M. Ernzerhof, Phys. Rev. Lett. 77, 3865 (1996).
- [31] C. Lee, W. Yang, and R. Parr, Phys. Rev. B 37, 785 (1988).
- [32] L. C. Wilson and M. Levy, Phys. Rev. B 41, 12930 (1990).
- [33] M. Levy, Proc. Natl. Acad. Sci (USA) 76, 6062 (1979).
- [34] M. Levy, Bull. Am. Phys. Soc. 24, 626 (1979).
- [35] J. P. Perdew, E. R. McMullen, and A. Zunger, Phys. Rev. A 23, 2785 (1981).
- [36] A. Görling and M. Levy, Int. J. Quantum Chem. S 29, 93 (1995); M. Levy and A. Görling, Phys. Rev. A 51, 2851 (1995).
- [37] M. Levy, S. Ivanov, and A. Görling, to appear in "Electronic Density Functional Theory: Recent Progress and New Directions", edited by J. F. Dobson, G. Vignale, and M. P. Das, Plenum Press, New York and London, 1997.
- [38] M. Stoll and A. Savin, in Density Functional Methods in Physics, edited by R. M. Dreizler and J. Da Providencia, Plenum Press, New York, 1985.

- [39] A. Seidl, A. Görling, P. Vogl, J. A. Majewski, and M. Levy, Phys. Rev. B 53, 3764 (1996).
- [40] A. Görling and M. Levy, J. Chem. Phys. 106, 2675 (1997).
- [41] M. Levy, Int. J. Quantum Chem. 61, 281 (1997).
- [42] J. Linderberg and H. Shull, J. Mol. Spectroscopy 5, 1 (1960); and references therein.
- [43] S. J. Chakravorty and E. R. Davidson, J. Phys. Chem. 100, 6167 (1996).
- [44] E. P. Ivanova and U. I. Safronova, J. Phys. B: Atom. Mol. Phys. 8, 1591 (1975); and references therein.
- [45] S. J. Chakravorty, S. R. Gwaltney, E. R. Davidson, F. A. Parpia and C. F. Fisher, Phys. Rev. A 47, 3649 (1993);
- [46] E. R. Davidson, S. A Hagstrom, S. J. Chakravorty, V. M. Umar, and C. F. Fisher, Phys. Rev. A 44, 7071 (1991).
- [47] P. Fuentealba and A. Savin, Chem. Phys. Lett. 217, 566 (1994).
- [48] C. J. Umrigar and X. Gonze, Phys. Rev. A 50, 3827 (1994).
- [49] C. Filippi, X. Gonze and C. J. Umrigar, in "Recent Developments and Applications of Density Functional Theory", Theoretical and Computational Chemistry, Vol. 4, edited by J. Seminario, Elsevier, Amsterdam, 1996.
- [50] R. van Leeuwen and E. J. Baerends, Phys. Rev. A 51, 170 (1995).
- [51] S. K. Ghosh and R. G. Parr, J. Chem. Phys. 82, 3307 (1985).
- [52] S. Ivanov, K. Burke, and M. Levy, unpublished.

Asymptotic Properties of the Optimized Effective Potential

T. Kreibich^a, S. Kurth^b, T. Grabo^a and E.K.U. Gross^a

^a Institut für Theoretische Physik, Universität Würzburg, Am Hubland, 97074 Würzburg, Germany

^b Dept. of Physics, University of Antwerpen (RUCA), Groenenborgerlaan 171, 2020 Antwerpen, Belgium

Abstract

Rigorous properties of the optimized effective potential (OEP) are derived. We present a detailed analysis of the asymptotic form of the OEP, going beyond the leading term. Furthermore, the asymptotic properties of the approximate OEP scheme of Krieger, Li and Iafrate [Phys. Lett. A **146**, 256 (1990)] are analysed, showing that the leading asymptotic behavior is preserved by this approximation.

1 Introduction

Density Functional Theory (DFT) has become a powerful tool for ab-initio electronic structure calculations of atoms, molecules and solids [1, 2, 3]. The success of DFT relies on the availability of accurate approximations for the exchange-correlation (xc) energy functional E_{xc} or, equivalently, for the xc potential v_{xc} . Though these quantities are not known exactly, a number of properties of the exact xc potential $v_{xc}(r)$ are well-known and may serve as valuable criteria for the investigation of approximate xc functionals. In this contribution, we want to focus on one particular property, namely the asymptotic behavior of the xc potential: For finite systems, the exact xc potential $v_{xc}(r)$ is known to decrease like $-1/r$ as $r \rightarrow \infty$, reflecting also the proper cancellation of spurious self-interaction effects induced by the Hartree potential.

Most of the conventional xc functionals including the local density approximation (LDA) as well as more refined generalized gradient approximations (GGAs) fail to reproduce this asymptotic behavior correctly. As a consequence, these approximations yield rather poor results for properties where the asymptotic region of the xc potential is of crucial importance, e.g. for ionization potentials [4] or excitation energies [5] of atoms and molecules.

In recent years, a different type of approximate xc functionals has gained increasing interest: It was found that the correct asymptotic behavior can be obtained by employing xc functionals depending explicitly on the set of Kohn-Sham (KS) single-particle orbitals rather than the density [6]. The implementation of orbital functionals in the KS scheme is known as the optimized effective potential (OEP) method [7, 8]. It was recognized early on [9] that with the exact Hartree-Fock expression for the exchange energy functional, the OEP method is equivalent to the *exact* x-only implementation of KS theory. The fact that the correct asymptotics as well as other exact properties are reproduced within the OEP scheme turned out to be an important advantage over the conventional xc functionals beyond the x-only limit. Consequently, approaches using orbital-dependent xc functionals have been shown to yield highly accurate results comparable to those of quantum chemical calculations [4].

The original proof [8] of the asymptotic behavior of the OEP was based on the asymptotic form of the Green's function which is easily accessible only in 1D. Considering the 3D Green's function, Krieger, Li and Iafrate [6] made it plausible that the statement holds true in the 3D case as well. An alternative proof was recently given [10] for the x-only case.

This proof uses the exact scaling behavior of the x-energy functional and can therefore not be extended to the correlation potential. The purpose of the present contribution is to provide a rigorous proof valid for both exchange and correlation. Our investigation confirms the statement of Ref. [6] for a particular well-defined class of orbital functionals for the correlation energy. Furthermore, we investigate how exactly the asymptotically leading term is approached. The paper is organized as follows: After a brief introduction to the OEP method in section 2.1, the asymptotic form of the OEP is investigated in detail in section 2.2. The central result is a lemma proven in section 2.2.1. In the final chapter 3, the analysis of section 2 is applied to the approximate OEP scheme of Krieger, Li and Iafrate (KLI) [6, 11, 12, 13, 14, 15, 16, 17, 18, 19, 20, 21, 22, 23].

2 The OEP method

2.1 Derivation of the OEP integral equation

In this section, we derive the OEP equations for the spin-dependent version of DFT [24, 25], where the basic variables are the spin-up and spin-down densities $\rho_\uparrow(\mathbf{r})$ and $\rho_\downarrow(\mathbf{r})$, respectively. They are obtained by self-consistently solving the single-particle Schrödinger equations

$$\left(-\frac{\nabla^2}{2} + V_{S\sigma}[\rho_\uparrow, \rho_\downarrow](\mathbf{r})\right) \varphi_{j\sigma}(\mathbf{r}) = \varepsilon_{j\sigma} \varphi_{j\sigma}(\mathbf{r}) \quad j = 1, \dots, N_\sigma \quad \sigma = \uparrow, \downarrow \quad (1)$$

where

$$\rho_\sigma(\mathbf{r}) = \sum_{i=1}^{N_\sigma} |\varphi_{i\sigma}(\mathbf{r})|^2. \quad (2)$$

For convenience we shall assume in the following that infinitesimal symmetry-breaking terms have been added to the external potential to remove any possible degeneracies. The KS orbitals can then be labeled such that

$$\varepsilon_{1\sigma} < \varepsilon_{2\sigma} < \dots < \varepsilon_{N_\sigma\sigma} < \varepsilon_{(N_\sigma+1)\sigma} < \dots \quad (3)$$

The Kohn-Sham potentials $V_{S\sigma}(\mathbf{r})$ may be written in the usual way as

$$V_{S\sigma}(\mathbf{r}) = v_0(\mathbf{r}) + \int d^3r' \frac{\rho(\mathbf{r}')}{|\mathbf{r} - \mathbf{r}'|} + V_{xc\sigma}(\mathbf{r}), \quad (4)$$

$$\rho(\mathbf{r}) = \sum_{\sigma=\uparrow,\downarrow} \rho_\sigma(\mathbf{r}) \quad (5)$$

where $v_0(\mathbf{r})$ represents the external potential and $V_{xc\sigma}(\mathbf{r})$ is a local exchange-correlation (xc) potential defined by the functional derivative of the xc energy:

$$V_{xc\sigma}(\mathbf{r}) := \frac{\delta E_{xc}[\rho_\uparrow, \rho_\downarrow]}{\delta \rho_\sigma(\mathbf{r})}. \quad (6)$$

At this point we want to emphasize that, by virtue of the Hohenberg-Kohn theorem applied to non-interacting systems, all single-particle orbitals are formally functionals of the densities, i.e.

$$\varphi_{j\sigma}(\mathbf{r}) = \varphi_{j\sigma}[\rho_\uparrow, \rho_\downarrow](\mathbf{r}). \quad (7)$$

As a consequence, any orbital functional $E_{xc}[\{\varphi_{j\tau}\}]$ is an (implicit) functional of ρ_\uparrow and ρ_\downarrow , provided the orbitals come from a local potential. Having this in mind, we may equivalently start out with an approximation for the xc energy functional depending explicitly on the set of KS orbitals, i.e.

$$E_{xc} = E_{xc}[\{\varphi_{j\tau}\}] \quad (8)$$

rather than the conventional density-dependent approximations for E_{xc} . However, the calculation of the corresponding xc potentials $v_{xc\sigma}(\mathbf{r})$ becomes somewhat more complicated: For the case of orbital-dependent xc functionals $v_{xc\sigma}(\mathbf{r})$ has to be determined by the solution of an integral equation, the so-called OEP integral equation. To demonstrate this, we may start out from the very definition of the local KS xc potential, Eq. (6), following a derivation first given by Görling and Levy [26]: In order to use Eq. (6) for orbital-dependent functionals, we employ the chain rule for functional derivatives, leading to

$$\begin{aligned} V_{xc\sigma}^{\text{OEP}}(\mathbf{r}) &= \frac{\delta E_{xc}^{\text{OEP}}[\{\varphi_{j\tau}\}]}{\delta \rho_\sigma(\mathbf{r})} \\ &= \sum_{\alpha=\uparrow,\downarrow} \sum_{i=1}^{N_\alpha} \int d^3r' \frac{\delta E_{xc}^{\text{OEP}}[\{\varphi_{j\tau}\}]}{\delta \varphi_{i\alpha}(\mathbf{r}')} \frac{\delta \varphi_{i\alpha}(\mathbf{r}')}{\delta \rho_\sigma(\mathbf{r})} + c.c.. \end{aligned} \quad (9)$$

Here and in the following we assume that the xc functional $E_{xc}[\{\varphi_{i\sigma}\}]$ only depends on the occupied KS orbitals. By applying the functional chain rule once more, we obtain

$$V_{xc\sigma}^{\text{OEP}}(\mathbf{r}) = \sum_{\alpha,\beta=\uparrow,\downarrow} \sum_{i=1}^{N_\alpha} \int d^3r' \int d^3r'' \left(\frac{\delta E_{xc}^{\text{OEP}}[\{\varphi_{j\tau}\}]}{\delta \varphi_{i\alpha}(\mathbf{r}')} \frac{\delta \varphi_{i\alpha}(\mathbf{r}')}{\delta V_{S\beta}(\mathbf{r}'')} + c.c. \right) \frac{\delta V_{S\beta}(\mathbf{r}'')}{\delta \rho_\sigma(\mathbf{r})}. \quad (10)$$

The last term on the right-hand side is readily identified with the inverse $\chi_S^{-1}(\mathbf{r}, \mathbf{r}')$ of the density response function of a system of non-interacting particles

$$\chi_{S\alpha,\beta}(\mathbf{r}, \mathbf{r}') := \frac{\delta \rho_\alpha(\mathbf{r})}{\delta V_{S\beta}(\mathbf{r}')} \quad (11)$$

This quantity is diagonal with respect to the spin variables so that Eq. (10) reduces to

$$V_{xc\sigma}^{\text{OEP}}(\mathbf{r}) = \sum_{\alpha=\uparrow,\downarrow} \sum_{i=1}^{N_\alpha} \int d^3r' \int d^3r'' \left(\frac{\delta E_{xc}^{\text{OEP}}[\{\varphi_{j\tau}\}]}{\delta \varphi_{i\alpha}(\mathbf{r}')} \frac{\delta \varphi_{i\alpha}(\mathbf{r}')}{\delta V_{S\sigma}(\mathbf{r}'')} + c.c. \right) \chi_{S\sigma}^{-1}(\mathbf{r}'', \mathbf{r}). \quad (12)$$

Acting with the response operator (11) on both sides of Eq. (12) one obtains

$$\int d^3r' V_{xc\sigma}^{\text{OEP}}(\mathbf{r}') \chi_{S\sigma}(\mathbf{r}', \mathbf{r}) = \sum_{\alpha=\uparrow,\downarrow} \sum_{i=1}^{N_\alpha} \int d^3r' \frac{\delta E_{xc}^{\text{OEP}}[\{\varphi_{j\tau}\}]}{\delta \varphi_{i\alpha}(\mathbf{r}')} \frac{\delta \varphi_{i\alpha}(\mathbf{r}')}{\delta V_{S\sigma}(\mathbf{r})} + c.c.. \quad (13)$$

The second functional derivative on the right-hand side of Eq. (13) is calculated using first-order perturbation theory. This yields

$$\frac{\delta \varphi_{i\alpha}(\mathbf{r}')}{\delta V_{S\sigma}(\mathbf{r})} = \delta_{\alpha,\sigma} \sum_{\substack{k=1 \\ k \neq i}}^{\infty} \frac{\varphi_{k\sigma}(\mathbf{r}') \varphi_{k\sigma}^*(\mathbf{r})}{\varepsilon_{i\sigma} - \varepsilon_{k\sigma}} \varphi_{i\sigma}(\mathbf{r}). \quad (14)$$

Using this equation, the response function

$$\chi_{S\alpha,\beta}(\mathbf{r}, \mathbf{r}') = \frac{\delta}{\delta V_{S\beta}(\mathbf{r}')} \left(\sum_{i=1}^{N_\alpha} \varphi_{i\alpha}^*(\mathbf{r}) \varphi_{i\alpha}(\mathbf{r}) \right) \quad (15)$$

is readily expressed in terms of the orbitals as

$$\chi_{S\sigma}(\mathbf{r}, \mathbf{r}') = \sum_{i=1}^{N_\sigma} \sum_{\substack{k=1 \\ k \neq i}}^{\infty} \frac{\varphi_{i\sigma}^*(\mathbf{r}) \varphi_{k\sigma}(\mathbf{r}) \varphi_{k\sigma}^*(\mathbf{r}') \varphi_{i\sigma}(\mathbf{r}')}{\varepsilon_{i\sigma} - \varepsilon_{k\sigma}} + c.c.. \quad (16)$$

Inserting (14) and (16) in Eq. (13), we obtain the standard form of the OEP integral equation:

$$\sum_{i=1}^{N_\sigma} \int d^3 r' \left(V_{xc\sigma}^{\text{OEP}}(\mathbf{r}') - u_{xci\sigma}(\mathbf{r}') \right) G_{Si\sigma}(\mathbf{r}', \mathbf{r}) \varphi_{i\sigma}(\mathbf{r}) \varphi_{i\sigma}^*(\mathbf{r}') + c.c. = 0 \quad (17)$$

where

$$u_{xci\sigma}(\mathbf{r}) := \frac{1}{\varphi_{i\sigma}^*(\mathbf{r})} \frac{\delta E_{xc}^{\text{OEP}}[\{\varphi_{j\sigma}\}]}{\delta \varphi_{i\sigma}(\mathbf{r})}. \quad (18)$$

The quantity $G_{Si\sigma}(\mathbf{r}', \mathbf{r})$, given by

$$G_{Si\sigma}(\mathbf{r}', \mathbf{r}) := \sum_{\substack{k=1 \\ k \neq i}}^{\infty} \frac{\varphi_{k\sigma}(\mathbf{r}') \varphi_{k\sigma}^*(\mathbf{r})}{\varepsilon_{i\sigma} - \varepsilon_{k\sigma}}, \quad (19)$$

represents the Green's function of the KS equation projected onto the subspace orthogonal to $\varphi_{i\sigma}(\mathbf{r})$, i.e., it satisfies the equation

$$\left(\hat{h}_{S\sigma}(\mathbf{r}) - \varepsilon_{i\sigma} \right) G_{Si\sigma}(\mathbf{r}', \mathbf{r}) = -(\delta(\mathbf{r}' - \mathbf{r}) - \varphi_{i\sigma}(\mathbf{r}') \varphi_{i\sigma}^*(\mathbf{r})) \quad (20)$$

where $\hat{h}_{S\sigma}(\mathbf{r})$ is a short-hand notation for the KS Hamiltonian

$$\hat{h}_{S\sigma}(\mathbf{r}) := -\frac{\nabla^2}{2} + V_{S\sigma}[\rho_\uparrow, \rho_\downarrow](\mathbf{r}). \quad (21)$$

Now, the OEP scheme is complete: The integral equation (17), determining the local xc potential $v_{xc}(\mathbf{r})$ corresponding to an orbital-dependent approximation of E_{xc} , has to be solved self-consistently with the KS equation (1) and the differential equation for $G_{Si\sigma}(\mathbf{r}', \mathbf{r})$, Eq. (20).

The main advantage of such an approach is that it allows for greater flexibility in the choice of appropriate xc functionals. In particular, the OEP method can be used for the treatment of the exact exchange energy functional, defined by inserting KS orbitals in the Fock term, i.e.

$$E_x^{\text{exact}}[\rho] = -\frac{1}{2} \sum_{\sigma=\uparrow, \downarrow} \sum_{j,k=1}^{N_\sigma} \int d^3 r \int d^3 r' \frac{\varphi_{j\sigma}^*(\mathbf{r}) \varphi_{k\sigma}^*(\mathbf{r}') \varphi_{k\sigma}(\mathbf{r}) \varphi_{j\sigma}(\mathbf{r}')}{|\mathbf{r} - \mathbf{r}'|}. \quad (22)$$

2.2 Asymptotic properties of the OEP

In this section a number of rigorous statements on the optimized effective potential for finite systems will be derived. For this purpose, the exchange-only potential and the correlation potential have to be treated separately within the OEP scheme. The exact exchange potential of DFT is defined as

$$V_{x\sigma}[\rho_{\uparrow}, \rho_{\downarrow}](\mathbf{r}) = \frac{\delta E_x^{\text{exact}}}{\delta \rho_{\sigma}(\mathbf{r})}, \quad \sigma = \uparrow, \downarrow \quad (23)$$

where the exact exchange-energy functional is given by Eq. (22). In an ordinary OEP calculation, one only determines the potential $V_{x\sigma}[\rho_{\uparrow 0}, \rho_{\downarrow 0}](\mathbf{r})$ corresponding to the self-consistent ground-state spin densities $(\rho_{\uparrow 0}, \rho_{\downarrow 0})$ of the system considered. If one were to calculate $V_{x\sigma}[\rho_{\uparrow}, \rho_{\downarrow}]$ for an arbitrary given set $(\rho_{\uparrow}, \rho_{\downarrow})$ of spin densities one would have to perform the following three steps:

1. Determine the unique potentials $V_{S\sigma}[\rho_{\uparrow}, \rho_{\downarrow}](\mathbf{r})$, $\sigma = \uparrow, \downarrow$, corresponding to the given spin densities $(\rho_{\uparrow}, \rho_{\downarrow})$
2. Solve the Schrödinger equation (1) for the spin-up and spin-down orbitals with the potentials of step (1)
3. Plug the orbitals obtained in step (2) into the OEP integral equation

$$\sum_{i=1}^{N_{\sigma}} \int d^3 r' (V_{x\sigma}(\mathbf{r}') - u_{xi\sigma}(\mathbf{r}')) G_{Si\sigma}(\mathbf{r}', \mathbf{r}) \varphi_{i\sigma}(\mathbf{r}) \varphi_{i\sigma}^*(\mathbf{r}') + c.c. = 0 \quad (24)$$

and solve this equation for $V_{x\sigma}$ keeping the orbitals of step (2) fixed.

In this way Filippi, Umrigar and Gonze [27] have recently calculated the exchange potentials corresponding to the *exact* (not the x-only) densities of some atoms where the exact densities were determined in a quantum Monte-Carlo calculation. Likewise, for any given approximate functional $E_c[\{\varphi_{i\sigma}\}]$, the corresponding correlation potential

$$V_{c\sigma}[\rho_{\uparrow}, \rho_{\downarrow}](\mathbf{r}) = \frac{\delta E_c}{\delta \rho_{\sigma}(\mathbf{r})} \quad (25)$$

is obtained by the above steps (1) and (2), and step (3) replaced by the solution of

$$\sum_{i=1}^{N_{\sigma}} \int d^3 r' (V_{c\sigma}(\mathbf{r}') - u_{ci\sigma}(\mathbf{r}')) G_{Si\sigma}(\mathbf{r}', \mathbf{r}) \varphi_{i\sigma}(\mathbf{r}) \varphi_{i\sigma}^*(\mathbf{r}') + c.c. = 0. \quad (26)$$

Whenever, in the following derivations, the OEP equations (24) and (26) are used or transformed it is understood that the orbitals $\{\varphi_{i\sigma}\}$ are kept fixed so that they always correspond to a unique fixed set $(\rho_{\uparrow}, \rho_{\downarrow})$ of spin densities.

For the following analysis we find it more convenient not to work with the standard form (17), but with a transformed representation of the OEP integral equation. Following KLI [18] we define

$$\begin{aligned} \psi_{i\sigma}^*(\mathbf{r}) &:= \sum_{\substack{k=1 \\ k \neq i}}^{\infty} \frac{\int d^3 r' \varphi_{i\sigma}^*(\mathbf{r}') (V_{xc\sigma}^{\text{OEP}}(\mathbf{r}') - u_{xci\sigma}(\mathbf{r}')) \varphi_{k\sigma}(\mathbf{r}')}{\varepsilon_{i\sigma} - \varepsilon_{k\sigma}} \varphi_{k\sigma}^*(\mathbf{r}) \\ &= \int d^3 r' \varphi_{i\sigma}^*(\mathbf{r}') (V_{xc\sigma}^{\text{OEP}}(\mathbf{r}') - u_{xci\sigma}(\mathbf{r}')) G_{Si\sigma}(\mathbf{r}', \mathbf{r}). \end{aligned} \quad (27)$$

With this abbreviation, the OEP integral equation (17) can be rewritten in the simple form:

$$\sum_{i=1}^{N_{\sigma}} \psi_{i\sigma}^*(\mathbf{r}) \varphi_{i\sigma}(\mathbf{r}) + c.c. = 0. \quad (28)$$

Now, the defining equation for $G_{Si\sigma}(\mathbf{r}', \mathbf{r})$ enables us to deduce a differential equation satisfied by the newly defined quantity $\psi_{i\sigma}^*(\mathbf{r})$: Acting with the operator $(\hat{h}_{S\sigma} - \varepsilon_{i\sigma})$ on Eq. (27) readily leads to

$$(\hat{h}_{S\sigma}(\mathbf{r}) - \varepsilon_{i\sigma}) \psi_{i\sigma}^*(\mathbf{r}) = - \left[V_{xc\sigma}^{\text{OEP}}(\mathbf{r}) - u_{xci\sigma}(\mathbf{r}) - (\bar{V}_{xci\sigma} - \bar{u}_{xci\sigma}) \right] \varphi_{i\sigma}^*(\mathbf{r}) \quad (29)$$

where $\bar{V}_{xci\sigma}$ denotes the average of $V_{xc\sigma}(\mathbf{r})$ with respect to the i th orbital, i.e.

$$\bar{V}_{xci\sigma} := \int d^3r \varphi_{i\sigma}^*(\mathbf{r}) V_{xc\sigma}^{\text{OEP}}(\mathbf{r}) \varphi_{i\sigma}(\mathbf{r}) \quad (30)$$

and

$$\bar{u}_{xci\sigma} := \int d^3r \varphi_{i\sigma}^*(\mathbf{r}) u_{xci\sigma}(\mathbf{r}) \varphi_{i\sigma}(\mathbf{r}). \quad (31)$$

The differential equation (29) will serve as the starting point of the analysis below.

Before doing this, we discuss some properties of the quantity $\psi_{i\sigma}^*(\mathbf{r})$. First, since the KS orbitals $\{\varphi_{i\sigma}\}$ span an orthonormal set, we readily conclude from Eq. (27) that the function $\psi_{i\sigma}(\mathbf{r})$ is orthogonal to $\varphi_{i\sigma}(\mathbf{r})$:

$$\int d^3r \psi_{i\sigma}^*(\mathbf{r}) \varphi_{i\sigma}(\mathbf{r}) = 0. \quad (32)$$

Secondly, we note that Eq. (29), having the structure of a KS equation with an additional inhomogeneity term, plus the boundary condition that $\psi_{i\sigma}^*(\mathbf{r})$ tends to zero as $r \rightarrow \infty$ uniquely determines $\psi_{i\sigma}^*(\mathbf{r})$. We can prove this statement by assuming that there are two independent solutions $\psi_{i\sigma,1}^*(\mathbf{r})$ and $\psi_{i\sigma,2}^*(\mathbf{r})$ of Eq. (29). Then the difference between these two solutions, $\Psi_{i\sigma}^*(\mathbf{r}) := \psi_{i\sigma,1}^*(\mathbf{r}) - \psi_{i\sigma,2}^*(\mathbf{r})$, satisfies the homogeneous KS equation

$$(\hat{h}_{S\sigma} - \varepsilon_{i\sigma}) \Psi_{i\sigma}^*(\mathbf{r}) = 0, \quad (33)$$

which has a unique solution

$$\Psi_{i\sigma}^*(\mathbf{r}) = \varphi_{i\sigma}^*(\mathbf{r}), \quad (34)$$

if the above boundary condition is fulfilled. However, this solution leads to a contradiction with the orthogonality relation (32) so that $\Psi_{i\sigma}^*(\mathbf{r})$ can only be the trivial solution of Eq. (33),

$$\Psi_{i\sigma}^*(\mathbf{r}) \equiv 0. \quad (35)$$

This completes the proof.

Finally, it seems useful at this point to attach some physical meaning to the quantity $\psi_{i\sigma}$: From Eq. (27) it is obvious that $\psi_{i\sigma}$ is the usual first-order shift in the wave function caused by the perturbing potential $\delta V_{i\sigma} = V_{xc\sigma}^{\text{OEP}} - u_{xci\sigma}$. This fact also motivates the boundary condition assumed above. In x -only theory, $u_{xci\sigma}$ is the local, orbital-dependent HF exchange potential so that $-\psi_{i\sigma}$ is the first order shift of the KS wave function towards the HF wave function. One has to realize, however, that the first-order change of the orbital dependent potential $u_{xci\sigma}[\{\varphi_{i\sigma}\}]$ has been neglected. This change can be expected to be small compared to $\delta V_{i\sigma}$ [18].

2.2.1 An important lemma

We now first prove an important *lemma* concerning the constants defined by Eqs. (30) and (31). The lemma states that

(i)

$$\bar{u}_{xN_\sigma\sigma} = \bar{V}_{xN_\sigma\sigma}$$

is satisfied for

$$u_{x\sigma}(\mathbf{r}) = \frac{1}{\varphi_{i\sigma}^*(\mathbf{r})} \frac{\delta E_x^{\text{exact}}}{\delta \varphi_{i\sigma}(\mathbf{r})} \quad (36)$$

with the exact exchange-energy functional;

(ii)

$$\bar{u}_{cN_\sigma\sigma} = \bar{V}_{cN_\sigma\sigma}$$

is satisfied for any approximate correlation energy functional $E_c[\{\varphi_{i\sigma}\}]$ having the property

$$u_{ci\sigma}(\mathbf{r}) = \frac{1}{\varphi_{i\sigma}^*(\mathbf{r})} \frac{\delta E_c}{\delta \varphi_{i\sigma}(\mathbf{r})} \xrightarrow{r \rightarrow \infty} \text{const}, i = 1 \dots N_\sigma. \quad (37)$$

We begin with the proof of statement (ii). To this end we use Eq. (29) for the correlation part only:

$$\left(-\frac{\nabla^2}{2} + V_{S\sigma}(\mathbf{r}) - \varepsilon_{i\sigma} \right) \psi_{i\sigma}^*(\mathbf{r}) = (V_{c\sigma}(\mathbf{r}) - u_{ci\sigma}(\mathbf{r}) - C_{i\sigma}) \varphi_{i\sigma}^*(\mathbf{r}) \quad (38)$$

where we have introduced the abbreviation

$$C_{i\sigma} = \bar{V}_{ci\sigma} - \bar{u}_{ci\sigma}. \quad (39)$$

If Eq. (38) is satisfied with potentials $V_{S\sigma}(\mathbf{r})$, $V_{c\sigma}(\mathbf{r})$ and $u_{ci\sigma}(\mathbf{r})$ it will also be satisfied with the constantly shifted potentials

$$\bar{V}_{S\sigma}(\mathbf{r}) := V_{S\sigma}(\mathbf{r}) + B_{S\sigma} \quad (40)$$

$$\bar{V}_{c\sigma}(\mathbf{r}) := V_{c\sigma}(\mathbf{r}) + B_{c\sigma} \quad (41)$$

$$\bar{u}_{ci\sigma}(\mathbf{r}) := u_{ci\sigma}(\mathbf{r}) + B_{i\sigma} \quad (42)$$

and the corresponding eigenvalues $\bar{\varepsilon}_{i\sigma}$ and the constants $\bar{\bar{V}}_{ci\sigma}$, $\bar{\bar{u}}_{ci\sigma}$, reflecting the fact that the eigenvalues as well as the various potentials are only determined up to an arbitrary constant. The constants $B_{S\sigma}$, $B_{c\sigma}$, $B_{i\sigma}$ cancel out in Eq. (38) because the eigenvalues $\bar{\varepsilon}_{i\sigma}$ resulting from solving the Schrödinger equation (1) with the potential (40) are given by

$$\bar{\varepsilon}_{i\sigma} = \varepsilon_{i\sigma} + B_{S\sigma} \quad (43)$$

and the constants $\bar{\bar{V}}_{c\sigma}$, $\bar{\bar{u}}_{ci\sigma}$ obtained from the correlation parts of Eqs. (30), (31) with the potentials (41), (42) are

$$\bar{\bar{V}}_{ci\sigma} = \bar{V}_{ci\sigma} + B_{c\sigma} \quad (44)$$

$$\bar{\bar{u}}_{ci\sigma} = \bar{u}_{ci\sigma} + B_{i\sigma}. \quad (45)$$

Hence we can assume *without restriction* that

$$V_{S\sigma}(\mathbf{r}) \xrightarrow{r \rightarrow \infty} 0 \quad (46)$$

$$V_{c\sigma}(\mathbf{r}) \xrightarrow{r \rightarrow \infty} 0 \quad (47)$$

$$u_{ci\sigma}(\mathbf{r}) \xrightarrow{r \rightarrow \infty} 0. \quad (48)$$

In the following we shall investigate the asymptotic behavior of the KS orbitals $\varphi_{i\sigma}(\mathbf{r})$ and of the quantities $\psi_{i\sigma}(\mathbf{r})$ defined by Eq. (38). As a shorthand we write

$$\varphi_{i\sigma}(\mathbf{r}) \xrightarrow{r \rightarrow \infty} \Phi_{i\sigma}(r) f_{i\sigma}(\Omega) \quad (49)$$

$$\psi_{i\sigma}(\mathbf{r}) \xrightarrow{r \rightarrow \infty} \Psi_{i\sigma}(r) g_{i\sigma}(\Omega). \quad (50)$$

The aim is to determine the asymptotically dominant functions $\Phi_{i\sigma}(r)$ and $\Psi_{i\sigma}(r)$. The angular parts $f_{i\sigma}(\Omega)$ and $g_{i\sigma}(\Omega)$ are not of interest in the present context. Using the fact that the KS potential of finite neutral systems behaves asymptotically as [28]

$$V_{S\sigma}(\mathbf{r}) \xrightarrow{r \rightarrow \infty} -\frac{1}{r} \quad (51)$$

the KS equation (1) leads to the following asymptotic equation

$$\left(-\frac{1}{2} \frac{1}{r} \frac{d^2}{dr^2} r - \frac{1}{r} - \varepsilon_{i\sigma} \right) \Phi_{i\sigma}(r) = 0. \quad (52)$$

The asymptotic form of $\Phi_{i\sigma}(r)$ is easily found to be

$$\Phi_{i\sigma}(r) \xrightarrow{r \rightarrow \infty} r^{1/\beta_{i\sigma}} \frac{e^{-\beta_{i\sigma} r}}{r} \quad (53)$$

with

$$\beta_{i\sigma} := \sqrt{-2\varepsilon_{i\sigma}}. \quad (54)$$

By virtue of Eqs. (38) and (53), $\Psi_{i\sigma}(r)$ must satisfy the asymptotic equation

$$\left(-\frac{1}{2} \frac{1}{r} \frac{d^2}{dr^2} r - \frac{1}{r} - \varepsilon_{i\sigma} \right) \Psi_{i\sigma}(r) = (W_{i\sigma}(r) - C_{i\sigma}) r^{1/\beta_{i\sigma}} \frac{e^{-\beta_{i\sigma} r}}{r} \quad (55)$$

where we have introduced the quantity $W_{i\sigma}(r)$ defined by

$$(V_{c\sigma}(\mathbf{r}) - u_{ci\sigma}(\mathbf{r})) \xrightarrow{r \rightarrow \infty} W_{i\sigma}(r) w_{i\sigma}(\Omega). \quad (56)$$

From Eqs. (47) and (48) we know that

$$W_{i\sigma}(r) \xrightarrow{r \rightarrow \infty} 0. \quad (57)$$

Inserting the ansatz

$$\Psi_{i\sigma}(r) = p_{i\sigma}(r) \frac{e^{-\beta_{i\sigma} r}}{r} \quad (58)$$

in Eq. (55) we find that the function $p_{i\sigma}(r)$ must satisfy the equation

$$\frac{1}{2} p_{i\sigma}'' - \beta_{i\sigma} p_{i\sigma}' + \frac{p_{i\sigma}}{r} = C_{i\sigma} r^{1/\beta_{i\sigma}} \quad \text{if } C_{i\sigma} \neq 0 \quad (59)$$

and

$$\frac{1}{2}p''_{i\sigma} - \beta_{i\sigma}p'_{i\sigma} + \frac{p_{i\sigma}}{r} = -W_{i\sigma}(r)r^{1/\beta_{i\sigma}} \quad \text{if } C_{i\sigma} = 0. \quad (60)$$

The asymptotic solution of Eq. (59) is immediately recognized as

$$p_{i\sigma}(r) \xrightarrow{r \rightarrow \infty} -\frac{C_{i\sigma}}{\beta_{i\sigma}} r^{(1/\beta_{i\sigma}+1)} \quad (61)$$

so that

$$\Psi_{i\sigma}(r) = -\frac{C_{i\sigma}}{\beta_{i\sigma}} r^{1/\beta_{i\sigma}} e^{-\beta_{i\sigma}r} \quad \text{if } C_{i\sigma} \neq 0. \quad (62)$$

Writing

$$p_{i\sigma}(r) = F_{i\sigma}(r)r^{1/\beta_{i\sigma}+1} \quad \text{if } C_{i\sigma} = 0 \quad (63)$$

one readily verifies by insertion in Eq. (60) that

$$F_{i\sigma}(r) \xrightarrow{r \rightarrow \infty} 0 \quad (64)$$

as a consequence of (57).

We now prove statement (ii) of the lemma by reductio ad absurdum: Assume that $C_{N_\sigma\sigma} \neq 0$. Then the asymptotic form of $\Psi_{N_\sigma\sigma}(r)$ is given by (62) and we conclude that

$$\psi_{N_\sigma\sigma}^*(\mathbf{r})\varphi_{N_\sigma\sigma}(\mathbf{r}) \xrightarrow{r \rightarrow \infty} -\frac{C_{N_\sigma\sigma}}{\beta_{N_\sigma\sigma}} r^{\left(\frac{2}{\beta_{N_\sigma\sigma}}-1\right)} e^{-2\beta_{N_\sigma\sigma}r} \cdot g_{N_\sigma\sigma}^*(\Omega) f_{N_\sigma\sigma}(\Omega). \quad (65)$$

For $i \neq N_\sigma$, on the other hand, we obtain

$$\psi_{i\sigma}^*(\mathbf{r})\varphi_{i\sigma}(\mathbf{r}) \xrightarrow{r \rightarrow \infty} G_{i\sigma}(r)r^{\left(\frac{2}{\beta_{i\sigma}}-1\right)} e^{-2\beta_{i\sigma}r} \cdot g_{i\sigma}^*(\Omega) f_{i\sigma}(\Omega) \quad (66)$$

where

$$G_{i\sigma}(r) = \begin{cases} -C_{i\sigma}/\beta_{i\sigma} & \text{if } C_{i\sigma} \neq 0 \\ F_{i\sigma}(r) \xrightarrow{r \rightarrow \infty} 0 & \text{if } C_{i\sigma} = 0 \end{cases}. \quad (67)$$

From this we conclude that the OEP integral equation

$$\psi_{N_\sigma\sigma}^*(\mathbf{r})\varphi_{N_\sigma\sigma}(\mathbf{r}) + \sum_{i=1}^{N_\sigma-1} \psi_{i\sigma}^*(\mathbf{r})\varphi_{i\sigma}(\mathbf{r}) + c.c. \equiv 0 \quad (68)$$

is not satisfied for $r \rightarrow \infty$ because the dominant term given by (65) cannot be canceled by any of the other contributions (66) which all fall off more rapidly (cf. Eq. (3)). Consequently the $\psi_{j\sigma}$ cannot be solutions of the OEP equation which is the desired contradiction. This implies that $C_{N_\sigma\sigma} = 0$ which completes the proof of statement (ii).

In order to prove statement (i) of the lemma we first investigate the asymptotic form of the quantities $u_{xi\sigma}(\mathbf{r})$. Employing the exact exchange-energy functional (22) we find

$$u_{xi\sigma}(\mathbf{r}) = -\sum_{j=1}^{N_\sigma} \frac{\varphi_{j\sigma}^*(\mathbf{r})}{\varphi_{i\sigma}^*(\mathbf{r})} K_{ji\sigma}(\mathbf{r}) \quad (69)$$

with

$$K_{j i \sigma}(\mathbf{r}) := \int d^3 r' \frac{\varphi_{j \sigma}(\mathbf{r}') \varphi_{i \sigma}^*(\mathbf{r}')}{|\mathbf{r} - \mathbf{r}'|}. \quad (70)$$

Performing a multipole expansion of $K_{j i \sigma}(\mathbf{r})$ and using the orthonormality of the KS orbitals we find

$$K_{i i \sigma}(\mathbf{r}) \xrightarrow{r \rightarrow \infty} \frac{1}{r} \quad (71)$$

$$K_{j i \sigma}(\mathbf{r}) \xrightarrow{r \rightarrow \infty} \frac{1}{r^m} k_{j i \sigma}(\Omega) \quad i \neq j \quad (72)$$

with some integer $m \geq 2$ that depends on i and j . Hence the sum in Eq. (69) must be dominated asymptotically by the $j = N_\sigma$ term:

$$u_{x i \sigma}(\mathbf{r}) \xrightarrow{r \rightarrow \infty} -\frac{\varphi_{N_\sigma \sigma}^*(\mathbf{r})}{\varphi_{i \sigma}^*(\mathbf{r})} K_{N_\sigma i \sigma}(\mathbf{r}). \quad (73)$$

Using Eqs. (71), (72) and the asymptotic behavior (53) of the KS orbitals we obtain

$$u_{x N_\sigma \sigma}(\mathbf{r}) \xrightarrow{r \rightarrow \infty} -\frac{1}{r} \quad (74)$$

and

$$u_{x i \sigma}(\mathbf{r}) \xrightarrow{r \rightarrow \infty} -r^{\left(\frac{1}{\beta_{N_\sigma \sigma}} - \frac{1}{\beta_{i \sigma}} - m\right)} e^{(\beta_{i \sigma} - \beta_{N_\sigma \sigma})r} \omega_{i \sigma}(\Omega). \quad (75)$$

We recognize that $u_{x i \sigma}(\mathbf{r})$ diverges exponentially to $-\infty$ for $i < N_\sigma$. In the x-only case, the quantities $\psi_{i \sigma}(\mathbf{r})$ satisfy the equation

$$\left(-\frac{\nabla^2}{2} + V_{S\sigma}(\mathbf{r}) - \varepsilon_{i\sigma}\right) \psi_{i\sigma}^*(\mathbf{r}) = (V_{x\sigma}(\mathbf{r}) - u_{x i \sigma}(\mathbf{r}) - C_{i\sigma}) \varphi_{i\sigma}^*(\mathbf{r}) \quad (76)$$

where

$$C_{i\sigma} = \bar{V}_{x i \sigma} - \bar{u}_{x i \sigma}. \quad (77)$$

In the following we prove statement (i) of the lemma by reductio ad absurdum: Assume that $C_{N_\sigma \sigma} \neq 0$. Then, by Eq. (74), the right-hand side of Eq. (76) for $i = N_\sigma$ is asymptotically dominated by $-C_{N_\sigma \sigma} \varphi_{N_\sigma \sigma}^*(\mathbf{r})$ and we obtain, in complete analogy to the correlation-only case:

$$\Psi_{N_\sigma \sigma}(r) = -\frac{C_{N_\sigma \sigma}}{\beta_{N_\sigma \sigma}} r^{1/\beta_{N_\sigma \sigma}} e^{-\beta_{N_\sigma \sigma} r} \quad \text{for } C_{N_\sigma \sigma} \neq 0. \quad (78)$$

For $i < N_\sigma$, the right-hand side of Eq.(76) is dominated by $-u_{x i \sigma}(\mathbf{r}) \varphi_{i \sigma}^*(\mathbf{r})$. Using Eqs. (53) and (75) $\Psi_{i \sigma}(r)$ satisfies the asymptotic differential equation

$$\left(-\frac{1}{2} \frac{1}{r} \frac{d^2}{dr^2} r - \frac{1}{r} - \varepsilon_{i\sigma}\right) \Psi_{i\sigma}(r) = r^{\left(\frac{1}{\beta_{N_\sigma \sigma}} - 1 - m\right)} e^{-\beta_{N_\sigma \sigma} r}. \quad (79)$$

From this equation one readily concludes that

$$\Psi_{i\sigma}(r) \xrightarrow{r \rightarrow \infty} \frac{1}{\varepsilon_{N_\sigma \sigma} - \varepsilon_{i\sigma}} r^{\left(\frac{1}{\beta_{N_\sigma \sigma}} - 1 - m\right)} e^{-\beta_{N_\sigma \sigma} r}, \quad i < N_\sigma. \quad (80)$$

We note in passing that all the functions $\psi_{i\sigma}$, $i = 1 \dots N_\sigma$, have the *same* exponential decay, $e^{-\beta_{N_\sigma\sigma}r}$, determined by the highest occupied orbital energy $\beta_{N_\sigma\sigma} = \sqrt{-2\varepsilon_{N_\sigma\sigma}}$. This fact further supports the interpretation of the quantities $\psi_{i\sigma}$ (in the x-only case) as a shift from the KS orbitals towards the HF orbitals: The HF orbitals $\varphi_{i\sigma}^{\text{HF}}$ are known [29] to be asymptotically dominated by the exponential decay $e^{-\beta_{N_\sigma\sigma}r}$ of the highest occupied orbital. The same holds true for the shifted KS orbitals $(\varphi_{i\sigma} + \psi_{i\sigma})$.

From Eqs. (53), (78) and (80) we obtain

$$\psi_{N_\sigma\sigma}^*(\mathbf{r})\varphi_{N_\sigma\sigma}(\mathbf{r}) \xrightarrow{r \rightarrow \infty} -\frac{C_{N_\sigma\sigma}}{\beta_{N_\sigma\sigma}} r^{\left(\frac{2}{\beta_{N_\sigma\sigma}} - 1\right)} e^{-2\beta_{N_\sigma\sigma}r} \cdot g_{N_\sigma\sigma}^*(\Omega) f_{N_\sigma\sigma}(\Omega). \quad (81)$$

and

$$\psi_{i\sigma}^*(\mathbf{r})\varphi_{i\sigma}(\mathbf{r}) \xrightarrow{r \rightarrow \infty} \frac{1}{\varepsilon_{N_\sigma\sigma} - \varepsilon_{i\sigma}} r^{\left(\frac{1}{\beta_{N_\sigma\sigma}} + \frac{1}{\beta_{i\sigma}} - 2 - m\right)} e^{-(\beta_{N_\sigma\sigma} + \beta_{i\sigma})r} \cdot g_{i\sigma}^*(\Omega) f_{i\sigma}(\Omega), \quad (82)$$

$i < N_\sigma.$

Once again we conclude that in the OEP equation (68) the asymptotically dominant term (81) cannot be canceled by any of the other terms (82), leading to the contradiction that the $\psi_{j\sigma}(\mathbf{r})$ are not solutions of the OEP integral equation. Hence we conclude that $C_{N_\sigma\sigma} = 0$ which completes the proof of the lemma.

Görling and Levy [10] recently gave a proof of statement (i) of the above lemma. This proof is based on the scaling properties of the exchange-energy functional and can therefore not be generalized to the case of correlation. The proof presented above for the correlation part of the OEP (statement (ii) of the lemma) is valid for all correlation energy functionals leading to asymptotically bounded functions $u_{ci\sigma}(\mathbf{r})$. For asymptotically diverging $u_{ci\sigma}(\mathbf{r})$ the lemma might still be valid. In particular, if the divergence is the same as the one (Eq.(75)) found in the exchange case, the proof of statement (i) carries over. This lemma will be used in the subsequent section in the derivation of the asymptotic form of the OEP.

2.2.2 Asymptotic form of the OEP

In this section we shall investigate the asymptotic form of the exchange and correlation potentials. It will be shown that $V_{x\sigma}(\mathbf{r})$ and $u_{xN_\sigma\sigma}(\mathbf{r})$ approach each other exponentially fast for $r \rightarrow \infty$, and that the difference between $V_{c\sigma}(\mathbf{r})$ and $u_{cN_\sigma\sigma}(\mathbf{r})$ decays exponentially as well. Using the notation of the last section the detailed statements read as follows:

Theorem 1:

$$V_{x\sigma}(\mathbf{r}) - u_{xN_\sigma\sigma}(\mathbf{r}) \xrightarrow{r \rightarrow \infty} r^{\left(\frac{1}{\beta_{(N_\sigma-1)\sigma}} - \frac{1}{\beta_{N_\sigma\sigma}} - m\right)} e^{-(\beta_{(N_\sigma-1)\sigma} - \beta_{N_\sigma\sigma})r} \quad (83)$$

where m is an integer satisfying $m \geq 2$.

Theorem 2: *If the constant $C_{(N_\sigma-1)\sigma}$ defined by Eq. (39) does not vanish then*

$$V_{c\sigma}(\mathbf{r}) - u_{cN_\sigma\sigma}(\mathbf{r}) \xrightarrow{r \rightarrow \infty} C_{(N_\sigma-1)\sigma} r^{\left(\frac{2}{\beta_{(N_\sigma-1)\sigma}} - \frac{2}{\beta_{N_\sigma\sigma}} + 1\right)} e^{-2(\beta_{(N_\sigma-1)\sigma} - \beta_{N_\sigma\sigma})r}. \quad (84)$$

If $C_{(N_\sigma-1)\sigma} = 0$ the right-hand side of (84) is an upper bound of $|V_{c\sigma}(\mathbf{r}) - u_{cN_\sigma\sigma}(\mathbf{r})|$ for $r \rightarrow \infty$, i.e. for $C_{(N_\sigma-1)\sigma} = 0$, $V_{c\sigma}(\mathbf{r})$ and $u_{cN_\sigma\sigma}(\mathbf{r})$ approach each other even faster than given by the right-hand side of Eq. (84).

To prove theorem 1 we write

$$\Psi_{N_\sigma\sigma}(r) = q(r) \frac{e^{-\beta_{N_\sigma\sigma}r}}{r}. \quad (85)$$

Using the lemma of the last section ensuring that $C_{N_\sigma\sigma} = 0$, $q(r)$ must satisfy the following asymptotic differential equation:

$$-\frac{1}{2} r^{-\frac{1}{\beta_{N_\sigma\sigma}}} q''(r) + \beta_{N_\sigma\sigma} r^{-\frac{1}{\beta_{N_\sigma\sigma}}} q'(r) - r^{-\left(\frac{1}{\beta_{N_\sigma\sigma}} + 1\right)} q(r) = V_{x\sigma}(\mathbf{r}) - u_{xN_\sigma\sigma}(\mathbf{r}). \quad (86)$$

This is readily verified by inserting (51), (53) and (85) in Eq. (76). By virtue of Eqs. (3) and (82) the sum

$$\sum_{i=1}^{N_\sigma-1} \psi_{i\sigma}^*(\mathbf{r}) \varphi_{i\sigma}(\mathbf{r}) \quad (87)$$

must be asymptotically dominated by the $i = (N_\sigma - 1)$ term which decays as

$$\psi_{(N_\sigma-1)\sigma}^*(\mathbf{r}) \varphi_{(N_\sigma-1)\sigma}(\mathbf{r}) \xrightarrow{r \rightarrow \infty} \frac{1}{\varepsilon_{N_\sigma\sigma} - \varepsilon_{(N_\sigma-1)\sigma}} r^{\left(\frac{1}{\beta_{N_\sigma\sigma}} + \frac{1}{\beta_{(N_\sigma-1)\sigma}} - 2 - m\right)} e^{-(\beta_{N_\sigma\sigma} + \beta_{(N_\sigma-1)\sigma})r}. \quad (88)$$

This term cannot be canceled by any other term of the sum (87). Hence, for the OEP equation (28) to be asymptotically satisfied, the expression (88) must be canceled by the $i = N_\sigma$ term which behaves as

$$\psi_{N_\sigma\sigma}^*(\mathbf{r}) \varphi_{N_\sigma\sigma}(\mathbf{r}) \xrightarrow{r \rightarrow \infty} q(r) r^{\left(\frac{1}{\beta_{N_\sigma\sigma}} - 2\right)} e^{-2\beta_{N_\sigma\sigma}r}. \quad (89)$$

Equating the right-hand side of Eqs. (88) and (89), the function $q(r)$ is readily determined to be

$$q(r) = \frac{1}{\varepsilon_{N_\sigma\sigma} - \varepsilon_{(N_\sigma-1)\sigma}} r^{\left(\frac{1}{\beta_{(N_\sigma-1)\sigma}} - m\right)} e^{-(\beta_{(N_\sigma-1)\sigma} - \beta_{N_\sigma\sigma})r}. \quad (90)$$

Finally, by inserting this result in the left-hand side of Eq. (86), we confirm that the right-hand side of this equation decays asymptotically as stated in theorem 1.

To prove theorem 2 we write for the correlation-only case

$$\Psi_{N_\sigma\sigma}(r) = p(r) \frac{e^{-\beta_{N_\sigma\sigma}r}}{r}. \quad (91)$$

Since $C_{N_\sigma\sigma} = 0$, $p(r)$ must satisfy the following asymptotic differential equation (cf. Eq. (60)):

$$-\frac{1}{2}r^{-\frac{1}{\beta_{N_\sigma\sigma}}}p''(r) + \beta_{N_\sigma\sigma}r^{-\frac{1}{\beta_{N_\sigma\sigma}}}p'(r) - r^{-\left(\frac{1}{\beta_{N_\sigma\sigma}}+1\right)}p(r) = V_{c\sigma}(\mathbf{r}) - u_{cN_\sigma\sigma}(\mathbf{r}) . \quad (92)$$

If $C_{(N_\sigma-1)\sigma} \neq 0$, the sum

$$\sum_{i=1}^{N_\sigma-1} \psi_{i\sigma}^*(\mathbf{r})\varphi_{i\sigma}(\mathbf{r}) \quad (93)$$

is asymptotically dominated by the $i = (N_\sigma - 1)$ term which, according to Eqs. (66) and (67), decays as

$$\begin{aligned} & \psi_{(N_\sigma-1)\sigma}^*(\mathbf{r})\varphi_{(N_\sigma-1)\sigma}(\mathbf{r}) \\ & \xrightarrow{r \rightarrow \infty} -\frac{C_{(N_\sigma-1)\sigma}}{\beta_{(N_\sigma-1)\sigma}} r^{\left(\frac{2}{\beta_{(N_\sigma-1)\sigma}}-1\right)} e^{-2\beta_{(N_\sigma-1)\sigma}r} . \end{aligned} \quad (94)$$

Once again this term cannot be canceled by any other term of the sum (93). Hence it must be canceled asymptotically by the $i = N_\sigma$ term which behaves as

$$\psi_{N_\sigma\sigma}^*(\mathbf{r})\varphi_{N_\sigma\sigma}(\mathbf{r}) \xrightarrow{r \rightarrow \infty} p(r)r^{\left(\frac{1}{\beta_{N_\sigma\sigma}}-2\right)} e^{-2\beta_{N_\sigma\sigma}r} . \quad (95)$$

Equating the right-hand sides of Eqs. (94) and (95) we can identify the asymptotic form of $p(r)$:

$$p(r) = -\frac{C_{(N_\sigma-1)\sigma}}{\beta_{(N_\sigma-1)\sigma}} r^{\left(\frac{2}{\beta_{(N_\sigma-1)\sigma}}-\frac{1}{\beta_{N_\sigma\sigma}}+1\right)} e^{-2(\beta_{(N_\sigma-1)\sigma}-\beta_{N_\sigma\sigma})r} . \quad (96)$$

Insertion of this expression in the left-hand side of Eq. (92) proves Eq. (84) for the case $C_{(N_\sigma-1)\sigma} \neq 0$. If $C_{(N_\sigma-1)\sigma} = 0$ the asymptotic form of $V_{c\sigma}(\mathbf{r}) - u_{cN_\sigma\sigma}(\mathbf{r})$ cannot be stated explicitly. It is clear, however, that the $i = N_\sigma$ term (95) must be canceled asymptotically by some contribution to the sum (93). Since, by Eqs. (66) and (67), *all* contributions to the sum (93) fall off more rapidly than the right-hand side of (94), $p(r)$ must decay more rapidly than the right-hand side of (96). Hence, by Eq. (92), the right-hand side of (84) provides an upper bound of $|V_{c\sigma}(\mathbf{r}) - u_{cN_\sigma\sigma}(\mathbf{r})|$ for $r \rightarrow \infty$ if $C_{(N_\sigma-1)\sigma} = 0$. This completes the proof.

Since the asymptotic form of $u_{cN_\sigma\sigma}(\mathbf{r})$, as derived in Eq. (74), is $-\frac{1}{r}$, theorem 1 immediately implies that

$$V_{x\sigma}(\mathbf{r}) \xrightarrow{r \rightarrow \infty} -\frac{1}{r} . \quad (97)$$

This is a well-known result that has been obtained in several different ways [8, 30, 28, 31, 32]. The exact correlation potential of DFT is known [28] to fall off as $-\alpha/(2r^4)$ for atoms with spherical N and $(N-1)$ -electron ground states, with α being the static polarizability of the $(N-1)$ -electron ground state. Theorem 2 provides a simple way of checking how the OEP correlation-only potential $V_{c\sigma}(\mathbf{r})$ falls off for a given approximate orbital functional $E_c^{\text{approx}}[\{\varphi_{i\sigma}\}]$: One only needs to determine the asymptotic decay of $u_{cN_\sigma\sigma}(\mathbf{r})$.

3 Approximation of Krieger, Li and Iafrate

3.1 Derivation of the KLI approximation

The OEP method, discussed in the preceding paragraph, opens up a way for using orbital-dependent functionals within the KS scheme. However, as a price to pay, one has to solve an integral equation self-consistently with the KS equation. Due to the rather large computational effort involved in this scheme, it has not been used extensively. Indeed, the solution of the OEP integral equation has been achieved so far only for systems of high symmetry such as spherical atoms [6, 8, 16, 17, 33] and for solids within the linear muffin tin orbitals atomic sphere approximation [13, 34, 35, 36]. Therefore, practical applications of the OEP scheme to a greater variety of systems require some simplification.

Krieger, Li and Iafrate have suggested an approximation leading to a highly accurate but numerically tractable scheme preserving many important properties of the exact OEP method [6, 11, 13, 14, 15, 16, 17, 18, 19]. It is most easily derived by replacing the energy denominator of the Green's function (19) by a single constant, i.e.

$$G_{Si\sigma}(\mathbf{r}', \mathbf{r}) \approx \frac{1}{\Delta\epsilon} (\delta(\mathbf{r}' - \mathbf{r}) - \varphi_{i\sigma}(\mathbf{r}')\varphi_{i\sigma}^*(\mathbf{r})) . \quad (98)$$

Substituting this into the OEP integral equation (17) leads to an approximate equation, known as the KLI approximation:

$$V_{xc\sigma}^{\text{KLI}}(\mathbf{r}) = \frac{1}{2\rho_{\sigma}(\mathbf{r})} \sum_{i=1}^{N_{\sigma}} |\varphi_{i\sigma}(\mathbf{r})|^2 \left[u_{xci\sigma}(\mathbf{r}) + (\bar{V}_{xci\sigma}^{\text{KLI}} - \bar{u}_{xci\sigma}) \right] + c.c. \quad (99)$$

where $\bar{V}_{xci\sigma}^{\text{KLI}}$ is defined in analogy to Eq. (30). In contrast to the full OEP equation (17), the KLI equation, still being an integral equation, can be solved explicitly in terms of the orbitals $\{\varphi_{i\sigma}\}$: Multiplying Eq. (99) by $|\varphi_{j\sigma}(\mathbf{r})|^2$ and integrating over space yields

$$\bar{V}_{xcj\sigma}^{\text{KLI}} = \bar{V}_{xcj\sigma}^S + \sum_{i=1}^{N_{\sigma}-1} M_{ji\sigma} \left(\bar{V}_{xci\sigma}^{\text{KLI}} - \frac{1}{2} (\bar{u}_{xci\sigma} + \bar{u}_{xci\sigma}^*) \right), \quad (100)$$

where

$$\bar{V}_{xcj\sigma}^S := \int d^3r \frac{|\varphi_{j\sigma}(\mathbf{r})|^2}{\rho_{\sigma}(\mathbf{r})} \sum_{i=1}^{N_{\sigma}} |\varphi_{i\sigma}(\mathbf{r})|^2 \frac{1}{2} (u_{xci\sigma}(\mathbf{r}) + u_{xci\sigma}^*(\mathbf{r})) \quad (101)$$

and

$$M_{ji\sigma} := \int d^3r \frac{|\varphi_{j\sigma}(\mathbf{r})|^2 |\varphi_{i\sigma}(\mathbf{r})|^2}{\rho_{\sigma}(\mathbf{r})}. \quad (102)$$

The term corresponding to the highest occupied orbital $\varphi_{N_{\sigma}\sigma}$ has been excluded from the sum in Eq. (100) because $\bar{V}_{xcN_{\sigma}\sigma}^{\text{KLI}} = \bar{u}_{xcN_{\sigma}\sigma}$, which will be proven in the next section. The remaining unknown constants $(\bar{V}_{xci\sigma}^{\text{KLI}} - \bar{u}_{xci\sigma})$ are determined by the linear equation

$$\sum_{i=1}^{N_{\sigma}-1} (\delta_{ji} - M_{ji\sigma}) \left(\bar{V}_{xci\sigma}^{\text{KLI}} - \frac{1}{2} (\bar{u}_{xci\sigma} + \bar{u}_{xci\sigma}^*) \right) = \left(\bar{V}_{xcj\sigma}^S - \frac{1}{2} (\bar{u}_{xcj\sigma} + \bar{u}_{xcj\sigma}^*) \right), \quad (103)$$

with $j = 1, \dots, N_{\sigma} - 1$. Solving Eq. (103) and substituting the result into Eq. (99), we obtain an explicitly orbital dependent functional. The approximation 98 might appear rather crude. However, it can be justified by a much more rigorous derivation, showing that the KLI equation can be interpreted as a mean-field type approximation [6, 18].

3.2 Asymptotic properties of the KLI potential

In this section we shall demonstrate that the above rigorous properties of the full OEP discussed above are preserved by the KLI approximation. As for the OEP equation, we first write the KLI approximation (99) separately for the exchange and correlation potentials:

$$\sum_{i=1}^{N_\sigma} |\varphi_{i\sigma}(\mathbf{r})|^2 \left(V_{x\sigma}^{\text{KLI}}(\mathbf{r}) - U_{xi\sigma}(\mathbf{r}) - \left(\bar{V}_{xi\sigma}^{\text{KLI}} - \bar{U}_{xi\sigma} \right) \right) = 0 \quad (104)$$

$$\sum_{i=1}^{N_\sigma} |\varphi_{i\sigma}(\mathbf{r})|^2 \left(V_{c\sigma}^{\text{KLI}}(\mathbf{r}) - U_{ci\sigma}(\mathbf{r}) - \left(\bar{V}_{ci\sigma}^{\text{KLI}} - \bar{U}_{ci\sigma} \right) \right) = 0. \quad (105)$$

where, for convenience, we have introduced

$$U_{xi\sigma}(\mathbf{r}) = \frac{1}{2} (u_{xi\sigma}(\mathbf{r}) + u_{xi\sigma}^*(\mathbf{r})) \quad (106)$$

and

$$U_{ci\sigma}(\mathbf{r}) = \frac{1}{2} (u_{ci\sigma}(\mathbf{r}) + u_{ci\sigma}^*(\mathbf{r})) \quad (107)$$

in order to deal with real-valued quantities only. Following the argument given in the beginning of section 2.2.1 (Eqs. (40) - (48)) we can assume *without restriction* that

$$V_{x\sigma}^{\text{KLI}}(\mathbf{r}) \xrightarrow{r \rightarrow \infty} 0 \quad (108)$$

$$V_{c\sigma}^{\text{KLI}}(\mathbf{r}) \xrightarrow{r \rightarrow \infty} 0 \quad (109)$$

$$U_{ci\sigma}(\mathbf{r}) \xrightarrow{r \rightarrow \infty} 0. \quad (110)$$

This is because the structure of Eqs. (104) and (105) is again such that an additive constant in the potentials (108) - (110) cancels out. Of course, Eq. (110) is valid only for those approximate orbital functionals $E_c[\{\varphi_{j\sigma}\}]$ leading to bounded functions $u_{ci\sigma}(\mathbf{r})$ for $r \rightarrow \infty$ (cf. condition (37)).

In order to determine the asymptotic form of the KLI-x-only potential $V_{x\sigma}^{\text{KLI}}(\mathbf{r})$, we first investigate the asymptotic behavior of the term $\sum_{i=1}^{N_\sigma} |\varphi_{i\sigma}(\mathbf{r})|^2 \cdot u_{xi\sigma}(\mathbf{r})$ appearing in the KLI equation (104): By Eqs. (69) and (70) the expression

$$|\varphi_{N_\sigma\sigma}(\mathbf{r})|^2 u_{xN_\sigma\sigma}(\mathbf{r}) + \sum_{i=1}^{N_\sigma-1} |\varphi_{i\sigma}(\mathbf{r})|^2 u_{xi\sigma}(\mathbf{r})$$

can be written as

$$\begin{aligned} &= |\varphi_{N_\sigma\sigma}(\mathbf{r})|^2 u_{xN_\sigma\sigma}(\mathbf{r}) + \sum_{i=1}^{N_\sigma-1} \sum_{j=1}^{N_\sigma} \varphi_{i\sigma}(\mathbf{r}) \varphi_{j\sigma}^*(\mathbf{r}) K_{jio}(\mathbf{r}) \\ &= |\varphi_{N_\sigma\sigma}(\mathbf{r})|^2 \left(u_{xN_\sigma\sigma}(\mathbf{r}) + \sum_{i=1}^{N_\sigma-1} \sum_{j=1}^{N_\sigma} \left(\frac{\varphi_{i\sigma}(\mathbf{r})}{\varphi_{N_\sigma\sigma}(\mathbf{r})} \right) \left(\frac{\varphi_{j\sigma}^*(\mathbf{r})}{\varphi_{N_\sigma\sigma}^*(\mathbf{r})} \right) K_{jio}(\mathbf{r}) \right). \end{aligned}$$

Since $K_{jio}(\mathbf{r})$ decays as an inverse power the double sum over i and j must be asymptotically dominated by the term with $i = N_\sigma - 1$, $j = N_\sigma$ so that

$$\xrightarrow{r \rightarrow \infty} |\varphi_{N_\sigma\sigma}(\mathbf{r})|^2 \left(u_{xN_\sigma\sigma}(\mathbf{r}) + \frac{\varphi_{(N_\sigma-1)\sigma}(\mathbf{r})}{\varphi_{N_\sigma\sigma}(\mathbf{r})} K_{N_\sigma(N_\sigma-1)\sigma}(\mathbf{r}) \right).$$

The KLI equation (104) then yields

$$\begin{aligned}
& \sum_{i=1}^{N_\sigma} |\varphi_{i\sigma}(\mathbf{r})|^2 \left[V_{x\sigma}^{\text{KLI}}(\mathbf{r}) - U_{x i \sigma}(\mathbf{r}) - \left(\bar{V}_{x i \sigma}^{\text{KLI}} - \bar{U}_{x i \sigma} \right) \right] \\
& \xrightarrow{r \rightarrow \infty} |\varphi_{N_\sigma \sigma}(\mathbf{r})|^2 \left[V_{x\sigma}^{\text{KLI}}(\mathbf{r}) - U_{x N_\sigma \sigma}(\mathbf{r}) - \left(\bar{V}_{x N_\sigma \sigma}^{\text{KLI}} - \bar{U}_{x N_\sigma \sigma} \right) \right. \\
& \quad + \left(\frac{\varphi_{(N_\sigma-1)\sigma}(\mathbf{r})}{\varphi_{N_\sigma \sigma}(\mathbf{r})} K_{N_\sigma(N_\sigma-1)\sigma}(\mathbf{r}) + \text{c.c.} \right) \\
& \quad \left. + \sum_{i=1}^{N_\sigma-1} \frac{|\varphi_{i\sigma}(\mathbf{r})|^2}{|\varphi_{N_\sigma \sigma}(\mathbf{r})|^2} \left(V_{x\sigma}^{\text{KLI}}(\mathbf{r}) - U_{x i \sigma}(\mathbf{r}) - \left(\bar{V}_{x i \sigma}^{\text{KLI}} - \bar{U}_{x i \sigma} \right) \right) \right] \equiv 0.
\end{aligned} \tag{111}$$

Since the KLI equation must be satisfied in the asymptotic region, the expression in square brackets on the right-hand side of Eq. (111) must vanish identically for $r \rightarrow \infty$. The term involving $\varphi_{(N_\sigma-1)\sigma}(\mathbf{r})/\varphi_{N_\sigma \sigma}(\mathbf{r})$ cannot be canceled by any of the terms involving $|\varphi_{i\sigma}(\mathbf{r})|^2/|\varphi_{N_\sigma \sigma}(\mathbf{r})|^2$ because the latter decay more rapidly. From this we conclude that

$$\begin{aligned}
& V_{x\sigma}^{\text{KLI}}(\mathbf{r}) - U_{x N_\sigma \sigma}(\mathbf{r}) - \left(\bar{V}_{x N_\sigma \sigma}^{\text{KLI}} - \bar{U}_{x N_\sigma \sigma} \right) \\
& \xrightarrow{r \rightarrow \infty} - \frac{\varphi_{(N_\sigma-1)\sigma}(\mathbf{r})}{\varphi_{N_\sigma \sigma}(\mathbf{r})} K_{N_\sigma(N_\sigma-1)\sigma}(\mathbf{r}) + \text{c.c.} \\
& \xrightarrow{r \rightarrow \infty} -r^{\left(\frac{1}{\beta_{(N_\sigma-1)\sigma}} - \frac{1}{\beta_{N_\sigma \sigma}} - m\right)} e^{-(\beta_{(N_\sigma-1)\sigma} - \beta_{N_\sigma \sigma})r}
\end{aligned} \tag{112}$$

where, in the second step, we have used Eqs. (53) and (72). $U_{x N_\sigma \sigma}(\mathbf{r})$ goes to zero asymptotically (cf. Eq. (74)) and the arbitrary additive constant in $V_{x\sigma}^{\text{KLI}}(\mathbf{r})$ had been fixed in such a way that $V_{x\sigma}^{\text{KLI}}(\mathbf{r})$ vanishes asymptotically (cf. Eq. (108)). Hence Eq. (112) immediately implies that

$$\bar{V}_{x N_\sigma \sigma}^{\text{KLI}} = \bar{U}_{x N_\sigma \sigma} \tag{113}$$

and thereby

$$V_{x\sigma}^{\text{KLI}}(\mathbf{r}) - U_{x N_\sigma \sigma}(\mathbf{r}) \xrightarrow{r \rightarrow \infty} -r^{\left(\frac{1}{\beta_{(N_\sigma-1)\sigma}} - \frac{1}{\beta_{N_\sigma \sigma}} - m\right)} e^{-(\beta_{(N_\sigma-1)\sigma} - \beta_{N_\sigma \sigma})r}. \tag{114}$$

We thus conclude that both the lemma of section 2.2.1 and the theorem 1 in section 2.2.2 are preserved in the KLI approximation. Once again, Eqs. (74) and (114) immediately imply that [6, 15, 16]

$$V_{x\sigma}^{\text{KLI}} \xrightarrow{r \rightarrow \infty} -\frac{1}{r}. \tag{115}$$

For the correlation potential $V_{c\sigma}^{\text{KLI}}(\mathbf{r})$ the considerations are even simpler. Dividing the KLI equation by $|\varphi_{N_\sigma \sigma}(\mathbf{r})|^2$ we find:

$$0 \equiv V_{c\sigma}^{\text{KLI}}(\mathbf{r}) - U_{c N_\sigma \sigma}(\mathbf{r}) - C_{N_\sigma \sigma} + \sum_{i=1}^{N_\sigma-1} \frac{|\varphi_{i\sigma}(\mathbf{r})|^2}{|\varphi_{N_\sigma \sigma}(\mathbf{r})|^2} \left(V_{c\sigma}^{\text{KLI}}(\mathbf{r}) - U_{c i \sigma}(\mathbf{r}) - C_{i\sigma} \right) \tag{116}$$

where

$$C_{i\sigma} := \bar{V}_{c i \sigma}^{\text{KLI}} - \bar{U}_{c i \sigma}. \tag{117}$$

By Eqs. (53), (109) and (110) all the r -dependent functions in (116) vanish asymptotically. Since the KLI equation (116) must be satisfied for $r \rightarrow \infty$ as well we readily conclude that

$$C_{N_\sigma\sigma} = 0 \quad (118)$$

so that

$$V_{c\sigma}^{\text{KLI}}(\mathbf{r}) - U_{cN_\sigma\sigma}(\mathbf{r}) = \sum_{i=1}^{N_\sigma-1} \frac{|\varphi_{i\sigma}(\mathbf{r})|^2}{|\varphi_{N_\sigma\sigma}(\mathbf{r})|^2} \left(C_{i\sigma} - V_{c\sigma}(\mathbf{r}) + U_{ci\sigma}^{\text{KLI}}(\mathbf{r}) \right). \quad (119)$$

If $C_{(N_\sigma-1)\sigma} \neq 0$, the right-hand side of (119) is asymptotically dominated by the $i = (N_\sigma - 1)$ term and we obtain

$$V_{c\sigma}^{\text{KLI}}(\mathbf{r}) - U_{cN_\sigma\sigma}(\mathbf{r}) \xrightarrow{r \rightarrow \infty} C_{(N_\sigma-1)\sigma} r^{\left(\frac{2}{\beta_{(N_\sigma-1)\sigma}} - \frac{2}{\beta_{N_\sigma\sigma}} \right)} e^{-2(\beta_{(N_\sigma-1)\sigma} - \beta_{N_\sigma\sigma})r} \quad (120)$$

If $C_{(N_\sigma-1)\sigma} = 0$, the right-hand side of (120) is an upper bound of $|V_{c\sigma}^{\text{KLI}}(\mathbf{r}) - U_{cN_\sigma\sigma}(\mathbf{r})|$ for $r \rightarrow \infty$. We note that $V_{c\sigma}^{\text{KLI}}(\mathbf{r})$ and $U_{cN_\sigma\sigma}(\mathbf{r})$ approach each other exponentially fast for $r \rightarrow \infty$ with the same exponential function as theorem 2 predicts for the full OEP. However, the power of r multiplying the exponential function in (120) differs by 1 from the power in theorem 2.

Acknowledgments

One of us (T.K.) gratefully acknowledges a fellowship of the Studienstiftung des deutschen Volkes. We thank the Deutsche Forschungsgemeinschaft for partial financial support.

References

- [1] *Density Functional Theory*, Vol. 337 of *NATO ASI Series B*, edited by E.K.U. Gross and R.M. Dreizler (Plenum Press, New York, 1995).
- [2] R.M. Dreizler and E.K.U. Gross, *Density Functional Theory* (Springer, Berlin, 1990).
- [3] R.G. Parr and W. Yang, *Density-Functional Theory of Atoms and Molecules* (Oxford University Press, New York, 1989).
- [4] T. Grabo and E.K.U. Gross, *Chem. Phys. Lett.* **240**, 141 (1995).
- [5] M. Petersilka, U.J. Gossmann, and E.K.U. Gross, *Phys. Rev. Lett.* **76**, 1212 (1996).
- [6] J.B. Krieger, Y. Li, and G.J. Iafrate, *Phys. Rev. A* **45**, 101 (1992).
- [7] R.T. Sharp and G.K. Horton, *Phys. Rev.* **90**, 317 (1953).
- [8] J.D. Talman and W.F. Shadwick, *Phys. Rev. A* **14**, 36 (1976).
- [9] J.P. Perdew and M.R. Norman, *Phys. Rev. B* **26**, 5445 (1982).
- [10] M. Levy and A. Görling, *Phys. Rev. A* **53**, 3140 (1996).
- [11] J.B. Krieger, Y. Li, and G.J. Iafrate, *Phys. Lett. A* **146**, 256 (1990).
- [12] J.B. Krieger, Y. Li, and G.J. Iafrate, *Phys. Lett. A* **148**, 470 (1990).

- [13] J.B. Krieger, Y. Li, M.R. Norman, and G.J. Iafrate, *Phys. Rev. B* **44**, 10437 (1991).
- [14] J.B. Krieger, Y. Li, and G.J. Iafrate, *Phys. Rev. A* **46**, 5453 (1992).
- [15] J.B. Krieger, Y. Li, and G.J. Iafrate, *Int. J. Quantum Chem.* **41**, 489 (1992).
- [16] Y. Li, J.B. Krieger, and G.J. Iafrate, *Chem. Phys. Lett.* **191**, 38 (1992).
- [17] Y. Li, J.B. Krieger, and G.J. Iafrate, *Phys. Rev. A* **47**, 165 (1993).
- [18] J.B. Krieger, Y. Li, and G.J. Iafrate, in *Density Functional Theory*, edited by R.M. Dreizler and E.K.U. Gross (Plenum Press, New York, 1995).
- [19] J.B. Krieger, J. Chen, Y. Li, and G.J. Iafrate, *Int. J. Quantum Chem. Symp.* **29**, 79 (1995).
- [20] J.B. Krieger, J. Chen, and G.J. Iafrate, *Bull. Am. Phys. Soc.* **41**, 748 (1996).
- [21] J. Chen, J.B. Krieger, and G.J. Iafrate, *Bull. Am. Phys. Soc.* **41**, 748 (1996).
- [22] J. Chen, J.B. Krieger, Y. Li, and G.J. Iafrate, *Phys. Rev. A* **54**, 3939 (1996).
- [23] J.B. Krieger, Y. Li, Y. Liu, and G.J. Iafrate, *Int. J. Quantum Chem.* **61**, 273 (1997).
- [24] U. von Barth and L. Hedin, *J. Phys. C* **5**, 1629 (1972).
- [25] M.M. Pant and A.K. Rajagopal, *Sol. State Commun.* **10**, 1157 (1972).
- [26] A. Görling and M. Levy, *Phys. Rev. A* **50**, 196 (1994).
- [27] C. Filippi, C.J. Umrigar, and X. Gonze, *Phys. Rev. A* (1996), (submitted).
- [28] C.O. Almbladh and U. von Barth, *Phys. Rev. B* **31**, 3231 (1985).
- [29] N.C. Handy, M.T. Marron, and H.J. Silverstone, *Phys. Rev.* **180**, 45 (1969).
- [30] L. Sham, *Phys. Rev. B* **32**, 3876 (1985).
- [31] M. K. Harbola and V. Sahni, *Phys. Rev. Lett.* **62**, 489 (1989).
- [32] E. Engel, J.A. Chevary, L.D. Macdonald, and S.H. Vosko, *Z. Phys. D* **23**, 7 (1992).
- [33] E. Engel and S.H. Vosko, *Phys. Rev. A* **47**, 2800 (1993).
- [34] T. Kotani, *Phys. Rev. B* **50**, 14816 (1994), and Erratum (submitted).
- [35] T. Kotani, *Phys. Rev. Lett.* **74**, 2989 (1995).
- [36] T. Kotani and H. Akai, *Phys. Rev. B* **52**, 17153 (1995).

RECENT DEVELOPMENTS IN THE LOCAL-SCALING TRANSFORMATION VERSION OF DENSITY FUNCTIONAL THEORY

E.V. Ludeña^{a,*}, R. López-Boada^a, V. Karasiev^a, R. Pino^a
E. Valderrama^a, J. Maldonado^a, R. Colle^b and J. Hinze^c

^aQuímica, Instituto Venezolano de Investigaciones Científicas, IVIC
Apartado 21827, Caracas 1020-A, Venezuela

^bDipartimento de Chimica Applicata, Università di Bologna, Bologna, Italy
and Scuola Normale Superiore, Pisa, Italy

^cFakultät für Chemie, Universität Bielefeld, Bielefeld, Germany

1. INTRODUCTION

The local-scaling transformation version of density functional theory (LS-DFT), [1-12] is a constructive approach to DFT which, in contradistinction to the usual Hohenberg-Kohn-Sham version of this theory (HKS-DFT) [13-18], is not based on the Hohenberg-Kohn theorem [13]. Moreover, in the context of LS-DFT it is possible to generate explicit energy density functionals that satisfy the variational principle [8-12]. This is achieved through the use of local-scaling transformations. The latter are coordinate transformations that can be expressed as functions of the one-particle density [19].

When these transformations are applied to an initial arbitrary N -particle wavefunction, Ψ_g , one obtains a density-dependent transformed wavefunction, Ψ_ρ . An energy functional containing both the one-particle density and the initial arbitrary wavefunction arises when the (density-dependent) transformed

* Author to whom all correspondence should be addressed

wavefunction is employed to calculate the expectation value of the Hamiltonian. For this reason we may write

$$E[\Psi_\rho] = \langle \Psi_\rho | \widehat{H} | \Psi_\rho \rangle \equiv \mathcal{E}[\rho, \Psi_g] \quad (1)$$

Because a local-scaling transformation establishes a one to one correspondence between a transformed wavefunction Ψ_ρ and the density ρ , there also arises (by construction) a one to one correspondence between the functional of the transformed wavefunction, $E[\Psi_\rho]$, and that of the one-particle density (and of the initial arbitrary wavefunction Ψ_g), $\mathcal{E}[\rho, \Psi_g]$. This property guarantees [3] that the minimization of the energy with respect to the one-particle density is variational [20].

One of the advantages of LS-DFT is the availability of specific prescriptions for building up energy density functionals [8-12]. In fact, we have been able to generate explicit functionals for the kinetic and exchange energy of atoms that lead to quite accurate values. In addition, general formulas have been obtained within the formalism of LS-DFT for the correlation energy of atoms.

In the present article we compare in Section 2 several kinetic energy functionals advanced in the context of the Hohenberg-Kohn-Sham version of density functional theory, HKS-DFT, with those constructed in LS-DFT by means of local-scaling transformations. In Section 3, we use LS-DFT in order to analyze the dynamic and non-dynamic components of the correlation energy and provide explicit values for the helium atom. We present explicit expressions for the correlation energy functional corresponding to the dominant term of a cluster expansion. Finally, we illustrate the use of local-scaling transformations for the purpose of improving the energy of correlated wavefunctions for the helium atom.

2. KINETIC AND EXCHANGE ENERGY FOR ATOMS IN LS-DFT

Consider a local-scaling transformation that carries the vector \vec{r} into the vector $\lambda(\vec{r})\vec{r}$. Applying this transformation to the arbitrary “generating” atomic orbital set $\{\phi_{g,i}(\vec{r}) = R_{g,n_i l_i}(r) Y_{l_i m_i}(\theta, \phi)\}_{i=1}^N$ one obtains the following set of transformed orbitals: $\{\phi_{\rho,i}(\vec{r}) = R_{\rho,n_i l_i}(r) Y_{l_i m_i}(\theta, \phi)\}_{i=1}^N$ where the locally-scaled (density-dependent) radial functions are given by

$$R_{\rho,n_i l_i}(r) = \sqrt{\frac{\rho(r)}{\rho_g(\lambda(r)r)}} R_{g,n_i l_i}(\lambda(r)r), \quad (2)$$

The radial densities $\rho(r)$ and $\rho_g(r)$ are obtained by spherically-averaging the one-particle densities $\rho(\vec{r}) = \sum_{i=1}^N |\phi_{\rho,i}(\vec{r})|^2$ and $\rho_g(\vec{r}) = \sum_{i=1}^N |\phi_{g,i}(\vec{r})|^2$.

Consider now a single Slater determinant Φ_ρ

$$\Phi_\rho(\vec{r}_1, s_1, \dots, \vec{r}_N, s_N) = \frac{\det}{N!^{1/2}} [\phi_{\rho,1}(\vec{r}_1)\sigma_1(s_1) \cdots \phi_{\rho,N}(\vec{r}_N)\sigma(s_N)] \quad (3)$$

formed by products of the transformed orbitals and spin functions. We assume that the above determinant is a micro-state of an atomic spectroscopic term labelled by the orbital and spin quantum numbers L and S . Thus, it satisfies the equations

$$\begin{aligned} \hat{L}^2 \Phi_\rho &= L(L+1) \Phi_\rho, & \hat{S}^2 \Phi_\rho &= S(S+1) \Phi_\rho, \\ \hat{L}_z \Phi_\rho &= M_L \Phi_\rho, & \hat{S}_z \Phi_\rho &= M_S \Phi_\rho \end{aligned} \quad (4)$$

(the generalization to a micro-state given as a linear combination Slater determinants is straightforward). Note that in LS-DFT, by construction, we always deal with a wavefunction that includes the symmetry of a given physical system (in the sense that it is an eigenfunction of the set of operators that commute with the Hamiltonian).

The expectation value of the Hamiltonian operator with respect to the transformed single Slater determinant is

$$E[\Phi_\rho] = \langle \Phi_\rho | \hat{H} | \Phi_\rho \rangle = T[\Phi_\rho] + E_x[\Phi_\rho] + E_{Coulomb}[\rho] + E_{ext}[\rho] \quad (5)$$

where we have decomposed it into its kinetic-, exchange-, Coulomb- and external-energy components, respectively. Note that only the kinetic and exchange terms depend on the full transformed wavefunction. We consider the generation of density functionals for these two terms in what follows.

2.1 Kinetic Energy Functional for Atoms in LS-DFT

Let us consider now the kinetic energy expression for the transformed wavefunction Φ_ρ :

$$T[\Phi_\rho] = \frac{1}{2} \sum_{i=1}^N \int_0^\infty dr r^2 \left[\left(\frac{dR_{\rho,n_i l_i}(r)}{dr} \right)^2 + \frac{l_i(l_i+1)}{r^2} (R_{\rho,n_i l_i}(r))^2 \right]. \quad (6)$$

Because a local-scaling transformation relates the densities $\rho(r)$ and $\rho_g(r)$ by means of the following first-order differential equation [8]:

$$\frac{\rho(r)}{\rho_g(\lambda(r)r)} = \lambda(r)^3 \{1 + \vec{r} \cdot \nabla_{\vec{r}} \ln \lambda(r)\} \quad (7)$$

the kinetic energy expression given by Eq. (6) becomes (after some manipulation [11])

$$\begin{aligned} T[\Phi_\rho] &= \frac{1}{8} \int_0^\infty dr r^2 \frac{(\nabla \rho(r))^2}{\rho(r)} + \int_0^\infty dr r^2 \rho^{5/3}(r) \left(1 + \vec{r} \cdot \nabla \ln \lambda(r)\right)^{4/3} \tau_N \\ &+ \int_0^\infty dr r^2 \rho^{5/3}(r) \left(1 + \vec{r} \cdot \nabla \ln \lambda(r)\right)^{-2/3} \kappa_N. \end{aligned} \quad (8)$$

where the modulating factors τ_N and κ_N (with $f = \lambda(r)r$) are:

$$\tau_N = \frac{1}{\rho_g^{8/3}(f)} \frac{1}{2} \sum_{i < j} \left[R_{g,n_i l_i}(f) \frac{dR_{g,n_j l_j}(f)}{df} - R_{g,n_j l_j}(f) \frac{dR_{g,n_i l_i}(f)}{df} \right]^2, \quad (9)$$

and

$$\kappa_N = \frac{1}{\rho_g(f)} \sum_{i=1}^N \frac{l_i(l_i + 1)}{2} \left(\frac{R_{g,n_i l_i}(f)}{f} \right)^2, \quad (10)$$

2.2 Exchange Energy Functional for Atoms in LS-DFT

The exchange energy for the transformed single Slater determinant Φ_ρ is:

$$E_x[\Phi_\rho] = -\frac{1}{2} \sum_{i=1}^N \sum_{j=1}^N \delta(m_{s_i}, m_{s_j}) \int d^3 \vec{r}_1 \int d^3 \vec{r}_2 \frac{\phi_{\rho,i}^*(\vec{r}_1) \phi_{\rho,j}(\vec{r}_1) \phi_{\rho,j}^*(\vec{r}_2) \phi_{\rho,i}(\vec{r}_2)}{|\vec{r}_1 - \vec{r}_2|}. \quad (11)$$

Bearing in mind Eqs. (2) and (7), upon integration over angular coordinates, Eq. (11) becomes [8,11]:

$$E_x[\Phi_\rho] = -\frac{1}{2} \int_0^\infty dr_1 r_1^2 \sum_{k=0} \rho(r_1)^{(4+k)/3} \left(\frac{1}{1 + \vec{r}_1 \cdot \nabla_{\vec{r}} \ln \lambda(r_1)} \right)^{(k+1)/3} \chi_N^k(f_1). \quad (12)$$

There appears in this Equation an exchange-modulating factor $\chi_N^k(f_1)$ which depends on the angular momentum quantum numbers:

$$\chi_N^k(f_1) = \frac{1}{f_1^{k+1} \rho_g(f_1)^{(4+k)/3}} \sum_{i=1}^N \sum_{j=1}^N \delta(m_{s_i}, m_{s_j}) b^k(l_i, m_{l_i}; l_j, m_{l_j}) G_{ij}^k(f_1). \quad (13)$$

The angular coefficient [21]

$$b^k(l_i, m_{l_i}; l_j, m_{l_j}) = [c^k(l_i, m_{l_i}; l_j, m_{l_j})]^2 \quad (14)$$

results from the integration over Legendre polynomials. Note that because of the triangular condition on the angular coefficients the sum over k in Eq. (12) is finite. The function

$$G_{ij}^k(f_1) = A_{ij}(f_1) P_{ji}^k(f_1) + A_{ji}(f_1) P_{ij}^k(f_1), \quad (15)$$

is the modified exchange integral. In Eq. (15) we have defined

$$A_{ij}(f_1) \equiv R_{g,n_i l_i}(f_1) R_{g,n_j l_j}(f_1), \quad (16)$$

and

$$P_{ij}^k(f_1) = \int_0^{f_1} df_2 f_2^2 r_2^k(f_2) A_{ij}(f_2). \quad (17)$$

2.3 Comparison Between Kinetic Energy Functionals in LS-DFT and HKS-DFT

The kinetic and exchange energy functionals given by Eqs. (8) and (12), respectively, contain universal terms that just depend upon the one-particle density. In the case of the former, such term is $\rho^{5/3}$, the Thomas-Fermi term [22,23] and for the latter, the set $\{\rho(r_1)^{(4+k)/3}\}$, where the first term $\rho^{4/3}$ (for $k = 0$) is the Dirac exchange expression [24]. But in addition, in Eq. (8) we observe the presence of a factor, which we call $F_{LS}([\rho], r)$ defined as:

$$F_{LS}([\rho], r) = \left(1 + \vec{r} \cdot \nabla \ln \lambda(r)\right)^{4/3} \tau_N + \left(1 + \vec{r} \cdot \nabla \ln \lambda(r)\right)^{-2/3} \kappa_N, \quad (18)$$

such that the kinetic energy can be written as

$$T[\Phi_\rho] = T_W[\rho] + \int_0^\infty dr r^2 \rho^{5/3}(r) F_{LS}(r). \quad (19)$$

Because both τ_N and κ_N depend upon the “generating” orbitals $\{R_{g,n_i,l_i}(f)\}$ (see Eqs. (9) and (10)), the realization of $F_{LS}([\rho], r)$ depends on our choice of these orbitals. Thus, for example, when we consider plane-waves of the type

$$R_{g,k}(r) = \sqrt{\frac{3}{4\pi}} e^{2\pi i(k-(N+1)/2)q(r)} \quad (20)$$

normalized in the unit sphere with $q(r) = r^3/3$, then the corresponding locally-scaled functions are

$$R_{\rho,k}(r) = \sqrt{\frac{\rho(r)}{N}} e^{2\pi i(k-(N+1)/2)q(f)}. \quad (21)$$

These locally-scaled plane-waves are precisely the equidensity orbitals of Hariman [25]. When the “generating” orbitals of Eq. (20) are substituted into Eqs. (9) and (10) (for the latter we assume spherical symmetry, viz., $l_i = 0$ for all i) we obtain the following constant term for the local-scaling plane-wave modulating function

$$F_{LS}^{pw}(r) = C_F \left(\frac{2\pi}{3}\right)^{4/3} \frac{5}{3} \left(1 - \frac{1}{N^2}\right). \quad (22)$$

We have set, in the above derivation, $r = r_s$, where the Fermi radius is

$$r_s = (3/4\pi)\rho^{-1/3}. \quad (23)$$

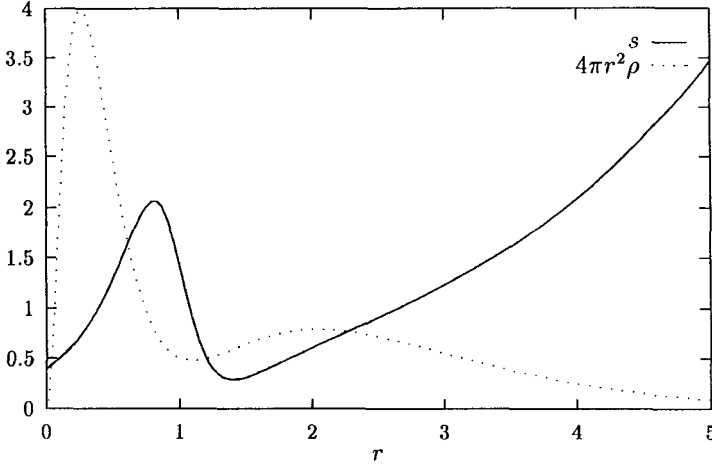


Figure 1: Graphical representation of the radial distribution function $D(r) = 4\pi r^2 \rho(r)$ and of the variable $s = (1/(2(3\pi^2)^{2/3})|\nabla \rho(\vec{r})|/\rho^{4/3}(\vec{r}))$ for the beryllium atom.

Another realization of this modulating function can be obtained by using generalized Slater-type orbitals (GSTO). For the particular case of the beryllium atom, these orbitals adopt the form [26]:

$$\begin{aligned} R_{g,1s}(r) &= N_1 \exp(-\alpha_1 r^\beta), \\ R_{g,2s}(r) &= N_2(1 + Br) \exp(-\alpha_2 r^\beta). \end{aligned} \quad (24)$$

The modulating function F_{LS}^{GSTO} is given by Eq. (18). Since in this example $\kappa_4 = 0$, this function is determined by τ_4 which for this choice of orbitals becomes [26]:

$$\tau_4^{GSTO}(f) = \frac{2}{\rho_g(f)^{8/3}} N_1^2 N_2^2 \exp(-(2\alpha_1 + 2\alpha_2)f^\beta) \left[(\alpha_1 - \alpha_2)\beta f^{\beta-1} (1 + Bf) + B \right]^2, \quad (25)$$

where

$$\rho_g(f) = 2 \left(N_1^2 \exp(-2\alpha_1 f^\beta) + N_2^2 (1 + Bf)^2 \exp(-2\alpha_2 f^\beta) \right). \quad (26)$$

For a single Slater determinant, the exact behaviour of the modulating function is attained when we use Hartree-Fock orbitals as the generating ones. The behavior of this modulating function F_{LS}^{HFF} can be easily determined. In fact, by inspection of Eqs. (8) and (9), we see that it is a positive function (the density is positive definite and tends to zero at infinity, the multiplicative

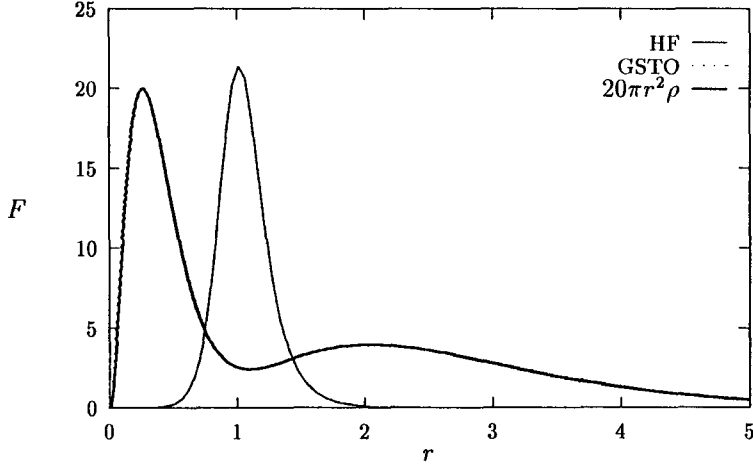


Figure 2: Graphical representation of the LS-DFT modulating functions $F_{LS}^{HF}(r)$ and $F_{LS}^{GSTO}(r)$ for the beryllium atom. For comparison, the radial distribution function $D(r) = 4\pi r^2 \rho(r)$ is also shown.

factors are squared and $(1 + \vec{r} \cdot \nabla \ln \lambda(r)) > 0$ according to Eq. (7)). The modulating functions F_{LS}^{HF} and F_{LS}^{GSTO} are depicted in Fig. 2.

In HKS-DFT there have been a number of proposals for approximating the kinetic energy functional [27]. Of particular importance are those based in the “conjoint gradient correction” hypothesis [27]. This stems from the conjecture made in 1991 by Lee et al. [28] that the kinetic energy functional could be constructed from the modulating function $G(x)$ appearing in the exchange energy functional. In fact, for the exchange energy functional, Becke [29,30] has introduced an approximate closed analytical expression

$$E_x[\rho] = -2^{1/3} C_x \int d^3 \vec{r} \rho^{4/3}(\vec{r}) [1 + \beta G(x)]. \quad (27)$$

(with $C_x = \frac{3}{4}(3/\pi)^{1/3}$ and $x = \frac{|\nabla \rho(\vec{r})|}{\rho(\vec{r})^{4/3}}$) where the convergent gradient expansion effects are embodied into the single function $G(x)$. Although there can be many choices for the function $G(x)$, the particular one advocated by Becke [29] is:

$$G(x) = \frac{x^2}{1 + \gamma x \sinh^{-1}(x)}, \quad (28)$$

where γ is a constant. Evaluations of the exchange energy of atoms and molecules using Eq. (27) give values whose rms percentage error is of the order of 0.5% [28].

According to the conjecture of Lee et al., [28] the kinetic energy functional adopts the following form:

$$T[\rho] = 2^{2/3} C_F \int d^3\vec{r} \rho^{5/3}(\vec{r}) [1 + \alpha G(x)]. \quad (29)$$

Application of this formula to atoms produced kinetic energy values whose rms percentage errors were also of the order of 0.5%. The absolute error is, however, an order of magnitude larger than those for exchange due to the fact that the absolute kinetic energy values are an order of magnitude larger than those for exchange.

Table 1: Kinetic energy values (in hartrees) for the beryllium atom obtained in the context of LS-DFT, with the several conjoint gradient expansion functionals discussed in the text. For comparison purposes, the Hartree-Fock value [40] is included.. $T_W[\rho]$ and $T_{NW}[\rho]$ are the Weizsäcker and non-Weizsäcker components, respectively. $T_{NW}^+[\rho]$ and $T_{NW}^-[\rho]$ are the positive and negative components of the non-Weizsäcker term.

Method	$T[\rho]$	$T_W[\rho]$	$T_{NW}[\rho]$	$T_{NW}^+[\rho]$	$T_{NW}^-[\rho]$
Hartree-Fock ^a	14.57302	13.66910	0.91112	0.91112	0.00000
LS-DFT(GSTO)	14.57349	13.66910	0.91159	0.91159	0.00000
TF $_{\frac{1}{9}}$ W	14.64648	13.66910	0.98458	4.34330	3.35872
Padé43 [37]	14.42220	13.66910	0.76030	4.42772	3.66742
Pearson [36]	14.00688	13.66910	0.34498	4.28898	3.94400
LLP [28]	14.61897	13.66910	0.95707	4.43936	3.48229
PW86 [32]	14.74650	13.66910	1.08460	4.49456	3.40997
PW91 [33]	14.60001	13.66910	0.93811	4.42981	3.49170
OL1 [38]	14.78732	13.66910	1.12542	4.42798	3.30256
OL2 [38]	14.74198	13.66910	1.08008	4.41186	3.33178
Thakkar [39]	14.66955	13.66910	1.00765	4.40595	3.39830
LCh [35]	14.63621	13.66910	0.97431	4.42784	3.45352
B86A [30]	14.68142	13.66910	1.01952	4.45214	3.43263
B86B [34]	14.64565	13.66910	0.98375	4.45117	3.46742

^a Clementi-Roetti [40]

The approach initiated by Lee et al. [28], was rapidly adopted and as a consequence, several kinetic energy “conjoint gradient correction” functionals were generated. In order to compare the behavior of kinetic energy density functionals constructed in the context of LS-DFT and some members of the

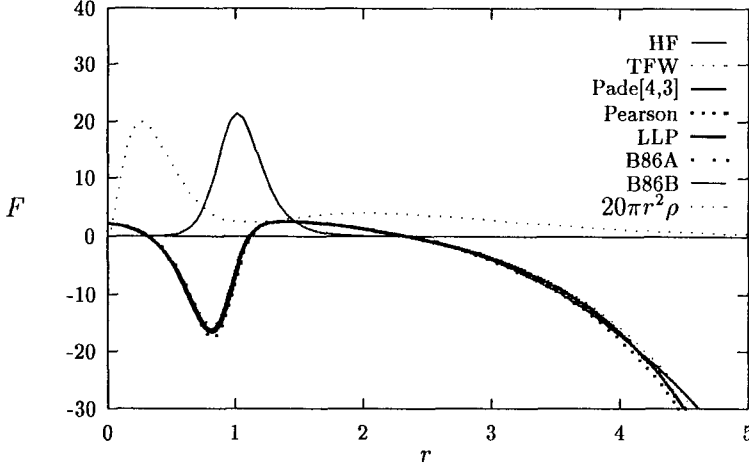


Figure 3: Graphical representation of the conjoint gradient correction functions – for the beryllium atom – of Padé43 [37], Pearson [36], LLP [28], TFW_9^1 , B86A [30] and B86B [34] advanced in HKS-DFT. For comparison the exact Hartree-Fock modulating function and radial distribution $D(r) = 4\pi r^2 \rho(r)$ are also shown.

family of “conjoint gradient correction” functionals developed in the HKS-DFT, let us rewrite the “conjoint” kinetic energy functionals given by

$$T[\rho] = A_k \int_0^\infty dr r^2 \rho^{5/3}(r) \tilde{F}(r) \quad (30)$$

where $A_k = \frac{3}{10}(3\pi^2)^{2/3}$ as

$$T[\rho] = T_W[\rho] + \int_0^\infty dr r^2 \rho^{5/3}(r) F(r), \quad (31)$$

where

$$F(r) = A_k \tilde{F}(r) - B_k s^2 \quad (32)$$

with $B_k = \frac{1}{2}(3\pi^2)^{2/3}$. Note that $B_k s^2$ just subtracts the contribution due to the Weizsäcker term [31]. Here, $s = (1/(2(3\pi^2)^{2/3})|\nabla\rho(\vec{r})|/\rho^{4/3}(\vec{r}))$. The kinetic energy functionals obtained from the exchange ones are those of Lee, Lee and Parr (LLP) [28], Perdew (PW86) [32], Perdew et al. (PW91) [33], Becke (B86A) [30], Becke (B86B) [34], and Lembarki and Chermette (LCh)[35]. We have also included the kinetic energy functionals of Pearson [36], DePristo and Kress based on a Padé approximant [4,3] (Pade43) [37], Ou-Yang and Levy in their two versions (OL1) and (OL2) [38], and Thakkar [39]. In addition

we have also included the functional $TF_{\frac{1}{9}}W$ comprising the Thomas Fermi contribution plus $\frac{1}{9}$ of the Weizsäcker term. Below, we list the functions $\tilde{F}(r)$ employed in these comparisons:

$$\tilde{F}_{Pade43}(s) = \frac{1 + 0.95s + 14.28111x^2 - 19.57962x^3 + 26.6477x^4}{1 - 0.05x + 9.99802x^2 + 2.96085x^3} \quad (33)$$

$$\tilde{F}_{Pearson}(s) = 1 + \frac{B_k s^2}{9A_k[1 + (s/\zeta)^6]} \quad (34)$$

$$\tilde{F}_{LLP}(s) = 1 + \frac{0.0045b^2 s^2}{1 + 0.0253bs \sinh^{-1}(bs)} \quad (35)$$

$$\tilde{F}_{TF_{\frac{1}{9}}W}(s) = \frac{1}{9} \quad (36)$$

$$\tilde{F}_{PW86}(s) = (1 + 1.296s^2 + 14s^4 + 0.2s^6)^{1/15} \quad (37)$$

$$\tilde{F}_{PW91}(s) = \frac{1 + 0.19645s \sinh^{-1}(7.7956s) + [0.2743 - 0.1508e^{-100s^2}]s^2}{1 + 0.19645s \sinh^{-1}(7.7956s) + 0.004s^2} \quad (38)$$

$$\tilde{F}_{OL1}(s) = 1 + \frac{5}{27}s^2 + 0.00187bs \quad (39)$$

$$\tilde{F}_{OL2}(s) = 1 + \frac{5}{27}s^2 + \frac{0.0245bs}{1 + 2^{5/3}bs} \quad (40)$$

$$\tilde{F}_{Thakkar}(s) = 1 + \frac{0.0055b^2 s^2}{1 + 0.0253bs \sinh^{-1}(bs)} - \frac{0.072bs}{1 + 2^{5/3}bs} \quad (41)$$

$$\begin{aligned} \tilde{F}_{LCh}(s) &= \frac{1 + 0.093907s \sinh^{-1}(76.320s)}{1 + 0.093907s \sinh^{-1}(76.320s) + 0.000057767s^4} \\ &+ \frac{[0.26608 - 0.0809615 \exp(-100s^2)]s^2}{1 + 0.093907s \sinh^{-1}(76.320s) + 0.000057767s^4} \end{aligned} \quad (42)$$

$$\tilde{F}_{B86A}(s) = 1 + 0.0039 \frac{b^2 s^2}{1 + 0.004b^2 s^2} \quad (43)$$

$$\tilde{F}_{B86B}(s) = 1 + 0.00403 \frac{b^2 s^2}{(1 + 0.007b^2 s^2)^{4/5}} \quad (44)$$

In Fig. 1, we show the behavior of the variable s as a function of r for the beryllium atom. Note that this function has the important peculiarity of having a local maximum in a region nearby the shell boundary.

The behavior of $F_{LS}^{HF}(r)$, and $F_{LS}^{GSTO}(r)$ for the beryllium atom is depicted in Fig. 2. The location of the maxima of these sharp bell-shaped curves coincides with the minimum of the radial distribution functions both for Be. This clearly shows that the modulating factor is essential in describing the

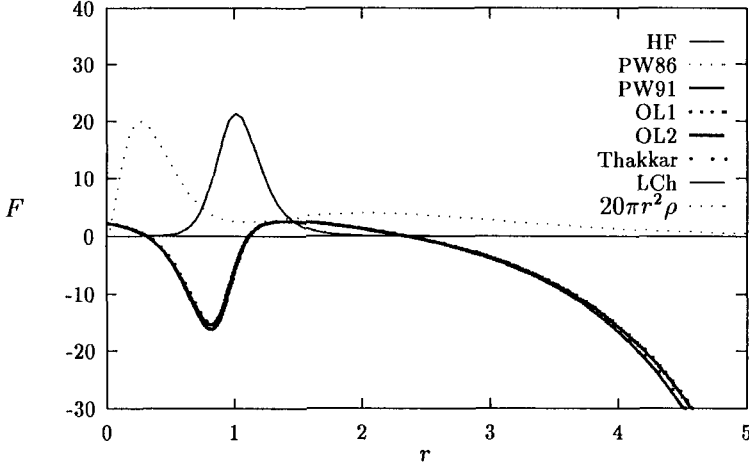


Figure 4: Graphical representation of the conjoint gradient correction functions – for the beryllium atom – of PW86 [32], PW91 [33], OL1 [38], OL2 [38], Thakkar [39] and LCh [35] advanced in HKS-DFT. For comparison the exact Hartree-Fock modulating function and radial distribution $D(r) = 4\pi r^2 \rho(r)$ are also shown.

proper physics underlying the arising of shell structure. It is important to remark that the values of the kinetic energy for these atoms – computed using the locally-scaled one particle functions obtained from the above set – are quite close to the “exact” Hartree-Fock values [40] (see Table 1).

In Fig. 3, we present a graphical display of the modulating functions $F(r)$ labelled as Padé43 [37], Pearson [36], LLP [28], $TF_{\frac{1}{9}}W$, B86A [30] and B86B [34] and compare them with the exact Hartree-Fock modulating function. In Fig. 4, we present the remaining cases PW86 [32], PW91 [33], OL1 [38], OL2 [38], Thakkar [39] and LCh [35].

In spite of the very different form of these functionals, the behavior of their corresponding modulating functions is amazingly similar. But, as can be seen from Figs. 3 and 4, they deviate considerably from that of the Hartree-Fock case. In fact, instead of showing a hump in the intershell region all the above modulating functions used in HKS-DFT present a sink. Moreover, they also show differences near the origin with respect to the Hartree-Fock modulating function.

Although for the Hartree-Fock case, the modulating function is positive for all r , the corresponding modulating functions arising from the HKS-DFT approximations lead to both negative and positive components of the kinetic

energy. Thus, as can be seen from Table 1, the fairly reasonable values for the kinetic energy obtained using the conjoint-gradient functionals actually result from a cancellation of errors among the positive and negative contributions. Note, on the other hand, that the LS-DFT(GSTO) modulating function resulting from the generalized Slater-type orbitals quite accurately reproduces the behavior of the Hartree-Fock modulating function.

3. ELECTRONIC CORRELATION IN LS-DFT

3.1 Dynamical and Non-dynamical Correlation in LS-DFT

Note that in terms of the energy functionals described by Eq. (1), the Hartree-Fock and exact (ground-state) energies E_0^{HF} and E_0^{exact} are given by:

$$E_0^{HF} = \mathcal{E}[\rho_{HF}, \Psi^{HF}], \text{ and } E_0^{exact} = \mathcal{E}[\rho_{exact}, \Psi^{exact}]. \quad (45)$$

Moreover, the correlation energy functional

$$\mathcal{E}_c[\rho] = \mathcal{E}[\rho, \Psi^{exact}] - \mathcal{E}[\rho_{HF}, \Psi^{HF}] \quad (46)$$

yields the quantum mechanical correlation energy at $\rho = \rho_{exact}$.

In order to decompose the correlation energy into its dynamical and non-dynamical components consider the following energy functionals: $\mathcal{E}[\rho_{HF}, \Psi^{HF}]$, $\mathcal{E}[\rho_{exact}, \Psi^{HF}]$, $\mathcal{E}[\rho_{exact}, \Psi^{exact}]$ and $\mathcal{E}[\rho_{HF}, \Psi^{exact}]$. Clearly, the functional $\mathcal{E}[\rho_{exact}, \Psi^{HF}]$ can be generated from $\mathcal{E}[\rho_{HF}, \Psi^{HF}]$ by applying a local-scaling transformation that carries the Hartree-Fock wavefunction into another one whose density is ρ_{exact} . Similarly, the functional $\mathcal{E}[\rho_{HF}, \Psi^{exact}]$ can be generated from $\mathcal{E}[\rho_{exact}, \Psi^{exact}]$ by locally-scaling the exact wavefunction so that it associates with the Hartree-Fock density.

A non-dynamical contribution to the correlation energy corresponds to the change in energy produced by a density transformation. On the other hand, the dynamical contribution arises from a wavefunction change at fixed density. Thus, the two following decompositions of the correlation energy (labelled as I and II) are possible [41]:

$$\begin{aligned} E_c &= (\mathcal{E}[\rho_{HF}, \Psi^{exact}] - \mathcal{E}[\rho_{HF}, \Psi^{HF}]) + (\mathcal{E}[\rho_{exact}, \Psi^{exact}] - \mathcal{E}[\rho_{HF}, \Psi^{exact}]) \\ &= E_c^{d(I)} + E_c^{nd(I)}. \end{aligned} \quad (47)$$

and

$$\begin{aligned} E_c &= (\mathcal{E}[\rho_{exact}, \Psi^{HF}] - \mathcal{E}[\rho_{HF}, \Psi^{HF}]) + (\mathcal{E}[\rho_{exact}, \Psi^{exact}] - \mathcal{E}[\rho_{exact}, \Psi^{HF}]) \\ &= E_c^{nd(II)} + E_c^{d(II)}. \end{aligned} \quad (48)$$

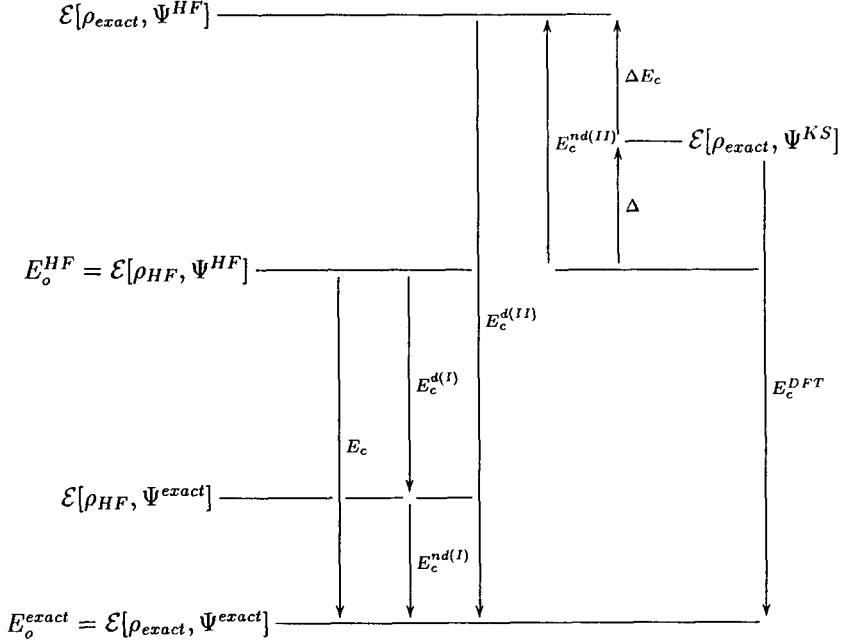


Figure 5: Graphical representation of the correlation energy decomposition into its dynamical and non-dynamical components and of their connection with other correlation energy components generated in DFT

A comprehensive view of the above correlation energy decomposition is presented in Fig. 5. For completeness we have also included the energy functional $\mathcal{E}[\rho_{exact}, \Psi^{KS}]$, namely, the Kohn-Sham energy. We see from Fig. 5 that the DFT correlation energy, E_c^{DFT} , defined as

$$E_c^{DFT} = \mathcal{E}[\rho_{exact}, \Psi^{exact}] - \mathcal{E}[\rho_{exact}, \Psi^{KS}] \quad (49)$$

does not coincide with the quantum mechanical correlation energy. However, it can be seen from this Figure that E_c^{DFT} is approximated by the dynamical component $E_c^{d(II)}$. We also observe in Fig. 5 the quantities Δ and ΔE_c . These have been introduced by Gross et al. [42] and by Görling and Ernzerhof [43], respectively. Notice that the non-dynamical component $E_c^{nd(II)}$ is the sum of Δ and ΔE_c .

A quantitative analysis of the non-dynamical and dynamical components of the correlation energy for the helium atom is given in Table 2.

Table 2: Comparison of quantum mechanical and density functional correlation energies for the helium isoelectronic series ^a. The values for the non-dynamical and dynamical components correspond closely to the already reported values^b for Δ and E_c^{DFT} , respectively. The last column shows the values obtained using the exact energies (μ hartrees) from Davidson^c [44].

Z	E_c	$E_c^{nd(II)}$	$E_c^{d(II)}$	Δ	E_c^{DFT}	$E_c^{DFT(c)}$
2	-41 963.4	63.2	-42 026.7	63	-42 107	-42 107
3	-43 389.4	17.2	-43 406.6			-43 515
4	-44 134.1	7.7	-44 141.8	7	-44 274	-44 275
5	-44 580.6	4.4	-44 585.0			-44 741
6	-44 911.9	2.8	-44 914.7			-45 057

^aDecomposition at the final MCSCF wavefunction

^bGross et. al. [42]

^cEstimated by $E_c^{DFT} = E_c - \Delta(MCSCF)$; E_c values from Davidson [44]

3.2 Correlation energy functional in LS-DFT

In view of the fact that in Section 2 we have presented energy density functionals which are in a one to one correspondence with energy functionals of a single Slater determinant, we consider in what follows the inclusion of electron correlation – in a first approximation – in terms of a modified Hamiltonian acting again on a single Slater determinant. This approach, of course is not new; it was introduced some time ago by Boys and Handy [45]. The novelty lies in that using this framework we obtain functionals for the electron correlation energy that can be explicitly given as functionals of the one-electron density.

A general way of writing a correlated wavefunction is as a product Ψ_g of a single Slater determinant Φ_g times a correlation factor C

$$\Psi_g(\vec{r}_1, \dots, \vec{r}_N) = C(\vec{r}_1, \dots, \vec{r}_N) \Phi_g(\vec{r}_1, \dots, \vec{r}_N), \quad (50)$$

Applying local-scaling transformation to this initial wavefunction, we obtain the transformed wavefunction

$$\Psi_\rho(\vec{r}_1, \dots, \vec{r}_N) = C(\vec{f}_1, \dots, \vec{f}_N) \prod_{i=1}^N \sqrt{\frac{\rho(\vec{r}_i)}{\tilde{\rho}_g(\vec{f}_i)}} \Phi_g(\vec{f}_1, \dots, \vec{f}_N)$$

$$= C(\vec{f}_1, \dots, \vec{f}_N) \Phi_\rho(\vec{r}_1, \dots, \vec{r}_N) \quad (51)$$

where again, $f(\vec{r}) = \lambda(\vec{r})r$. Note that in order to be consistent, the local-scaling transformation must connect the density $\tilde{\rho}_g$ coming from the correlated wavefunction Ψ_g and the final density ρ (the unknown variational quantity).

It is clear that the variational principle is observed because the expectation value of the Hamiltonian \widehat{H} with respect to the transformed wavefunction Ψ_ρ satisfies the inequality

$$\langle \Psi_\rho | \widehat{H} | \Psi_\rho \rangle \geq E_0. \quad (52)$$

According to the transcorrelated function method of Boys and Handy [45], we can take advantage of the fact that $CC^{-1} = 1$, to rewrite Eq. (52) as:

$$\langle C\Phi_\rho C | C^{-1}\widehat{H}C | C^{-1}C\Phi_\rho \rangle = \quad (53)$$

$$\langle C^2\Phi_\rho | \widehat{H} + \widehat{H}^{(1)} + \widehat{H}^{(2)} | \Phi_\rho \rangle \geq E_0. \quad (54)$$

In Eq. (54) there appears a new Hamiltonian containing the additional Hamiltonians $\widehat{H}^{(1)}$ and $\widehat{H}^{(2)}$. The latter contain two- and three-particle operators, respectively. Although the new Hamiltonian operates to the right over the single Slater determinant Φ_ρ we have on the left the presence of the correlation term C^2 . For a Jastrow-type correlating factor $C = \prod_{i>j} (1 + \phi_{ij})$ the energy expression gives rise to a cluster expansion

$$\begin{aligned} E[\Psi_\rho] &= \langle (1 + c_{12} + c_{123} + c_{1234} + \dots + c_{12\dots N}) \Phi_\rho | \widehat{H} + \widehat{H}^{(1)} + \widehat{H}^{(2)} | \Phi_\rho \rangle \\ &= \langle \Phi_\rho | \widehat{H} | \Phi_\rho \rangle + \langle \Phi_\rho | \widehat{H}^{(1)} | \Phi_\rho \rangle + \dots \langle c_{12\dots N} \Phi_\rho | \widehat{H}^{(2)} | \Phi_\rho \rangle. \end{aligned} \quad (55)$$

where c_{12} , c_{123} , up to $c_{12\dots N}$ are cluster functions (see, Clark et al. [46]).

The first term

$$E[\Phi_\rho] = \langle \Phi_\rho | \widehat{H} | \Phi_\rho \rangle, \quad (56)$$

gives the expectation value of the original Hamiltonian with respect to a single Slater determinant. As the only terms in this expectation value that do not directly give functionals of the one-particle density are the non-Weizsäcker part of the kinetic energy and the exchange energy, it is clear that this term can be transformed into a functional of ρ using the procedures developed in Section 2.

The second term

$$E_C^{(1)}[\Phi_\rho] = \langle \Phi_\rho | \widehat{H}^{(1)} | \Phi_\rho \rangle \quad (57)$$

contains, on the other hand, electron correlation contributions coming from the two-particle interactions appearing in the Hamiltonian $\widehat{H}^{(1)}$ and is given by

$$E_C^{(1)}[\Phi_\rho] = \int d^3\vec{r}_1 \int d^3\vec{r}_2 (\hat{u}_1(\vec{f}_1, \vec{f}_2) + \hat{u}_2(\vec{f}_1, \vec{f}_2)) D_\rho^2(\vec{r}_1, \vec{r}_2; \vec{r}_1, \vec{r}_2), \quad (58)$$

where D_ρ^2 is the two matrix corresponding to the single Slater determinant Φ_ρ :

$$D_\rho^2(\vec{r}_1, \vec{r}_2; \vec{r}_1, \vec{r}_2) = d(\vec{r}_1)d(\vec{r}_2)D_g^2(\vec{f}_1, \vec{f}_2; \vec{f}_1, \vec{f}_2), \quad (59)$$

with $d(\vec{r}_i) = \rho(r_i)/\rho_g(f_i)$. The two-particle operator is:

$$\begin{aligned} \hat{u}_1(\vec{f}_1, \vec{f}_2) &= \left(\frac{df_1}{dr_1}\right)^2 \left(\frac{2}{g(\vec{f}_1, \vec{f}_2)} \frac{\partial g(\vec{f}_1, \vec{f}_2)}{\partial f_1} \frac{\partial}{\partial f_1} - \frac{1}{2g(\vec{f}_1, \vec{f}_2)} \frac{\partial^2 g(\vec{f}_1, \vec{f}_2)}{\partial f_1^2} \right) \\ &+ \left(\frac{df_1}{dr_1}\right) \left(-\frac{1}{r_1 g(\vec{f}_1, \vec{f}_2)} \frac{\partial g(\vec{f}_1, \vec{f}_2)}{\partial f_1} \right) \\ &+ \frac{1}{2r_1^2 g(\vec{f}_1, \vec{f}_2)} \left(-\frac{1}{2r_1^2 g(\vec{f}_1, \vec{f}_2)} \nabla_{\Omega_1}^2 g(\vec{f}_1, \vec{f}_2) + \frac{2\nabla_{\Omega_1} g(\vec{f}_1, \vec{f}_2) \cdot \nabla_{\Omega_1}}{r_1^2 g(\vec{f}_1, \vec{f}_2)} \right) \\ &= \left(\frac{df_1}{dr_1}\right)^2 (\hat{a}_0(\vec{f}_1, \vec{f}_2) + a_1(\vec{f}_1, \vec{f}_2)) + \left(\frac{df_1}{dr_1}\right) b_0(\vec{f}_1, \vec{f}_2) \\ &+ (c_0(\vec{f}_1, \vec{f}_2) + \hat{c}_1(\vec{f}_1, \vec{f}_2)). \end{aligned} \quad (60)$$

Substituting Eq.(60) into Eq. (58) and using Eq. (7) one obtains:

$$\begin{aligned} E_C^{(1)}[\Phi_\rho] &= \int dr r^2 \rho^{5/3}(r) \left[(1 + \vec{r} \cdot \nabla_{\vec{r}} \lambda(r))^{4/3} C_N^{(1)} + (1 + \vec{r} \cdot \nabla_{\vec{r}} \lambda(r))^{-2/3} C_N^{(3)} \right] \\ &+ \int dr r^2 \rho^{4/3}(r) (1 + \vec{r} \cdot \nabla_{\vec{r}} \lambda(r))^{2/3} C_N^{(2)} \\ &+ \int dr r^2 \rho^{2/3}(r) \left[(1 + \vec{r} \cdot \nabla_{\vec{r}} \lambda(r))^{4/3} C_N^{(4)} + (1 + \vec{r} \cdot \nabla_{\vec{r}} \lambda(r))^{-2/3} C_N^{(5)} \right] \end{aligned} \quad (61)$$

where the correlation modulating factors are:

$$\begin{aligned} C_N^{(1)}(f_1) &= \frac{1}{\bar{\rho}_g^{5/3}(f_1)} \int d\Omega_1 \int df_2 f_2^2 \int d\Omega_2 (\hat{a}_0(\vec{f}_1, \vec{f}_2) + a_1(\vec{f}_1, \vec{f}_2)) D_g^1(\vec{f}_1, \vec{f}_2), \\ C_N^{(2)}(f_1) &= \frac{1}{\bar{\rho}_g^{4/3}(f_1)} \int d\Omega_1 \int df_2 f_2^2 \int d\Omega_2 b_0(\vec{f}_1, \vec{f}_2) D_g^1(\vec{f}_1, \vec{f}_2), \\ C_N^{(3)}(f_1) &= \frac{1}{f_1^2 \bar{\rho}_g^{5/3}(f_1)} \int d\Omega_1 \int df_2 f_2^2 \int d\Omega_2 (c_0(\vec{f}_1, \vec{f}_2) + \hat{c}_1(\vec{f}_1, \vec{f}_2)) D_g^1(\vec{f}_1, \vec{f}_2), \\ C_N^{(4)}(f_1) &= \frac{1}{\bar{\rho}_g^{2/3}(f_1)} \int d\Omega_1 \int df_2 f_2^2 \int d\Omega_2 (\hat{a}_0(\vec{f}_1, \vec{f}_2) d(\vec{r}_1)) D_g^1(\vec{f}_1, \vec{f}_2), \\ C_N^{(5)}(f_1) &= \frac{1}{f_1^2 \bar{\rho}_g^{2/3}(f_1)} \int d\Omega_1 \int df_2 f_2^2 \int d\Omega_2 (\hat{c}_1(\vec{f}_1, \vec{f}_2) d(\vec{r}_1)) D_g^1(\vec{f}_1, \vec{f}_2). \end{aligned}$$

The last integral in Eq. (61) includes effects not considered in the correlation energy functional advanced in Ref. [11].

Table 3: Improvement of correlated helium atom wavefunctions by local-scaling transformations. The functional $\mathcal{E}[\rho, \Psi_g]$ is defined in Eq. (1). Energies in hartrees

Ψ_g	$\mathcal{E}[\rho_g, \Psi_g]$	$\mathcal{E}[\rho_{HF}, \Psi_g]$	$\mathcal{E}[\rho_{exact}, \Psi_g]$
Ψ_g^I	-2.9022		-2.9025
Ψ_g^{II}	-2.9025		-2.9030
Ψ_g^{III}	-2.9000	-2.90189	-2.90182

3.3 Improvement of Correlated Wave Functions for Helium by Means of Local-Scaling Transformations

We consider here the application of local-scaling transformations as a means to improve a correlated generating wavefunction. We take as examples correlated wavefunctions for the helium atom. The basic idea behind this approach is that any wavefunction (correlated or not) whose parameters have been optimized by finding the extremum of the energy functional, is still capable of undergoing improvements when it is subjected to a local-scaling transformation. The reason is that the energy minimum within an orbit (for the concept of “orbit” see Ref. [3]) is attained by searching over acceptable one-particle densities – which are generally different from that of the “orbit-generating” wavefunction $\Psi_g^{[i]}$ (the superscript $[i]$ labels the orbit). Note that the optimal one-particle density within a given orbit need not be the exact one, viz., ρ_{exact} , unless, of course, one is dealing with the “Hohenberg-Kohn” orbit, which by definition yields the exact ground-state energy: $E_o = \mathcal{E}[\rho_{exact}, \Psi_g^{[HK]}]$. This is due to the fact that any wavefunction in this orbit is related to the exact ground-state wavefunction Ψ_o^{exact} by a local-scaling transformation between the densities ρ_g and ρ_{exact} .

Moreover, the global minimum can be reached by “inter-orbit jumping”. This may be accomplished by modifying the generating wavefunction at fixed final density. In the present case, this inter-orbit optimization is carried out by varying the parameters at fixed density.

As is well-known, the difficulty in improving a wavefunction increases by orders of magnitude when one sets on the next higher decimal the accuracy with which the energy is to be determined. In fact, few configurations beyond Hartree-Fock are required to account for most of the correlation energy of the helium atom (configurations $1s^2$, $2s^2$ and $2p^2$ yield already 85% of the correlation energy). However, inclusion of ns^2 configurations up to $n = 12$ just

lead to a 2% improvement on the correlation energy and a similar inclusion up to $10p^2$, to 4% [41]. Thus, in order to describe the finer details of the correlation energy it becomes indispensable to introduce either very large CI (or MCSCF) expansions or highly complicated correlated wavefunctions. It is in this respect, that local-scaling transformations can be quite useful, as they lead to an improvement of 1% to 2% of the correlation energy corresponding to a simple wavefunction just by adjusting the latter so that it associates with a different density (either ρ_{exact} or ρ_{HF}).

The following correlated wavefunctions are considered in the present work:

$$\Psi_g^I(r_1, r_2, r_{12}) = c_1^I \Phi_{1s^2}(r_1, r_2) \chi_{1s^2}^I(r_{12}) + c_2^I \Phi_{1s^2}(r_1, r_2) \chi_{1s2s}^I(r_{12}) \quad (62)$$

$$\Psi_g^{II}(r_1, r_2, r_{12}) = c_1^{II} \Phi_{1s^2}(r_1, r_2) \chi_{1s^2}^{II}(r_{12}) + c_2^{II} \Phi_{1s^2}(r_1, r_2) \chi_{1s2s}^I(r_{12}) \quad (63)$$

$$\Psi_g^{III}(r_1, r_2, r_{12}) = B[\Phi_{1s^2}^{III}(r_1, r_2) + \Phi_{1s^2}^{III}(r_2, r_1)] \chi_{1s2s}^{III}(r_{12}) \quad (64)$$

where the uncorrelated wavefunctions are

$$\Phi_{1s^2}(r_1, r_2) = N_1 e^{-\alpha_1 \cdot r_1} e^{-\alpha_2 \cdot r_2} \quad (65)$$

$$\Phi_{1s2s}(r_1, r_2) = N_2 (e^{-\alpha_1 \cdot r_1} e^{-\alpha_2 \cdot r_2} + e^{-\alpha_1 \cdot r_2} e^{-\alpha_2 \cdot r_1}) \quad (66)$$

$$\Phi_{1s2s}^{III}(r_1, r_2) = e^{-Zr_1} e^{-\beta r_2} (1 + cr_2)^{(Z-1)/\beta-1} \quad (67)$$

and the correlation factors are given by:

$$\chi_{1s^2}^I(r_{12}) = (1 + a_1 r_{12}) \quad (68)$$

$$\chi_{1s2s}^I(r_{12}) = (1 + b_1 r_{12}) \quad (69)$$

$$\chi_{1s^2}^{II}(r_{12}) = (1 + a_1 r_{12} + a_2 (r_1 + r_2)^2 + a_3 (r_1 - r_2)^2) \quad (70)$$

$$\chi_{1s2s}^{III}(r_{12}) = 1 - e^{-\lambda r_{12}} / (1 + 2\lambda) \quad (71)$$

The wavefunction $\Psi_g^{III}(r_1, r_2, r_{12})$ has been recently described [47]. The results are presented in Table 3. As it can be seen, in all cases the energy is improved by a local-scaling transformation. Also, note that as discussed above, a transformation to ρ_{exact} does not necessarily lead to the lowest energy (it does not yield a minimum in an arbitrary orbit).

4. DISCUSSION

In the present review of LS-DFT the constructive nature of this approach leading to the actual formulation of density functionals has been emphasized. We have shown explicit expressions for the kinetic and exchange energy functionals and have compared the former to a number of the usual representations advanced in conventional DFT. We have further analyzed the correlation problem from the point of view of local-scaling transformations and have made some

incipient suggestions as to the form of certain terms appearing in the highly complex correlation energy functional.

We do not wish, however, to leave the reader with the impression that LS-DFT is either the only or the best constructive version of DFT. In the first place, let us remember that LS-DFT is closely related to Levy's "constrained-search" reformulation of DFT [48] which in the words of Cioslowski [19] "... yielded an *implicit construction* for the functional $E[\rho]$." In fact, several attempts have been made [49] in the context the constrained-search formulation for the purpose of attaining an *explicit construction* for $E[\rho]$. In this vein, a vast array of known properties have been determined for the exact functionals [50-55]; these properties, clearly, can be and have been incorporated into the construction of approximate functionals [56]. (In this respect, it is pertinent, however, to remark that the functionals obtained in LS-DFT satisfy by construction the requirements derived from ordinary scaling as the latter is a particular instance of local-scaling.)

In the second place, a quite useful characteristic of LS-DFT is that it renders possible to transform an arbitrary wavefunction, say, the Hartree-Fock single Slater determinant into a locally-scaled one associated with a given one-particle density such as the exact one. Thus, one can easily generate a locally-scaled Hartree-Fock wavefunction that yields the exact ρ . In this sense, one finds much common ground between LS-DFT and those constructive realizations of the constrained-search approach which reformulate the Hartree-Fock method as well as with those developments which pose the optimized potential method as a particular instance of density functional theory [42,43,57-61].

There is still a very important area of contact between LS-DFT and other approaches having to do with the direct evaluation of the Kohn-Sham potentials [6,62-66] from known densities. In this respect, the work of Zhao, Morrison and Parr [66] is of particular interest as it provides an alternative to local-scaling transformations for a fixed-density variation of the kinetic energy functional.

ACKNOWLEDGMENTS

E.V.L. would like to express his gratitude to the Commission of European Communities for its support of this work through contract No. CII*-CT93 - 0333. He also gratefully acknowledges support by Conicit of Venezuela through Project S1-95000702.

REFERENCES

- [1] I.Zh. Petkov, M.V. Stoitsov and E.S. Kryachko, *Int. J. Quantum Chem.* **29**, 149 (1986).
- [2] E.S. Kryachko and E.V. Ludeña, *Energy Density Functional Theory of Many-Electron Systems*, Kluwer Academic Publishers, Dordrecht, 1990.
- [3] E.S. Kryachko and E.V. Ludeña, *Phys. Rev. A* **43**, 2179 (1991).
- [4] E.S. Kryachko, E.V. Ludeña and T. Koga, in: *Methods and Techniques in Computational Chemistry, METECC-94, Vol. B: Medium Size Systems*, E. Clementi (ed.), STEF, Cagliari, 1993, p. 23.
- [5] E.V. Ludeña, E.S. Kryachko, T. Koga, R. López-Boada, J. Hinze, J. Maldonado and E. Valderrama, in: *Theoretical and Computational Chemistry: Density Functional Calculations*. J.M. Seminario and P. Politzer (eds.), Elsevier, Amsterdam, 1995, p. 75.
- [6] E.V. Ludeña, J. Maldonado, R. López-Boada, T. Koga, E.S. Kryachko, *J. Chem. Phys.* **102**, 318 (1995).
- [7] E.V. Ludeña, R. López-Boada, J. Maldonado, E. Valderrama, T. Koga, E.S. Kryachko, J. Hinze, *Int. J. Quantum Chem.* **56**, 285 (1995).
- [8] E.V. Ludeña, R. López-Boada, *Top. Current Chem.* **180**, 169 (1996).
- [9] E.V. Ludeña, R. López-Boada, R. Pino, *Can. J. Chem.* **74**, 1097 (1996).
- [10] R. López-Boada, R. Pino and E.V. Ludeña, *Int. J. Quantum Chem.* **63**, 1025 (1997).
- [11] E.V. Ludeña, R. López-Boada, R. Pino, in: *Recent Developments and Applications of DFT 1*. J.M. Seminario (ed.), Elsevier, Amsterdam, 1996, p. 25.
- [12] E.V. Ludeña, R. López-Boada and R. Pino, in: *Condensed Matter Theories. 11*. E.V. Ludeña, P. Vashishta and R.F. Bishop (eds.), Nova Science Publishers, Commack, N.Y., 1996, p. 51.
- [13] P.C. Hohenberg and W. Kohn, *Phys. Rev. B* **136**, 864 (1964).
- [14] W. Kohn and L.J. Sham, *Phys. Rev. A* **140**, 1133 (1965).
- [15] P.C. Hohenberg, W. Kohn and L.J. Sham, *Adv. Quantum Chem.* **21**, 7 (1990).
- [16] R.G. Parr and W. Yang, *Density Functional Theory of Atoms and Molecules*, Oxford University Press, Oxford, 1989.
- [17] R.M. Dreizler and E.K.U. Gross, *Density Functional Theory*, Springer-Verlag, Berlin, 1990.
- [18] N.H. March, *Electron Density Theory of Atoms and Molecules*, Academic Press, New York, 1992.
- [19] For a finite-basis formulation of LS-DFT see: J. Cioslowski, *Adv. Quantum Chem.* **21**, 303 (1990); E.S. Kryachko and E.V. Ludeña, *J. Chem. Phys.* **95**, 9054 (1991).

- [20] E.S. Kryachko and E.V. Ludeña, in: *Condensed Matter Theories*. 7. J. Aliaga and A. Proto (eds.), Plenum Press, New York, 1992, p 229.
- [21] J.C. Slater, *Quantum Theory of Atomic Structure*, McGraw-Hill, New York, 1960, Vol. I, p. 309.
- [22] L.H. Thomas, Proc. Cambridge Phil. Soc. **23**, 542 (1927).
- [23] E. Fermi, Rend. Accad. Naz. Lincei **6**, 602 (1927).
- [24] P.A.M. Dirac, Proc. Cambridge Phil. Soc. **26**, 376 (1930).
- [25] J.E. Harriman, Phys. Rev. A **24** 680, (1981).
- [26] R. López-Boada, R. Pino and E.V. Ludeña. Hartree-Fock energy density functionals generated by local-scaling transformations: Applications to first-row atoms. J. Chem. Phys. (submitted).
- [27] D.J. Lacks and R.G. Gordon, J. Chem. Phys. **100**, 4446 (1994).
- [28] H. Lee, C. Lee and R.G. Parr, Phys. Rev. A **44**, 768 (1991).
- [29] A.D. Becke, J. Chem. Phys. **84**, 4522 (1986).
- [30] A.D. Becke, Phys. Rev. A **38**, 3098 (1988).
- [31] C.F. von Weizsäcker, Z. Phys. **96**, 431 (1934).
- [32] J.P. Perdew, Phys. Rev. Lett. **55**, 1665 (1985); J.P. Perdew and W. Yue, Phys. Rev. B **33**, 8800 (1986).
- [33] J.P. Perdew, J.A. Cevary, S.H. Vosko, K.A. Jackson, M.R. Pederson, D.J. Singh, and C. Fiolhais, Phys. Rev. B **46**, 6671 (1992).
- [34] A.D. Becke, J. Chem. Phys. **85**, 7184 (1986)
- [35] A. Lembarki and H. Chermette, Phys. Rev. A **50**, 5328 (1994).
- [36] E. Pearson, Ph.D. thesis, Harvard University (1982) (cited in [27]).
- [37] A.E. DePristo and J.D. Kress, Phys. Rev. A **35**, 438 (1987).
- [38] H. Ou-Yang and M. Levy, Int. J. Quantum Chem. **40**, 379 (1991).
- [39] A. Thakkar, Phys. Rev. A **46**, 6920 (1992).
- [40] E. Clementi and C. Roetti, At. Data and Nucl. Data Tables **14**, 177 (1974).
- [41] E. Valderrama, E.V. Ludeña and J. Hinze, J. Chem. Phys. **106**, 9227 (1997).
- [42] Gross, E. K. U., Petersilka, M. and Grabo, T. *Density Functional Methods in Chemistry*, ACS Series, Vol. 629, p. 42 (1996).
- [43] A. Görling and M. Ernzerhof, Phys. Rev. A **51**, 4501 (1995)
- [44] E.R. Davidson, S.A. Hagstrom, S.J. Chakravorty, V.M. Umar and C. Froese-Fischer, Phys. Rev. A **44**, 7071 (1991).
- [45] S.F. Boys and N.C. Handy, Proc. Roy. Soc. A **310**, 43 (1969).
- [46] J.W. Clark, R.L. Mead, E. Krotscheck, K.E. Kürten and M.L. Ristig, Nucl. Phys. A **328**, 45 (1979).
- [47] U. Kleinekathöfer, S.H. Patil, K.T. Tang and J.P. Toennies, Phys. Rev. A **54**, 2840 (1996).
- [48] M. Levy, Proc. Natl. Acad. Sci. USA **79**, 6062 (1979).

- [49] M. Levy, in: *Recent Developments and Applications of DFT 1*. J.M. Seminario (ed.), Elsevier, Amsterdam, 1996, p. 3.
- [50] O. Gunnarsson and B.I. Lundquist, Phys. Rev. B **13**, 4274 (1976).
- [51] M. Levy and J.P. Perdew, Phys. Rev. A **32**, 2010 (1985).
- [52] M. Levy, Phys. Rev. A **43**, 4637 (1991).
- [53] A. Görling and M. Levy, Phys. Rev. A **45**, 1509 (1992).
- [54] M. Levy and J.P. Perdew, Phys. Rev. B **48**, 11638 (1993).
- [55] M. Levy and J.P. Perdew, Int. J. Quantum Chem. **49**, 539 (1993).
- [56] C. Filippi, X. Gonze and C.J. Umrigar, in: *Recent Developments and Applications of DFT 1*. J.M. Seminario (ed.), Elsevier, Amsterdam, 1996, p. 295.
- [57] A. Holas, N.H. March, Y. Takahashi and C. Zhang, Phys. Rev. A **48**, 2708 (1993).
- [58] A. Holas and N.H. March, Top. Current Chem. **180**, 57 (1996).
- [59] A. Görling and M. Ernzerhof, Phys. Rev. **51**, 4501 (1995).
- [60] J.B. Krieger, Y. Li and G.J. Iafrate, Phys. Rev. A **45**, 101 (1992).
- [61] Y. Li, J.B. Krieger, and G.J. Iafrate, Phys. Rev. A **47**, 165 (1993).
- [62] E.V. Ludeña, R. Lopez-Boada and J. Maldonado, Phys. Rev. A **48**, 1937 (1993).
- [63] A. Görling, Phys. Rev. A **46**, 3753 (1992).
- [64] R. van Leeuwen, O.V. Gritsenko and E.J. Baerends, Top. Current Chem. **180**, 107 (1996).
- [65] F. Aryasetiawan and M.J. Stott, Phys. Rev. B **38**, 2974 (1988).
- [66] Q. Zhao, R.C. Morrison and R.G. Parr, Phys. Rev. A **50**, 2138 (1994).

In Search of the Correlation Potential

R.K. Nesbet

IBM Almaden Research Center, 650 Harry Road, San Jose, California

95120-6099

Abstract

Recent developments in density-functional theory (DFT) provide a new way of thinking about the effective correlation potential in atoms and molecules. In reference-state DFT the kinetic energy and exchange functionals take the same form as in Hartree-Fock theory, and the correlation potential is expressed as a nonlocal operator of known form, evaluated for a ground state. An equivalent local correlation potential is determined by the functional derivative of an implicitly defined density functional. An approximation to this local potential is needed for practical applications. While a useful short-range form of this potential is given by the local-density approximation, the long-range form requires a nonlocal theory, since it is asymptotically equal to the dipole polarization potential. It has recently been shown that a local-response model provides systematically good results for the van der Waals interaction, given only the local density as specified by DFT. Application of these ideas to the generalized polarization potential (bound-free correlation potential) is discussed here.

- 1.Introduction
- 2.Reference-state density functional theory
- 3.Local response theory
- 4.The bound-free correlation potential
- 5.Conclusions

I. INTRODUCTION

An electron scattered by an atom or molecule experiences a generalized polarization potential due to bound-free correlation. In general this takes the form of a nonlocal, energy-dependent optical potential [1]. The density-functional theory (DFT) of Hohenberg, Kohn, and Sham [2,3] provides a rationale for replacing this optical potential by a parametrized local potential, defined as the functional derivative of a universal correlation energy functional with respect to the local electronic spin-density. In the local density approximation (LDA), the exchange-correlation functional is a local function of electron spin-density, so that the correlation potential is a function of the local density. The LDA has been very widely used, but it cannot describe the essentially nonlocal correlation of an external electron with a polarizable charge density [4]. Inclusion of density-gradient corrections [5-7] still involves a local expansion and cannot describe polarization by a distant charged particle.

In the recently proposed reference-state DFT (RDFT), the separation between exchange and correlation energy functionals is made explicit. The exchange functional is given by the exchange energy of a single-configuration reference state [8]. An explicit formal expression for the nonlocal correlation potential follows from the relevant many-body theory.

Although screening of the short-range Coulomb singularity is important to the success of the LDA for bound systems, it has recently been recognized that a model of long-range electronic correlation should use a very different aspect of the physics of an electron gas. Especially for interactions between spatially separated density fluctuations, energy relationships are determined by the dynamical property of polarization response. This leads to a local response model of polarization, dependent on local electron density. This theory has been applied with considerable success to compute van der Waals inter-

action coefficients for rare-gas, alkali, and alkali-earth atoms and molecular hydrogen [9]. It has been shown [10] that fundamental principles of charge conservation and reciprocity, when applied to modify an earlier Ansatz for local-density response theory [11], are consistent with the practical formula tested by Andersson et al [9].

The local response model of the van der Waals interaction implies a corresponding model of the polarization potential, hence of the long-range limit of the bound-free correlation potential for an electron outside a polarizable charge distribution [12]. The implications of this observation are discussed in the present paper.

II. REFERENCE-STATE DENSITY FUNCTIONAL THEORY

It is often convenient to define an independent-electron reference state Φ that represents a mean-field approximation to a true correlated eigenfunction Ψ of an N -electron system. For any ground state, the kinetic energy functional of Kohn and Sham [3] can be defined by postulating the existence of a reference state that has the same spin-density as the eigenfunction Ψ . In RDFT, this postulate is replaced by taking Φ to be that model wave function (Slater determinant) whose projection onto Ψ is greatest [13–15]. This construction ensures that first-order variations of Φ are orthogonal to Ψ , and in particular that Φ has no one-electron matrix elements with Ψ [14]. Using the normalization condition $(\Phi|\Psi) = (\Phi|\Phi) = 1$, a second basic theorem [16,17] implies that the unsymmetric energy formula $E = (\Phi|H|\Psi)$ is exact if Ψ is an eigenfunction of H with eigenvalue E . The Brenig theorem implies that $(\Phi|H1|\Psi) = (\Phi|H1|\Phi)$ for any one-electron Hamiltonian operator $H1$. The full N -electron Hamiltonian is $H = T + V + U$, where U is the two-electron Coulomb interaction and T and V are the one-electron kinetic energy and

external potential operators. In the Brueckner-Brenig representation, the unsymmetric energy formula implies that the contributions of these one-electron operators to N -electron energy eigenvalues can be evaluated as mean values in the reference state. Hence the external potential function can be taken to interact with the electronic density of the reference state Φ rather than with that of the corresponding eigenstate Ψ . These two density functions are in general not identical.

The electron density of a correlated wave function is denoted here by $\hat{\rho}$ such that $\Psi \rightarrow \hat{\rho}$ and the reference-state electron density by ρ such that $\Psi \rightarrow \Phi \rightarrow \rho$. The external potential operator V is the sum over all electrons of some physically realizable one-electron potential function v . The ground-state energy is a functional $E[v]$. A ground state eigenfunction whose correlated density is $\hat{\rho}$ defines an expression of the form

$$\hat{F}[\hat{\rho}] = (\Psi|T + U|\Psi)/(\Psi|\Psi). \quad (1)$$

Hohenberg-Kohn theory proves this to be a functional of $\hat{\rho}$, universal in the sense that it does not depend explicitly on v .

RDFT can be derived in close analogy to the constrained-search argument by Levy [18], valid for standard DFT, if the Rayleigh quotient is replaced by the unsymmetric formula $(\Phi|T + U|\Psi)$ and $\hat{\rho}$ is replaced by ρ . Because the unsymmetric formula is not itself a variational expression, but rather a formula for a stationary value, the argument must be modified in some points, which will be indicated below. A universal functional is defined by

$$F[\rho] = (\Phi|T + U|\Psi), \quad (2)$$

where Ψ is a ground-state eigenfunction such that $\Psi \rightarrow \Phi \rightarrow \rho$. To show that this is a functional of ρ , the one-electron potential function v_ρ can be derived as a spin-indexed Lagrange multiplier field from a variational expression

$$F_v[\rho] = \min_{\Psi_t} [(\Phi_t|T + U|\Psi_t) + \int v(\rho_t - \rho)d^3\mathbf{r}], \quad (3)$$

where Ψ_t determines Φ_t and ρ_t . The Lagrange multiplier field $v = v_\rho$ is chosen so that $\rho_v = \rho$ for the minimizing trial function Ψ_v . If the constant integral $\int v\rho d^3\mathbf{r}$ is added to both sides of this equation, the right-hand side is the minimal value of $(\Phi|H_v|\Psi)$ for the potential function v_ρ . If the minimizing trial function is an eigenfunction of H_v , then the left-hand side defines an energy functional

$$E[\rho] = F[\rho] + \int v_\rho \rho d^3\mathbf{r}. \quad (4)$$

The wave function and reference function defined by this minimization condition, Ψ_ρ and by Φ_ρ , respectively, are functionals of ρ . The kinetic energy functional $T[\rho]$ is defined simply by $(\Phi_\rho|T|\Phi_\rho)$. Denoting the Coulomb part of $(\Phi_\rho|U|\Phi_\rho)$ by $U[\rho]$, a universal exchange-correlation energy functional is defined by

$$E_{xc}[\rho] = F[\rho] - T[\rho] - U[\rho] = (\Phi_\rho|U|\Psi_\rho) - U[\rho]. \quad (5)$$

Because $(\Phi|H_v|\Psi)$ is not in itself a variational expression, its unconstrained minimum value is not simply related to an eigenstate of the Hamiltonian H_v defined by v in Eq.(3), whereas Eq.(2) defines $F[\rho]$ only for such eigenstates. Any arbitrary trial function $\Psi \rightarrow \Phi$ can be expressed in the form $\Phi + \Delta c_\Delta$ with $c_\Delta = 1$. If the minimizing trial function in Eq.(3) were not an eigenfunction of H_v , then for some subset of trial functions, using the Brueckner-Brenig condition,

$$(\Phi|H_v|\Psi) = (\Phi|H_v|\Phi) + (\Phi|U|\Delta) \leq E[v]. \quad (6)$$

It should be noted that $(\Phi|H_v|\Phi) \geq E[v]$, and $(\Phi|U|\Delta)$ is a generalized correlation energy. The construction proposed here for any trial function Ψ in

this subset is to diagonalize the 2×2 variational matrix for H_v in the orthogonal basis (Φ, Δ) , replacing Ψ by the function determined by the lowest matrix eigenvalue. The unsymmetric energy expression is valid for such an eigenvalue, which is an upper bound for $E[v]$. This retains the form of Ψ , modifying only the coefficient c_Δ , and retains Φ as reference state. An eigenstate remains unchanged, and the ground state is in the trial set. Hence the minimum in Eq.(3) for the modified set of trial functions corresponds to the ground state of H_v .

Because the restricted set of trial functions includes the complete set of eigenfunctions of the Hamiltonian H_v determined by the given one-electron potential function v , and the unsymmetric energy formula is valid for each such trial function, the minimum value in Eq.(3) is a lower bound for $E[v] - \int v \rho d^3r$. This proves that $E[\rho] \leq E[v]$, and proves equality if the minimizing trial function is an eigenfunction of H_v . The construction given above ensures this condition, but restricts the set of variational trial functions by requiring the scale coefficient c_Δ to be determined as specified above. Eq.(3) implies that $F[\rho]$ is the minimum value of $(\Phi|T+U|\Psi)$ for the constrained-search condition $\Psi \rightarrow \Phi \rightarrow \rho$, following Levy [18], for the restricted trial set.

Eq.(5) provides a simple and natural definition of the correlation energy functional. The Coulomb energy functional of the reference-state density ρ is the non-exchange part of $(\Phi|U|\Phi)$, and the exchange energy functional is the exchange part, both including self-interaction. Thus $E_x[\rho]$, expressed in terms of the occupied orbital functions of the reference state, has the same form as in Hartree-Fock theory. The residual formula $(\Phi|U|\Psi - \Phi)$ defines the correlation energy functional. This has an explicit representation in the orbital basis specified by the reference state Φ using the coefficients c_{ij}^{ab} for virtual two-particle excitations of Φ in the configuration interaction (CI) expansion of the eigenstate Ψ [8,19]. Introducing orbital occupation numbers n_p , this is

$$E_c[\rho] = \sum_{i < j} n_i n_j \sum_{a < b} (1 - n_a)(1 - n_b)(ij|\bar{u}|ab)c_{ij}^{ab}, \quad (7)$$

where \bar{u} indicates an antisymmetrized Coulomb-exchange matrix element. For a ground state all quantities here are functionals of the reference-state density.

The local ground-state correlation potential is defined in RDFT as the functional derivative of Eq.(7) with respect to ρ . When infinitesimal variation of occupation numbers is allowed, a more practical definition follows from the fact that the unsymmetrical energy formula used to construct Eq.(7) is itself a Landau functional of the occupation numbers [19]. Correlation energies of Landau quasiparticles, expressed as diagonal elements of a one-electron Hamiltonian matrix, are defined by differentiating with respect to occupation numbers to give

$$(i|v_c|i) = (i|\frac{\delta E_c[\rho]}{\delta \rho}|i) = \frac{\partial E_c}{\partial n_i}. \quad (8)$$

For occupied orbital ϕ_i , the correlation potential derived from Eq.(7) has diagonal matrix elements

$$\begin{aligned} (i|v_c|i) = & \sum_j n_j \sum_{a < b} (1 - n_a)(1 - n_b)(ij|\bar{u}|ab)c_{ij}^{ab} \\ & - \sum_{k < j} n_k n_j \sum_b (1 - n_b)(kj|\bar{u}|ib)c_{kj}^{ib}. \end{aligned} \quad (9)$$

III. LOCAL RESPONSE MODEL

In the local response model each electron density volume element is separately characterized by a two-parameter formula giving electric dipole oscillator strength as a function of frequency [12]. One of the two parameters is fixed by the oscillator strength sum rule, while the other is an effective mean excitation energy, taken to be the plasma energy $\hbar\omega_p$ by Andersson et al [9]. This model requires introduction of a low-density cutoff of the dipole response, because a

plasma resonance is not well-defined when a momentum-transfer scale parameter exceeds the value at which a collective plasma excitation of the electron gas (jellium model) disappears into the particle-hole excitation continuum [20].

The basic postulate of the model is that the frequency-dependent polarizability of each electron density volume element is given by

$$\alpha(z) \simeq \frac{e^2}{m} \frac{f_1}{\omega_p^2 - z^2} = \frac{e^2}{m} \frac{n(\mathbf{r})d^3\mathbf{r}}{(4\pi e^2/m)n(\mathbf{r}) - z^2}, \quad (10)$$

where $f_1 = n(\mathbf{r})d^3\mathbf{r}$, $\omega_p^2 = 4\pi ne^2/m$, and z is a complex-valued frequency. In the limit of static polarizability, $z = 0$, this formula reduces to a universal constant polarizability $1/4\pi$ per unit volume, because the local density $n(\mathbf{r})$ cancels between numerator and denominator. This seemingly bizarre result would imply infinite integrated polarizability for any atom or molecule if it were not for the low-density cutoff. The implied static polarizability still depends only on the volume of the polarizable charge distribution, implying that the cutoff radius of a spherical atom can be parametrized by the observed static polarizability. This has been shown [12] to give radii comparable the those deduced by Andersson et al [9] from the Langreth-Mehl criterion [20]. The van der Waals interaction between two separated polarizable charge distributions is characterized by the coefficient

$$C_6(A, B) = \frac{3}{\pi} \int_0^\infty \alpha_A(iu)\alpha_B(iu)du, \quad (11)$$

defined by an integral over imaginary frequency [21]. Combined with Eq.(10), this gives an integrated formula that was evaluated by Andersson et al [9] for rare-gas, alkali, and alkali-earth atoms and for molecular hydrogen, obtaining results in good agreement with existing experimental and theoretical data.

When combined with the classical Clausius-Mossotti theory of a dielectric medium, this version of the local response model gives the correct asymptotic form of the polarization potential of a spherical atom, $-\alpha(0)/2r^4$, where

$\alpha(0)$ is the static electric dipole polarizability [12]. This can be shown most clearly in a classical electrostatic model, in which spatial variation of the electric field is computed explicitly. This model, however, indicates a possible inconsistency in the assumption that the effective mean excitation energy of a volume element of electron density is given by the plasma excitation energy. The plasma model (jellium) assumes that a local charge displacement induces a restoring electric field given by $\delta\mathcal{E} = -4\pi\delta\mathbf{P}$. This differs from the dielectric response model used to derive the Clausius-Mossotti formula [22], which assumes $\delta\mathcal{E} = -(4\pi/3)\delta\mathbf{P}$. If the first formula here is used consistently, which requires modifying the Clausius-Mossotti formula, it does not give the correct asymptotic form of the polarization potential [12]. Alternatively, the correct asymptotic form is obtained by consistent use of the second formula, retaining Clausius-Mossotti but replacing the plasma frequency ω_p by a dielectric response frequency defined by

$$\omega_d^2 = \frac{4\pi ne^2}{3m}. \quad (12)$$

Thus ω_d is reduced from the classical plasma frequency by a factor $3^{-1/2}$. This has the effect of reducing the cutoff radius (response radius) by a factor $3^{-1/3}$ for a spherical atom. It has been shown that this resolves another difficulty with the plasma-response model, which implies response radii greater than the classical turning radius of the most weakly bound electron in an atom. The dielectric-response radius is in general less than the classical turning radius [12].

IV. THE BOUND-FREE CORRELATION POTENTIAL

DFT implies the existence of a local correlation potential valid for any ground state, and by extension valid as an approximation for small perturba-

tions of a ground state. Since a scattered electron makes only an infinitesimal change of the target density, in RDFT the bound-free correlation potential for ground-state scattering can be identified with the potential v_c in Eq.(8). The local-response model produces a correlation potential that is an explicit functional of the electron density, and has been shown to have the correct asymptotic form, given by the classical dipole polarization potential, for a suitable definition of the excitation-energy parameter. However, this is strictly valid only as an asymptotic form. The classical electrostatic model of a point charge outside a polarizable charge distribution has a singularity as the particle approaches the response boundary [12]. Such a singularity is symptomatic of a well-known property of models of the polarization-response optical potential [23,24]. The leading asymptotic terms in an equivalent local potential are known [25,26] as a series of inverse powers of r . The purely attractive asymptotic potential $-\alpha/2r^4$ is dominated at smaller distances by repulsive terms, whose leading asymptotic term has the form $3\beta/r^6$ [26]. These terms remove the attractive singularity, but the inverse-power expansion is not appropriate to smaller distances and there is no generally accepted closed form for the short-range potential.

V. CONCLUSIONS

The short-range form of the correlation potential has been considered in DFT primarily in terms of density-gradient corrections to the LDA [6,7]. The correlation energy functional given by Eq.(7) here is not expressed explicitly as a functional of the electronic density, but is a formally exact expression which could be used to calibrate proposed functionals in particular cases where an accurate CI expansion of a correlated ground-state wave function is known. When occupied orbital functions are expressed in a localized representation,

Eq.(7) is a sum of electron-pair correlation energies with characteristic properties [16,17]. The pair correlation energy of two electrons in an atomic shell, localized bond, or lone pair is approximated by a nearly constant correction to the corresponding Hartree-Fock energy, while distant pairs interact primarily through virtual excitations, giving the asymptotic van der Waals potential. In a systematic theory, short-range correlation must be augmented by terms treated as in the local response model in order to describe such effects as non-bonded interactions in large molecules.

ACKNOWLEDGMENTS

The author is indebted to M. A. Morrison for helpful comments.

REFERENCES

- [1] R. K. Nesbet, *Variational Methods in Electron-Atom Scattering Theory*, (Plenum, New York, 1980).
- [2] P. Hohenberg and W. Kohn, Phys. Rev. **136**, B864 (1964).
- [3] W. Kohn and L. J. Sham, Phys. Rev. **140**, A1133 (1965).
- [4] R. O. Jones and O. Gunnarsson, Rev. Mod. Phys. **61**, 689 (1989).
- [5] A. D. Becke, Phys. Rev. A **38** 3098 (1988).
- [6] C. Lee, W. Yang and R. G. Parr, Phys. Rev. B **37** 785 (1988).
- [7] J. P. Perdew, J. A. Chevary, S. H. Vosko, K. A. Jackson, M. R. Pederson, D. J. Singh and C. Fiolhais, Phys. Rev. B **46** 6671 (1992).
- [8] R. K. Nesbet, J. Phys. B **29**, L173 (1996).
- [9] Y. Andersson, D. C. Langreth and B. I. Lundqvist, Phys. Rev. Lett. **76**, 102 (1996).
- [10] J. F. Dobson and B. P. Dinte, Phys. Rev. Lett. **76**, 1780 (1996).
- [11] K. Rapcewicz and N. W. Ashcroft, Phys. Rev. B **44**, 4032 (1991).
- [12] R. K. Nesbet, Phys. Rev. A (1997), in the press.
- [13] K. A. Brueckner and W. Wada, Phys. Rev. **103** 1008 (1956).
- [14] W. Brenig, Nucl. Phys. **4**, (1957).
- [15] R. K. Nesbet, Phys. Rev. **109** 1632 (1958).
- [16] R. K. Nesbet, Adv. Chem. Phys. **9** 321 (1965).
- [17] R. K. Nesbet, Adv. Chem. Phys. **14** 1 (1969).

- [18] M. Levy, Proc. Natl. Acad. Sci. **76** 6062 (1979); Bull. APS **24** 626 (1979).
- [19] R. K. Nesbet, Phys. Rev. B **34** 1526 (1986).
- [20] D. C. Langreth and M. J. Mehl, Phys. Rev. Lett. **47**, 446 (1981).
- [21] C. Mavroyannis and M. J. Stephen, Mol. Phys. **5**, 629 (1962).
- [22] J. D. Jackson, *Classical Electrodynamics*, 2nd edition, (Wiley, New York, 1975). Chapter 4, pp136-167.
- [23] T. L. Gibson and M. A. Morrison, Phys. Rev. A **29**, 2497 (1984).
- [24] M. A. Morrison, B. C. Saha and T. L. Gibson, Phys. Rev. A **36**, 3682 (1987).
- [25] M. Born and W. Heisenberg, Z. Phys. **23**, 388 (1924).
- [26] G. Peach, in *Atoms in Astrophysics*, edited by P. G. Burke, W. B. Eissner, D. G. Hummer and I. C. Percival (Plenum, New York, 1983), pp.115-171.

The n-particle Picture and the Calculation of the Electronic Structure of Atoms, Molecules, and Solids

A. Gonis*, T. C. Schulthess[†], P. E. A. Turchi[‡], and J. van Ek[§]

1 Introduction

There are several problems in the physics of quantum systems whose importance is attested to by the time and effort that have been expended in search of their solutions. A class of such problems involves the treatment of interparticle correlations with the electron gas in an atom, a molecule (cluster) or a solid having attracted significant attention by quantum chemists and solid-state physicists. This has led to the development of a large number of theoretical frameworks with associated computational procedures for the study of this problem. Among others, one can mention the local-density approximation (LDA) to density functional theory (DFT) [1, 2, 3, 4, 5], the various forms of the Hartree-Fock (HF) approximation[1, 2, 6, 7], the so-called GW approximation[8, 9, 10], and methods based on the direct study of two-particle quantities[11, 12, 13], such as two-particle reduced density matrices[14, 15, 16, 17, 18], and the closely related theory of geminals[17, 18, 19, 20], and configuration interactions (CI's)[21]. These methods, and many of their generalizations and improvements[22, 23, 24] have been discussed in a number of review articles and textbooks[2, 3, 25, 26].

The great formal variety that characterizes these methods provides evidence of the complexity of the problem at hand. This diversity has evolved

*Department of Chemistry and Materials Science, L-268, Lawrence Livermore National Laboratory, Livermore, California, 94550, USA

[†]2. Metals and Ceramics Division, Oak Ridge National Laboratory, Oak Ridge, TN 37831, USA

[‡]Department of Chemistry and Materials Science, L-268, Lawrence Livermore National Laboratory, Livermore, California, 94550, USA

[§]Department of Physics, Tulane University, New Orleans, LA 70118, USA

out of attempts to treat specific features of this complex problem, ranging from the electron gas in “small systems”, e.g., atoms and molecules, and atomic clusters, where HF-based methods and CI’s, for example, have been found very useful, or electrons in solids where the LDA has met with considerable success in determining ground-state densities and energies. Even a cursory review of the advantages and limitations of the various methods that have been proposed to study the inhomogeneous electron gas is far beyond the scope of the present work. Suffice it to say that each of these methods have come to be accepted as the most appropriate for a particular aspect of this very complex problem, while having only limited and even questionable applicability in other domains.

However, in spite of much progress along different directions and in different areas, there exists no unified conceptual framework[26] capable of providing systematic improvements to the study of correlations across a broad spectrum of materials types, while possessing well-defined convergence characteristics. Furthermore, the disparity between so-called single-particle methods, such as the LDA, and many-body techniques, e.g, Green-function theory, has led to the perception that these two approaches are irreparably divorced and disjoined from one another in a formal sense.

This perception, however, may be premature. It appears that it is possible to adopt a point of view which provides for a unified approach to the problem of correlations for systems of any size or structure. This viewpoint is the natural outgrowth of work initiated as far back as the 1930’s and which has continued in certain areas to the present.

Initially, Pauling used the concept of a single state (bond state) to describe the behavior of two electrons participating in molecular binding[27]. In the late 1950’s and early 1960’s, Brueckner[11] and collaborators, and Kadanoff and Baym[12, 28] showed, respectively, how the two-particle t -matrix and the two-particle Green function could be used in the study of interacting quantum systems in a straightforward generalization of the methods based on the corresponding single-particle quantities. However, the most telling developments have accrued from a particular approach initiated in the field of atomic and molecular physics. In this methodology, it has proved profitable to study the electronic structure and related properties of atoms by considering *all* the N electrons in the system as forming a single particle in a space of $3N$ dimensions. There is a large body of work on this approach, from which a single representative reference is given here[29].

In this method, the problem of N particles in 3-dimensional space is mapped onto a problem of a single-particle in a hyperspace of $3N$ dimensions, moving under the influence of an external potential. This potential is made up of the external potentials acting on the particles, as well as their

mutual interactions. This reduction to a single-particle in an external field has the formal nicety of allowing the use of single-particle methods in the solution of a many-particle problem. Not to downplay the significance of the computational ramifications of this formalism, we note that applying single-particle methods to hyperspace, e.g., partial-wave analysis of scattering, can be an extremely difficult task. In fact, it becomes quickly intractable when the number of particles increases beyond even some fairly small number, say $N = 4$. This feature has limited the application of this method to fairly small systems such as the He atom and the molecule H_2^+ , (where the two particles combined into one in a space of six dimensions are the nuclei). Applications to extended systems characterized by a large number of centers of force seems to be hopelessly out of reach. (However, for some innovative approaches to atoms with infinite charge and the interpretation of the results, the reader is referred to the literature[29].)

The works referred to above indicate the usefulness of viewing an N -particle system from a higher-dimensional perspective. In doing so, one should attempt to strike a balance between conceptual clarity and computational efficiency, which mitigates against considering calculations in $3n$ -dimensional space except for rather small values of n . It appears that such a procedure may be profitably employed if a system of N particles were to be considered as consisting of a collection of units or sets, $\{I_k\}$, each containing n_k particles, so that

$$\sum_k n_k = N. \quad (1)$$

The resulting problem associated with these sets of particles that interact with one another is obviously formally identical to the original one (only the meaning of the term particle having been redefined in the present case). However, it possesses the formal advantage of allowing, in principle, the systematic approach to an exact solution by treating the entire system as a single unit (N -particle picture). The operative words here are “in principle”, as practical applications do not seem to be possible but for the smallest number of particles in a unit, say $n = 2$ or $n = 3$. However, in such an implementation, the interparticle correlation is treated directly and explicitly within a unit, resulting in a more accurate treatment of the system the larger the number of particle in a unit. Furthermore, this methodology can be applied to a broad spectrum of systems, such as atoms, molecules, and solids, with fairly strong expectations that it will yield improved results compared to its corresponding use within strictly single-particle methods. For example, one can determine the ground-state two-particle, correlated density and energy in terms of two-particle states by using a generalization of DFT and LDA to the appropriate hyperspace, as was presented in an earlier publications

[30] and will be highlighted below. Similarly, alloy phase stability and transport properties (which can be expressed directly in terms of the two-particle Green function) can also be studied, as can the ground state properties of small clusters, molecules, and atoms, within appropriate generalizations of the HF method. Finally, this method may provide a more realistic description of the electronic structure of a system than can be achieved within a single-particle framework. Even if its computational implementation is only possible for small values of particles in a unit, the method to be developed below has one very important conceptual characteristic: it tends to obscure the sharp boundaries that divide single-particle (band-theory) methods from many-body approaches, leading to a broader viewpoint and providing a possibly deeper insight into the effects of correlations than has been hitherto possible.

2 Basic Notions

We begin with the Hamiltonian for a system of N interacting particles,

$$\begin{aligned} H &= \sum_i -\nabla_i^2 + \sum_i v_i + \frac{1}{2} \sum_{i \neq j} v_{ij} \\ &= \sum_i h_i + \frac{1}{2} \sum_{i \neq j} v_{ij}. \end{aligned} \quad (2)$$

Here, ∇_i^2 is the kinetic energy operator for particle i , (with $\hbar = 1$, $2m_i = 1$, for all i), v_i represents the interaction of particle i with an external potential, such as that associated with nuclei in the system, and v_{ij} represents the mutual interaction between particles i and j . The definition of the single-particle Hamiltonian, h_i , is evident. We are interested in the solutions of the many-particle time-independent Schrödinger equation,

$$H\Psi = E\Psi, \quad (3)$$

where Ψ is the many-particle wave function for the system.

At least two different possible viewpoints present themselves immediately as alternative procedures for solving Eq.(3). One may consider the entire interacting system as a single particle in a configuration space of $3N$ dimensions, or one may consider the system wave function as consisting of certain combinations of wave functions of individual particles. In either case, of course, one is obligated to incorporate into the solution the statistics, either Fermi or Bose, governing the behavior of the system.

The first viewpoint defines the N -particle picture and leads in principle to an exact solution of Eq.(3). Leaving aside the question of whether or not one could extract useful information from the complicated form that such an exact solution for large values of N would be bound to take, the computational hindrance associated with this approach as N increases has mitigated against widespread use of such a direct procedure. At the same time, where it has been implemented[29], such as in connection with the He atom, this approach has yielded results which agree to great precision with those of exact numerical procedures.

The second viewpoint defines what will be referred to as the single-particle picture, in which one attempts the construction of the many-body solution of Eq.(3) through the use of solutions associated with individual particles. It should be emphasized that in the language used here, the single-particle picture is not synonymous to what has come to be known as single-particle theory, in which the properties of the entire system are studied through judiciously chosen single-particle solutions of an effective Schrödinger equation. In the present terminology, the methods of single-particle theory, as well as canonical many-body theory are developed within the single-particle picture as defined above. Not to belabor the possibly obvious point, we should note that the N -particle picture mentioned above lends itself to computational procedures which are themselves generalizations of methods developed within single-particle theories. In any case, because of relative ease of implementation, the study of interacting quantum systems has proceeded almost exclusively within the single-particle picture.

Unlike the N -particle picture, which in principle leads naturally to the exact solution of the many-particle Schrödinger equation, the single-particle picture has led to the development of a number of different approximation schemes designed to address particular issues in the physics of interacting quantum systems. A particularly pointed example of this state of affairs is the strict dichotomy that has set in between so-called single-particle theories and canonical many-body theory[31, 32]. Each of the two methodologies can claim a number of successful applications, which tends to reinforce the perceived formal gap between them.

Under these conditions, one is moved to ask if indeed this gap is real or perhaps could be bridged in a way that may reveal the unified features of the problem and possibly lead to a deeper understanding of the behavior of interacting quantum systems. The work described here is an attempt to bridge this gap in a computationally viable way. It is based on a point of view bounded by the single-particle picture at one end and the N -particle picture at the other. In this point of view an interacting quantum system of N particles is taken to consist of non-overlapping units or sets of particles,

$I_k = \{\mathbf{r}_1^{I_k}, \mathbf{r}_2^{I_k}, \dots, \mathbf{r}_k^{I_k}\}$, so that a particle belongs to only one such unit, and the particles in all these sets equal N , the total number of particles in the system. Denoting the number of particles in a set I_i by n_i , leads to Eq.(1). At this point, there is no restriction as to the number of sets chosen or the numbers of particles in each set. This seems to raise the danger of possibly mishandling the statistics of the system by treating some particles in a preferential way. It will be shown below that, even though this is a “real” danger, it can be avoided.

With these considerations in mind, we return to the Hamiltonian of Eq.(2). If we denote the Hamiltonian describing the particles in a unit or subsystem I_k by H_{I_k} ,

$$H_{I_k} = \sum_{i \in I_k} \nabla_i^2 + \sum_{i \in I_k} v_i + \sum_{i \in I_k, j \in I_k} v_{ij}, \quad (4)$$

we can write the Hamiltonian of the original system in the form,

$$H = \sum_k H_{I_k} + \frac{1}{2} \sum_{k \neq l} v_{I_k, I_l}, \quad (5)$$

where

$$v_{I_k, I_l} = \frac{1}{2} \sum_{i \in I_k, j \in I_l} v_{ij}, \quad I_k \neq I_l, \quad (6)$$

where $i \in I$ indicates that i belongs to the set I and the last expression defines the mutual interaction of particles across two different units.

Now, the Hamiltonian in the form of Eq.(5) looks formally identical to that in Eq.(2), with the sets of particles I_k in the new description playing the role of individual particles in the original (single-particle) picture. We will refer to this point of view as the n -particle picture. It is seen that the traditional single-particle picture corresponds to $n = 1$, while the N -particle picture is obtained when $n = N$, the total number of particles in the system. Therefore, if we treat the Hamiltonian of Eq.(5) as consisting of individual “particles” in appropriately defined higher-dimensional spaces, we go a long way toward obtaining the unifying viewpoint alluded to above. In fact, however the Hamiltonian of Eq.(5) may be treated, and two different ways are presented below, one is assured of an exact limit as the number of units or subsystems approaches one and, correspondingly, $n \rightarrow N$.

There are, however, some very important issues still to be addressed before specific techniques are introduced for solving the Schrödinger equation in connection with the form of the Hamiltonian of Eq.(5). These have to do with retaining the proper symmetry in the wave function for the system as a

whole when written in terms of wave functions of the higher-dimensional particles on which the n -particle picture is based. In the following, we shall use the generic term “particle” to refer either to an ordinary particle in three dimensions, or to single point in a space of $3n$ dimensions, $\mathbf{x}_n = (\mathbf{r}_1, \mathbf{r}_2, \dots, \mathbf{r}_n)$, describing n ordinary particles. It is hoped that the context of the discussion will provide sufficient indication as to what is meant to avoid confusion.

Let us first consider the case of distinguishable particles and take the wave function of the system, $\Psi(\mathbf{r}_1, \mathbf{r}_2, \dots, \mathbf{r}_N)$, to be a product of single-particle states. Denoting these states by $\Phi_{I_k}(\{\mathbf{r}\}_{I_k})$, where $\{\mathbf{r}\}_{I_k}$ denotes the set of coordinates of the ordinary particles assigned to I_k , we have

$$\begin{aligned}\Psi &= \Pi_k \Phi_{\alpha_k}(\{\mathbf{r}\}_{I_k}) \\ &= \Pi_k \Phi_{\alpha_k}(\mathbf{x}_{I_k}),\end{aligned}\quad (7)$$

where α_k is a state of the particle I_k . These states can be chosen to be both orthonormal and complete in the usual sense. These states can be found by the usual procedure of minimizing the quantity,

$$I = \langle \Psi | H | \Psi \rangle - \sum_k \epsilon_{\alpha_k} \int d^{3n} x_{I_k} |\Phi_{\alpha_k}(\mathbf{x}_{I_k})|^2, \quad (8)$$

with respect to $\Phi_{\alpha_k}^*(\mathbf{x}_{I_k})$, where an asterisk denotes a complex conjugate. This leads to an eigenvalue equation determining the levels ϵ_{α_k} ,

$$[H_{I_k} + v^{\text{eff}}] \Phi_{\alpha_k} = \epsilon_{\alpha_k} \Phi_{\alpha_k}, \quad (9)$$

where v^{eff} denotes the interaction of the particles in I_k with an external field, (e.g., the nuclei in the system), as well as their interactions with the particles in other units, $I_l \neq I_k$. This term takes the form of a Hartree-like expression involving the density of the particle I_k , and reduces to the conventional Hartree expression in the canonical single-particle description.

We now consider the case of indistinguishable particles, treating explicitly a system of Fermions. It is convenient to write the wave function for a system of *free* Fermions in the form,

$$\Psi_{i_1 i_2 \dots i_N}^0(\mathbf{r}_1, \mathbf{r}_2, \dots, \mathbf{r}_N) = \begin{bmatrix} i_1 & i_2 & \dots & i_N \\ \mathbf{r}_1 & \mathbf{r}_2 & \dots & \mathbf{r}_N \end{bmatrix}, \quad (10)$$

In this notation, we designate a single-particle state by the symbol $\phi_i(\mathbf{r}) = \begin{bmatrix} i \\ \mathbf{r} \end{bmatrix}$. This notation is meant to emphasize the fact that a fully antisymmetrized wave function for non-interacting particles may be obtained

by distributing individual particles over all possible states written in some order or, alternatively, by distributing all possible states over *particles* which have been labeled in a permanent way. Thus, a fully antisymmetrized wave function is obtained from the last expression as a sum of terms resulting from keeping the particle labels in the order given in the lower row, and performing all possible permutations on the state indices in the top row. From now on, we take this expression to denote this fully antisymmetrized wave function.

Let us now partition the particles in the system according to some scheme which assigns n_i particles to distinct sets I_i in accordance with Eq.(1). As this partitioning depends only on the number of particles in each unit, it can be effected by dividing the lower row in the expression for the wave function, Eq.(10), into sets of n_i particles beginning from the left. Thus, particles 1, 2, ..., n_1 are taken to form the first set, particles $n_1 + 1$, $n_1 + 2$, ..., $n_1 + n_2$, to form the second set, and so on. Each set is marked off by means of vertical lines as given in the following expression written explicitly for the case of pairs, (assuming that the total number of particles is divisible by two),

$$\begin{aligned} & \left[\begin{array}{cc|cc|ccc} i_1 i_2 & i_3 i_4 & \cdots & i_{N-1} i_N \\ \mathbf{r}_1 \mathbf{r}_2 & \mathbf{r}_3 \mathbf{r}_4 & \cdots & \mathbf{r}_{N-1} \mathbf{r}_N \end{array} \right] = \hat{A} \left[\begin{array}{cc} i_1 & i_2 \\ \mathbf{r}_1 & \mathbf{r}_2 \end{array} \right] \\ & \times \left[\begin{array}{cc} i_3 & i_4 \\ \mathbf{r}_3 & \mathbf{r}_4 \end{array} \right] \cdots \left[\begin{array}{cc} i_{N-1} & i_N \\ \mathbf{r}_{N-1} & \mathbf{r}_N \end{array} \right], \end{aligned} \quad (11)$$

where the antisymmetrizing operator, \hat{A} , acts on the state indices, and the vertical lines indicate the partitioning of the system into pairs of particles and their corresponding pair states. In this expression, we can use the combined notation \mathbf{x}_k to denote the particles in I_k as a single point in a space of $3n_k$ dimensions. In the present case, we have $\mathbf{x}_1 = (\mathbf{r}_1, \mathbf{r}_2)$, $\mathbf{x}_2 = (\mathbf{r}_3, \mathbf{r}_4)$, and so on. It is, therefore, seen that because of the equivalence of distributing states over particles to distributing particles over states, the wave function of a system of free Fermions is not affected by a partitioning into sets of specific particles.

To proceed with formal developments, we now associate with each particle I_k in hyperspace a coordinate \mathbf{x}_k , and a state α_k , which in the form employed here is such as to correspond to all possible independent combinations of the free particle states into the units I_k . *As long as the particles remain free*, a fully antisymmetrized wave function can be obtained by antisymmetrizing with respect to *particle* indices a product of the type given in Eq.(7).

It is tempting to think that this procedure can be used when the states α_k are obtained directly through the solution of an appropriate Schrödinger equation in $3n_k$ -dimensional space. This, however, is not the case. As a spe-

cific example, let us consider the Be atom whose ground state configuration is $1s^2 2s^2$. The states involved are (in a hopefully obvious notation), $\chi_1 = 1s \uparrow$, $\chi_2 = 1s \downarrow$, $\chi_3 = 2s \uparrow$, and $\chi_4 = 2s \downarrow$. Using these wave functions, an approximate wave function for the system in the form of a Slater determinant can be obtained by antisymmetrizing the product $\chi_1(1)\chi_2(2)\chi_3(3)\chi_4(4)$ *either* with respect to state or particle indices. However, suppose that we are given states of pairs of particles, (each fully antisymmetrized and consistent with the Pauli principle), and choose the two of the lowest energies to construct the ground-state wave function of the system. In this case these would be determinantal wave functions denoted by $(\chi_1(1)\chi_2(2))$ and $(\chi_3(3)\chi_4(4))$, since the state of immediately higher energy than the ground state of two particles is obtained by exciting *one* of them to the next level. Now, forming the product of these two states and antisymmetrizing with respect to particle indices *does not* cause the final wave function to vanish for violating the exclusion principle, and thus this incorrect state is not excluded from the final wave function as it should be. This feature is obviously retained when the pair states are obtained directly, rather than as products of single-particle states. Because of it, the ordinary theory of geminals, depending on the determination of two-particle states, does not allow the construction of a properly antisymmetrized wave function that is consistent with the Pauli exclusion principle. Hence, the well-known absence of an *aufbau prinzip* (building-up principle) in terms of *independently* determined n -particle states. Of course, antisymmetrization with respect to single-particle-state indices would take care of the problem, and eliminate inappropriate wave functions, but this procedure is not viable when n -particle states are determined directly and independently of one another.

One of the applications of the n -particle picture made below involves the generalization of the Hatree-Fock approximation to n -particle states. If one attempted to determine n -particle states directly from the equations, coupled with an antisymmetrization procedure with respect to particle indices, one would encounter precisely the same difficulty as noted above. Instead, the problem must be approached from a different perspective.

In this approach, we consider the evolution of a system of particles described by means of the generalized HF equations as the interparticle interaction is turned on, starting from a single Slater determinant. The determinantal state corresponding to the zero-interaction limit provides an "initial condition" for solving the generalized HF equations within the n -particle picture. The states which evolve out of this procedure are known to satisfy the Pauli principle in the zero-interaction limit, and the generalized HF procedure to be described below maintains the correct symmetry as well as the requirements of the exclusion principle.

We also discuss the generalization of density-functional theory to n -partical states, n DFT, and the possible extension of the local density approximation, n LDA. We will see there that the difficulty of describing the state of a system properly in terms of n -particle states presents no formal difficulties since DFT is directed only at the determination of the particle density rather than individual-particle wave functions. The extent to which practical applications of n DFT within a generalized Kohn-Sham scheme will provide a viable procedure is commented upon below.

3 Generalization of the Hartree-Fock Approximation

The equations of the HF approximation are derived by taking expectation values of the Hamiltonian with respect to a determinantal wave function written in terms single-particle states, incorporating the orthonormality condition by means of a Lagrange multiplier, and minimizing the expression $\left\{ \langle \Psi | H | \Psi \rangle - \sum_i \epsilon_i \int d^3r \begin{bmatrix} i \\ \mathbf{r} \end{bmatrix}^* \begin{bmatrix} i \\ \mathbf{r} \end{bmatrix} \right\}$ with respect to $\begin{bmatrix} i \\ \mathbf{r} \end{bmatrix}^*$. In the coordinate representation, this yields the "eigenvalue" equation

$$\begin{aligned} & \left[-\nabla^2 + v(\mathbf{r}) + \sum_{j \neq i}^{N/2} \int d^3r' \frac{|\phi_j(\mathbf{r}')|^2}{|\mathbf{r} - \mathbf{r}'|} \right] \phi_i(\mathbf{r}) \\ & - \sum_{j \neq i}^N \int d^3r' \frac{\phi_j^*(\mathbf{r}') \phi_i(\mathbf{r}')}{|\mathbf{r} - \mathbf{r}'|} \phi_j(\mathbf{r}) = \epsilon_i \phi_i^*(\mathbf{r}). \end{aligned} \quad (12)$$

We note the presence of the direct or Hartree term and the exchange term, third term inside the brackets and first term outside, respectively. The term $i = j$ can be included in the direct term since it is canceled by the corresponding inclusion into the exchange term. Therefore, we have the well-known result that the HF approximation does not include self-interaction terms.

We now extend the formalism just summarized to two-particle states. We begin by writing the wave function of the system of N particles as the sum of products of two-particle states each of which possesses the proper symmetry under exchange of ordinary particles, and with the total wave function being fully symmetrized or antisymmetrized with respect to exchange of individual particles. Denoting such a two-particle state by the symbol $\begin{bmatrix} i & j \\ \mathbf{r}_1 & \mathbf{r}_2 \end{bmatrix}$ we have for the full wave function the expression given in Eq.(11).

We now envision these pair states to evolve out of free and non-interacting plane-wave states as the interaction with the nuclei and between the particles

are introduced. This is a natural way of viewing the evolution of a set of initially free particles under the action of an external field (e.g. nuclear attraction) and their mutual interaction. Under the action of the external field the particles form a bound system, described approximately through the solutions of the HF equations. The n -particle picture allows an approximate description of the way in which the interaction among the particles now modifies these HF states. Clearly, this description becomes exact as $n \rightarrow N$. At the same time, the solutions for the n -particle states should yield a lowering of the total energy of the system compared to the HF method because of the more accurate treatment in the former of correlation effects that would tend to keep the particles apart thus lowering their potential energy.

In the procedure just outlined, the final wave function retains the proper symmetry under exchange of state indices or particle exchange. This wave function, described in more detail below, corresponds to a particular partition of the particles into pairs, and each of the pairs is associated with every possible two- particle state that can be formed by and evolves out of an original set of single-particle free and non-interacting states. Denoting by a zero subscript two-particle states in free space, we have the following orthonormality

$$\begin{aligned} & \int d^3r_1 d^3r_2 \begin{bmatrix} i & j \\ \mathbf{r}_1 & \mathbf{r}_2 \end{bmatrix}_0^* \begin{bmatrix} k & l \\ \mathbf{r}_1 & \mathbf{r}_2 \end{bmatrix}_0 \\ &= \int d^3r_1 d^3r_2 \begin{bmatrix} i & j \\ \mathbf{r}_1 & \mathbf{r}_2 \end{bmatrix}_0^* \begin{bmatrix} k & l \\ \mathbf{r}_1 & \mathbf{r}_2 \end{bmatrix}_0 = \delta_{ik} \delta_{jl} \end{aligned} \quad (13)$$

and completeness

$$\begin{aligned} & \sum_{ij} \begin{bmatrix} i & j \\ \mathbf{r}_1 & \mathbf{r}_2 \end{bmatrix}_0^* \begin{bmatrix} i & j \\ \mathbf{r}'_1 & \mathbf{r}'_2 \end{bmatrix}_0 \\ &= \sum_{ij} \begin{bmatrix} i & j \\ \mathbf{r}_1 & \mathbf{r}_2 \end{bmatrix}_0^* \begin{bmatrix} i & j \\ \mathbf{r}'_1 & \mathbf{r}'_2 \end{bmatrix}_0 = \delta(\mathbf{x} - \mathbf{x}') \end{aligned} \quad (14)$$

relations.

In order to generalize the HF equations to n -particle states, we perform a variational procedure. In this procedure, it is convenient to identify clearly and uniquely the particle space in which the two-particle wave functions are acting. This identification is considerably easier when the particle pairings are uniquely and distinctly defined, as is done in constructing the wave function or in partitioning the Hamiltonian. We can now obtain an eigenvalue-like

equation for the two-particle states $\begin{bmatrix} i & j \\ \mathbf{r}_1 & \mathbf{r}_2 \end{bmatrix}$ by following the same formal procedure as in the single-particle case. From the variational condition

$$\delta \left[\langle \Psi | H | \Psi \rangle - \sum_{ij} \epsilon_{ij} \int d^6x \begin{bmatrix} i & j \\ \mathbf{x} \end{bmatrix}^* \begin{bmatrix} i & j \\ \mathbf{x} \end{bmatrix} \right] = 0 \quad (15)$$

with respect to $\begin{bmatrix} i & j \\ \mathbf{x} \end{bmatrix}^*$ we obtain the equation in the coordinate representation

$$\begin{aligned} & \left[-\nabla_{\mathbf{x}}^2 + V(\mathbf{x}) + \int d^6x' V(\mathbf{x}, \mathbf{x}') \rho_{(ij)}(\mathbf{x}') \right] \begin{bmatrix} i & j \\ \mathbf{x} \end{bmatrix} \\ & + \sum_{nm} \int d^6x' \begin{bmatrix} n & m \\ \mathbf{x}' \end{bmatrix}^* V(\mathbf{x}, \mathbf{x}') \\ & \times \left\{ \begin{bmatrix} i & j & | & n & m \\ \mathbf{x} & | & \mathbf{x}' \end{bmatrix} - \begin{bmatrix} i & j \\ \mathbf{x} \end{bmatrix} \begin{bmatrix} n & m \\ \mathbf{x}' \end{bmatrix} \right\} = \epsilon_{ij} \begin{bmatrix} i & j \\ \mathbf{x} \end{bmatrix}, \end{aligned} \quad (16)$$

where the two-particle density, $\rho_{(ij)}(\mathbf{x})$, is given by the expression

$$\rho_{(ij)}(\mathbf{x}) = \sum_{nm \neq ij} \begin{bmatrix} n & m \\ \mathbf{x} \end{bmatrix}^* \begin{bmatrix} n & m \\ \mathbf{x} \end{bmatrix}. \quad (17)$$

It should be emphasized that the combinations of “single-particle” indices, such as i, j , are to be viewed as a single combined index denoting the pair state that has evolved out of the individual particle states, i and j , under the interparticle interaction (and the interaction with an external potential).

The generalized two-particle HF equations are seen to have a structure equivalent to their single-particle counterparts, exhibiting the presence of a direct term, written in terms of the density, and an “exchange” term. As the canonical HF equations, the present expressions do not contain spurious self-interaction terms. However, unlike the single-particle equations, they allow the determination of fully correlated two-particle states removing to this extent the most basic objection to the HF method.

3.1 Numerical illustration

We present the resulting calculations of single-particle spectra for four electrons (2 of each spin direction) on a linear ring of four sites. The single-particle single-band Hamiltonian describing the *non-interacting* system is

defined by its matrix elements in a tight-binding representation,

$$H_{ij}^{(1)} = \epsilon_i \delta_{ij} + t_{ij}, \quad (18)$$

where ϵ_i is an on-site energy, and t_{ij} represents electron hopping from site i to site j and is taken to connect only nearest neighbor sites. In the calculations reported here, we set $\epsilon_i = 0$ and $t = 1.0$. Also, the energies were assigned an imaginary part of $t/4.0$ for ease of presenting the spectra. Within this picture, a description of interparticle interactions is often given by means of a term $U_{ij}n_i n_j$ being added to the Hamiltonian of non-interacting particles, where U_{ij} represents the Coulomb repulsion between two electrons on sites i and j , and n_i is the number operator for an electron on site i . Usually, U is taken to be site diagonal and we will also take this to be the case. In a (restricted) HF treatment of this model Hubbard Hamiltonian, the pair of number operators $n_i n_i$ is decoupled by replacing one of the two operators by its expectation value. This in turn leads to a Hamiltonian of the non-interacting type, Eq.(18), but with all on-site energies displaced by an amount $U\langle n_i \rangle$. In this description the structure of the single particle spectrum remains identical to that for non-interacting particles.

We now generalize the HF treatment just described to two-particle space. The two-particle space associated with a ring of four sites is a torus of 16 sites and the Hamiltonian describing two non-interacting particles has the form,

$$H_{ij;kl}^{(2)} = [\epsilon_i + \epsilon_j] \delta_{ik} \delta_{jl} + t [(1 - \delta_{ik}) \delta_{jl} + (1 - \delta_{jl}) \delta_{ik}]. \quad (19)$$

This describes a single particle on a torus with site energies $\epsilon_i + \epsilon_j$ (corresponding to two particles on the linear ring being on sites i and j), and nearest-neighbor hopping t . The interaction between the particles is described by the operator $f(U)n_i n_j n_k n_l$, where $f(U)$ is a function of configuration. Thus, when the indices i, j, k, l are all different from one another, $f(U) = 0.0$. When only two of the indices are identical, $f(U) = U$, and in the case of two different pairs of identical indices, $f(U) = 2U$. In the present version of the HF approximation, we decouple the four number operators by replacing two of them by their expectation value (average). In this case, we find that the sites along the main diagonal of the torus have their on-site energies shifted by an amount $2U\langle n_k n_k \rangle + U\langle n_k n_l \rangle = \frac{5}{4}U$, while the energies on sites off the diagonal are shifted by $U\langle n_i n_i \rangle = \frac{U}{4}$. Thus, the two-particle interacting Hamiltonian, which would contain a term U along the main diagonal of the torus, has all on-site energies shifted by the average energy of a pair of opposite-spin electrons on a site.

Figures 1 shows, for $U = 10.0$, the single-particle spectra for four electrons on a ring of four sites (half-filled band) obtained in the ordinary version of HF

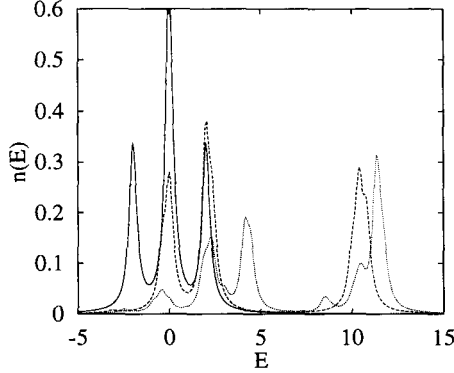


Figure 1: Single-particle spectra for a ring with four sites with $U = 10.0$. The solid line is the spectrum calculated from the restricted HF while the dashed line is the spectrum obtained with the 2HF, and the dotted line is the exact spectrum.

treatment (restricted HF) (solid lines) and in the two-particle generalization of this approach described above (dashed lines), compared to the exact results (dotted line). The exact results were obtained from the exact Green function of the four-electron system by inverting the full configurational matrix in four-particle space, and integrating out (summing over) the coordinates of three of the particles. Also, for the sake of ease of comparisons, we do not display the shift in the on-site energies since they do not affect the structure of the spectra.

As the present results indicate, the single-particle HF approximation is completely insensitive to the presence of interparticle interactions. On the other hand, the use of 2HF, the present method, which essentially consists of the treatment of two-particles, provides a much improved representation of the exact spectra.

4 Generalization of DFT

Given the formal similarity between the Hamiltonians defined in Eqs.(2) and (5), it follows that the ground-state energy, E , is given in terms of a universal functional of the pair (or n -particle) density, $n(\mathbf{x})$, which attains its minimum value for the exact pair density. Furthermore, within a Kohn-Sham scheme, the form of this functional is identical to the functional of ordinary DFT but is given in terms of the correlated pair density. The details of this derivation

are similar to those of ordinary DFT and are presented elsewhere [30, 33]. We thus confine ourselves to the final result. The energy functional which determines the density in two-particle phase space can be written in the form,

$$E[n(\mathbf{x})] = T_s[n(\mathbf{x})] + U[n(\mathbf{x})] + E_{xc}[n(\mathbf{x})], \quad (20)$$

where $T_s[n(\mathbf{x})]$ represents the kinetic energy of a system of non-interacting particles at the density $[n(\mathbf{x})]$, the quantity $U[n(\mathbf{x})]$ is defined by

$$\begin{aligned} U[n(\mathbf{x})] &= \int d^6x V(\mathbf{x})n(\mathbf{x}) \\ &+ \int d^6x_1 \int d^6x_2 n(\mathbf{x}_1)V(\mathbf{x}_1, \mathbf{x}_2)n(\mathbf{x}_2), \end{aligned} \quad (21)$$

and $E_{xc}[n(\mathbf{x})]$ contains the difference between the exact kinetic energy $T[n(\mathbf{x})]$ and that represented by $T_s[n(\mathbf{x})]$, as well as the difference between the exact interparticle interaction and its “classical” approximation given by Eq.(21),

$$\begin{aligned} E_{xc}[n(\mathbf{x})] &= T[n(\mathbf{x})] - T_s[n(\mathbf{x})] + \int d^6x_1 \int d^6x_2 \\ &\times V(\mathbf{x}_1, \mathbf{x}_2) [n(\mathbf{x}_1, \mathbf{x}_2) - n(\mathbf{x}_1)n(\mathbf{x}_2)]. \end{aligned} \quad (22)$$

Here, $n(\mathbf{x}_1, \mathbf{x}_2)$ represents the two-particle correlated density in two-particle space or, equivalently, the correlated density of four ordinary particles. As in ordinary DFT, the exchange-correlation functional is not known but can be used in a local density approximation (LDA) sense through, for example, the study of 6-dimensional jellium.

Both formal analysis and computational developments associated with DFT can be carried over intact to n DFT. For example, the exact two-particle ground-state density, $n_0(\mathbf{x})$, can be determined through a constrained search[34] for that many-particle, properly symmetrized or antisymmetrized wave function, with symmetry imposed with respect to ordinary particles, which yields n_0 and also minimizes the many-particle energy, $T + V_{pp}$, where V_{pp} denotes the interparticle interaction in two-particle space. Essentially any method developed within a single-particle application of DFT for the study of electronic structure can, with appropriate technical modifications, be extended to two-, or n -particle states. The use of multiple-scattering theory to calculate fully correlated two-particle densities in solids will be given in a future publication.

4.1 Numerical illustration

In order to illustrate the role played by the two-particle density in the determination of the electronic structure, we study the single-particle spectrum of

four electrons of total spin zero on a four site single-band linear ring described by a Hubbard Hamiltonian

$$H = \sum_i \epsilon_i c_i^\dagger c_i + \frac{1}{2} \sum_{i>j} t_{ij} c_i^\dagger c_j + U \sum_i n_{i\sigma} n_{i\bar{\sigma}}, \quad (23)$$

where c_i^\dagger and c_i are creation and annihilation operators for an electron on site i , the site energies ϵ_i are chosen equal to zero, the hopping term t_{ij} is confined to near neighbors and set equal to 1.0, and the on-site Coulomb interaction felt by electrons of opposite spin is taken to have the values 1.0 and 10.0, with the respective results shown in Figs. 2 and 3. Exact two-particle and single-particle Green functions and spectra are obtained in down-folding procedure by summing over (integrating out) the coordinates of one and three of the particles, respectively, in the four-particle Green function. This, in turn, is obtained through the usual procedure as a “single-particle” Green function in a four-particle phase space which in the present case leads to a 256-dimensional matrix. We also include results obtained within a version of the GW approximation in which the self-energy,

$$\Sigma_{ij}(E) = \lim_{\eta \rightarrow 0} \frac{1}{2\pi} \int e^{-i\omega\eta} W_{ij}(\omega) G_{ij}(E - \omega) d\omega. \quad (24)$$

is given in terms of the exact single-particle Green function and the exact screened interaction which is determined in terms of the non-interacting, zero superscript, and exact two-particle Green functions, $W_{ij;kl}(E) = \{G_{ij;kl}^{(0)}\}^{-1} - G_{ij;kl}^{-1}$.

Finally, we also show the single-particle spectra derived through down-folding from an averaged two-particle Green function in which two-particle states are obtained in the presence of another pair of particles. These states are consistent with the Pauli exclusion principle but neglect the interactions among configurations of two-particle spaces. In all cases the energy was assigned an imaginary part of $0.25t$ for presentation purposes.

As is seen in these figures, these averaged results are in considerably better agreement with the exact spectra than those obtained in the present version of the GW approximation, particularly for large values of U . One also sees that the averaged results overestimate the gap in the strong U limit as may be expected in a non-self-consistent procedure of this type. Even for $U/t = 1.0$, a region in which the GW approximation has been found to give accurate results for real systems, the averaging of the two-particle Green function in the presence of a finite density resolves the band structure much more accurately. We note the resonance at $U = 1.0$ which is missed in the GW results, and that both approximate results are displaced somewhat with

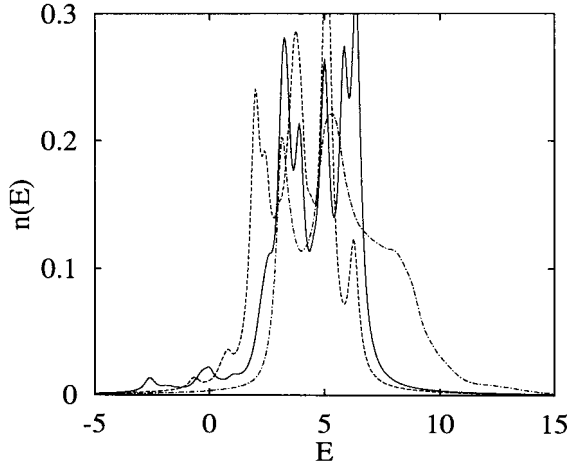


Figure 2: Exact single-particle spectrum (solid line) for four electrons on a four-site ring compared with the results of a GW approximation (dash-dotted line) and those obtained from an effective two-particle Green-function (dashed line) for $U = 1.0$.

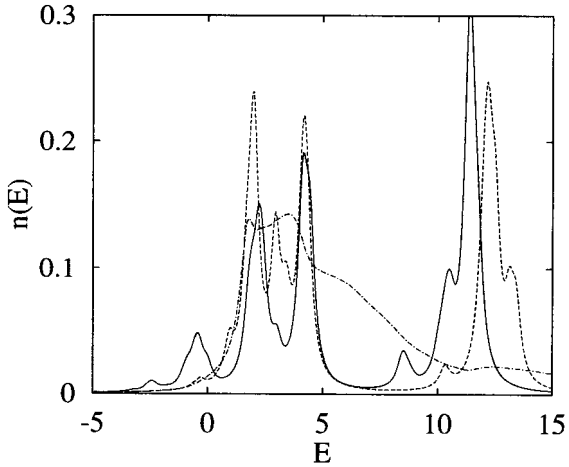


Figure 3: Results analogous to those of the previous figure but for $U = 10.0$.

respect to the exact ones. Much of this effect, along with the wider gap in the strong U limit mentioned above can be traced back to the incomplete treatment of the Pauli principle, i.e., the neglect of configuration interactions. Both of these approximations can be expected to improve with increased dimensionality and lattice connectivity. More detailed discussions of these and other similar numerical results than can be presented here will be given in a future publication.

5 Discussion

The formalism presented here indicates the unifying power of the n -particle picture and provides an extension of the HF and density functional theories to the treatment of fully correlated two-particle states, (and by a straightforward extension of n -particle states). In the case of the HF method, it allows the study of correlation effects in a systematic way in terms of increasing the unit size, becoming exact as $n \rightarrow N$. In the case of DFT, it leads to a general minimum principle governing correlated densities in quantum systems which is analogous to the principle governing single-particle densities. This formalism also becomes exact in the limit in which the entire system of particles is treated as a single unit. Thus, within an n -particle picture, HF theory and DFT are seen to be two different methods leading to exact results in the same limiting procedure.

Although its computational implementation of the method, say within a partial-wave analysis, increases in difficulty rapidly with increasing dimensionality of the n -particle phase space, its application to two-particle states is well within the domain of present computational technology.

6 Acknowledgment

One of the authors (AG) is grateful to John Perdew, Mel Levy, Kreion Burke, W. H. Butler, and X.-G. Zhang for clarifying discussions. Support for this work was provided by Lawrence Livermore National Laboratory under the auspices of the U.S. Department of Energy under Contract No. W-7405-ENG-48. Work at Oak Ridge was supported by the Division of Materials Sciences, U.S. Department of Energy under contract DE-AC05-96OR22464 with Lockheed Martin Energy Research Corporation.

References

- [1] P. Hohenberg and W. Kohn, Phys. Rev. **136**, B864 (1964).
- [2] R. G. Par and Weitao Yang, *Density Functional Theory of Atoms and Molecules*, (Oxford University Press, New York, 1989).
- [3] R. M. Dreitzler and E. U. K. Gross, *Density Functional Theory*, (Springer Verlag, Berlin, New York, 1990).
- [4] *Theory of the Inhomogeneous Electron Gas*, Edited by S. Lundqvist and N. H. March, (Plenum, New York, 1983).
- [5] R. O. Jones and O. Gunarson, Rev. Mod. Phys. **61**, 689 (1989).
- [6] S. Massida, M. Posternak, and A. Baldereschi, Phys. Rev. **B48**, 5058 (1993).
- [7] C. Pisani, R. Dovesi, and C. Roetti, *Hartree-Fock Ab Initio Treatment of Crystalline Systems*, (Springer-Verlag, Berlin, 1988).
- [8] Lars Hedin, Phys. Rev. **139**, A796 (1965).
- [9] M. S. Hybertsen and S. G. Louie, Phys. Rev. Lett. **55**, 1418 (1985); Phys. Rev. **B34**, 5390 (1986).
- [10] R. W. Godby, M. Schlütter, and L. J. Sham, Phys. Rev. Lett. **56**, 2415 (1986); Phys. Rev. **B37**, 10159 (1988).
- [11] K. A. Bruckner and C. Levinson, Phys. Rev. **97**, 1344 (1955).
- [12] Gordon Baym and Leo P. Kadanoff, Phys. Rev. **124**, 287 (1961).
- [13] Paul Ziesche, Phys. Lett. **A195**, 213 (1994).
- [14] P. -O. Löwdin, Phys. Rev. **97**, 1474 (1955).
- [15] R. McWeeny, Rev. Mod. Phys. **32**, 335 (1969).
- [16] A. J. Coleman, Rev. Mod. Phys. **35**, 668 (1960).
- [17] E. R. Davidson, *Reduced Density Matrices in Quantum Chemistry*, (Academic Press, New York, 1976).
- [18] R. Erdahl and V. H. Smith, eds. *Density Matrices and Density Functionals*, (Reidel, Dordrecht, 1987).

- [19] A. C. Hurley, *Electron Correlation in Small Molecules*, (Academic Press, New York, 1976).
- [20] W. Kutzelnigg, *Einführung in die Theoretische Chemie*, Bd.2, 2nd Ed. (VCH, Weinheim 1994).
- [21] Ralph E. Chistoffersen, *Basic Principles and Techniques of Molecular Quantum Mechanics* (Springer Verlag, New York, 1989).
- [22] R. D. Cowan, Phys. Rev. **163**, 54 (1967).
- [23] J. P. Perdew and G. L. Oliver, Solid State Commun. **34**, 933 (1980).
- [24] J. P. Perdew and A. Zunger, Phys. Rev. B23, 5048 (1981).
- [25] Lars Hedin and Stig Lundqvist, Solid State Physics, (Academic Press, New York, 1969), Supplement **23**.
- [26] Peter Fulde, *Electron Correlations in Molecules and Solids*, (Springer Verlag, Berlin, New York 1995).
- [27] L. Pauling, *The Nature of the Chemical Bond and the Structure of Molecules and Solids*, (Cornell University Press, Ithaca, NY 1960).
- [28] Leo P. Kadanoff and Gordon Baym, *Quantum Statistical Mechanics*, (Benjamin, New York, 1962).
- [29] John Avery, *Hyperspherical Harmonics*, (Kluwer, Dordrecht, 1989), and references therein.
- [30] A. Gonis, T. C. Schulthess, Jan van Ek, and P. E. A. Turchi, Physical Review Letters **77**, 2981 (1996).
- [31] Alexander L. Fetter and John Tirk Wallecka, *Quantum Theory of Many Particle systems* (McGraw-Hill, New York 1971).
- [32] E. K. U. Gross and E. Runge, *Vielteilchentheorie*, (Teubner, Stuttgart 1986).
- [33] A. Gonis, T. C. Schulthess, P. E. A. Turchi, and Jan van Ek, Phys. Rev. B **56**, 8970 (1997).
- [34] Mel Levy and John P. Perdew in *Density Functional Methods in Physics*, edited by Reiner M. Dreizler and Joao da Providencia (Plenum, New York, 1985), p. 11.

Gradient-corrected Exchange Potential Functional with the correct asymptotic behaviour

H. Chermette*, A. Lembarki, H. Razafinjanahary,
and F. Rogemond*

Laboratoire de Chimie-Physique Théorique,
Université Claude Bernard Lyon1,
and (*) Inst. Recherches sur la Catalyse, UPR 5401-CNRS
43, Bd du 11 Novembre 1918,
F-69622 Villeurbanne Cedex, France

October 1, 1997

Abstract

Among the various conditions which should be satisfied by any exchange-correlation functional, some classes of conditions are less important for some practical applications to molecular systems. In this article, emphasis is brought to the $\frac{1}{2r}$ and $\frac{1}{r}$ asymptotic behaviour which should be satisfied by energy functionals and potential functionals. It is shown that the rigorous derivation of the potential from the energy functional is not a critical requirement, and that, as far as preliminary results are concerned, the present potential functionals having the correct asymptotic behavior do not necessarily improve the theoretical determination of geometries of molecules. Some trends are deduced from calculations of molecular geometries with potential functionals possessing the correct asymptotic behaviour, and some hypotheses about missing features in the potential, like an improved shell structure are discussed.

1 Introduction

It is well known that many sets of conditions should be fulfilled by density functionals. A somewhat arbitrary but hopefully useful personal classification scheme may be the division of these conditions, most of them being summarized in the "shopping list" of Perdew *et al.* [1], into 4 classes of properties:

1. the scaling properties of the exchange-correlation energy functionals E_{xc} , which can be subdivided in properties of the exchange functionals E_x and the properties of the correlation functionals E_c [2, 3, 4, 5].
2. the sum rules which involve the exchange-correlation hole, and which also can be subdivided into relations for the Fermi (exchange) hole $\rho_x(\mathbf{r}, \mathbf{r}')$ [1, 3, 4, 6, 7] :

$$\int \rho_x(\mathbf{r}, \mathbf{r}') d\mathbf{r}' = -1 \quad (1)$$

$$\rho_x(\mathbf{r}, \mathbf{r}') \leq 0 \quad (2)$$

$$\epsilon_x(\mathbf{r}) < 0 \quad (3)$$

and for the Coulomb (correlation) hole $\rho_c(\mathbf{r}, \mathbf{r}')$. [1, 7, 8]

$$\int \rho_c(\mathbf{r}, \mathbf{r}') d\mathbf{r}' = 0 \quad (4)$$

$$\rho_c(\mathbf{r}, \mathbf{r}') \leq 0 \quad (5)$$

$$\epsilon_c(\mathbf{r}) < 0 \quad (6)$$

$\epsilon_{xc}(\mathbf{r})$ being the exchange-correlation energy density.

3. the asymptotic properties of the E_{xc} energy functionals and the V_{xc} potential functionals. Let us recall that, in the Kohn-Sham formalism [9], this last one is related to the E_{xc} functional through the functional derivation:

$$V_{xc\sigma}(\mathbf{r}) = \frac{\delta E_{xc}[\rho_\sigma]}{\delta \rho_\sigma(\mathbf{r})} \quad (7)$$

Now, whereas the long range behaviour of the exchange-correlation energy density should follow [10]:

$$\lim_{r \rightarrow \infty} \epsilon_{xc} \rightarrow \frac{-1}{2r} \quad (8)$$

which turns out to be (*vide infra*)

$$\lim_{r \rightarrow \infty} \epsilon_x \rightarrow \frac{-1}{2r} \quad (9)$$

one should have, simultaneously, for the long range behaviour of the exchange-correlation potential:

$$\lim_{r \rightarrow \infty} V_{xc} \rightarrow \frac{-1}{r} \quad (10)$$

which also turns out to be (*vide infra*)

$$\lim_{r \rightarrow \infty} V_x \rightarrow \frac{-1}{r} \quad (11)$$

4. the fourth class of condition assumes that, for a slowly varying density, one should recover the uniform gas limit and its gradient expansion. This very last requirement is sometimes called the Kohn-Sham (KS) quadratic condition.

These conditions have been used as guideline for the elaboration of accurate exchange-correlation functionals and have permitted the obtention of some of the most popular exchange and correlation functionals of the time being. Called "non local functionals" at the beginning, all these functionals are function of ρ and $\nabla\rho$ and for that reason they are often called gradient-corrected functionals to emphasize the fact that the use of gradient dependent terms corrects some deficiencies of the LDA (local density approximation). Following Perdew [8], most of them, derived from a gradient expansion of the energy functional, are called GGAs (generalised gradient approximation). According to Ziegler's classification [11, 12], these functionals belong to the so-called second generation of functionals of the DFT, the first one corresponding to LDA functionals. However, as it has already been shown by Umrigar, Gonze [13] and others, none of them satisfies all the four classes of conditions. This is rapidly summarized in Table 1 where it is easily seen that on the one hand, the Becke exchange energy functional (Be88), [14]) is the unique one which satisfies the condition (9), provided it is used with an exponential density (e.g. not a gaussian one). On the other hand the PW91 exchange energy functional [8] satisfies much more scaling relations than any others, and, although possessing an analytical form which derives from Be88, it does not fulfil the condition (9).

In this paper, we would like to address the following questions:

Table 1: Known properties of the exact density functional. (+- means some, ++ means most)

Properties	LDA	Be88	PW91(X)	LYP	PW91(C)
Sum rules [†]					
$\int \rho_x(r, r') dr' = -1$	+	-	+		
$\rho_x(r, r') \leq 0$	+	-	+		
$E_x[\rho] < 0$	+	+	+		
$\int \rho_c(r, r') dr' = 0$	+			-	-
$\rho_c(r, r') \leq 0$	+			-	-
$E_c[\rho] < 0$	+			-	+
Scaling properties ^{††}	+ -	+ -	++	-	++
Asymptotic behaviors					
$\lim_{x \rightarrow \frac{-1}{2r}} \epsilon_x \rightarrow$	-	+ -	-		
$\lim_{x \rightarrow \frac{-1}{r}} v_x \rightarrow$	-	-	-		
LDA limit for constant $\rho(r)$ quadratic LDA limit.	+	+	+	-	+
		-	+	-	+

† see ref.[13], [5] and [2].

†† see ref.[13] and [7].

- are there any significant difference in the optimized geometries obtained using the present potential functionals satisfying the asymptotic condition (9) and other standard pure or hybrid DFT functionals?
- is there an increased sensitivity to the so-called auxiliary basis sets used in most DFT codes for this class of potential functionals?
- how sensitive are other electronic properties like the dipole moment to this class of potential functionals?
- how sensitive are the optimized geometries obtained using the present potential to the energy functional selected for the computation of the exchange energy?
- how sensitive are the optimized geometries obtained using the present potential to the correlation energy and potential functional selected for the computation?

2 Towards a hierarchy in the conditions fulfilled by the functionals

We are skeptical about the possibility of finding an exchange-correlation functional in the near future, satisfying simultaneously all the following requirements:

1. it is quasi-universal, *i.e.* applicable to both quasi-uniform systems (like metals band structures) and strongly non uniform systems such as small hydrogenated molecules.
2. it fulfils simultaneously all the scaling relations [2, 6] and the sum rules [8] (*cf.* Table 1) prescribed by Levy, Perdew and others [5, 4].
3. it is analytically simple and smooth: whereas this feature may look important for the computational time necessary for the description of extended molecular systems, this is not the point we want to underline. What is important is to have a smooth energy functional and smooth successive derivatives. In particular, the potential (first derivative) and its derivative control the KS density, so that any abrupt feature in the potential may lead to oscillations in the density. This point has been highly neglected up to now, but it is important because a potential which is not smooth everywhere may generate spurious peaks in the density in some parts of the space, which may lead to difficulties or impossibilities to converge properly calculations, in particular geometry optimisations. This occurs mainly when extra terms are added to the E_{xc} functional in order to satisfy more scaling properties, whereas the numerical value of the energy itself, is not significantly modified. Unfortunately, this is especially the case of the PW91 functional, which has been designed in order to fulfil a maximum of scaling relations and to provide an analytical formulation of the numerical PW91 functional. This last one contains sharp cut-offs used in its elaboration and introduced in order to satisfy the sum rules. This has been underlined by the authors themselves [15, 16, 17, 18] and others, and is illustrated in Fig. 1 in the case of the correlation hole of the helium atom. (see [15] and references therein or [3]). Similar features are present in the exchange functional, although less visible on a small graph.

Whereas extra terms added in the energy functional can be of little numerical significance in the energy determination, because it is an integral property which is not sensitive to the parts of space where the

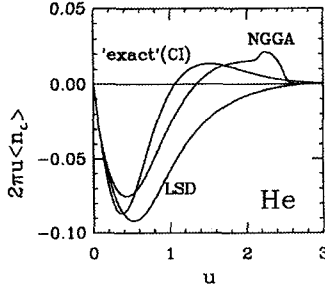


Figure 1: System-averaged correlation hole density in the Helium atom (LDA, Numerical GGA, exact, from ref. [16]).

density is small, they can be of larger significance in the corresponding potential. In other words, a potential which is not smooth in the whole space leads to both numerical instabilities which make more difficult the SCF convergence of Kohn-Sham equations and the reliability of the corresponding density. This conclusion may be emphasized by the expansion of the basis set used, the largest one leading not necessarily to the best results (*vide infra*). Therefore, and unfortunately, the increase in the size of the basis set does not necessarily leads to more accurate theoretical properties, as it has been already found by many DFT practitioners [19, 20, 21]. In a recent paper, Gill [20] have shown that some numerical terms present in the Lee-Yang-Parr (LYP) [22] functional are of little significance since for a set of 56 molecules, namely the G2 set [23], only one half of molecules exhibit improved descriptions (bond energies, geometrical structures) when these terms are present, whereas one third of these molecules were more poorly described!

4. it possess asymptotic properties for both E_{xc} and V_{xc} . Indeed, it has been shown by Engel *et al.* [24, 25] that requirements given by Eq. (8) and (10) can be satisfied only if the functionals depending on the density and the gradient of the density contain also density laplacian terms. This immediatly suggests that accurate calculations will be necessary because of the well known numerical instabilities of successive derivations. Nevertheless, quite encouraging results have been already obtained with $E_x(\rho, \nabla\rho, \Delta\rho)$ functionals, in particular for the description of loosely bonded systems [26, 27, 28].

5. it is “Kohn-Sham quadratic”, *i.e.* which lets recover the gradient expansion for densities slowly varying from the uniform systems.

Therefore, at least for pragmatic reasons, it is necessary to choose among the 1-5 requirements which ones are less (or most) important for the description of electronic properties. We will briefly comment these classes of requirements.

- It is clear that in the description of finite or infinite systems, some of the non-uniform scaling properties pointed out by Perdew, Levy and others are of little importance because they may be quenched by the vanishing density through the energy determination. In a similar vein, for the study of 3D-periodic systems, the density never vanishes, and problems related to the divergence of the reduced gradients $x = \frac{|\nabla\rho(\mathbf{r})|}{\rho^{4/3}(\mathbf{r})}$ should not be relevant, at least for other systems than Van der Waals solids. On the other hand, the satisfaction of some sum rules may remain important. For instance, the integration of the Fermi hole to -1, property which is fulfilled by the LDA and PW91(X) exchange functional, but not by other exchange functionals, [13], should remain a promising direction for improving functionals. Indeed, as already said, the PW91(X) exchange functional, through its elaboration, just truncates the gradient expansion when the sum rule becomes satisfied [15]. Although it is smoothed through its analytic form, one can see (Fig.2) that it is possible that it could undercompensate and overcompensate the deviation of the exchange-correlation energy *w.r.t.* the LDA in some parts of the space, in particular at large (reduced) gradients.
- In a recent paper [20], Gill showed that the necessity for a good functional to be “Kohn-Sham quadratic” is a weak constrain, since we know exchange functionals which are not KS quadratic (*e.g.* Be88), and which perform at least as well as the best KS quadratic exchange functional available (*e.g.* PW91(X)) (the two being very similar). However, this assumption does not necessarily hold for all systems and it is probably restricted to many theoretical properties (mostly energetics), whereas some properties may remain more sensitive to the exchange-correlation functional quality.
- The necessity to have a simple analytical form is certainly a condition which has no physical basis, but which is necessary if one wants to avoid spurious noise in the determination of molecular structures, an effect which is generally emphasized by the use of large basis sets. This point has been recently underlined by better results obtained with

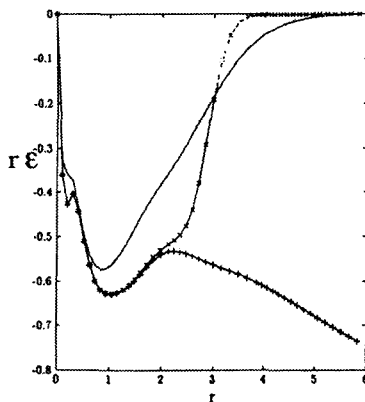


Figure 2: Radial exchange energy density $r\epsilon(r)$ for neon atom for LDA (line), LDA + Be88 exchange functional (+), and PW91 exchange functional (x)(from ref. [2]. The broken part of the PW91 curve should be related to an over/undercorrection of the LDA.

basis sets of medium size compared to results calculated with extended basis sets [20]. This clearly indicates that, at least, small density regions described by diffuse functions, are not energetically properly described by some of the GGAs. As a consequence, the grid used for the numerical integrations has to be increased significantly. For example, the radial grid in deMon [29] which is sufficiently accurate with 32 points for LDA calculations, has to be extended to 64 points for GGAs [30] calculations. This point is, however, not true for fully numerical, basis set free, programs like NUMOL [31, 32, 33] which are unfortunately scarcely used in the world, although in these conditions, such a code has also to increase considerably the number of points to keep the required numerical accuracy.

- The necessity to fulfil condition Eq. (8) for E_{xc} is possibly responsible of the preferred choice of the exchange Be88 functional by many DFT practitioners which select the functional leading to results in the best agreement with what they expect. This is certainly amplified by the presence of this functional in most widely distributed DFT codes, but this preference takes essentially its origin in the fact that Be88 leads statistically to the most accurate bond energies of molecules (provided

a reasonable choice is made for the correlation functional). This good performance is certainly related to the fact that it is important to fulfil the condition Eq.(9) and among all the exchange energy functionals, only Be88, although approximately, does. (*vide supra*). Of course, as already said, the choice of the correlation functional used together is important, but, at least to begin, it may be considered as less essential for two reasons:

- for molecular systems, the correlation energy is approximately one order of magnitude smaller than the exchange one,
- the correlation is more a short range property (superconductors excepted, which are far from molecular systems we refer to), so that the long range behaviour is mostly driven by the exchange functional.

It is remarkable that, LDA excepted, no correlation functional satisfies Equation (4) (PW91(C) does not, because it contains corrections to deficiencies of the exchange part of the PW91 exchange-correlation functional, which fulfils Equations (1)+(4) for the whole exchange-correlation functional). However, on the one hand, the separation of correlation energy from exchange, although being always possible, is not necessary since this is only the sum of Equations (1)+(4) which has to be satisfied. On the other hand, the decomposition for a many electrons system of the exact exchange-correlation potential into exchange and correlation components has seldom been done[34, 35, 36].

3 Importance of the asymptotic behavior for the potential

The signification of the HOMO eigenvalue in “exact” KS calculations (*i.e.* with the true (unknown) exchange-correlation has been clearly identified by Levy, Perdew and Sahni as equal to the chemical potential $\mu = \delta E / \delta \rho$ because the long range exponential decay of the electron density is $\exp(-(-2\mu)^{1/2}r)$ [37]. These authors [37], as well as Almbladh and von Barth [38] proved that this eigenvalue should equal the ionisation potential I , provided that the derivation is taken on the electron deficient side of the integer number of electrons. This is related to the proof by Perdew, Parr,

Levy and Balduz that [39]

$$\mu = -I \text{ for } Z - 1 < N < Z$$

$$\mu = -A \text{ for } Z < N < Z + 1$$

(A being the electroaffinity). This rises the point of the discontinuity of μ , therefore of ϵ_{HOMO} as N passes through an integer value (ϵ_i being the eigenvalue of the spinorbital i). Accordingly, the correct asymptotic behaviour of the V_{xc} potential for a closed shell system should not be $-1/r$, but $-1/r + (I - A)/2$ [39, 3]. Moreover, one should have for open shell systems $\epsilon_{HOMO} = -I$ and $\epsilon_{LUMO} = -A$, the difference between them being brought by the spin polarization. This holds for any atom, if no spherical average is made, but for a delocalised system (e.g. metal), this difference vanishes. For a detailed discussion of the impact of the sphericity of the density on the total energy, see Baerends *et al.* [40], and for a documented discussion on the relation between ϵ_{HOMO} , ϵ_{LUMO} , I and A , see Russier [41].

Nevertheless recently were proposed V_{xc} functionals which exhibit the correct asymptotic behaviour (in the following, when not explicitly stated, the correct asymptotic behaviour means $-1/r$). Van Leeuwen and Baerends (VLB) proposed the first one, based on the Be88 exchange analytical form [42], and parametrized in order to recover the true KS density of the beryllium atom. They proposed to compute the E_{xc} through a line integral [43]. A few months later, Lembarki, Rogemond and Chermette (LRC) proposed two V_x functionals [44] exhibiting the correct asymptotic behaviour. Since the correlation potential is short range, only the V_x was derived, and a correlation potential was further added in the computation of densities and total energies of systems. These V_x potentials were parametrized in such a way that they had either the Be88 analytical form, or a form derived from the PW91 exchange form. Roughly speaking, the parameters were fitted in order to recover the ionisation potentials (IP) of a panel of atoms, since the HOMO eigenvalue should be equal to the IP. More precisely, the fit was performed in order to recover the optimized potential model (OPM) eigenvalues [44]. Whereas the Be88 form requires only one parameter to be fitted, the (modified) PW91 form in LRC has 5 independant parameters, only 2 of them being fitted. The exchange energy E_x is obtained either through a formula derived from the virial theorem, or, as in VLB work, with a line integral [42]. Most exchange-correlation potential functionals do not show the correct asymptotic behaviour. In fact, besides the aforementioned potentials, one should also mention the potential based on the weighted density approximation (WDA) which is much more computationally expensive [45, 46, 47, 48, 49], the functional proposed by Jemmer and Knowles, which

appears to be numerically instable [50], and the recently proposed functional by Santamaria [51].

In section 5 are reported some results obtained with such V_{xc} potentials: our hope was to obtain better densities, and therefore better related properties, and finally better geometries. Simultaneously we expected to get reasonable energies: although the theory requires that the potential is a functional derivative, otherwise the energy minimum point does not coincide with the energy gradient zero area, we expected to get rather small discrepancies because of the closeness of the energy functionals used and the potential functional: we will develop this point a little further (section 6).

4 Calculation details

Calculations have been performed with deMon-KS 0.1 [29, 52] and ADF 2.0 [53, 54, 55] in which these functionals have been implemented. Geometry optimisations have been performed for a panel of molecules which are extracted from the G2 set [23]. These molecules are already well described by most of the GGAs and hybrid functionals such as B3LYP [56, 57]. The DZP2 basis sets were taken from Godbout *et al.* [58] for deMon calculations, and from the so-called base V [53] for ADF calculations. The calculations were made using the fine random grid, with 64 radial points within deMon, and a required accuracy better or equal to 10^{-6} in the energy in the SCF cycles, (deMon, ADF), and 10^{-6} in the energy gradient in the geometry optimisations. The quality of these basis sets for this class of molecules has been established in many works. Without anticipating the following discussion, we will see that the results are not as good as expected. We first thought that it could be related to the quality of the auxiliary basis set, which is used for the fit of the density, and for the exchange-correlation potential. Consequently, in both kinds of codes, namely deMon which uses GTOs for orbitals and auxiliary functions, and ADF, which uses STOs for orbitals and auxiliary functions, we tested the saturation of the auxiliary basis set, by inclusion of more diffuse functions which were expected to be lacking to a correct description of low densities domains.

Unfortunately, it turns out that, whereas the energies may be different, as expected, the geometries were not significantly modified.

5 Results and Discussion

The point that if one starts from an optimised V_{xc} potential, one can not fulfill exactly the relation (7) has for a long time been responsible of the absence of endeavours to parametrize V_{xc} , whereas many attempts to propose new E_{xc} have been published [8, 14, 16, 59, 60, 61, 62, 63, 64, 65, 66, 67, 68, 69].

Nevertheless, for many years, the GGA has been used successfully for the computation of energies together with a LDA expression for the potential V_{xc} . Moreover, the geometrical structures are not significantly improved by GGA potentials [11, 56, 70, 71, 72]. Therefore one can think of forgetting the necessity to satisfy Eq. (7) and one could reasonably expect that accurate calculations of energies and molecular structures could be obtained using "senior" GGAs like Be88/P86, Be88/LYP or PW91/PW91 exchange-correlation couples of functionals for the energy [14, 73, 22, 8], together with V_x functional satisfying the asymptotic condition (in the E_{xc} labels, the first acronym describes the exchange functional and the second one designates the correlation functional).

In order to investigate this point, we performed a series of calculations bearing on a subset of molecules constituting the G2 set [23] with various strategies:

- the form of the potential, namely:
 1. the use of the $V_x(B)$ potential with a correct asymptotic behaviour as parametrized in [44],

$$V_x(B) = V_x^{LDA} - 2\beta \sum_{\sigma} \rho_{\sigma}^{1/3} \frac{x_{\sigma}^2}{1 + 3\beta x_{\sigma} \sinh^{-1}(x_{\sigma})} \quad (12)$$

where the reduced gradient is $x_{\sigma} = \frac{|\nabla \rho_{\sigma}(\mathbf{r})|}{\rho_{\sigma}^{4/3}(\mathbf{r})}$ and β is a constant fitted on IP of atoms (σ is the spin label).

2. the use in some cases of the $V_x(PW)$ potential with a correct asymptotic behaviour as parametrized in [44],

$$V_x(PW91) = V_x^{LDA} - 2^{4/3} \sum_{\sigma} \rho_{\sigma}^{1/3} \frac{(a_2 - a_3 e^{-a_4 s_{\sigma}^2}) s_{\sigma}^2}{1 + a_2 b_2 s_{\sigma} \sinh^{-1}(a_1 s_{\sigma})} \quad (13)$$

where the inhomogeneity wavevector is $s_{\sigma} = \frac{|\nabla \rho_{\sigma}(\mathbf{r})|}{2k_F \rho_{\sigma}(\mathbf{r})}$, k_F is the Fermi vector $= (6\pi^2 \rho_{\sigma}(\mathbf{r}))^{1/3}$ and a_1 , a_2 , a_3 and a_4 are constants fitted on IP of atoms or kept equal to PW91's parametrisation of

the E_x exchange energy functional [8]. The constant b_2 is set to $\frac{3}{(3\pi)^{\frac{1}{3}}}$ in order to satisfy (11).

- the technique for calculating the exchange energy
 1. the calculation of the exchange energy via the virial formula [74], relating the exchange energy to its potential, as proposed by Lembarki *et al.* [44] and Neumann *et al.* [3].
 2. the calculation of the exchange energy through a “senior” GGA energy functional like Be88 or PW91(X).
 3. in some cases, some line integral have been performed, as did VLB [42], and similar trends were obtained.
- the choice of the code, which is related to the nature of the basis sets (*i.e.* STOs *vs* GTOs). No statistically significant deviation in the structures have been found between the results obtained with deMon and ADF codes, these codes exhibiting comparable computation times for the geometry optimisations.

Three kinds of properties will be discussed in the following: the geometry parameters deduced from geometry optimisations, the eigenvalues of the HOMOs, and the dipole moments.

5.1 Molecular geometries

The results, which are summarized in Tables 2 and 3 have to be split into geometries obtained by scans of the potential energy surfaces (PES), and those obtained through optimisation codes included in ADF or deMon packages.

1. It is very unsatisfactory to see that the geometrical structures obtained via standard geometry optimisations are generally worse than the LDA ones. Let us recall that the LDA underestimates 80% of the bond lengths of molecular systems, and overestimates only 10% of them. GGAs, which reduce the overestimated bond energies, increase the bond lengths in almost all the cases, leading to a small improvement of most of the 80% of the bond lengths, but, with a few exceptions, not for the 20% of the already correct or too long ones. The use of V_x with correct asymptotic behaviour leads to an overestimated weakening of the bonds, and consequently to rather erratic, often too long bond lengths.

From Table 2 one can see that strong deviations are obtained when the two LRC forms of exchange potential are used, whatever the nature of

Table 2: Bond lengths (pm) for selected molecules, as calculated with various functionals. Summary of results (deviations from experimental values) obtained for a subset of the G2 set of molecules. Geometries determined either through standard optimizations (opt) or PES scans (scan).

Functional and method	Average (absolute) deviation	Average relative deviation	comment
LRC(B) (opt) Equ.(12) ADF	52 (2.2)		31 molecules (reduced subset of 25 molecules)
LRC(B) (opt) Equ.(12) deMon	7		15 molecules average over 3 correlation funct.
LRC(PW) (opt) Equ.(13) deMon	70		13 molecules average over 3 correlation funct.
LDA (opt)	2.1	2.5%	
B3LYP		2.5%	literature data
LRC(B)(scan) Equ.(12) deMon	1.5	1%	15 molecules
LRC(PW)(scan) Equ.(13) deMon	3.5	4%	15 molecules

the correlation functional used in connection. The largest discrepancy stems from the bond angles which are even more erratic. From the data set reported in Tables 3 and 2 the average relative absolute deviations *w.r.t* experimental data amount 5 to 15 %, whereas it was only 2.5% for LDA.

We calculated also some molecular geometries with the exchange-correlation VLB potential functional, and similar trends can be observed, in agreement with Neuman *et al.*'s observations [3].

Table 3: Angles (degrees) for a subset of the G2 set of molecules (summary), as calculated with various functionals.

Functional and method†	Average deviation	Average absolute deviation	Average relative absol. deviation	comment
LRC(B) (opt) Equ.(12) ADF	0.9	5.9	1.1%	10 molecules
LRC(B) (opt) Equ.(12) deMon	1.0	10.0	2%	average 3 correl. functionals 6 molecules
LRC(PW) (opt) Equ.(13) deMon	1.2	16.	3%	average 3 correl. functionals 4 molecules
LDA (opt)	-1.6	2.3		
LRC(B)(scan) Equ.(12) deMon	0.5	1.2		3 molecules

† LRC(B)(scan) geometries determined through PES scans.

Therefore, one is tempted to conclude that the condition Eq. (10) should not be considered as most important, at least for the determination of molecular structures. Whereas it is now well accepted that GGAs for the E_{xc} functional is clearly superior to that of the LDA, this is less clear for the functional derivative of this functional, namely the exchange-correlation potential V_{xc} . Indeed, Neumann, Nobes and Handy came to the same conclusion on test cases they performed on 2 molecular systems, namely HF and NH_3 , with the VLB potential [3]. They underlined the fact that the VLB functional does not give good energies, could be related to the point that V_{xc} is not the exact functional derivative of the exchange-correlation energy, and this point will be discussed later on.

If one postulates that functionals with the correct asymptotic behaviour

are good for the description of regions far from the molecule nuclei, one has to admit that those which have been used here are incorrect in regions closer to the bonding domain, namely near the Van der Waals - Connolly surfaces, or/and in the core shells. Indeed, further work is necessary to assess such a conclusion.

2. However, in the second set of data, reporting scans of the PES for a limited set of small molecules, it appears that the geometries obtained are satisfactory. Moreover, the nature of the technique used for the determination of E_{xc} , namely the use of a "senior" E_{xc} functional, or the use of the virial theorem, as well as the use of a line integration (not reported here), leads to quite similar geometries. This point is in accord with a similar conclusion obtained by van Gisbergen *et al.* in their frequency-dependent polarizabilities [75]: they choose to use a "mixed scheme" where a different approximation for f_{xc} and V_{xc} were used, whereas f_{xc} is the functional derivative of the exchange-correlation potential V_{xc} , with respect to the time-dependent density. Indeed, although the geometries parameters look fine, they are not significantly improved towards the experimental values, relatively to the GGA values. Further calculations are still needed in order to give confidence intervals, since the basis sets choices may affect the accuracy.

5.2 Eigenvalues

Let us recall that the LRC potential, which is fitted on a panel of atomic IP, leads to good IP for most (if not any) atomic IPs. This is unfortunately not true anymore for the molecular systems for which a shift between experimental IPs and the eigenvalues spectrum remains [76]. This shift is definitely smaller than those of the LDA or other GGAs, but it is significantly larger than for atoms. Indeed, it corresponds to an overcorrection with respect to the LDA, and this could be related to a proportionally smaller importance of low density domains in molecules than in atoms. This overcorrection was also noticed by Casida with the VLB potential [77].

5.3 Dipole moments

It is well known that the dipole moment is an electronic property which is very sensitive to the quality of the theoretical approach used, so that, for example, only trends can be discussed from results issued from semi-empirical calculations. Therefore, an other measure of the efficiency of the V_x potential

is given by the accuracy of the dipole moment calculated with the corresponding density; for sake of comparison, calculations have to be performed at the same reference geometry as, for instance the experimental one. Table 4 summarizes the deviations (with respect to experimental values) obtained at both the self-consistently optimised geometries and the experimental geometries, in regard to the dipole moments calculated within the LDA approximation.

Table 4: Dipole moments (debye) for selected molecules, as calculated with various functionals for a subset of the G2 set of molecules (summary).

Functional and method†	Average absolute deviation	Average relative deviation	comment
LRC(B) (opt) Equ.(12) ADF	0.23	25%	11 molecules
LRC(B) (opt) Equ.(12) deMon	0.32		average of 3 correl. funct. 5 molecules
LRC(PW) (opt) Equ.(13) deMon	0.98		average of 3 correl. funct. 5 molecules
LDA (opt)	0.085	13%	
LRC(B)(exp) Equ.(12)	0.15	27%	10 molecules
ADF	0.12	6%	subset of 9 molecules

† LRC(exp) = calculation with LRC densities calculated at experimental geometries.

† LRC (opt) = calculation with LRC densities calculated at LRC optimised geometries.

It appears that the results obtained at the experimental geometries are not far from the results obtained at the LDA level of approximation, whereas the dipole moments determined at the optimised geometries are definitely worse, underlining the lack of accuracy in the standard geometry optimisations. Indeed, these preliminary conclusions need the completion of statistics bearing on a larger number of molecules. Casida [78] lead to similar conclusions with the VLB potential, obtaining dipole moments generally

comparable to, and sometimes worse than, dipole moments calculated with the LDA. The relatively small incidence of the V_{xc} exchange-correlation potential in the KS equations for the determination of properties like the dipole moment has already been pointed out in different problems. For instance, Wesolowski found similar trends in the Kohn-Sham with constrained density (KSCED) method [79]: Let us recall that, in this approach, the electronic system is divided in two parts, one of them is just a frozen density, whereas the second part is described by KS orbitals in presence of the frozen density [80]. These orbitals obey to KS-like equations in which the Hamiltonian contains supplementary terms, in particular the functional derivative of the non-additive kinetic energy with respect to the density. Wesolowski *et al.* showed recently that the choice of the kinetic energy functional is important in an accurate description of hydrogen-bonded systems (kinetic energy functionals with GGAs form being the best), in particular for the bonding energy and the equilibrium distance [79, 81]. However the dipole moment was shown to be rather insensitive to the choice of the kinetic energy functional used for the description of the non-additive kinetic energy term [79].

5.4 Other properties

We did not look at other properties, but it is worthwhile to mention the work performed by Casida *et al.* with the time dependent DFT formalism for the determination of polarizabilities and excitation energies within the linear response approach, both properties being very sensitive to the large r behavior of the exchange-correlation potential [78]. They made use of the VLB functional and obtained a strong improvement of the polarizabilities over the LDA, although they observed also an overcorrection of LDA *vs* experiment [82].

6 Concluding remarks

Although the set of studied molecules was strongly limited, it is worth noting that molecules involving only σ bonds look rather better described than molecules involving π bonds. It is interesting to underline that this qualitative classification was already true, but less pronounced, for GGAs [83]. Let us recall that systems like cumulenes are unsatisfactorily described by GGAs [84]. We can conjecture that all systems for which π orbitals, and more generally orbitals with nodal planes or nodal surfaces playing an important role in the electronic structure, are badly described by pure DFT functionals. This means that the self-interaction correction which is described only

to a small extent via gradient terms, is more poorly taken into account for these π orbitals than for others. One is lead to conclude that this is directly connected to a weak description of the shell structure of atomic or molecular systems.

The third generation of density functionals [11, 12], tries to improve the deficiency of GGAs by at least three different approaches:

- the use of explicitly self-interaction corrected functionals, for which the price to pay is to handle orbital-dependent functionals. We will refer to Gross *et al.*'s work in this area [85, 86], which uses the Krieger, Li and Iafrate approximation [87, 88], and to Goedecker and Umrigar's recent work [89]. It is interesting to note these authors found better atomic properties, but worse geometries of small molecules.
- the introduction of a part of pure exchange part in the V_x exchange potential, as proposed by Becke in 1993 [90]. Such use of an hybrid functional is now widely used through the functionals called B3xxx in Gaussian code [91] and (misleadingly) adiabatic connection method (ACM) in MSI softwares [72]. The interesting point is that the amount of correlation, optimised by Becke with the Perdew-Wang 91 correlation functional [92], which does not fulfill the same scaling conditions as PW91, as discussed in section 2. This is a consequence of the short range of the correlation, which lets the geometry of molecules to be driven by the exchange functional. In a recent paper, Ernzerhof, Perdew and Burke [15] underlined the fact that the part of pure exchange in hybrid functionals is not universal, and should amount 0.25 or more. This amount should be higher for π systems, and even higher for strongly inhomogeneous systems like hydrogen-only compounds. For these last ones, we showed recently that an amount of *ca.* 45% of pure exchange is the best [93]. Anyhow, the just discussed weakness of GGAs in the description of multiple bonds, *i.e.* of π orbitals, is strikingly improved by the use of hybrid functionals [94].
- A somewhat different and promising approach has been proposed recently by Gritsenko, van Leeuwen and Baerends [95]. These authors decomposed the potential into the Slater potential v_S and the response to density variations v_{resp} . They showed that the latter exhibits the peaks which reflect the atomic shell structure which is poorly described by usual GGAs potentials. The potential they proposed possesses correct asymptotic and scaling properties. Although there is still room for improvements, it would be worthwhile to see how molecular properties

can be described with densities calculated using this potential. Work in this direction looks promising [96].

In conclusion, the obtention of molecular structures by the use of an exchange potential possessing the correct asymptotic behaviour has not yet lead to the expected accuracy, and a large room for improvement exists. We have shown that the use of functionals especially designed for recovering the ionisation energy as the HOMO energy (as they should) does not lead to molecular structures sufficiently accurate. Since one remembers that usual DFT assumes a continuous spectrum of eigenvalues, the so-called gap problem is directly connected to the failure of the attempt to build a V_{xc} starting from Eq. (10). In finite systems like molecules, V_{xc} should be shifted by a constant which is directly related to the gap value, or in molecular terms, to the HOMO-LUMO energy differences (i.e. to the hardness). At a first glance, this would preclude a simple use of an universal explicit formula for V_{xc} , since the HOMO-LUMO energy gap should not be given as an input of a first principle calculation. However this hindrance could be turned round by the use of the linear response of the exchange pair-correlation function to density variations as proposed recently by Gritsenko *et al.* [95, 96, 97]. Moreover, in a documented review, Casida [78] showed that the ionisation threshold in time dependent DF response theory depends on the asymptotic behavior of V_{xc} , and is related to the treatment of fractional particle numbers in the E_{xc} energy functional. He gave a detailed survey of the status of the present exchange-correlation potentials for time dependent DF response theory.

However, if one sticks to the type of functional discussed here, it appears that the geometry optimizations may lead to rather good structures, provided the geometry optimizer does not make use of gradients. This has been seen on Table 2 for diatomics, and also for a few molecules for which the geometry optimization has been performed step by step. One knows that standard calculations of analytical derivatives of the exchange-correlation integrals assume that V_{xc} is the true functional derivative of E_{xc} . The results summarized in this work have shown that geometry optimisations conducted through standard, gradient-conjugated-like, optimisers included in deMon or ADF codes lead to erratic structures, pointing out the necessity to handle an energy functional which is closely related to the potential functional. On the contrary, the inclusion of an optimiser like the simplex algorithm, which does not make use of energy derivatives [98] should give satisfactory results, although less efficient for the computer time point of view.

Acknowledgments

Mark Casida, Mel Levy and Andreas Savin are acknowledged for stimulating discussions and helpful comments on the manuscript.

References

- [1] J.P. Perdew, K. Burke, *Int. J. Quant. Chem.*, **57**, 309 (1996).
- [2] M. Levy, J.P. Perdew, *Int. J. Quant. Chem.*, **49**, 539, (1994).
- [3] R. Neumann, R.H. Nobes and N.C. Handy, *Mol. Phys.*, **87**, 1 (1996).
- [4] J.P. Perdew, K. Burke, Y. Wang, *Phys. Rev. B* **54**, 16533 (1996).
- [5] M. Levy, in *Density Functional Theory*, E.K.U. Gross, R.M. Dreizler, eds. Plenum, New-York, (1995) 11.
- [6] M. Levy, J.P. Perdew, *Phys Rev. B* **48**, 11638 (1993).
- [7] R.O. Jones, O. Gunnarson, *Rev. Mod. Phys.* **61**, 689 (1989).
- [8] J.P. Perdew, in "Electronic Structure of Solids'91", Eds.; P. Ziesche and H. Eschrig, (Academic Verlag, Berlin, 1991).
- [9] W. Kohn and L. J. Sham, *Phys. Rev. A* **140**, 1133 (1965).
- [10] N. H. March, *Phys. Rev. A* **36**, 5077 (1987).
- [11] T. Ziegler, *Can. J. Chem.*, **73**, 743 (1995).
- [12] H. Chermette, *L'Actualité Chimique (Paris)* **7**, 10 (1996).
- [13] C. Umrigar, X. Gonze, *High Performance Computing and its Application to the Physical Sciences, Proceedings of the Mardi Gras 1993 Conference*, ed D.A. Browne *et al.*, World Scientific, Singapore, 1993).
- [14] A. D. Becke, *Phys. Rev. A* **38**, 3098 (1988).
- [15] M. Ernzerhof, J.P. Perdew and K. Burke, *Density Functional methods in Chemistry*, eds. B.B. laird, R. Ross and T. Ziegler, American Chemical Society Symposium Series (1996).
- [16] M. Ernzerhof, J.P. Perdew and K. Burke, in *Density Functional Theory*, eds. R. Nalewajski, Springer, Berlin (1996).

- [17] M. Ernzerhof, J.P. Perdew and K. Burke, in *Recent Developments in Density Functional Theory, Theoretical and Computational Chemistry*, J.M. Seminario ed., Elsevier, Amsterdam (1997).
- [18] J.P. Perdew, K. Burke and M. Ernzerhof, *Phys. Rev. Lett.* **77**, 3865 (1996).
- [19] B.G. Johnson, P.M.W. Gill and J.A. Pople, *J. Chem. Phys.*, **98**, 5612 (1993).
- [20] P.M.W. Gill, *Mol. Phys.*, **89**, 433 (1996).
- [21] P. A. Stewart, P.M.W. Gill, *J. Chem Soc. Trans.*, **91**, 4337 (1995).
- [22] C. Lee, W. Yang and R.G. Parr, *Phys. Rev.* **B37**, 785 (1988).
- [23] L.A. Curtiss, K. Raghavachari, G.W. Trucks and J.A. Pople, *J. Chem. Phys.*, **94**, 7221 (1991).
- [24] E. Engel, J.A. Chevary, L.D. MacDonald, S.H. Vosko, *Phys. Rev. B* **46**, 6671 (1992).
- [25] C.J. Umrigar, X. Gonze, *Phys. Rev. A*, **50**, 3827 (1994).
- [26] E.I. Proynov, A. Vela and D.R. Salahub, *Chem. Phys. letters*, **230**, 419 (1994).
- [27] E.I. Proynov, E. Ruiz, E. Vela, D. R. Salahub, *Int. J. Quant. Chem.* **S29**, 61 (1995).
- [28] H. Guo, S. Sirois, E.I. Proynov and D.R. Salahub, in "Theory of Hydrogen Bonds", John Wiley, in press (1997).
- [29] D.R. Salahub, R. Fournier, P. Mlynarski, I. Papai, A. StAmant, J. Ushio, in "Density Functional in Chemistry", J.K. Labanowski and J. Andzelm, eds, Springer-Verlag, 77 (1991).
- [30] A. Goursot, I. Papai and C.A. Daul, *Int. J. of Quantum Chem.*, **52**, 799 (1994).
- [31] A. D. Becke, *J. Phys. Chem.*, **88**, 2547 (1988).
- [32] A. D. Becke, R.M. Dickson, *J. Phys. Chem.*, **89**, 2993 (1988).
- [33] A. D. Becke, R.M. Dickson, *J. Phys. Chem.*, **92**, 3610 (1990).
- [34] A. G orling, M. Levy, *Int. J. Quant. Chem.*, **29**, 93 (1994).

- [35] A. G. Orling, M. Levy, Phys. Rev. A **50**, 196 (1995).
- [36] C. Filippi, C.J. Umrigar, X. Gonze, Phys. Rev. A **54**, 4810 (1996).
- [37] M. Levy, J.P. Perdew, V. Sahni, Phys. Rev. A **30**, 2745 (1984).
- [38] C.O. Almbladh, U. von Barth, Phys. Rev. B **31**, 3231 (1985).
- [39] J.P. Perdew, R.G. Parr, M. Levy and J.L. Balduz, Phys. Rev. Lett. **49**, 1691 (1982).
- [40] E.J. Baerends, V. Branchadell, M. Sodupe, Chem. Phys. Lett., **265**, 481 (1997).
- [41] V. Russier, Phys. Rev. B **45**, 8894 (1992).
- [42] R. van Leeuwen, E.J. Baerends, Phys. Rev. A **49**, 2421 (1994).
- [43] R. van Leeuwen, E.J. Baerends, Phys. Rev. A **51**, 170 (1995).
- [44] A. Lembarki, F. Rogemond and H. Chermette, Phys. Rev. A **52**, 3704 (1995).
- [45] H. Przybylski, G. Borstel, Sol. State Comm., **49**, 317 (1984); **52**, 713 (1984).
- [46] J.A. Alonso, L.A. Girifalco, Phys. Rev. B, **17**, 3735 (1978).
- [47] O. Gunnarson, M. Jonson, B.I. Lundqvist, Phys. Rev. B, **20**, 3136 (1979).
- [48] O. Gritsenko, N.A. Cordero, A. Rubio, L.C. Balbas, J.A. Alonso, Phys. Rev. A, **48**, 4197 (1993).
- [49] J. Charlesworth, Phys. Rev. B, **53**, 12667 (1996).
- [50] P. J  mmer, P.J. Knowles, Phys. Rev. A **51**, 3575 (1995).
- [51] R. Santamaria, Int. J. Quant. Chem. **61**, 891 (1997).
- [52] A. StAmant, th  se, Universit   de Montreal, (1991).
- [53] B. teVelde, E.J. Baerends, J. Comp. Physics, **99**, 84 (1992).
- [54] E.J. Baerends, D.E. Ellis, P. Ros, Chem. Phys., **2**, 41 (1993).
- [55] Amsterdam Density Functional, Theoretical Chemistry, Vrije Universiteit, Amsterdam, The Netherlands (1995).

- [56] V. Barone, J. Chem. Phys., **101**, 6834 (1994); *ibid* **102**, 384 (1994).
- [57] V. Barone, L. Orlandini, C. Adamo, J. Phys. Chem., **98**, 13185 (1994).
- [58] N. Godbout, D. R. Salahub, J. Andzelm and E. Wimmer, Can. J. Chem. **70**, 750 (1992).
- [59] A. D. Becke, J. Phys. Chem., **85**, 7184 (1986).
- [60] A. D. Becke, J. Phys. Chem., **84**, 4524 (1986).
- [61] J.P. Perdew and Y. Wang, Phys. Rev. **B33**, 8800 (1986).
- [62] D.J. Lacks, R.G. Gordon, Phys. Rev. A **47**, 4681 (1993).
- [63] A.E. dePristo, J.D. Kress, J. Chem. Phys., **86** 1425 (1987).
- [64] L.C. Wilson, M. Levy, **B41**, 12930 (1990).
- [65] A. D. Becke, M.E. Roussel, Phys. Rev. A **39**, 3761 (1989).
- [66] J.P. Perdew, J.A. Chevary, S.H. Vosko, K.A. Jackson, M.R. Pederson, D.J. Singh, C. Fiolhais, Z. Phys. D **23**, 7 (1992).
- [67] E.I. Proynov and D.R. Salahub, Int. J. of Quantum Chem., **49**, 67 (1994).
- [68] E.I. Proynov and D.R. Salahub, Phys. Rev. **B49**, 7874 (1994).
- [69] A.D. Becke, J. Chem. Phys. **104**, 1040 (1996).
- [70] R. G. Parr and W. Yang, "Density-Functional Theory of Atoms and Molecules", (Oxford University Press, 1989).
- [71] L. Fan, T. Ziegler, J. Chem. Phys. **94**, 6057 (1991).
- [72] C. Lee, G. Fitzgerald, W. Yang, J. Chem. Phys. **98**, 2971 (1993).
- [73] J.P. Perdew, Phys. Rev., **B33**, 8822 (1986), erratum **38**, 7406 (1986).
- [74] M. Levy, J.P. Perdew, Phys. Rev. **A32**, 2010 (1985).
- [75] S.J.A. van Gisbergen, V.P. Osinga, O. Gritsenko, R. van Leeuwen, J.G. Snijders, E.J. Baerends, J. Phys. Chem., **105**, 3142 (1996).
- [76] H. Chermette, unpublished.
- [77] M.E. Casida, private communication.

- [78] M.E. Casida, in *Recent Developments and Applications of Modern Density Functional Theory*, J.M. Seminario ed., Elsevier, Amsterdam, 391 (1996).
- [79] T.A. Wesolowski, *J. Chem. Phys.* **106**, 8516 (1997).
- [80] T.A. Wesolowski, A. Warshel, *J. Phys. Chem.* **97**, 8050 (1993).
- [81] T.A. Wesolowski, H. Chermette, J. Weber, *J. Chem. Phys.* **105**, 9182 (1996).
- [82] C. Jamorski, M.E. Casida, D.R. Salahub, *J. Chem. Phys.* **104**, 5134 (1997).
- [83] P.M.W. Gill, B.G. Johnson, J.A. Pople, *Chem. Phys. Lett.*, **197**, 499 (1992).
- [84] D.A. Plattner, K.N. Houk, *J. Am. Chem. Soc.*, **117**, 4405 (1995).
- [85] T. Grabo, E.K.U. Gross, *Chem. Phys. Lett.*, **240**, 141 (1995).
- [86] E.K.U. Gross, M. Petersilka, T. Grabo, *Density Functional methods in Chemistry*, eds. B.B. Laird, R. Ross and T. Ziegler, American Chemical Society Symposium Series (1996).
- [87] J.B. Krieger, Y. Li, G.J. Iafrate, *Density Functional theory*, edited by E.K.U. Gross and R.M. Dreizler, Plenum Press, New York (1995).
- [88] J.B. Krieger, Y. Li, G.J. Iafrate, *Phys. Rev. B*, **46**, 5453 (1992).
- [89] S. Goedecker, C.J. Umrigar, *Phys. Rev. A* **55**, 1765 (1997).
- [90] A.D. Becke, *J. Chem. Phys.* **98**, 5648 (1993).
- [91] GAUSSIAN 94 (Revision B.3), M.J. Frisch, G.W. Trucks, H.B. Schlegel, P.M.W. Gill, M.A. Robb, J.R. Cheeseman, T.A. Keith, G.A. Petersson, J.A. Montgomery, K. Raghavachari, M.A. Al-Laham, V. G. Zakrzewski, J.V. Ortiz, J.B. Foresman, J. Cioslowski, B.B. Stefanov, A. Nanayakkara, M. Challacombe, C.Y. Peng, P. Y. Ayala, W. Chen, M.W. Wong, J.L. Andres, G. Johnson, E. S. Replogle, R. Gomperts, R.L. Martin, D.J. Fox, J.S. Binkley, D.J. Defrees, J. Baker, J.P. Stewart, M. Head-Gordon, C. Gonzalez, and J.A. Pople, Gaussian, Inc., Pittsburgh PA, 1995.
- [92] V. Barone, *Chem. Phys. Lett.*, **233**, 129 (1995).

- [93] H. Chermette, H. Razafinjanahary, L. Carrion, *J. Chem. Phys.*, to appear (1997).
- [94] W. Kohn, A.D. Becke, R.G. Parr, *J. Phys. Chem.* **100**, 12974 (1996).
- [95] O. Gritsenko, R. van Leeuwen, E.J. Baerends, *Int. J. Quant. Chem.* **57**, 17 (1995).
- [96] O. Gritsenko, R. van Leeuwen, E. van Lenthe, E.J. Baerends, *Phys. Rev. A* **51**, 1944 (1995).
- [97] O. Gritsenko, E.J. Baerends, *Phys. Rev. A* **54**, 1957 (1996).
- [98] J.A. Nelder, R. Mead, *Comp. J.*, **7**, 308 (1965).

Auxiliary Field Representation of Fermion Kinetic Energy Density Functional *

J. K. Percus

Courant Institute of Mathematical Sciences
and Physics Department
New York University, New York, N.Y.

The kinetic energy, or thermodynamic potential, of a non-interacting Fermion system, as a functional of the non-uniform density pattern evoked by an external potential, serves as a crucial tool in the analysis of interacting system ground states. Examples from classical lattice gas and continuum fluid theory are cited to show that analytic tractability can be dramatically enhanced by the introduction of auxiliary density fields with respect to which a suitable thermodynamic potential is stationary. This strategy is developed for the prototype of one-dimensional spinless Fermions, resulting in an exact highly overcomplete representation. A semi-classical variational ansatz recovers the familiar Thomas-Fermi plus renormalized Weiszacker expression, as well as leading corrections, and a simple extension creates a simple modification of the former. The corresponding 3-dimensional format is set up, and evaluated by extrapolation from the 1-dimensional case.

1 Introduction

It is hardly necessary to discourse on the importance of determining the structure of many-electron systems. If one focuses on molecules and adopts a Born-Oppenheimer viewpoint¹, it is often sufficient to analyze the ground state of such a system, and this will be our domain of interest. To this end, the density functional approach² has become an increasingly effective tool. What we want to do is to obtain information on the structural characteristics of valid density functionals in order to more reliably construct the parametrized empirical

*Following presentation at Density Functional International Conference, Curie Institute, Paris 1995

models that seem the most useful practical computational tools. For this purpose, we will confine our attention to non-interacting spinless Fermions with Newtonian kinetic energy. The crucial simplification is that of no interaction, and even this assumes significance in the Kohn-Sham version³ of approximate density functionals, or in the Hubbard-Stratonovich⁴ representation. However, our aim is rather that of understanding how the physical underpinning is manifested in the final structural form.

The vehicle we employ is that of overcomplete description, in which the electron density, the independent function of density functional theory, is augmented by a set of auxiliary functions with respect to which the system (free) energy is stationary. Primitive lattice gases and one-dimensional classical fluids are first used to indicate the genesis of such descriptions. The one-dimensional free Fermion ground state kinetic energy (in an external field) is then decomposed into auxiliary field contributions in preparation for the overcomplete description, two versions of which are presented in a general form and verified. An explicit computation of the component free energies is carried out, in which form a literal decomposition into Weiszacker and Thomas-Fermi contributions is observed. Applications of the WKB approximation to the whole set of auxiliary fields results in one approximate variational expression for the kinetic energy involving only the density, and others with an auxiliary coarse-grained density. Some details are discussed, and a leading extrapolation made to the 3-dimensional domain.

2 Background

A simple fluid in thermal equilibrium, at its most primitive level of description, is characterized by a particle density $n(r)$ controlled by an applied external potential $u(r)$. In the grand ensemble, it is only the combination

$$\mu(r) = \mu - u(r), \quad (2.1)$$

where μ is the imposed chemical potential, that appears. Here, r denotes a point in the full physical space, but if the fluid is not simple, it must be expanded to include additional degrees of freedom. The system properties are succinctly expressed by $\Omega[\mu(r)]$, the grand potential, as a concave functional (strictly concave, we assume) of the local chemical potential $\mu(r)$. In particular, the density profile is given by

$$n(r) = -\delta\Omega[\mu]/\delta\mu(r), \quad (2.2)$$

with higher functional derivatives bringing in higher distribution functions. Near a thermodynamic singularity, Ω is very sensitive to change in $\mu(r)$, and a

more robust “inverse” formulation is preferable which turns out as well to be that in which almost all explicitly solvable model systems assume their solvable forms. The inverse formulation depends upon the fact that at given profile $\{n(r)\}$, not only is (2.2) reproduced by the stationary principle

$$\delta \left(\Omega[\mu] + \int n(r)\mu(r)dr \right) = 0, \quad (2.3)$$

but also the concavity of the expression varied shows that it is a maximum, and the maximizing $\{\mu(r)\}$ is uniquely determined by $\{n(r)\}$,

$$\mu(r) = \mu[r; n]. \quad (2.4)$$

Thus, we can switch to $n(r)$ as independent function, and introduce the Legendre transformation

$$\bar{F}[n] = \Omega[\mu[r; n]] + \int n(r)\mu(r; n)dr. \quad (2.5)$$

Since $\bar{F} = \Omega + N\mu - \int n(r)u(r)dr$, \bar{F} is identified as the intrinsic (Helmholtz) free energy, i.e. the free energy with external field energy subtracted out.

From $\delta\bar{F} = \delta\Omega + \int \mu\delta n + \int n\delta\mu = \int \mu\delta n$, we have the inverse profile relation

$$\mu(r) = \delta\bar{F}[n]/\delta n(r). \quad (2.6)$$

It follows that $\delta^2\bar{F}/\delta n(r)\delta n(r') = \delta\mu(r)/\delta n(r') = (\delta n/\delta\mu)^{-1}(r, r') = -(\delta^2\Omega/\delta\mu\delta\mu)^{-1}(r, r')$, so that \bar{F} is convex in $\{n(r)\}$. Thus, (2.6), written as

$$\delta\Omega = 0 \quad (2.7)$$

$$\text{where} \quad \Omega[n] = \bar{F}[n] - \int \mu(r)n(r)dr,$$

is in fact a minimum principle. The “traditional” format (2.6, 2.7) requires the functional $\bar{F}[n]$ which, unfortunately, can rarely be exhibited explicitly for systems of interest. Under these circumstances, an expansion of the concept of explicit solvability may be preferable to poorly controlled perturbation expansions or empirical modifications. This entails the introduction of auxiliary, nominally independent, variables $\{C_\alpha\}$ or fields $\{C_\alpha(r)\}$, often but not necessarily of global or collective origin, in terms of which the profile relation at fixed C ,

$$\mu(r) = \delta\bar{\bar{F}}[n, C]/\delta n(r)|_C \quad (2.8)$$

is valid, and $\bar{\bar{F}}[n, C]$ is explicit. The utility of (2.6) arises from a readily proven formal theorem⁵ which we quote for the case of auxiliary fields:

If (2.6) is valid, then there exists (not uniquely) a functional $\Delta[C]$ of the $\{C_\alpha\}$ alone such that on defining

$$\bar{F}[n, C] = \bar{\bar{F}}[n, C] + \Delta[C], \quad (2.9)$$

one has

$$\begin{aligned} \mu(r) &= \delta \bar{F}[n, C] / \delta n(r)|_C \\ 0 &= \delta \bar{F}[n, C] / \delta C_\alpha(r)|_n. \end{aligned} \quad (2.10)$$

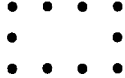
The second of (2.10) allows one to solve for $C_\alpha[r; n]$, and we then have

$$\bar{F}[n] = \bar{F}[n, C[n]]. \quad (2.11)$$

Although the convexity of $\bar{F}[n, C]$ is not guaranteed, one does have the very concise

$$\delta \left(\bar{F}[n, C] - \int \mu(r) n(r) dr \right) = 0 \quad (2.12)$$

for all variations of $\{n\}$ and $\{C\}$.

Ex 1.  A classical lattice gas on a ring, in thermal equilibrium

at reciprocal temperature β , with next neighbor exclusion as the only site to site interaction⁶. Because of the presence of an interaction loop, there is no local formulation for the free energy of this system (as there would be for an open interval or any simply connected lattice), but instead one finds that with the single additional “collective” amplitude C , and

$$\begin{aligned} \beta \bar{\bar{F}}[n, C] &= \sum_x \left[\left(C - \frac{1}{2} + n_x \right) \ln \left(C - \frac{1}{2} + n_x \right) \right. \\ &\quad \left. + \left(C + \frac{1}{2} - n_x \right) \ln \left(C + \frac{1}{2} - n_x \right) \right. \\ &\quad \left. - (1 - n_{x-1} - n_x) \ln (1 - n_{x-1} - n_x) \right], \end{aligned} \quad (2.13)$$

the discrete version of (2.6) is satisfied. Furthermore, setting

$$\beta \Delta(C) = \left(C + \frac{1}{2} \right) \ln \left(C + \frac{1}{2} \right) - \left(C - \frac{1}{2} \right) \ln \left(C - \frac{1}{2} \right), \quad (2.14)$$

the system behavior is fully determined by (2.10). A similar conclusion is reached for a lattice of arbitrary connectivity, with $\Delta[C, K]$ now depending upon a C_α for each chain of 2-coordinated sites, and a K_x for each site of higher coordination number, but of course explicit expressions are available only in special cases.

Ex 2. A classical one-dimensional continuum fluid with next neighbor interaction⁷ $\varphi(x, y)$ and corresponding one-sided Boltzmann factor

$$e(x, y) = e^{-\beta\varphi(x, y)} \theta(y - x), \quad (2.15)$$

where θ is the Heaviside step function. Now, two auxiliary fields are required, ω and v , in terms of which

$$\beta\bar{F}[n, \omega, v] = \int n(x)(\ln n(x) - 1 + \beta v(x))dx. \quad (2.16)$$

Here, $\mu(x) = \delta\bar{F}/\delta n(x)$ implies $n(x) = \exp \beta(\mu(x) - v(x))$, identifying $v(x)$ as the effective potential field seen by equivalent ideal gas particles. The field ω enters via

$$\beta\Delta[\omega, v] = \beta \int \omega(x)dx + \int \int e^{-\frac{\beta}{2}v(x)} e^{-\frac{\beta}{2}v(y)} e^{-\beta \int_y^x \omega(t)dt} e^{-1}(x, y) dy dx, \quad (2.17)$$

and we find without difficulty that $\Omega = \int \omega(x)dx$, so that $\omega(x)$ plays the role of specific grand potential.

3 Free Fermions, General

Now we turn to the topic of interest, that of the ground state of a many - Fermion system represented by a grand ensemble at chemical potential μ . The appropriate Rayleigh-Ritz principle for such a system is

$$\Omega = \text{Min}_\Psi \left(\langle \Psi | T | \Psi \rangle + \langle \Psi | \Phi | \Psi \rangle - \int \mu(r)n(r)dr \right) \quad (3.1)$$

where Ψ is the normalized second quantized wave function, T the kinetic energy operator, Φ the internal interaction, $n(r) = \langle \Psi | \sum \delta(r - r_j) | \Psi \rangle = \langle \Psi | \psi^\dagger(r)\psi(r) | \Psi \rangle$, and $\mu(r)$ is the local chemical potential, as in (2.1). Despite the grand ensemble context, the number operator $\hat{N} = \int \hat{n}(r)dr = \int \psi^\dagger(r)\psi(r)dr$ is concentrated on only one integer value for almost all choices of μ , except those for which μ becomes the excitation energy on adding a particle, and then N has contributions from both integers. The resulting highly involved

structure of $\Omega[\mu]$ is rarely mirrored in approximation methods. Conversion of (3.1) to a density functional formalism is in principle routine⁸. One defines the minimizing wave function at fixed $\{n(r)\}$:

$$\begin{aligned} & \langle \Psi | T | \Psi \rangle + \langle \Psi | \Phi | \Psi \rangle = \min, \\ \text{subject to } \{n(r)\} &= \left\langle \Psi \left| \sum \delta(r - r_j) \right| \Psi \right\rangle, \text{ at } \Psi = \Psi[n], \end{aligned} \quad (3.2)$$

in terms of which (3.1) assumes the form

$$\begin{aligned} \Omega &= \text{Min}_{\{n\}} \left(\bar{F}[n] - \int \mu(r) n(r) dr \right) \\ \text{where } \bar{F}[n] &= \langle \Psi[n] | T | \Psi[n] \rangle + \langle \Psi[n] | \Phi | \Psi[n] \rangle. \end{aligned} \quad (3.3)$$

$\bar{F}[n]$ is the intrinsic free energy (here simply the intrinsic energy because the entropic contribution TS vanishes at $T = 0$) that we have met before, and carries with it all of the standard consequences.

In one version of the familiar approach of Kohn and Sham, we define

$$T[n] = \text{Min}_{\Psi | \{\langle \Psi | \hat{n}(r) | \Psi \rangle = n(r)\}} \langle \Psi | T | \Psi \rangle, \quad (3.4a)$$

and then

$$\bar{F}[n] = T[n] + \frac{1}{2} \iint \varphi(r, r') n(r) n(r') dr dr' + \Psi_{xc}[n] \quad (3.4b)$$

where

$$\begin{aligned} \Phi_{xc}[n] &= \text{Min}_{\Psi | \{\langle \Psi | \hat{n}(r) | \Psi \rangle = n(r)\}} \langle \Psi | T + \Phi | \Psi \rangle \\ &- \text{Min}_{\Psi | \{\langle \Psi | \hat{n}(r) | \Psi \rangle = n(r)\}} \langle \Psi | T | \Psi \rangle - \frac{1}{2} \iint \varphi(r, r') n(r) n(r') dr dr'. \end{aligned} \quad (3.4c)$$

The exchange-correlation functional $\Phi_{xc}(n)$ is estimated by one of many semi-empirical recipes. A major problem, then, and the one we devote our attention to, is that of determining $T[n]$, the intrinsic free energy of a non-interacting Fermion system. Let us be explicit. We ignore spin and set units so that $\hbar = 2m = 1$, with Newtonian kinetic energy. Then the system ground state is constructed by filling up all energy levels of $H_1 = u(r) - \nabla^2$ until the Fermi energy μ , together with anti-symmetry. For the one-body density matrix γ of the system, one simply adds the one-body density matrices of the orbitals thereby occupied, yielding in operator form

$$\gamma = \theta(\mu(r) + \nabla^2). \quad (3.5)$$

Consequently, the particle density is given by

$$n(r) = \langle r | \theta(\mu(r) + \nabla^2) | r \rangle, \quad (3.6)$$

which we recognize as $n(r) = -\delta\Omega/\delta\mu(r)$, where

$$\Omega = -\text{Tr}((\mu + \nabla^2)\theta(\mu + \nabla^2)). \quad (3.7)$$

To complete the description, we Legendre transform to $\bar{F} = \Omega + \int \mu(r)n(r)dr = \text{Tr}(-(\mu + \nabla^2)\theta(\mu + \nabla^2)) + \mu\theta(\mu + \nabla^2) = -\text{Tr} \nabla \cdot \theta(\mu + \nabla^2)\nabla$, so that

$$\bar{F} = \int -\langle r | \nabla \cdot \theta(\mu + \nabla^2) \nabla | r \rangle dr, \quad (3.8)$$

which is of course the kinetic energy.

Our objective is to express \bar{F} of (3.8) in terms of $n(r)$ of (3.6), if necessary via a controllable set of auxiliary fields. To start this process, we introduce the auxiliary fields, arranged to contribute independently to both \bar{F} and $n(r)$. This is accomplished through the complex contour integral representation

$$\theta(\mu) = \oint \frac{1}{\mu + \nu} \frac{d\nu}{2\pi i}, \quad (3.9)$$

where O encircles the negative real axis counterclockwise:

$$O: \quad \begin{aligned} \text{Im}(\nu) < 0 \text{ for } \nu: -i\epsilon - \infty \rightarrow 0 \\ \text{Im}(\nu) > 0 \text{ for } \nu: 0 \rightarrow i\epsilon - \infty, \end{aligned} \quad (3.10)$$

but in fact can close about any point below the lowest spectral value of μ . We will act as if there are no problems associated with interchanges of operations when this representation is used; this is true in one-dimension, but will require a minor modification in 3 dimensions. Now we can write

$$n(r) = \oint n_\nu(r) d\nu / 2\pi i \text{ where } n_\nu(r) = \langle r | (\mu + \nu + \nabla^2)^{-1} | r \rangle. \quad (3.11)$$

At fixed ν , evaluating the logarithm according to the cut real axis, so that $\text{Im} \ln \nu > 0$ for $\text{Im} \nu > 0$, we have

$$\begin{aligned} n_\nu(r) &= \frac{\delta}{\delta\mu(r)} \text{Tr} \ln(\mu + \nu + \nabla^2) \\ &= -\delta\Omega_\nu / \delta\mu(r) \end{aligned} \quad (3.12)$$

$$\text{where } \Omega_\nu = -\text{Tr} \ln(\mu + \nu + \nabla^2),$$

and the corresponding Legendre transform free energy $\bar{F}_\nu[n_\nu] = \Omega_\nu + \int n_\nu(r)\mu(r)dr$ is

$$\bar{F}_\nu[n_\nu] = \text{Tr}[\mu(\mu + \nu + \nabla^2)^{-1} - \ln(\mu + \nu + \nabla^2)], \quad (3.13)$$

in terms of which

$$\mu(r) = \delta \bar{F}_\nu[n_\nu] / \delta n_\nu(r). \quad (3.14)$$

To conclude at this level, we observe that, as expected, not only does the density decompose, but also $\oint \bar{F}_\nu d\nu / 2\pi i = \text{Tr}[\mu\theta(\mu + \nabla^2) - (\mu + \nabla)\theta(\mu + \nabla^2)] = -\text{Tr} \nabla \cdot \theta(\mu + \nabla^2)\nabla = \bar{F}$. It follows from (3.14) that

$$\begin{aligned} \text{If } \hat{F}\{n_\gamma\} &= \oint \bar{F}_\nu[n_\nu] d\nu / 2\pi i \\ \text{then } \mu(r) &= 2\pi i \delta \hat{F}\{n_\gamma\} / \delta n_\sigma(r) \text{ for any } \sigma \\ &\text{and } \hat{F}\{n_\gamma[n]\} = \bar{F}[n]. \end{aligned} \quad (3.15)$$

Here n_γ is a functional of n by virtue of μ being a functional of n .

4 Extended Generating Functionals

It will develop that $\bar{F}_\nu[n_\nu]$ of (3.13) can be found exactly for one-dimensional systems, and in suggestive approximations otherwise. But this does not solve the problem of finding explicitly suitable thermodynamic potentials to generate the relation between $\{\mu(r)\}$ and $\{n(r)\}$, with auxiliary fields appended as needed. Overcomplete representations are far from unique, but at least two of these arise very simply. The first is in the context of the grand potential, and starts with the observation that if we define

$$\Omega[\mu; n] = \bar{F}[n] - \int n(r)\mu(r)dr, \quad (4.1)$$

then $\{n\}$ serves to extend the chemical potential space $\{\mu\}$, and we have the trivial overcomplete variational principle

$$\begin{aligned} n(r) &= -\delta\Omega[\mu, n] / \delta\mu(r)|_n \\ 0 &= \delta\Omega[\mu, n] / \delta n(r)|_\mu. \end{aligned} \quad (4.2)$$

Now the supplementary space $\{n\}$ can be replaced by the larger supplementary space $\{n_\nu\}$, with $n = \oint \bar{F}_\nu d\nu / 2\pi i$ and $\bar{F} = \oint \bar{F}_\nu[n_\nu] d\nu / 2\pi i$ to yield

$$\Omega[\mu, \{n_\nu\}] = \oint \bar{F}_\nu[n_\nu] d\nu / 2\pi i - \int \oint n_\nu(r)\mu(r) d\nu / 2\pi i dr, \quad (4.3)$$

and then indeed we have

$$\begin{aligned} n(r) &= -\delta\Omega[\mu, \{n_\nu\}] / \delta\mu(r)|_{\{n_\nu\}} \\ 0 &= \delta\Omega[\mu, \{n_\nu\}] / \delta n_\nu(r)|_\mu. \end{aligned} \quad (4.4)$$

Thus the problem in practice is to devise a sufficiently accurate parametrized ansatz $\{n_\nu[\rho]\}$ for the set $\{n_\nu\}$ that the resulting $\Omega[\mu, \rho]$ leads to feasible solution.

On the other hand, a free energy functional of the same genesis can be obtained. One way of doing so entails the elimination of μ from the (2.5) - derived

$$\bar{F}[\mu, n, \{n_\nu\}] = \hat{F}\{n_\nu\} + \int \oint \left(\frac{n(r)}{\oint n_\nu(r) \frac{d\nu}{2\pi i}} - 1 \right) n_\nu(r) \mu(r) \frac{d\nu}{2\pi i} dr, \quad (4.5)$$

most easily as

$$\bar{F}[n, \{n_\nu\}] = \hat{F}\{n_\nu\} + \int \left(\frac{n(r)}{\oint n_\nu(r) \frac{d\nu}{2\pi i}} - 1 \right) \oint n_\nu(r) \frac{\delta \hat{F}\{n_\nu\}}{\delta n_\nu(r)} d\nu dr. \quad (4.6)$$

Since $\Delta(r) = n(r)/\oint n_\nu(r) d\nu/2\pi i - 1$ vanishes in the stationary configuration, it can be replaced in (4.6) by any function with which it agrees through first order:

$$\bar{F}[n, \{n_\nu\}] = \hat{F}\{n_\nu\} + \int W \left(\frac{n(r)}{\oint n_\nu(r) \frac{d\nu}{2\pi i}} \right) \oint n_\nu(r) \frac{\delta \hat{F}\{n_\nu\}}{\delta n_\nu(r)} d\nu dr, \quad (4.7)$$

where $W(1) = 0, W'(1) = 1$.

A special choice of W will quickly guarantee the equivalence of the stationarity of (4.3) and (4.7). In condensed notation,

$$\bar{F} = \hat{F} + \int W(\xi(r)) Q_r \hat{F} dr \text{ where } Q_r = \oint n_\nu(r) \delta / \delta n_\nu(r), \quad (4.8)$$

but $Q_{r'} \bar{F} = 0$ now becomes $0 = Q_{r'} \hat{F} + \int W(\xi(r)) Q_{r'} Q_r \hat{F} dr - \xi(r') W'(\xi(r')) Q_{r'} \hat{F}$,
or

$$(\xi(r') W'(\xi(r')) - 1) Q_{r'} \hat{F} = \int W(\xi(r)) Q_r dr Q_{r'} \hat{F}. \quad (4.9)$$

Hence if $K(r', r) = Q_{r'} Q_r \hat{F}$ is non-singular, the choice $W(\xi) = \ln \xi$ implies $W(\xi) = 0$, or $n(r) = \oint n_\nu(r) d\nu/2\pi i$. Furthermore, if this is the case, then $\delta \bar{F} / \delta n_\sigma(r) = 0$ becomes

$$\delta \hat{F} / \delta n_\sigma(r) = \frac{1}{n(r)} \oint n_\nu(r) \delta \hat{F} / \delta n_\nu(r) d\nu / 2\pi i \text{ for any } \sigma, \quad (4.10)$$

and the remaining $\mu(r) = \delta \bar{F} / \delta n(r) = \frac{1}{n(r)} \oint n_\nu(r) \delta F / \delta n_\nu(r) d\nu$ converts (4.10) to the full set of auxiliary profile relations

$$2\pi i \delta \hat{F}\{n_\nu\} / \delta n_\nu(r) = \mu(r). \quad (4.11)$$

We therefore have the second overcomplete representation

$$\bar{F}[n, \{n_\nu\}] = \oint \bar{F}_\nu[n_\nu] \frac{d\nu}{2\pi i} + \int \ln \frac{n(r)}{\oint n_\nu(r) \frac{d\nu}{2\pi i}} \oint n_\nu(r) \frac{\delta \bar{F}_\nu[n_\nu]}{\delta n_\nu(r)} \frac{d\nu}{2\pi i} dr. \quad (4.12)$$

While (4.3) and (4.12) are of course equivalent, this equivalence does not extend to the consequences of a parametrized variational ansatz for the set $\{n_\nu(r)\}$, since (4.12) will no longer imply that $n(r) = \oint n_\nu(r) d\nu / 2\pi i$. We will point out this distinction in the sequel.

5 $\hat{F}\{n_\nu\}$ in One Dimension

Even the one-dimensional problem is not trivial, but it is also not difficult. We want to establish the density functional structure accompanying

$$n_\nu(x) = \langle x | (\mu_\nu(x) + d^2)^{-1} | x \rangle \text{ where } \mu_\nu(x) = \mu(x) + \nu, \quad d \equiv d/dx. \quad (5.1)$$

For this purpose, we introduce the corresponding Green's function

$$G_\nu(x, y) = \langle x | (\mu_\nu + d^2)^{-1} | y \rangle. \quad (5.2)$$

In standard fashion⁹, if

$$\begin{aligned} (\mu_\nu + d^2) \varphi_\nu^+(x) &= 0, & \varphi_\nu^+(\infty) &= 0 \\ (\mu_\nu + d^2) \varphi_\nu^-(x) &= 0, & \varphi_\nu^-(-\infty) &= 0, \end{aligned} \quad (5.3)$$

then we have

$$\begin{aligned} W_\nu G_\nu(x, y) &= \varphi_\nu^+(x) \varphi_\nu^-(y) \theta(x - y) + \varphi_\nu^-(x) \varphi_\nu^+(y) \theta(y - x) \\ \text{where } W_\nu &= \varphi_\nu^{+'}(x) \varphi_\nu^-(x) - \varphi_\nu^{-'}(x) \varphi_\nu^+(x). \end{aligned} \quad (5.4)$$

The Wronskian W_ν is a constant, and we readily verify that, indeed, $\mu_\nu(x) G_\nu(x, y) + G_\nu''(x, y) = \delta(x - y)$.

It follows now that

$$\begin{aligned} n_\nu(x) &= \varphi_\nu^+(x) \varphi_\nu^-(x) / W_\nu \\ n'_\nu(x) &= (\varphi_\nu^{+'}(x) \varphi_\nu^-(x) + \varphi_\nu^{-'}(x) \varphi_\nu^+(x)) / W_\nu \\ n''_\nu(x) &= (2\varphi_\nu^{+'}(x) \varphi_\nu^{-'}(x) - 2\mu_\nu(x) \varphi_\nu^+(x) \varphi_\nu^-(x)) / W_\nu, \end{aligned} \quad (5.5)$$

from which φ^\pm can be eliminated to yield the profile equation

$$\mu_\nu(x) = \frac{1}{4} \frac{n'_\nu(x)^2 - 1}{n_\nu(x)^2} - \frac{1}{2} \frac{n''_\nu(x)}{n_\nu(x)}. \quad (5.6)$$

It is easily shown that $\mu(x) = 2\pi i \delta \widehat{F}\{n_\nu\} / \delta n_\nu(x)$ is derived from

$$\widehat{F}\{n_\nu\} = \int \oint \left[-\nu n_\nu(x) + \frac{1}{4} \frac{n'_\nu(x)^2 + 1}{n_\nu(x)} \right] \frac{d\nu}{2\pi i} dx, \quad (5.7)$$

and we see as well that

$$\oint n_\sigma(x) \delta \widehat{F}\{n_\nu\} / \delta n_\sigma(x) d\sigma = \oint \left[-\nu n_\nu(x) + \frac{1}{4} \frac{n'_\nu(x)^2 - 1}{n_\nu(x)} - \frac{1}{2} n''_\nu(x) \right] \frac{d\nu}{2\pi i}. \quad (5.8)$$

Thus, $\widehat{F}[n_\nu\{n_\nu\}]$ of (4.12) is fully determined.

Since the $n_\nu(x)$ are bound by a common $\mu(x)$, they must be related, and this relationship can now be found by computing $\dot{n}_\nu(x) \equiv \partial n_\nu(x) / \partial \nu = \frac{\partial}{\partial \nu} \langle x | (\mu_\nu + d^2)^{-1} | x \rangle = -\int \langle x | (\mu_\nu + d^2)^{-1} | y \rangle \langle y | (n_\nu + d^2)^{-1} | x \rangle dy = -\int G_\nu(x, y)^2 dy$. According to (5.4),

$$\begin{aligned} G_\nu(x, y) &= n_\nu(x)^{1/2} \mu_\nu(y)^{1/2} \left[\left(\frac{\varphi_\nu^+(x) \varphi_\nu^-(y)}{\varphi_\nu^-(x) \varphi_\nu^+(y)} \right)^{1/2} \theta(x - y) \right. \\ &\quad \left. + \left(\frac{\varphi_\nu^-(x) \varphi_\nu^+(y)}{\varphi_\nu^+(x) \varphi_\nu^-(y)} \right)^{1/2} \theta(y - x) \right], \end{aligned} \quad (5.9)$$

but from $1/n_\nu(x) = \varphi_\nu^{+'}(x)/\varphi_\nu^+(x) - \varphi_\nu^{-'}(x)/\varphi_\nu^-(x)$, we have $\ln(\varphi_\nu^+(x)/\varphi_\nu^-(x)) - \ln(\varphi_\nu^+(y)/\varphi_\nu^-(y)) = \int_y^x dz/n_\nu(z)$. Hence

$$G_\nu(x, y) = n_\nu(x)^{1/2} n_\nu(y)^{1/2} \left[e^{\frac{1}{2} \int_y^x dz/n_\nu(z)} \theta(x - y) + e^{\frac{1}{2} \int_x^y dz/n_\nu(z)} \theta(y - x) \right], \quad (5.10)$$

and it follows that

$$\dot{n}_\nu(x) = -n_\nu(x) \int n_\nu(y) e^{\int_y^x dz/n_\nu(z)} \operatorname{sgn}(x-y) dy. \quad (5.11)$$

This, in principle, allows all $n_\nu(x)$ to be obtained in terms of one of them.

6 Semi-Classical Viewpoint

Recapitulating, we have shown that the one-dimensional

$$\Omega[\mu, \{n_\nu\}] = \int \oint \left[-(\mu(x) + \nu)n_\nu(x) + \frac{1}{4} \frac{n'_\nu(x)^2 + 1}{n_\nu(x)} \right] \frac{d\nu}{2\pi i} dx \quad (6.1)$$

and

$$\begin{aligned} \bar{F}[n, \{n_\nu\}] = & \int \oint \left[-\nu n_\nu(x) + \frac{1}{4} \frac{n'_\nu(x)^2 + 1}{n_\nu(x)} \right] \frac{d\nu}{2\pi i} dx \\ & + \int \ln \left(\frac{n(x)}{\oint \frac{n_\sigma(x) d\sigma}{2\pi i}} \right) \oint \left[-\nu n_\nu(x) + \frac{1}{4} \frac{n'_\nu(x)^2 - 1}{n_\nu(x)} - \frac{1}{2} n''_\nu(x) \right] \frac{d\nu}{2\pi i} dx \end{aligned} \quad (6.2)$$

are valid grand potential and free energy in the respective expanded spaces $[\mu, \{n_\nu\}]$ and $[n, \{n_\nu\}]$ in the sense that

$$\begin{aligned} \delta(\Omega[\mu, \{n_\nu\}] + \int n(x)\mu(x)dx) &= 0 \\ \delta(\bar{F}[n, \{n_\nu\}] - \int n(x)\mu(x)dx) &= 0 \end{aligned} \quad (6.3)$$

for all variations in their respective spaces. With an uncountable set of auxiliary fields to be determined, these hardly seem to be practical tools. If the number of auxiliary fields could be reduced, perhaps to one, that would make more sense. In fact, we have seen in (5.11) that such a reduction to a single function is in principle possible, but it is unclear how to take advantage of this. A simpler but cruder method of parametrizing the $\{n_\nu\}$ by a single function is to use a semi-classical expansion to an appropriate order. In fact, we will start by observing that the semi-classical context enters our considerations in an unexpected and suggestive way as well.

Let us examine more closely the expression

$$\bar{F}_\nu[n_\nu] = \int \left(-\nu n_\nu(x) + \frac{1}{4} \frac{n'_\nu(x)^2}{n_\nu(x)} + \frac{1}{4} \frac{1}{n_\nu(x)} \right) dx \quad (6.4)$$

that gave rise to (6.1) and (6.2). The first term of course is due to the fact that the ν -component chemical potential is not μ but $\mu + \nu$. The second term is the Weiszacker or ideal gas kinetic energy¹⁰, present whenever a single particle wave function is relevant, due e.g. to low density or to a strong decoupling force; it therefore is given by $\int \psi'(x)^2 dx$, or since $n(x) = \psi(x)^2$, by

$$\bar{F}_\nu[n_\nu]_w = \frac{1}{4} \int \frac{n'_\nu(x)^2}{n_\nu(x)} dx. \quad (6.5)$$

To pick up the third term in (6.4), we instead evaluate $n_\nu(x) = \langle x | (\mu_\nu + d^2)^{-1} | x \rangle$ in semi-classical approximation¹¹. Since $\hbar = 1$ in our units, $dx dp / \hbar \rightarrow dx dp / 2\pi$, so that

$$\begin{aligned} n_\nu(x) &\simeq \frac{1}{2\pi} \int_{-\infty}^{\infty} (\mu_\nu(x) - p^2)^{-1} dp \\ &= \frac{1}{2i} \mu_{\nu+}(x)^{-1/2}, \end{aligned} \quad (6.6)$$

where $\mu_{\nu+}^{1/2}$ selects that square root for which $\text{Im } \mu_{\nu+}^{1/2} \geq 0$; hence

$$\mu(x) = -\nu - \frac{1}{4 n_\nu(x)^2}, \quad (6.7)$$

arising from the semi-classical free (kinetic) energy

$$\bar{F}_\nu[n_\nu]_{sc} = \int \left(-\nu n_\nu(x) + \frac{1}{4} \frac{1}{n_\nu(x)} \right) dx. \quad (6.8)$$

We see that the exact expression can be written as

$$\bar{F}_\nu[n_\nu] = \bar{F}_\nu[n_\nu]_w + \bar{F}_\nu[n_\nu]_{sc}. \quad (6.9)$$

The semi-classical density expression (6.6) is adequate for computing expectations of quantities varying slowly on the scale of local wavelength. It need not be adequate when non-linear combinations of n_ν and spatial derivatives are at issue. For this purpose, a more detailed semi-classical wave function analysis is required, or in the present context, a semi-classical analysis of (5.6) – dropping subscript ν for the moment –

$$\mu(x) = \frac{1}{4} \frac{n'(x)^2 - 1}{n(x)^2} = \frac{1}{2} \frac{n''(x)}{n(x)}. \quad (6.10)$$

Let us imagine that $\mu(x)$ is real, saving suitable modifications for later. We know that we will have to distinguish between the non-classical region $\mu(x) < 0$, in which $n(x)$ typically decays monotonically, and the classical region $\mu(x) > 0$, in which $n(x)$ oscillates. We also know from standard WKB or Airy function analysis that $n(x)$ will have an amplitude $\sim |\mu(x)|^{-1/2}$ with a phase argument going as $\int^x |\mu(x)|^{1/2} dx$.

Consider the non-classical case first, with turning point x_0 , $\mu(x_0) = 0$, and $x > x_0$. Set

$$n(x) = (-\mu(x))^{1/2} f \left(\int_{x_0}^x (-\mu(x))^{1/2} dx \right) \quad (6.11)$$

and neglect derivatives from $\mu'(x)$ on, so that

$$\begin{aligned} n'(x) &= f' \left(\int_{x_0}^x (-\mu(x))^{1/2} dx \right) \\ n''(x) &= (-\mu(x))^{1/2} f'' \left(\int_{x_0}^x (-\mu(x))^{1/2} dx \right); \end{aligned} \quad (6.12)$$

substituting into (6.10) gives the requirement

$$\frac{1}{2} \frac{f''(y)}{f(y)} - \frac{1}{4} \frac{f'(y)^2 - 1}{f(y)^2} = 1. \quad (6.13)$$

Multiplying by $f'(y)$, (6.13) integrates at once to yield

$$f'^2 = 1 + 4(f^2 - Kf), \quad (6.14)$$

with a non-diverging solution only at $K = 1$, and then

$$f(y) = \frac{1}{2}(1 + Ce^{-2y}), \quad (6.15)$$

C determined by WKB matching¹² with the classical domain; here then

$$n(x) = \frac{1}{2}(-\mu(x))^{-1/2} \left(1 + C \exp -2 \int_{x_0}^x (-\mu(x'))^{1/2} dx' \right) \quad (6.16)$$

in the non-classical region.

In the classical region, $\mu(x) > 0$, let us suppose that $\mu(x)$ is an even function of x , and similarly set

$$n(x) = \frac{1}{i} \mu(x)^{-1/2} f \left(\int_0^x \mu(x')^{1/2} dx \right). \quad (6.17)$$

Then $n' = 1/if'$, $n'' = 1/i\mu^{1/2}f''$ inserted into (6.10) yield

$$f' = 4fK - 1 - 4f^2, \quad (6.18)$$

with the corresponding even solution

$$n(x) = \frac{1}{2i} (\mu(x))^{-1/2} \left(K + \sqrt{K^2 - 1} \cos \left(2 \int_0^x \mu(x')^{1/2} dx \right) \right). \quad (6.19)$$

Eqs (6.16) and (6.19), with μ replaced by $\mu + \nu$, are then the true reference semi-classical forms.

7 Explicit Functionals

The art now is to adopt variational forms for the $n_\nu(x)$, with one or more functions as parameters, to produce explicit expressions for either of the generating functionals Ω or \bar{F} of (6.1) and (6.2), themselves only a small selection of available formalisms for the task. In all cases, a key role is played by the combination

$$\rho(x) = \oint n_\nu(x) d\nu / 2\pi i. \quad (7.1)$$

In the Ω formulation, this *is* the density $n(x)$; if $\{n_\nu(x)\}$ is parameterized by the single function $\rho(x)$, Ω then gives rise at once to the ordinary density functional $\bar{F}[n]$. In the \bar{F} formulation, $\rho(x)$ is not necessarily $n(x)$, the generating functional takes the form $\bar{F}[n, \rho]$ and corrections for the ansatz are automatically included. However, we can also impose the requirement that for a set of supplementary densities $\rho(x)$, $\{\rho_\alpha(x)\}$, the relation $n(x) = \rho(x)$ is guaranteed; this greatly restricts the class of acceptable $\Omega[n, \rho, \{\rho_\alpha\}]$ and is clearly to be carried out when feasible.

The equivalence of $\bar{F}[n, \{\rho_\alpha\}]$ and $\Omega[\mu, \rho, \{\rho_\alpha\}]$ can be guaranteed, as was that of (4.3) and (4.7). That is, if we write

$$\bar{F}[n, \rho, \{\rho_\alpha\}] = \hat{F}[\rho, \{\rho_\alpha\}] + \int \ln(n(x)/\rho(x)) \phi(x|\rho, \{\rho_\alpha\}) dx, \quad (7.2)$$

then under weak invertibility conditions, it suffices to have

$$\phi(x|\rho, \{\rho_\alpha\}) = \left(\rho(x) \frac{\delta}{\delta \rho(x)} + \sum_\alpha \rho_\alpha(x) \frac{\delta}{\delta \rho_\alpha(x)} \right) \hat{F}[\rho, \{\rho_\alpha\}]. \quad (7.3)$$

More restrictive, but perhaps more convenient, one can separate out “ideal gas” and excess contributions:

$$\begin{aligned} \hat{F}_{id}[\rho, \{\rho_\alpha\}] &= \int \oint \frac{1}{4} \left(\frac{n'_\nu(x)^2}{n_\nu(x)} \right) [\rho, \{\rho_\alpha\}] d\nu / 2\pi i dx \\ \hat{F}_{ex}[\rho, \{\rho_\alpha\}] &= \int \oint \left(-\nu n_\nu(x) + \frac{1}{4} \frac{1}{n_\nu(x)} \right) [\rho, \{\rho_\alpha\}] d\nu / 2\pi i dx \end{aligned} \quad (7.4)$$

and

$$\begin{aligned} \phi_{id}[x|\rho, \{\rho_\alpha\}] &= \oint \left(\frac{1}{4} \frac{n'_\nu(x)^2}{n_\nu(x)} - \frac{1}{2} n''_\nu(x) \right) [\rho, \{\rho_\alpha\}] d\nu / 2\pi i \\ &= \oint \left(\frac{1}{4} \frac{n'_\nu(x)^2}{n_\nu(x)} \right) [\rho, \{\rho_\alpha\}] d\nu / 2\pi i - \frac{1}{2} \rho''(x) \\ \phi_{ex}[x|\rho, \{\rho_\alpha\}] &= \oint \left(-\nu n_\nu(x) - \frac{1}{4} \frac{1}{n_\nu(x)} \right) [\rho, \{\rho_\alpha\}] d\nu / 2\pi i, \end{aligned} \quad (7.5)$$

where $f[\rho, \{\rho_\alpha\}]$ means that f has been expressed in terms of the set $\rho, \{\rho_\alpha\}$, and require (7.3) to hold for each part separately. In the special case in which the only supplementary density is $\rho(x)$ itself, (7.3) applied to ϕ_{id} says that

$$\text{if } W[x|\rho] = \oint \left(\frac{1}{4} \frac{n'_\nu(x)^2}{n_\nu(x)} \right) [\rho] d\nu / 2\pi i \nu, \quad (7.6)$$

$$\text{then } W[x|\rho] - \frac{1}{2} \rho''(x) = \rho(x) \delta / \delta \rho(x) \int W[y|\rho] dy.$$

It is readily verified that (7.6) has the solution

$$W[x|\rho] = \frac{1}{4} \rho'(x^2) / \rho(x), \quad (7.7)$$

and if this is satisfied, the remaining condition is that

$$\begin{aligned} & \oint \left(\nu n_\nu(x) - \frac{1}{4} \frac{1}{n_\nu(x)} \right) [\rho] d\nu / 2\pi i \\ &= \rho(x) \delta / \delta \rho(x) \int \oint \left(-\nu n_\nu(y) + \frac{1}{4} \frac{1}{n_\nu(y)} \right) [\rho] d\nu / 2\pi i dy. \end{aligned} \quad (7.8)$$

The simplest variational ansatz we can make is the narrowly semi-classical approximation of (6.6), with effective $\bar{\mu}(x)$:

$$n_\nu(x) = \frac{1}{2i} (\bar{\mu}(x) + \nu)^{-1/2}. \quad (7.9)$$

Here, if $\bar{\mu}(x) < 0$, the square root with $\text{Im}(\bar{\mu}(x) + \nu)^{1/2} \geq 0$ is continuous across the line $\text{Re}(\nu) \leq 0$, and so the contour integral (7.1) vanishes. If $\bar{\mu}(x) > 0$, this root reverses sign across the segment $-\bar{\mu}(x) \leq \text{Re}(\nu) \leq 0$, and so we find that

$$\rho(x) = \frac{1}{\pi} \bar{\mu}(x)^{1/2} \theta(\bar{\mu}(x)). \quad (7.10)$$

Consequently

$$n_\nu(x) = \frac{1}{2\pi} (\pi^2 \rho(x)^2 + \nu)^{-1/2} \quad (7.11)$$

will indeed satisfy (7.1). To complete the evaluation of \hat{F} and ϕ , we similarly integrate $\nu n_\nu(x)$, $1/n_\nu(x)$, and $n'_\nu(x)^2/n_\nu(x)$, taking advantage of the observation accompanying (3.10) to close the contour across $\nu = -\bar{\mu}(x) + \epsilon$; then $n_\nu(x)$ is analytic along the contour, with only the values $\pm(1/2i)\bar{\mu}(x)^{1/2}$ at the endpoints $\nu = 0 \pm i\epsilon$ to be used for the square root in the integration limits.

We therefore find

$$\begin{aligned}\oint \nu n_\nu(x) d\nu / 2\pi i &= -\frac{2}{3\pi} \bar{\mu}^{3/2} = -\frac{2\pi^2}{3} \rho(x)^3 \\ \oint 1/n_\nu(x) d\nu / 2\pi i &= -\frac{4}{3\pi} \bar{\mu}^{3/2} = -\frac{4\pi^2}{3} \rho(x)^3 \\ \oint n'_\nu(x)^2 / n_\nu(x) d\nu / 2\pi i &= -\frac{1}{3\pi} \bar{\mu}^2 \bar{\mu}^{-3/2} = -\frac{4}{3} \frac{\rho'(x)^2}{\rho(x)},\end{aligned}\quad (7.12)$$

giving rise to the components

$$\hat{F}_{id}[\rho] = \int -\frac{1}{3} \frac{\rho'(x)^2}{\rho(x)} dx, \quad \phi_{id}[x|\rho] = -\frac{1}{3} \frac{\rho'(x)^2}{\rho(x)} - \frac{1}{2} \rho''(x) \quad (7.13)$$

and

$$\hat{F}_{ex}[\rho] = \int \frac{\pi^2}{3} \rho(x)^3 dx, \quad \phi_{ex}[x|\rho] = \pi^2 \rho(x)^3 \quad (7.14)$$

\bar{F}_{ex} and ϕ_{ex} are indeed related by (7.3), but not \hat{F}_{id} and ϕ_{id} . If we now impose the required form (7.7) to replace (7.13), our conclusion is that

$$\bar{F}[n] = \int \left(\frac{\pi^2}{3} n(x)^3 + \frac{1}{4} \frac{n'(x)^2}{n(x)} \right) dx, \quad (7.15)$$

precisely the sum of one-dimensional Thomas-Fermi and Weiszacker terms.

Our derivation of (7.15) was of course very much ad hoc, since (7.7) did not arise from the ansatz (7.11). Clearly, a more realistic representation than (7.11) must be used. The simplest extension that can still be carried out without difficulty is the renormalized density expression

$$n_\nu(x) = \frac{\rho(x)}{2i\gamma(x)} (\pi^2 \gamma(x)^2 + \nu)^{-1/2}, \quad (7.16)$$

with two functional parameters, which would reduce to (7.11) in the special case $\gamma(x) = \rho(x)$. Proceeding precisely as in (7.12), we now find

$$\begin{aligned}\oint n_\nu(x) d\nu / 2\pi i &= \rho(x) \\ \oint 1/n_\nu(x) d\nu / 2\pi i &= -\frac{4}{3} \pi^2 \gamma(x)^4 / \rho(x) \\ \oint \nu n_\nu(x) d\nu / 2\pi i &= -\frac{2}{3} \pi^2 \gamma(x)^2 \rho(x) \\ \oint n'_\nu(x)^2 / n_\nu(x) d\nu / 2\pi i &= \rho(x) \left(\frac{\rho'(x)}{\rho(x)} - \frac{\gamma'(x)}{\gamma(x)} \right)^2 \\ &\quad + 2\rho(x) \left(\frac{\rho(x)}{\rho(x)} - \frac{\gamma(x)}{\gamma(x)} \right) \frac{\gamma'(x)}{\gamma(x)} - \frac{1}{3} \rho(x) \left(\frac{\gamma'(x)}{\gamma(x)} \right)^2.\end{aligned}\quad (7.17)$$

Hence, inserting into $\Omega[\mu, \rho, \gamma]$, we have

$$\begin{aligned} \bar{F}[n, \gamma] = & \int \frac{\pi^2}{3} \left(2n(x)\gamma(x)^2 - \frac{1}{n(x)}\gamma(x)^4 \right) dx \\ & + \int \left[\frac{1}{4}n'(x)^2/n(x) - \frac{1}{3}n(x) \left(\frac{\gamma'(x)}{\gamma(x)} \right)^2 \right] dx. \end{aligned} \quad (7.18)$$

We have now allowed enough functional leeway that it is not necessary to go to the formulation (4.12). For example, instead of varying over γ , just choose

$$\gamma(x) = \lambda n(x)^\alpha, \quad (7.19)$$

converting (7.18) to the simple

$$\begin{aligned} \bar{F}[n, \alpha, \lambda] = & \int \frac{\pi^2}{3} (2\lambda^2 n(x)^{1+2\alpha} - \lambda^4 n(x)^{4\alpha-1}) dx \\ & + \left(\frac{1}{4} - \frac{1}{3}\alpha^2 \right) \int \frac{n'(x)^2}{n(x)} dx, \end{aligned} \quad (7.20)$$

with a modified Thomas-Fermi energy and a reduced - coefficient Weiszacker term¹³. And then minimize with respect to λ :

$$\begin{aligned} \bar{F}[n, \alpha] = & \frac{\pi^2}{3} \left(\int n(x)^{1+2\alpha} dx \right)^2 / \int n(x)^{4\alpha-1} dx \\ & + \left(\frac{1}{4} - \frac{\alpha^2}{3} \right) \int n'(x)^2/n(x) dx, \end{aligned} \quad (7.21)$$

a non-linear version of the same.

8 Prospects

Even without taking advantage of the known detailed semi-classical structure, (6.16) and (6.19), and without making use of the correction procedure inherent in (6.2), the variational character of the basic grand potential expression (6.1) produces reasonable results at low cost. But the one-dimensional study is to be regarded mainly as a warm-up for the three-dimensional Fermion fluid of physical interest. In three-dimensions, the basic problem in the current formulation is that of finding the generating functional appropriate to $n_\nu(r)$. But a little care must be exercised, because the diagonal elements of a 3-dimensional Green's function diverge, i.e. integrating $(\mu_\nu(r) + \nabla^2)G(r, r') = \delta(r - r')$ over the sphere $|r - r'| \leq \epsilon$ tells us that $|\nabla G(r, r')| \sim 1/4\pi\epsilon^2$ at

$|r - r'| = \epsilon$, and hence that $|G(r, r')| \sim 1/4\pi\epsilon$. We will thus replace $n_\nu(r)$ of (3.11) by

$$n_\nu(r) = \langle r | (\mu + \nu + \nabla^2)^{-1} - (\nabla^2)^{-1} | r \rangle \quad (8.1)$$

since the additional term does not contribute to $n(r) = \oint n_\nu(r) d\nu/2\pi i$ but does eliminate the divergence.

Direct solution of (8.1) in the fashion of (5.6, 5.7) does not seem to be feasible, although expansions about a locally isotropic reference patterned after (5.6) can be carried out. Let us in this preliminary discussion note instead that a more elegant, but initially more poorly controlled alternative is to extrapolate the previously observed

$$\overline{F}_\nu[n_\nu] = \overline{F}_\nu[n_\nu]_w + \overline{F}_\nu[n_\nu]_{sc} \quad (8.2)$$

directly to 3-dimensions. The Weiszacker component is essentially unchanged:

$$\overline{F}_\nu[n_\nu]_w = \frac{1}{4} \int \frac{|\nabla n_\nu(r)|^2}{n_\nu(r)} d^3r. \quad (8.3)$$

For the semi-classical component, we translate (8.1) to $(1/2\pi)^3 \int [(\mu_\nu(r) - p^2)^{-1} + (p^2)^{-1}] 4\pi p^2 dp = \frac{1}{2\pi^2} \mu_\nu(r) \int dp/(\mu_\nu(r) - p^2)$, or

$$n_\nu(r) = \frac{1}{2\pi i} \mu_\nu(r)^{1/2} \quad (8.4)$$

for $\mu_\nu(r) > 0$. Hence $\mu_\nu(r) = -4\pi^2 n_\nu(r)^2$, or

$$\overline{F}_\nu[n_\nu]_{sc} = -\frac{4\pi^2}{3} \int n_\nu(r)^3 d^3r - \int \nu n_\nu(r) d^3r. \quad (8.5)$$

We conclude that the extrapolated 3D kinetic energy is given by

$$\widehat{F}\{n_\nu\} = \int \oint \left[-\nu n_\nu(r) + \frac{1}{4} \frac{|\nabla n_\nu(r)|^2}{n_\nu(r)} - \frac{4\pi^2}{3} n_\nu(r)^3 \right] d\nu/2\pi i d^3r. \quad (8.6)$$

Thereafter, the 1-dimensional technology can be taken over without essential change.

In summary then, we have shown that the construction of an exact density functional representation of one-dimensional Fermions with Newtonian kinetic energy can be carried out via the expansion of the control space to an infinite set of densities. The variational character of the formulation allows for the insertion of reasonable forms for the control fields, reducing their effective number to only a few. A very similar formulation has been proposed in three dimensions, whose utility is now under intense investigation.

References

- [1] See R. Car and M. Parrinello, "Unified Approach for Molecular Dynamics and Density-Functional Theory", *Phys. Rev. Lett.* 55, 2471 (1985) for a modern realization.
- [2] P. Hohenberg and W. Kohn, "Inhomogeneous Electron Gas", *Phys. Rev.* 136, B864 (1964).
- [3] W. Kohn and L.J. Sham, "Self-consistent Equations Including Exchange and Correlation Effects", *Phys. Rev.* 140, A1133 (1965).
- [4] J. Hubbard, *Phys. Rev. Lett.* 3, 77 (1959); R.L. Stratonovich, *Sov. Phys. Dokl.* 2, 416 (1958).
- [5] J.K. Percus and M.Q. Zhang, "One-dimensional Inhomogeneous Ising Model with Periodic Boundary Conditions", *Phys. Rev. B*, 11737 (1988).
- [6] J.K. Percus, "Interaction-driven Modification of Local Response", *Inverse Problems* 6, 789 (1990).
- [7] J.K. Percus, "Expanded Density Functionals", in "Density-Functional Theory", ed. Laird, Ross, Ziegler, ACS Symp. Series 629, 185 (1996).
- [8] J.K. Percus, "The Role of Model Systems in the Few-body Reduction of the N-Fermion Problem", *Int. J. Quantum Chem.* 13, 89 (1978).
M. Levy, "Universal Variational Functionals of Electron Densities", *Proc. Natl. Acad. Sci. USA* 76, 6062 (1979).
- [9] See e.g. R. Courant and D. Hilbert, "Methods of Mathematical Physics", p. 355 (Interscience Pub., 1953).
- [10] C.F. Von Weizsacker, "Zur theorie der kernmassen", *Z Physik* 96, 431 (1935).
- [11] E. Wigner, "On the Quantum Correction for Thermodynamic Equilibrium", *Phys. Rev.* 40, 749 (1932).
- [12] See e.g. L.I. Scheff, "Quantum Mechanics", see 28 (McGraw-Hill 1955).
- [13] See e.g. D.A. Kirzhnits, "Quantum Corrections to the Thomas-Fermi Equation", *Sov. Phys. JETP* 5, 64 (1957).

USING THE EXACT KOHN-SHAM EXCHANGE ENERGY
DENSITY FUNCTIONAL AND POTENTIAL TO STUDY
ERRORS INTRODUCED BY APPROXIMATE
CORRELATION FUNCTIONALS

Leonard Kleinman and D.M. Bylander
Department of Physics
University of Texas
Austin, Texas 78712-1081

ABSTRACT

We compare total atomic valence energies, total crystal energies, lattice constants, bulk moduli, and cohesive energies using several different Kohn-Sham exchange and correlation functionals with experimental values for Si and Ge. In particular, we have used the KLI approximation to the exact Kohn-Sham exchange potential together with different correlation functionals. The KLI approximation yields the exact Kohn-Sham exchange energy to one part in 10^5 allowing us to obtain accurate estimates of the errors arising from the correlation functionals.

1. INTRODUCTION

If one could know the exact exchange and correlation energy density functionals¹ along with their Kohn-Sham² potentials, one would have the exact many body solution for the ground state properties of any electronic system at hand. The exact exchange energy density functional is simply the expectation value of the Fock operator with Kohn-Sham (KS) eigenfunctions. Because the KS eigenfunctions are functionals of the charge density, so is the expectation value of the Fock operator. Although the functional dependence is unknown, the exchange energy may be evaluated directly from the KS eigenfunctions just as the KS kinetic energy is and just as the difference between the kinetic energy of Hartree Fock (HF) and KS eigenfunctions is included in the correlation energy, so is the difference between the exchange energy evaluated with HF and KS eigenfunctions.

In 1953, twelve years before the seminal paper² of Kohn-Sham, Sharp and Horton³ wrote down the integral equation for that multiplicative potential (which, unlike the HF potential, is the same for every electron) whose eigenfunctions minimize the expectation value of the HF Hamiltonian. This potential, subsequently called the optimized effective potential (OEP), is the exact KS potential for the HF equation because the exact KS potential for any density functional Hamiltonian is that multiplicative potential whose eigenfunctions minimize its expectation value.⁴ Apparently unaware of Sharp and Horton,³ Talman and Shadwick⁵ derived the OEP integral equation and solved it in one dimension, enabling them to perform atomic calculations. It was only very recently that Görling⁶ showed how to solve the OEP equation in three dimensions, making OEP energy band calculations possible. Krieger, Li, and Iafrate⁷⁻⁹ (KLI) had previously discovered an approximation to the OEP which makes energy band calculations straightforward and which is extremely accurate for total energy calculations but which may not yield a good approximation to the OEP energy bands.

It is well known that when exchange and correlation are treated on an equal footing as in the local density approximation (LDA) or generalized gradient approximation^{10,11} (GGA), their errors tend to cancel. It is the purpose of this work to treat exchange essentially exactly with the KLI approximation in order to examine the effect of LDA and GGA correlation on the four-fold ionization energy of Si and Ge and on the total energy, equilibrium lattice constant, bulk modulus, and cohesive energy of their crystals. We shall also see their effect on the energy bands although this is less meaningful since density functional theory does not yield excitation energies. We will also compare all these results with those obtained when both exchange and correlation are treated in the LDA or GGA.

2. KLI METHOD AND ATOMIC ENERGIES

The derivation of the OEP integral equation is straightforward and may be found in ref. 5 and in spin polarized form in refs. 8a and 12. By replacing an energy denominator with a constant which then dropped out of the integral equation, KLI were able to obtain an approximation to the OEP. They also obtained the KLI approximation in an entirely different manner; we now give a slight variation of that derivation.

In 1951 Slater¹³ obtained an average of the HF potential (in Ry atomic units)

$$v_{\text{HF}}^{i\sigma}(\mathbf{r}) = -2 \sum_{j=1}^{N_\sigma} \int \psi_{j\sigma}^*(\mathbf{r}') \psi_{i\sigma}(\mathbf{r}') |\mathbf{r} - \mathbf{r}'|^{-1} d\mathbf{r}' \psi_{j\sigma}(\mathbf{r}) / \psi_{i\sigma}(\mathbf{r}) \quad (1)$$

(where N_σ is the number of occupied states with spin σ) by weighting (1) with a factor $\psi_{i\sigma}^*(\mathbf{r}) \psi_{i\sigma}(\mathbf{r}) / \rho_\sigma(\mathbf{r})$ where $\rho_\sigma(\mathbf{r}) = \sum_i \psi_{i\sigma}^*(\mathbf{r}) \psi_{i\sigma}(\mathbf{r})$ to obtain what we¹⁴ have called the averaged Fock approximation (AFA) to distinguish it from other approximations of Slater. We have

$$V_{\text{AFA}}^\sigma(\mathbf{r}) = -2 \sum_{i,j=1}^{N_\sigma} \int \psi_{j\sigma}^*(\mathbf{r}') \psi_{i\sigma}(\mathbf{r}') |\mathbf{r} - \mathbf{r}'|^{-1} d\mathbf{r}' \psi_{j\sigma}(\mathbf{r}) \psi_{i\sigma}^*(\mathbf{r}) / \rho_\sigma(\mathbf{r}). \quad (2)$$

The KLI approximation is obtained by noting that $v_{\text{HF}}^{i\sigma}(\mathbf{r}) + C_{i\sigma}$, where $C_{i\sigma}$ is an arbitrary constant, also yields the $i\sigma$ HF eigenfunction, and then taking the Slater weighted average to obtain

$$V_{\text{KLI}}^\sigma(\mathbf{r}) = V_{\text{AFA}}^\sigma(\mathbf{r}) + \sum_{i=1}^{N_\sigma-1} C_{i\sigma} n_{i\sigma}(\mathbf{r}) / \rho_\sigma(\mathbf{r}) \quad (3)$$

where $n_{i\sigma}(\mathbf{r}) = \psi_{i\sigma}^*(\mathbf{r}) \psi_{i\sigma}(\mathbf{r})$. Because an i independent constant added to each of the $C_{i\sigma}$ has no effect on the \mathbf{r} dependence of V_{KLI}^σ , any relationship we find to optimize V_{KLI}^σ must leave the $C_{i\sigma}$ linearly related. Therefore one of them will remain arbitrary and so we have set $C_{N_\sigma\sigma} = 0$. We wish the eigenfunctions $\psi_{i\sigma}(\mathbf{r})$ of $V_{\text{KLI}}^\sigma(\mathbf{r})$ to closely resemble those of the $v_{\text{HF}}^{i\sigma}(\mathbf{r})$. If one takes $\langle \psi_{i\sigma} | V_{\text{KLI}}^\sigma | \psi_{i\sigma} \rangle = \langle \psi_{i\sigma} | v_{\text{HF}}^{i\sigma} + C_{i\sigma} | \psi_{i\sigma} \rangle$ or, in briefer notation $C_{i\sigma} = \bar{V}_{\text{KLI}}^i - \bar{v}_{\text{HF}}^{i\sigma}$ this will be the case. Substituting for $C_{i\sigma}$ in Eq. (3) we have

$$V_{\text{KLI}}^\sigma(\mathbf{r}) = V_{\text{AFA}}^\sigma(\mathbf{r}) + \sum_{i=1}^{N_\sigma-1} (\bar{V}_{\text{KLI}}^{i\sigma} - \bar{v}_{\text{HF}}^{i\sigma}) \hat{n}_{i\sigma}(\mathbf{r}) / \rho_\sigma(\mathbf{r}). \quad (4)$$

Because symmetry requires that degenerate states (other than accidental degeneracies) have the same $C_{i\sigma}$ to remain degenerate, the $n_{i\sigma}$ of those degenerate states have been added to give the $\hat{n}_{i\sigma}$ of which there are $\hat{N}_{i\sigma}$ in Eq. (4). Because $\hat{n}_{N_{\sigma}\sigma}$ is not included in the sum, $V_{KLI}^{\sigma}(\mathbf{r}) \rightarrow 0$ as $r \rightarrow \infty$. This choice of $C_{N_{\sigma}\sigma} = 0$ can also be shown^{8a,12} to cause the KLI potential in the local density approximation to be

$$V_{KLI}^{LDA} = -2 \left[\frac{6}{\pi} \rho_{\sigma}(\mathbf{r}) \right]^{\frac{1}{3}} = V_{KS}^{LDA} = \frac{2}{3} V_S^{LDA} \quad (6)$$

where the last two V 's are the Kohn-Sham² and Slater¹³ LDA. To obtain the $\bar{V}_{KLI}^{i\sigma}$ in Eq. (4) one multiplies Eq. (4) by $\hat{n}_j(\mathbf{r})$ and integrates over \mathbf{r} to obtain after a little algebra

$$\bar{V}_{KLI}^{j\sigma} - \bar{v}_{HF}^{j\sigma} = \sum_{k=1}^{\hat{N}_{\sigma}-1} [(D^{\sigma} - M^{\sigma})^{-1}]_{jk} D_{kk}^{\sigma} (\bar{V}_{AFA}^{k\sigma} - \bar{v}_{HF}^{k\sigma}) \quad (6)$$

where D^{σ} is a diagonal matrix of the degeneracies and

$$M_{jk}^{\sigma} = \int d\mathbf{r} \hat{n}_{j\sigma}(\mathbf{r}) \hat{n}_{k\sigma}(\mathbf{r}) / \rho_{\sigma}(\mathbf{r}). \quad (7)$$

It may be possible to avoid using a plane wave expansion when using the KLI potential in a crystal, but we do not advise it. Thus we here discuss the construction of our ionic pseudopotentials together with the calculation of the atomic total valence energies, i.e. minus the four-fold ionization energies of Si and Ge. We¹⁵ first performed an all electron Dirac atom calculation in which each electron sees a HF potential from the core electrons and an LDA exchange-correlation (xc) potential from the valence electrons where $v_{xc}^{val} = v_{xc}(\rho_{total}) - v_{xc}(\rho_{core})$. The core electrons are then taken to be rigid and the Dirac equation solved twice again, with the valence electrons seeing a HF potential from the core and either an LDAxc potential $v_{xc}^{val} = v_{xc}(\rho_{val})$ or KLI exchange plus LDA correlation among themselves. Because our valence electrons see a HF potential from the core, only the valence charge density enters a GGA calculation. Because $|\nabla \rho_{val}|/\rho_{val}$ becomes huge at the first node of the valence s functions, the GGA becomes unphysical and we must wait until we have a pseudopotential at which point we can apply the GGA to the pseudofunctions. (Very recently a simplified GGA has been obtained¹⁶ which can be applied when $|\nabla \rho_{val}|/\rho_{val}$ becomes huge.)

The four-fold ionization energies for these two full potential rigid core calculations are listed in the first row of Tables I and II. The relaxation

energy, obtained by calculating the difference between the total energy of the rigid and self-consistent ions is listed in the second row. This energy is almost identical in the atom and crystal and therefore will not contribute to the cohesive energy.¹⁷ In earlier work^{18,19} we took the KLI average of the total exchange seen by valence electrons, i.e. the sum over i in Eqs. (2) and (4) was over valence electrons whereas the j summation in (2) was over all electrons. However almost all of the difference with the earlier calculations can be attributed to using different LDA exchange and correlation functionals, which are now taken from ref. 11 where nonrelativistic exchange is employed.

The pseudofunctions are obtained by extending the large component of the Dirac eigenfunctions from some cutoff radius r_c back to $r = 0$ in a smooth and norm conserving manner. The pseudopotentials are obtained by inserting the pseudofunctions and their Dirac eigenvalues into the Schrödinger equation and inverting it. Then the ionic pseudopotential is obtained by subtracting off the contribution of the valence pseudofunctions to the atomic pseudopotential. There are two sources of error in pseudopotentials which are not usually discussed. One is that they are constructed to yield exact eigenvalues but do not yield correct total energies and the other is that they may not equal the true potential for $r > r_c$. When they overlap neighboring atoms in the crystal, these pseudopotential "tails" can cause substantial errors. They are usually negligible because the pseudofunctions are identical to the eigenfunctions for $r > r_c$ and have the same total charge for $r < r_c$. Thus the pseudo and true valence charge densities result in the same Coulomb potential for $r > r_c$ as long as they are spherical for $r < r_c$. The LDA or GGA xc potentials, being local, also are identical for $r > r_c$. Note however that the integrals in Eqs. (1), (4) and (7) depend upon whether true or pseudo wave functions are used and these integrals effect the KLI exchange potential due to the valence electrons for all r . Thus when the potential arising from the valence pseudo electrons is subtracted from the atomic pseudopotential, the ionic pseudopotential which is obtained differs from the true ionic potential for all r . We were able to reduce these pseudopotential tails to negligible size by using a method used by Rappe, *et al.*²⁰ to minimize $\int_Q^\infty q^2 |\hat{\varphi}(\mathbf{q})|^2 d\mathbf{q}$ where $\hat{\varphi}(\mathbf{q})$ is the fourier transform of a pseudofunction and the integral represents the momentum content of $\hat{\varphi}(\mathbf{r})$ above some cutoff Q . One writes $\hat{\varphi}_\ell(r) = \varphi_\ell(r) + \sum_k b_k j_\ell(kr)$ where $\varphi_\ell(r)$ is the original pseudofunction and the spherical Bessel functions $j_\ell(kr)$ vanish at r_c . The b_k are chosen to maintain the norm conservation and derivative continuity, and to minimize the momentum content and, in our case, the magnitude of the pseudopotential tail.

The third rows of Tables I and II list the valence electron total energies obtained from the pseudopotentials which have been spin-orbit averaged. The HF potential that the valence electrons see from the core electrons is subsumed into the pseudopotential and the xc potential that they see from themselves head the four columns: LDAxc, GGAXc and KLI exchange with LDA or GGA correlation. The fourth row lists the discrepancy Δ_{P_s} between the pseudo and full potential total valence energy calculations. In the LDAxc and GGAXc cases a particular choice of r_c causes the error to vanish (because of the discreteness of our integration mesh it does not exactly vanish). No matter what r_c was chosen Δ_{P_s} could not be made to vanish when we forced the KLI pseudopotential tails to be negligible. We previously found¹⁹ two pseudopotentials with different r_c 's gave atomic total energies differing by 19.0 mRy but their cohesive energies differed by only 0.9 mRy. Even if the atomic total energy error were made to vanish, one would expect the crystal total energy error to be at least that large because pseudopotentials created in one system are only approximately transferable to another. Thus we will assume the Δ_{P_s} for the crystal is identical to that calculated for the atom. One third of the spin-orbit splitting of the p -electrons obtained from the Dirac equation (shown in row 5) is the spin-orbit contribution to $-E(\uparrow\uparrow)$, the four-fold ionization energy of the spin polarized pseudoatom shown in row 6 with the core relaxation added and the pseudopotential energy error corrected.

We note for Si that gradient corrections to LDAxc increase the four-fold ionization energy but gradient corrections to the LDA correlation, when exchange is calculated essentially exactly, decrease the ionization energy. In both cases this causes the agreement with experiment to be quite good. For Ge the signs of the gradient corrections are as in Si and cause the GGAXc and KLI-GGA total energies to agree to better than one part in 10^5 but their agreement with experiment is only fair. Some or most of this error may be due to treating the Ge d electrons as core electrons. We did not include any core-valence correlation energy (other than core relaxation) in the calculation but an LDA estimate of its contribution shows it accounts for less than 25% of the error. The error is not a result of approximating the OEP with the KLI potential. We have compared KLI (with no correlation functional) and HF calculations and found the HF four-fold ionization energy to be only 0.18 and 0.20 mRy larger for Si and Ge. All-electron calculations⁹ indicate that only 25% of this arises from approximating the OEP with the KLI potential.

Table I. Four-fold ionization energy $-E_{\text{FP}}(j)$ of Si obtained from a rigid core full potential Dirac equation calculation. Δ_{Rlx} is the reduction of $E_{\text{FP}}(j)$ when the core relaxes. $-E(j)$ is the ionization energy obtained from a pseudopotential calculation and $\Delta_{\text{Ps}} = E_{\text{FP}}(j) - E(j)$. Δ_{SO} is the spin-orbit splitting obtained from a pseudopotential calculation. $-E(\uparrow\uparrow)$ is the ionization energy obtained from a pseudopotential calculation for parallel spin valence electrons and $-(E(\uparrow\uparrow) + \Delta_{\text{Rlx}} + \Delta_{\text{Ps}})$ is compared with experiment for four different exchange-correlation potentials. All energies are in Ry.

	LDAxc	GGAxc	KLI-LDA	KLI-GGA
$-E_{\text{FP}}(j)$	7.46411		7.63139	
Δ_{Rlx}	-0.00811	-0.00811	-0.00811	-0.00811
$-E(j)$	7.46404	7.51391	7.62361	7.50786
Δ_{Ps}	0.00007	0.00007	0.00778	0.00778
Δ_{SO}	0.00204	0.00211	0.00215	0.00216
$-(E(\uparrow\uparrow) + \Delta)$	7.50491	7.56250	7.66083	7.55534
$-E_{\text{EXP}}$	7.578	7.578	7.578	7.578

Table II. Same as Table I but for Ge.

	LDAxc	GGAxc	KLI-LDA	KLI-GGA
$-E_{\text{FP}}(j)$	7.44580		7.61273	
Δ_{Rlx}	-0.04524	-0.04524	-0.04524	-0.04524
$-E(j)$	7.44578	7.49694	7.60990	7.49337
Δ_{Ps}	0.00002	0.00002	0.00283	0.00283
Δ_{SO}	0.01172	0.01273	0.01218	0.01199
$-(E(\uparrow\uparrow) + \Delta)$	7.40447	7.45490	7.57155	7.45496
$-E_{\text{EXP}}$	7.624	7.624	7.624	7.624

3. GRADIENT CORRECTIONS IN CRYSTALS

We expanded our crystal pseudofunctions in all plane waves with $k^2 < 60$ Ry using a conjugate gradient scheme for solving the secular equation.²¹ This high cutoff was required because in the LDA case a small r_c was needed to obtain the correct atomic total energy and the reduction of the KLI pseudopotential tail increased the high k content of the pseudofunctions in that case. Convergence errors, determined by expanding the atomic pseudofunctions in spherical Bessel functions up to 60 Ry were 0.36 and 0.09 mRy for Si in the KLI-LDA and LDAxc cases while for Ge these were 0.16 and 0.17 mRy.

The most time consuming part of the calculation is the evaluation of V_{AFA}^σ because of the double sum in Eq.(2). Taking advantage of symmetry, one may restrict one of the \mathbf{k} 's to being one of the ten sampled in the irreducible wedge of the Brillouin zone (BZ) but the other is one of the 256 in the full BZ. With four bands at each \mathbf{k} , there are 40,960 integrals to be evaluated in every iteration toward self-consistency. The integrals can be simplified with the help of fast fourier transforms (FFT). Let $\psi_{i\sigma} = e^{-i\mathbf{k}_i \cdot \mathbf{r}} u_{i\sigma}(\mathbf{r})$ where $u_{i\sigma}(\mathbf{r})$ is a periodic function and let $\mathcal{F}_{ij}^\sigma(\mathbf{K})$ be the FFT of $u_{i\sigma}(\mathbf{r}') u_{j\sigma}^*(\mathbf{r}')$ in Eq. (2) which then becomes

$$V_{\text{AFA}}^\sigma(\mathbf{r}_1) = -2 \sum_{i,j,\mathbf{K}} \mathcal{F}_{ij}^\sigma(\mathbf{K}) \int e^{i(\mathbf{K}+\mathbf{k}_i-\mathbf{k}_j) \cdot \mathbf{r}_{12}} r_{12}^{-1} d\mathbf{r}_{12} u_{j\sigma}(\mathbf{r}_1) u_{i\sigma}(\mathbf{r}_1) / \rho_\sigma(\mathbf{r}_1) \quad (8)$$

where the \mathbf{K} are reciprocal lattice vectors. Performing the integration over r_{12}^{-1} yields a factor of $8\pi \mathcal{F}_{ij}^\sigma(\mathbf{K}) / |\mathbf{K} + \mathbf{k}_i - \mathbf{k}_j|^2$ and defining $\Gamma_{ij}^\sigma(\mathbf{r})$ to be its FFT yields

$$V_{\text{AFA}}^\sigma(\mathbf{r}) = \sum_{ij} \Gamma_{ij}^\sigma(\mathbf{r}) u_{j\sigma}(\mathbf{r}) u_{i\sigma}(\mathbf{r}) / \rho_\sigma(\mathbf{r}). \quad (9)$$

Note that the $\mathbf{k}_i = \mathbf{k}_j$ and $\mathbf{K} = 0$ contribution to $\Gamma_{ij}^\sigma(\mathbf{r})$ appears to be singular. However because of the orthonormality of the $\psi_{j\sigma}(\mathbf{r})$, $\mathcal{F}_{ij}^\sigma(0)$ vanishes when $\mathbf{k}_i = \mathbf{k}_j$ unless $i = j$. The BZ is sampled on a mesh of m \mathbf{k} -points. Each point represents all the \mathbf{k} 's in its proximity volume. Thus when $i = j$ and $\mathbf{K} = 0$, we average \mathbf{k}_j over a sphere with the proximity volume of \mathbf{k}_i to obtain a constant contribution of $-4(6/m\pi\Omega)^{\frac{1}{3}}$ where Ω is the unit cell volume. Because the $\hat{n}_{j\sigma}(\mathbf{r})$ contain contributions from all states degenerate with a state in the irreducible wedge of the BZ, the matrix M_{ij}^σ is 37×37 . There are two pairs of degenerate states sampled in the wedge, leaving 38 separate $\hat{n}_{j\sigma}$ of which that of the highest lying states is not included. Inserting Eq. (7) into (6) and Eqs. (6) and (9) into (4), we have $V_{\text{KLI}}^\sigma(\mathbf{r})$.

We calculated the total energy, self consistent to 2 μRy , for lattice constants differing from the experimental value in steps of one percent and fit two points on one side and one on the other of the energy minimum with the "universal" curve²² to obtain the total energy, equilibrium lattice constant, and bulk modulus for each of the four xc potentials. In the first row of Table III we list the total valence energy per atom for Si, including the relaxation energy and pseudopotential total energy error correction. The second row lists the equilibrium lattice constants and the third the bulk moduli. For Si our fits were all made at $0.99a_0^{\text{EXP}}$, a_0^{EXP} , and $1.01a_0^{\text{EXP}}$. For two of the cases a_0 is closer to $1.01a_0^{\text{EXP}}$ than to a_0^{EXP} so one could argue that $1.02a_0^{\text{EXP}}$ should replace $0.99a_0^{\text{EXP}}$ in their fit. E_0 is independent of which set of lattice

constants are used in the fit and the equilibrium lattice constant depends by no more than one in the last decimal place. The bulk moduli, however, are quite sensitive to the lattice points used in the fit (but less so than if the “universal” curve is replaced by a parabola). For example, if $1.02a_0^{\text{EXP}}$ is used in the GGAXc fit, the bulk modulus becomes $9.330 \times 10^{10} \text{ N/m}^2$. To obtain accurate numerical values for the bulk modulus at the calculated equilibrium lattice constant a_0 one should perform a second fit using a_0 , $0.99a_0$, and $1.01a_0$. Because the KLI calculations are very computationally intensive, this was not done. We note that, just as for the atomic energy, applying the GGA to LDAXc and KLI-LDA makes the larger numerical value smaller and the smaller one larger whether it be for E_0 , a_0 , or B. These changes are fairly small but note the changes in $E_{\text{coh}} = [E(\uparrow\uparrow) + \Delta] - [E_0 + \Delta]$. Adding GGA corrections to LDAXc decreases E_{coh} by 498 meV so that it is in near perfect agreement with experiment while adding them to KLI-LDA increases E_{coh} by 489 meV, reducing the error by 40% but still leaving it 731 meV below the experimental value. Although the GGA corrections had the same effect on the LDAXc and KLI-LDA results for Ge (in Table IV) as they did for Si, all the results save one are in much poorer agreement with experiment. The equilibrium lattice constants all have errors a factor of 2 or 3 times those of Si and were all obtained by fitting at a_0^{EXP} , $1.01a_0^{\text{EXP}}$, and $1.02a_0^{\text{EXP}}$. Nevertheless the largest error in a_0 is 1.57% which is not atypical. Whereas the GGAXc cohesive energy error for Si was only 12 meV, for Ge it is 653 meV. The only number in Table IV which is closer to experiment than the corresponding number in Table III is the KLI-GGA E_{coh} .

Band energies at symmetry points in the Brillouin zone are listed in Tables V and VI for Si and Ge. We see in every case, for both valence and conduction bands, that GGA corrections cause a lowering of the KLI levels and a raising of the LDAXc levels relative to the top of the valence band. We note that the Ge direct gap to $\Gamma_{2'}^c$, which was negative in our earlier LDA calculation,¹⁹ where the total (valence plus core) charge density was used to calculate the xc potential, is reasonably satisfactory in every case here, where the core presents a HF potential to the valence electrons. This is because the LDA exchange potential in the core is appropriate for core electrons and thus too strong for valence electrons. Furthermore the GGA corrections improve both the LDAXc and KLI-LDA results. The LDAXc indirect gap to L_1^c , although much improved over the old LDA result by the use of the HF core potential, is in pretty poor agreement with experiment. The addition of GGA corrections reduces the discrepancy by 30%. On the other hand, the excellent agreement of the KLI-LDA L_1^c gap with experiment is completely ruined by GGA corrections to the correlation potential. For Si the Γ_{15}^c direct

gap is in neither very good agreement with experiment nor very sensitive to the xc potential but the GGA corrections slightly improve the LDAxc and worsen the KLI-LDA agreement with experiment. The indirect gap at Δ_1^c is close to X_1^c where the GGA corrections improve the LDAxc and very severely worsen the KLI-LDA agreement with experiment.

Table III. Minus the total Si crystal valence electron energy per atom with relaxation energy and pseudopotential corrections included, along with the equilibrium lattice constant, bulk modulus, and cohesive energy calculated with four different exchange-correlation functionals (defined in the caption of Table I) are compared with experimental values. The experimental total energy is the sum of E_{coh} plus the four-fold ionization energy.

	LDAxc	GGAxc	KLI-LDA	KLI-GGA	EXP
$-(E_0 + \Delta)(\text{Ry})$	7.8827	7.9037	7.9115	7.8419	7.918
$a_0(\text{bohr})$	10.309	10.325	10.328	10.289	10.261
$B(10^{10}\text{N/m}^2)$	9.743	9.691	10.779	10.884	9.88
$E_{\text{coh}}(\text{eV})$	5.140	4.642	3.410	3.899	4.63

Table IV. Same as Table III except for Ge.

	LDAxc	GGAxc	KLI-LDA	KLI-GGA	EXP
$-(E_0 + \Delta)(\text{Ry})$	7.7633	7.7859	7.7785	7.7097	7.907
$a_0(\text{bohr})$	10.819	10.845	10.785	10.733	10.677
$B(10^{10}\text{N/m}^2)$	8.752	8.656	9.774	9.845	7.72
$E_{\text{coh}}(\text{eV})$	4.881	4.503	2.816	3.466	3.85

Table V. Band energies of Si calculated at the experimental lattice constant and compared with experimental values in eV. The column headings are defined in the caption of Table I.

	LDAxc	GGAxc	KLI-LDA	KLI-GGA	EXP
Γ_1^v	-12.186	-12.108	-12.050	-12.232	-12.5
$\Gamma_{25'}^v$	0	0	0	0	0
Γ_{15}^c	2.570	2.655	2.871	2.633	3.4
$\Gamma_{2'}^c$	3.176	3.275	3.738	3.474	4.2
X_1^v	-7.990	-7.940	-7.857	-7.981	
X_4^v	-2.951	-2.900	-2.864	-2.988	-2.9,-3.3 \pm 0.2
X_1^c	0.599	0.803	0.935	0.492	1.3
$L_{2'}^v$	-9.820	-9.771	-9.694	-9.818	-9.3 \pm 0.4
L_1^v	-7.152	-7.057	-6.997	-7.215	-6.7 \pm 0.2
$L_{3'}^v$	-1.246	-1.230	-1.200	-1.245	-1.2 \pm 0.2,-1.5
L_1^c	1.428	1.563	1.818	1.506	2.1,2.4 \pm 0.15
L_3^c	3.371	3.493	3.650	3.352	4.15 \pm 0.1

Table VI. Band energies of Ge (in eV) calculated at the experimental lattice constant and compared with experimental values. The column headings are defined in the caption of Table I. The experimental values have been spin-orbit averaged.

	LDAxc	GGAxc	KLI-LDA	KLI-GGA	EXP
Γ_1^v	-12.721	-12.661	-12.646	-12.788	-12.6 \pm 0.3
$\Gamma_{25'}^v$	0	0	0	0	0
$\Gamma_{2'}^c$	0.820	0.873	1.261	1.085	1.00
Γ_{15}^c	2.538	2.614	2.796	2.594	3.25 \pm 0.1
X_1^v	- 8.769	- 8.734	- 8.676	- 8.771	- 9.3 \pm 0.2
X_4^v	- 3.106	- 3.058	- 3.084	- 3.192	- 3.15 \pm 0.2
X_1^c	0.565	0.778	0.871	0.429	1.3 \pm 0.2
$L_{2'}^v$	-10.586	-10.551	-10.501	-10.597	-10.6 \pm 0.5
L_1^v	- 7.570	- 7.494	- 7.483	- 7.656	- 7.7 \pm 0.2
$L_{3'}^v$	- 1.395	- 1.381	- 1.383	- 1.421	- 1.4 \pm 0.2
L_1^c	0.424	0.552	0.772	0.477	0.84
L_3^c	3.607	3.730	3.869	3.584	4.3 \pm 0.2

4. CONCLUSIONS

Städele et al.²³ have recently reported the gaps to the conduction band minima at Γ , X and L in Si and Ge from a full OEP calculation with LDA correlation, but with a pseudopotential obtained from an LDA atom. They repeated their Si calculation using our KLI pseudopotential which reduced all of the gaps slightly.²⁴ For Si their Γ and X gaps are 3.25 and 1.49 eV which are larger than experiment and the L gap of 2.26 eV is slightly smaller. Their Ge gaps were quite sensitive to the choice of pseudopotential. Using our KLI pseudopotential, these gaps were all larger than experiment but were not quite converged in that they used fewer plane waves than they did for Si. Assuming that the effect of replacing LDA correlation with GGA is similar to that which we found for KLI calculations, the OEP gaps will not be in good agreement with experiment but still will be in much better agreement than LDAxc or GGAXc calculations and also better than our KLI calculations.

Because the exact KS eigenvalues do not represent excitation energies, the OEP with the exact KS correlation potential will not yield correct energy gaps. Whether the gaps will all be much smaller than experiment, as are the LDA and as was previously believed, we now doubt. Godby, Schlüter and Sham²⁵ found the exact KS potential resulted in only small improvements over the LDA using an exact expression involving two Green's functions and the self energy. The approximations they made in evaluating the Green's functions and self energy make their result suspect. Because the dielectric function is a ground state property which must be given correctly by an exact KS calculation and because it can be obtained by perturbation theory, we find it hard to believe that every energy gap can be too small.

We do not understand why the GGAXc and KLI-GGA total energies are in such remarkable agreement in the atoms. What we believe we do understand is why, irrespective of the atomic and crystal total energy errors, the KLI-LDA and KLI-GGA cohesive energies considerably underestimate the experimental value. Since the KLI approximation for HF total energies is near perfect agreement with the OEP, the error resides in the correlation functional. The exchange functional is the expectation value of the Fock operator with the ground state KS eigenfunctions but the correlation functional cannot be simply written in terms of the KS ground state charge density or eigenfunctions. Because the correlation energy results from an expansion in a complete set of Slater determinants, the correlation functional of the ground state charge density must contain information about the excited state Slater determinants, at least in some average way. No simple functional can contain this information and if one should yield the correct total energy for an atom, it should not be expected to do so for the crystal where the excited state

spectrum will be different. For example, in the semiconductors a large part of the correlation energy comes from the low lying antibonding states. There are no corresponding states in the atom and therefore any density functional which is incapable of “knowing” that the crystal has these excited states whereas the atom does not will underestimate the magnitude of the crystal’s total energy relative to that of the atom. That GGA correlation is a marked improvement over LDA in this regard may be its strongest recommendation.

Things will become much worse when one considers magnetic systems, although these calculations may not be made for some time because accurate calculations for metals require about eight times more BZ points to be sampled than need be for semiconductors. Thus the double sum in Eq. (9) will require about a factor of 50 more time²⁶ to evaluate. We²⁷ have argued that a HF core, LDA valence exchange potential should be superior to a full LDA exchange potential because if one expands the latter in a Taylor series where the core charge density is large, one obtains

$$V_{\sigma}^{\text{KS}} \approx -2(6/\pi)^{\frac{1}{3}} [\rho_{\text{core}\sigma}^{\frac{1}{3}} + \frac{1}{3}(\rho_{\text{val}\sigma}/\rho_{\text{core}\sigma})^{\frac{2}{3}}\rho_{\text{val}\sigma}^{\frac{1}{3}}]. \quad (10)$$

Thus the exchange interaction between valence electrons in the core region is vastly reduced by the factor $\frac{1}{3}(\rho_{\text{val}\sigma}/\rho_{\text{core}\sigma})^{\frac{2}{3}}$ from its HF core, LDA valence value. This reduction is unphysical because the core electrons cannot reduce the exchange interaction between a pair of valence electrons. We²⁷ obtained a surface magnetization of $1.8\mu_B$ per Rh(001) unit cell extending over the first two surface planes. A full LDA calculation²⁸ results in no surface magnetization although experiment²⁹ indicates about $0.2\mu_B$ at room temperature and a recent GGA calculation³⁰ suggests it maybe $0.5\mu_B$ at low temperatures. Thus for Rh(001) as well as other systems²⁸ the HF core, LDA valence exchange potential overestimates the ferromagnetism. Because the core electrons do not reduce the exchange interactions between valence electrons in the OEP or KLI approximation, we also expect them to considerably overestimate ferromagnetism when used with LDA or GGA correlation. We can suggest an *ad hoc* correlation functional and potential to be used with OEP or KLI exchange:

$$V_{c\sigma} = \frac{1}{2}(V_{x\bar{\sigma}} - V_{x\sigma}) + \frac{1}{2}(V_{x\sigma}^{sc} - V_{x\bar{\sigma}}^{sc}) + \frac{1}{2}(V_{c\sigma} + V_{c\bar{\sigma}}) \quad (11)$$

with a similar equation for the energy functional. Here $V_{x\sigma}^{sc}$ is a screened exchange which in the KLI case would be obtained by replacing $\Gamma_{ij}^{\sigma}(\mathbf{r})$ in Eq. (9) by

$$\Gamma_{ij}^{sc\sigma}(\mathbf{r}) = FFT\{8\pi\mathcal{F}_{ij}^{\sigma}(\mathbf{K})/(|\mathbf{K} + \mathbf{k}_i - \mathbf{k}_j|^2 + K_s^2)\} \quad (12)$$

where K_s could be taken to be the Thomas-Fermi wave vector or simply a parameter chosen to yield the correct magnetization. Note that when $V_{x\sigma}$ is added to Eq. (11), $V_{xc\sigma}$ contains the spin averaged exchange plus half the screened spin difference exchange. Since this screening accounts for the effect of correlation on the spin difference, we have added a spin averaged correlation potential. While all this is very physical and should even lead to reasonable results for a magnetic crystal it is not very physical for an atom and if it were to be used for an atom, a different K_s would be required, making the cohesive energy calculation meaningless. This is just another example of how difficult it will be (if not impossible) to find an exact or even nearly exact correlation functional and potential, applicable to both atoms and crystals, to accompany the exact KS exchange functional and potential which is now coming into use.

ACKNOWLEDGMENT

This work was supported by the University of Texas High Performance Computing Facility, the Welch Foundation (Houston, TX) and the NSF under Grant no. DMR9614040.

REFERENCES

1. P. Hohenberg and W. Kohn, Phys. Rev. **136**, B864 (1964).
2. W. Kohn and L.J. Sham, Phys. Rev. **140**, A1133 (1965).
3. R.T. Sharp and G.K. Horton, Phys. Rev. **90**, 317 (1953).
4. The first authors to realize that the OEP is the exact Kohn-Sham potential at the exchange-only level were apparently V. Sahni, J. Gruenebaum, and J.P. Perdew, Phys. Rev. B **26**, 4371 (1982).
5. J.D. Talman and W.F. Shadwick, Phys. Rev. A **14**, 36 (1976).
6. A. Görling, Phys. Rev. B **53**, 7024 (1996).
7. J.B. Krieger, Y. Li, and G.J. Iafrate, Phys. Lett. A **146**, 256 (1990).
8. J.B. Krieger, Y. Li, and G.J. Iafrate, (a) Phys. Rev. A **45**, 101 (1992); (b) *ibid.* **46**, 5453 (1992).
9. Y. Li, J.B. Krieger, and G.J. Iafrate, Phys. Rev. A **47**, 165 (1993).
10. J.P. Perdew in *Electronic Structure of Solids '91*, edited by Paul Ziesche and Helmut Eschrig (Akademie Verlag, Berlin, 1991).
11. J.P. Perdew, J.A. Chevary, S.H. Vosko, K.A. Jackson, M.R. Pederson, D.J. Singh, and C. Fiolhais, Phys. Rev. B **46**, 6671 (1992).

12. D.M. Bylander and Leonard Kleinman, *Int. J. Mod. Phys. B* **10**, 399 (1996).
13. J.C. Slater, *Phys. Rev.* **81**, 385 (1951).
14. Leonard Kleinman, *Phys. Rev. B* **49**, 14197 (1994).
15. D.M. Bylander and Leonard Kleinman, *Phys. Rev. B* **55**, (1997).
16. J.P. Perdew, K. Burke, and M. Ernzerhof, *Phys. Rev. Lett.* **77**, 3865 (1996).
17. U. von Barth and C.D. Gelatt, *Phys. Rev. B* **21**, 2222 (1980).
18. D.M. Bylander and Leonard Kleinman, *Phys. Rev. B* **52**, 14566 (1995).
19. D.M. Bylander and Leonard Kleinman, *Phys. Rev. B* **54**, 7891 (1996).
20. A. Rappe, K. Rabe, E. Kaxiras, and J.D. Joannopoulos, *Phys. Rev. B* **41**, 1227 (1990).
21. D.M. Bylander, Leonard Kleinman, and Seongbok Lee, *Phys. Rev. B* **42**, 1394 (1990). Appendix A.
22. J.H. Rose, J. Ferrante and J.R. Smith, *Phys. Rev. Lett.* **47**, 675 (1981).
23. M. Städele, J.A. Majewski, P. Vogl, and A. Görling in *Proceedings of the 23rd International Conference on the Physics of Semiconductors*, Berlin, 1996 (World Scientific, Singapore) p. 613.
24. A. Görling, private communication.
25. R.W. Godby, M. Schlüter, and L.J. Sham, *Phys. Rev. Lett.* **56**, 2415 (1986) and *Phys. Rev. B* **36**, 6497 (1987).
26. The number of points in the irreducible wedge increases by slightly less than a factor of eight.
27. Ian Morrison, D.M. Bylander and Leonard Kleinman, *Phys. Rev. Lett.* **71**, 1083 (1993).
28. M. Weinert, S. Blugel and P.D. Johnson, *Phys. Rev. Lett.* **71**, 4097 (1993).
29. S.C. Wu, K. Garrison, A.M. Begley, F. Jona and P.D. Johnson, *Phys. Rev. B* **49**, 14081 (1994).
30. J.-H. Cho and M. Scheffler, *Phys. Rev. Lett.* **78**, 1299 (1997).

QUANTUM CHEMICAL MOLECULAR DYNAMICS

BRETT. I. DUNLAP AND ROBERT W. WARREN[†]

Theoretical Chemistry Section, Code 6179, Naval Research Laboratory, Washington, DC 20375-5342

ABSTRACT

Two new methods of performing *ab initio* molecular dynamics calculations are discussed. The first method is a completely general approach requiring variational fitting of the exchange-correlation energy density on a grid of points. The second method avoids the grid of points, but is restricted to the $X\alpha$ functional. These methods are based on Kohn-Sham density functional theory in which the charge density is fitted variationally. The linear combination of Gaussian-type orbitals approach is used to construct the orbital and local-potential basis sets. Variable occupation numbers for the Kohn-Sham orbitals are used to model the configurational mixing which occurs upon bond formation/dissociation. Applications to the reaction of two linear ozone molecules, a collinear $(NO)_{12}$ system, and the excited state dynamics of halide photodissociation are presented.

1. INTRODUCTION

The study of chemical reactions has profoundly affected quantum chemistry. There are certain dynamical processes, such as the hindered internal rotation of ethane, that can be accurately computed from first-principles using quantum chemical methods that include no electron correlation. For the most part, however, even a qualitative description of a chemical reaction requires correlated methods. The breaking of any single covalent chemical bond involves a transition state in which two singlet-coupled electrons have begun to localize in different parts of the molecule. Ultimately the two unpaired electrons are completely isolated on different molecular fragments. The minimal pure-state description of this process involves two electronic configurations. Greater accuracy requires higher levels of correlation. As a consequence, quantum chemical descriptions of bond breaking and bond formation must include correlation from the outset. This drawback of Hartree-Fock theory is so great that today many quantum chemists are reluctant to use it as a terminal level of theory even when it would be appropriate.

The best traditional quantum-chemical descriptions of chemical reactions involve three different demanding calculations. First, one performs correlated electronic structure calculations at a few most important geometries, minimally those of the reactants, of the transition state, and of the products. The results of these few calculations are then fitted to extrapolate a full potential-energy

surface (or surfaces) of the chemical reaction. Next dynamical calculations are performed on the surfaces, and finally the results analyzed statistically to compare to experiment [1,2].

Using density-functional theory (DFT), Car and Parrinello [3] showed that an adequate first-principles description of at least some chemical reactions can be achieved on-the-fly in a single type of calculation, *ab-initio* molecular dynamics (AIMD). As reactions become more and more complicated, involving more and more atoms, or the relevant portions of the potential energy surface(s) become more difficult to determine *a priori*, AIMD becomes the only practical method. These two approaches can be combined to a degree, by doing molecular dynamics on a small region of the potential energy surface (PES) where a Taylor-series expansion of the potential is adequate and as the system leaves that region generating a new Taylor-series expansion of the potential that is appropriate in the new region [4].

AIMD need not be based on DFT and the treatment of correlation in density-functional theory is not, yet at least, exact. Thus AIMD based on traditional quantum chemistry is being developed in parallel. To study chemical reactions using such methods, treating more than one electronic configuration is essential and treating a very large number of configurations is prohibitive; thus the generalized-valence-bond (GVB) or other similar multiconfiguration self-consistent-field (MCSCF) method appears most appropriate [5]. Within DFT the best description of two electrons singlet coupled in two orbitals, which provides the minimal description of covalent bond rupture or formation, is not practical. The simplest, and only practical, approach for this case is an unrestricted calculation that assigns different spins to the two electrons. A more rigorous approach notes that this configuration is half singlet and half triplet and thus projects out the triplet component of the wavefunction to obtain the singlet energy [6]. This more sophisticated approach does not yield a smooth PES at the seam where the unrestricted and restricted surfaces are degenerate. Smooth potential energy surfaces require that this projection be done self-consistently, which leads to a coupled set of MCSCF-like equations [7]. The MCSCF-like approach to DFT may be practical for pure states, but not for the ensemble of electronic states populated at finite temperature. In finite temperature DFT, one occupies the spin-unrestricted but usually symmetry-restricted Kohn-Sham one-electron orbitals [8] according to a Fermi distribution. In the limit as the electronic temperature goes to zero, finite-temperature DFT becomes the fractional-occupation-number (FON) method [9]. Varying the orbital occupation numbers during the course of a density-functional AIMD simulation is a practical way to study chemical reactions.

The Gaussian basis set is the basis set of *ab initio* quantum chemistry. It is rapidly becoming the basis set of choice for density-functional treatments of finite systems [10-13]. Gaussian-based density-functional AIMD is being established [14-15] using an accurate and efficient method to fit the charge density variationally [16]. In general, the exchange-correlation (XC) energy

operator or kernel can also be fit variationally [17]. For the special case of $X\alpha$ the exchange energy density can also be fit analytically [18-21]. Complete variational fitting of the local potential of DFT leads to a 3-center quantum chemistry with all the chemically meaningful characteristics of traditional 4-center quantum chemistry yet enabling facile molecular dynamics calculations.

Our AIMD simulations are all-electron and self-consistent at each 0.4 femtoseconds (fs) time step. Variational fitting ensures accurate forces for any finite orbital or fitting basis sets and any finite numerical grid. These forces are used to propagate the nuclear motion according to the velocity Verlet algorithm [22]. The accuracy of these methods is indicated by the fact that during the 500 time-step simulations of methyl iodide dissociation described below, the center of mass moved by less than 10^{-6} Å.

Section 2 reviews the linear-combination-of-atomic-orbitals AIMD forces when the orbital occupations are allowed to vary [23]. Section 3 considers the effect of constraints on orbital occupancy on the dynamics of reaction between two linear O_3 molecules [24]. Section 4 considers larger 1-D molecular collisions, the symmetric collision between two twelve-atom collections of van der Waals bonded NO dimers. Section 5 considers the role of bending in organic halide photodissociation using 3-D AIMD.

2. FORCES AND FRACTIONAL OCCUPATION NUMBERS

We use fractional occupation number solutions to describe the configurational mixing which occurs in molecules upon bond formation or fissure. A simple example is found in the diatomic species, C_2 , which has two low-lying $^1\Sigma_g^+$ states that differ in having either two or four electrons in ϕ_{π_u} molecular orbitals. The latter configuration is lower in energy at internuclear separations less than about 1.55 Å, whereas the π_u^2 configuration is the more stable singlet at larger bond lengths. This discontinuity in the ground-state surface can be treated smoothly using FON solutions [25].

The question arises whether there exists any contribution to the force resulting from variations in orbital occupation numbers in those regions of configuration space where FON solutions occur. Alternatively expressed, we seek to determine whether a term arising from the implicit dependence of the occupation numbers on the nuclear coordinates contributes to the analytic derivative of the electronic energy. This question is of concern also when implementing molecular dynamics using a finite-electronic-temperature formalism based on Fermi broadening.

Consider the total nonrelativistic fitted electronic energy [26] functional, \mathcal{E} , which in Kohn-Sham density functional theory takes the form (in atomic units)

$$\begin{aligned} \mathcal{E} = & \sum_{a,b,b \neq a} \frac{Z_a Z_b}{R_{ab}} + \sum_{i\mu\nu} n_i c_{\mu i}^* c_{\nu i} H_{\mu\nu} + 2(\rho|\mathbf{F}) \cdot \mathbf{d} \\ & + \langle \rho \mathbf{G} \rangle \cdot [\mathbf{G} \frac{\rho}{U} \mathbf{G}]^{-1} \cdot [\mathbf{G} \rho] - \mathbf{d} \cdot (\mathbf{F}|\mathbf{F}) \cdot \mathbf{d}. \end{aligned} \quad (1)$$

Here, R_{ab} is the scalar distance between nucleus a and b , n_i and $c_{\mu i}$ are the occupation number and the μ th LCGTO coefficient of the i th molecular orbital, and $H_{\mu\nu}$ is an element of the one-electron (kinetic energy and nuclear-electron attraction) matrix in the primitive basis. \mathbf{F} and \mathbf{G} are the Gaussian fitting bases for the charge density, ρ ($= \sum_i n_i \phi_i^* \phi_i$), and XC operator, U , respectively. In this equation square and angular braces indicate, respectively, numerical and analytic integration over all space. Curved braces indicate Coulombic integration. For analytic $X\alpha$ the term involving numerical integration is replaced by the completely analytical expression,

$$C_\alpha \langle \rho \mathbf{G} \rangle \cdot \mathbf{x} - C_\alpha \mathbf{x} \mathbf{x} : \langle \mathbf{G} \mathbf{G} \mathbf{Y} \rangle \cdot \langle \mathbf{Y} \mathbf{Y} \rangle^{-1} \cdot \langle \mathbf{Y} \mathbf{G} \mathbf{G} \rangle : \mathbf{x} \mathbf{x} / 4, \quad (2)$$

where \mathbf{Y} is the basis for fitting the 2/3 root of the charge density and

$$C_\alpha = -\alpha \frac{3}{4} \left(\frac{3}{2\pi} \right)^{1/3}, \quad (3)$$

for a spin-restricted calculation.

These energy functionals are made variational by requiring they be stationary with respect to variation of the orbital coefficients, occupation numbers, \mathbf{x} for analytic $X\alpha$, and \mathbf{d} subject to the constraints that the orbitals be orthonormal and the sum of the occupation numbers be the total number of electrons, N_e , and optional constraints on the fits.

Differentiation of this energy functional using the chain rule with respect to an arbitrary component of a nuclear coordinate, \mathbf{R}_α , yields several terms which can be grouped conveniently as containing either derivatives of the orbital coefficients, *i.e.* $\partial c_{\mu i} / \partial \mathbf{R}_\alpha \equiv c_{\mu i}^\alpha$, derivatives of the fitting basis expansion coefficients for the charge density and exchange-correlation energy, derivatives of the orbital occupation numbers, and finally, terms which result from any explicit dependence on \mathbf{R}_α . These latter are straightforward to obtain, whereas a brute force approach to compute the former kinds of terms, those with an implicit dependence on \mathbf{R}_α , require solution of the coupled-perturbed Kohn-Sham equations (CPKS). Fortunately, it has been shown that the variational condition (and the appropriate constraint equation) allow the derivatives of the orbital coefficients [27] and the fitting coefficients [17] to be replaced by expressions which do not require an iterative, and thereby costly, calculation.

In the case of variable occupation numbers, we are interested in the term

$$\sum_i \left(\frac{\partial \mathcal{E}}{\partial n_i} \right) n_i^\alpha = \sum_i \epsilon_i n_i^\alpha . \quad (4)$$

The variational condition, together with the constraint $\sum_i n_i - N_e = 0$, allows one to show that the energy eigenvalues of the fractionally occupied orbitals are degenerate [28], and thus for an FON solution, the above summation vanishes. Gradients calculated analytically and numerically (using a three point central difference formula with the functional, \mathcal{E}) agree to within 10^{-5} atomic units (au) for a FON solution in C_2 over a range of appropriate internuclear separations [23]. There is no contribution to the force from the variation of the occupation numbers with nuclear configuration in the FON formalism. Note that this result is distinct, for example, from the case of the orbital coefficients. Terms containing the derivatives $c_{\mu i}^\alpha$ do not vanish; rather they are replaced by a computationally more convenient expression containing the perturbed overlap matrix, $S_{\mu\nu}^\alpha$.

When the occupation numbers are given by a Fermi distribution

$$n_i = \left[1 + \exp\{\sigma(\epsilon_i - \epsilon_F)\} \right]^{-1} , \quad (5)$$

characterized by a width, σ , and Fermi energy, ϵ_F , orbitals with non-integer occupations need not be degenerate. This property means that the sum of terms given in Eq. 2 does not vanish identically. Evaluation of n_i^α for Fermi broadening requires solution of the CPKS equations to obtain the perturbed eigenvalues, ϵ_i^α [23]. If one considers rather the modified energy functional $\mathcal{E}' = \mathcal{E} + \mathcal{N}$, where \mathcal{E} is given by Eq. 1 and the term, \mathcal{N} , is defined [29]

$$\mathcal{N} = \frac{1}{\sigma} \sum_i \left\{ (1 - n_i) \ln(1 - n_i) + n_i \ln n_i \right\} , \quad (6)$$

then the property, $\partial \mathcal{N} / \partial n_i = \epsilon_F - \epsilon_i$, leads to a cancellation of all terms involving n_i^α . Gradients for a Fermi broadening solution ($\sigma = 0.025$ eV) in C_2 analogous to those discussed above, show poor agreement, only to the order of 10^{-2} a.u., between the analytic and numerical results computed using the functional \mathcal{E} . Use of the modified functional, \mathcal{E}' , leads to agreement between the analytic and numerical forces to within 10^{-5} a.u. Clearly, the difficult terms containing n_i^α are of appreciable magnitude, and it is a distinct advantage to avoid their calculation using the free energy functional, \mathcal{E}' .

3. COLLINEAR OZONE COLLISIONS

The ozone reaction is a challenge to DFT. The ground state of ozone is singlet and has a bent geometry. The ground state of two such ozone molecules is thereby necessarily singlet. The oxygen molecule however, has a triplet ground state. How best to describe the product state of three oxygen molecules singlet coupled is an open question in DFT [30]. The exact Kohn-Sham potential is symmetric and thus commutes with the total spin operator [31]. The way current functionals are derived, however, is most consistent with broken-symmetry calculations [32]. Thus the most accurate DFT description of the ozone reaction currently available probably comes from allowing the spin of the system to be variationally determined as the reaction proceeds. This approach necessarily involves fractional occupation numbers when applied to the $2O_3 \rightarrow 3O_2$ gas-phase chemical reaction.

The selection of a model system for initial studies of chemical reactions using AIMD and variable occupation numbers was influenced by several considerations, including the requirements that the system be reactive, sample significant regions of the XC potential, avoid the nonessential complications of a large number of internal degrees of freedom, and be nontrivial. The collinear reaction of two linear O_3 moieties is such a system; the collinear reaction $2O_3 \rightarrow 3O_2$ is characterized by the creation of a bond to form dioxygen and the breaking of an O-O bond in each ozone. Performing the calculation in D_{6h} symmetry avoids the complexity of rotational motion and allows the trajectories to be described completely in terms of three degrees of freedom. Although the reaction of two linear ozone molecules is somewhat less complex than is the case for the bent system, nevertheless the orbital occupation numbers must be allowed to change for the reaction to occur. Thus, we believe that the collinear ozone reaction captures the essential physics necessary to examine reactive molecular dynamics using DFT.

Orbital occupation numbers define the electronic state in Kohn-Sham density functional theory. As discussed above, we model the configurational mixing which occurs upon bond formation or rupture using fractional occupation numbers. Changes in spin state which could occur in a complex reaction such as $2O_3 \rightarrow 3O_2$ are implemented using an iterative procedure which establishes a common Fermi (CF) level for α - and β -electrons in each SCF cycle. In this way, electrons can change spin orbitals to minimize the electronic energy at each step in the dynamical trajectory. The software includes an option that allows the orbitals to be reoccupied (including fractionally) with a Separate Fermi (SF) energy for each spin to hold constant the number of electrons for that spin. The occupation numbers also may be held fixed throughout the dynamics and such trajectories are referred to as fixed occupation (FO) trajectories.

The orbital basis set for oxygen [33] is $9s/5p$ contracted to $4s/2p$ according to a same-orbitals-for-different-spins atomic calculation using the appropriate

Table 1. Linear O_3 Energies and $O - O$ Bond Lengths in a.u.

Functional	Electronic Energy	Atomization Energy ^a	$O - O$ Length (a_0)
PZ	-223.839535	0.253087	2.417
GGA	-225.383253	0.174291	2.498
X α	-222.176913	0.245724	2.473

$$^a 3E(O) - E(O_3)$$

functional and augmented with a d exponent of 1.154 atomic units [34]. The contractions are not segmented, but are the cores of the occupied atomic orbitals together with the appropriate number of uncontracted diffuse Gaussians. The s orbital exponents were scaled by factors of 2, 4/3 and 2/3, respectively, to obtain the s bases for fitting the charge density (CD), its 2/3 power, and the XC operator. The Gaussians with the five largest exponents in these fits were contracted. Three p exponents, 7.8, 1.56, and 0.39 a.u. [35] were added to all auxiliary bases. Bond-centered s exponents of 1.0, 0.65, and 0.3 a.u., respectively, were added to the CD, its 2/3 power, and XC bases. The grid of points used was one with 30 different radial points and approximately 590 total points about each symmetrically distinct atom and 4 additional points about each bond center; this set of points is essentially equivalent to the course option of the DGAUSS code [36].

The trajectories presented here have certain common features. The collision is collinear between two linear ozone moieties and the calculation is performed in D_{6h} symmetry. The optimized O–O bond length for linear ozone was calculated for each functional and these data are found in Table 1. The trajectories begin with the distance between the interior oxygen atoms of each ozone moiety set to 2.00 Å. The internal O–O bond lengths are set to those of the isolated O_3 species or suitably compressed or expanded relative to that length. The ground state for the $O_3 - O_3$ system in this arrangement is the $S = 2$ (quintet) configuration $7\sigma_g \uparrow 7\sigma_g \downarrow 7\sigma_u \uparrow 7\sigma_u \downarrow 6\pi_u \uparrow 4\pi_u \downarrow 6\pi_g \uparrow 4\pi_g \downarrow$ (where $\sigma_g \equiv a_{1g}$, $\pi_g \equiv e_{1g}$, $\sigma_u \equiv a_{2u}$, and $\pi_u \equiv e_{1u}$). Each oxygen atom within a O_3 molecule is given the same initial velocity, v_0 , so that they begin the dynamical path with no internal vibrational motion. The velocities for the second O_3 moiety are equal but opposite by symmetry. Due to the enforced symmetry, there are three independent degrees of freedom that define the potential energy hypersurface of the collision. For simplicity, the trajectories are plotted using only two of these, specifically the distance between the interior oxygen atoms, R , and the distance between the interior and the central oxygen atom, r , within an O_3 moiety. The reaction $2O_3 \rightarrow 3O_2$ ($3O_2 \rightarrow 2O_3$) is characterized by bond formation in the coordinate, R (r), and bond fissure in the coordinate, r (R). The position of the exterior oxygen atom is updated at each time step, but its position is not indicated by the plots. It undergoes vibrational motion relative to the central atom as the dynamics proceed.

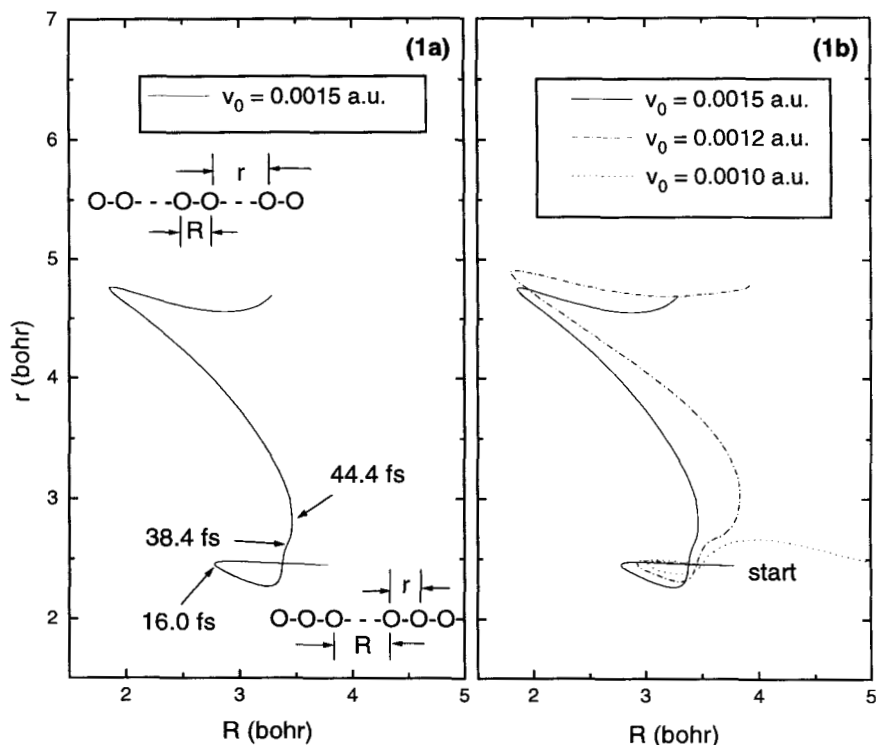


Figure 1. (a) Representative LDA trajectory with time points indicating significant changes in electronic structure. (b) Effect of initial velocity, v_0 .

A representative trajectory obtained using the Perdew-Zunger (PZ) parameterization [37] in the local density approximation (LDA) is found in Figure 1a. As indicated by the diagrams, the lower right hand portion of the plot corresponds to separated O_3 species, whereas the upper left hand section is characteristic of three separated molecules of dioxygen. The trajectory begins in the lower right, plotted as a solid line. The calculation is of the Common Fermi type described above. The initial velocity for each oxygen atom was 0.0015 a.u. and the interior $O-O$ bond lengths were set to 1.015 times that of the isolated O_3 moiety (r_0). The distance, R , between the interior oxygen atoms of each ozone is plotted along the abscissa and the internal $O-O$ separation, r , is plotted along the ordinate.

Until the 16 fs time point, the ozone molecules approach one another, but decelerate since the intermolecular potential is repulsive. There is little change in the internal bond length, r . At the 16 fs time point however, the interior oxygen atoms are seen to reverse their direction and the internal $O - O$ bond is compressed; the ozone moieties “bounce off” one another. This initial scattering event continues until $R \approx 3.4 a_0$ when the interior O atoms essentially stop (R varies only slowly) whereas the central and exterior oxygen atoms continue to move outwards. At 38.4 fs into the dynamics, the geometrical arrangement of the nuclei is such that a FON solution is obtained; the orbital reoccupation occurs over 3 steps (1.2 fs) resulting in a state where an electron has been transferred from an orbital of $\pi_g \uparrow$ symmetry to one of $\sigma_g \uparrow$ symmetry. The trajectory propagates in this new state until at 44.4 fs a spin flip (*vide infra*) occurs to an ($S=1$) state via the transfer of the electron remaining in the partially filled $\pi_g \uparrow$ orbital to a $\sigma_g \downarrow$ orbital. After this change of electronic state, the interior oxygen atoms rapidly move inwards whilst the outer oxygens continue outwards. The remaining part of the trajectory can be considered as the oscillation of a vibrationally hot central O_2 species with O_2 fragments departing the collision region.

The solid trajectory in Figure 1b is the same as that given in Figure 1a. The other trajectories shown are for different values of the initial velocity, v_0 , beginning from the same starting configuration. The dynamics with $v_0 = 0.0010$ a.u. are unreactive with the ozone molecules scattering intact with some vibrational excitation. Interestingly, the slower reactive collision, $v_0 = 0.0012$ a.u., leads to a greater degree of vibrational excitation in the central O_2 product fragment.

The trajectories plotted in Figure 2a indicate the effect of the electronic state on the dynamics of the collision. All trajectories were computed using the LDA with $v_0 = 0.0015$ a.u. Again, the solid curve is the same trajectory as presented in Figure 1a. Note that curves SF and CF diverge at the 44.4 fs point indicated in Figure 1a, namely where the spin flip in the latter occurs, but that both trajectories are reactive. A trajectory during which the occupation numbers are held fixed to the initial values corresponding to the ground state of the initial configuration is labeled as FOQ (Fixed Occupation Quintet). Curves CF and FOQ diverge at 38.4 fs, at the point where a FON solution is obtained in the CF (and SF) calculation, and exhibit a dramatic difference in dynamics – the former being a reactive trajectory whereas the latter is not. The curve labeled FOT (Triplet) is a fixed occupation calculation similar to FOQ, but with the initial occupation numbers corresponding to the lowest energy $S=1$ state; this state is excited relative to the $S=2$ state in the initial configuration, but is the ground state for the products. This significantly changes the dynamics, in particular the interior oxygen atoms do not bounce off before “reacting”. In this context, “reacting” means the six oxygen atoms attain a configuration which looks more like products (three molecules of dioxygen) than reactants (two molecules of linear ozone). The interior oxygen atoms are accelerated inwards smoothly approaching each other

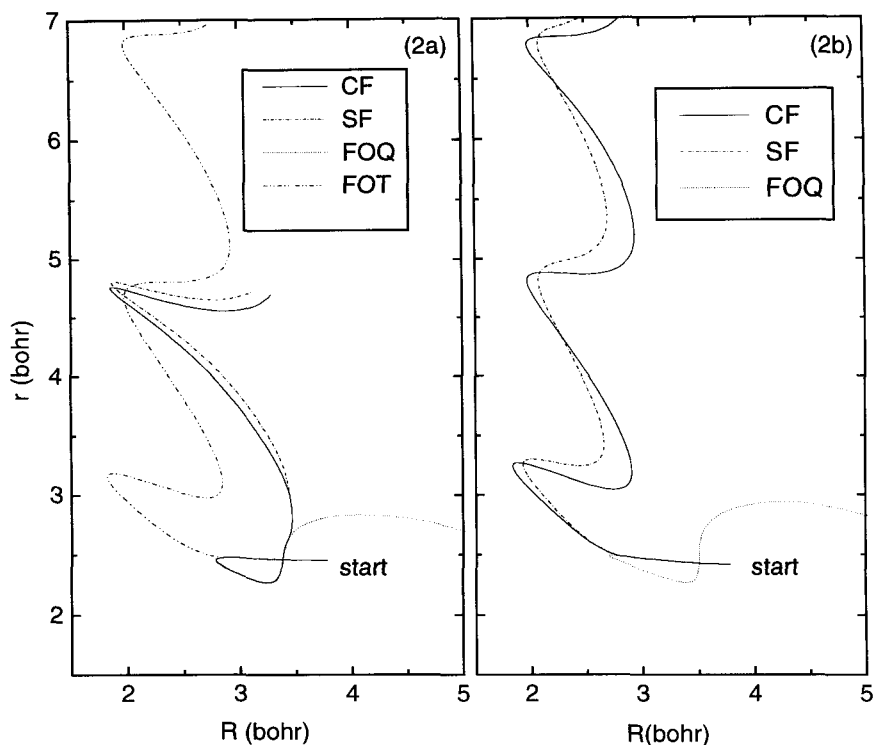


Figure 2. Effect of electronic structure constraints on LDA trajectories. (a) O-O length set to $1.015r_0$. (b) O-O length set to r_0 .

to a distance of $1.8 a_0$ before recoiling; the overall atomic arrangement thus resembles the final products very much earlier in the dynamics. The interior O_2 moiety vibrates over several periods in the coordinate R , as the exterior O_2 fragments move outwards from the collision center. This vibrational motion oscillates about a mean distance of ($R =$) 1.3 \AA , very close to the equilibrium bond length for O_2 .

Figure 2b presents trajectories analogous to those found in Figure 2a, but beginning from a starting configuration in which the $O - O$ bond length is set equal to the calculated monomer equilibrium distance. Again, the FOQ trajectory is unreactive. From this starting geometry however, the CF and SF trajectories exhibit reaction during the initial collision event (somewhat like the FOT trajectory in Figure 2a rather than after an initial unreactive recoil.

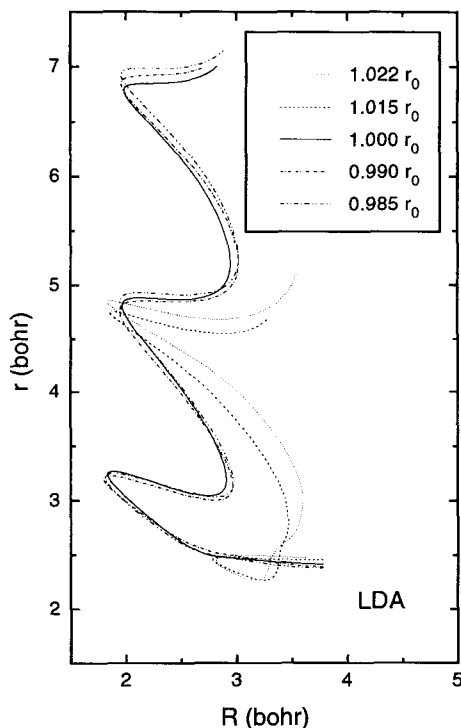


Figure 3. LDA trajectories (CF) for a range of starting configurations. All have $v_0 = 0.0015$ a.u.

Common Fermi trajectories starting from a variety of initial configurations with $v_0 = 0.0015$ a.u. are given in Figure 3. By expanding or compressing the $O-O$ bond in this way, a kind of phase was imparted to the internal dynamics.

We also investigated the dependence of the trajectory on the nature of the approximation to the XC energy. The generalized gradient approximation (GGA) was developed to correct the overbinding often seen in calculations using the LDA. In Figure 4a are shown CF trajectories using the Perdew-Wang (PW) GGA functional [38]. The initial velocity of 0.002 a.u. is different from that used for the LDA results because an initial velocity of 0.0015 a.u. is just at threshold for reaction when using the PW-GGA. None of the trajectories exhibit the curious behavior of reacting after an initial scattering, although that behavior is seen when v_0 is very close to the threshold value. Shown in Figure 4b are analogous trajectories using the analytic $X\alpha$ functional, with α

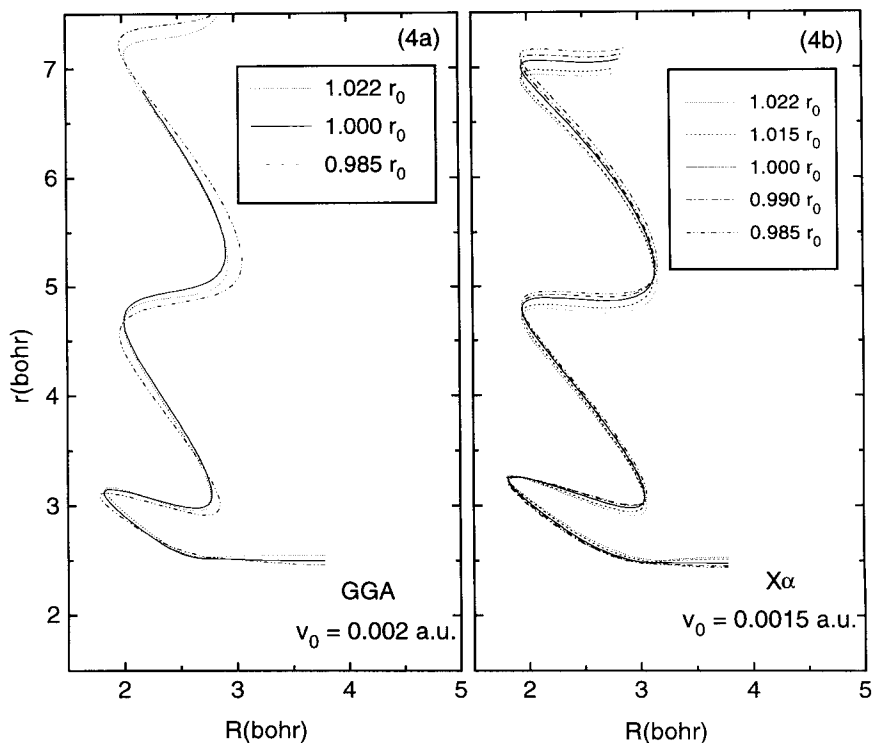


Figure 4. (a) GGA trajectories. (b) Analytic $X\alpha$ trajectories.

set (to four significant digits) to the Gáspár-Kohn-Sham value of two thirds [39]. This functional requires no numerical evaluation of the XC energy, thus the method is very efficient computationally. For direct comparison with the LDA results, these trajectories were performed at $v_0 = 0.0015$ because the $X\alpha$ threshold velocity is on the order of 0.0008 a.u. [24]. All of the trajectories are reactive during the initial approach of the reactants. For this system, the efficient analytic $X\alpha$ approach appears to reproduce well the trajectories attained using the more sophisticated GGA, albeit that there is a distinct difference in the threshold velocity required to initiate reaction.

4. COLLINEAR $(\text{NO})_{12}$ COLLISIONS

The code can be used to study large collections of atoms. At one time it held the record for the largest number of contracted orbital basis functions,

4560, used in an *ab initio* or first-principles SCF calculation [40]. Of course AIMD requires hundreds of SCF calculations and the size of system that can be treated with similar computational effort is significantly smaller, but fitting the local potential of density-functional theory should provide the same relative advantage in AIMD as it does in single-point calculations.

The nitric oxide system has also been studied as a model explosive [41-43]. The NO dimer, ONNO, is slightly bent, with a weak NN bond. The bond is weakened only slightly more by constraining it to be straight. Under this approximation one can make one-dimensional models of the solid nitric oxide explosive that are clearly tractable using AIMD, yet that allow energetic chemistry.

It is energetically favorable for the atoms of the NO dimer to rearrange to form O₂ and N₂. Thus under the right circumstances a collection of dimers would be expected to explode giving predominantly molecular nitrogen and oxygen. This might be particularly facile for a linear array of dimers, which has oxygen atoms from adjacent dimers as nearest neighbors. Thus chemical reactions could sustain a linear explosion simply by having each oxygen atom break a bond to its neighboring nitrogen atom and form a bond in the other direction to a neighboring oxygen atom.

The obvious problem with this picture concerns end effects. The oxygen atoms at both ends must either break away free or become attached to its neighboring nitrogen molecule. If the chains are made long enough, then what happens to the ends should not matter. In a sense, however, these end effects propagate inward, necessarily affecting the dynamics. Only in a concerted reaction can all the atoms be viewed as reacting simultaneously. A concerted reaction can only involve a few atoms. That concerted reaction propagating down a linear chain of ONNO molecules will necessarily have an endothermic leading edge, which results in the oxygen atom or N₂O molecule when the concerted reaction reaches the end of the chain.

These edge effects do not prohibit chemical reaction on energetic grounds. It is endothermic to convert two dimers into two N₂O molecules and two oxygen atoms, but it is exothermic to convert them into two N₂O molecules and an oxygen molecule. Thus independent of chain length, the creation of two terminal N₂O molecules and everything else into oxygen and nitrogen molecules is significantly exothermic. A linear array of six NO dimers is clearly big enough to contain any concerted reaction that might be involved in a linear (NO)₂ explosion. The collision can be exothermic by 10 eV or more. Estimating the barrier to reaction is far from obvious, however. Is the barrier to more or less complete reaction the creation of the first oxygen atom or molecule or some larger number of oxygen and nitrogen molecules? This is a question that can be studied with AIMD.

The O basis set is the same as that used in the ozone study. The N basis set is the same apart from adjusting the values of each exponent where necessary;

those of $9s/5p$ orbital basis [33], the d polarization exponent to 0.864 a.u. [34], and the p fitting exponents to 0.32, 1.28, and 6.4 a.u. [35]. The calculations are analytic $X\alpha$, $\alpha = 0.6667$ and no grids of points are necessary. With this basis and the $X\alpha$ functional, changing each NO dimer to O_2 and N_2 releases 1.58 eV. The optimized structure of the isolated system of three van der Waals bonded NO dimers in D_{6h} symmetry is given in Table 2. The N-N distances are 1.15 Å, the N-O distances are 1.25 Å and the O-O distances are 2.88 Å. The AIMD calculations were of the CF type; spin unrestricted to allow for the possibility of forming paramagnetic oxygen.

Table 2. Symmetry inequivalent $(ON_2O)_3$ distances in Å.

Element	Distance from Center
N	0.574
O	1.818
O	4.696
N	5.941
N	7.088
O	8.334

Two of these $(ON_2O)_3$ 'solids' were placed 3.0 Å apart and fired towards each other at a relative velocity of 5 km/sec or 0.05 Å/fs. It takes quite a long time for all the separate dimers to bounce off of each other and exit the collision zone. In the process the two interior dimers have collided three times. After one thousand time steps all dimers have velocities opposite their initial velocities. During this time no chemical reaction was seen, and afterward no further chemical reactions are possible. Doubling the relative velocity to 10 km/sec leads to the same qualitative result. Quadrupling the original velocity leads to the breaking of the outer ONN-O bond, but all other bonds remain intact.

The dynamics is quite similar if internal potential energy is added to the two collision partners. For a fixed relative initial velocity of 5 km/sec, internal energy can be added to the system by compressing or expanding various bonds from their equilibrium values. Moving each oxygen atom 0.04 Å towards its nitrogen neighbor has the effect of raising the energy of the colliding system 1/40 eV per degree of freedom which if equilibrated would give room temperature vibrational motion. The collision of two such compressed moieties at 5 km/sec relative velocity results in no reaction. Doubling and quadrupling the compression similarly does not lead to reaction. During the course of the latter trajectory various N-O bonds become extremely elongated before being pulled back by the density-functional forces.

It is not clear why this linear NO system is so unreactive. While analytic $X\alpha$ was shown to reproduce accurately the dynamics of the ozone system, perhaps it is the problem in this system. We are looking at these same dynamics using the GGA, which unfortunately requires more than a factor of two increase in computer time.

5. HALIDE PHOTODISSOCIATION

A halogen atom lacks a single electron to complete its p electronic subshell. As it interacts with a ligand, a bonding p_σ molecular orbital drops in energy while an antibonding p_σ molecular orbital rises relative to the nonbinding p_π halide orbitals. Assuming the ligand is not a chromophore, the first electronic excitation then corresponds to exciting a halide π electron to the anti-bonding p_σ (σ^*) orbital [44]. This will break the bond formed by the p_σ -containing molecular orbital, and the molecule will dissociate. This Σ to Π transition of the total molecular wavefunction breaks axial symmetry. As symmetry no longer requires the bond to remain straight, it will bend.

In both ICN [45] and ICH_3 [46,47], as well as other cyanohalides [48-50] this excitation is called the \tilde{A} continuum. The existence of highly rotationally excited CN fragments in ICN photodissociation suggests that there are strong bending forces on at least some of the excited PES's in the Franck-Condon region relevant to photodissociation [51]. Heavy halogen photodissociation is complicated by the fact that the atomic halogen wavefunction can have large spin-orbit splitting.

For chlorine the spin-orbit splitting is not significant, and a fitted $X\alpha$ ClCN photoexcited-state potential energy surface with strong bending forces [52] gives good agreement with the experimental data [50,53,54] showing high rotational excitation of the CN fragment. In contrast, ICH_3 shows little rotational excitation of the methyl fragment. The electronic structure of these molecules is similar and one should expect similarity in their photodissociation dynamics.

Accurate theoretical treatment of the photodissociation of ICN [55] and ICH_3 [56] requires spin-orbit-split potential energy surfaces and a model of how the molecule hops from one spin-orbit surface to another as it dissociates to produce spin-orbit split $J=1/2$ and ground-state $J=3/2$ iodine atoms. Ref. 57 points out that there are two π to σ^* transitions to a bent upper state in ClCN that are Renner-Teller paired to correlate to a Π state in the linear geometry and that there are many other still higher lying, but still close in energy, states in the Franck-Condon region. It is possible that the interference of multiple potential energy surfaces leads to the very different rotational distributions in XCN and XCH_3 . The best traditional molecular dynamics studies [55,56] based on fits to *ab initio* PES's suggest, however, that bending forces are important the photodissociation of both molecules. Such forces should be apparent in spin-free (and thus spin-orbit-interaction-free) AIMD simulations

of these photodissociation processes as such effects will change slowly on any diabatic potential energy surface.

For ICN the Renner-Teller states have A' and A'' symmetry in C_s symmetry. AIMD can be used to follow the dynamics of these states in ICN and the corresponding states in ICH_3 . The A'' state of both molecules are the ground electronic states of that symmetry, thus even though they photodissociate, DFT can in principle exactly provide the relevant PES [58]. There is no tendency for broken-symmetry solutions [30], thus one should expect reliable DFT descriptions of the A'' dynamics. The A' states are first excited states of their symmetry, but it is hard to imagine that if DFT is appropriate for one member of a Renner-Teller pair of electronic states that it is inappropriate for the other or by analogy the corresponding states of ICH_3 .

For use with analytic $X\alpha$, the orbital basis set for I was $18s/14p/8d$ [33] modified to $19s/15p/9d$ by replacing the most diffuse s orbital exponent by two exponents 0.05 and 0.12 a.u. and the third and fourth most diffuse s orbital exponents by 0.5 and 1.0 a.u. exponents. The p and d exponents were augmented with exponents 0.03 and 0.2 a.u., respectively. The orbitals were contracted to $10s/8p/6d$. The Iodine p orbital exponents numbered 4, 8, 10, and 13, ordered least to greatest, were doubled to get r^2 fitting functions. The N, C, and H, orbital basis sets were $11s/7p$, $11s/7p$, and $6s$ [33], augmented with polarization functions 0.6, 0.78, and 1.0 a.u. [34], respectively, and contracted $5s/3p/1d$, $5s/3p/1d$, and $3s/1p$. For N p exponents 4 and 6 were doubled to get r^2 fitting exponents. All s orbital exponents were scaled properly to obtain the s functions for the auxiliary bases. The 7, 5, 4 tightest s CD fitting exponents, respectively, for I, N, and C as well as the tightest r^2 CD fitting exponent on I were contracted. Five p and d exponents were added to both auxiliary bases for I, N, and C. For I the exponents were 0.01, 0.07, 0.2, 0.7 and 3.0 a.u., for N and C they were 0.25, 0.37, 0.7, 2.0 and 5.0 a.u., and for H the single auxiliary p exponent was 1.0 a.u. Bond-centered s exponents of 1.0, 0.65 and 0.3 au, respectively, were added to the CD, its 2/3 power, and the XC bases.

Basis sets of this size are highly accurate, capable of obtaining exact DFT binding energies to 0.1 eV/atom. Calculations of such accuracy left little doubt that local density functionals significantly overbind [59]. For molecular dynamics, where relative energies are the only quantities of interest, smaller Gaussian basis sets, such as used in the calculations described above, probably strike a better balance between accuracy and computer resource usage. (This ICN basis was designed to study higher lying Rydberg states.) Highly contracted basis sets are inappropriate for reactive AIMD, which must necessarily treat the great amount of change in the valence region during the breaking and formation of chemical bonds. Similar care should be taken in designing auxiliary bases. A single bond-centered fitting function can affect the energy as much as an entire set of d fitting functions; d fitting functions are not essential if

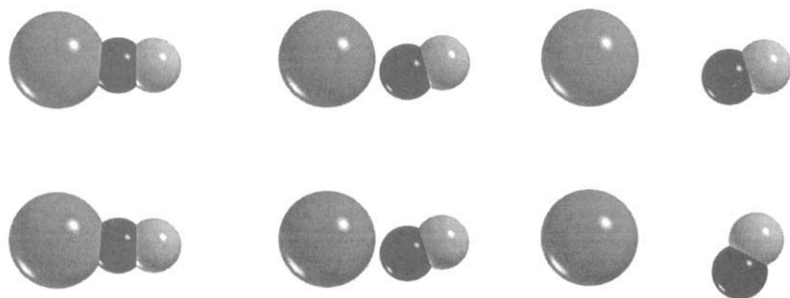


Figure 5. AIMD on the A' (above) and A'' (below) surfaces of slightly bent ICN. I is grey, C black, and N lightest. The structure of these two states evolve in time; from left to right immediately after, 28 fs into, and 120 fs into the dynamics.

bond-centered functions are used. Variational fitting is stable if bonds become break with bond-centered fitting function remaining in the basis.

Vertically excited in a linear configuration, ICN cannot bend because bending in either direction is equivalent by symmetry. Thus we chose to start our dynamics with the I atom displaced from equilibrium in a direction perpendicular to the C-N bond to make the ICN angle 175° . At this geometry the A'' state lies higher than the A' state, which has the excitation in the plane of the molecule, by 600 cm^{-1} . The the A' and A'' states were then propagated from rest. Three snapshots of the motion are given in Figure 5. The initial configurations are almost linear. A short time later, both states are quite bent. The bending forces gradually die out on the A' surface, but continue on the A'' surface, ultimately giving a bimodal rotational distribution like the experimental rotational distribution.

ICH₃ photodissociation is similar to ICN, except that bending is allowed upon any vertical ' σ ' to ' π ' excitation preserving C_{3v} symmetry. The molecule does not have to be bent slightly to enable it to experience bending forces, yet high end-over-end CH₃ rotation is not seen in any of its photodissociation decay channels. Like ICN, the A' state, with a hydrogen atom in the plane containing the excitation, is the lowest-energy excitation. The A'' state lies 5200 cm^{-1} higher in energy, however, almost ten times more so than the corresponding bent ICN state. This great energy difference prevents the methyl group from rotating freely after photoexcitation, consequently the molecule can and will immediately bend. This is seen in Fig. 6 which compares A' and A'' dissociation. The significant difference between ICN and ICH₃ photodissociation is that the methyl group is too big to keep on rotating throughout the dissociation. Instead the methyl group bounces off the I atom and ultimately

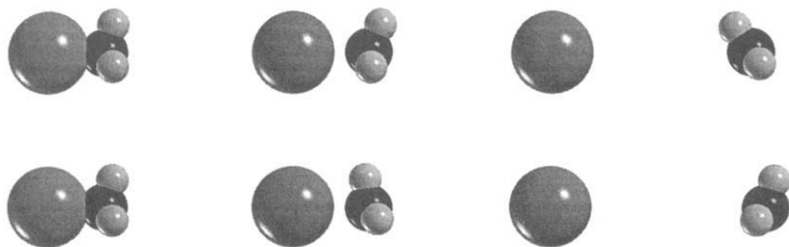


Figure 6. AIMD on the A' (above) and A'' (below) surfaces of slightly bent ICH₃. I is grey, C black, and H lightest. The structure of these two states evolve in time; from left to right immediately after, 34 fs into, and 200 fs into the dynamics.

dissociates rotating in the opposite sense to its initial rotation on in both surfaces. Thus the end-over-end rotational distribution of the methyl fragment from ICH₃ is much colder than the hot component of the CN rotational distribution from ICN, but the axial rotational temperature of the methyl fragment is even colder than the end-over-end rotational distribution because the initial photoexcitation locks to the methyl rotation.

Snapshots of ICH₃ photodissociation can be seen in Figure 6. The maximal amount of bending in the two decay channels do not occur at the same time step. The upper-state dynamics is ahead of that of the lower. The middle snapshots show both CH₃ fragments bent near the maximal amount in the initial direction. The upper state is bending in the opposite sense and the initial rotation is about to stop in the lower state. The right-hand panels of the figure show the CH₃ fragments bent in the other direction. In both molecules and both photoexcited states the initial motion is the same in the sense of involving strong bending.

5. CONCLUSIONS

The FON method enables the study of complex chemical reactions in Kohn-Sham DFT. In order for ground-state singlet ozone to react and form ground-state triplet oxygen molecules in DFT AIMD the occupations of the Kohn-Sham orbitals need to change from being all doubly occupied to having six half-filled orbitals. The situation is less dramatic for two linear ozone molecules reacting to form oxygen, but the orbital occupation numbers still must change for a ground-state to ground-state reaction to occur. The FON method can be used to change orbital occupation numbers smoothly during a complex chemical reaction. Exactly how the FON method is applied and which exchange-correlation functional is used can dramatically affect the course of an AIMD

simulation of a chemical reaction. The dynamics with analytical $X\alpha$ is rather similar to that with the GGA exchange correlation functional, which is expected to be more accurate. Because it avoids numerical integration of the exchange-correlation energy, analytic $X\alpha$ is less expensive computationally than either the LDA or the even more demanding GGA.

Variational fitting enables a completely analytic treatment of the $X\alpha$ exchange correlation functional. This practical first-principles AIMD method enables studies of detonations, photodissociation, and ultimately the even more complex chemical reactions that can be driven tribologically.

ACKNOWLEDGEMENT

RWW gratefully acknowledges an NRC/NRL Postdoctoral Research Associateship. This work was supported by the Office of Naval Research through the Naval Research Laboratory and directly through contracts N0001497WX20237 and N0001497WX20175.

REFERENCES

- † Current Address: Department of Chemistry, Saint Michael's College, Winooski Park, Colchester, VT 05439.
1. M. A. Collins, *Adv. Chem. Phys.* **93**, 389 (1996).
 2. J. M. Bowman and G. C. Schatz, *Ann. Rev. Phys. Chem.* **46**, 169 (1995).
 3. R. Car and M. Parrinello, *Phys. Rev. Lett.* **55**, 2471, (1985).
 4. T. Helgaker, E. Uggerud, and H. J. Aa. Jensen, *Chem. Phys. Lett.* **173**, 145 (1990).
 5. B. Hartke and E. A. Carter, *J. Chem. Phys.* **97**, 6569 (1992).
 6. T. Ziegler and A. Rauk, *Theoret. Chim. Acta* **46**, 1 (1977).
 7. B. I. Dunlap *Phys. Rev. A* **29**, 2902 (1984).
 8. W. Kohn and L. J. Sham, *Phys. Rev.* **140** A1133 (1965).
 9. B. I. Dunlap and N. Rösch, *Adv. in Quantum Chem.* **21**, 317 (1990).
 10. C. van Wüllen, *Chem. Phys. Lett.* **219**, 8 (1994).
 11. C. A. White and M. Head-Gordon, *J. Chem. Phys.* **104**, 2620 (1996).
 12. M. C. Strain, G. E. Scuseria, and M. Frisch, *Science* **271**, 51 (1996).
 13. R. Neuman and N. C. Handy, *Chem. Phys. Lett.* **252**, 19 (1996).
 14. A. St-Amant and D. R. Salahub, *Chem. Phys. Lett.* **169**, 387 (1990).
 15. D. Wei and D. R. Salahub, *Chem. Phys. Lett.* **224**, 291 (1994); *J. Chem. Phys.* **101**, 7633 (1994).
 16. B. I. Dunlap, J. W. D. Connolly, and J. R. Sabin, *J. Chem. Phys.* **71**, 3396 (1979).
 17. B. I. Dunlap, J. Andzelm, and J. W. Mintmire *Phys. Rev. A* **42**, 6354 (1990); B. I. Dunlap and J. Andzelm, *Phys. Rev. A* **45**, 81 (1992).
 18. B. I. Dunlap, *J. Phys. Chem.* **84**, 5524 (1986).
 19. B. I. Dunlap and N. Rösch, *J. Chim. Phys. Phys-chim. Biol.* **86**, 671 (1989).

20. K. S. Werpetinski and M. Cook, *Phys. Rev. A* **52**, 3397 (1995); *J. Chem. Phys.* **106**, 7124 (1997).
21. F. Sato, Y. Shigemitsu, I. Okazaki, S. Yahiro, M. Fukue, S. Kozuru and H. Kashiwagi, *Int. J. Quantum Chem.* **63**, 246 (1997).
22. C. Swope, H. C. Anderson, P. H. Berens, and K. R. Wilson, *J. Chem. Phys.* **76**, 637 (1982).
23. R. W. Warren and B. I. Dunlap, *Chem. Phys. Lett.* **262**, 384 (1996).
24. R. W. Warren and B. I. Dunlap, *Phys. Rev. A* **57**, 899 (1998).
25. B. I. Dunlap and W. N. Wei, *J. Chem. Phys.* **78**, 4997 (1983).
26. B. I. Dunlap, *Int. J. Quant. Chem.* **64**, 193 (1997).
27. J. A. Pople, H. Krishnan, H. B. Schlegel, and J. S. Binkley, *Int. J. Quant. Chem.* **S13**, 225 (1979).
28. J. F. Janek, *Phys. Rev. B* **18**, 7165 (1978).
29. M. Weinert and J. W. Davenport, *Phys. Rev. B* **45**, 13709 (1992).
30. B. I. Dunlap, *Adv. Chem. Phys.* **69**, 287 (1987).
31. A. Görling, *Phys. Rev. A* **47**, 2783 (1993).
32. J. P. Perdew, A. Savin, and K. Burke, *Phys. Rev. A* **51**, 4531 (1995).
33. R. Poirier, R. Kari, I. G. Csizmadia, *Handbook of Gaussian Basis Sets* (Elsevier, Amsterdam, 1985).
34. S. Huzinaga, ed., *Gaussian Basis Sets for Molecular Calculations* (Elsevier, Amsterdam, 1984).
35. N. Godbout, D. R. Salahub, J. Andzelm, and E. Wimmer, *Can. J. Chem.* **70**, 560 (1992).
36. J. Andzelm and E. Wimmer, *J. Chem. Phys.* **96**, 1280 (1992).
37. J. P. Perdew and A. Zunger, *Phys. Rev. B* **23**, 5048 (1981).
38. J. P. Perdew, J. A. Chevary, S. H. Vosko, K. A. Jackson, M. D. Peterson, D. J. Singh, and C. Fiolhais, *Phys. Rev. B* **46**, 6671 (1992).
39. J. C. Slater, *The Self-consistent Field for Molecules and Solids* (Quantum Theory of Molecules and Solids Vol. 4) (McGraw-Hill, New York, 1974).
40. B. I. Dunlap, D. W. Brenner, J. W. Mintmire, R. C. Mowrey, and C. T. White, *J. Phys. Chem.* **95**, 8737 (1991).
41. D. H. Robertson, D. W. Brenner, and C. T. White, *Phys. Rev. Lett.* **67**, 3132 (1991).
42. C. T. White, D. H. Robertson, and D. W. Brenner, *Physica (Amsterdam)* **188A**, 357 (1992).
43. D. W. Brenner, D. H. Robertson, M. L. Elert, and C. T. White, *Phys. Rev. Lett.* **67**, 2471 (1993).
44. A. Gedanken and M. D. Rowe, *Chem. Phys. Lett.* **34**, 39 (1975).
45. J. F. Black, *J. Chem. Phys.* **98**, 6853 (1993).
46. R. O. Loo, H.-P. Haerri, G. E. Hall, and P. L. Houston, *J. Chem. Phys.* **90**, 4222 (1989).
47. D. Y. Kim, N. Brandstater, L. Pipes, T. Garner, and D. Baugh, *J. Phys. Chem.* **99**, 4364 (1995).
48. W. S. Felps, K. Rupnik, and S. P. McGlynn, *J. Phys. Chem.* **95**, 639 (1991).
49. E. A. J. Wannemacher, H. Lin, W. H. Fink, A. J. Paul, and W. M. Jackson, *J. Chem. Phys.* **95**, 3431 (1991).

50. S. A. Barts and J. B. Halpern, *J. Phys. Chem.* **93**, 7346 (1989).
51. B. A. Waite, H. Helvajian, B. I. Dunlap, and A. P. Baronavski, *Chem. Phys. Lett.* **111**, 544 (1984).
52. B. A. Waite and B. I. Dunlap, *J. Chem. Phys.* **84**, 1391 (1986).
53. R. Schinke, *J. Chem. Phys.* **92**, 2397 (1990).
54. T. Seideman, *J. Chem. Phys.* **98**, 1989 (1993); **102**, 6487 (1995).
55. Y. Amatatsu, S. Yabushita, and K. Morokuma, *J. Chem. Phys.* **100**, 4894 (1994).
56. Y. Amatatsu, S. Yabushita, and K. Morokuma, *J. Chem. Phys.* **104**, 9783 (1996).
57. Y. Y. Bai, G. A. Segal, and H. Reisler, *J. Chem. Phys.* **94**, 331 (1991).
58. O. Gunnarsson and B. I. Lundqvist, *Phys. Rev. B* **13** 4274 (1976).
59. B. I. Dunlap, J. W. D. Connolly, and J. R. Sabin, *J. Chem. Phys.* **71**, 4993 (1979).

A Quantum Monte Carlo Approach to the Adiabatic Connection Method

Maziar Nekovee and W.M.C. Foulkes
The Blackett Laboratory, Imperial College,
Prince Consort Road, London SW7 2BZ, UK

A.J. Williamson, G. Rajagopal and R.J. Needs
TCM group, Cavendish Laboratory,
Madingley Road, Cambridge CB3 0HE, UK

Abstract

We present a new method for realizing the adiabatic connection approach in density functional theory, which is based on combining accurate variational quantum Monte Carlo calculations with a constrained optimization of the ground state many-body wavefunction for different values of the Coulomb coupling constant. We use the method to study an electron gas in the presence of a cosine-wave potential. For this system we present results for the exchange-correlation hole and exchange-correlation energy density, and compare our findings with those from the local density approximation and generalized gradient approximation.

1. Introduction
2. The Adiabatic connection
3. Quantum Monte Carlo realization
 - 3.1 Variational Monte Carlo
 - 3.2 Fixed-density variance minimization
4. Cosine-wave jellium
 - 4.1 Many-body wavefunction
5. Results and discussion

1 Introduction

Density functional theory (DFT) (1, 2) is the main computational tool for the treatment of many-body effects in solid state electronic structure calculations and is now widely used to determine ground-state properties of atoms and molecules (3). In the Kohn-Sham formulation of DFT (2) the problem of finding the ground state energy and density of an interacting N -electron system is transformed into an equivalent problem involving non-interacting electrons. The central quantity in this formulation is the exchange-correlation energy E_{xc} , which is a universal functional of the electron density $n(\mathbf{r})$. The exchange-correlation energy functional, a complicated many-body object, is the big unknown of the theory and the core problem in the density functional approach is to find accurate approximations for E_{xc} . The most frequently used approximations to date are the local density approximation (LDA) (2) and various generalized gradient approximations (GGA) (4, 5, 6).

An entirely different approach to the ground-state many-body problem is quantum Monte Carlo (QMC) (7). QMC calculations are computationally more demanding than density functional calculations. However, unlike the density functional approach, in which the ground-state density is the basic variable, quantum Monte Carlo methods focus on sampling the full ground-state many-body wavefunction of the system under consideration and hence yield a more detailed description of many-body effects. Quantum Monte Carlo calculations can therefore be used to investigate density functional theory from “outside” and to test the performance of approximations to E_{xc} . In the last few years a number of quantum Monte Carlo investigations of DFT have been reported for atoms and molecules (8, 9), model solids (10, 11) and silicon (12). Most of these investigations focused on extracting the exchange-correlation potential and components of exchange-correlation energy from accurate electron densities obtained from Monte Carlo calculations. Except for a very recent calculation by Hood *et al.*(12), other key quantities in DFT, namely the exchange-correlation hole n_{xc} and the exchange-correlation energy density ϵ_{xc} , have not been investigated with Monte Carlo methods. These quantities, however, are important in understanding the success of the LDA beyond its formal limits of validity, and play a key role in constructing more accurate approximations to E_{xc} . A better knowledge of these quantities is therefore crucial for a better understanding of the performance of the LDA and various corrections to it such as GGAs, and can guide the construction of more accurate functionals. Unlike V_{xc} which can be directly obtained from the electron density (by inversion of the Kohn-Sham equations (10, 8)) evaluating ϵ_{xc} and n_{xc} is more demanding. These quantities are derived from an adiabatic connection procedure in which one scales the Coulomb interaction by a factor λ

while keeping the density fixed at the ground state density of the system under consideration. To extract n_{xc} and e_{xc} from Monte Carlo data one therefore needs to calculate not only the ground state many-body wavefunction of the fully interacting system ($\lambda = 1$), but also the many-body wavefunction in the range $0 \leq \lambda < 1$.

Within variational quantum Monte Carlo, we have developed a new scheme for realizing the above adiabatic connection procedure which allows us to extract n_{xc} and e_{xc} from Monte Carlo data. Our method is based on a constrained optimization of the many-body wavefunction at different Coulomb coupling constants using the technique of variance minimization (13, 14). In this paper we will discuss aspects of our method and illustrate it with a first application to an electron gas exposed to a cosine-wave potential. For this system we calculate the exchange-correlation energy, exchange-correlation energy density and exchange-correlation hole, and compare our findings with those obtained from the LDA and the most commonly used version of GGA (6, 15).

2 The Adiabatic Connection

The idea of an adiabatic connection to determine E_{xc} has been developed by several authors (16-18). Here we closely follow the review by Parr and Yang (3). We consider a system of N interacting electrons in the presence of an external potential $V_{ex}(\mathbf{r})$ and characterized by the Hamiltonian (atomic units are used throughout, with $e = \hbar = m = 1$)

$$\hat{H} = \hat{T} + \hat{V}_{ee} + \hat{V}_{ex} \quad (1)$$

with

$$\hat{T} = \sum_{i=1}^N -\frac{1}{2} \nabla_i^2 \quad (2)$$

$$\hat{V}_{ee} = \frac{1}{2} \sum_{i=1}^N \sum_{j \neq i}^N \frac{1}{|\mathbf{r}_i - \mathbf{r}_j|} \quad (3)$$

$$\hat{V}_{ex} = \sum_{i=1}^N V_{ex}(\mathbf{r}_i) \quad (4)$$

In the Kohn-Sham formulation of DFT the problem of finding the ground state energy of this system is exactly mapped onto one of finding the electron density which minimizes the total energy functional

$$E[n(\mathbf{r})] = T_0[n(\mathbf{r})] + E_H[n(\mathbf{r})] + \int d\mathbf{r} V_{ex}(\mathbf{r})n(\mathbf{r}) + E_{xc}[n(\mathbf{r})] \quad (5)$$

Here T_0 is the kinetic energy of a fictitious non-interacting system of N electrons having the same electron density $n(\mathbf{r})$ as the interacting system and $E_H[n]$ is the Hartree (electrostatic) energy. The exchange-correlation energy functional $E_{xc}[n]$ is usually defined by equation (5) and contains all the many-body terms not considered elsewhere in (5).

An exact expression for E_{xc} is obtained by scaling the electron-electron interaction with a factor λ and varying λ between 1 (real system) and 0 (non-interacting system). The exchange-correlation functional E_{xc} is then given by (3)

$$E_{xc}[n] = \int_0^1 d\lambda < \Psi^\lambda | \hat{V}_{ee} | \Psi^\lambda > - E_H[n] \quad (6)$$

where Ψ^λ is the anti-symmetric many-body wavefunction which minimizes

$$F^\lambda = < \hat{T} + \lambda \hat{V}_{ee} > \quad (7)$$

under the fixed-density constraint

$$< \Psi^\lambda | \hat{n}(\mathbf{r}) | \Psi^\lambda > = n(\mathbf{r}) \quad (8)$$

and $\hat{n}(\mathbf{r})$ is the density operator

$$\hat{n}(\mathbf{r}) = \sum_{i=1}^N \delta(\mathbf{r} - \mathbf{r}_i). \quad (9)$$

A minimum for F^λ always exists (20) and, except under some unusual conditions (21), Ψ^λ can be obtained from the following Schrödinger equation

$$[\hat{T} + \lambda \hat{V}_{ee} + \hat{V}^\lambda] \Psi^\lambda = \hat{H}_\lambda \Psi^\lambda = E^\lambda \Psi^\lambda \quad (10)$$

with

$$\hat{V}^\lambda = \sum_{i=1}^N V^\lambda(\mathbf{r}_i). \quad (11)$$

The potential $V^\lambda(\mathbf{r})$ at point \mathbf{r} is a Lagrange multiplier corresponding to the fixed-density constraint at that point. As λ varies between 0 and 1, $V^\lambda(\mathbf{r})$ must be adjusted such that the electron density remains fixed at $n(\mathbf{r})$. At $\lambda = 1$, V^λ coincides with the actual external potential $V_{ex}(\mathbf{r})$ while at $\lambda = 0$, it coincides with the Kohn-Sham effective potential,

$$V^{\lambda=0}(\mathbf{r}) = V_{eff}(\mathbf{r}) = V_{ex}(\mathbf{r}) + V_H(\mathbf{r}) + V_{xc}(\mathbf{r}) \quad (12)$$

where V_H is the Hartree (electrostatic) potential

$$V_H(\mathbf{r}) = \int d\mathbf{r}' \frac{n(\mathbf{r}')}{|\mathbf{r} - \mathbf{r}'|} \quad (13)$$

and

$$V_{xc}(\mathbf{r}) = \frac{\delta E_{xc}[n]}{\delta n(\mathbf{r})} \quad (14)$$

is the Kohn-Sham exchange-correlation potential. Note also that $\Psi^{\lambda=0}$ corresponds to the Slater determinant of the exact Kohn-Sham orbitals corresponding to the density $n(\mathbf{r})$.

The adiabatic expression (6) allows us to obtain several useful decompositions of E_{xc} . Inserting (3) in (6) gives

$$E_{xc}[n(\mathbf{r})] = \frac{1}{2} \int d\mathbf{r} \int d\mathbf{r}' \frac{n(\mathbf{r})n_{xc}(\mathbf{r},\mathbf{r}')}{|\mathbf{r} - \mathbf{r}'|} \quad (15)$$

where n_{xc} is the density-functional exchange-correlation hole defined by (3)

$$\bar{n}(\mathbf{r},\mathbf{r}') = n(\mathbf{r})n(\mathbf{r}') + n(\mathbf{r})n_{xc}(\mathbf{r},\mathbf{r}') \quad (16)$$

Here $\bar{n}(\mathbf{r},\mathbf{r}')$ is the diagonal part of the two-particle density matrix averaged over λ ,

$$\bar{n}(\mathbf{r},\mathbf{r}') = \int_0^1 d\lambda \, n^\lambda(\mathbf{r},\mathbf{r}') \quad (17)$$

and

$$n^\lambda(\mathbf{r},\mathbf{r}') = \langle \Psi^\lambda | \sum_{i=1}^N \sum_{j \neq i}^N \delta(\mathbf{r} - \mathbf{r}_i) \delta(\mathbf{r}' - \mathbf{r}_j) | \Psi^\lambda \rangle. \quad (18)$$

Integrating (15) over \mathbf{r}' yields

$$E_{xc}[n(\mathbf{r})] = \int d\mathbf{r} \, e_{xc}(n[\mathbf{r}],\mathbf{r}) \quad (19)$$

where e_{xc} is the exchange-correlation energy density derived from the adiabatic connection procedure

$$e_{xc}([n(\mathbf{r})],\mathbf{r}) = \int_0^1 d\lambda \, e_{xc}^\lambda([n(\mathbf{r})],\mathbf{r}) \quad (20)$$

with e_{xc}^λ given by

$$e_{xc}^\lambda([n(\mathbf{r})],\mathbf{r}) = \langle \Psi^\lambda | \frac{1}{2} \sum_{i=1}^N \sum_{j \neq i}^N \frac{\delta(\mathbf{r} - \mathbf{r}_i)}{|\mathbf{r} - \mathbf{r}_j|} | \Psi^\lambda \rangle - \frac{1}{2} \int d\mathbf{r}' \frac{n(\mathbf{r})n(\mathbf{r}')}{|\mathbf{r} - \mathbf{r}'|} \quad (21)$$

For further reference we note that $n_{xc}^{\lambda=0}$ corresponds to the *density functional* exchange hole n_x . The corresponding exachange energy density is $e_x = e_{xc}^{\lambda=0}$ and the correlation energy density is given by $e_c = e_{xc} - e_x$. Note, however, that the exachange-correlation energy density, and hence its exchange and

correlation components, are not uniquely defined quantities since we can always add to e_{xc} any function which integrates to zero without affecting the exchange-correlation energy. Our definition of these quantities emerges in a natural way from the adiabatic connection. An alternative definition of the correlation energy density has been suggested by Baerends and Gritsenko (22) and by Huang and Umrigar (23).

3 Quantum Monte Carlo realization

Given an interacting many-body system with ground-state density $n(\mathbf{r})$, the main ingredient for evaluating n_{xc} and e_{xc} is the many-body wavefunction Ψ^λ for a number of systems corresponding to different values of the coupling constant λ satisfying the fixed-density constraint. In this section we describe our variational quantum Monte Carlo algorithm for obtaining Ψ_λ .

3.1 Variational Monte Carlo

In variational Monte Carlo calculations (7) one starts off with an explicit parameterized *Ansatz* for the ground-state many-body wavefunction of the system under consideration. The total energy of the system is then calculated as the expectation value of the Hamiltonian \hat{H} with respect to the variational wavefunction Ψ_T . Monte Carlo integration is used to perform the multi-dimensional integrals required for evaluating this expectation value and the variational parameters in Ψ_T are adjusted until an optimized wavefunction is obtained. The state-of-the-art method for performing the optimization procedure is the variance minimization scheme (13, 14). In this scheme one minimizes the variance of the local energy $\hat{H}\Psi_T/\Psi_T$ (rather than expectation value of \hat{H}) with respect to variational parameters over a set of particle configurations. The use of energy optimized wavefunctions may give unsatisfactory results when quantities other than the energy are evaluated, while minimization of the variance tends to give a better fit for the wavefunction as a whole, so that satisfactory results are obtained for a range of quantities including both energy and electron density. The electron density plays a central role in the adiabatic connection procedure making variance minimization a more suitable choice for optimizing Ψ^λ .

3.2 Fixed-density variance minimization

We consider an N-electron system having ground-state density $n(\mathbf{r})$. At a given coupling constant λ the corresponding many-body wavefunction Ψ^λ satisfies

equation (10). Therefore, at an arbitrary point $\mathbf{R} = (\mathbf{r}_1, \mathbf{r}_2, \dots, \mathbf{r}_N)$ in the $3N$ dimensional configuration space of electron coordinates, we have

$$\frac{H^\lambda \Psi^\lambda(\mathbf{R})}{\Psi^\lambda(\mathbf{R})} - E^\lambda \equiv 0. \quad (22)$$

In conventional variance minimization calculations (14) (i.e. the unconstrained $\lambda = 1$ case), the above property is used to find an overall fit to Ψ (we drop the λ superscript for simplicity). The procedure is to determine the parameters $\{\alpha\}$ in the trial function $\Psi_T(\mathbf{R}, \{\alpha\})$ by minimizing the variance of local energy σ^2

$$\sigma^2 = \int d\mathbf{R} \left[\frac{H^\lambda \Psi_T(\mathbf{R})}{\Psi_T^\lambda(\mathbf{R})} - E[\Psi_T] \right]^2 |\Psi_T(\mathbf{R})|^2 \quad (23)$$

where $E[\psi_T]$ is the expectation value of the Hamiltonian.

The above unconstrained optimization cannot be directly applied at intermediate values of λ for which the Hamiltonian contains the unknown potential V_λ . We found, however, that a simultaneous determination of Ψ_λ and V_λ can be achieved by performing the following constrained optimization. We assume that the trial many-body wavefunction Ψ_T^λ results in the electron density $n^\lambda(\mathbf{r})$ and expand both $n^\lambda(\mathbf{r})$ and the ground state density $n(\mathbf{r})$ in a complete and orthonormal set of basis functions $\{f_s\}$

$$n(\mathbf{r}) = \sum_{s=1}^{N_d} n_s f_s(\mathbf{r}) \quad (24)$$

$$n^\lambda(\mathbf{r}) = \sum_{s=1}^{N_d} n_s^\lambda f_s(\mathbf{r}) \quad (25)$$

where N_d is a cut-off chosen such that the above expansions converge to $n(\mathbf{r})$ and $n_\lambda(\mathbf{r})$ within a specified accuracy. Subsequently, we define the modified penalty function μ^2

$$\mu^2 = \sigma^2 + W \sum_{s=1}^{N_d} [n_s - n_s^\lambda]^2 \quad (26)$$

where W is a weight factor the magnitude of which determines the emphasis laid on the fixed-density constraint. The above penalty function reaches its lower bound (of zero) if and only if Ψ^λ is the exact many-body wavefunction satisfying the fixed density constraint (within the accuracy set by N_d) and V^λ is the corresponding exact potential. Hence minimization of μ^2 will, in principle, result in the *simultaneous* determination of Ψ^λ and V^λ . In practice, however, our constrained search is restricted to a sub-space of many-body wavefunctions and minimization of μ^2 yields an optimal fit to Ψ^λ and a corresponding optimal

fit to V^λ , the deviations of which from the exact V^λ reflect the errors in the many-body wavefunction.

Our numerical implementation of the above scheme works as follows. We start off with an initial guesses Ψ_0^λ for the many-body wavefunction and a corresponding guess for V^λ . A fixed number N_c of statistically independent configurations \mathbf{R}_i are then sampled from $|\Psi_0^\lambda|^2$ and the Monte Carlo estimator of μ^2 over these configurations is evaluated

$$\mu^2 = \sum_{i=1}^N (E_L(\mathbf{R}_i) - \langle E_L \rangle)^2 \left[\frac{\omega_i}{\sum_{j=1}^{N_c} \omega_j} \right] + W \sum_{s=1}^{N_d} [n_s - n_s^\lambda]^2 \quad (27)$$

with

$$E_L(\mathbf{R}_i) = \frac{H\Psi_T^\lambda(\mathbf{R}_i)}{\Psi_T^\lambda(\mathbf{R}_i)} \quad (28)$$

$$\omega_i = \left| \frac{\Psi_T^\lambda}{\Psi_0^\lambda} \right|^2 \quad (29)$$

$\langle E_L \rangle$ the average energy

$$\langle E_L \rangle = \sum_{i=1}^{N_c} E_L(\mathbf{R}_i) \left[\frac{\omega_i}{\sum_{j=1}^{N_c} \omega_j} \right] \quad (30)$$

The expansion coefficients of the electron density, n_s^λ , are evaluated from

$$n_s^\lambda = \sum_{i=1}^{N_c} \sum_{k=1}^N f^*(\mathbf{r}_k^i) \left[\frac{\omega_i}{\sum_{j=1}^{N_c} \omega_j} \right] \quad (31)$$

where \mathbf{r}_k^i denotes the coordinates of the electron k belonging to configuration i . Finally, we vary the parameters in Ψ_T^λ and V^λ , using a standard NAG routine for optimization, until μ^2 is minimized. We found that setting W equal to the number of configurations results in a satisfactory minimization of both the variance in energy and the error in electron density.

Following (14) we set the reweighting factors ω_i in equations (27) and (30) equal to unity in order to avoid a numerical instability in the variance minimization procedure which occurs for systems with a large number of electrons (these factors, however, are included in calculating the expansion coefficients of the electron density). The above fixed-density variance minimization is then repeated several times until the procedure converges.

4 Cosine-wave jellium

We performed adiabatic connection calculations for the inhomogeneous spin-unpolarized electron gas with average electron density $n_0 = 3/(4\pi r_s^3)$ corresponding to $r_s = 2$. In the QMC simulations we model this system by a finite

system of $N = 64$ electrons satisfying periodic boundary conditions in a FCC simulation cell. Density modulations can be induced by applying an external potential of the form $V_{\mathbf{q}} \cos(\mathbf{q} \cdot \mathbf{r})$ where, because of periodic boundary conditions, \mathbf{q} is restricted to be a reciprocal lattice vector of the simulation cell. Alternatively, we can fix the ground-state electron density *a priori* and use our fixed-density variance minimization method to obtain the corresponding many-body wavefunction at a given Coulomb coupling constant which produces the specified density. In the calculations reported here we chose this second option, with the “target” electron density for the system generated in the following way. We expose the non-interacting electrons (i.e. the $\lambda = 0$ system) to the potential $V(\mathbf{r})$

$$V(\mathbf{r}) = V_{\mathbf{q}} \cos(\mathbf{q} \cdot \mathbf{r}) \quad (32)$$

with $V_{\mathbf{q}} = 2.084\epsilon_F^0$ and $\mathbf{q} = 2\mathbf{B}_3$. Here ϵ_F^0 is the Fermi energy of the unperturbed electron gas, \mathbf{B}_3 is a primitive vector of the reciprocal (simulation) cell with $|2\mathbf{B}_3| = 1.11k_F^0$, and k_F^0 is the Fermi wavevector. We then solve the following self-consistent single-particle Schrödinger equations

$$[-\frac{1}{2}\nabla^2 + V_{eff}]\phi_i = \epsilon_i\phi_i \quad (33)$$

with

$$V_{eff}(\mathbf{r}) = V(\mathbf{r}) + V_H(\mathbf{r}) + V_{xc}^{LDA}(\mathbf{r}) \quad (34)$$

to obtain the electron density

$$n(\mathbf{r}) = 2 \sum_{i=1}^{N/2} |\phi_i(\mathbf{r})|^2 \quad (35)$$

We *define* this density to be the exact ground-state density of our interacting system. In this way, the single-particle orbitals ϕ_i are by construction the exact Kohn-Sham orbitals and their Slater determinant corresponds exactly to the many-body wavefunction at $\lambda = 0$. Having obtained this non-interacting v -representable density we then perform fixed-density variance minimization to produce variational many-body wavefunctions at non-zero Coulomb coupling constants (including the ground-state many-body wavefunction at $\lambda = 1$) which reproduce this density and (variationally) satisfy the Schrödinger equation (10). Once the $\Psi_{\lambda S}$ are obtained, we use the Monte Carlo Metropolis algorithm to evaluate the required expectation values and perform a numerical coupling constant integration using Gaussian quadrature.

4.1 Many-body wavefunction

The quality of a variational quantum Monte Carlo calculation is determined by the choice of the many-body wavefunction. The many-body wavefunction we use is of the parameterized Slater-Jastrow type which has been shown to yield accurate results both for the homogeneous electron gas and for solid silicon (14) (In the case of silicon, for example, 85% of the fixed-node diffusion Monte Carlo correlation energy is recovered). At a given coupling λ , Ψ^λ is written as

$$\Psi^\lambda = D^\uparrow D^\downarrow \exp \left[- \sum_{i>j} u_{\sigma_i, \sigma_j}^\lambda(r_{ij}) + \sum_i \chi^\lambda(\mathbf{r}_i) \right] \quad (36)$$

where $r_{ij} = |\mathbf{r}_i - \mathbf{r}_j|$ and D^\uparrow and D^\downarrow are Slater determinants of spin-up and spin-down Kohn-Sham orbitals respectively. $u_{\sigma_i, \sigma_j}^\lambda$ is the two-body term correlating the motion of pairs of electrons and σ_i denotes the spin of electron i . Finally, χ^λ is a one-body function which is absent in the homogeneous electron gas but is crucial for a satisfactory description of systems with inhomogeneity. Both u^λ and χ^λ contain variational parameters. We write u^λ as (14)

$$u^\lambda(r) = u_0^\lambda(r) + f^\lambda(r), \quad (37)$$

where u_0^λ is a fixed function and f^λ is given by

$$\begin{aligned} f^\lambda(r) &= B^\lambda \left(\frac{L_{WS}}{2} + r \right) (L_{WS} - r)^2 + r^2 (L_{WS} - r)^2 \sum_{l=0}^M \alpha_l^\lambda T_l(\bar{r}) & 0 \leq r \leq L_1 \\ &= 0 & r > L_{WS} \end{aligned} \quad (38)$$

where B^λ and α_l^λ are variational coefficients, T_l is the l th Chebyshev polynomial, and

$$\bar{r} = \frac{2r - L_{WS}}{L_{WS}}. \quad (39)$$

In the last two equations L_{WS} is the radius of the sphere touching the Wigner-Seitz cell of the simulation cell.

The fixed part of u^λ at full coupling constant $\lambda = 1$ is the short-ranged Yukawa form (14)

$$u_0^1(r) = \frac{A^1}{r} \left(1 - \exp\left(-\frac{r}{F^1}\right) \right) \exp\left(-\frac{r^2}{L_0^2}\right), \quad (40)$$

where A^1 is fixed by the plasma frequency of the unperturbed electron gas

$$A^1 = \frac{1}{\omega_p^0} \quad (41)$$

and F^1 is fixed by imposing the cusp condition (7) leading to $F_{\sigma_i, \sigma_j}^1 = \sqrt{(2A^1)}$ for parallel spins and $F_{\sigma_i, \sigma_j}^1 = \sqrt{(A^1)}$ for anti-parallel spins. L_0 is a cut-off parameter chosen so that $u_0(L_{WS})$ is effectively zero and is set equal to $0.25L_{WS}$ in the present calculations. In the case of the unperturbed electron gas, scaling arguments (24) applied to the Hamiltonian (10) result in the following relation for the exact many-body wavefunction at coupling constant λ

$$\Psi_{r_s}^\lambda(\mathbf{r}_1, \mathbf{r}_2, \dots \mathbf{r}_n) = C^\lambda \Psi_{r'_s}^{\lambda=1}(\lambda \mathbf{r}_1, \lambda \mathbf{r}_2, \dots \lambda \mathbf{r}_n) \quad (42)$$

where $\Psi_{r'_s}^{\lambda=1}$ is the ground-state wavefunction of a homogeneous electron gas with the density parameter $r'_s = \lambda r_s$ and C^λ is a normalization constant. For the unperturbed electron gas ($\chi \equiv 0$) imposing condition (42) on the fixed-part of our Slater-Jastrow wavefunction yields

$$u_0^\lambda(r) = \frac{A^\lambda}{r} \left(1 - \exp\left(-\frac{r}{F^\lambda}\right) \right) \exp\left(-\frac{r^2}{L_0^2}\right), \quad (43)$$

where $A^\lambda = \lambda^{1/2} A^1$, $F^\lambda = \lambda^{-1/4} F^1$. We note that with the above choice for A^λ and F^λ the λ -dependent cusp conditions are automatically satisfied. The electron density is modulated only in the \mathbf{B}_3 direction and hence both the one-body part of the Jastrow factor and V^λ can be expanded as

$$\chi^\lambda(\mathbf{r}) = \sum_{m=1}^M \chi^\lambda(m\mathbf{B}_3) \cos(m\mathbf{B}_3 \cdot \mathbf{r}) \quad (44)$$

$$V^\lambda(\mathbf{r}) = \sum_{m=1}^M V^\lambda(m\mathbf{B}_3) \cos(m\mathbf{B}_3 \cdot \mathbf{r}) \quad (45)$$

The electron density is expanded in a similar way (with the inclusion of the $m = 0$ term). We use 7 Fourier coefficients in the expansion of electron density, 6 Fourier coefficients in the expansions of χ_λ and V_λ (only the first four coefficients turned out to be significantly different from zero), and 8 coefficients (for each of the spin-parallel and spin-antiparallel cases) in the two-body term.

5 Results and discussion

We performed adiabatic connection calculations for cosine-wave jellium using six values of λ : 0, 0.2, 0.4, 0.6, 0.8, 1. The many-body wavefunctions for $\lambda > 0$ were optimized by fixed-density variance minimization using 10000 independent N -electron configurations at each λ . These configurations were regenerated several times. The weight factor in expression (27) was set equal

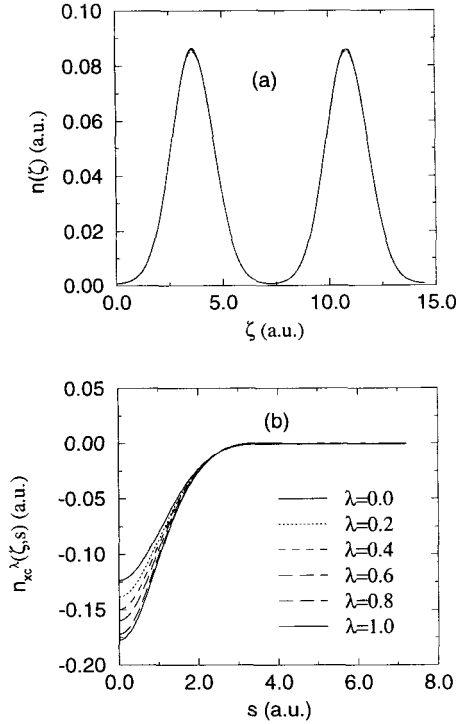


Figure 1: (a) Electron density for different values of λ plotted along ζ (the direction of inhomogeneity). (b) The λ -dependent spherically averaged exchange-correlation hole for an electron sitting at $\zeta = 10.85$ a.u.

to 10000 in order to obtain a satisfactory minimization of both the variance in energy and the error in electron density. Once Ψ_λ was optimized, quantities of interest were accumulated with the Metropolis Monte Carlo algorithm using 500000 statistically uncorrelated configurations.

We found that our method results in electron densities $n^\lambda(\mathbf{r})$ which deviate from the reference density by less than 1%. This is shown in figure 1(a) where the density is plotted as a function of λ along a line parallel to the direction in which the external potential varies (we call this the ζ direction). While the density is fixed, all other physical quantities vary smoothly and monotonically with λ . As an example we consider the spherically-averaged exchange-correlation hole

$$\tilde{n}_{xc}^\lambda(\mathbf{r}, s) = \frac{1}{4\pi} \int_{\Omega} d\mathbf{r}' n_{xc}^\lambda(\mathbf{r}, \mathbf{r}'), \quad \Omega : |\mathbf{r} - \mathbf{r}'| = s \quad (46)$$

as a function of λ . In figure 1(b) this quantity is shown around an electron sitting at one of the maxima of the electron density ($\zeta = 10.85$ a.u.). The $\lambda = 0$ curve corresponds to the spherically-averaged exchange hole. The ex-

change hole is relatively shallow and negative everywhere. As the interaction is switched on, the hole around the electron becomes gradually deeper. The spherically-averaged hole obeys the sum-rule (3)

$$4\pi \int s^2 \tilde{n}_x^\lambda(\mathbf{r}, s) = -1 \quad (47)$$

and the deepening of the hole for $\lambda > 0$ is compensated by the fact that the hole becomes slightly positive far away from the electron. Note that the hole does not “narrow” as it deepens, but actually broadens. In evaluating $\tilde{\rho}_{xc}^\lambda$ we expanded the exchange-correlation hole in a double Fourier series, sampled the corresponding expansion coefficients and subsequently performed the spherical averaging. Our calculated ρ_{xc}^λ does not satisfy the Kimball cusp-condition (25, 29) because of the finite number of plane-waves in its Fourier expansion. As a result $\tilde{\rho}_{xc}^\lambda$ has zero slope at $s = 0$. We note, however, that this deficiency does not affect E_{xc} and e_{xc}^λ because these quantities are evaluated directly from equations (6) and (21).

Before discussing our findings for this system, we would like to pause and give a short outline of the errors present in our simulations. First of all, the small ($< 1\%$) deviations of the electron density at different λ from the reference density $n(\mathbf{r})$ will induce errors in the adiabatically calculated quantities such as the correlation energy density. By recalculating the exchange energy density with a density which deviates from the reference density by 1% and extrapolating the resulting deviation $e_x[n(\mathbf{r})] - e_x[n(\mathbf{r}) + \delta n(\mathbf{r})]$ to the correlation energy density, we estimate the errors in e_c due to these density deviations to be also $\sim 1\%$.

Further, there are two other kind of errors in our calculations: (i) statistical errors; and (ii) finite size errors (i.e. those caused by the fact that we are using a finite number of electrons to model a supposedly infinite system). With 500000 configurations used in sampling all physical quantities, we found statistical errors to be unimportant, except for the exchange-correlation hole. By evaluating the exchange hole both directly and by Monte Carlo sampling, and assuming that the errors in n_{xc} for $\lambda \neq 0$ are similar, we estimate the statistical error in this quantity to be less than 7%. Another source of errors is finite size effects. These errors occur because a finite simulation cell is used to model an infinite system, with the Coulomb interaction energy evaluated using the Ewald formula (26). The use of a finite simulation cell with periodic boundary conditions affects the wavefunction, of course, and the use of Ewald interaction also produces a Coulomb finite size error in the interaction energy (26, 27). We found the effect of the finite cell on the exchange-correlation hole to be unimportant, except for the asymptotic behavior of this quantity which cannot be correctly described with the present system size. Coulomb finite size

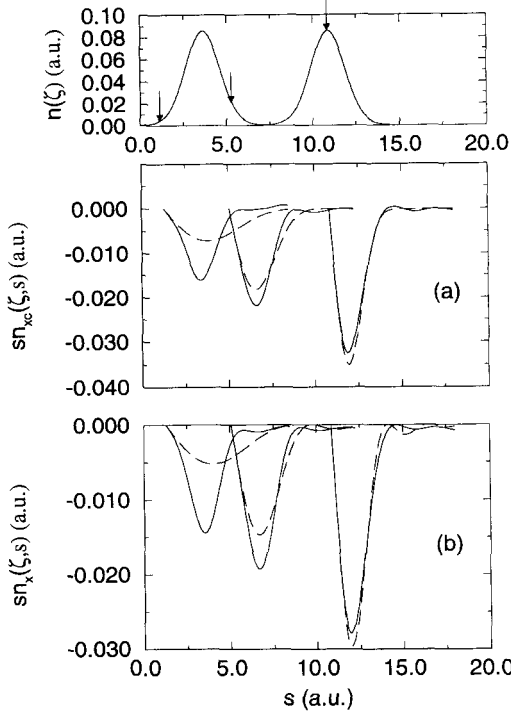


Figure 2: (a) VMC (solid lines) and LDA (dashed lines) $s\tilde{n}_{xc}(\mathbf{r}, s)$ plotted for an electron moving along ζ . Arrows on the electron density (plotted on top), mark the position of the electron. (b) Exact $s\tilde{n}_x(\mathbf{r}, s)$ plotted in the same direction and at the same points as in (a) (solid lines) and the corresponding LDA approximation (dashed lines).

effects do not significantly affect the many-body wavefunctions, and hence their effect on quantities such as the electron density and the exchange-correlation hole is negligible. The exchange-correlation energy density, however, is directly affected by Coulomb finite size effects since in evaluating e_{xc}^λ the $1/|\mathbf{r} - \mathbf{r}'|$ Coulomb interaction in (21) is replaced by the periodic Ewald interaction. By calculating the exchange energy density of the homogeneous electron gas using our finite simulation cell and comparing it with the exact result (28)

$$e_x = -\frac{0.45805}{r_s} n_0 \quad (48)$$

we estimate the total finite-size error in e_x to be of the order of -2×10^{-4} a.u.; the errors in the correlation energy density e_c is expected to be somewhat

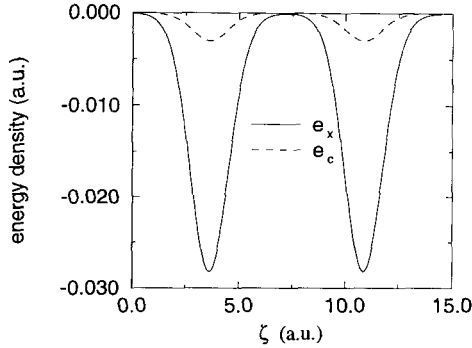


Figure 3: Exchange (solid line) and correlation (dashed line) contributions to e_{xc} plotted along ζ .

smaller.

We now turn to our results for n_{xc} and e_{xc} . The spherically averaged exchange-correlation hole, $\tilde{n}_{xc}^\lambda(\mathbf{r}, s)$, obtained from our adiabatic calculations is shown in figure 2(a) together with the LDA approximation (28) to this quantity

$$n_{xc}^{LDA}(\mathbf{r}, s) = n(\mathbf{r})(\bar{g}^{hom}(n(\mathbf{r}), s) - 1) \quad (49)$$

where \bar{g}^{hom} is the λ -averaged pair-correlation function of a homogeneous electron gas with density $n(\mathbf{r})$ (we use the Perdew-Wang parameterization of \bar{g} (29)). In this figure we plot $n_{xc}(\mathbf{r}, s)$ for an electron moving along ζ , and hence fully experiencing the strong variations in electron density. The hole is shown multiplied by s so that the area under each curve is directly proportional to the exchange-correlation energy per electron e_{xc}/n . At $\zeta = 1.30$ a.u. the electron density is very low and n_{xc} is shallow. As electron moves to higher densities ($\zeta = 5.6$ and $\zeta = 10.85$ a.u.) the hole becomes deeper and its asymptotic tail less pronounced. Unlike the LDA hole which depend only on the local density $n(\mathbf{r})$ and is dug out of a homogeneous electron gas of that density, the VMC

hole depends on the density everywhere in the vicinity of \mathbf{r} . At $\zeta = 1.30$ a.u., where the electron density is very low, the LDA “probes” only this density and for this reason the LDA exchange-correlation hole is very different from the VMC hole, even close to the electron. As the electron moves to the high density region, the LDA description becomes more satisfactory and at $\zeta = 10.85$ a.u., where the electron density has a maximum, the agreement between the LDA and the VMC hole is rather good. In figure 2(b) we compare the exact exchange hole (obtained from our exact Kohn-Sham orbitals) for the same electron positions with the LDA hole given by (28)

$$\tilde{n}_x^{LDA}(\mathbf{r}, s) = -\frac{9}{2}n(\mathbf{r}) \left[\frac{j_1(k_F(\mathbf{r})s)}{k_F(\mathbf{r})s} \right]^2, \quad (50)$$

where $k_F(\mathbf{r}) = (3\pi^2 n(\mathbf{r}))^{1/3}$ is the local Fermi wavevector and j_1 the first order spherical Bessel function. Once again, the LDA description is unsatisfactory at low densities but improves as we move to the high density region.

Next we consider exchange-correlation energy densities. In figure 3 the exchange and correlation contributions to this quantity are shown. The differences $e_x^{VMC} - e_x^{LDA}$ and $e_c^{VMC} - e_c^{LDA}$ are shown in figure 4 (a). The difference in e_c follows the variations in electron density and is largest at points where $n(\mathbf{r})$ has a maximum. The differences in e_x shows a more complicated structure and $e_x^{VMC} < e_x^{LDA}$ everywhere in the system. This result is in line with the well-known fact that LDA almost always underestimates the exchange energy of an inhomogeneous system. However, because of the finite size errors, we expect the true e_x to be slightly ($\sim 2 \times 10^{-4}$ a.u.) less negative than e_x^{VMC} so that $e_x < e_x^{LDA}$ must holds in most points of the structure but not necessarily everywhere.

The GGAs for exchange and correlation of a spin-unpolarized system are written as (15)

$$E_x = \int d\mathbf{r} n(\mathbf{r}) \epsilon_x^{unif}(n(\mathbf{r})) F_x(s) \quad (51)$$

$$E_c = \int d\mathbf{r} n(\mathbf{r}) [\epsilon_c^{unif}(n(\mathbf{r})) + H(n(\mathbf{r}), t)] \quad (52)$$

In the above equations ϵ_x^{unif} and ϵ_c^{unif} are the exchange and correlation energies per particle of a uniform electron gas with density $n(\mathbf{r})$, $t = |\nabla n|/2k_s(\mathbf{r})$, $s = |\nabla n|/2k_F(\mathbf{r})$ with k_s the local Thomas-Fermi wavevector $k_s(\mathbf{r}) = \sqrt{4k_F(\mathbf{r})/\pi}$. In analogy with (19) one may define the GGA e_x and e_c as

$$e_x^{GGA}(\mathbf{r}) = n(\mathbf{r}) \epsilon_x^{unif}(n(\mathbf{r})) F_x(s) \quad (53)$$

and

$$e_c^{GGA}(\mathbf{r}) = n(\mathbf{r}) [\epsilon_c^{unif}(n(\mathbf{r})) + H(n(\mathbf{r}), t)] \quad (54)$$

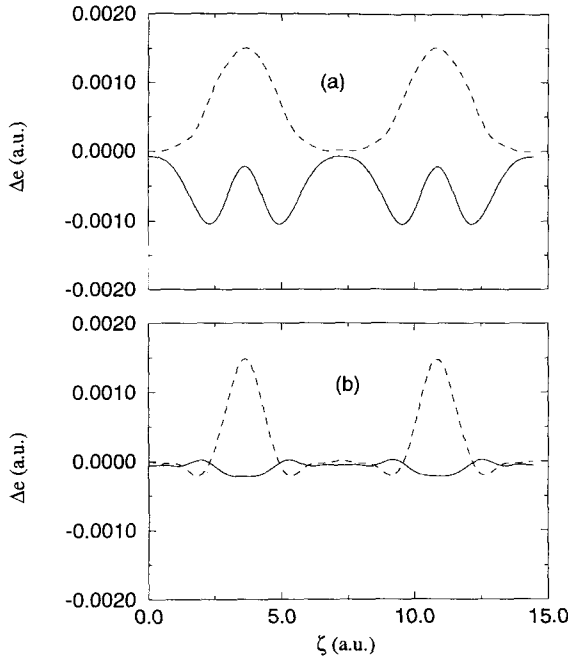


Figure 4: (a) The differences $e_x^{VMC} - e_x^{LDA}$ (solid line) and $e_c^{VMC} - e_c^{LDA}$ (dashed line) plotted along ζ . (b) The same as (a) but for $e_x^{VMC} - e_x^{GGA}$ and $e_c^{VMC} - e_c^{GGA}$.

We note that the above quantities do not directly correspond to the physical e_x and e_c as defined by equation (21) (i.e. via the exchange-correlation hole). Nevertheless, they present pointwise corrections to the LDA exchange and correlation energy densities and for this reason we found it interesting to compare them with our VMC results. In figure 4(b) we show $e_x^{VMC} - e_x^{GGA}$ and $e_c^{VMC} - e_c^{GGA}$. The GGA results were obtained from the ground state density $n(\mathbf{r})$ using the Perdew-Burke-Ernzerhof scheme (15), which we found to give results slightly different from PW91 (6). Note that the difference between the VMC and the GGA exchange energy densities is significantly smaller than that between the VMC and the LDA exchange energy densities, indicating that the GGA improves upon the LDA in describing this quantity. As for e_c , the differences are of the same order as for the LDA, although the shape is

different. It is interesting that the LDA errors in e_x and e_c partially cancel each other, even on a local scale, but that these cancellations do not occur for the GGA. In summary, the GGA seems to do a good job in improving the LDA description of the exchange energy density but is less successful in the case of the correlation energy density. The resulting exchange correlation energy per electron obtained from VMC, LDA and GGA are $E_{xc}^{VMC}/N = -0.328 \pm 0.009$, $E_{xc}^{LDA}/N = -0.3296$, $E_{xc}^{GGA}/N = -0.3347$ a.u.

Acknowledgments

We thank Randy Hood and Mei-Yin Chou for helpful discussions. Part of this work has been supported by the Human Capital and Mobility Program through contract No. CHRX-CT94-0462.

References

- (1) P. Hohenberg and W. Kohn, Phys. Rev. **136**, B864 (1964).
- (2) W. Kohn and L.J. Sham, Phys. Rev. **140**, A1133 (1965).
- (3) R.G. Parr and W. Yang, *Density Functional Theory of Atoms and Molecules* (Oxford University Press, New York, 1989).
- (4) D.C. Langreth and M.J. Mehl, Phys. Rev. B **28**, 1809 (1983).
- (5) A.D. Becke, Phys. Rev. A **38**, 3098 (1988).
- (6) J.P. Perdew *et al.*, Phys. Rev. B **46**, 6671 (1992); **48**, 4978 (1993) (E).
- (7) B.L. Hammond, W.A. Lester, Jr. and R.J. Reynolds, *Monte Carlo Methods in Ab Initio Quantum Chemistry* (World Scientific, Singapore, 1994).
- (8) C.J. Umrigar and X. Gonze in *High Performance Computing and its Applications to the Physical Science*, edited by D.A. Browne *et al.* (World Scientific, Singapore, 1993).
- (9) C. Filippi, C.J. Umrigar and X. Gonze, Phys. Rev. A **54**, 4810 (1996).
- (10) W. Knorr and R.W. Godby, Phys. Rev. Lett. **68**, 639 (1992).
- (11) G.E. Engel, Y. Kwon and R.M. Martin, Phys. Rev. B **51** (1995).
- (12) R.Q. Hood *et al.* Phys. Rev. Lett. **78**, 3350 (1997).

- (13) C.J. Umrigar, K.G. Wilson and J.W. Wilkins, Phys. Rev. Lett. **60**, 1719 (1988).
- (14) A.J. Williamson *et al.*, Phys. Rev. B **53**, 9640 (1996).
- (15) J.P. Perdew, K. Burke and M. Ernzerhof, Phys. Rev. Lett. **77**, 3865 (1996).
- (16) J. Harris and R.O. Jones, J. Phys. F **4**, 1170 (1974).
- (17) D.C. Langreth and J.P. Perdew, Phys. Rev. B **21**, 5469 (1980).
- (18) O. Gunnarson and B.I. Lundqvist, Phys. Rev. B **13**, 4274 (1976).
- (19) M. Levy in *Density Functional Theory*, edited by J. Keller and J.L. Gasquez (Springer, New York, 1983).
- (20) E.H. Lieb, in *Physics as Natural Philosophy*, edited by A. Shimony, H. Feshbach (MIT Press, Cambridge, Mass, 1982).
- (21) H. Englisch and R. Englisch, Physica (Utrecht) **21A**, 253 (1983).
- (22) E.J. Baerends and O.V. Gritsenko J. Phys. Chem., **101**, 5383 (1997).
- (23) Chien-Juang Huang and C.J. Umrigar, Phys. Rev. A, **56**, 290 (1997).
- (24) M. Levy and J.P. Perdew, Phys. Rev. A **32**, 2010 (1985).
- (25) A.K. Rajagopal, J.C. Kimball and M. Banerjee, Phys. Rev. B **18**, 2339 (1978); J.C. Kimball, Phys. Rev. A **7**, 1648 (1973).
- (26) L.M. Fraser *et al.*, Phys. Rev. B **53**, 1814 (1996).
- (27) A.J. Williamson *et al.*, Phys. Rev. B **55**, R4851 (1997).
- (28) R.M. Dreizler and E.K.U. Gross, *Density Functional Theory, An approach to the Quantum Many-Body Problem*, (Springer-Verlag, Berlin 1990).
- (29) J.P. Perdew and Y. Wang, Phys. Rev. B **46**, 12947 (1992).
- (30) J.P. Perdew and K. Burke, private communication.

Full potential linearized-augmented-plane-wave calculations for 5d transition metals using the relativistic generalized gradient approximation

R. N. Schmid, E. Engel, and R. M. Dreizler

Institut für Theoretische Physik, Universität Frankfurt, Robert-Mayer-Str. 8-10,
D-60054 Frankfurt/Main, Germany

P. Blaha and K. Schwarz

Institut für Technische Elektrochemie, Technische Universität Wien,
Getreidemarkt 9/158, A-1060 Wien, Austria

Abstract

The importance of relativistic exchange-correlation effects for the description of 5d transition metals is examined by application of a relativistic extension of the Perdew-Wang generalized gradient approximation to Pt and Au, using a full potential linearized-augmented-plane-wave approach. It is found that the relativistic corrections to exchange affect both the band structure and the cohesive properties on the 1% level, while the relativistic corrections to correlation can be safely neglected.

I. Introduction and Summary of Results

Establishing fully relativistic methods for *ab-initio* electronic structure calculations in atomic, molecular and solid state physics has been as a major activity during recent years. As density functional theory (DFT) has proven to be rather successful in nonrelativistic applications [1–3], its relativistic version [4–8] is a promising tool for the investigation of systems with heavy elements. The crucial quantity of the DFT formalism is the exchange-correlation (*xc*) energy functional $E_{xc}[n]$, which, together with the corresponding single particle *xc*-potential $v_{xc}(\mathbf{r}) = \delta E_{xc}[n]/\delta n(\mathbf{r})$, provides the DFT description of *xc*-effects.

A considerable amount of work has been devoted to the development of suitable approximations for $E_{xc}[n]$, which are efficient and at the same time reliable

and sufficiently accurate. For a long time, the nonrelativistic local density approximation (LDA), based on the homogeneous electron gas (HEG), has been the standard for $E_{xc}[n]$ in both nonrelativistic and relativistic calculations. During the last years, gradient corrections to the LDA have attracted widespread interest. Nonrelativistic generalized gradient approximations (GGAs) [9,10] have improved the quality of DFT results for a variety of systems, most notably for the structural properties of small molecules [11,12] and metallic iron [13]. However, it has become clear by now that for solids GGA functionals are not systematically superior to the LDA [14–20]. In particular, while GGA functionals are remarkably successful for 3d transition metals [13,14], they overcorrect the LDA's errors for 5d transition metals [17,18,20]. This even worsens the agreement with experiment for some systems, with Gold being the prime example.

On the other hand, Gold shows large relativistic effects (the *Gold maximum* — see eg. [21]). In fact, it has been explicitly demonstrated that for Au relativistic and xc -effects are nonadditive [22]. This is most obvious for its electron affinity: While a nonrelativistic CI-calculation [23] gives a value of 1.02 eV and a fully relativistic Coupled-Cluster calculation [22] yields 2.28 eV, the corresponding nonrelativistic and relativistic Hartree-Fock values are 0.10 eV [22] and 0.67 eV, respectively. Thus immediately the question arises to which extent the GGA's failure for metallic Au is due to the neglect of relativistic xc -contributions in $E_{xc}[n]$.

In the atomic context the need for relativistic corrections to $E_{xc}[n]$ is obvious and has led to the development of the relativistic LDA (RLDA) [5,6,24]. On the basis of RLDA calculations for metallic Au and Pt, MacDonald *et al.* [25,26] have concluded that in solids relativistic contributions to $E_{xc}[n]$ can produce small but significant modifications of measurable quantities, as eg. the Fermi surface area. On the other hand, it has been shown [7] that the RLDA suffers from several shortcomings, eg. from a drastic overestimation of transverse exchange contributions, thus making the RLDA a less reliable tool than its nonrelativistic counterpart. As relativistic corrections are clearly misrepresented by the RLDA, it seems worthwhile to reinvestigate the role of relativistic xc -effects in solids on the basis of a more accurate form for $E_{xc}[n]$.

For this purpose, the generalization of the GGA approach to the relativistic domain (RGGA) [27,28] offers itself. An x -only form of the RGGA [27], based on the Becke GGA [9], has been shown to correct the RLDA's failure for the description of transverse exchange, thus leading to rather accurate results for atomic systems. Recently, also a relativistic extension of the Perdew-Wang GGA (PW91) [10] has been derived [28], including a relativistic form of the correlation energy functional. The latter RGGA thus provides an ideal starting point for the study of the importance of relativistic xc -effects in solids.

In this contribution we present a comparative analysis of (R)LDA and (R)GGA results for both the band structure and the cohesive properties of metallic Au and Pt, as examples for systems for which relativistic xc -effects are expected to be prominent. We find that the relativistic corrections resulting from the RGGA are smaller than those produced by the RLDA. Nevertheless, the corrections are still visible in the band structure, the changes of the valence levels being of the order of 1%. On the other hand, the predictions for lattice constants are only marginally affected when going from the nonrelativistic to the relativistic form of a given type of xc -functional, in contrast to the well-known lattice expansion due to the inclusion of gradient corrections. Cohesive energies experience somewhat larger shifts, i.e. they are reduced by about 1% for both Au and Pt. These relativistic modifications are not only too small in their absolute magnitude in order to close the gap between non-relativistic GGA results and experiment [17,18,20], but even go into the wrong direction. The results are in agreement with a recent, weakly relativistic study of diatomic molecules involving Au, which has led to the conclusion that relativistic corrections to $E_{xc}[n]$ have only a very limited impact on the structural properties of molecules [29].

The inclusion of relativistic corrections in the GGA thus does not resolve the problems of the GGA with the 5d transition metals, suggesting that the nonlocal contributions to $E_{xc}[n]$ beyond the first density gradient are important in these systems. In addition, the spin-orbit coupling of the valence electrons, neglected in this work, could be partially responsible for this discrepancy [25,30].

II. Theoretical background

An extensive review of relativistic DFT has recently been given in [8]. For this reason we restrict ourselves to presenting only the relevant details of the xc -functionals used in this work. Among the various xc -functionals proposed for DFT calculations the nonrelativistic LDA,

$$E_{xc}^{LDA} = \int d^3r e_{xc}^{HEG}(n) , \quad (1)$$

plays a central role as it is the most simple approximation and also serves as basis for the construction of most nonlocal functionals. While the exchange contribution of the HEG can be calculated exactly, the correlation energy of the HEG is only known from Monte-Carlo studies [31,32], for which a number of slightly different parametrizations have been suggested [31–34]. As nonrelativistic LDA correlation functional we here use the Vosko-Wilk-Nusair (VWN) parametrization [33].

The RLDA is obtained from the relativistic HEG [5,6,24] and can be written as

$$\begin{aligned} E_{xc}^{RLDA}[n] &= \int d^3r e_{xc}^{RHEG}(n) \\ &= \int d^3r \left[e_x^{HEG}(n) \Phi_{x,0}(\beta) + e_c^{HEG}(n) \Phi_{c,0}(\beta) \right], \end{aligned} \quad (2)$$

where β is defined by

$$\beta = \frac{(3\pi^2 n)^{1/3}}{mc}, \quad (3)$$

and both the exchange and correlation energy densities of the relativistic HEG have been decomposed into their respective nonrelativistic limits and relativistic corrections factors $\Phi_{x,c,0}(\beta)$. While $\Phi_{x,0}$ has been known for quite some time [35],

$$\Phi_{x,0}(\beta) = 1 - \frac{3}{2} \left[\frac{\sqrt{1+\beta^2}}{\beta} - \frac{\text{Arsh}(\beta)}{\beta^2} \right], \quad (4)$$

$\Phi_{c,0}$ has only been evaluated within the RPA [24,7]. We have parametrized the resulting correction factor as

$$\Phi_{c,0}^{RPA}(\beta) = \frac{1 + a_1\beta^3 \ln(\beta) + a_2\beta^4 + a_3(1+\beta^2)^2\beta^4}{1 + b_1\beta^3 \ln(\beta) + b_2\beta^4 + b_3[A \ln(\beta) + B]\beta^7}, \quad (5)$$

utilizing the known high-density limits of both the relativistic RPA (RRPA) [36] as well as its nonrelativistic counterpart,

$$e_c^{RRPA}/n \xrightarrow{n \rightarrow \infty} -0.197464 \frac{(1+\beta^2)^2}{\beta^3} \quad (6)$$

$$e_c^{RPA}/n \xrightarrow{n \rightarrow \infty} -[A \ln(\beta) + B]. \quad (7)$$

With the parameters given in Table 1 the numerical data for $\Phi_{c,0}^{RPA}$ are reproduced with an accuracy better than 10^{-3} . Note that for small β the numerical results clearly allow the extraction of a $\beta^3 \ln(\beta)$ -dependence of the lowest order weakly relativistic contribution, rather than a β^2 -dependence which one might have expected. To further check the accuracy of the parametrization (5) we have applied both (5) and a direct spline interpolation of the numerical data to atoms, finding differences for eigenvalues to be on the $0.1 mRy$ -level. The form (5) is thus sufficiently accurate for the present purpose. Lacking the full density dependence of all contributions to e_c^{RHEG} beyond the RPA we have used $\Phi_{c,0}^{RPA}$ with the complete nonrelativistic e_c^{HEG} for the RLDA, utilizing the VWN-parametrization for e_c^{HEG} [33].

In the x -only limit the general form of the RGGA is [27]

$$E_x^{RGGA} = \int d^3r e_x^{HEG}(n) [\Phi_{x,0}(\beta) + g(\xi)\Phi_{x,2}(\beta)], \quad (8)$$

Parameter	Exchange		Correlation	
	$\Phi_{x,2}^L$	$\Phi_{x,2}^T$	$\Phi_{c,0}^{RPA}$	Φ_c^{GGA}
a_1	2.2156	3.5122	-2.44968	1.9407
a_2	0.66967	0.62525	1.91853	0.14435
a_3	—	—	0.0718854	—
b_1	1.3267	1.3313	-1.59583	0.28142
b_2	0.79420	0.10066	1.29176	0.004723
b_3	—	—	0.364044	—

Table 1: Parameter sets for the relativistic correction factors (5,9,10).

with $\xi = [\nabla n / (2(3\pi^2 n)^{1/3})]^2$ and $g(\xi)$ being the gradient part of the corresponding nonrelativistic GGA. In [27] the longitudinal (L) and transverse (T) contributions to the x -only energy (compare [7,8]) have been separated, leading to a corresponding decomposition of $\Phi_{x,2} = \Phi_{x,2}^L + \Phi_{x,2}^T$. For both $\Phi_{x,2}^L$ and $\Phi_{x,2}^T$ sufficiently flexible Padé approximants have been used,

$$\Phi_{x,2}^L = \frac{1 + a_1^L \beta^2 + a_2^L \beta^4}{1 + b_1^L \beta^2 + b_2^L \beta^4} \quad ; \quad \Phi_{x,2}^T = \frac{a_1^T \beta^2 + a_2^T \beta^4}{1 + b_1^T \beta^2 + b_2^T \beta^4}. \quad (9)$$

The coefficients have been determined by a least squares fit to the exact relativistic x -only energies of a number of closed subshell atoms keeping the form of $g(\xi)$ fixed. For the PW91 GGA this procedure leads to the parameters listed in Table 1 [28]. As has been demonstrated in [28] the resulting RGGA produces much more accurate atomic results than both the RLDA and the corresponding nonrelativistic GGA.

The correlation energy requires a slightly different scheme, as on the one hand $\Phi_{c,0}$ is not known completely, and, on the other hand, some GGAs for correlation [37] are not even based on the LDA. Therefore only one overall correction factor for the complete GGA has been used in [28],

$$E_c^{RGGA}[n] = \int d^3r \, e_c^{GGA}(n, (\nabla n)^2, \dots) \Phi_c^{GGA}(\beta), \quad (10)$$

keeping the nonrelativistic form $e_c^{GGA}(n, (\nabla n)^2, \dots)$ fixed. In view of the fact that the relativistic corrections to atomic E_c are much smaller than those to atomic E_x this less sophisticated approach should be sufficient (compare Section IV). Using again a Padé approximant of the form (9) as ansatz for Φ_c^{GGA} and fitting its coefficients to the most systematic set of atomic relativistic correlation energies available to date (second order perturbation theory results for the Ne isoelectronic series on the basis of the Dirac-Coulomb-Breit

Hamiltonian [38]) one finds the parameters of Table 1 for the PW91 correlation GGA [28]. Again, compared with the RLDA or the nonrelativistic GGA atomic correlation energies are clearly improved by this RGGA.

Eqs.(8-10) with the PW91 parameters of Table 1 define the RGGA used in this work (the longitudinal and transverse components of the x -only GGA have always been combined).

III. Computational details

The calculations for solids have been performed using a full potential linearized augmented plane wave (LAPW) code (WIEN95 [39]). For an extensive discussion of the LAPW method the reader is referred to [40,41]. We only comment on the handling of the Kohn-Sham kinetic energy of the electrons. In the calculations a fully relativistic core is used, whereas the valence electrons are treated in a scalar relativistic approximation (see [42] for details) inside the muffin tins and completely nonrelativistically in the interstitial regime. As for Pt spin-orbit coupling has been shown to be important near high-symmetry lines in the Brillouin-zone [25] this neglect of spin-orbit coupling for the valence electrons may not be justified. However, one would expect the small relativistic xc -contributions studied in this work to be additive to the spin-orbit effects. Thus, while eg. the bands will change when including spin-orbit coupling, our conclusions concerning the size of the relativistic xc -corrections should be unaffected.

For transition elements like Pt and Au the linear orbital extension to the LAPW method [43] has been used. We have employed the procedure proposed in [20], in which the $5p$ -states for Au and Pt are included in the core for total energy calculations, but corresponding local orbitals are also included in the basis for the valence states in order to allow the basis functions for the actual valence electrons to orthogonalize to the extended core states.

The convergence of the calculations has been carefully checked by varying the plane wave cutoff and the number of \mathbf{k} -points used for the Brillouin-zone integration. Employing $(RK)_{min} = 10$ our results were converged to mRy -accuracy. The \mathbf{k} -integration has been performed using 165 \mathbf{k} -points in the irreducible Brillouin-zone. Adding further \mathbf{k} -points affected the total energy by less than $0.1mRy$. All xc -functionals have been treated identically, so that the differences between the results obtained with the various functionals should be even more accurate than the corresponding absolute values. For the calculation of the cohesive energy of Pt the required atomic ground state energy has been obtained by solving the fully relativistic Kohn-Sham equations for the occupation $[Xe]4f^{14}5d^96s$, using a spherical average for the density. The equilibrium lattice constant has been derived via the standard fitting procedure

Level	Functionals				
	x : LDA	x :RLDA	x : GGA	x :RGGA	x :RGGA
	c : LDA	c :RLDA	c : GGA	c : GGA	c :RGGA
1s1/2	5923.193	5885.536	5928.439	5901.832	5902.042
2s1/2	1044.186	1038.687	1045.009	1040.946	1040.999
2p1/2	1001.487	996.678	1001.983	997.494	997.553
2p3/2	866.695	863.557	867.011	863.952	863.999
3s1/2	246.250	245.104	246.479	245.656	245.670
3p1/2	227.035	226.109	227.162	226.304	226.318
3p3/2	197.296	196.702	197.378	196.799	196.810
3d3/2	165.328	165.043	165.356	165.051	165.061
3d5/2	158.932	158.686	158.956	158.690	158.699
4s1/2	53.238	52.980	53.348	53.172	53.175
4p1/2	45.049	44.860	45.113	44.940	44.943
4p3/2	37.899	37.786	37.969	37.860	37.863
4d3/2	24.486	24.457	24.511	24.478	24.479
4d5/2	23.155	23.133	23.181	23.155	23.157
4f5/2	5.933	5.959	5.924	5.947	5.947
4f7/2	5.652	5.679	5.644	5.667	5.667
5s1/2	7.767	7.724	7.763	7.737	7.737
5p1/2	5.099	5.074	5.093	5.070	5.070
5p3/2	3.869	3.857	3.875	3.864	3.864

Table 2: Core levels ($-\epsilon_{nlj}$) of solid Au relative to the Fermi level for various xc -functionals (in Ry).

to the Murnaghan equation of state [44]. The speed of light has been set to $\alpha = 137.0359895$ and point nuclei have been employed.

IV. Results

We start with a discussion of the role of relativistic xc -contributions for the band structure of Au and Pt on the basis of the RGGA, thus repeating the analysis of MacDonald et al. [25,26] with a more appropriate form for $E_{xc}[n]$. As relativistic effects are most important near the atomic nucleus, first the core levels are analyzed (on the basis of the Kohn-Sham eigenvalues, as usual). Table 2 shows the core levels of Au (relative to the Fermi level) for several xc -functionals, i.e. the nonrelativistic LDA, the RLDA, the nonrelativistic GGA, the RGGA for both exchange and correlation as well as a combination of the

Level	Functionals						Ref. [29]
	<i>x</i> : LDA	<i>x</i> :RLDA	<i>x</i> : GGA	<i>x</i> :RGGA	<i>x</i> :RGGA	<i>x</i> : LDA	<i>x</i> : LDA
	<i>c</i> : LDA	<i>c</i> :RLDA	<i>c</i> : GGA	<i>c</i> : GGA	<i>c</i> :RGGA	<i>c</i> :RGGA	
1s _{1/2}	5923.389	5885.733	5928.619	5902.013	5902.223		5893.484
2s _{1/2}	1044.379	1038.880	1045.185	1041.122	1041.175		1040.889
2p _{1/2}	1001.679	996.870	1002.160	997.670	997.729		905.731
2p _{3/2}	866.887	863.750	867.187	864.128	864.176		
3s _{1/2}	246.449	245.303	246.662	245.839	245.853		245.782
3p _{1/2}	227.234	226.308	227.345	226.486	226.500		206.230
3p _{3/2}	197.495	196.901	197.560	196.981	196.993		
3d _{3/2}	165.526	165.241	165.538	165.232	165.243		161.632
3d _{5/2}	159.130	158.884	159.138	158.871	158.881		
4s _{1/2}	53.441	53.182	53.533	53.357	53.360		53.314
4p _{1/2}	45.251	45.062	45.299	45.126	45.129		40.233
4p _{3/2}	38.101	37.989	38.155	38.046	38.049		
4d _{3/2}	24.688	24.659	24.697	24.663	24.665		23.901
4d _{5/2}	23.357	23.335	23.367	23.340	23.342		
4f _{5/2}	6.135	6.162	6.110	6.133	6.133		5.953
4f _{7/2}	5.855	5.881	5.830	5.853	5.853		
5s _{1/2}	7.976	7.933	7.954	7.927	7.928		7.952
5p _{1/2}	5.310	5.285	5.286	5.264	5.264		4.442
5p _{3/2}	4.084	4.072	4.073	4.061	4.061		
5d _{5/2}	0.594	0.596	0.580	0.581	0.581		0.511
5d _{7/2}	0.481	0.483	0.468	0.470	0.470		
6s _{1/2}	0.448	0.445	0.430	0.428	0.428		0.442

Table 3: Single-particle levels ($-\epsilon_{nlj}$) of atomic Au for various xc -functionals (in Ry). Also given are the j -averaged weakly relativistic LCGTO results of [29].

RGGA for exchange and the GGA for correlation. All these calculations have been performed for the experimental lattice constant. A comparison with the corresponding single-particle energies of the free Au atom, listed in Table 3, demonstrates immediately that the atomic eigenvalue shifts by relativistic xc -corrections are essentially transferred to the solid without any modification: This is not only true for the innermost levels, but also for the relative stabilization of the $4f$ -eigenvalues with respect to the $5p$ -levels. Consequently also the overestimation of relativistic effects by the RLDA can be observed: Eg. for the $5s_{1/2}$ -level the RLDA shift of $43mRy$ with respect to the nonrelativistic LDA

is almost twice as large as the $26mRy$ difference between the RGGA and the GGA eigenvalues. Comparing the results obtained with the full RGGA with those from the combination of the x -only RGGA with the correlation GGA demonstrates that at least on the present level of sophistication relativistic corrections to the correlation energy functional can be neglected. Even for the innermost levels the corresponding shifts are rather small.

On the other hand, the shift induced by inclusion of relativistic corrections in the x -only GGA is larger than that resulting from the addition of gradient corrections to the LDA: Even for the $5p_{3/2}$ -level the eigenvalue difference of $11mRy$ between RGGA and GGA is larger than the $6mRy$ difference between GGA and LDA (for solid Au). The eigenvalues for Pt, which are not explicitly given here, show a similar picture. In view of the fact that in the x -only limit the atomic RGGA eigenvalues are much closer to the exact Kohn-Sham single particle energies [27] than the GGA eigenvalues these substantial core level shifts indicate that an accurate microscopic description of solids requires relativistic contributions to $E_x[n]$.

A similar analysis of the relative importance of gradient and relativistic contributions has been presented by Mayer et al. [29] on the basis of weakly relativistic LCGTO results. The various relative atomic eigenvalue shifts given in [29] are consistent with those extracted from Table 3. The absolute size of the eigenvalues of Ref. [29], on the other hand, allows to estimate the importance of higher order $1/c$ -corrections to the kinetic energy. In Table 3 we thus also list the j -averaged LCGTO eigenvalues for the nonrelativistic LDA, which is the only functional used in both [29] and this study. For all core levels the differences between the weakly relativistic LCGTO data and the fully relativistic eigenvalues are of the same order of magnitude as the contributions of the relativistic xc -corrections. On the other hand, for the valence levels the higher order $1/c$ -corrections to the kinetic energy lead to roughly 3-5 times larger shifts than the relativistic xc -corrections.

The valence levels for Au obtained with the various xc -functionals for a number of selected \mathbf{k} -points in the Brillouin-zone are given in Table 4 (all results for the experimental lattice constant). In contrast to the substantial modifications of the core levels, only small effects of the relativistic xc -corrections on the valence levels are found. For instance, at the Γ -point the d -bands are lowered with respect to the s -band by about $2.5mRy$ when going from the GGA to the RGGA. On the other hand, the nonrelativistic gradient corrections, which set the scale for judging the importance of this shift, lower the d -bands with respect to the s -band by about $8mRy$ (see Tables 4a,4c). While the eigenvalue shifts are different at other \mathbf{k} -points, the relative impact of relativistic and gradient corrections is roughly the same. Although the importance of the latter becomes larger if the lattice constant is relaxed, i.e. if the bands

k	$\epsilon_{n,k} - \epsilon_F$					
	a) x : LDA, c : LDA					
W	-454	-393	-393	-253	-123	344
L	-558	-360	-360	-148	-148	-84
Γ	-750	-357	-357	-357	-240	-240
X	-538	-514	-150	-123	-123	63
K	-492	-444	-293	-218	-158	277
	b) x : RLDA, c : RLDA					
W	-456	-395	-395	-255	-125	349
L	-559	-362	-362	-150	-150	-83
Γ	-748	-360	-360	-360	-242	-242
X	-540	-517	-153	-125	-125	64
K	-494	-446	-295	-220	-160	281
	c) x : GGA, c : GGA					
W	-456	-395	-395	-256	-127	349
L	-557	-363	-363	-152	-152	-80
Γ	-745	-360	-360	-360	-244	-244
X	-539	-516	-155	-127	-127	68
K	-493	-446	-294	-222	-162	282
	d) x : RGGA, c : GGA					
W	-457	-396	-396	-258	-129	352
L	-559	-364	-364	-154	-154	-79
Γ	-744	-362	-362	-362	-246	-246
X	-541	-518	-157	-129	-129	68
K	-495	-447	-296	-224	-164	285
	e) x : RGGA, c : RGGA					
W	-457	-396	-396	-258	-129	352
L	-559	-364	-364	-154	-154	-79
Γ	-744	-362	-362	-362	-246	-246
X	-541	-518	-157	-129	-129	68
K	-495	-447	-296	-224	-164	285

Table 4: Valence levels of Au at selected k -points relative to the Fermi level for various xc -functionals (in mRy).

corresponding to the lattice constants which give the minimum total energy for the functional of interest are compared, this nevertheless indicates that relativistic xc -corrections are not completely negligible even for valence levels.

Similar to the core levels, the relativistic corrections to eigenvalues calcu-

Functionals		a_0	$-E_{coh}$	$-E_0(\text{solid})$	$-E_0(\text{atom})$
x	c	[bohr]	[eV]	[Ry]	[Ry]
LDA	LDA	7.68	4.12	38075.445	38075.132
RLDA	RLDA	7.68	4.09	37997.970	37997.669
GGA	GGA	7.87	2.91	38100.029	38099.815
RGGA	GGA	7.88	2.89	38048.438	38048.225
RGGA	RGGA	7.88	2.89	38049.253	38049.040
expt		7.67	3.78		

Table 5: Lattice constants and cohesive energies of Au obtained from LAPW calculations with various xc -functionals in comparison to experiment [45,20].

Functionals		a_0	$-E_{coh}$	$-E_0(\text{solid})$	$-E_0(\text{atom})$
x	c	[bohr]	[eV]	[Ry]	[Ry]
LDA	LDA	7.36	6.76	36873.465	36872.968
RLDA	RLDA	7.37	6.73	36799.369	36798.875
GGA	GGA	7.51	5.34	36897.502	36897.109
RGGA	GGA	7.52	5.30	36848.219	36847.829
RGGA	RGGA	7.52	5.30	36849.005	36848.616
expt		7.40	5.85		

Table 6: Lattice constants and cohesive energies of Pt obtained from LAPW calculations with various xc -functionals in comparison to experiment [45,20].

lated with the RLDA are too large by a factor of 1.5 to 2. Moreover, the inclusion of relativistic corrections in the correlation energy functional has almost no impact on the valence states as can be seen from a comparison of Tables 4d,4e. This then *a posteriori* justifies the rather crude treatment of these contributions in both the RLDA and RGGA.

The situation is somewhat different for Pt, for which the relativistic xc -corrections only affect the s -band in the interior of the Brillouin-zone: Its bottom is shifted upwards by $3mRy$. The absolute and relative positions of the d -bands remain more or less unchanged.

The limited importance of relativistic xc -potentials for the cohesive properties of Au and Pt is demonstrated in Tables 5,6: Lattice constants remain nearly unchanged when one replaces the LDA by the RLDA or the GGA by the RGGA. Also, only a small reduction is observed for the corresponding cohesive energy E_{coh} (evaluated at the lattice constant corresponding to the

energy minimum for the functional of interest). While the total ground state energies change by almost $50 Ry$, the energy difference between the solid state and the free atom experiences only a $1 mRy$ shift, which represents roughly 1% of the total cohesive energy. This percentage correction is on the same level as the shifts observed for the valence bands and for the dissociation energy of the Au-dimer [29].

Like its nonrelativistic counterpart, the RGGA predicts lattice constants which are too large by $0.21 bohr$ for Au and $0.12 bohr$ for Pt. The corresponding RGGA cohesive energies are roughly 25% too small for Au and 10% below the experimental value for Pt. Thus the reduction of E_{coh} , which is always found when going from the LDA to the GGA, by far overcorrects the LDA's error, in particular in the case of Au for which the LDA result is fortuitously close to the experimental energy. In fact, the inclusion of relativistic corrections in the GGA even worsens the agreement with experiment, although only marginally. The nonadditivity of relativistic and xc -effects [22] is thus not responsible for the GGA's failure for some $5d$ transition elements.

In summary, there can be little doubt that for the cohesive properties of solids the relativistic contributions to $E_{xc}[n]$ are much less important than the 'nonlocal' contributions to $E_{xc}[n]$ not contained in the LDA. It should be pointed out, however, that the RGGA is as efficiently applied as the GGA, so that there seems to be no reason to rely on error cancellation in the calculation of E_{coh} . Moreover, at least for some systems (as Au) the relativistic xc -corrections are visible in the band structure, indicating that a complete description of these systems requires a relativistic form for $E_{xc}[n]$. Finally, if relativistic xc -corrections are to be included at all this should be done on the GGA- rather than the LDA-level.

Acknowledgements: Financial support by the Deutsche Forschungsgemeinschaft within the program *Theorie relativistischer Effekte in der Chemie und Physik schwerer Elemente* (Project Dr 113/20-2) is gratefully acknowledged. P.B. was supported by the Austrian Science Foundation Project No P10847.

References

- [1] R. O. Jones and O. Gunnarson, *Rev. Mod. Phys.* **61**, 689 (1989).
- [2] R. M. Dreizler and E. K. U. Gross, *Density functional theory* (Springer, Berlin, 1990).
- [3] *Density Functional Theory*, ed. by E. K. U. Gross and R. M. Dreizler, NATO ASI Series B, Vol. 337 (Plenum, New York, 1995).

- [4] A. K. Rajagopal and J. Callaway, Phys. Rev. B **7**, 1912 (1973).
- [5] A. K. Rajagopal, J. Phys. C **11**, L943 (1978).
- [6] A. H. MacDonald and S. H. Vosko, J. Phys. C **12**, 2977 (1979).
- [7] E. Engel, S. Keller, A. Facco Bonetti, H. Müller, and R. M. Dreizler, Phys. Rev. A **52**, 2750 (1995).
- [8] E. Engel and R. M. Dreizler, Top. Curr. Chem. **181**, 1 (1996).
- [9] A. D. Becke, Phys. Rev. B **33**, 3098 (1988).
- [10] J. P. Perdew, in *Electronic Structure of Solids 1991* ed. by P. Ziesche and H. Eschrig (Akademie Verlag, Berlin, 1991), p.11.
- [11] A. D. Becke, J. Chem. Phys. **96**, 2155 (1992).
- [12] B. G. Johnson, P. M. W. Gill, and J. A. Pople, J. Chem. Phys. **98**, 5612 (1993).
- [13] P. Bagno, O. Jepsen, and O. Gunnarsson, Phys. Rev. B **40**, 1997 (1989).
- [14] T. C. Leung, C. T. Chan, and B. N. Harmon, Phys. Rev. B **44**, 2923 (1991).
- [15] D. J. Singh and J. Ashkenazi, Phys. Rev. B **46**, 11570 (1992).
- [16] A. Garcia, C. Elsässer, J. Zhu, S. G. Louie, and M. L. Cohen, Phys. Rev. B **46**, 9829 (1992).
- [17] M. Körling and J. Häglund, Phys. Rev. B **45**, 13293 (1992).
- [18] V. Ozoliņš and M. Körling, Phys. Rev. B **48**, 18304 (1993).
- [19] P. Dufek, P. Blaha and K. Schwarz, Phys. Rev. B **50**, 7279 (1994).
- [20] A. Khein, D. J. Singh, and C. J. Umrigar, Phys. Rev. B **51**, 4105 (1995).
- [21] P. Pyykkö, Chem. Rev. **97**, 597 (1997).
- [22] E. Eliav, U. Kaldor, and Y. Ishikawa, Phys. Rev. A **49**, 1724 (1994).
- [23] A. Pizlo, G. Jansen, B. A. Heß, and W. von Niessen, J. Chem. Phys. **98**, 3945 (1993).
- [24] M. V. Ramana and A. K. Rajagopal, Phys. Rev. A **24**, 1689 (1981).

- [25] A. H. MacDonald, J. M. Daams, S. H. Vosko, and D. D. Koelling, *Phys. Rev. B* **23**, 6377 (1981).
- [26] A. H. MacDonald, J. M. Daams, S. H. Vosko, and D. D. Koelling, *Phys. Rev. B* **25**, 713 (1982).
- [27] E. Engel, S. Keller, and R. M. Dreizler, *Phys. Rev. A* **53**, 1367 (1996).
- [28] E. Engel, S. Keller, and R. M. Dreizler, in *Electronic Density Functional Theory: Recent Progress and New Directions*, ed. by J. F. Dobson, G. Vignale and M. P. Das (Plenum, New York, 1997).
- [29] M. Mayer, O. D. Häberlein, and N. Rösch, *Phys. Rev. A* **54**, 4775 (1996).
- [30] H. Bross, private communication (1997).
- [31] D. M. Ceperley and B. J. Alder, *Phys. Rev. Lett.* **45**, 566 (1980).
- [32] G. Ortiz and P. Ballone, *Phys. Rev. B* **50**, 1391 (1994).
- [33] S. H. Vosko, L. Wilk, and M. Nusair, *Can. J. Phys.* **58**, 1200 (1980).
- [34] J. P. Perdew and Y. Wang, *Phys. Rev. B* **45**, 13244 (1992).
- [35] I. A. Akhiezer and S. V. Peletminskii, *Sov. Phys. JETP* **11**, 1316 (1960).
- [36] H. Müller, unpublished (1995).
- [37] C. Lee, W. Yang, and R. G. Parr, *Phys. Rev. B* **37**, 785 (1988).
- [38] Y. Ishikawa and K. Koc, *Phys. Rev. A* **50**, 4733 (1994).
- [39] P. Blaha, K. Schwarz, P. Dufek and R. Augustyn, WIEN95, Technical University of Vienna 1995 (improved and updated Unix version of the original copyrighted WIEN-code, by P. Blaha, K. Schwarz, P. Sorantin, and S. B. Trickey, *Comput. Phys. Commun.* **59**, 399 (1990)).
- [40] O. K. Andersen, *Phys. Rev. B* **12**, 3060 (1975).
- [41] D. J. Singh, *Planewaves, Pseudopotentials and the LAPW Method* (Kluwer Academic, Boston, 1994).
- [42] D. D. Koelling and B. N. Harmon, *J. Phys. C: Sol. St. Phys.* **10**, 3107 (1977).
- [43] D. Singh, *Phys. Rev. B* **43**, 6388 (1994).

- [44] F. D. Murnaghan, Proc. Natl. Acad. Sci. U.S.A. **30**, 244 (1944).
- [45] L. Brewer, Report LBL-3720 Rev. Lawrence Berkeley Laboratory (Univ. of California, Berkeley, 1977).

INTERATOMIC FORCE CONSTANTS IN PERIODIC SOLIDS FROM DENSITY FUNCTIONAL PERTURBATION THEORY

Xavier Gonze

Unité P.C.P.M.,
Université Catholique de Louvain,
1, Place Croix du Sud,
B-1348 Louvain-la-Neuve, BELGIUM

Abstract

Interatomic Force Constants (IFCs) are the proportionality coefficients between the displacements of atoms from their equilibrium positions and the forces they induce on other atoms (or themselves). Their knowledge allows to build vibrational eigenfrequencies and eigenvectors of solids. This paper describes IFCs for different solids (SiO_2 -quartz, SiO_2 -stishovite, BaTiO_3 , Si) obtained within the Local-Density Approximation to Density-Functional Theory. An efficient variation-perturbation approach has been used to extract the linear response of wavefunctions and density to atomic displacements. In mixed ionic-covalent solids, like SiO_2 or BaTiO_3 , the careful treatment of the long-range IFCs is mandatory for a correct description of the eigenfrequencies.

1. Introduction

In the present paper, a particular technique for the computation of the Interatomic Force Constants of periodic solids in the framework of Density-Functional Theory (DFT) will be described, as well as some of its applications.

In the description of the technique, the particular aspects that make it different of other schemes aimed at the computation of IFCs in solids or molecules [1-9] will be emphasized. These aspects are connected to the central use of a variational principle in order to find the changes in the wavefunctions due to atomic displacements, on one hand, and to find the change in electronic energy due to the changes in wavefunctions, on the other hand. Some technical details, related with the presence of relatively long-ranged interatomic force constants, caused by

dipole-dipole interactions will also been discussed. In SiO_2 or BaTiO_3 , these are the leading terms in the asymptotic behaviour of the IFCs. Since they can be parametrized exactly in terms of Born effective charges (also called atomic polar tensors) and the macroscopic dielectric tensor, their separate treatment allows to put the major computational effort on the short-range IFCs, and generate a tractable scheme.

The analysis of the IFC behaviour, for the different solids, will proceed along two lines : the comparison of the strength and anisotropy of the potential well that each atom feels when the other atoms are kept fixed; and the decomposition of the IFCs in their dipole-dipole part and the remaining part. Each material has its own characteristics, in term of the respective strength of ionic and covalent bonding, and their balance.

More details on the formalism and results can be found in Refs. [10-21]. Atomic (Hartree) units are used throughout.

2. Formalism

As usual in the treatment of dynamical properties of nuclei-electron systems, the Born-Oppenheimer potential energy is expanded with respect to the displacement of the N nuclei around their equilibrium positions (where the energy is minimal) as follows :

$$E(\mathbf{R}_1, \dots, \mathbf{R}_N) = E(\mathbf{R}_{01}, \dots, \mathbf{R}_{0N}) + \sum_{\alpha\kappa\beta\kappa'} \frac{1}{2} (\mathbf{R} - \mathbf{R}_0)_{\alpha\kappa} (\mathbf{R} - \mathbf{R}_0)_{\beta\kappa'} \frac{\partial^2 E}{\partial R_{\alpha\kappa} \partial R_{\beta\kappa'}} (\mathbf{R}_{01}, \dots, \mathbf{R}_{0N}) + \dots \quad (1)$$

\mathbf{R}_κ is the position of atom κ , while α and β label directions in the three-dimensional space. The interatomic force constants appear in the second-order term of this expansion,

$$\Phi_{\alpha\beta}(\kappa; \kappa') = \frac{\partial^2 E}{\partial R_{\alpha\kappa} \partial R_{\beta\kappa'}} (\mathbf{R}_{01}, \dots, \mathbf{R}_{0N}) \quad , \quad (2)$$

and relate linearly the force on one atom to the displacement of other atoms (or itself) with respect to their equilibrium position :

$$\mathbf{F}_{\kappa\alpha} = - \sum_{\kappa\beta} \Phi_{\alpha\beta}(\kappa; \kappa') (\mathbf{R} - \mathbf{R}_0)_{\kappa\beta} \quad . \quad (3)$$

The knowledge of these quantities, coupled with the equation of motion, allows to find the vibrational eigenfunctions and eigenvalues, in the harmonic approximation. In order to compute the IFCs, a variation-perturbation approach to the DFT has been used.

In the Kohn-Sham approach to DFT, the energy of the electronic system can be written as

$$E_{el}[\psi_\alpha] = s \sum_{\alpha=1}^N \langle \psi_\alpha | T + v | \psi_\alpha \rangle + E_{Hxc}[n] \quad (4)$$

(α runs from 1 to N , where N is the number of occupied orbitals, $s=2$ stands for the spin degeneracy), where the "interaction energy" $E_{Hxc}[n]$ is the sum of Hartree and exchange-correlation parts :

$$E_{Hxc}[n] = E_H[n] + E_{xc}[n] . \quad (5)$$

$E_{Hxc}[n]$ depends on the occupied Kohn-Sham orbitals $|\psi_\alpha\rangle$ through the density

$$n(\mathbf{r}) = s \sum_{\alpha=1}^N \psi_\alpha^*(\mathbf{r}) \cdot \psi_\alpha(\mathbf{r}) \quad . \quad (6)$$

Focusing on the variational principle present at the heart of the Density Functional formalism (actually a minimum principle), Eq.(4) must be minimised with respect to the variations of the wavefunctions, subject to the following orthonormalisation constraints :

$$\langle \psi_\alpha | \psi_\beta \rangle = \delta_{\alpha\beta} \quad (7)$$

(α and β run from 1 to N).

The Lagrange multiplier method, applied to this minimisation problem, allows to recover the usual Kohn-Sham equations, modulo an unitary transform within the space of occupied orbitals, as follows. One Lagrange multiplier for each orthonormalisation constraint is introduced, such that :

$$E_{el}^+[\psi_\alpha] = s \sum_{\alpha=1}^N \langle \psi_\alpha | T + v | \psi_\alpha \rangle + E_{Hxc}[n] \\ - s \sum_{\alpha,\beta=1}^N \varepsilon_{\alpha\beta} [\langle \psi_\alpha | \psi_\beta \rangle - \delta_{\alpha\beta}] \quad (8)$$

The corresponding Lagrange-Euler equation are

$$H | \psi_{\alpha} \rangle = \sum_{\beta=1}^N \epsilon_{\alpha\beta} | \psi_{\beta} \rangle \quad (9)$$

where the Hamiltonian

$$H = T + v_{KS} = T + v + v_{Hxc} \quad (10)$$

is self-consistently determined : it includes the Hartree and exchange-correlation potential (a local potential)

$$v_{Hxc}(\mathbf{r}) = \frac{\delta E_{Hxc}[n]}{\delta n(\mathbf{r})} \quad (11)$$

The Hamiltonian being hermitian, one can recover the canonical Kohn-Sham equations from Eq.(9) by a unitary transformation on the wavefunctions, so that :

$$H | \psi_{\alpha} \rangle = \epsilon_{\alpha} | \psi_{\alpha} \rangle \quad (12)$$

Eq.(8) is the starting point for a direct variational approach to Density Functional Theory, proposed by Teter, Payne and Allan [23,24], and called band-by-band (or state-by-state) conjugate-gradient (CG) algorithm. By contrast, Eqs.(10-12) have been in use since many years. They parallel the well-known SCF approach to the Hartree-Fock approximation. In the spirit of Teter, Payne and Allan, a variational approach to the treatment of perturbations within DFT is now presented.

The nuclei displacement perturbation κ_{μ} is such that the nucleus labelled κ is displaced by the small amount λ along the direction μ (the unit vector along μ is written \mathbf{e}_{μ}). Supposing a nucleus with charge Z_{κ} , the change of potential operator is:

$$\Delta v(\mathbf{r}) = - \frac{Z_{\kappa}}{|\mathbf{r} - (\mathbf{R}_{\kappa} + \lambda \mathbf{e}_{\mu})|} + \frac{Z_{\kappa}}{|\mathbf{r} - \mathbf{R}_{\kappa}|} \quad (13)$$

All quantities, like this external potential, the ground-state total energy of the system (placed in the slightly perturbed external potential), or the corresponding density, will be written as a perturbation series, as follows (for a generic quantity $X(\lambda)$) :

$$X(\lambda) = X^{(0)} + \lambda X^{(1)} + \lambda^2 X^{(2)} + \lambda^3 X^{(3)} + \dots \quad (14)$$

In view of the applications, one can consider a general form of interaction between nuclei and electrons, represented by a pseudopotential $v(\mathbf{r})$. The first-order change in atomic potential due to the atomic displacement of atom \mathbf{K} in the direction α is

$$v^{(1)}(\mathbf{r}) = \frac{d}{d\mathbf{R}_{\alpha\mathbf{K}}} (v_{\mathbf{K}}(\mathbf{r} - \mathbf{R}_{\mathbf{K}})) = - \left. \frac{dv_{\mathbf{K}}}{d\mathbf{r}_{\alpha}} \right|_{(\mathbf{r} - \mathbf{R}_{\mathbf{K}})} \quad (15)$$

When perturbation theory is applied to a quantity for which a variational principle holds, like Eq.(8), an interesting mathematical structure is observed : there exist variational principles for even orders of perturbation, as well as a generic "2n+1 theorem".

Be $E_{\min}(\lambda)$ an "energy", function of λ , obtained by minimisation of the functional $E_{(\lambda)}[\Phi_{\text{trial}}]$ in the space of possible wavefunctions Φ_{trial} :

$$E_{\min}(\lambda) = \min_{\Phi_{\text{trial}}} \{E_{(\lambda)}[\Phi_{\text{trial}}]\} \quad (16)$$

The value of Φ_{trial} at the minimum, for a given value of λ , is written $\Phi_{\min}(\lambda)$. The knowledge of the expansion of $\Phi_{\min}(\lambda)$ up to order n allows to know the expansion of $E_{\min}(\lambda)$ up to order $2n+1$. Explicitly [11] :

$$E_{\min}^{(2n+1)} = \left\{ E_{(\lambda)} \left[\sum_{i=0}^n \lambda^i \Phi_{\min}^{(i)} \right] \right\}^{(2n+1)} . \quad (17)$$

At order $2n$, one even finds a variational (minimum) principle :

$$E_{\min}^{(2n)} = \min_{\delta\Phi_{\text{trial}}} \left\{ \left(E_{(\lambda)} \left[\sum_{i=0}^{n-1} \lambda^i \Phi_{\min}^{(i)} + \lambda^n \delta\Phi_{\text{trial}} \right] \right)^{(2n)} \right\} . \quad (18)$$

At the minimum, $\delta\Phi_{\text{trial}}$ is equal to the n -th order Φ_{\min} : a minimization algorithm can be used to generate it.

The application of these results to DFT gives, at the second order,

$$E_{\text{el}}^{(2)} = \min_{\Phi_{\text{trial}}^{(1)}} \{ E_{\text{el}}^+ [\Phi_{\text{min}}^{(0)} + \lambda \Phi_{\text{trial}}^{(1)}] \}^{(2)} \quad (19)$$

More explicitly, one has to minimize

$$\begin{aligned} E_{\text{el}}^{(2)} = s \sum_{\alpha=1}^N & (\langle \Phi_{\alpha}^{(1)} | v^{(1)} | \Phi_{\alpha}^{(0)} \rangle + \langle \Phi_{\alpha}^{(1)} | (H - \epsilon_{\alpha})^{(0)} | \Phi_{\alpha}^{(1)} \rangle \\ & + \langle \Phi_{\alpha}^{(0)} | v^{(2)} | \Phi_{\alpha}^{(0)} \rangle + \langle \Phi_{\alpha}^{(0)} | v^{(1)} | \Phi_{\alpha}^{(1)} \rangle) \\ & + \frac{1}{2} \iint \frac{\delta^2 E_{\text{Hxd}}[n^{(0)}]}{\delta n(\mathbf{r}) \delta n(\mathbf{r}')} n^{(1)}(\mathbf{r}) n^{(1)}(\mathbf{r}') d\mathbf{r} d\mathbf{r}' \end{aligned} \quad (20)$$

with

$$n^{(1)}(\mathbf{r}) = s \sum_{\alpha=1}^N \psi_{\alpha}^{(0)*}(\mathbf{r}) \cdot \psi_{\alpha}^{(1)}(\mathbf{r}) + \psi_{\alpha}^{(1)*}(\mathbf{r}) \cdot \psi_{\alpha}^{(0)}(\mathbf{r}) \quad (21)$$

by varying the first-order wavefunctions, subject to the following constraints :

$$\langle \Phi_{\alpha}^{(0)} | \Phi_{\beta}^{(1)} \rangle + \langle \Phi_{\alpha}^{(1)} | \Phi_{\beta}^{(0)} \rangle = 0 \quad (22)$$

The state-by-state CG algorithm of Teter, Payne and Allan can now be adapted to the variational principle Eq.(20), under constraints Eq.(22). By construction, such an algorithm will be unconditionnally stable, since the second-order derivative of the electronic energy is always decreased in the successive steps of the CG algorithm. It is presented in detail in Ref. [13], where its specific advantages are discussed. Now, let us turn to the specific features related to the treatment of an extended system of electrons and nuclei [1,6,13,14].

In order to manage the infinite number of atoms contained in a periodic solid, one has to take advantage of its translational symmetry. In short, instead of trying to compute the interatomic force constants by considering the infinitesimal displacement of one atom placed in a huge supercell (hoping that the images of the displaced atom in neighbouring cells will not see each other), it is possible to use Fourier's theorem to decompose exactly the infinitesimal displacement of one atom in a sum of collective infinitesimal displacements characterized by different wavelengths, then use Bloch's theorem to map each wavelength perturbation to a problem with the periodicity of the small periodic unit cell. This leads to a considerable gain in computing time. However, some care has to be taken in the treatment of the long-range part of the IFCs, as I explain now.

When an atom is displaced from its original position, in an insulating material, a dipole is created. The proportionality coefficient between the dipole and the displacement is the Born effective charge tensor (or atomic polar tensor). Such a dipole will create a force field in the whole material, whose propagation is governed by the macroscopic dielectric tensor. By this mechanism, long-ranged IFCs appear, with an average $1/d^3$ decay (d being the distance between the atoms), corresponding to dipole-dipole interactions, that are difficult to treat by a Fourier decomposition. Interestingly, they can be parametrized in terms of Born effective charges and the macroscopic dielectric tensor, and then separated from the remaining short-ranged part of the IFCs. This separate treatment allows to put the major computational effort on the short-range IFCs, and get an altogether tractable scheme. The Born effective charges and macroscopic dielectric tensor can be computed from first principles, in a way that is rather similar to the one used to build the derivative of the energy with respect to atomic displacements.

3. Interatomic Force Constants in ionic and covalent solids.

At this stage, the formalism can be implemented in a computer program. The applications described below [15-21] rely on the expansion of the electronic wavefunctions in terms of a large number of plane waves, as well as on the replacement of nuclear bare potentials by accurate norm-conserving pseudopotentials. The Local Density Approximation was used, with the Ceperley and Alder data for the exchange-correlation energy of the homogeneous electron gas.

The atomic geometries of Si (2-atom unit cell), SiO₂-quartz (9-atom unit cell), SiO₂-stishovite (6-atom unit cell), and BaTiO₃ (5-atom unit cell) can be found in Refs.[18,21,22]. The characteristics of each material will now be described.

In bulk silicon, each silicon atom is bonded covalently to four other silicon atoms, with a sp^3 configuration. The large number of symmetry operations leaving the silicon atomic sites invariant, coupled with the fact that only one kind of atom make this solid imposes the Born effective charge to vanish. So, a dipole will not be created when a silicon atom is displaced. A quadrupole can appear, but the quadrupole-quadrupole interaction, with an average $1/d^5$ decay, can be considered short-range for the present study.

In quartz, each oxygen atom is bonded to two silicon atoms, with a rather open 145° angle between the vectors pointing toward these atoms. The silicon atoms are bonded to four oxygen atoms, in a tetrahedral configuration. By contrast, in stishovite, the high-pressure form of SiO₂, the silicon atoms are six-fold coordinated, and the oxygen atoms are three-fold coordinated, with the oxygen and three silicon atoms lying in a plane. In these materials, the Born effective charge tensors do not vanish. The nominal charge of the oxygen and silicon ions

(respectively) being -2 and +4 (resp.), the elements of the Born effective charge tensor should be on this order of magnitude. The environment of the silicon atoms is rather isotropic, and their Born effective charge tensor also, with calculated principal values ranging from +3.02 to +4.15. The effective charge for a motion of an oxygen atom towards a silicon atom is between -2.027 and -2.76, and less than -1.345 in other directions : the effective charge tensor of oxygen atoms is rather anisotropic. This dependence on the direction is a typical effect observed in mixed ionic-covalent bonds. Also, from these geometrical considerations, one expects the oxygen atoms in quartz to have a considerable freedom of displacement in a two-dimensional plane, while their motion in stishovite will be restricted in a line perpendicular to the plane containing its three nearest silicon atoms. By contrast, the potential well of the silicon atoms should be rather isotropic. Because each atom in stishovite is more coordinated than in quartz, each bond will be relatively weaker.

Material	(atom)	Eigenvalues (Ha/Bohr ²)		
Silicon	(Si atom)	0.139		
Quartz	(Si atom)	0.525	0.475	0.464
	(O atom)	0.590	0.126	0.055
Stishovite	(Si atom)	0.437	0.315	0.265
	(O atom)	0.362	0.269	0.131
BaTiO ₃	(Ba atom)	0.081		
	(Ti atom)	0.152		
	(O atom)	0.127	0.067	

Table 1. Eigenvalues of the potential well for each atom, in Hartree/Bohr².

In BaTiO_3 , one considers the high-temperature cubic structure as the reference one. This ferroelectric material undergoes three phase transitions when the temperature is lowered, with slight departure of the atomic positions from their reference ones. In the reference structure, the titanium atom is at the center of an oxygen octahedron. The oxygens are aligned in Ti-O-Ti-O-Ti linear chains, and also surrounded by 4 barium atoms, in the plane perpendicular to the chain, but at longer distances. The barium atoms have twelve oxygen nearest neighbours. The mixed ionic-covalent character is very pronounced in BaTiO_3 . It is the source of so-called "anomalous" Born effective charges, much bigger than the nominal charge of the ions. For the titanium atom, the nominal charge is +4, while the Born effective charge (the tensor is diagonal due to the highly symmetric environment of this atom) has the value +7.29. For the oxygen atom, in line with two titanium atoms, the Born effective charge tensor is strongly anisotropic : along the Ti-O-Ti chains, the Born effective charge is -5.75, much higher than the -2 nominal charge, while perpendicular to it, it is -2.13. For the barium atoms, placed in a local site of cubic symmetry, the Born effective charge is +2.74, for a nominal value of +2. As a last, important, information, the bond lengths in BaTiO_3 are significantly longer than in Si, and SiO_2 , the smallest bond lengths being obtained in the quartz polymorphs.

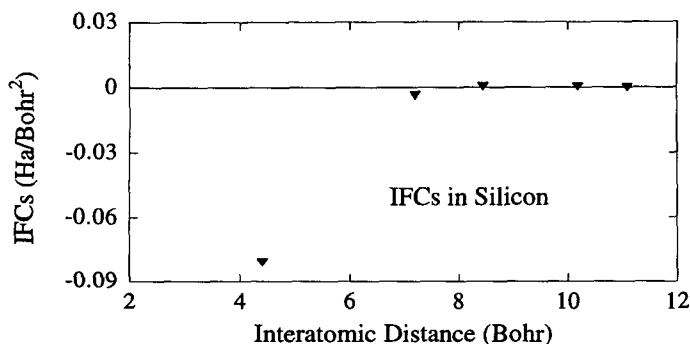


Fig. 1. Longitudinal interatomic force constants in Si, as a function of the distance between the pair of atoms.

Thus, in comparing these four materials, one will monitor the balance between ionic and covalent effects, as well as the anisotropy of each local site. Let us now focus on the potential well that each atom feels, and on the decomposition of the longitudinal interatomic force constants in its dipole-dipole component and its short range part. A more complete account of the results obtained thanks to the application of the above-described formalism can be found in Refs.[15-22], together with comparison with experiments. At the level of vibrational frequencies, the LDA is consistently within 3-5% of the experimental data for all these materials.

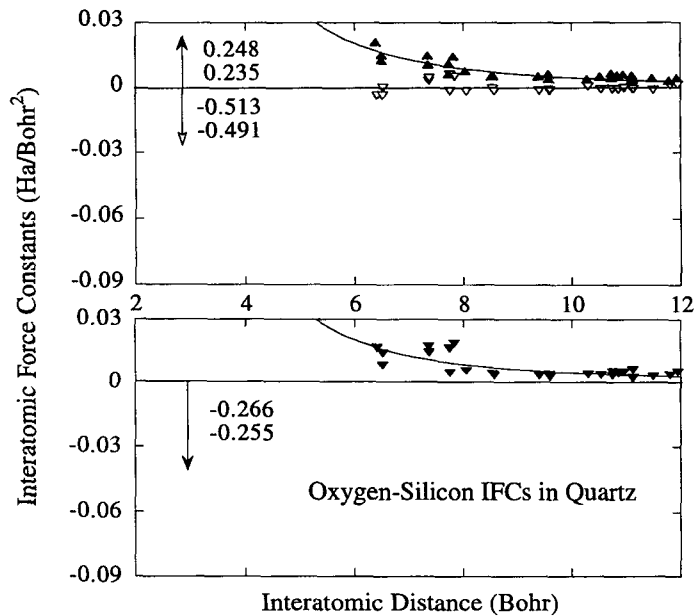


Fig. 2. (lower part of the figure) Oxygen-silicon longitudinal interatomic force constants in quartz, as a function of the distance between the pair of atoms. The full line is a guide for the eyes, and represents a decay proportional to the cube of the distance. The arrow indicates values that are larger than the range allowed by the coordinates.
(upper part) Filled triangles, the dipole-dipole part of the IFCs; empty triangles, the short-ranged part of the IFCs. The full line is the same as in the lower part, and arrows have the same meaning.

Table 1 presents the characteristics of the potential wells. The largest potential wells are observed in SiO_2 , for movements related with bond length changes. The smallest is observed for the Ba atom in BaTiO_3 . The anisotropy of the well is particularly high for the oxygen in quartz, with a factor of 10 between the direction parallel to the Si-Si nearest neighbour line and the out-of-plane direction. This anisotropy is about 2...3 for the oxygen in stishovite or BaTiO_3 . The potential well of other atoms is rather isotropic.

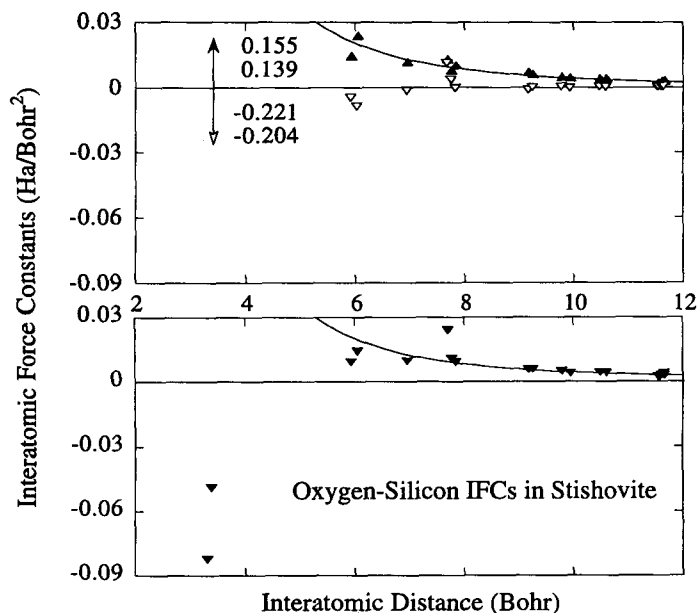


Fig. 3. The analysis of oxygen-silicon longitudinal interatomic force constants in stishovite. See the caption of Fig. 2.

The longitudinal IFCs (IFCs for displacement and forces projected along the line connecting the two nuclei) are presented in Figs. 1-4, as a function of the distance between pairs of atoms. In SiO_2 , only the behaviour of the force constants between Si and O has been monitored, while in BaTiO_3 , the Ti-O pairs were chosen. In Si, the IFCs decrease rapidly. By contrast, due to the long range dipole-dipole interaction, the IFCs are still sizeable for separations as large as 12 Bohr in all the other materials. The decomposition of the total IFCs in their dipole-dipole and short-range components is presented in the upper part of Figs. 2-4. The short-range part tends rapidly to zero for most pairs of atoms. The nearest-neighbour interaction is also worth to study. The short-range part is the largest one in quartz and stishovite, by contrast, due to the large Born effective charges in BaTiO_3 , they compensate, so that the sign of the IFC can be positive or negative. This is actually connected with the ferroelectric instabilities of this material.

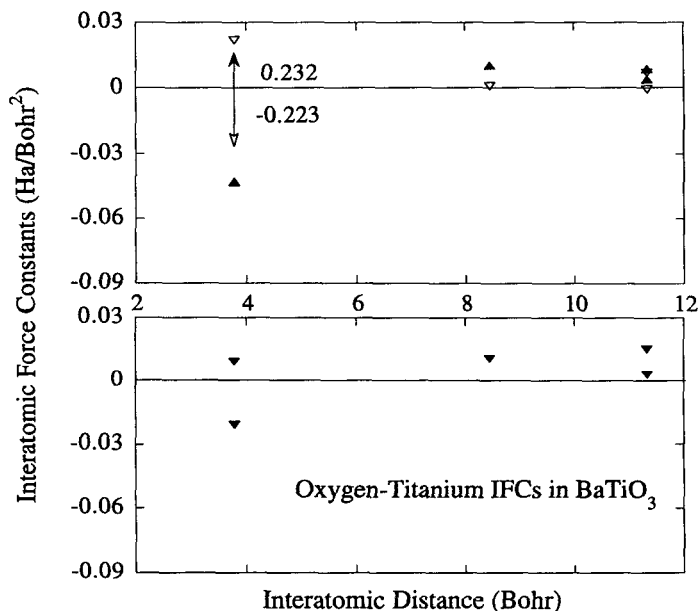


Fig. 4. The analysis of longitudinal interatomic force constants in BaTiO_3 . See the caption of Fig. 2.

Summary - Perspectives.

The present paper aimed at presenting a particular technique for the computation of IFCs in solids, and its application to Si, SiO₂ quartz and stishovite, and BaTiO₃. The variational principle is used for two purposes : it determines the response of the wavefunctions and density to the different perturbations, and also gives an accurate evaluation of the second derivative of the total energy. The IFCs in the above-mentioned materials were compared at the level of the potential well that each atom feels and the decrease of the IFC longitudinal component with the distance between the atoms.

Acknowledgements.

I would like to thank my collaborators in the different studies presented here: D. C. Allan, J.-C. Charlier, P. Ghosez, C. Lee, G.-M. Rignanese, M. P. Teter. This work has been supported by FNRS-Belgium, FDS-UCL, the PAI IUAP P4/10, and the research contract between UCL, FUNDP and IBM.

References.

- [1] N.E. Zein, "Density functional calculations of elastic moduli and phonon spectra of crystals," *Sov. Phys. Solid State* **26** (1984), 1825-1828.
- [2] K. Kunc and P. Gomes Davosta, "Real-space convergence of the force series in the lattice dynamics of germanium," *Phys. Rev. B* **32** (1985), 2010-2021.
- [3] S. Baroni, P. Giannozzi, and A. Testa, "Green's functions approach to linear response in solids," *Phys. Rev. Lett.* **58** (1987), 1861-1864.
- [4] S. Yu. Savrasov, "A linearized direct approach for calculating the static response in solids," *Solid State Commun.* **74** (1990), 69-72.
- [5] S. Wei and M.Y. Chou, "Ab Initio calculation of force constants and full phonon dispersion," *Phys. Rev. Lett.* **69** (1992), 2799-2802.
- [6] P. Giannozzi, S. de Gironcoli, P. Pavone, and S. Baroni, "Ab Initio calculation of phonon dispersions in semiconductors," *Phys. Rev. B* **43** (1991), 7231-7242.

- [7] A. Komornicki and G. Fitzgerald, "Molecular gradients and Hessians implemented in density functional theory," *J. Chem. Phys.* **98** (1993), 1398-1421.
- [8] N.C. Handy, D.J. Tozer, G.J. Laming, C.W. Murray, and R. Amos, "Analytic second derivatives of the potential energy surface," *Isr. J. of Chem.* **33** (1993), 331-344.
- [9] See also the references mentioned in Refs.[12-14].
- [10] X. Gonze, D.C. Allan and M.P. Teter, "Dielectric tensor, effective charges and phonons in α -quartz by variational density-functional perturbation theory," *Phys. Rev. Lett.* **68** (1992), 3603-3606.
- [11] X. Gonze, "On the perturbation expansion of variational principles at arbitrary order," *Phys. Rev. A* **52** (1995), 1086-1095.
- [12] X. Gonze, "Adiabatic Density Functional Perturbation Theory," *Phys. Rev. A* **52** (1995), 1096-1114.
- [13] X. Gonze, "First-principle responses of solids to atomic displacements and homogeneous electric fields: a conjugate-gradient algorithm, used with plane waves and pseudopotentials," *Phys. Rev. B* **55** (1997), 10337-10354.
- [14] X. Gonze and C. Lee, "Dynamical matrices, Born effective charges, dielectric permittivity tensors, and interatomic force constants from density-functional perturbation theory," *Phys. Rev. B* **55** (1997), 10355-10368.
- [15] C. Lee and X. Gonze, "Lattice dynamics and dielectric properties of SiO₂-stishovite," *Phys. Rev. Lett.* **72** (1994), 1686-1689.
- [16] X. Gonze, J.-C. Charlier, D.C. Allan and M.P. Teter, "Interatomic force constants from first-principles : the case of α -quartz," *Phys. Rev. B* **50** (1994), 13035-13038.
- [17] C. Lee and X. Gonze, "Ab initio calculation of the thermodynamical properties of α -quartz and stishovite," *Phys. Rev. B* **51** (1995), 8610-8613.
- [18] G.-M. Rignanese, J.-P. Michenaud and X. Gonze, "Ab Initio study of the volume dependence of dynamical and thermodynamical properties of silicon," *Phys. Rev. B* **53** (1996), 4488-4497.

- [19] Ph. Ghosez, X. Gonze and J.-P. Michenaud, "Coulomb interaction and ferroelectric instability of BaTiO_3 ," *Europhys. Letters* **33** (1996), 713-718.
- [20] C. Lee, "Analyses of the ab initio harmonic interatomic force constants of stishovite," *Phys. Rev. B* **54** (1996), 8973-8976.
- [21] Ph. Ghosez, X. Gonze and J.-P. Michenaud, "Ab Initio phonon dispersion curves and interatomic force constants of barium titanate," accepted for publication in *Ferroelectrics*.
- [22] C. Lee and X. Gonze, " SiO_2 -stishovite under high pressure : dielectric and dynamical properties, ferroelastic phase transition," accepted for publication in *Phys. Rev. B*.
- [23] M.P. Teter, M.C. Payne, and D.C. Allan, "Solution of Schrödinger's equation for large systems," *Phys. Rev. B* **40** (1989), 12255-12263.
- [24] M.C. Payne, M.P. Teter, D.C. Allan, T.A. Arias, and J.D. Joannopoulos, "Iterative minimization techniques for Ab Initio total-energy calculations: molecular dynamics and conjugate gradients," *Rev. Mod. Phys.* **64** (1992), 1045-1097.

RECENT DEVELOPMENTS IN THE ELECTRONIC

STRUCTURE OF METAL SURFACES

Viraht Sahni and Alexander Solomatin

**Department of Physics, Brooklyn College of the City University of New York
2900 Bedford Avenue, Brooklyn, New York 11210**

and

**The Graduate School and University Center of the City University of New
York**

33 West 42nd Street, New York, New York 10036

Contents

- I. Introduction**
- II. A. Physical interpretation of Kohn-Sham theory exchange-correlation energy functional and its derivative**
 - B. Physical interpretation of Kohn-Sham theory exchange energy functional and its derivative**
 - C. Physical interpretation of Kohn-Sham theory correlation energy functional and its derivative**
- III. Asymptotic structure in vacuum region**
- IV. Structure of the Pauli and correlation-kinetic components of Kohn-Sham exchange potential**
- V. Construction of approximate Kohn-Sham exchange energy functional and derivative with exact asymptotic structure**
- VI. Concluding remarks**
- VII. Acknowledgements**
- VIII. References**

I. INTRODUCTION

In this article we describe the results and conclusions of recent work of ours¹⁻⁷ on the electronic structure of the many-electron nonuniform density system at a metal surface⁸. These results are of significance from the perspective of surface probes such as the scanning-tunnelling microscope, the interaction of ions and positrons with the surface, and properties such as the surface energy, curvature energy and work function. The surface is described by the jellium⁹ and structureless-pseudopotential¹⁰ models, so that the electrons are confined to within the metal by a local effective potential. This local potential has a rigorous mathematical definition within Hohenberg-Kohn-Sham^{11,12} density-functional theory¹³. Recently, Kohn-Sham (KS) theory has also been provided a rigorous physical interpretation^{14,15} based on the original ideas of Harbola and Sahni^{16,17}, and of their extension by Holas and March¹⁸. As such, our calculations are performed both within conventional KS theory as well as in the context of its physical description.

In KS theory¹² a model system of *noninteracting* fermions is constructed such that it possesses the same ground-state density $\rho(\mathbf{r})$ and energy $E[\rho]$ as the interacting system described by the Schrödinger equation. As the fermions are noninteracting, the corresponding electron-interaction energy functional component of the theory is representative of correlations due to the Pauli exclusion principle, Coulomb repulsion and the correlation contribution to the kinetic energy. The local potential which incorporates these electron correlations is then derived to be the functional derivative of the KS electron-interaction energy functional. Within this framework, the dependence of this energy functional and of its derivative on these correlations is not known explicitly. That understanding is provided by the physical interpretation^{14,15} of the theory. This description is in terms of a field which is the sum of two fields, one representative of the quantum-mechanical Pauli and Coulomb correlations, and the other of the correlation-kinetic effects. The sources of these fields are expectations of Hermitian operators taken with respect to the system wavefunction. Thus, within this picture, the representation of these correlations in the KS electron-interaction energy functional and of its derivative is explicitly known. This then allows for the determination of the separate Pauli, Coulomb and correlation-kinetic contributions to the energy and potential.

For the details and derivation of the physical interpretation we refer the reader to the original literature^{14,15}. Since the Coulomb self-energy component of the KS electron-interaction energy functional and its derivative, the Hartree potential, are known functionals of the density, we provide in Section IIA the expressions governing the interpretation of the KS exchange-correlation energy

component and its derivative. We note, however, that the functional derivative of the Coulomb self-energy too has a rigorous physical interpretation. In Sections IIB and IIC we provide the interpretation of the separate KS exchange and correlation energy functionals and their derivatives (potentials). It can be shown¹⁹ that the KS exchange potential is comprised of a Pauli component as well as *part* of the correlation-kinetic contribution. The KS correlation potential is therefore representative of Coulomb correlations and the remaining contribution of the correlation-kinetic effects. In Section III we present and discuss the results of *rigorous analytical* calculations of the asymptotic structure in the vacuum of the Slater potential²⁰, the KS exchange potential, and of its Pauli and correlation-kinetic components. If it is *assumed* that the asymptotic structure of the KS exchange-correlation potential is the image potential, then the asymptotic structure of the KS correlation potential is then also known exactly. These analytical results are all valid for *fully-self-consistently* determined orbitals and for arbitrary metal. In this section we also briefly describe the work of others²¹⁻²⁷ as well as provide an alternate 'classical' description^{1,2} of the physical origin of the asymptotic structure of the KS exchange-correlation potential. In Section IV we present the structure of the Pauli and correlation-kinetic components of the KS exchange potential for a high and low density metal. These calculations are performed for the highly accurate²¹ orbitals of the jellium and finite-linear-potential models²⁸ of a metal surface. In Section V we show how the exact results described in Section III may be employed to improve upon existing approximate functionals and their derivatives. We do this by constructing an approximate exchange energy functional which improves upon the local density approximation by ensuring that the latter has the correct KS asymptotic structure in the vacuum. Concluding remarks are made and directions for future work given in Section VI.

II. A. PHYSICAL INTERPRETATION OF KOHN-SHAM THEORY EXCHANGE-CORRELATION ENERGY FUNCTIONAL AND ITS DERIVATIVE

The KS theory exchange-correlation energy functional $E_{xc}^{KS}[\rho]$ and its derivative (potential) $v_{xc}(\mathbf{r})$ can both be expressed as a sum of two terms, one representative of the quantum-mechanical Pauli and Coulomb correlations and the other of the correlation-kinetic effects. Thus, we may write

$$E_{xc}^{KS}[\rho] = E_{xc}[\rho] + T_c[\rho] \quad , \quad (1)$$

and

$$v_{xc}(\mathbf{r}) = \frac{\delta E_{xc}^{KS}[\rho]}{\delta \rho(\mathbf{r})} = W_{xc}(\mathbf{r}) + W_t(\mathbf{r}) \quad . \quad (2)$$

The quantum-mechanical exchange-correlation energy $E_{xc}[\rho]$ and the Pauli-Coulomb component $W_{xc}(\mathbf{r})$ of the potential can be expressed in terms of a field $\mathcal{E}_{xc}(\mathbf{r})$. This field is derived via Coulomb's law from the quantum-mechanical Fermi-Coulomb hole charge distribution $\rho_{xc}(\mathbf{r}, \mathbf{r}')$ at \mathbf{r}' for an electron at \mathbf{r} as

$$\mathcal{E}_{xc}(\mathbf{r}) = \int \frac{\rho_{xc}(\mathbf{r}, \mathbf{r}') (\mathbf{r} - \mathbf{r}')}{|\mathbf{r} - \mathbf{r}'|^3} d\mathbf{r}' \quad . \quad (3)$$

The Fermi-Coulomb hole $\rho_{xc}(\mathbf{r}, \mathbf{r}')$ is in turn defined in terms of the density $\rho(\mathbf{r}) = \langle \Psi | \sum_i \delta(\mathbf{r}_i - \mathbf{r}) | \Psi \rangle$ and pair-correlation density $g(\mathbf{r}, \mathbf{r}') = \langle \Psi | \sum_{i,j} \delta(\mathbf{r}_i - \mathbf{r}) \delta(\mathbf{r}_j - \mathbf{r}') | \Psi \rangle / \rho(\mathbf{r}) \rho(\mathbf{r}')$ as $\rho_{xc}(\mathbf{r}, \mathbf{r}') = g(\mathbf{r}, \mathbf{r}') - \rho(\mathbf{r}')$, and where $\Psi(\mathbf{x}_1, \dots, \mathbf{x}_N)$ is the system wavefunction with $\mathbf{x} = \mathbf{r}\sigma$. The total charge of the Fermi-Coulomb hole is negative unity: $\int \rho_{xc}(\mathbf{r}, \mathbf{r}') d\mathbf{r}' = -1$. Note that the density and pair-correlation density are expectations of Hermitian operators. In terms of the field $\mathcal{E}_{xc}(\mathbf{r})$, the energy $E_{xc}[\rho]$ may be written in virial form as

$$E_{xc}[\rho] = \int d\mathbf{r} \rho(\mathbf{r}) \mathbf{r} \cdot \mathcal{E}_{xc}(\mathbf{r}) \quad , \quad (4)$$

whereas $W_{xc}(\mathbf{r})$ is the work done to move an electron from infinity to its position at \mathbf{r} in this field so that

$$W_{xc}(\mathbf{r}) = - \int_{\infty}^{\mathbf{r}} \mathcal{E}_{xc}(\mathbf{r}') \cdot d\mathbf{l}' \quad . \quad (5)$$

The correlation-kinetic energy $T_c[\rho]$ and potential component $W_t(\mathbf{r})$ are also expressed in terms of a field $Z_t(\mathbf{r})$. The field $Z_t(\mathbf{r})$ is the difference of two fields $\mathbf{z}(\mathbf{r};[\gamma_s])$ and $\mathbf{z}(\mathbf{r};[\gamma])$ for the KS noninteracting and Schrödinger interacting systems respectively, each field being derived from the corresponding system kinetic-energy-density tensor $t_{\alpha\beta}(\mathbf{r})$. Thus

$$\mathbf{Z}_c(\mathbf{r}) = \frac{1}{\rho(\mathbf{r})} [\mathbf{z}(\mathbf{r}; [\gamma_s]) - \mathbf{z}(\mathbf{r}; [\gamma])] , \quad (6)$$

where

$$z_\alpha(\mathbf{r}; [\gamma]) = 2 \sum_{\beta=1}^3 \frac{\partial}{\partial r_\beta} t_{\alpha\beta}(\mathbf{r}; [\gamma]) , \quad (7)$$

$$t_{\alpha\beta}(\mathbf{r}; [\gamma]) = \frac{1}{4} \left[\frac{\partial^2}{\partial r'_\alpha \partial r''_\beta} + \frac{\partial^2}{\partial r'_\beta \partial r''_\alpha} \right] \gamma(\mathbf{r}', \mathbf{r}'') \Big|_{\mathbf{r}' = \mathbf{r}'' = \mathbf{r}} , \quad (8)$$

and $\gamma(\mathbf{r}, \mathbf{r}')$, $\gamma_s(\mathbf{r}, \mathbf{r}')$ are the spinless single-particle and Dirac density matrices:

$$\gamma(\mathbf{r}, \mathbf{r}') = N \sum_{\sigma} \int \Psi^*(\mathbf{r}\sigma, \mathbf{x}_2 \dots \mathbf{x}_N) \Psi(\mathbf{r}'\sigma, \mathbf{x}_2 \dots \mathbf{x}_N) d\mathbf{x}_2 \dots d\mathbf{x}_N , \quad (9)$$

$$\gamma_s(\mathbf{r}, \mathbf{r}') = \sum_{\sigma} \sum_i \phi_i^*(\mathbf{r}\sigma) \phi_i(\mathbf{r}'\sigma) , \quad (10)$$

where $\phi_i(\mathbf{x})$ are the KS orbitals with $\gamma_s(\mathbf{r}, \mathbf{r}) = \rho(\mathbf{r})$, and $\int d\mathbf{x} = \sum_{\sigma} \int d\mathbf{r}$. Note that the density matrices too can be expressed^{14,15} as expectations of a Hermitian operator. The energy $T_c[\rho]$ is written in terms of the field $\mathbf{Z}_c(\mathbf{r})$ in virial form as

$$T_c[\rho] = \frac{1}{2} \int d\mathbf{r} \rho(\mathbf{r}) \mathbf{r} \cdot \mathbf{Z}_c(\mathbf{r}) , \quad (11)$$

and the component $W_c(\mathbf{r})$ is the work done to move an electron in the field $\mathbf{Z}_c(\mathbf{r})$:

$$W_c(\mathbf{r}) = - \int_{\infty}^{\mathbf{r}} \mathbf{Z}_c(\mathbf{r}') \cdot d\mathbf{l}' . \quad (12)$$

Defining the field $\mathbf{R}(\mathbf{r})$ as the sum of the fields $\mathcal{E}_{xc}(\mathbf{r})$ and $\mathbf{Z}_c(\mathbf{r})$:

$$\mathbf{R}(\mathbf{r}) = \mathbf{Z}_{xc}(\mathbf{r}) + \mathbf{Z}_t(\mathbf{r}) \quad , \quad (13)$$

the KS exchange-correlation potential $v_{xc}(\mathbf{r})$ is then the work done in the field $\mathbf{R}(\mathbf{r})$:

$$v_{xc}(\mathbf{r}) = - \int_{\infty}^{\mathbf{r}} \mathbf{R}(\mathbf{r}') \cdot d\mathbf{l}' \quad . \quad (14)$$

This work done is *path-independent* since $\nabla \times \mathbf{R}(\mathbf{r}) = 0$. For systems of certain symmetry such as closed shell atoms or open-shell atoms in the central-field approximation, the jellium and structureless-pseudopotential models of a metal surface considered here, etc., the work $W_{xc}(\mathbf{r})$ and $W_t(\mathbf{r})$ are separately path-independent since for these cases $\nabla \times \mathbf{Z}_{xc}(\mathbf{r}) = \nabla \times \mathbf{Z}_t(\mathbf{r}) = 0$.

B. PHYSICAL INTERPRETATION OF KOHN-SHAM THEORY EXCHANGE ENERGY FUNCTIONAL AND ITS DERIVATIVE

In conventional KS theory, the exchange-correlation energy functional $E_{xc}^{KS}[\rho]$ is normally split into its exchange $E_x^{KS}[\rho]$ and correlation $E_c^{KS}[\rho]$ energy components. The exchange energy functional $E_x^{KS}[\rho]$ is known in terms of the KS orbitals $\phi_i(\mathbf{x})$ and may be expressed via the corresponding Fermi hole charge $\rho_x^{KS}(\mathbf{r}, \mathbf{r}')$ through the Slater potential $V_x^S(\mathbf{r})$ as

$$E_x^{KS}[\rho] = \frac{1}{2} \int \rho(\mathbf{r}) V_x^S(\mathbf{r}) d\mathbf{r} \quad , \quad (15)$$

where

$$V_x^S(\mathbf{r}) = \int \frac{\rho_x^{KS}(\mathbf{r}, \mathbf{r}')}{|\mathbf{r} - \mathbf{r}'|} d\mathbf{r}' \quad , \quad (16)$$

and

$$\rho_x^{KS}(\mathbf{r}, \mathbf{r}') = - |\gamma_s(\mathbf{r}, \mathbf{r}')|^2 / 2\rho(\mathbf{r}) \quad . \quad (17)$$

The total charge of the Fermi hole is also (negative) unity: $\int \rho_x^{KS}(\mathbf{r}, \mathbf{r}') d\mathbf{r}' = -1$, and it satisfies the constraints of negativity

$\rho_x^{\text{KS}}(\mathbf{r}, \mathbf{r}') \leq 0$, and value at electron position $\rho_x^{\text{KS}}(\mathbf{r}, \mathbf{r}) = -\rho(\mathbf{r})/2$. The derivative $v_x(\mathbf{r})$ of the functional $E_x^{\text{KS}}[\rho]$ is then

$$v_x(\mathbf{r}) = \frac{\delta E_x^{\text{KS}}[\rho]}{\delta \rho(\mathbf{r})} = \frac{1}{2} V_x^{\text{S}}(\mathbf{r}) + \frac{1}{2} \int \rho(\mathbf{r}') \frac{\delta V_x^{\text{S}}(\mathbf{r}')}{\delta \rho(\mathbf{r})} d\mathbf{r}' \quad (18)$$

Note that the leading term of the KS exchange potential is $(1/2)V_x^{\text{S}}(\mathbf{r})$.

The physical interpretation of the derivative $v_x(\mathbf{r})$ is that it is the sum of two terms, one representative of Pauli correlations $W_x^{\text{KS}}(\mathbf{r})$, and the other $W_{t_c}^{(1)}(\mathbf{r})$ part of the contribution of the correlation-kinetic effects¹⁹:

$$v_x(\mathbf{r}) = \frac{\delta E_x^{\text{KS}}[\rho]}{\delta \rho(\mathbf{r})} = W_x^{\text{KS}}(\mathbf{r}) - W_{t_c}^{(1)}(\mathbf{r}) \quad (19)$$

Here $W_x^{\text{KS}}(\mathbf{r})$ is the work done to move an electron in the field $\mathcal{E}_x^{\text{KS}}(\mathbf{r})$ determined via Coulomb's law from the Fermi hole charge $\rho_x^{\text{KS}}(\mathbf{r}, \mathbf{r}')$ so that

$$W_x^{\text{KS}}(\mathbf{r}) = - \int_{\infty}^{\mathbf{r}} \mathcal{E}_x^{\text{KS}}(\mathbf{r}') \cdot d\mathbf{l}' \quad (20)$$

with

$$\mathcal{E}_x^{\text{KS}}(\mathbf{r}) = \int \frac{\rho_x^{\text{KS}}(\mathbf{r}, \mathbf{r}') (\mathbf{r} - \mathbf{r}')}{|\mathbf{r} - \mathbf{r}'|^3} d\mathbf{r}' \quad (21)$$

The Pauli component $W_x^{\text{KS}}(\mathbf{r})$ of the exchange potential $v_x^{\text{KS}}(\mathbf{r})$ may also be expressed as

$$W_x^{\text{KS}}(\mathbf{r}) = \frac{1}{2} V_x^{\text{S}}(\mathbf{r}) + \int_{\infty}^{\mathbf{r}} d\mathbf{l}' \cdot \int d\mathbf{r}'' \frac{(\nabla'' - \nabla') \rho_x^{\text{KS}}(\mathbf{r}', \mathbf{r}'')}{|\mathbf{r}' - \mathbf{r}''|} \quad (22)$$

so that the leading term of this work done is $(1/2)V_x^{\text{S}}(\mathbf{r})$. The work $W_{t_c}^{(1)}(\mathbf{r})$ is that done to move an electron in the field $\mathcal{Z}_{t_c}^{(1)}(\mathbf{r})$:

$$W_{t_c}^{(1)}(\mathbf{r}) = - \int_{\infty}^{\mathbf{r}} \mathbf{Z}_{t_c}^{(1)}(\mathbf{r}') \cdot d\mathbf{l}' , \quad (23)$$

with

$$\mathbf{Z}_{t_c}^{(1)}(\mathbf{r}) = \frac{\mathbf{z}(\mathbf{r}; [\gamma_1^c])}{\rho(\mathbf{r})} , \quad (24)$$

where $\gamma_1^c(\mathbf{r}, \mathbf{r}')$ is the first-order correction to the KS density matrix $\gamma_s(\mathbf{r}, \mathbf{r}')$ as obtained via perturbation theory by an expansion of the system wavefunction in terms of the electron-interaction coupling constant. Once again the sum of the work $[W_x^{KS}(\mathbf{r}) - W_{t_c}^{(1)}(\mathbf{r})]$ is path-independent since $\nabla \times [\mathbf{Z}_x^{KS}(\mathbf{r}) - \mathbf{Z}_{t_c}^{(1)}(\mathbf{r})] = 0$. For systems with the symmetry discussed in the previous section, the work $W_x^{KS}(\mathbf{r})$ and $W_{t_c}^{(1)}(\mathbf{r})$ are separately path-independent. The expression for the functional derivative $v_x(\mathbf{r})$ of Eq. (19) in terms of the work $W_x^{KS}(\mathbf{r})$ and $W_{t_c}^{(1)}(\mathbf{r})$ is *exact*¹⁹ because it incorporates *all* terms *linear* in the coupling constant.

There is no explicit correlation-kinetic contribution to the KS exchange energy $E_x^{KS}[\rho]$. The contribution, however, is manifested via the KS orbitals, so that $E_x^{KS}[\rho]$ which is related to its functional derivative $v_x^{KS}(\mathbf{r})$ by the virial theorem²⁹ is expressed entirely in terms of the field $\mathbf{Z}_x^{KS}(\mathbf{r})$ as

$$E_x^{KS}[\rho] = - \int \rho(\mathbf{r}) \mathbf{r} \cdot \nabla v_x(\mathbf{r}) d\mathbf{r} = \int \rho(\mathbf{r}) \mathbf{r} \cdot \mathbf{Z}_x^{KS}(\mathbf{r}) d\mathbf{r} , \quad (25)$$

with

$$\int \rho(\mathbf{r}) \mathbf{r} \cdot \mathbf{Z}_{t_c}^{(1)}(\mathbf{r}) d\mathbf{r} = 0 . \quad (26)$$

In the KS representation of Hartree-Fock theory, an exchange energy functional and its derivative which give rise to the Hartree-Fock density and energy can also be defined¹⁵. Once again this functional and derivative can be described in terms of a field representative of Pauli correlations and one representing the corresponding correlation-kinetic effects. A similar interpretation can also be provided³⁰ the exchange potential³¹ of exchange-only Kohn-Sham theory, viz., that of the optimized potential method³².

C. PHYSICAL INTERPRETATION OF KOHN-SHAM THEORY CORRELATION ENERGY FUNCTIONAL AND ITS DERIVATIVE

The KS theory Coulomb hole $\rho_c^{\text{KS}}(\mathbf{r}, \mathbf{r}')$ is defined as the difference

$$\rho_c^{\text{KS}}(\mathbf{r}, \mathbf{r}') = \rho_{\text{xc}}(\mathbf{r}, \mathbf{r}') - \rho_x^{\text{KS}}(\mathbf{r}, \mathbf{r}') \quad , \quad (27)$$

so that it satisfies the constraint $\int \rho_c^{\text{KS}}(\mathbf{r}, \mathbf{r}') d\mathbf{r}' = 0$. The KS correlation energy $E_c^{\text{KS}}[\rho]$ is then the sum of the Coulomb $U_c[\rho]$ and correlation-kinetic $T_c[\rho]$ energies:

$$E_c^{\text{KS}}[\rho] = U_c[\rho] + T_c[\rho] \quad , \quad (28)$$

where

$$U_c[\rho] = \frac{1}{2} \int \rho(\mathbf{r}) V_c^S(\mathbf{r}) d\mathbf{r} \quad , \quad (29)$$

and

$$V_c^S(\mathbf{r}) = \int \frac{\rho_c^{\text{KS}}(\mathbf{r}, \mathbf{r}')}{|\mathbf{r} - \mathbf{r}'|} d\mathbf{r}' \quad , \quad (30)$$

is the Slater correlation potential. The corresponding KS correlation potential $v_c(\mathbf{r})$ is the functional derivative

$$v_c(\mathbf{r}) = \frac{\delta E_c^{\text{KS}}[\rho]}{\delta \rho(\mathbf{r})} = \frac{1}{2} V_c^S(\mathbf{r}) + \frac{1}{2} \int \rho(\mathbf{r}') \frac{\delta V_c^S(\mathbf{r}')}{\delta \rho(\mathbf{r})} d\mathbf{r}' + \frac{\delta T_c[\rho]}{\delta \rho(\mathbf{r})} \quad . \quad (31)$$

With the KS theory Fermi and Coulomb holes defined by Eq. (27), the derivative $v_{\text{xc}}(\mathbf{r})$ can also be expressed in terms of its separate Pauli, Coulomb and correlation-kinetic contributions as

$$v_{\text{xc}}(\mathbf{r}) = \frac{\delta E_{\text{xc}}^{\text{KS}}[\rho]}{\delta \rho(\mathbf{r})} = W_x^{\text{KS}}(\mathbf{r}) + W_c^{\text{KS}}(\mathbf{r}) + W_t(\mathbf{r}) \quad , \quad (32)$$

where $W_c^{KS}(\mathbf{r})$ is the work done in the field $\mathcal{E}_c^{KS}(\mathbf{r})$ due to the Coulomb hole charge $\rho_c^{KS}(\mathbf{r}, \mathbf{r}')$:

$$W_c^{KS}(\mathbf{r}) = - \int_{\infty}^{\mathbf{r}} \mathcal{E}_c^{KS}(\mathbf{r}') \cdot d\mathbf{l}' ; \quad \mathcal{E}_c^{KS}(\mathbf{r}) = \int \frac{\rho_c^{KS}(\mathbf{r}, \mathbf{r}')(\mathbf{r} - \mathbf{r}')}{|\mathbf{r} - \mathbf{r}'|^3} d\mathbf{r}' \quad (33)$$

Since $v_{xc}(\mathbf{r}) = v_x(\mathbf{r}) + v_c(\mathbf{r})$, where $v_x(\mathbf{r})$ is given by Eq. (19), the *exact* expression for the derivative $v_c(\mathbf{r})$ is then

$$v_c(\mathbf{r}) = \frac{\delta E_c^{KS}[\rho]}{\delta \rho(\mathbf{r})} = W_c^{KS}(\mathbf{r}) + W_{t_c}(\mathbf{r}) + W_{t_c}^{(1)}(\mathbf{r}) , \quad (34)$$

where $W_{t_c}(\mathbf{r})$ and $W_{t_c}^{(1)}(\mathbf{r})$ are as defined previously. The Coulomb correlation energy $U_c[\rho]$ is also expressed in terms of the field $\mathcal{E}_c^{KS}(\mathbf{r})$ as

$$U_c[\rho] = \int d\mathbf{r} \rho(\mathbf{r}) \mathbf{r} \cdot \mathcal{E}_c^{KS}(\mathbf{r}) . \quad (35)$$

Perturbation theory expressions for $W_c^{KS}(\mathbf{r})$, $W_{t_c}(\mathbf{r})$, $U_c[\rho]$ and $T_c[\rho]$ can be derived but we do not give these here. We note, however, that the KS correlation potential $v_c(\mathbf{r})$ commences¹⁹ in second order in the coupling constant. The term quadratic in the coupling constant $v_{c,2}(\mathbf{r})$ is then

$$v_{c,2}(\mathbf{r}) = W_c^{(1)}(\mathbf{r}) - W_{t_c}^{(2)} , \quad (36)$$

where the work $W_c^{(1)}(\mathbf{r})$ depends on the first-order correction to the pair-correlation density, and $W_{t_c}^{(2)}$ on the second-order correction $\gamma_2^c(\mathbf{r}, \mathbf{r}')$ of the density-matrix $\gamma(\mathbf{r}, \mathbf{r}')$. Similarly, it can be shown that for $E_c^{KS}[\rho]$ the term quadratic in the coupling constant is due to correlation-kinetic effects arising from the field of $\gamma_2^c(\mathbf{r}, \mathbf{r}')$.

III. ASYMPTOTIC STRUCTURE IN VACUUM REGION

In the jellium and structureless pseudopotentials models of a metal surface, there is translational symmetry in the plane parallel to the surface and the effective potential in which the electrons move is local. Thus, the structure of the *self-consistent* KS orbitals for these models is of the form

$$\psi_{\mathbf{k}}(\mathbf{r}) = \sqrt{\frac{2}{V}} e^{i\mathbf{k}_{\parallel} \cdot \mathbf{x}_{\parallel}} \phi_{\mathbf{k}}(x) , \quad (37)$$

where $(\mathbf{k}_{\parallel}, \mathbf{x}_{\parallel})$ are the momentum and position vectors parallel to the surface, and (k, x) the components perpendicular to it. The semi-infinite metal, assigned the negative half-space, is defined by its Fermi energy $\epsilon_F = k_F^2/2$, where $k_F = 1/\alpha r_S$ is the Fermi momentum, $\alpha^{-1} = (9\pi/4)^{1/3}$, and r_S is the Wigner-Seitz radius.

For the self-consistent orbitals, we have determined¹⁻⁴ the exact analytical asymptotic structure in the classically forbidden vacuum region of (i) the Slater potential $V_S^S(\mathbf{r})$, (ii) the functional derivative (exchange potential) $v_x(\mathbf{r}) = \delta E_x^{KS}[\rho]/\delta\rho(\mathbf{r})$, (iii) the Pauli component $W_x^{KS}(\mathbf{r})$ of the derivative (exchange-correlation potential) $v_{xc}(\mathbf{r}) = \delta E_{xc}^{KS}[\rho]/\delta\rho(\mathbf{r})$ (or of $v_x(\mathbf{r})$), and hence (iv) the correlation-kinetic component $W_c^{(1)}(\mathbf{r})$ of $v_x(\mathbf{r})$. Further, if it is *assumed* that the asymptotic structure of the functional derivative $v_{xc}(\mathbf{r})$ is the image potential $-1/4x$, the asymptotic structure of (v) the derivative (correlation potential) $v_c = \delta E_c^{KS}[\rho]/\delta\rho(\mathbf{r})$ is then also known exactly.

The asymptotic structure of the exchange potential $v_x(\mathbf{r})$ was derived via the relationship between density functional theory and many-body perturbation theory as established by Sham²⁶. The integral equation relating $v_{xc}(\mathbf{r})$ to the nonlocal exchange-correlation component $\Sigma_{xc}(\mathbf{r}, \mathbf{r}'; \omega)$ of the self-energy $\Sigma(\mathbf{r}, \mathbf{r}'; \omega)$ is

$$\begin{aligned} & \int d\mathbf{r}' v_{xc}(\mathbf{r}') \int \frac{d\omega}{2\pi} G_s(\mathbf{r}, \mathbf{r}'; \omega) G(\mathbf{r}', \mathbf{r}; \omega) \\ &= \int d\mathbf{r}' \int d\mathbf{r}'' \int \frac{d\omega}{2\pi} G_s(\mathbf{r}, \mathbf{r}'; \omega) \Sigma_{xc}(\mathbf{r}', \mathbf{r}''; \omega) G(\mathbf{r}'', \mathbf{r}; \omega) , \end{aligned} \quad (38)$$

where $G(\mathbf{r}, \mathbf{r}'; \omega)$ is the one-particle Green function and $G_s(\mathbf{r}, \mathbf{r}'; \omega)$ the KS Green function. From this equation, Sham derived the asymptotic structure of $v_{xc}(\mathbf{r})$ to be

$$v_{xc}(\mathbf{r}) = \frac{1}{2\psi_{\mathbf{k}}(\mathbf{r})} \int d\mathbf{r}' \Sigma_{xc}(\mathbf{r}, \mathbf{r}'; \epsilon_F) \psi_{\mathbf{k}}(\mathbf{r}') \\ + \frac{1}{2\psi_{\mathbf{k}}^*(\mathbf{r})} \int d\mathbf{r}' \psi_{\mathbf{k}}^*(\mathbf{r}') \Sigma_{xc}(\mathbf{r}', \mathbf{r}; \epsilon_F) , \quad (39)$$

where the electron is at the Fermi level ϵ_F . The asymptotic structure of the exchange component $v_x(\mathbf{r})$ is obtained by substituting the self-energy $\Sigma_x(\mathbf{r}, \mathbf{r}') = -\gamma_s(\mathbf{r}, \mathbf{r}')/2|\mathbf{r} - \mathbf{r}'|$ into the above equation. The result derived^{1,3} is

$$\lim_{x \rightarrow \infty} v_x(\mathbf{r}) = -\frac{\alpha_{KS,x}(\beta)}{x} , \quad (40)$$

where

$$\alpha_{KS,x}(\beta) = \frac{\beta^2 - 1}{2\beta^2} \left[1 - \frac{\ln(\beta^2 - 1)}{\pi(\beta^2 - 1)^{1/2}} \right] , \quad (41)$$

the parameter $\beta^2 = W/\epsilon_F$, and W is the surface barrier height.

Now if it *assumed* that the asymptotic structure of the exchange-correlation potential $v_{xc}(\mathbf{r})$ is the image potential, the analytical asymptotic structure of the KS correlation potential is

$$\lim_{x \rightarrow \infty} v_c(\mathbf{r}) = -\frac{\alpha_{KS,c}(\beta)}{x} ; \quad \alpha_{KS,c}(\beta) = [1 - 4\alpha_{KS,x}(\beta)]/4 . \quad (42)$$

The asymptotic structure of the Pauli component $W_x^{KS}(\mathbf{r})$ is derived⁴ to be

$$\lim_{x \rightarrow \infty} W_x^{KS}(x) = -\frac{\alpha_W(\beta)}{x} , \quad (43)$$

where the coefficient

$$\alpha_W(\beta) = \frac{\beta^2 - 1}{\beta^2} \left[\frac{2}{\pi\sqrt{\beta^2 - 1}} \left(1 - \frac{(\beta^2 - 1)\ln(\beta^2 - 1)}{\beta^2} \right) + \frac{\beta^2 - 2}{\beta^2} \right] . \quad (44)$$

As such, the asymptotic structure of the correlation-kinetic component $W_{t_c}^{(1)}(\mathbf{r})$ is also known to decay *exactly* as

$$W_{t_c}^{(1)}(x) = \frac{\alpha_{t_c}^{(1)}(\beta)}{x} , \quad x \rightarrow \infty \quad (45)$$

where the decay coefficient is

$$\alpha_{t_c}^{(1)}(\beta) = \frac{\beta^2 - 1}{2\beta^2} \left[1 - 2 \frac{\beta^2 - 2}{\beta^2} - \frac{4}{\pi\sqrt{\beta^2 - 1}} \left\{ 1 + \frac{4 - 3\beta^2}{\beta^2} \ln(\beta^2 - 1) \right\} \right] . \quad (46)$$

Finally, the asymptotic structure of the Slater potential is derived^{1,2} as

$$V_x^S(x) = - \frac{\alpha_S(\beta)}{x} ; \quad \alpha_S(\beta) = 2\alpha_{KS,x}(\beta) . \quad (47)$$

We refer the reader to the original literature for details of the derivation of these results. What the derivations all show, however, is that the asymptotic structure in the vacuum region is governed by and arises entirely from the orbitals deep in the metal interior where the structure of $\phi_k(x) = \sin[kx + \delta(k)]$. The orbitals in the regions at and outside the surface do not contribute to the structure far in the vacuum.

The most significant point of the results is that the KS exchange potential $v_x(\mathbf{r})$, the Pauli component $W_x^{KS}(\mathbf{r})$, and the Slater potential $V_x^S(\mathbf{r})$ all decay asymptotically as $-x^{-1}$. This is consistent with the work of Harbola and Sahni²¹⁻²⁴ who also determined these structures but did so numerically and for specific metals only. Furthermore, their calculations were performed for model potential orbitals. The present results are valid for *fully-self-consistently* determined orbitals, and the decay coefficients for *arbitrary* metal can be obtained

exactly. It can also be shown^{1,2} analytically that for *jellium slab metal*, these potentials must decay as $-x^{-2}$. This is consistent with the work of Eguiluz, et al.²⁷ who solved the Sham²⁶ integral equation numerically in the exchange-only case for specific metals and slab metal geometry.

In Fig. 1 we plot the decay coefficients $\alpha_s(\beta)$, $\alpha_{KS,x}(\beta)$, $\alpha_W(\beta)$, $\alpha_{t_c}^{(1)}(\beta)$ and $\alpha_{KS,c}(\beta)$ as a function of the barrier height parameter β . The corresponding values of the Wigner-Seitz radius r_s for both the jellium and structureless-pseudopotential models are also given. The relationship between the parameters r_s and β is through fully-self-consistent calculations (see Appendix of Ref. 21 and Ref. 10), within the local density approximation¹². The values of the coefficients for jellium metal corresponding to $r_s = 2, 4, 6$ are given in Table I.

TABLE 1. The asymptotic structure coefficients of the Slater potential $V_x^S(r)$: $\alpha_s(\beta)$, the KS exchange potential $v_x(r)$: $\alpha_{KS,x}(\beta)$, the potential $W_x^{KS}(r)$: $\alpha_W(\beta)$, the potential $W_t^{(1)}(r)$: $\alpha_{t_c}^{(1)}(\beta)$, and the KS correlation potential $v_c(r)$: $\alpha_{KS,c}(\beta)$, as a function of the Wigner-Seitz radius r_s for the jellium metal surface. The parameter $\beta = \sqrt{W/\epsilon_F}$, where W is the barrier height and ϵ_F the Fermi energy. The relationship between the parameter β and r_s , is determined via a self-consistent calculation within the local density approximation.

Coefficients	Wigner-Seitz radius r_s (a.u.)		
	2	4	6
$\alpha_s(\beta)$	0.390	0.496	0.548
$\alpha_{KS,x}(\beta)$	0.195	0.248	0.274
$\alpha_W(\beta)$	0.217	0.315	0.368
$\alpha_{t_c}^{(1)}(\beta)$	0.022	0.066	0.094
$\alpha_{KS,c}(\beta)$	0.055	0.002	-0.024

The KS exchange potential coefficient $\alpha_{KS,x}(\beta)$ is essentially the image-potential value of $1/4$, ranging from 0.195 to 0.274 over the metallic range of densities. Its value is precisely 0.250 for $\beta = \sqrt{2}$, which corresponds to a Wigner-Seitz radius of $r_s \sim 4.1$. The jellium model is stable for approximately this value of r_s . With the assumption that the asymptotic structure of $v_{xc}(r)$ is the image potential, we see that the correlation contribution to this structure is an

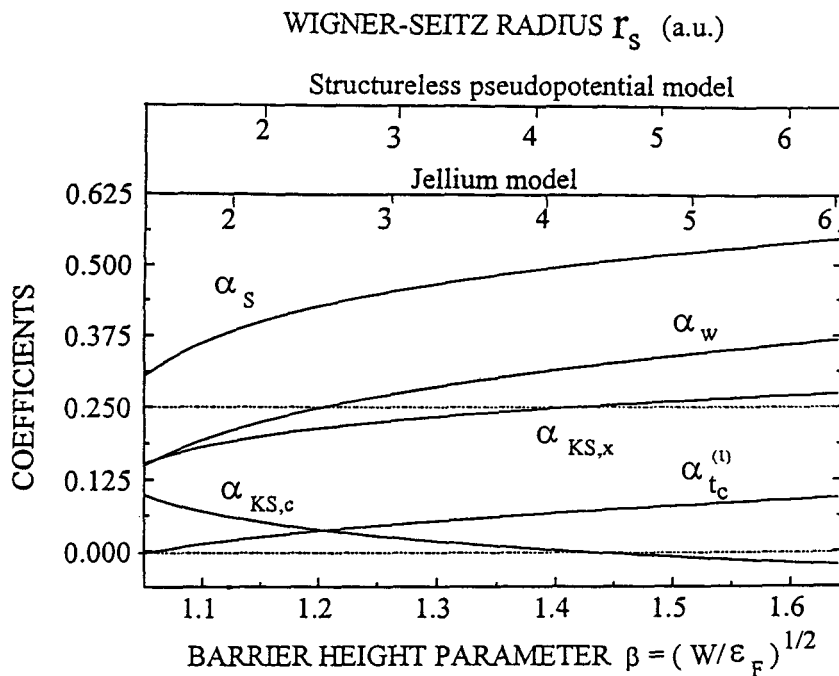


Fig. 1 Asymptotic structure coefficients $\alpha_s(\beta)$, $\alpha_{KS,x}(\beta)$, $\alpha_w(\beta)$, $\alpha_{t_c}^{(1)}(\beta)$, and $\alpha_{KS,c}(\beta)$ as function of barrier height parameter $\beta = \sqrt{W/\epsilon_F}$, where W is the barrier height and ϵ_F the Fermi energy. Corresponding values of the Wigner-Seitz radius r_s for jellium and structureless-pseudopotential models over the metallic range of densities are also given. The relationship between r_s and β is via self-consistent calculations in the local density approximation for exchange-correlation.

order of magnitude weaker, the coefficient $\alpha_{\text{KS},c}(\beta)$ ranging from 0.055 to - 0.024. There is then no KS correlation contribution for stable jellium.

For finite systems, such as atoms and molecules, the asymptotic structure of the KS exchange potential $v_x(\mathbf{r})$ in the classically forbidden region is due entirely to Pauli correlations⁵ as described by $W_x^{\text{KS}}(\mathbf{r})$. Thus,

$$v_x(\mathbf{r}) = W_x^{\text{KS}}(\mathbf{r}) = V_x^{\text{S}}(\mathbf{r}) = -\frac{1}{r}, \quad (48)$$

where the equality between $W_x^{\text{KS}}(\mathbf{r})$ and $V_x^{\text{S}}(\mathbf{r})$ is due to the fact that for asymptotic positions of the electron the Fermi hole is essentially a static charge distribution. The correlation-kinetic contribution $W_c^{(1)}(\mathbf{r})$ is *short-ranged*⁵ for these systems. In the metal surface case (see Eqs. 40 and 47), we have instead the asymptotic structure of $v_x(x)$ to be

$$v_x(x) = \frac{1}{2} V_x^{\text{S}}(x), \quad (49)$$

which is the same (see Eq. 18) as its leading term. It is also evident from Fig. 1 and Eq. (43) that the asymptotic structure of $W_x^{\text{KS}}(x)$ is not that of $(1/2)V_x^{\text{S}}(x)$ which is its leading term (see Eq. 22). Thus, ***there is both a Pauli $W_x^{\text{KS}}(x)$ as well as a correlation-kinetic $W_c^{(1)}(x)$ contribution to the KS exchange potential $v_x(x)$ in the asymptotic vacuum region.*** The correlation-kinetic component is therefore *long-ranged*. The principal contribution to $v_x(x)$, however, is still due to Pauli correlations, the correlation-kinetic contribution being an order of magnitude smaller. (Compare values of $\alpha_w(\beta)$ and $\alpha_c^{(1)}(\beta)$ given in Table I). Note also that for high density metals the correlation-kinetic contribution to $v_x(x)$ is small whereas for low density metals it is quite significant. Thus, for high density metals ($r_s \leq 2$), the asymptotic structure of $v_x(\mathbf{r})$ in the vacuum is essentially that of $W_x^{\text{KS}}(\mathbf{r})$ and therefore governed primarily by Pauli correlations. This result is consistent with the fact^{33,34} that for slowly varying densities for which the local density approximation is valid, the KS potential $v_x(\mathbf{r}) = \delta E_x^{\text{LDA}}[\rho]/\delta \rho(\mathbf{r}) = W_x^{\text{KS}}(\mathbf{r}) = -k_F(\mathbf{r})/\pi$. Finally, we note that since the Fermi hole remains dynamic for asymptotic positions of the electron in the vacuum, the asymptotic structure of the work $W_x^{\text{KS}}(\mathbf{r})$ and Slater potential $V_x^{\text{S}}(\mathbf{r})$ are not equivalent.

There is at present no rigorous analytical proof of the asymptotic structure of the KS exchange-correlation potential $v_{\text{xc}}(\mathbf{r})$ at a metal surface. For

completeness we discuss here the work of others on this structure. In their paper, Almladh and von Barth²⁵ state *without proof* that for microscopic systems, the exchange potential $v_x(r)$ decays *exponentially* to zero, and thus the asymptotic structure of $v_{xc}(r)$ is a Coulomb correlation effect. They then obtain the asymptotic structure of $v_{xc}(r)$ to be the image potential. The basis for the exponential decay of $v_x(r)$ is not explained. The calculations of Sham²⁶ based on Rudnick's³⁵ thesis, involves approximations such as using the free-space one-electron Green function to represent the electron in the classically forbidden region. The subsequent result that $v_x(r)$ decays as $-x^{-2}$ then leads to the conclusion that the asymptotic structure of $v_{xc}(r)$ is due entirely to $v_c(r)$, and that it is the image potential. As noted previously, the *jellium slab-metal* calculations of Egiluz et al.²⁷ show the exchange potential $v_x(r)$ to decay as $-x^{-2}$ as it must^{1,2}. The calculations of these authors for $v_{xc}(r)$ which are within the GW and random phase approximations, and in which the one-electron Green function is replaced by the KS noninteracting Green function, are performed numerically for specific metals. With these approximations, and to a distance of two Fermi wavelengths from the surface, they obtain the asymptotic structure of $v_{xc}(r)$ to be the image potential. As such the $-x^{-1}$ structure of $v_{xc}(r)$ is again attributed to Coulomb correlation effects. The conclusions of these various authors based on approximate calculations thus differ from those arrived at via our rigorous analytical derivations.

There is, however, another^{1,2} way of understanding the physical origin of the asymptotic structure of the KS exchange-correlation potential $v_{xc}(r)$ that is more 'classical' in its description. Recall that the total charge of the Fermi-Coulomb and Fermi holes is $-e$, whereas that of the Coulomb hole is zero. Furthermore, the Fermi hole is *delocalized*³⁶⁻³⁸ in the metal for asymptotic positions of the electron. Thus, for these positions, the Coulomb hole is comprised of two components: one of charge $(+e)$ *delocalized* in the metal which screens out the field of the delocalized Fermi hole, and the other of charge $(-e)$ *localized* to the surface region. If there is no correlation-kinetic contribution to the asymptotic structure of $v_{xc}(r)$, then this structure is the work done in the field of that *part* of the Coulomb hole that is localized to the surface region. In this manner, the asymptotic structure of $v_{xc}(r)$ will also be independent of the metal parameters, and therefore the same for all metals.

IV. STRUCTURE OF THE PAULI AND CORRELATION-KINETIC COMPONENTS OF KOHN-SHAM EXCHANGE POTENTIAL

In this section we present our results^{4,5} for the Pauli and correlation-kinetic component fields ($\mathcal{E}_x^{KS}(r), Z_{tc}^{(1)}(r)$) and potentials ($W_x^{KS}(r), W_{tc}^{(1)}(r)$) of the KS

exchange potential $v_x(\mathbf{r})$ at a jellium-metal surface. Our calculations were performed for the semi-analytical orbitals of the finite-linear-potential model²⁸. These orbitals are extremely accurate and lead to results essentially equivalent to those of fully-self-consistent calculations (see Appendix of Ref. 21). The KS effective potential for this model is

$$v_{\text{eff}}(z) = Fz[\theta(z) - \theta(z - z_b)] + W\theta(z - z_b) \quad , \quad (50)$$

for which the orbitals $\phi_k(z)$ are

$$\begin{aligned} \phi_k(z) = & \sin[kz + \delta(k)]\theta(-z) + [B_k \text{Ai}(\zeta_k) + C_k \text{Bi}(\zeta_k)][\theta(z) - \theta(z - z_b)] \\ & + D_k \exp(-\kappa_k z)\theta(z - z_b) \quad , \end{aligned} \quad (51)$$

where $k = \sqrt{2E}$, $\kappa_k = \sqrt{2(W - E)}$, $\zeta_k = zz_F^{-1/3} - \zeta_0$, $\zeta_0 = k^2 z_F^{2/3}$, $F = (k_F^2/2)/z_F$, $z_F = (k_F^2/2)z_b/W$, E is the energy, W the barrier height, and $\text{Ai}(\zeta_k)$ and $\text{Bi}(\zeta_k)$ the Airy functions. The phase factor $\delta(k)$ and the coefficients B_k , C_k and D_k are determined by the requirement of continuity of the wavefunction and its logarithmic derivative at $z=0$ and $z = z_b$.

To determine the correlation-kinetic field and potential we assume the KS exchange-potential $v_x(\mathbf{r})$ to be that derived^{6,7} by *restricted differentiation* of the exchange energy functional $E_x^{\text{KS}}[\rho]$. The resulting expression for the potential which is in terms of the density $\rho(\mathbf{r})$ and Slater potential $V_x^S(\mathbf{r})$ is

$$v_x^{(0)}(\mathbf{r}) = \frac{1}{2d\rho(\mathbf{r})/dk_F} \frac{d}{dk_F} (\rho(\mathbf{r}) V_x^S(\mathbf{r})) \quad . \quad (52)$$

The intrinsic nonlocality of the problem is thus incorporated in the potential $v_x^{(0)}(\mathbf{r})$ through the dynamic Fermi hole charge. Furthermore, $v_x^{(0)}(\mathbf{r})$ possesses the correct asymptotic structure of $v_x(\mathbf{r})$ in the vacuum as given by Eq. (40), as well as its correct limiting value of $-k_F/\pi$ in the metal bulk. Now for the orbitals of Eq. (51), expressions for the Slater potential $V_x^S(\mathbf{r})$ and the Pauli field $\mathcal{E}_x^{\text{KS}}(\mathbf{r})$ are derived which each reduce to a finite-region momentum-space double integral. Thus, the potentials $v_x^{(0)}(\mathbf{r})$ and $W_x^{\text{KS}}(\mathbf{r})$ can be determined accurately for arbitrary electron position. The differences $[\nabla v_x^{(0)}(\mathbf{r}) - \mathcal{E}_x^{\text{KS}}(\mathbf{r})]$ and

$[v_x^{(0)}(\mathbf{r}) - W_x^{KS}(\mathbf{r})]$ then represent the correlation-kinetic field $Z_c^{(1)}(\mathbf{r})$ and potential $W_{tc}^{(1)}(\mathbf{r})$, respectively.

In Fig. 2 we plot the Pauli field $\mathcal{P}_x^{KS}(z)$ in Fermi wavelengths about the surface for $r_s = 3.24$ and 6.00 . (The Fermi wavelength for $r_s = 3.24$ is 5.61\AA and for $r_s = 6.00$ it is 10.39\AA). The barrier height parameter $\beta = \sqrt{W/\epsilon_F}$ in the orbitals is determined by energy minimization in the local density approximation for the exchange-correlation energy functional. (See Appendix of Ref. 21). Observe that the field is concentrated about the surface, and is greater for $r_s = 6.00$ than for $r_s = 3.24$. The reason for this is that for electron positions near the jellium edge, the Fermi hole for low density metals is more localized³⁶⁻³⁸ in that region than it is for high density metals. The amplitude of the Bardeen-Friedel oscillations of the field within the metal are also greater as expected^{8,39} for the lower density metal. Observe that the field is long-ranged decaying in the vacuum as $\alpha_W(\beta)/z^2$.

In Fig. 3 we plot the approximate KS exchange potential $v_x^{(0)}(z)$ and the Pauli component $W_x^{KS}(z)$. The potential $v_x^{(0)}(z)$ achieves the exact asymptotic structure of $v_x(\mathbf{r})$ in the vacuum by about one Fermi wavelength from the surface. In the metal bulk, it has the correct limiting value of $-2/3$ (in units of $3k_F/2\pi$). For these metal densities, the Pauli component $W_x^{KS}(z)$ is distinct from the exchange potential $v_x^{(0)}(z)$. It has a different asymptotic structure in the vacuum as discussed in the previous section, but it is also different about the surface and in the metal bulk. The fact that the limiting value $W_x^{KS}(-\infty)$ is more negative for lower density metals is a reflection of the greater Pauli field at the surface. Further, the asymptotic coefficient $\alpha_W(\beta)$ is also greater for low density metals (see Fig. 1.) Thus, in integrating from $+\infty$ to inside the metal one obtains a greater limiting value in the bulk.

In Fig. 4 we plot the correlation-kinetic field $Z_c^{(1)}(z)$ and observe that it too is concentrated about the surface. It is long-ranged in the vacuum, decaying asymptotically as $\alpha_c^{(1)}(\beta)/z^2$. In the metal, it exhibits the requisite Bardeen-Friedel oscillations. The field $Z_c^{(1)}(z)$, however, is an order of magnitude smaller than the Pauli component field $\mathcal{P}_x^{KS}(z)$.

In Fig. 5 the correlation-kinetic potential component $W_{tc}^{(1)}(z)$ is plotted. For these densities, the potential is entirely positive, possesses the correct asymptotic structure of Eq. (45) in the vacuum, and exhibits the Bardeen-Friedel oscillations. Once again, the potential $W_{tc}^{(1)}(z)$ is an order of magnitude smaller than the Pauli component $W_x^{KS}(z)$. For higher density metals ($r_s \leq 2$), the correlation-kinetic contribution to $v_x(z)$ will be less significant. It will vanish entirely for the very slowly varying density case for which^{33,34} $v_x(z) = W_x^{KS}(z)$.

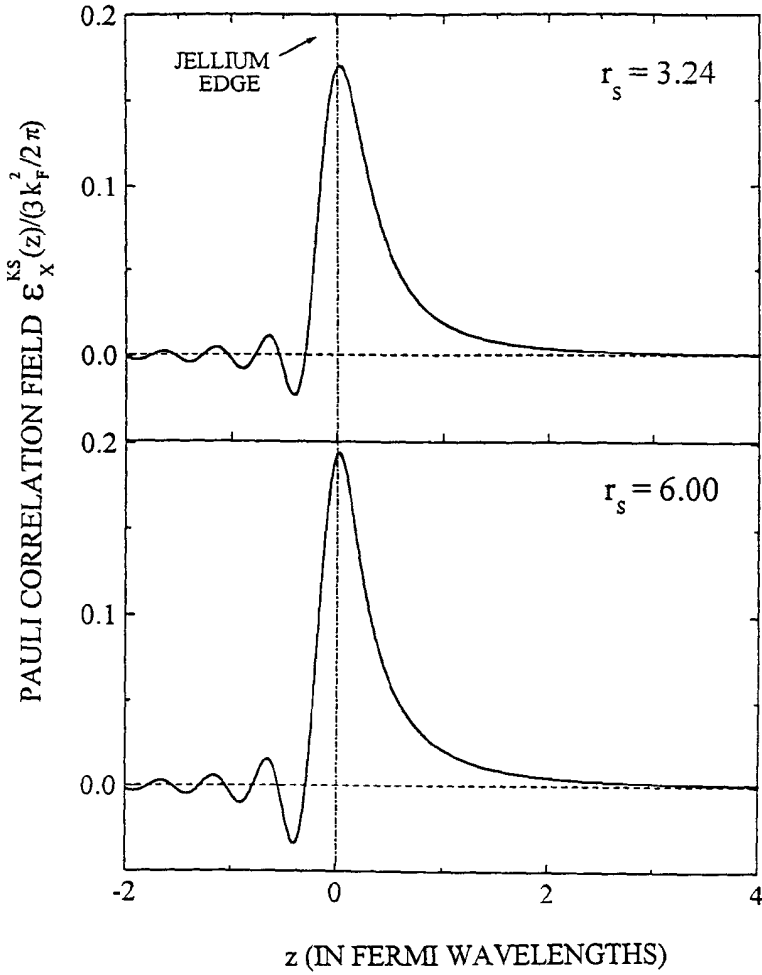


Fig. 2 The Pauli field $\mathcal{E}_x^{KS}(z)$ at the surface of metals of Wigner-Seitz radii $r_s = 3.24$ and 6.00 .

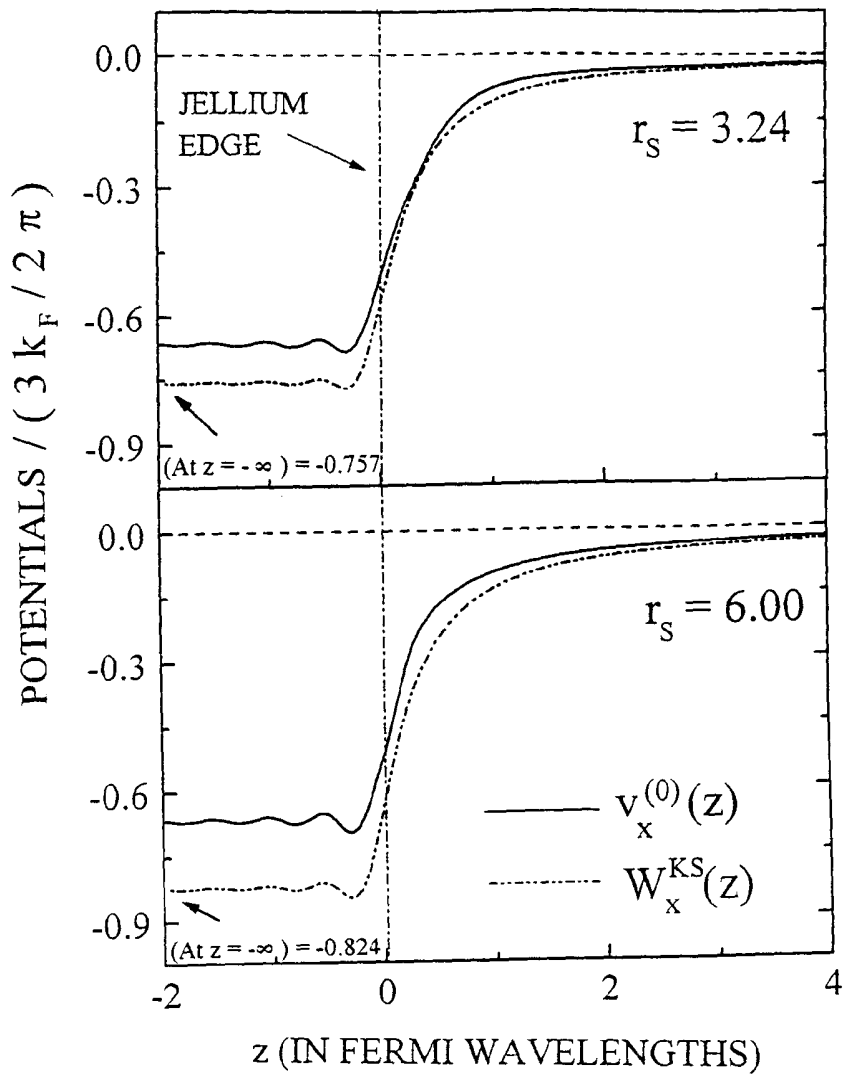


Fig. 3 The Kohn-Sham exchange potential $v_x^{(0)}(z)$, and the Pauli component potential $W_x^{KS}(z)$ at the surface of metals of Wigner-Seitz radii $r_s = 3.24$ and 6.00 .

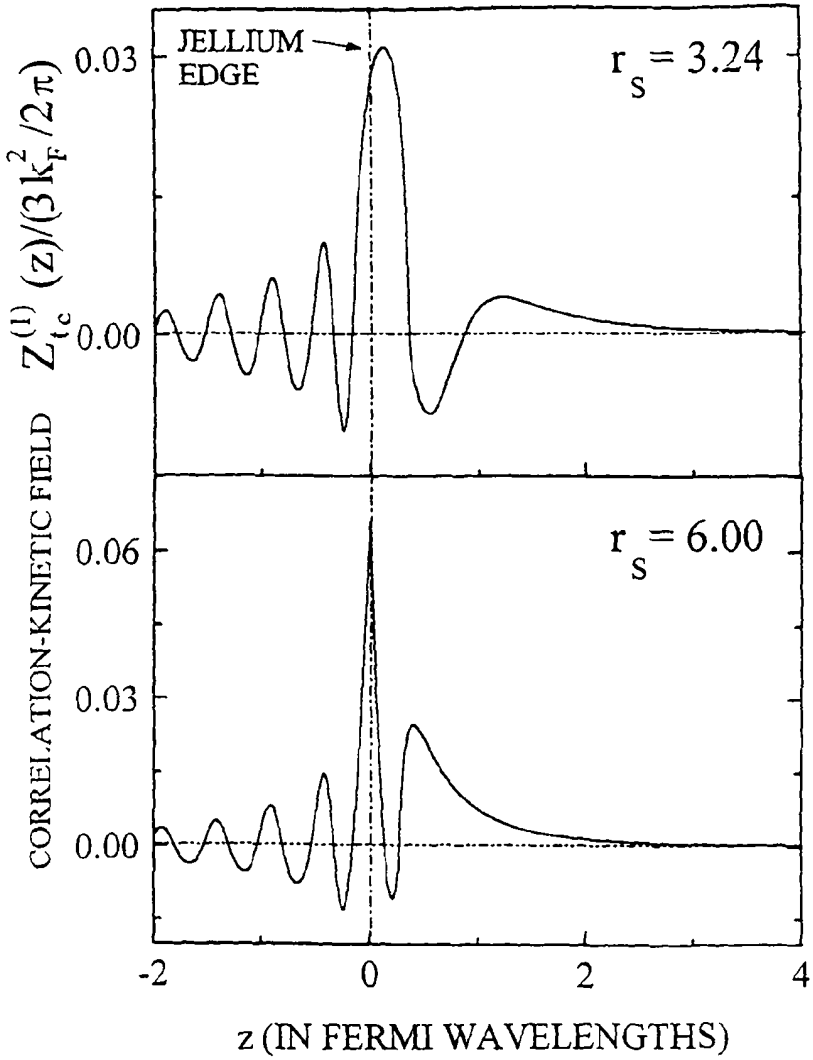


Fig. 4 The correlation-kinetic field $W_{tc}^{(1)}(z)$ at the surface of metals of Wigner-Seitz radii $r_s = 3.24$ and 6.00 .

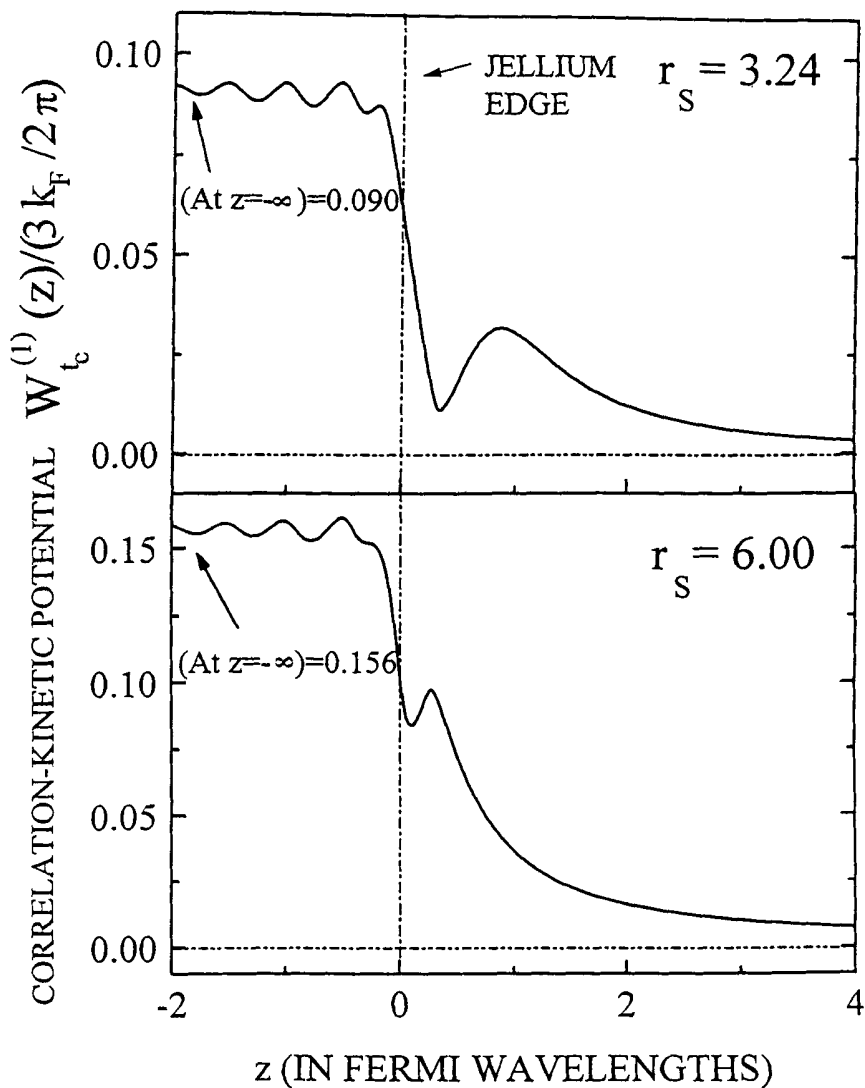


Fig. 5 The correlation-kinetic components potential $W_{tc}^{(1)}(z)$ at the surface of metals of Wigner-Seitz radii $r_s = 3.24$ and 6.00 .

V. CONSTRUCTION OF APPROXIMATE KOHN-SHAM EXCHANGE ENERGY FUNCTIONAL AND DERIVATIVE WITH EXACT ASYMPTOTIC STRUCTURE

In this section we derive a local density approximation-like expression for the KS exchange energy functional and its derivative such that the latter possesses the correct asymptotic structure both in the classically forbidden and metal-bulk regions.

We begin by constructing an approximate expression $V_x^{S,app}(\mathbf{r})$ for the Slater potential $V_x^S(\mathbf{r})$ as

$$V_x^{S,app}(\mathbf{r}) = \frac{3k_F}{2\pi} \left[p \rho_n^{1/3}(\mathbf{r}) + \frac{\bar{\alpha}_S(\beta)}{\ln \rho_n^{1/3}(\mathbf{r}) - \frac{\bar{\alpha}_S(\beta)}{p+1}} \right], \quad (53)$$

where

$$\bar{\alpha}_S(\beta) = \frac{4\pi}{9} (\beta^2 - 1)^{1/2} \alpha_S(\beta), \quad (54)$$

$\alpha_S(\beta)$ is the Slater asymptotic decay coefficient of Eq. (47), $\rho_n(\mathbf{r})$ is the electron density normalized to the bulk value $\bar{\rho} = k_F^3/3\pi^2$, $\beta^2 = W/\epsilon_F$, and p is a free parameter. Note that for $p = -1$, the potential $V_x^{S,app}(\mathbf{r})$ is equivalent to the local density approximation of the Slater potential which is $-3k_F\{\rho(\mathbf{r})\}/2\pi = -(3/2\pi)[3\pi^2\rho(\mathbf{r})]^{1/3}$.

It is easy to see that since $\lim_{z \rightarrow -\infty} \rho_n(z) = 1$, where $z = k_F x$, then for any value of the parameter p , the potential $V_x^{S,app}(\mathbf{r})$ reproduces the correct asymptotic structure of the exact Slater potential $V_x^S(\mathbf{r})$ in the metal bulk:

$$\lim_{z \rightarrow -\infty} V_x^{S,app}(z) = \frac{3k_F}{2\pi} [p - p - 1] = -\frac{3k_F}{2\pi}. \quad (55)$$

In the classically forbidden region we can write the normalized density as

$$\rho_n(z) \sim \exp[-2\sqrt{\beta^2 - 1} z] , \quad (56)$$

where we have omitted the pre-exponential factor, which in general depends upon z . This factor leads to higher order terms in the asymptotic expansion of $V_x^S(\mathbf{r})$ in the vacuum region. Thus, in the asymptotic vacuum region we have the result

$$\lim_{z \rightarrow +\infty} V_x^{S,app}(z) = \frac{3k_F}{2\pi} \frac{\bar{\alpha}_S(\beta)}{\ln \rho_n^{1/3}(z)} \sim -\frac{\alpha_S(\beta)}{x} , \quad (57)$$

for any value of p .

We next construct the approximate KS exchange energy $E_x^{app}[\rho]$ via the approximate Slater potential $V_x^{S,app}(\mathbf{r})$ as

$$\begin{aligned} E_x^{app}[\rho] &= \frac{1}{2} \int d\mathbf{r} \rho(\mathbf{r}) V_x^{S,app}(\mathbf{r}) \\ &= \frac{3k_F}{2\pi} \int d\mathbf{r} \rho(\mathbf{r}) \left[\frac{p}{\bar{\rho}^{1/3}} \rho^{1/3}(\mathbf{r}) + \frac{\bar{\alpha}_S(\beta)}{\ln \left[\frac{\rho(\mathbf{r})}{\bar{\rho}} \right]^{1/3} - \frac{\bar{\alpha}_S(\beta)}{p+1}} \right] . \end{aligned} \quad (58)$$

The functional derivative of $E_x^{app}[\rho]$ which is the approximate KS exchange potential $v_x^{app}(\mathbf{r})$ is then

$$v_x^{app}(\mathbf{r}) = \frac{3k_F}{4\pi} \left[\frac{4p}{3} \rho_n^{1/3}(\mathbf{r}) + \frac{\bar{\alpha}_S(\beta)}{\ln \rho_n^{1/3}(\mathbf{r}) - \frac{\bar{\alpha}_S(\beta)}{p+1}} - \frac{\bar{\alpha}_S(\beta)}{3 \left[\ln \rho_n^{1/3}(\mathbf{r}) - \frac{\bar{\alpha}_S(\beta)}{p+1} \right]^2} \right] . \quad (59)$$

It is readily seen that the potential $v_x^{app}(\mathbf{r})$ has the correct asymptotic structure of $-\alpha_S(\beta)/2x = -\alpha_{KS,x}(\beta)/x$ of Eq. (40) in the vacuum for any value of the parameter p except for $p = -1$. The parameter p is determined by the requirement that $v_x^{app}(\mathbf{r})$ have the correct asymptotic structure of $-k_F/\pi$ of the KS exchange potential $v_x(\mathbf{r})$ in the bulk. Thus

$$v_x^{\text{app}}(z) = \frac{3k_F}{4\pi} \left[\frac{4p}{3} - p - 1 - \frac{(p+1)^2}{3\bar{\alpha}_S(\beta)} \right] = -\frac{k_F}{\pi}, \quad (60)$$

so that the parameter p must satisfy the equation

$$(p+1) \left[1 - \frac{p+1}{\bar{\alpha}_S(\beta)} \right] = 0. \quad (61)$$

The first root of this equation $p = -1$ gives rise to the local density approximation exchange energy functional and corresponding derivative. The second root is

$$p = -1 + \bar{\alpha}_S(\beta), \quad (62)$$

which then leads to the following expressions for the exchange energy and derivative:

$$E_x^{\text{app}}[\rho] = -\frac{3k_F}{4\pi} \bar{\rho} \int d\mathbf{r} \left[\{1 - \bar{\alpha}_S(\beta)\} \rho_n^{4/3}(\mathbf{r}) + \frac{\bar{\alpha}_S(\beta) \rho_n(\mathbf{r})}{1 - \ln \rho_n^{1/3}(\mathbf{r})} \right], \quad (63)$$

$$v_x^{\text{app}}(\mathbf{r}) = -\frac{k_F}{\pi} \left[\{1 - \bar{\alpha}_S(\beta)\} \rho_n^{1/3}(\mathbf{r}) + \frac{3\bar{\alpha}_S(\beta)}{4\{1 - \ln \rho_n^{1/3}(\mathbf{r})\}} + \frac{\bar{\alpha}_S(\beta)}{4\{1 - \ln \rho_n^{1/3}(\mathbf{r})\}^2} \right] \quad (64)$$

A plot of $v_x^{\text{app}}(z)$ for $r_s = 3.24$ employing the orbitals of the finite-linear-potential model²⁸ is given in Fig. 6. The corresponding local density approximation (LDA) potential is also plotted. In the interior and about the surface of the metal the two potentials are equivalent. But outside the surface $v_x^{\text{app}}(z)$ improves upon the LDA significantly and approaches the exact structure asymptotically. We thus expect that properties such as the surface energy and work function obtained with $E_x^{\text{app}}[\rho]$ and $v_x^{\text{app}}(\mathbf{r})$ to be superior to those of the LDA. Such self-consistent calculations are in progress.

In a manner similar to that described above, it is possible to correct other exchange energy functionals more accurate than the LDA, such as the generalized gradient approximation⁴⁰. Similarly it is also possible to obtain the correction to

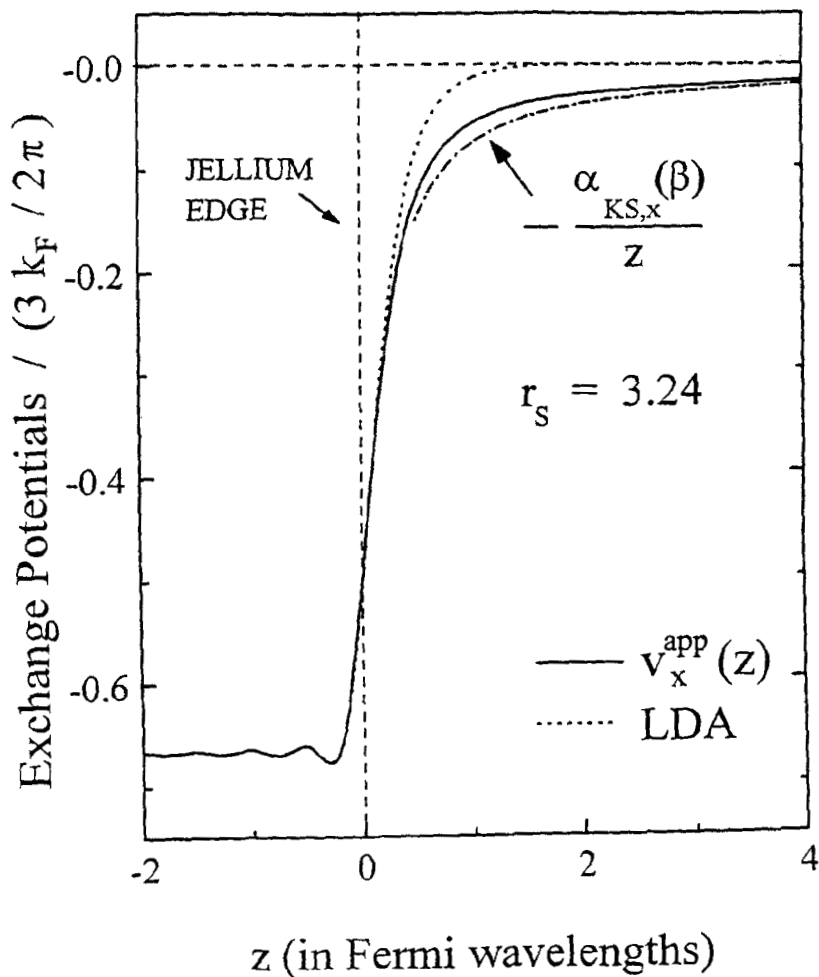


Fig. 6 The approximate exchange potential $v_x^{\text{app}}(z)$ of Eq. (64) at the surface of a metal of Wigner-Seitz radius $r_s = 3.24$. The potential in the local density approximation (LDA) is also plotted, as is the exact asymptotic structure $-\alpha_{KS,x}(\beta)/z$ of the KS exchange potential.

the LDA or other correlation energy functionals such that the correct asymptotic structure is ensured.

VI. CONCLUDING REMARKS

In this paper we have described recent developments in our understanding of the electronic structure of metal surfaces. These developments are based on rigorous analytical derivations of properties within conventional KS density-functional theory as well as its physical interpretation. The latter delineates between the separate Pauli and Coulomb correlations and correlation-kinetic effects incorporated in the KS exchange-correlation energy functional $E_{xc}^{KS}[\rho]$ and its derivative $v_{xc}(r)$. The exact asymptotic structure in the vacuum of the KS exchange potential $v_x(r) = \delta E_x^{KS}[\rho]/\delta\rho(r)$, where $E_x^{KS}[\rho]$ is the exchange energy functional, has been determined and shown to be image-potential-like. It is *precisely* the image potential for a value of the Wigner-Seitz radius r_s which corresponds to that of stable jellium. If then it is assumed that the asymptotic structure of the potential $v_{xc}(r)$ is the image potential, then the contribution of the KS correlation potential $v_c(r) = \delta E_c^{KS}[\rho]/\delta\rho(r)$ to this structure is also exactly known, and thereby shown to be weak. With a knowledge of the exact asymptotic structure of these potentials in the vacuum and metal-bulk regions, it is then possible to construct corresponding energy functionals such that their derivatives possess this structure. An example of such a construction has been provided.

The physical interpretation of the functional derivative $v_x(r)$ shows that it is comprised of a term $W_x^{KS}(r)$ representative of Pauli correlations, and a term $W_{t_c}^{(1)}(r)$ that constitutes *part* of the total correlation-kinetic contribution $W_{t_c}(r)$. The exact asymptotic structure of these components in the vacuum has been determined and shown to also be image-potential-like. Although the structure of $v_x(r)$ about the surface and asymptotically in the vacuum and metal-bulk regions is comprised primarily of its Pauli component, the correlation-kinetic contribution is not insignificant for medium and low density metals. It is only for high density systems ($r_s \leq 2$) that $v_x(r)$ is represented essentially by its Pauli component $W_x^{KS}(r)$. Thus, we see that the uniform electron gas result of $-k_F/\pi$ for the functional derivative $v_x(r)$, which is the asymptotic metal-bulk value, is not a consequence of Pauli correlations alone as is thought to be the case. There is also a small correlation-kinetic contribution. The Pauli and correlation-kinetic contributions have now been quantified.

As discussed in the text, the asymptotic structure of $v_{xc}(r)$ in the vacuum can be thought of as arising from that *part* of the Coulomb hole localized to the

surface, provided there is no correlation-kinetic contribution asymptotically. A further understanding of the overall structure of $v_c(r)$ and properties such as the surface correlation energy can therefore be achieved by determining the structure of the Coulomb hole charge $\rho_c^{KS}(r, r')$ as a function of electron position. This would also show how, for electron positions in the vacuum, the field due to the Coulomb hole component delocalized in the metal bulk screens out that of the delocalized Fermi hole. The work done in the field of the Coulomb hole component localized to the surface region is then the asymptotic structure of the Coulomb correlation part of $v_{xc}(r)$ in the vacuum. One approach to determining an accurate approximation to the Coulomb hole is to combine the random phase⁴¹ and generalized gradient expansion⁴² approximations. The former represents long-range and the latter short-range correlations accurately. We are presently investigating the feasibility of such a calculation.

VII. ACKNOWLEDGEMENTS

The authors thank Prof. Jorge Seminario for the invitation to write this article. This work was supported in part by the Research Foundation of the City University of New York.

VIII. REFERENCES

1. A. Solomatin and V. Sahni, Phys. Lett. A212, 263 (1996).
2. A. Solomatin and V. Sahni, Annals of Physics 259, 97 (1997).
3. A. Solomatin and V. Sahni, Phys. Rev. B 56, 3655 (1997).
4. A. Solomatin and V. Sahni, Annals of Physics (to be published).
5. A. Solomatin and V. Sahni, Int. J. Quantum Chem. 65, 893 (1997).
6. A. Solomatin, V. Sahni, and N.H. March, Phys. Rev. B49, 16856 (1994).
7. A. Solomatin and V. Sahni, Int. J. Quantum Chem. Symp. 29, 31 (1995).
8. A. Kiejna and K.F. Wojciechowski, *Metal Surface Electron Physics*, (Pergamon 1996).
9. J. Bardeen, Phys. Rev. 49, 653 (1936).
10. J.P. Perdew, Prog. Surf. Sci. 48, 245 (1995); J.P. Perdew, H.Q. Tran, and E.D. Smith, Phys. Rev. B42, 11627 (1990); H.B. Shore and J.H. Rose, Phys. Rev. Lett. 66, 2519 (1991).
11. P. Hohenberg and W. Kohn, Phys. Rev. 136, B864 (1964).
12. W. Kohn and L.J. Sham, Phys. Rev. 140, A1133 (1965).

13. R.G. Parr and W. Yang, *Density Functional Theory of Atoms and Molecules* (Oxford University Press, Oxford, 1989); R.M. Dreizler and E.K.U. Gross, *Density Functional Theory* (Springer-Verlag, Berlin, 1990); N.H. March, *Electron Density Theory of Atoms and Molecules* (Academic, London, 1992).
14. V. Sahni in *Density Functional Theory III*, edited by R. Nalewajski, (Top. Curr. Chem. **182**, 1 (1996) (Springer-Verlag, Heidelberg 1996).
15. V. Sahni Phys. Rev. **A55**, 1846 (1997).
16. M.K. Harbola and V. Sahni, Phys. Rev. Lett, **62**, 489 (1989); V. Sahni and M.K. Harbola, Int. J. Quantum Chem. Symp. **24**, 569 (1990); M.K. Harbola and V. Sahni, J. Chem. Educ. **70**, 920 (1993).
17. M.K. Harbola, M. Slamet and V. Sahni, Phys. Lett. **A157**, 60 (1991); M. Slamet, V. Sahni and M.K. Harbola, Phys. Rev. **A49**, 809 (1994).
18. A. Holas and N.H. March, Phys. Rev. **A51**, 2040 (1995).
19. M. Levy and N.H. March, Phys. Rev. **A55**, 1885 (1997).
20. J.C. Slater, Phys. Rev. **81**, 385 (1951).
21. V. Sahni, Surf. Sci. **213**, 226 (1989).
22. M.K. Harbola and V. Sahni, Phys. Rev. **B36**, 5024 (1987).
23. M.K. Harbola and V. Sahni, Phys. Rev. **B39**, 10437 (1989).
24. M.K. Harbola and V. Sahni, Int. J. Quantum Chem. Symp. **27**, 101 (1993).
25. C.-O. Almbladh and U. von Barth, Phys. Rev. **31**, 3231 (1985); A.R. Williams and U. von Barth, in *Theory of the Inhomogeneous Electron Gas*, edited by S. Lundquist and N.H. March (Plenum, New York, 1983).
26. L.J. Sham, Phys. Rev. **B32**, 3876 (1985).
27. A.G. Eguiluz, M. Heinrichsmeier, A. Fleszar and W. Hanke, Phys. Rev. Lett. **68**, 1359 (1992); A.G. Eguiluz, J.J. Deisz, M. Heinrichsmeier, A. Fleszar and W. Hanke, Int. J. Quantum Chem. Symp. **26**, 837 (1992).
28. V. Sahni, C.Q. Ma and J.S. Flamholz, Phys. Rev. **B18**, 3931 (1978).
29. M. Levy and J.P. Perdew, Phys. Rev. **A32**, 2010 (1985).
30. M. Slamet and V. Sahni (manuscript in preparation).
31. V. Sahni, J. Gruenebaum, and J.P. Perdew, Phys. Rev. **B26**, 4371 (1982); V. Sahni and M. Levy, Phys. Rev. **B33**, 3869 (1986).
32. R.T. Sharp and G.K. Horton, Phys. Rev. **30**, 317 (1953); J.D. Talman and W.F. Shadwick, Phys. Rev. **A14**, 36 (1976).
33. Y. Wang, J.P. Perdew, J.A. Chevary, L.D. Macdonald and S.H. Vosko, Phys. Rev. **A41**, 78 (1990).
34. V. Sahni in *Density-Functional Theory*, Vol. 337 of *NATO Advanced Study Institute, series B: Physics*, edited by E.K.U. Gross and R.M. Dreizler (Plenum, New York, 1995); V. Sahni and M. Slamet, Phys. Rev. **B48**, 1910 (1993); M. Slamet and V. Sahni, Phys. Rev. **B45**, 4013 (1992).
35. J.A. Rudnick, Ph.D. thesis, University of California, San Diego, 1970, (unpublished).

36. V. Sahni and K.-P. Bohnen, Phys. Rev. B**29**, 1045 (1984).
37. V. Sahni and K.-P. Bohnen, Phys. Rev. B**31**, 7651 (1985).
38. M.K. Harbola and V. Sahni, Phys. Rev. B**37**, 745 (1988).
39. N.D. Lang and W. Kohn, Phys. Rev. B**1**, 4545 (1970).
40. J.P. Perdew, Phys. Rev. Lett. **55**, 1665 (1985).
41. E. Wikborg and J.E. Inglesfield, Solid State Commun. **16**, 335 (1975).
42. J.P. Perdew, Int. J. Quantum Chem. Symp. **27**, 93 (1993).

Density functional orbital reactivity indices. Fundamentals and applications.

T. Mineva and N. Neshev
Institute of Catalysis, Bulgarian Academy of Sciences,
1113 Sofia, Bulgaria

and

N. Russo, E. Sicilia and M. Toscano
Dipartimento di Chimica, Universita' della Calabria,
I-87030 Arcavacata di Rende (CS), Italy

Contents

- 1. Introduction**
- 2. Method**
 - 2.1 Orbital hardness tensor
 - 2.2 Orbital reactivity indices
- 3. Computational details**
- 4. Results and discussion for atoms and molecules**
 - 4.1 Absolute hardness
 - 4.2 Molecular orbital reactivity indices
 - 4.3 Hardness profiles of reaction paths
- 5. Conclusions**
- 6. References**

1. Introduction

In the 1963 Pearson introduced the concept of "hard and soft acids and bases" (HSAB) [1]. The root of the idea lies in the simple acid-base view of chemistry of Lewis and leads to the statement that "hard acids prefer to coordinate to hard bases and soft acids prefer to coordinate to soft bases".

Starting from this pioneering work, in the last three decades, a number of researches have developed and used Pearson's principle in order to explore its potentials for studying molecular electronic structure and predicting basic chemical features.

The HSAB principle can be considered as a condensed statement of a very large amount of experimental information, but cannot be labelled a law, since a quantitative definition of the intuitive concepts of chemical hardness (η) and softness (S) was lacking. This problem was solved when the hardness found an *exact*, and also an operational, definition in the framework of the Density Functional Theory (DFT) by Parr and co-workers [2]. In this context, the hardness is defined as the second order derivative of energy with respect to the number of electrons and has the meaning of resistance to change in the number of electrons. The softness is the inverse of the hardness [3]. Moreover, these quantities are defined in their local version [4, 5] as response functions [6] and have found a wide application in the chemical reactivity theory [7].

Different practical procedures for computing η have been proposed, that range from the computation of the difference between the energy values of the highest occupied (HOMO) and the lowest unoccupied (LUMO) molecular orbitals [8,9], to the atom in molecules based models [10, 11], to the charge sensitivity analysis [12, 13], to the use of Slater transition state theory [14], to the Janak's extension of DFT for fractional occupancies [15, 16]. Recently, Neshev and Mineva have proposed a scheme for the construction of the internally resolved hardness tensor in the framework of $X\alpha$ [17] and DFT [18] formalism. This procedure was applied in the study of the orbital hardness of the transition metal oxides [14, 17]. More recently a very similar protocol was used for the water molecule [19]. A rigorous procedure was proposed by Liu [20] for the molecular orbital hardness determination that is unfortunately time consuming and until now has been applied to the HCN hardness matrix computation.

The main goal of the present work is to formulate the relationship between the intuitive chemical concepts and the theoretical computation of the reactivity indices, in the dual space of the Kohn-Sham (KS) [21] eigenvalues (ϵ_j) and the occupation numbers (n_j), using the Janak theorem [22]. In this approach, the orbital reactivity indices are calculated directly from the hardness tensor. This opens the way to a more accurate analysis of the intrinsic properties of each orbital in chemical reactions.

Applications presented here include the computation of total hardness values of a selected number of atoms and molecules, orbital Fukui indices and orbital softness tensor (polarization) for test systems. In addition, the change of the hardness along the isomerization paths of HCN and O_3H^+ is reported.

2. Method

In the context of DFT the energy of a many-electron system can be expressed as a function of a one particle density $\rho(\mathbf{r})$:

$$E[\rho] = T_s[\rho] + J[\rho] + E_{xc}[\rho] + \int v(\mathbf{r})\rho(\mathbf{r})d\mathbf{r} \quad (1)$$

where $T_s[\rho]$, $J[\rho]$ and $E_{xc}[\rho]$ are the kinetic, coulomb and exchange-correlation energy terms, respectively. For a fixed external potential $v(\mathbf{r})$ the true density determines uniquely the minimum energy.

2.1 Orbital hardness tensor

The means to study the change from one ground state to another of electronic systems, is introduced through the fundamental energy differential expression [5, 23]:

$$dE = \mu dN + \int \rho(\mathbf{r})dv(\mathbf{r})d\mathbf{r} \quad (2)$$

where N is the total number of electrons and the chemical potential μ is the Lagrange multiplier in the minimization procedure, satisfying the stationary principle:

$$\delta\{E[\rho] - \mu N[\rho]\} = 0 \quad (3)$$

μ measures the sensitivity of the extremum $E[\rho]$ to a change in N :

$$\mu = \left(\frac{\partial E}{\partial N} \right)_v \quad (4)$$

Kohn et al. [23] have shown that "this result contains considerable chemistry. μ characterizes the escaping tendency of electrons from the equilibrium system. Systems (e.g. atoms or molecules) coming together must attain at equilibrium a common chemical potential. This chemical potential is none other the negative of the electronegativity concept of classical structural chemistry".

Before proceeding, we should mention that the ground state energy $E[N, v]$ is assumed to be continuous and differentiable function of the number of electrons N for a given external potential $v(\mathbf{r})$, as discussed in details by Parr and Yang [5].

The next reactivity index in importance is the second energy derivative, the absolute hardness [3, 24]:

$$\eta = \left(\frac{\partial^2 E}{\partial N^2} \right)_v \quad (5)$$

The mean sum of the ionization potential (I) and the electron affinity (A) is the approximation to μ :

$$\mu = -\frac{I + A}{2} \quad (6)$$

and the corresponding finite difference approximation to η is:

$$\eta = \frac{I - A}{2} \quad (7)$$

In a simple orbital theory η becomes the HOMO-LUMO energy difference [8]:

$$\eta = \frac{\epsilon_{\text{LUMO}} - \epsilon_{\text{HOMO}}}{2} \quad (8)$$

Softness is defined as the inverse of hardness:

$$S = \frac{1}{\eta} \quad (9)$$

The chemical hardness measures the resistance of a system to charge transfer and is directly connected to the degree of electron localization [3], while the softness is related to polarizability.

The equations 7, 8 and 9 fail to operate when the HOMO - LUMO energy gap becomes too small and do not consider the influence on chemical properties of other orbitals, besides the HOMO and LUMO's. Moreover, it is not possible to study the site selectivity of a chemical species considering only absolute hardness other than space-dependent (local) versions of hardness/softness concepts [5]. Thus in addition to the global definition of η and S , the local hardness [4] and local softness [5] have been introduced as follows:

$$\eta(\mathbf{r}) = \frac{1}{N} \int \frac{\delta^2 F[\rho]}{\delta \rho(\mathbf{r}) \delta \rho(\mathbf{r}')} \rho(\mathbf{r}') d\mathbf{r}' \quad (10)$$

$$s(\mathbf{r}) = \left[\frac{\partial \rho(\mathbf{r})}{\partial \mu} \right]_{v(\mathbf{r})} = \frac{1}{\eta} \left[\frac{\partial \rho(\mathbf{r})}{\partial N} \right]_{v(\mathbf{r})} \quad (11)$$

where $F[\rho]$ is the Hohenberg and Kohn universal functional [25].

These expressions are obtained through the integration of the hardness and softness kernels:

$$\eta(\mathbf{r}, \mathbf{r}') = \frac{\delta^2 F[\rho]}{\delta \rho(\mathbf{r}) \delta \rho(\mathbf{r}')} \quad (12)$$

$$s(\mathbf{r}, \mathbf{r}') = - \left[\frac{\partial \rho(\mathbf{r})}{\partial u(\mathbf{r}')} \right]_{v(\mathbf{r})} = - \frac{1}{\eta} \left[\frac{\partial \rho(\mathbf{r}')}{\partial u(\mathbf{r})} \right]_{v(\mathbf{r})} \quad (13)$$

where $u(\mathbf{r})$ is the modified potential [5]:

$$u(\mathbf{r}) = v(\mathbf{r}) - \mu = - \frac{\delta F[\rho]}{\delta \rho(\mathbf{r})} \quad (14)$$

The local hardness and local softness are reciprocals in the sense:

$$\int s(\mathbf{r}) \eta(\mathbf{r}) = 1 \quad (15)$$

The formalism of DFT allows one to introduce another important local variable, the Fukui function $f(\mathbf{r})$, originally defined by Parr and Yang [5] as the first derivative of the electronic chemical potential μ with respect to the external potential $v(\mathbf{r})$:

$$f(\mathbf{r}) = \left[\frac{\delta \mu}{\delta v(\mathbf{r})} \right]_N = \left[\frac{\partial \rho(\mathbf{r})}{\partial N} \right]_v \quad (16)$$

The Fukui function measures how sensitive a system's chemical potential is to an external perturbation at a particular point.

In order to compute local variables for a particular site in a molecule an approach is used which is based on the fractional occupation number concept. The original idea to exploit fractional occupation numbers in the framework of DFT is due to Janak [22] who generalized the earlier work of Slater [26], using the $X\alpha$ approach. The validation of the Janak theorem in DFT for N - and v -representable densities and the discontinuity of the energy functional versus the occupation numbers are subjects of discussion in the works of Rajagopal [27], Perdew and Zunger [28], Harris [29, 30], English and English [31], Valiev and Fernando [32] and Whithead [33]. Very recently Warren and Dunlap [34] have treated fractional occupation numbers in the computation of DF-energy gradient within the linear combination of Gaussian type orbitals approach.

In the Janak's formulation of DFT, the KS one-electron orbital energies are defined as the first derivatives of the total energy with respect to the occupation numbers, n_i , and can be interpreted as the orbital electronegativities [35]:

$$\varepsilon_i = \left(\frac{\partial E}{\partial n_i} \right) \quad i=1, \dots, N \quad (17)$$

The latter equation is obtained through the definition of the total electron density in

terms of Kohn-Sham orbital Ψ_i .

$$\rho(\mathbf{r}) = \sum_i n_i |\Psi_i(\mathbf{r})|^2 \quad 0 \leq n_i < 1 \quad \sum_{i=1}^N n_i = N \quad (18)$$

Now, in analogy with Slater's $X\alpha$, the total energy functional can be conveniently expanded in a Taylor's series around the steady state calculated in advance by a preliminary SCF procedure. This state is characterized by the set of occupation numbers n^0 ($n_1^0, n_2^0, \dots, n_N^0$) and by the corresponding eigenvalues of the DFT Hamiltonian $\epsilon^0 = (\epsilon_1^0, \dots, \epsilon_n^0)$.

$$\begin{aligned} \Delta E = & \sum_i \frac{\partial E}{\partial n_i} \Delta n_i + \frac{1}{2} \sum_{ij} \frac{\partial^2 E}{\partial n_i \partial n_j} \Delta n_i \Delta n_j + \\ & + \frac{1}{6} \sum_{ijk} \frac{\partial^3 E}{\partial n_i \partial n_j \partial n_k} \Delta n_i \Delta n_j \Delta n_k + \dots \end{aligned} \quad (19)$$

where $\Delta n_i = n_i - n_i^0$. The first derivative corresponds to the KS-eigenvalue (see eq. 17), the second one

$$\frac{\partial^2 E}{\partial n_i \partial n_j} = \eta_{ij} \quad (20)$$

to the hardness tensor [35-37] and the third derivative describes the change in the hardness with respect to the occupation number variation. For a nonsingular matrix η_{ij} , the Mor's lemma [38] states that accounting for the higher order terms of Taylor's expansion does not change qualitatively the properties of the function defined by eq. 19.

In order to get the hardness tensor elements, one needs a second derivative of the KS energy with respect to the occupation numbers. By taking the derivative of eq. 12 with respect to the occupation numbers, at constant $\nu(\mathbf{r})$, η_{ij} , becomes:

$$\begin{aligned} \eta_{ij} = & \frac{\delta^2 [J[\rho] + E_{xc}[\rho]]}{\delta \rho(\mathbf{r}) \delta \rho(\mathbf{r}')} \frac{\partial \rho(\mathbf{r})}{\partial n_i} \frac{\partial \rho(\mathbf{r}')}{\partial n_j} = \\ & \int \frac{\Psi_i^*(\mathbf{r}) \Psi_i(\mathbf{r}) \Psi_j^*(\mathbf{r}') \Psi_j(\mathbf{r}')}{|\mathbf{r} - \mathbf{r}'|} d\mathbf{r} d\mathbf{r}' + \\ & \int \frac{\delta^2 E_{xc}(\rho) \Psi_i^*(\mathbf{r}) \Psi_i(\mathbf{r}) \Psi_j^*(\mathbf{r}') \Psi_j(\mathbf{r}')}{\delta \rho(\mathbf{r}) \delta \rho(\mathbf{r}')} d\mathbf{r} d\mathbf{r}' \end{aligned} \quad (21)$$

Following the work of Garza and Robles [39], the kinetic hardness term is zero and the local hardness depends only on the second derivative of the Coulomb and exchange-correlation energies. The exchange-correlation contribution to η_{ij} is much smaller than the Coulomb one, but neglecting η_{ij}^{xc} term, for many systems, brings wrong hardness values.

The Janak's theorem (eq.17) and the hardness tensor definition (eq. 20) allows the calculations of η_{ij} as the first derivative of the Kohn-Sham orbital eigenvalues with respect to the orbital occupation numbers [17]:

$$\eta_{ij} = \frac{\partial \epsilon_i}{\partial n_j} \quad (22)$$

Numerically, the latter derivatives can be computed using the finite difference approximation:

$$\eta_{ij} = \frac{\epsilon_i(n_j - \Delta n_j) - \epsilon_i(n_j)}{\Delta n_j} \quad (23)$$

This expression takes into account the response of the i -th orbital to the change of the occupation number of the j -th orbital.

For nonsingular η_{ij} matrix, the calculation of the softness matrix follows immediately:

$$s_{ij} = [\eta]_{ij}^{-1} \quad (24)$$

Since the local softness is related to the total one in the sense [5]:

$$\int s(\mathbf{r}) d\mathbf{r} = S \quad (25)$$

the approximation to S used in the present approach is:

$$S = \sum_{ij} s_{ij} \quad (26)$$

Now it is easy to obtain the total hardness as:

$$\eta = \frac{1}{S} = \frac{1}{\sum_{ij} s_{ij}} \quad (27)$$

As motivated by a statement of Pearson [40] "there seems a rule of nature that molecules arrange themselves so as to be as hard as possible", the molecular

hardness value can be conceived as a measure of the stability of a system. As a consequence of this maximum hardness principle (MHP), since a chemical species is most reactive at the transition state, hardness would attain a minimum there, along a reaction path.

Parr and Chattaraj [41] have shown that if, a chemical species moves away from its equilibrium position, its hardness value decreases. Their proof demands that the chemical species in question maintains a constant chemical potential.

2.2 Orbital reactivity indices

It is well known that the algebraic theory of systems of non homogeneous linear equations with N -variables is equivalent to the geometric theory of a plane in the N -dimensional affine space [42]. Therefore the study of the total KS-energy variation around the equilibrium state (see eq. 19) in terms of metric geometry enables the calculations of orbital indices of reactivity. Both algebraic and geometric theories describe the same phenomena, but with different formalisms. If the Taylor's expansion of the energy functional is truncated up to the second order term and Janak's theorem (eq. 17) is considered, the orbital eigenvalues become linear functions of the occupation numbers:

$$\epsilon_i = \epsilon_i(n_i) \quad (28)$$

In the geometry formalism, the latter equation is the so called state equation, which defines a $2N$ -dimensional affine space with basis vectors ϵ_j and n_j . Thus, the energy functional E (eq. 19) appears to be a bilinear functional of the occupation numbers and eigenvalues. The energy behaviour around the equilibrium state, (ϵ_i^0, n_i^0) , can be studied topologically not as a function of the position in the real molecular space, but as a function of the eigenvalues and occupation numbers in the above defined $2N$ -dimensional affine space. The metric of this space is given through the hardness tensor, as defined in eq. (22) [17]. Thus, the critical points of the energy functional $\Delta E(n, \epsilon)$ with respect to the occupation number variation can be found as follows:

$$\frac{\partial \Delta E}{\partial n_i} = \epsilon_i + \sum_j^N \eta_{ij} \Delta n_j = 0 \quad i = 1 \dots N \quad (29)$$

The solution of eq. 29 at given ϵ_i and with $\text{Det}(\eta_{ij}) \neq 0$ with respect to Δn_j gives:

$$\Delta n_i = - \sum_{j=1}^N [\eta]_{ij}^{-1} \epsilon_j = - \sum_{j=1}^N s_{ij} \epsilon_j \quad (30)$$

Considering a "closed system" with a constant deviation of the i -th occupation number from its equilibrium value, $\sum_i \Delta n_i = \Delta N$, the set of equations (29) turns into:

$$\begin{aligned} \epsilon_i + \sum_{j=1}^N \eta_{ij} \Delta n_j + \lambda &= 0 \quad i = 1, \dots, N \\ \sum_i \Delta n_i &= \Delta N \end{aligned} \quad (31)$$

In the last equation λ is the Lagrange multiplier and can be interpreted, analogously to the Slater transition state formula [26], as the effective electronegativity, or the negative of the chemical potential. Using the set of equations 31, the response of the charge deviation with respect to the external potential (u) measured relative to the effective electronegativity λ is found as follows:

$$p_{ij} = \frac{\partial n_i}{\partial u_j} \quad (32)$$

where $u_i = \epsilon_i - \lambda$.

Now, the solution of the system of eq. 31 gives Δn_i for a "closed system":

$$\Delta n_i = - \sum_{j=1}^N p_{ij} \epsilon_j \quad (33)$$

The orbital Fukui indices, defined through the eq. (16) can be also calculated from eq. 31:

$$f_i = \frac{\partial \lambda}{\partial \epsilon_i} = \frac{\partial n_i}{\partial N} \quad \sum_i f_i = 1 \quad (34)$$

The relation between the orbital Fukui indices and the orbital softness, $s_i = \sum_j s_{ij}$, is:

$$f_i = \left(\frac{\partial n_i}{\partial \mu} \right) \left(\frac{\partial \mu}{\partial N} \right) = \eta s_i \quad (35)$$

Finally, the orbital polarization functions and the chemical potential can be expressed as:

$$\pi_i = \frac{\partial n_i}{\partial \lambda} = \sum_j s_{ij} \quad (36)$$

$$\mu \equiv \lambda = \frac{\partial E}{\partial N} = \sum_i \frac{\partial E}{\partial n_i} \left(\frac{\partial n_i}{\partial N} \right) = \sum_i \epsilon_i f_i \quad (37)$$

It is worth noting that the chemical potential can be computed simply as a root of the eq. 31.

Equations 29-37 provide a practical scheme to compute orbital reactivity indices, in vicinity of the system equilibrium point in the parametric space of the KS-eigenvalues and occupation numbers.

The relationship between p_{ij} and s_{ij}

$$-p_{ij} = s_{ij} + \frac{\pi_i \pi_j}{S} \quad (38)$$

is analogous to the relationship between the local softness and Fukui functions in the work of Berkowitz and Parr [4], where all functions were defined in the real space.

3. Computational details

The results presented here were obtained in the framework of DFT by using a modified version of deMon code [43]. All calculations were performed within the nonlocal density approximation employing the gradient-corrected functional of Perdew [44] for correlation and that of Perdew and Wang [45] for exchange energy (PPW) respectively. For some species test calculations using the local potential [46] were carried out.

In order to locate the extreme points on the potential energy hypersurface, the Broyden-Fletcher-Goldfarb-Shanno minimization algorithm [47] for the minima was used. For the saddle points search the Abashkin and Russo [48] algorithm was employed. Along the reaction path, critical points were classified as minima or transition states on the basis of vibrational analysis. The point along the reaction paths were obtained fixing the appropriate reaction coordinate and optimizing all the other geometrical parameters.

The orbital and auxiliary basis sets used are of triple-zeta quality [49]:

The $\epsilon_j(n_i)$ ensemble was obtained from the SCF procedure for the ground and excited states ($\Delta n_i=0.5$). The choice of Δn_i value equal to 0.5 comes from the Slater's transition state formula [26] for the computation of the ionization energies. This enables one to compute the relaxed hardness tensor elements. If a very small perturbation of the occupation number is used (e.g. 0.001) the unrelaxed hardness (η_{unrel}) is computed. The unrelaxed hardness can be analytically calculated, as the Slater's integral, F_0 , minus the exchange term. As previously shown [50], for the first and second row transition metal, $\eta_{rel} \approx 0.7\eta_{unrel}$ for 3d and 4d states and $\eta_{rel} \approx 0.9\eta_{unrel}$ for 4s and 5s ones. Here, in the framework of DFT, we are interested in rationalizing the relaxation effects on the absolute hardness values and the other reactivity indices, derived from the hardness tensor.

The computation of the hardness tensor elements and, consequentially, the absolute hardness values, has been carried out by taking into account the valence shell orbitals. The influence of LUMO on the global η values was found to be negligible in many test cases.

By using the elements of the hardness tensor, calculated through eq. (23) for k valence orbitals, as the coefficients of the equations (31) for a system with $\Delta N=0$ is obtained the following matrix:

$$\begin{pmatrix} \eta_{11} & \eta_{12} & \dots & \eta_{1k} & 1 \\ \eta_{21} & \dots & \dots & \eta_{2k} & 1 \\ \dots & \dots & \dots & \dots & \dots \\ \eta_{k1} & \dots & \dots & \eta_{kk} & 1 \\ 1 & \dots & \dots & 1 & 0 \end{pmatrix}$$

that by inversion gives:

$$\begin{pmatrix} p_{11} & p_{12} & \dots & p_{1k} & f_1 \\ p_{21} & \dots & \dots & p_{2k} & f_2 \\ \dots & \dots & \dots & \dots & \dots \\ p_{k1} & \dots & \dots & p_{kk} & f_k \\ f_1 & \dots & \dots & f_k & \eta \end{pmatrix}$$

4. Results and discussion

The performance of the method proposed above in the calculation of absolute hardness values of a set of neutral atoms and molecules is investigated. The Fukui indices and the polarization functions for the σ -bonds of test molecules are also reported. Finally, the maximum hardness principle was checked by studying the "hardness profile" along the reaction path for the isomerization of HCN and O_3H^+ systems.

4.1 Absolute hardness

Tables 1 and 2 list the absolute hardness values for a number of neutral atoms and molecules.

The experimental hardness [3, 40] was obtained from the experimental values of I and A by using the working definition of η given by eq. 7. In Table 1 are reported also the results obtained employing the SCF procedure ($\eta_{\Delta SCF}$) for the calculation of I and A , compared with those previously computed at different levels of theory [51]. Because they are very close to the experimental values, it is worth

confirming the ability of the *ab-initio* calculations to reproduce the ionization potential and electron affinity. Our hardness values (η) were computed through eq. 27 that is closer to the exact hardness definition of eq.5.

As an example of the application of the method for hardness calculation, the coefficients of equations (31) matrix and the corresponding inverted one (in eV) are reported for the occupied valence orbitals of H_2O :

$$\begin{matrix} & a_1 & b_2 & a_1 & b_1 \\ \begin{matrix} a_1 \\ b_2 \\ a_1 \\ b_1 \end{matrix} & \left(\begin{array}{cccc} 10.059 & & & \\ 9.340 & 9.300 & & \\ 8.504 & 8.027 & 9.293 & \\ 8.493 & 8.132 & 8.152 & 9.103 \\ 1 & 1 & 1 & 1 & 0 \end{array} \right) \end{matrix}$$

$$\begin{matrix} & a_1 & b_2 & a_1 & b_1 \\ \begin{matrix} a_1 \\ b_2 \\ a_1 \\ b_1 \end{matrix} & \left(\begin{array}{ccccc} 1.678 & & & & \\ -1.336 & 1.620 & & & \\ -0.231 & -0.041 & 0.601 & & \\ -0.112 & -0.243 & -0.329 & 0.683 & \\ -0.493 & 0.719 & 0.391 & 0.383 & -8.334 \end{array} \right) \end{matrix}$$

Table 1. Theoretical and experimental absolute hardness values (in eV).

Atom	η	η_{Slater}	$\eta_{\Delta\text{SCF}}$	$\eta_{\Delta\text{SCF}}$ B3LYP ^a	$\eta_{\Delta\text{SCF}}$ CCSD(T) ^a	$\eta_{\text{exp}}^{\text{b}}$
H	9.50			6.40	6.53	6.42
Li	2.06	2.25	2.55	2.53	2.57	2.38
Be	3.71	4.35	5.94	4.67	4.88	4.50
B	5.32	4.63	4.16	4.17	4.02	4.01
C	6.33	6.50	5.15	5.10	5.00	4.99
N	9.97	9.04	7.39	7.26	7.45	7.27
O	7.64	9.95	6.45	6.28	6.09	6.08
F	8.58	12.42	7.29	7.15	9.02	7.01

a) From ref. 40; b) From refs. 16, 28.

Table 2. Theoretical and experimental molecular hardness (in eV).

Molecule	η	η_{Slater}	$\eta_{\Delta\text{SCF}}$	η	η_{exp}^b
HF	11.35	9.07	9.21	11.44 ^a	11.00
HCl	6.79	6.60	6.78	8.77 ^a	8.00
HBr	5.44	5.70	6.05	7.79 ^a	/
HI	4.37	4.72	6.08	6.70 ^a	5.3
CO	5.26	5.92	7.73	6.0 ^b	7.9
H ₂ O	8.33	6.91	8.00	7.0 ^b	9.5
H ₂ S	5.00	5.40	6.20	5.3 ^b	6.2
NH ₃	7.60	6.83	6.98	8.59 ^a	8.2

a) From ref. 6; b) From ref. 16.

The values of absolute hardness, shown in the Tables, are highly satisfactory when compared with the known chemical behaviour of the selected systems. The expected chemical behaviour is well reproduced when the valence shell electrons in the absolute hardness calculation are taken into account. As previously mentioned [3], single atom chemistry is not so significant in terms of Lewis acid-base interaction, though Table 1 is still useful in showing how η can vary from element to element. More interesting are the reported molecular η values (Table 2) that can accounts for the chemical properties for a given series of compounds. Indeed, we found that absolute hardness of the halide acids follows the order of $\text{HF} \gg \text{HCl} > \text{HBr} > \text{HI}$. Analogously, water is harder than hydrogen sulphide. A hard base such as ammonia has a larger hardness value than CO, which is classified as a soft base. This trend occurs also when the Slater's transition state procedure is employed.

4.2 Molecular orbital reactivity indices

While the electronegativity and the absolute hardness are global properties of the system, the reaction between two molecules depends on the properties of the involved orbitals. In order to measure the chemical reactivity of a particular orbital in a molecule, different local variables, such as orbital softness (s_{σ}) and Fukui (f_{σ}) and polarization functions (π_{σ}), can be computed through equations 24, 34, 36.

Model test calculations were performed on the σ -bond of the same set of above reported molecules (Table 3), except for CO for which the valence orbital analysis is reported in Table 4.

Among the halide acids the σ -bond Fukui function of HF is found to be the smallest. This correlates well with the anomalous behaviour of hydrofluoric acid with respect to the other acids of the series. In fact, HF is a weak acid, whereas the other are strong (e.g. with about the same strength in water solvent). The Fukui indices for HCl, HBr and HI fall almost in the same range. The polarization functions π_{σ} indicates that σ -bond of HF is the less polarizable (0.051 eV), while HI σ -bond has a large values of the polarization function (0.165 eV). This behaviour is confirmed by the corresponding orbital softness, that is found to be of 0.37, 1.11, 1.13 and 1.34 eV for HF, HCl, HBr and HI respectively.

Furthermore, a good correlation between the orbital softness and the hydrogen Mulliken net charge (q_H) exists. Namely, as it is expected, the σ -bond softness increases with increasing of q_H . Similarly, the f_σ and π_σ of water and H_2S indicates that the latter would be more reactive.

Table 3. Fukui indices, polarizability functions (eV) and hydrogen Mulliken net charges for σ -bond of studied molecules.

Molecule	f_σ	$\pi_\sigma 10^2$	q_H
HF	0.58	5.1	0.26
HCl	0.77	8.8	0.57
HBr	0.80	14.7	0.64
HI	0.72	16.5	0.66
H ₂ O	1.02	12.8	0.38
H ₂ S	1.05	21.0	0.49
NH ₃	0.62	8.1	0.26

Table 4. Fukui indices, polarizability functions, local softness (eV) and Mulliken net charge of carbon for valence orbitals of CO.

Orbital	f_i	$\pi_i 10^2$	s_{ii}	q_C
4 σ	0.17	3.31	0.49	0.40
5 π	0.62	11.80	1.53	0.55
n	0.55	10.46	0.36	1.87

A full orbital analysis for CO (see Table 4) shows that the π -bond possesses the highest Fukui index (0.62 eV) as well as the highest polarization function (0.118 eV). This agrees with the fact that carbon monoxide works most efficiently as a π acceptor when it interacts with transition metal atoms.

4.3 Hardness profiles of reaction paths

Since it is well known that during a reaction the reactivity of a chemical species changes, the study of the "hardness profile" along the reaction path would be of great interest and numerical results have started accumulating [52-60]. In this context we have considered different isomerization processes studying the hardness values of the minima and the maxima (Table 5). In addition the value of η as a function of various reaction coordinates for O_3H^+ (Figure 1) and HCN (Figure 2) isomerizations was calculated.

The reported results show that the inclusion of the gradient corrected nonlocal effects is recommended to obtain data consistent with the maximum hardness principle. In fact, in the case of isomerization of HSiN the calculated hardness value for TS is higher than that of the minimum when local VWN potential is used. The introduction of the nonlocal corrections removes this error. The results for all

the studied reactions confirm that the hardness profile goes through a minimum at the transition state. On the contrary, the η values calculated by using the simple HOMO-LUMO approximation, η H-L, does not follow, in all the studied cases, the maximum hardness principle. Moreover, results for O_3H^+ and S_3H^+ evidence that this approximation gives zero hardness for TS.

As mentioned previously, the MHP can be rigorously applied only under the condition of constant chemical potential. To check this aspect the variation of η for the isomerization reaction of O_3H^+ and HCN was examined in some detail. The energetic and hardness profiles for the interconversion between *trans* and *cis* forms of O_3H^+ are drawn in Figure 1a, as a function of the dihedral angle $\text{O}_1\text{O}_2\text{O}_3\text{H}$ (α) (see Scheme). The *trans* isomer is more stable than the *cis* one by about 4 kcal/mol and the transition state occurs at $\alpha=90^\circ$ and lies at about 21 kcal/mol above the global minimum. Accordingly to this energy path, η decreases on going from its maximum value of 6.54 eV, for the *trans* form, to 5.81 eV for the transition state. Then, it increases and reaches the value of 6.45 eV which characterizes the *cis* isomer. At the same time the computed chemical potential along the reaction path is found to remain practically constant.

Table 5. Calculated hardnesses (eV) and energy differences (kcal/mol), for minima and maxima, for different isomerization reactions.

System	η LSD	η LSD H-L	ΔE LSD	η NLSD	η NLSD H-L	μ	ΔE NLSD
t- N_2H_2	6.51	1.19	0.0	6.36	1.27	-13.5	0.0
c- N_2H_2	6.72	1.22	8.2	6.28	1.33	-10.0	4.8
TS	6.12	0.41	45.6	5.94	1.26	-16.5	53.6
HCN	6.49	3.96	0.0	6.96	3.92	-3.9	0.0
HNC	6.38	3.23	14.6	6.42	3.31	-6.3	16.0
TS	6.36	2.64	46.4	6.35	2.65	-12.3	47.8
HSiN	3.97	1.82	71.1	4.48	1.72	-2.4	66.5
HNSi	4.18	2.40	0.0	4.59	2.30	-4.8	0.0
TS	4.13	0.72	82.9	4.41	0.76	-4.9	78.5
t- O_3H^+				6.54	0.88	-20.0	0.0
c- O_3H^+				6.45	0.93	-20.4	3.5
TS				5.81	0.00	-19.8	21.1
t- S_3H^+				3.37	0.58	-19.6	0.0
c- S_3H^+				3.26	0.61	-19.9	0.5
TS				3.02	0.00	-20.1	18.2

The interconversion path for going from *trans* to open-chain (C_{2v}) isomers of O_3H^+ was also studied.

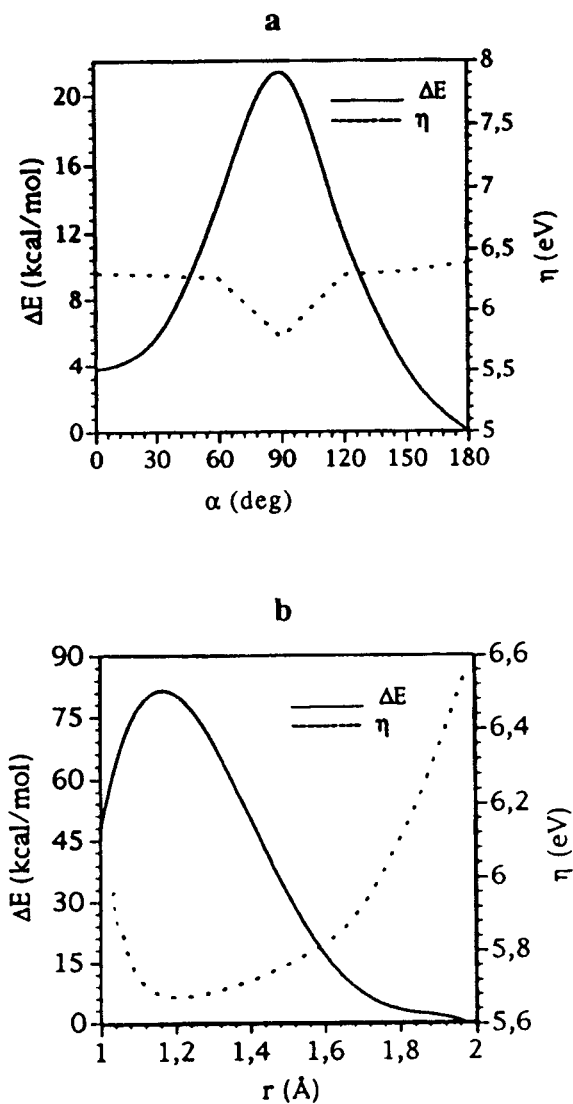


Figure 1. Energetic path for O_3H^+ trans \rightarrow cis (a) and trans \rightarrow C $_{2v}$ (b) isomerization together with hardness profiles.

In this case between the two minima there is an energy difference of about 46 kcal/mol and the *trans*→ C_{2v} energy barrier is very high (about 80 kcal/mol). In Figure 1b this path is depicted, together with the hardness profile as functions of the bond length r (see Scheme).

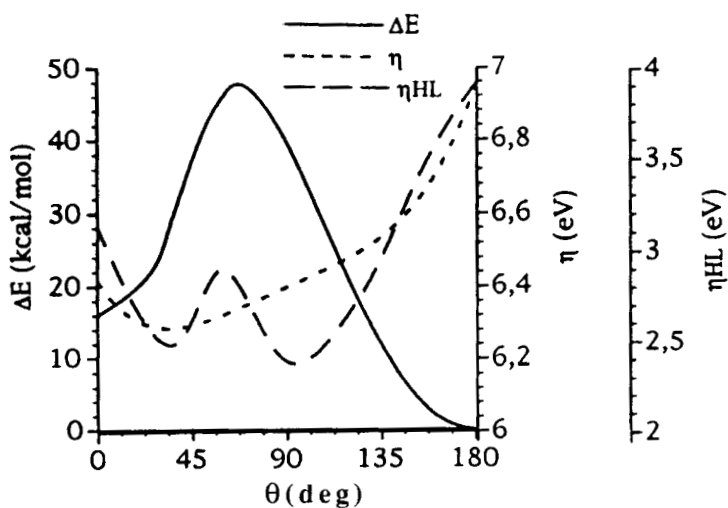
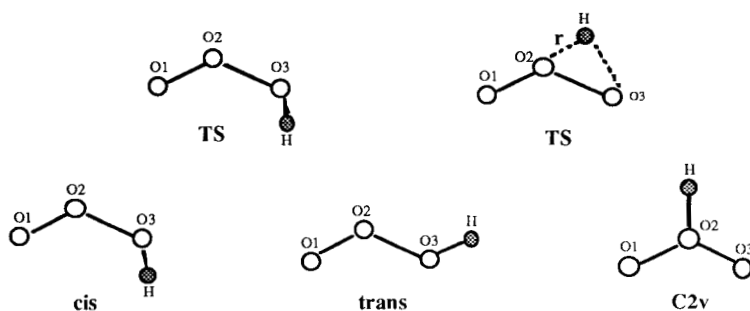


Figure 2. Dependence of relative energy (ΔE), valence shell hardness (η) and hardness computed taking into account the HOMO and LUMO orbitals (η_{HL}) of HCN isomerization.

It is evident that η goes through a minimum at the transition state and follows the reverse behaviour of the energy variation. Also in this case μ is constant throughout the reaction path.

As a representative case of a reaction that does not fulfil the constant chemical potential constraint, the 1,2-hydrogen shift in HCN was considered. The behaviour of the hardness along the reaction path of HCN isomerization was previously studied by Chattaraj et al. [57], Kar and Scheiner [59] and Ghanty and Ghosh [60].

The dependence of the total energy and the absolute hardness upon the HCN-angle (θ) is illustrated in Figure 2. Starting from HNC minimum, η (6.42) drops until reaching a minimum (6.28 eV) at $\theta=35^\circ$, whereas the energy maximum corresponds to a θ value of 68.4° . Going to the most stable isomer, HCN, η climbs to a maximum value of 6.96 eV. Also sketched, in the same Figure, is the profile of hardness, computed as a HOMO-LUMO energy difference (eq. 8), that differs significantly from that discussed above. In the cited work [59] an analogous behaviour of the hardness, calculated using equation 8, was found.

In general, the results presented in this section support the statement that greater hardness implies greater stability, however the MHP seems to be valid only when chemical potential does not vary significantly during the reaction.

5. Conclusions

The performance of the method, recently proposed by Neshev and Mineva for the computation of internal chemical hardness tensor and other reactivity indices, was investigated considering different systems and three isomerization reaction paths. Results indicates that:

- i. absolute hardness describes satisfactorily the chemical behaviour of the studied atoms and molecules;
- ii. the calculated Fukui and polarization functions explain well the known molecular reactivity;
- iii. the absolute hardness values along the reaction paths, here considered, are consistent with the maximum hardness principle. On the contrary the conventional HOMO-LUMO approximation fails in some cases. Having this indications we can conclude that also in the calculation of the absolute hardness the valence electrons should be taken into account;
- iv. in order to obtain good correlation between energy and hardness profiles in the reaction paths the use of nonlocal corrections is suggested.

Acknowledgements

We are grateful to the Italian MURST and CNR and Bulgarian National Scientific Foundation for financial support.

6. References

- [1] Pearson, R.G., *J. Am. Chem. Soc.*, **85**, 3533 (1963).
- [2] Parr, R.G., Donnelly, R.A., Levy, M. and Palke, W.E., *J. Chem. Phys.* **69**, 4491 (1978).

- [3] Parr, R.G and Pearson, R.G., *J. Am. Chem. Soc.*, **105**, 7512 (1983).
- [4] Berkowitz, M. and Parr, R.G., *J. Chem. Phys.*, **88**, 2554 (1988).
- [5] Parr, R.G and Yang, W., 1989, "*Density-Functional Theory of Atoms and Molecules*", Oxford University Press, New York.
- [6] Senet, P. *J. Chem. Phys.*, **105**, 6471 (1996); ibidem **107**, 2516, 1997.
- [7] Cohen, M. H., Ganduglia-Pirovano, M. V. and Kudrnovsky, J., *J. Chem. Phys.*, **101**, 8988 (1994); ibidem **103**, 3543 (1995).
- [8] Chattaraj, P.K. and Parr, R.G., *Struct. Bond.* **80**, 11 (1993).
- [9] Pearson, R.G., *Struct. Bond.*, **80**, 1 (1993).
- [10] Baekelandt, B.G., Mortier, W.J. and Schoonheydt, R.A., *Struct. Bond.* **80**, 187 (1993).
- [11] Balawender, R., Komorowski, L. and Roszak S., *Int. J. Quantum Chem.* **61**, 499 (1997).
- [12] Nalewajski, R.F., *Struct. Bond.* **80**, 115 (1993).
- [13] Nalewajski, R.F., *Int. J. Quantum Chem.* **61**, 181 (1997).
- [14] Neshev, N. and Proinov E., *J. Mol. Cat.* **54**, 484 (1989).
- [15] Kostyk, R. G. and Whitehead, M. A., *J. Mol. Struct. (THEOCHEM)*, **230**, 83 (1991).
- [16] Galvan, M., Dal Pino, A. Jr. and Joannopoulos, *Phys. Rev. Letters*, **70**, 21 (1993).
- [17] Neshev, N. and Mineva T. *Metal-Ligand Interactions: Structure and Reactivity*, N. Russo and D.R. Salahub (eds), Kluwer, Dordrecht, p. 361-407 (1996).
- [18] Neshev, N., Mineva T. and V. Parvanov, 1996, in "*Heterogeneous Catalysis*", Proc. 8th Int. Symp. Heterogeneous Catalysis, Varna, 5-9/10 1996, A. Andreev, L. Petrov, Ch. Bonev, G. Kadinov and I. Mitov (eds), Institute of Catalysis, Bulgarian Academy of Sciences, Sofia, p. 67-72, ibidem p. 79-84.
- [19] Grigorov, M., Weber, J., Chermette, H. and Tronchet, J.M.J., *Int. J. Quantum Chem.*, **61**, 551 (1997).
- [20] Liu, G., H., *J. Chem. Phys.*, **106**, 165, 1997.
- [21] Kohn, W. and Sham, L.J., *Phys. Rev.*, **140**, A1133 (1965).
- [22] Janak J.F., *Phys. Rev.*, **B 18**, 7165 (1978).
- [23] Kohn, W., Parr, R.G. and Becke, A.D., *J. Phys. Chem*, **100**, 12974 (1996).
- [24] Gazquez, J. L., *Struct. and Bond.*, **80**, 27 (1993). Note that the definition of the hardness, given in the text differs from the original one by a conventional factor of 2.
- [25] Hohenberg, P. and Kohn, W. *Phys. Rev. B*, **136**, 864 (1964).
- [26] Slater, J.C., 1974, "*The Self Consistent Field for Molecules and Solids*", McGraw-Hill, New York, v. 4.
- [27] Rajagopal, A.K., *Adv. Chem. Phys.*, **41**, 59 (1980).
- [28] Perdew, J.P. and Zunger, A. *Phys. Rev.*, **B23**, 5048 (1981).
- [29] Harris, J, *Int. J. Quantum Chem.*, **13**, 189 (1979).
- [30] Harris, J, *Phys. Rev.*, **A 29**, 1648 (1984).
- [31] Englisch, H. and Englisch, R., *Phys. Stat. Sol.*, **123**, 711 (1984), ibidem, **124**, 373 (1984).
- [32] Valiev, M.M. and Fernando, G.W., *Phys. Rev.*, **B 52**, 10697 (1995).
- [33] Gopinathan, M., S. and Withehead, M. A., *Israel J. Chem.*, **19**, 209 (1980).
- [34] Warren, R.W. and Dunlap, B.I., *Chem. Phys. Lett.*, **262**, 384 (1996).

- [35] Liu, G. H. and Parr, R. G., *J. Am. Chem. Soc.*, **117**, 3179 (1995).
- [36] Nalewajski, R. F. and Mrozek, J., *Int. J. Quantum Chem.*, **43**, 353 (1992).
- [37] Teter, M., *Phys. Rev. B*, **48**, 531 (1993).
- [38] R. Gilmore, "*Catastrophe theory for scientists and engineers*", J. Wiley and sons, New York, Chapt. 10 (1981)
- [39] Garza, J. and Robles, J., *Int. J. Quantum Chem.*, **49**, 159 (1994).
- [40] Pearson, R.G, *J. Chem. Educ.*, **64**, 561 (1987).
- [41] Parr, R.G and Chattaraj, P.K., *J. Am. Chem. Soc.*, **113**, 1854 (1991).
- [42] Postnikov, M., "*Linear Algebra*", Nauka, Moskow, chapt. 9 (1986), in Russian.
- [43] St-Amant, A., PhD Thesis, Universite de Montreal, Canada, 1992.
- [44] Perdew, J.P, *Phys. Rev.*, **B33**, 8822 (1986) .
- [45] Perdew, J.P. and Wang, Y., *Phys. Rev.*, **B33**, 8800 (1986).
- [46] Vosko, S.H., Wilk, L. and Nusair, M., *Can. J. Phys.*, **58**, (1980) 1200.
- [47] Broyden, C.C., *J. Inst. Math. Appl.*, **6**, 76 (1970) ; Fletcher, R, *Comput. J.*, **13**, 317 (1970) ; Goldfarb, D., *Math. Comput.*, **24**, 1385 (1970) .
- [48] Y. Abashkin, Y and Russo, N, *J. Chem. Phys.*, **100**, 4477 (1994).
- [49] Godbout, N., Salahub, D.R., Andzelm, J. and Wimmer, E., *Can. J. Chem.*, **70**, 560 (1992) .
- [50] Antonova, T. I., Neshev, N., Proinov E. and Nalewajski, R.F., *Acta Phys. Pol.*, **A 79**, 805 (1991).
- [51] De Proft, F. and Geerlings, P., *J. Chem. Phys.*, **106**, 3270 (1997).
- [52] Pearson, R. G. and Palke, W. E., *J. Phys. Chem.*, **96**, 3283 1992.
- [53] Datta, D. *J. Phys. Chem.* , **96**, 2409 (1992).
- [54] Pal, N.; Vaval, N. and Roy, S. *J. Phys. Chem.*, **97**, 4404 (1993).
- [55] Chattaraj, P. K.; Nath, S. and Sannigrahi, A. B. *Chem. Phys. Letters* , **212**, 223, (1993).
- [56] Gazquez, J. L., Martinez, A. and Mendez, F., *J. Phys. Chem.*, **97**, 4059 (1993).
- [57] Chattaraj, P. K.; Nath, S. and Sannigrahi, A. B. *J. Phys. Chem.* , **98**, 9143 (1994).
- [58] Nath, S., Sannigrahi, A. B and Chattaraj, P. K., *J. Mol. Struct. (THEOCHEM)*, **115**, 65 (1994).
- [59] Kar, T. and Scheiner, S. *J. Phys. Chem.*, **99**, 8121 (1995).
- [60] Ghanty, T. K. and Ghosh, S. K. *J. Phys. Chem.*, **100**, 12295 (1996).

DENSITY FUNCTIONAL CALCULATIONS OF REACTION ENERGETICS: APPLICATION TO ALKYL AZIDE DECOMPOSITION

Peter Politzer and Pat Lane

Department of Chemistry, University of New Orleans, New Orleans, LA 70148

Introduction

A continuing challenge in computational chemistry is to achieve a capability for calculating reaction energetics of practical significance with reliable accuracy. A major problem is that the ΔE or ΔH of a chemical process is generally a very small difference between numbers that are typically two or three orders of magnitude larger; any errors in the latter may consequently be greatly magnified in the former. While this might seem to suggest that the energies or enthalpies of the reactants and products need to be calculated at the highest possible level, this is not necessarily the case; what is important is that the maximum cancellation of intrinsic errors be achieved in obtaining the energy or enthalpy differences, ΔE or ΔH . Even Hartree-Fock results may be quite accurate if correlation effects change relatively little in going from reactants to products, as may be the case when the number of electron pairs remains constant [1].

Table I lists dissociation energies computed by a variety of methods for the four indicated bonds. Experimental data are included for comparison purposes. For these processes, the Hartree-Fock values are much too low, because the effects of electronic correlation, which are being neglected, are significantly greater in the molecules than in the fragments [1]. The correlated *ab initio* results demonstrate that the level of the computation is not necessarily reflected in the accuracy of the dissociation energy. While the individual molecular and fragment energies certainly improve in going from MP2 to MP4, $\Delta H(298\text{ K})$ does not in three of the four examples. It is notable that the coupled cluster value is also worse than the MP2 in these instances. The same point is brought out by the density functional (DF) calculations; increasing the size of the basis set, for a given functional combination, does not guarantee a more accurate dissociation energy. This can be seen, for example, from the DF/B3LYP/6-31G** and DF/B3LYP/6-31+G** results for $\text{H}_3\text{C-NH}_2$ and $\text{H}_3\text{C-OH}$.

The inclusion of electronic correlation is particularly important when molecules contain, in close proximity, several of the most "electron-rich" atoms (fluorine, oxygen and nitrogen), which have high outer-shell electronic densities [2]; failure to do so may lead to significant errors in optimized geometries as well as energetics [3-7]. Since systems of chemical interest are often too large to be treated by *ab initio* correlated procedures (e.g. many-body perturbation, configuration interaction, coupled cluster, etc.), density functional methods offer an attractive alternative [8-12]; they do include correlation, but require much less in terms of

Table I. Calculated bond dissociation energies for $\text{H}_3\text{C-NH}_2$, $\text{H}_3\text{C-OH}$, $\text{H}_3\text{C-CN}$ and $\text{H}_3\text{C-SiH}_3$.^a

Method	$\Delta\text{H}(298\text{ K}), \text{ kcal/mole}$			
	$\text{H}_3\text{C-NH}_2$	$\text{H}_3\text{C-OH}$	$\text{H}_3\text{C-CN}$	$\text{H}_3\text{C-SiH}_3$
HF/6-31G**//HF/6-31G**	49.6	51.5	96.0	61.9
MP2/CEP-TZDP++//MP2/CEP-TZDP	83.6	92.1	141.0	86.1
MP3/CEP-TZDP++//MP2/CEP-TZDP	77.1	83.6	131.8	84.0
MP4/CEP-TZDP++//MP2/CEP-TZDP	79.8	87.8	134.8	84.9
CCSD(T)/CEP-TZDP++//MP2/CEP-TZDP	78.3	85.9	121.4	83.9
DF/BLYP/6-31G**//BLYP/6-31G**	81.5	91.5	---	---
DF/B3LYP/6-31G**//B3LYP/6-31G**	81.5	89.4	123.3	83.3
DF/B3LYP/6-31+G*//B3LYP/6-31+G*	80.3	87.2	121.7	81.7
DF/B3LYP/6-31+G**//B3LYP/6-31+G**	79.8	86.9	---	---
DF/B3PW91/6-31G**//B3PW91/6-31G**	82.9	90.0	124.6	83.7
DF/B3PW91/6-31+G*//B3PW91/6-31+G*	82.1	88.4	123.3	82.5
DF/B3P86/6-31G**//B3P86/6-31G**	85.8	93.2	---	---
DF/B3P86/6-31+G*//B3P86/6-31+G*	85.1	91.7	126.2	85.0
DF/B3P86/6-31+G**//B3P86/6-31+G**	84.6	91.4	125.9	84.7
experimental	84.9 ^b	92.3 ^b	121.8 ^c	88.2 ^b

^aThe Hartree-Fock results were computed with Gaussian 94 [13], the MP and CCSD(T) are taken from reference [14], in which the basis sets are described, and the density functional (DF) are from reference [15], which identifies the exchange and correlation functionals.

^bReference [16].

^cReference [17].

computer resources, both time and space. The effectiveness of such approaches will be discussed in more detail in the next section.

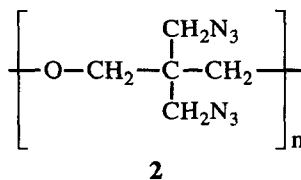
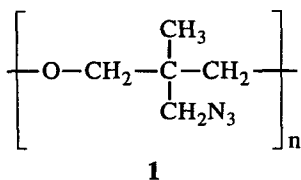
Density Functional Calculations of Energies and Enthalpies of Reaction

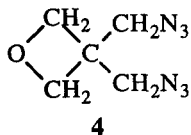
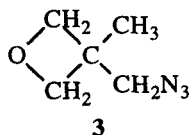
There is increasing evaluation and application of density functional techniques in computing ΔE and ΔH for chemical reactions of practical significance [15,18-22]. As part of this effort, we have recently tested the effectiveness for computing bond dissociation energies of six different combinations of exchange and correlation functionals and basis sets [15]. For 28 bonds in 26 molecules, the most accurate results, overall, were obtained with the DF/B3P86/6-31+G** procedure, followed by the DF/B3P86/6-31+G* and the DF/B3PW91/6-31G**; all three had average errors of less than 2.5 kcal/mole.

As a more demanding test, we have calculated $\Delta H(298\text{ K})$ at the DF/B3P86/6-31+G** level for 20 general chemical reactions, with as many as eight molecules in the balanced equation [20,22]. Since these processes involve breaking and forming as many as 16 bonds, they provide ample opportunity for both accumulation and cancellation of errors. On the average, the computed $\Delta H(298\text{ K})$ was within 5 kcal/mole of the experimental. Since, as mentioned earlier, the former are small differences between very large numbers, this degree of accuracy is quite gratifying. Thus, while some problems remain, and the DF/B3P86/6-31+G** $\Delta H(298\text{ K})$ is occasionally in error by more than 10 kcal/mole [20,22], it seems fair to say that density functional techniques are now capable of producing meaningful ΔE and ΔH for reactions of practical chemical interest. A specific example will be discussed in the next section.

An Application: Organic Azide Decomposition

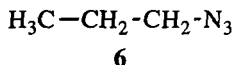
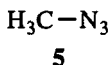
Poly(AMMO), **1**, and poly(BAMO), **2**, are energetic azide-containing polymers which are used as components of propellant formulations. They are prepared from the corresponding oxetanes AMMO, **3** (3-azidomethyl-3-methyloxetane) and BAMO, **4** (3,3'-bis(azidomethyl)oxetane) by opening the rings through C–O bond cleavage and subsequent linking of the monomer units through these carbons and oxygens.





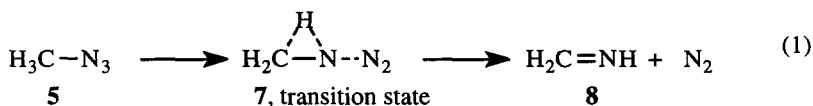
Due to the importance of **1** and **2** as propellant ingredients, there is considerable interest in their decomposition processes, and several experimental studies have sought to elucidate their key features [23-26]. We have now addressed some aspects of this problem computationally, using a density functional procedure, DF/B3PW91/6-31G**, and the Gaussian 94 code [13] for all geometry, energy and vibration frequency calculations. Transition states were established by confirming that they have one imaginary frequency [1].

The consensus of the experimental work is that the initial decomposition step is cleavage of the RN-N₂ bond, releasing N₂, with an activation energy of about 40 kcal/mole [23,25]. For completeness, however, we began our investigation by computing the R-N₃ dissociation energies for both **3** and **4**, as well as for two model systems, methyl azide, **5**, and *n*-propyl azide, **6**.



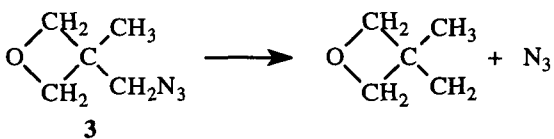
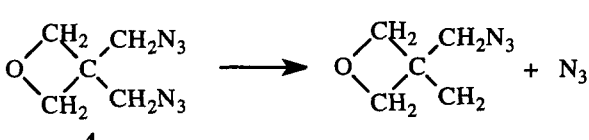
The results, presented in Table II, are very similar for all four systems, providing some reassurance that the C-N₃ portions of **3** and **4** (and hopefully **1** and **2**) can be modeled by **5** and **6**. All subsequent calculations have accordingly been only for **5** and **6**.

Since the values in Table II are considerably higher than the observed 40 kcal/mole activation energy, we moved next to an examination of N₂ elimination, via breaking of the RN-N₂ bond. The spin-allowed reaction might be expected to be formation of the singlet nitrene, RN. Instead we found, for methyl azide, a concerted process involving H₃CN-N₂ bond cleavage and hydrogen transfer, producing the imine H₂C=NH, **8**:



The computed activation barrier is 49 kcal/mole, while the overall ΔH(298 K) for eq. (1) is -36 kcal/mole (Table III), in very good agreement with the experimental -35 kcal/mole [27]. The rearrangement shown in eq. (1) has also been found in other theoretical and experimental studies [28-34]. (Elimination of N₂ from **5** to yield the

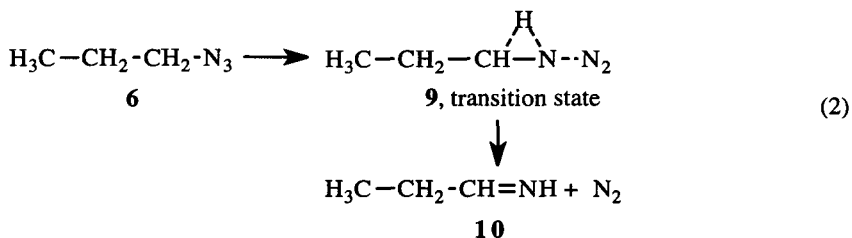
Table II. Computed (DF/B3PW91/6-31G**) dissociation energies for R-N₃ bonds.

Process	$\Delta H(298\text{ K}),$ kcal/mole
$\text{H}_3\text{C}-\text{N}_3 \longrightarrow \text{H}_3\text{C} + \text{N}_3$ <p style="text-align: center;">5</p>	68
$\text{H}_3\text{C}-\text{CH}_2-\text{CH}_2-\text{N}_3 \longrightarrow \text{H}_3\text{C}-\text{CH}_2-\text{CH}_2 + \text{N}_3$ <p style="text-align: center;">6</p>	68
 <p style="text-align: center;">3</p>	67
 <p style="text-align: center;">4</p>	66 ^a

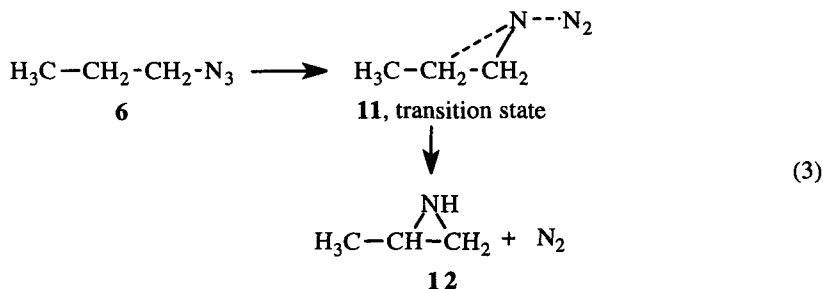
^aThe difference in the zero-point and thermal energies involved in the dissociation of **4** was assumed to be the same as for **3**.

spin-forbidden triplet nitrene, for which we find $\Delta H(298\text{ K}) = 10\text{ kcal/mole}$, has been observed as a minor decomposition channel [35,36].)

n-Propyl azide, **6**, can undergo an analogous process to form the imine **10**:



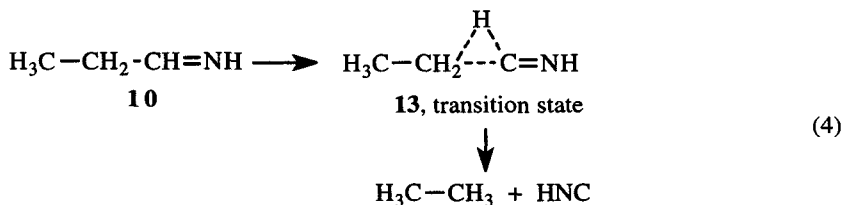
The calculated activation barrier is 47 kcal/mole, and the overall $\Delta H(298\text{ K})$ is -41 kcal/mole (Table III). However we found that there is now a second option: a concerted loss of N_2 and rearrangement to the aziridine **12**:



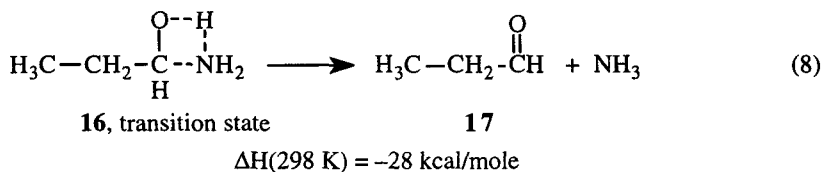
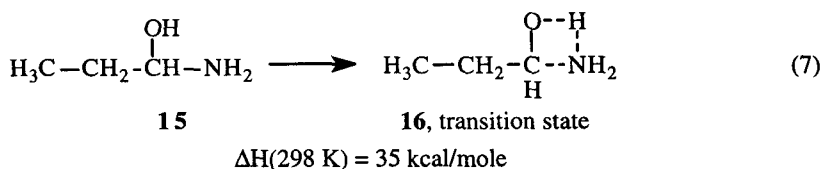
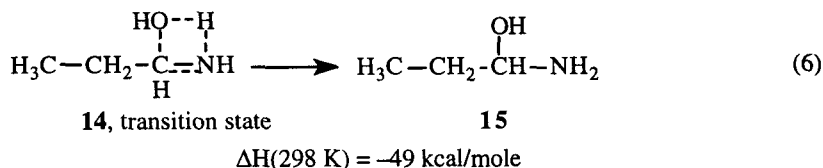
The activation barrier is 49 kcal/mole; the overall $\Delta H(298\text{ K})$ is -27 kcal/mole (Table III). It is interesting to note that earlier experimental studies of ethyl azide decomposition have reported the formation of the aziridine [29, 37, 38].

While reactions (2) and (3) are competitive, the latter is not relevant to our present objectives, since analogous aziridines are structurally impossible for polymers **1** and **2** (however azetidines are possible). Among the products that have been observed in the decompositions of these polymers are HCN and NH_3 [23-25], and we have therefore made some efforts to determine how these might be produced, taking the imine **10** as our starting point.

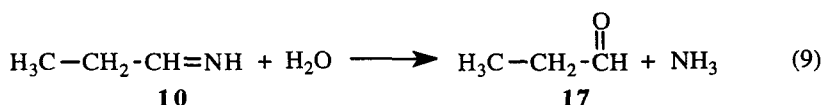
As a potential source of HCN, we examined the reaction in eq. (4); this could yield HNC, which might then isomerize to HCN. We did obtain the transition state **13**, but the activation barrier appears to be prohibitive, 84 kcal/mole.



Following a suggestion by Brill [39], we also investigated the possibility that NH_3 may be formed through the interaction of **10** with H_2O , which is another of the



For the overall process,



$\Delta\text{H}(298 \text{ K})$ is equal to -7 kcal/mole . Eqs. (5) - (8) are a possible explanation of the reported observation of NH_3 .

Summary

Density functional methods are now capable of giving meaningful ΔE and ΔH values for reactions of practical chemical significance. The decomposition of *n*-propyl azide was considered in some detail. Loss of N_2 is a likely initial step, accompanied by the rearrangement of the remainder of the molecule to either an imine

or an aziridine. The former can interact with water in a two-step process to yield propionaldehyde and ammonia.

Acknowledgements

We greatly appreciate discussions with Dr. Jane S. Murray and Dr. Thomas B. Brill, and the financial support provided by the Ballistic Missile Defense Organization and the Office of Naval Research through contract N00014-95-1-1339, Program Officers Dr. Leonard H. Caveny (BMDO), Dr. Richard S. Miller (ONR) and Dr. Jonah Goldwasser (ONR).

References

1. W. J. Hehre, L. Radom, P. v. R. Schleyer and J. A. Pople, *Ab Initio Molecular Orbital Theory*, Wiley-Interscience, New York, 1986.
2. P. Politzer, J. S. Murray and M. E. Grice, in *Chemical Hardness*, K. D. Sen, Ed., Springer-Verlag, Berlin, 1993.
3. D. J. DeFrees, B. A. Levi, S. K. Pollack, W. J. Hehre, J. S. Binkley and J. A. Pople, *J. Am. Chem. Soc.* **101**, 4085 (1979).
4. D. A. Clabo and H. F. Schaefer III, *Int. J. Quant. Chem.* **31**, 429 (1987).
5. J. M. Coffin and P. Pulay, *J. Phys. Chem.* **95**, 118 (1991).
6. J. M. Seminario, M. C. Concha and P. Politzer, *J. Comp. Chem.* **13**, 177 (1992).
7. D. H. Phillips and G. E. Quelch, *J. Phys. Chem.* **100**, 11270 (1996).
8. R. G. Parr and W. Yang, *Density-Functional Theory of Atoms and Molecules*, Oxford University Press, New York, 1989.
9. J. K. Labanowski and J. W. Andzelm, Eds., *Density Functional Methods in Chemistry*, Springer, Berlin, 1991.
10. J. M. Seminario and P. Politzer, Eds., *Modern Density Functional Theory*, Elsevier, Amsterdam, 1995.
11. R. G. Parr and W. Yang, *Ann. Rev. Phys. Chem.* **46**, 701 (1995).
12. J. M. Seminario, Ed. *Recent Developments and Applications of Modern Density Functional Theory*, Elsevier, Amsterdam, 1996.
13. M. J. Frisch, G. W. Trucks, H. B. Schlegel, P. M. W. Gill, B. G. Johnson, M. A. Robb, J. R. Cheeseman, T. A. Keith, G. A. Petersson, J. A. Montgomery, K. Raghavachari, M. A. Al-Laham, V. G. Zakrzewski, J. V. Ortiz, J. B. Foresman, J. Cioslowski, B. B. Stefanov, A. Nanayakkara, M. Challacombe, C. Y. Peng, P. Y. Ayala, W. Chen, M. W. Wong, J. L. Andres, E. S. Replogle, R. Gomperts, R. L. Martin, D. J. Fox, J. S. Binkley, D. J. DeFrees, J. Baker, J. P. Stewart, M. Head-Gordon, C. Gonzalez and J. A. Pople, Gaussian 94, (Gaussian, Inc., Pittsburgh, PA, 1995).

14. H. Basch, *Inorg. Chim. Acta* **252**, 265 (1996).
15. J. J. M. Wiener and P. Politzer, *J. Mol. Struct. (Theochem)*, in press.
16. D. F. McMillen and D. M. Golden, *Ann. Rev. Phys. Chem.* **33**, 493 (1982).
17. D. R. Lide, Ed. *Handbook of Chemistry and Physics*, 71st ed., CRC Press, Boca Raton, FL, 1990.
18. G. Fitzgerald and J. Andzelm, *J. Phys. Chem.* **95**, 10531 (1991).
19. G. Seifert and K. Krüger, in *The Reaction Path in Chemistry: Current Approaches and Perspectives*, D. Heidrich, Ed., Kluwer, Dordrecht (The Netherlands), 1995, p. 161.
20. P. Politzer, J. J. M. Wiener and J. M. Seminario, in *Recent Developments and Applications of Modern Density Functional Theory*, J. M. Seminario, Ed., Elsevier, Amsterdam, 1996, ch. 22.
21. A. C. Scheiner, J. Baker and J. W. Andzelm, *J. Comp. Chem.* **18**, 775 (1997).
22. P. Politzer and J. M. Seminario, in *Computational Thermochemistry*, K. K. Irikura and D. J. Frurip, Eds., American Chemical Society, Washington, DC, in press.
23. M. Farber, S. P. Harris and R. D. Srivastava, *Combust. Flame* **55**, 203 (1984).
24. Y. Oyumi and T. B. Brill, *Combust. Flame* **65**, 127 (1986).
25. J. K. Chen and T. B. Brill, *Combust. Flame* **87**, 157 (1991).
26. E. Kimura and Y. Oyumi, *J. Energ. Mat.* **14**, 201 (1996).
27. S. G. Lias, J. E. Bartmess, J. F. Liebman, J. L. Holmes, R. D. Levin and W. G. Mallard, *J. Phys. Chem. Ref. Data* **17**, suppl. 1 (1988).
28. J. A. Pople, K. Raghavachari, M. J. Frisch, J. S. Binkley and P. v. R. Schleyer, *J. Am. Chem. Soc.* **105**, 6389 (1983).
29. E. P. Kyba, in *Azides and Nitrenes*, E. F. V. Scriven, Ed., Academic, Orlando, FL, 1984, ch. 1.
30. C. Richards, Jr., C. Meredith, S.-J. Kim, G. E. Quelch and H. F. Schaefer, III, *J. Chem. Phys.* **100**, 481 (1994).
31. M. T. Nguyen, D. Sengupta and T.-K. Ha, *J. Phys. Chem.* **100**, 6499 (1996).
32. D. E. Milligan, *J. Chem. Phys.* **35**, 1491 (1961).
33. M. E. Jacox and D. E. Milligan, *J. Mol. Spectrosc.* **56**, 333 (1975).
34. H. Bock and R. Dammel, *J. Am. Chem. Soc.* **110**, 5261 (1988).
35. E. Wasserman, G. Smolinsky and W. A. Yager, *J. Am. Chem. Soc.* **86**, 3166 (1964).
36. L. Ying, Y. Xia, H. Shang, X. Zhao and Y. Tang, *J. Chem. Phys.* **105**, 5798 (1996).
37. G. Geiseler and W. König, *Z. Phys. Chem. (Wiesbaden)* **227**, 81 (1964).
38. W. Pritzkow and D. Timm, *J. Prakt. Chem.* **32**, 178 (1966).
39. T. B. Brill, private communication.

Density Functional Theory : A Source of Chemical Concepts and a Cost-Effective Methodology for Their Calculation

P. Geerlings* , F. De Proft and W. Langenaeker

Eenheid Algemene Chemie
Vrije Universiteit Brussel
Faculteit Wetenschappen
Pleinlaan 2
1050 Brussels
Belgium

Invited contribution to Advances in Quantum Chemistry, J. Seminario Editor.

* Author to whom correspondence should be sent

TABLE OF CONTENTS

1. Introduction

2. Computational vs. Conceptual DFT

3. Calculation of DFT based Quantities : Atomic Electronegativities and Hardnesses

3.1. Introduction and Methodology

3.2. Isolated Atom Electronegativity and Hardness

3.3. Atoms in Molecules Electronegativity and Hardness

4. Rationalizing Chemical Reactivity within the HSAB principle

4.1. Introduction : the HSAB Principle

4.2. The Global HSAB Principle : Stabilization of Endohedral Complexes of C_{60} , Si_{60} and Ge_{60} with Monoatomic Cations and Anions

4.3. The HSAB Principle at a Local Level : Regioselectivity of Diels-Alder Reactions

4.3.1. Introduction

4.3.2. The Local HSAB Principle : Importance of Equal Softness Between Reaction Sites

4.3.3. Results and Discussion

5. Conclusions

Acknowledgements

References

1. INTRODUCTION

Density Functional Theory (DFT) [1-7] provoked a revolution in quantum chemical research in the past 15 years. In the post war period, after formulation of the Hartree-Fock problem in matrix form by Roothaan [8], the fifties, sixties and seventies witnessed a continuous effort to improve Hartree-Fock and post-SCF calculations, thereby stressing the importance of the wave function as the source of all information about an atomic or molecular system. One noticeable exception to this evolution is Slater's X_α method [9] introduced in the 1950's, where the non-local Hartree-Fock exchange operator is substituted by Dirac's exchange formula for the free electron gas, function of the electron density. The eighties then witnessed the fullblast introduction in chemistry of the idea that the electron density can be used as the fundamental variable, as proved by Hohenberg and Kohn in 1964 [10] (for an intuitive approach, see Wilson, quoted in a paper by Löwdin [11]). It was finally the Kohn-Sham formalism [12], to be briefly described in section 2, which provoked a major computational breakthrough in the late eighties and the nineties. DFT thereby consolidated more and more its position, with a very promising outlook with the current development and refinement of methods, of which the computational cost scales linearly with the number of basis functions.

2. CALCULATIONAL VS. CONCEPTUAL DFT

A closer look at the Hohenberg-Kohn theorems [10] and their consequences reveals that two aspects of density functional theory are important in quantum chemistry.

The Hohenberg-Kohn theorems state that the electron density uniquely determines the external potential and the number of electrons of an atomic or molecular system. Since these determine in turn the Hamiltonian of the system, $\rho(r)$ will ultimately determine the energy of the system :

$$\begin{array}{ccccccc} \rho(r) & \longrightarrow & v(r) & \longrightarrow & H_{op} & \longrightarrow & E \\ & \searrow & & \nearrow & & & \\ & & N & & & & \end{array}$$

The calculation of the electron density, function of three spatial coordinates thus avoids the calculation of the over-complicated wave function, function of the spatial and spin coordinates of all the electrons of the system. The electronic energy $E[\rho]$ of the system can be written as

$$E[\rho] = T[\rho] + V_{NE}[\rho] + V_{EE}[\rho] \quad (1)$$

with $T[\rho]$ the kinetic energy, $V_{NE}[\rho]$ the nuclear-electron attraction energy and $V_{EE}[\rho]$ the electron-electron repulsion energy.

Minimizing the energy of the system with respect to the electron density, under the constraint that the integral of the electron density should yield the total number of electrons, yields the equation :

$$v(\underline{r}) + \frac{\delta F}{\delta \rho(\underline{r})} = \mu \quad (2)$$

with $v(\underline{r})$ the external (i.e. due to the nuclei) potential, F the Hohenberg-Kohn functional containing the electron-electron repulsion and kinetic energy. The Lagrange multiplier μ , will be identified later on. This equation is in fact the DFT analogue of the time-independent Schrödinger equation. The practical treatment of this equation (looking for $\rho(\underline{r})$ which makes the left hand side of Eq. (2) equal to an unknown constant) has been provided by Kohn and Sham [12], ingeniously turning it into a form showing high analogy with the Hartree-Fock equations, thereby facilitating its implementation in existing computer codes. This is achieved by introducing orbitals into the picture and starting from a non-interacting reference system. Expression (1) then becomes :

$$E[\psi_i] = \sum_{i=1}^N \left\langle \psi_i \left| -\frac{1}{2} \nabla^2 \right| \psi_i \right\rangle + \int \rho(\underline{r}) v(\underline{r}) d\underline{r} + \int \frac{\rho(\underline{r})\rho(\underline{r}')}{|\underline{r} - \underline{r}'|} d\underline{r} d\underline{r}' + E_{xc}[\rho(\underline{r})] \quad (3)$$

with $E_{xc}[\rho(\underline{r})]$ the exchange-correlation functional.

The electron density is then written as :

$$\rho(\underline{r}) = \sum_{i=1}^N |\psi_i|^2 \quad (4)$$

Minimization of the total energy function (3) with respect to the Kohn-Sham orbitals ψ_i , imposing their orthonormality, yields the Kohn-Sham orbital equations :

$$\left(-\frac{1}{2} \nabla^2 + v_{eff} \right) \psi_i = \epsilon_i \psi_i \quad (5)$$

where v_{eff} is the effective Kohn-Sham potential, having the form :

$$v_{eff}(\underline{r}) = v(\underline{r}) + \int \frac{\rho(\underline{r}')}{|\underline{r} - \underline{r}'|} d\underline{r}' + v_{xc}(\underline{r}) \quad (6)$$

It should be noted that $v_{xc}(\underline{r})$ remains unknown, and an approximation has to be chosen (for a recent review, see [13]). Moreover, in most applications, the

Kohn-Sham orbitals are expanded in a Gaussian basis set, so the problem remains to choose the type of basis set and the number of basis functions. Fortunately, the basis functions used are the same as in wave function calculations, offering maximum compatibility between DFT and ab initio MO calculations.

In this way, computational efficiency has been reached and high precision calculations are now possible at much more affordable calculation times than correlated methods. Although the search for $v_{XC}(r)$ remains a standing problem [14], the impression is that DFT may take over molecular orbital calculations when calculation of non-pathological molecular systems is concerned. High precision DFT calculations are indeed possible, e.g. on reaction energies [15, 16], charge distributions (including atomic populations [17, 18], dipole moments [17, 18] and infrared intensities [17, 18]), reactivity descriptors [18, 19] (such as the electrostatic potential and the Fukui function) and geometries [20]. The whole of the aforementioned developments, essentially aiming at a simplified but high quality calculation of atomic or molecular properties has been termed by Parr as *calculational DFT* [6]. However, DFT offers a second source of interest, especially to chemists. Looking at the above depicted scheme, it is clear that energy changes of a system will be ultimately due to changes in its number of electrons N or the external potential $v(r)$. These changes will be governed by the derivatives

$$\left(\frac{\partial^n E}{\partial N^n} \right)_v, \quad (7)$$

$$\left[\frac{\delta^n E}{\delta v^n} \right]_N \quad (8)$$

and their mixed derivatives. These quantities, which are called response functions, have been identified with atomic or molecular reactivity descriptors. When $n=1$, Eq. (7) yields the electronic chemical potential μ [21], the Lagrange multiplier in Eq. (1), and equal to the negative of the electronegativity χ [21–24]. When $n=2$, the response function is equal to the hardness [25], measuring the resistance of the system towards charge transfer. The inverse of the global hardness is the softness [26].

The derivative of the energy with respect to the external potential yields the electron density, which can be seen to contain two components, the number of electrons N , measuring the extent of the electron cloud and the shape factor $\sigma(r)$, measuring the shape of the electron density [27] :

$$\rho(r) = N\sigma(r) \quad (9)$$

with

$$\int \sigma(r) dr = 1 \quad (10)$$

since $\int \rho(r) dr = N$.

The first mixed derivative is the Fukui function $f(r)$ [28], a frontier molecular orbital reactivity index :

$$f(r) = \left[\frac{\delta \mu}{\delta v(r)} \right]_N = \left(\frac{\partial \rho(r)}{\partial N} \right)_v \quad (11)$$

Quantities of both types (i.e. local and global) can be combined, a well known example being the local counterpart of the softness, local softness, introduced as [29]:

$$s(r) = \left(\frac{\delta \rho(r)}{\delta \mu} \right)_v = Sf(r) \quad (12)$$

It can be noted that the local softness is obtained by multiplication of the Fukui function with the global softness ; the local softness can thus be considered as a weighted distribution of the global softness over the molecule. Due to this fact, the local softness should be used as a intermolecular reactivity index, whereas the Fukui function is an intramolecular reactivity index. The definition of local hardness is less trivial and remains a matter of current debate.

Equation (12) shows a remarkable resemblance with Eq. (9). Since ρ will determine the energy, N and σ are sufficient to determine all properties of the atomic or molecular system, implying a functional dependence $E[N, \sigma]$. The importance of the shape factor, which has only been spuriously recognized in the past, emerges when changes from one ground state to another are written as a function of N and σ . It appeared that the contribution of the shape of a system to the electronegativity and hardness of a system can be filtered out [30, 31]. For the electronegativity, one obtains :

$$\chi_v = \chi_\sigma - \frac{1}{N} \int \left[\frac{\delta E}{\delta \sigma(r)} \right]_N \left(f(r) - \frac{\rho(r)}{N} \right) dr \quad (13)$$

As can be seen, the electronegativity at constant external potential χ_v equals the electronegativity at a constant shape factor χ_σ and a term which describes the effect of a shape factor change on the energy at a constant number of electrons.

Moreover, the shape factor could play an important role when looking at molecular similarity, where the most often used similarity index SI is [32] :

$$SI = \frac{\int \rho_A(r) \rho_B(r) dr}{\left(\int \rho_A^2(r) \right)^{1/2} \left(\int \rho_B^2(r) \right)^{1/2}} \quad (14)$$

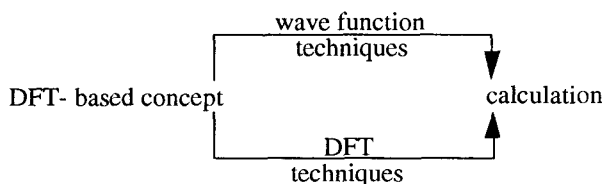
with $\rho_A(r)$ and $\rho_B(r)$ the electron densities of the molecules A and B. This expression can obviously be reduced to an index only involving the shape factors $\sigma_A(r)$ and $\sigma_B(r)$ of both molecules [33] :

$$SI = \frac{\int \sigma_A(r) \sigma_B(r) dr}{\left(\int \sigma_A^2(r)\right)^{1/2} \left(\int \sigma_B^2(r)\right)^{1/2}} \quad (15)$$

implying that similarity is essentially shape-determined.

Density functional theory thus offers precise definitions of previously poorly defined chemical quantities, enabling their first principles calculation. This part of DFT is termed by Parr as *conceptual DFT* [6].

Both aspects, calculational and conceptual DFT, can be elegantly linked, via the following scheme :



Our work in recent years has mainly concentrated on testing and using DFT based reactivity concepts, calculated via wave functional techniques, in order to avoid simultaneous testing of concepts and calculational techniques.

However, the development and elaboration of exchange correlation functionals now makes it possible to calculate these concepts at an accuracy comparable with correlated ab initio calculations, establishing a complete DFT evaluation of chemical reactivity. We studied, among others :

- Fukui functions and local softnesses and their application in typical organic reactions (electrophilic substitutions on aromatic systems, nucleophilic additions to activated carbon-carbon double and triple bonds) [34-39].
- The search for a true companion for local softness (local hardness) and its applications [40].
- Electronegativity equalization at the atomic, functional group and amino acid residue level [41-43].

In the substrates, special attention has been devoted to zeolites and fullerenes [34, 38, 39, 44], in the reactions to acid-base equilibria and the influence of hardness and softness on both sides of the equilibrium (acidity of carboxylic acids [45], alkyl [46] and halogenated alcohols [47], hydrides [48] and recently hydrofullerenes [49], basicity of amines [50, 51] and proton affinities of amino acids [52]). For reviews of these studies, see [18, 53, 54].

In the present contribution, the calculational and conceptual aspects of DFT will be illustrated together with some recent applications situated around a central theme : atomic hardnesses and softnesses and the Hard and Soft Acids

and Bases (HSAB) principle [55, 56]. In Section 3, we concentrate on the calculation of atomic electronegativities and hardnesses both for isolated atoms (3.2) [57] and atoms embedded in a molecule (3.3) [58]. In Section 4, after a short introduction to Pearson's Hard and Soft Acids and Bases (HSAB) principle [55, 56], the idea of hardness and softness (both in a global and a local sense) is applied to chemical interactions, concentrating on thermodynamic aspects (stability) [59] as well as on its kinetic aspects (reactivity) [60]. In Section 5, conclusions are drawn and an outlook to the future is given.

3. CALCULATION OF DFT-BASED QUANTITIES : ELECTRONEGATIVITY AND HARDNESS

3.1. Introduction and Methodology

The methodology in this section concerns global properties, which can be written as first or second order derivatives of the energy with respect to the number of electrons N . In practice, these derivatives cannot be calculated analytically and their numerical calculation is performed using a finite difference approximation ("faute de mieux") ; very recently, a variational ansatz has been proposed [61]. For the chemical potential (or minus the electronegativity), the finite difference approximation becomes :

$$\mu = -\chi = \left(\frac{\partial E}{\partial N} \right)_v \approx -\frac{1}{2} [(E_{N_0-1} - E_{N_0}) + (E_{N_0} - E_{N_0+1})] = -\frac{I + A}{2} \quad (16)$$

which is the Mulliken formula [23] for the electronegativity and for the hardness

$$\eta = \left(\frac{\partial^2 E}{\partial N^2} \right)_v \approx \frac{1}{2} [(E_{N_0-1} - E_{N_0}) - (E_{N_0} - E_{N_0+1})] = \frac{I - A}{2} \quad (17)$$

with I and A the ionization energy and the electron affinity respectively. Since all these derivatives should be evaluated at constant external potential $v(\underline{r})$, the $N_0 + 1$ and $N_0 - 1$ electron system are calculated at the same geometry as the N_0 electron system. The same methodology is used when local properties are calculated (Fukui function, local softness, ...), both in their non-condensed and condensed form.

3.2. Isolated Atom Electronegativity and Hardness

As the global hardness and softness concepts, together with the electronegativity are now well established [62, 63], we decided to examine to what extent DFT methods can be used to obtain high accuracy results, needed for the use of these properties in the HSAB principle and especially in electronegativity

equalization calculations. High quality calculations are indeed necessary as the calculation of the properties (cf. Eqs. (16) and (17)) involves a change in the number of electrons by one, thus making electron correlation effects important. Some testing on the calculation of ionization energies and electron affinities revealed that the best choice for $v_{xc}(r)$ are the "exact exchange" B3PW91 and B3LYP functionals [64, 65], containing a portion of exact Hartree-Fock exchange and using the PW91 [66] and LYP [67] correlation functionals respectively. The largest basis set used was Dunning's aug-cc-pVTZ (augmented correlation consistent polarized valence triple zeta) [68, 69]. The atomic and molecular systems considered are those from Pople's well known G2 set [70]. In the following table, the mean absolute deviations from experiment are listed for the B3LYP and B3PW91 functional, for the ionization energy (I) and the electron affinity (A), together with the number of systems considered.

	I	A
B3LYP	0.15 (38)	0.12 (27)
B3PW91	0.15 (36)	0.11 (27)

Table 1 : Mean absolute deviations (eV) from experiment for the ionization energies (I) and electron affinities (A), calculated with the B3LYP and B3PW91 functionals and the aug-cc-pVTZ basis set. Also listed are the number of systems included in the statistical analysis.

As can be seen, both methods show an excellent performance in the calculation of ionization energies and electron affinities. These results are in agreement with our previous experiences using these methods in the calculation of atomic populations, dipole moments, infrared intensities, electrostatic potentials and Fukui functions. Moreover, the results are very promising for the calculation of electronegativities and hardnesses. As a test, electronegativities and hardnesses were calculated using a finite difference approximation for the majority of first and second row atoms and for some ions, using the aug-cc-pVTZ and the Pople type 6-311++G(3df,2p) basis set [71]. Reference calculations at the correlated CCSD(T) [72] level were performed. Table 2 lists the performance of the two exact exchange functionals in the calculation of χ and η with the Pople basis set. The conclusions for the aug-cc-pVTZ basis set are completely analogous. A remark should be made concerning the experimental values for these two quantities. These values are denoted experimental in the sense that values of I and A from experiment were used in the finite difference expression for the electronegativity and hardness.

	B3LYP	B3PW91	CCSD(T)
χ	0.21	0.15	0.25
η	0.08	0.08	0.13

Table 2 Mean absolute deviations (eV) from "experiment" for the electronegativities and hardnesses calculated at the B3LYP, B3PW91 and CCSD(T) level with the 6-311++G(3df,2p). 15 atoms and 7 cations were considered.

As an example, a plot of the B3LYP electronegativities and hardnesses vs. the "experimental" values for these quantities is shown (Figures 1 and 2).

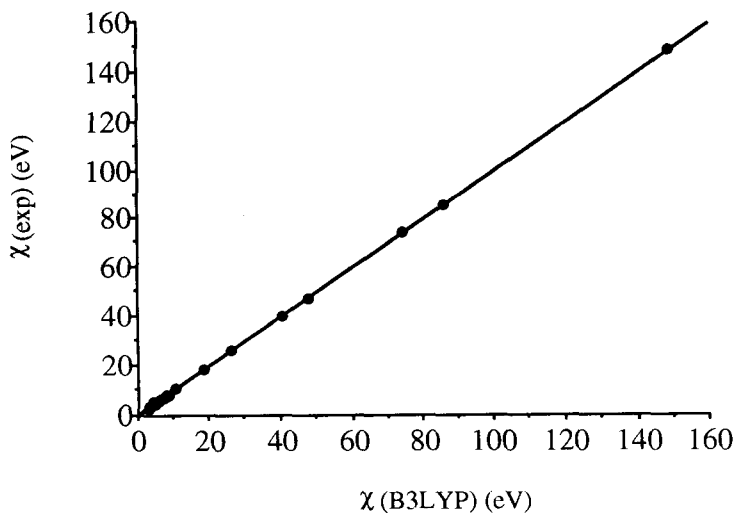


Figure 1. Correlation of the electronegativities, calculated at the B3LYP level with the 6-311++G(3df,2p) basis set, with experiment ($r^2=0.99998$, $n=22$)

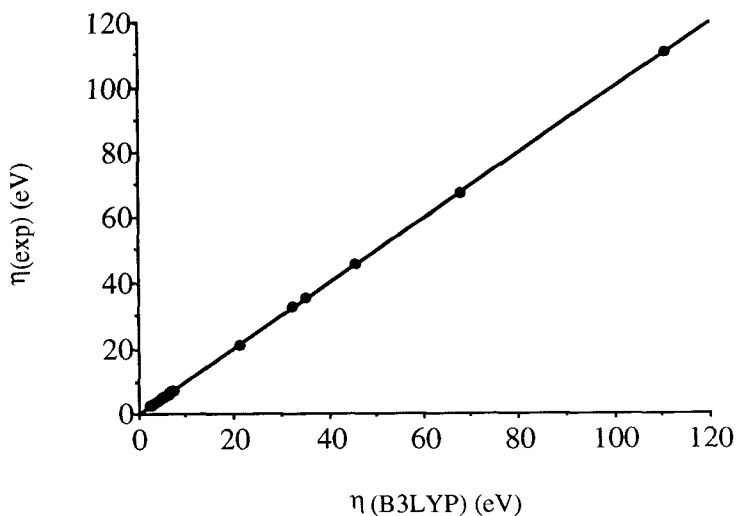


Figure 2. Correlation of the hardnesses, calculated at the B3LYP level with the 6-311++G(3df,2p) basis set, with "experiment" ($r^2=0.99999$, $n=22$).

As can be seen, an excellent correlation is found. From this work, it can be concluded that both the B3LYP and B3PW91 functional, combined with large Dunning or Pople type basis sets yields excellent results in the calculation of ionization energies and electron affinities of atoms and simple molecules. The same conclusions can be drawn for electronegativities and hardnesses. The extension of this methodology to groups and larger molecules will thus give rise to accurate reactivity descriptors for use in HSAB and electronegativity equalization studies.

3.3. Atoms-in-Molecules Electronegativities and Hardnesses

Already in the early fifties, Sanderson formulated his electronegativity equalization principle : "When two atoms or groups, initially different in electronegativity, unite to form a molecule, their electronegativities will be adjusted to the same intermediate value" [73, 74]. Although of extreme simplicity and appealing to chemical intuition, the use of the principle remained modest until its proof provided by Parr and coworkers[21, 75]. Although it was proved that the electronegativity is equalized in every point in space or for every spatial partitioning, the atomic resolution is mostly used. The total molecular energy should then be written as a sum of atomic contributions, as is done in the Electronegativity Equalization Method (EEM) of Mortier [76-78] :

$$E = \sum_{\alpha}^n \left(E_{\alpha}^{*} + \chi_{\alpha}^{*} q_{\alpha} + \eta_{\alpha}^{*} q_{\alpha}^2 + \frac{k}{2} \sum_{\alpha \neq \beta}^n \frac{q_{\alpha} q_{\beta}}{R_{\alpha\beta}} \right) \quad (18)$$

using a Taylor expansion in the charges on the atoms. The expansion coefficients E_{α}^{*} , χ_{α}^{*} and η_{α}^{*} , which differ from the isolated atom values of these quantities due to the influence of the molecular environment and connectivity on these properties, were determined for different types of atoms via calibration against ab initio STO-3G data. The interatomic interaction upon molecule formation is here approximated by Coulomb's law. The method thus has to be weaponed with parameters chosen as to reproduce experimental or high quality theoretical results, bringing however severe empiricism in the theory. An alternative is a non-empirical calculation of the parameters χ_{α}^{*} and η_{α}^{*} , taking into account molecular environment effects, thereby creating atoms-in-molecules (AIM) electronegativities and hardnesses. The procedure designed, taking into account the coordination type and the distance of the nearest neighbours, is schematically shown in Figure 3. Part A shows the usual situation upon ionization of an atom : the electron leaves the atom to infinity and the electron cloud contracts but remains spherically symmetrical. When taking an electron out of an atom in a molecule, as is shown in part B, the situation will be different as the atom is now embedded in the molecule. In a first approximation, one can distribute the electron symmetrically among its nearest neighbours ; as a result, a polarization of the remaining charge cloud will occur, thereby changing its shape. The AIM ionization energy will thus be obtained as the difference of the energy of the isolated atom and the positive ion surrounded by negative point charges. All calculations of the neutral atom, the

atom's positive ion surrounded by negative point charges and the atom's negative ion surrounded by positive point charges were performed using the CCSD(T) method (Coupled Cluster Theory with all Single and Double Substitutions and a quasiperturbative correction for triple substitutions) and the 6-31++G(d,p) basis set. For the ion in a field of point charges, the total energy E_{total} has the form :

$$E_{total} = E + \sum_i \frac{Qq_i}{R} - \sum_i \sum_{j \neq i} \frac{q_i q_j}{R_{ij}} \quad (19)$$

where Q is the charge of the ion, q the magnitude of the point charges and E the "self energy" of the ion including any interaction not reproduced by a simple Coulomb law.

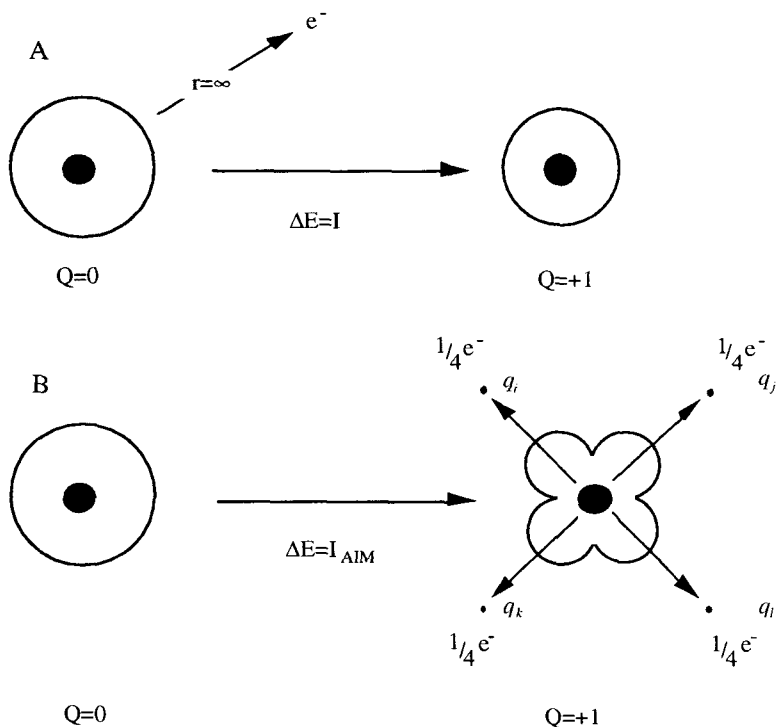


Figure 3. Definition of the ionization energy I for an isolated atom (A) and an atom in a molecule (B). In the first case, the electron is moved to infinite distance and does not interact with the cation. In the latter case, the charge of the electron is distributed in the vicinity of the cation. This results in a deformation of the electron cloud (in this case a tetrahedral one). The definition of an atom-in-molecule electron affinity is analogous.

It has to be remarked that by making this correction, a reasonable approximation to a constant external potential, necessary for the calculation of electronegativity and hardness, is obtained. An analogous reasoning was followed for the electron affinities. Using the ionization energies and electron affinities obtained in this manner, AIM electronegativities and hardnesses were calculated.

In Table 3, the isolated atom data, calculated using equations (16) and (17) are given for the elements H, C, O and Si, which were chosen as test cases in view of our long standing interest on the interaction of small organic molecules with zeolites [79-81].

	χ (eV) exp.	χ (eV) calc.	η (eV) exp.	η (eV) calc.
H	7.18	6.97	6.43	6.60
C	6.27	5.91	5.00	4.99
O	7.54	7.02	6.08	6.04
Si	4.77	4.40	3.38	3.37

Table 3 :CCSD(T)/6-31++G(d,p) electronegativities and hardnesses as compared with experiment.

The atoms-in-molecules hardnesses, calculated using equation (17) and the definition of the AIM ionization energy and electron affinity depicted in Figure 3, were higher than the isolated atom hardness for different coordinations of the point charges considered. This means that the softness and polarizability of an atom in a molecule will be lower than the corresponding isolated atom value. It can indeed be imagined that the change from the spherical symmetrical isolated atom case to the highly non-symmetrical atom-in-a-molecule will decrease the polarizability, thus increasing the hardness. The ratio increases with decreasing distance of the neighbours (point charges) to the atom. In Figure 4, the ratio

η/η_0 is plotted as a function of r for the carbon atom in a tetrahedral coordination. Note that recent findings have indicated that EEM calibrated hardnesses are about 50 % higher than experimental hardnesses. Analytically, the ratio was found to be well represented by the relationship :

$$\eta/\eta_0 = 1 + Ae^{-Br} \quad (20)$$

where the parameters A and B are different for each atom. These parameters were determined for the first row elements. Particularly interesting is the relationship between the polarizability and B , as plotted in Figure 5 for the first row elements. As can be seen, a higher polarizability means a slower fall off of the hardness.

For the electronegativity, a decrease is encountered with respect to the isolated atom case, again function of the distance, i.e. a larger decrease with decreasing distance. Furthermore, it could be noted that going from a tetrahedral to a trigonal and on to a digonal coordination, the increase of the hardness and the decrease of the electronegativity becomes less pronounced.

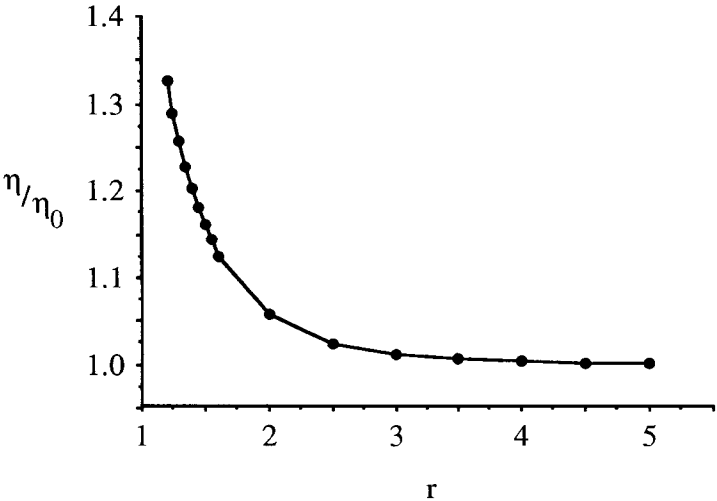


Figure 4. Dependence of the hardening coefficient on the distance of the test charges (Å) for the carbon atom.

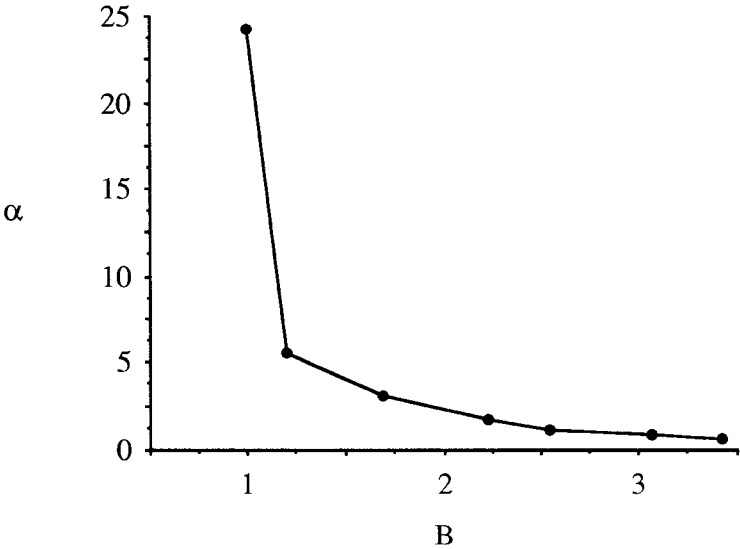


Figure 5. Relationship between the fall-off parameter B of the hardening coefficient and the atomic polarizability a (in 10^{-24} cm^3).

All these findings could ultimately lead to the construction of a non-parametrized electronegativity equalization scheme, permitting the calculation of very large molecular systems. For each element of the periodic table, χ and η values can be tabulated as a function of the distance and the environment and incorporated in a database. Inclusion of these parameters in electronegativity equalization schemes could indeed seriously decrease the degree of empiricism present.

4. RATIONALIZING CHEMICAL INTERACTIONS WITHIN THE HSAB PRINCIPLE

4.1. Introduction : the HSAB Principle

Just like Sanderson's electronegativity equalization principle, the Hard and Soft Acids and Bases principle was originally introduced without strong theoretical basis. Nevertheless, it was used widely from its formulation on. The principle states that hard acids prefer to coordinate with hard bases and soft acids with soft bases [82]. In 1983, Parr and Pearson provided a definition for the chemical hardness [25]

$$\eta = \frac{1}{2} \left(\frac{\partial \mu}{\partial N} \right)_v = \frac{1}{2} \left(\frac{\partial^2 E}{\partial N^2} \right)_v \quad (21)$$

offering possibilities for its quantitative study.

Moreover, a partial proof was provided for the HSAB principle. Consider the formation of a diatomic molecule AB. Upon neglect of the external potential perturbation, the chemical potential change for the atoms A and B will be :

$$\mu_A = \mu_A^0 + 2\eta_A^0 \Delta N_A \quad (22)$$

$$\mu_B = \mu_B^0 + 2\eta_B^0 \Delta N_B \quad (23)$$

Since, after molecule formation $\mu_A = \mu_B$ and $\Delta N = \Delta N_A = -\Delta N_B$, the charge transfer ΔN between A and B at a constant external potential equals

$$\Delta N = \frac{\mu_B^0 - \mu_A^0}{2(\eta_B^0 + \eta_A^0)} \quad (24)$$

The energy change associated with this is

$$\Delta E = -\frac{(\mu_B^0 - \mu_A^0)^2}{4(\eta_B^0 + \eta_A^0)} = -\frac{(\Delta \mu)^2}{2} \frac{S_A S_B}{S_A + S_B} \quad (25)$$

As can be seen, stabilization will be bigger when the softness values are both small, i.e. "soft likes soft".

Two proofs for the HSAB principle were provided under the restriction of a common chemical potential of the reaction partners [83, 84]. Later on, a local HSAB principle was provided by Gazqu   and M  ndez [85]. They showed that the interaction between two chemical species will not necessarily occur through their softest atoms, but through those whose softnesses are approximately equal. In Section 4.2, an intuitive application of the HSAB concept is provided, followed by an application of the local HSAB principle in the interpretation of regioselectivity in Diels Alder reactions.

4.2. The Global HSAB Principle : Stabilization Energies of Endohedral Complexes of C₆₀, Si₆₀ and Ge₆₀ with Monoatomic Cations and Anions.

For the first time, a systematic uniform ab initio study of endohedral complexes of C₆₀, Si₆₀ and Ge₆₀ with monoatomic cations (Li⁺, Na⁺, K⁺ and Rb⁺) and anions (F⁻, Cl⁻, Br⁻ and I⁻) was performed. The 3-21 G level (3-21+G for the anions) was used. This could be achieved by application of the multiplicative integral approximation [86], as implemented in the program BRABO [87]. The sequence studied for the cages bears a close resemblance with isomorphic substitution in zeolites modifying its catalytic activity via bridging hydroxyls. In a first step, the populations of the encapsulated ions were determined via numerical integration. The electron density was integrated from the center of the cage along the C₅ axis to its minimum, which can be considered as the border between the ion and the cage. The results are shown in Table 4.

	C ₆₀	Si ₆₀	Ge ₆₀
Li ⁺	2.004	2.002	2.002
Na ⁺	10.00	9.996	9.997
K ⁺	18.05	18.00	18.00
Rb ⁺	36.05	36.02	36.01
F ⁻	9.920	9.98	9.99
Cl ⁻	17.86	17.98	17.98
Br ⁻	35.78	35.93	35.94
I ⁻	53.72	53.93	53.94

Table 4 : Atomic population (in a.u.) of the ions within the different fullerene cages, as determined from numerical integration.

As can be seen, the populations are very close to the isolated ion populations. Almost no charge transfer occurs between the ions and the surrounding cage, justifying the term "endohedral complexes". Moreover, it turned out that the typical shell structure of the ions is completely conserved. In a second step, the complexation energies ΔE were computed as :

$$\Delta E = E_{X^+Y_{60}} - (E_{X^+} + E_{Y_{60}}) \quad (26)$$

where a correction for the so-called basis set superposition error (BSSE) [88] was applied. The complexation energies can be found in Table 5.

Ion	$\Delta E_{C_{60}}$	$\Delta E_{Si_{60}}$	$\Delta E_{Ge_{60}}$
Li ⁺	-9.37	-30.27	-23.37
Na ⁺	-8.66	-30.30	-29.86
K ⁺	-2.21	-30.36	-29.83
Rb ⁺	3.90	-30.09	-22.34
F ⁻	-22.54	6.69	6.73
Cl ⁻	-5.29	5.49	5.97
Br ⁻	7.73	4.45	5.24
I ⁻	39.27	5.02	5.55

Table 5 : BSSE corrected stabilization energies of the endohedral complexes. All values are in kcal/mol.

As can be seen, for C_{60} , the largest stabilization occurs for F^- . The positive ions are also stabilized, but to a lesser extent. In Si_{60} and Ge_{60} however, it appears that the positive ions are the most stabilized. These findings indicate that the electrostatic potential within the C_{60} cage should be positive, whereas in Si_{60} and Ge_{60} , it should be negative. As a test, the molecular electrostatic potential in the three cages was calculated along the C_5 symmetry axes. It was indeed encountered that the electrostatic potential in C_{60} is positive, in contrast with Si_{60} and Ge_{60} [59]. This finding confirms the double layer model proposed by Cioslowski [89] stating that C_{60} can be considered as a double layer, with the electrons located outside the cage. For Si_{60} and Ge_{60} , an inversion of this layer seems to occur.

Finally, the influence of the cage and guest ion hardness on the complexation energies was studied. In a first step, the hardness of the fullerene cage was calculated using ionization energies and electron affinities from Koopmans' theorem. It was found that $\eta_{C_{60}} > \eta_{Si_{60}} > \eta_{Ge_{60}}$. Within the C_{60} cage, the stabilization energy within the two ion series goes as follows : $Rb^+ < K^+ < Na^+ < Li^+$ and $I^- < Br^- < Cl^- < F^-$, which runs parallel with the ion hardnesses ($\eta_{Rb^+} < \eta_{K^+} < \eta_{Na^+} < \eta_{Li^+}$ and $\eta_{I^-} < \eta_{Br^-} < \eta_{Cl^-} < \eta_{F^-}$). It thus appears that in this case, within each ion series, the hardest ion is stabilized the most. In Si_{60} and Ge_{60} , a partial inversion of this sequence occurs, indicating a larger stabilization (or a smaller destabilization) for the softest ions. These trends can be explained using the HSAB principle. Within the hardest cage, the hardest ions will be stabilized to a larger extent, whereas in the softer cages, the softest ions will be more stabilized. As a test, the local hardness $\tilde{\eta}(r)$, approximated as [90] :

$$\tilde{\eta}(r) \approx -\frac{1}{2N} \int \frac{\rho(r')}{|r-r'|} dr' \quad (27)$$

was calculated at the center of the three fullerene cages. The results are shown in Table 6.

Molecule	η	$\tilde{\eta}(r) (r=0)$
C ₆₀	3.81	0.0751
Si ₆₀	2.22	0.0477
Ge ₆₀	2.13	0.0450

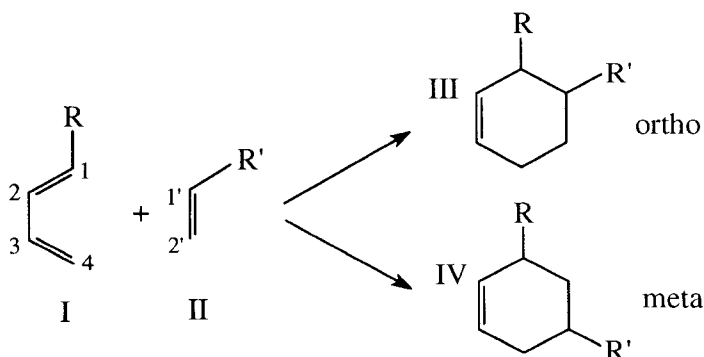
Table 6 : Global hardness (eV), together with the local hardness at the center of the fullerene cage (a.u.).

As can be seen, the local hardness at the cage centre is indeed the largest for C₆₀, in accordance with the stabilization energies for the ions.

4.3. The HSAB Principle at a Local Level : Regioselectivity of Diels-Alder Reactions

4.3.1. Introduction

The Diels-Alder reaction, a pericyclic reaction between a diene and a dienophile, is of utmost importance in synthetic organic chemistry. In the case of a reaction between asymmetrically substituted dienes (I) and asymmetrical dienophiles (II) :

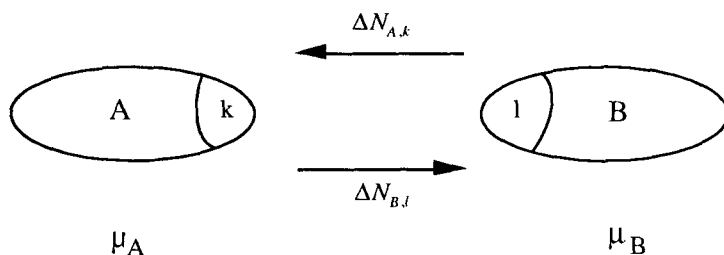


it is already known for a long time that the formation of one of the two possible regio isomers (III) will predominate or that the ortho isomer will be formed exclusively. Since the ortho product is more crowded, one can consider it as a kinetic product, formed via a concerted mechanism. Numerous FMO studies (for a listing of references, see [60]), considering HOMO-LUMO orbital interactions, have been conducted in the past concerning the regioselectivity and reaction rate of this reaction. In this part, DFT based reactivity descriptors

are used to interpret the orientation in Diels-Alder reactions. Moreover, the HSAB principle will be applied in a local sense.

4.3.2. The Local HSAB Principle : Importance of Equal Softness Between Reaction Sites

The work by Gazqu   and M  ndez [85], later on completed by our group in collaboration with M  ndez uses a DFT formalism to formulate simple requirements which should be obeyed if a local HSAB principle is at work. Consider two systems A and B interacting through atoms k and l and with chemical potentials μ_A and μ_B :



Adopting an atoms in molecules viewpoint, the atoms can be regarded as "open subsystems" and it thus becomes natural to use the grand potential Ω_i [83] as the basic thermodynamic function to describe the system :

$$\Omega_i = E_i - \mu_i(N_i - N_i^0) \quad (28)$$

Neglecting changes in the external potential, the energy changes of atom k in molecule A and atom l in molecule B can be written as :

$$\Delta E_{A,k} = \mu_A \Delta N_{A,k} + \eta_{A,k} (\Delta N_{A,k})^2 \quad (29)$$

$$\Delta E_{B,l} = \mu_B \Delta N_{B,l} + \eta_{B,l} (\Delta N_{B,l})^2 \quad (30)$$

Note that μ_A and μ_B do not depend on k or l as the chemical potential is equalized throughout the system (which is not the case for the hardness). Turning to the grand potential, one obtains after some algebra :

$$\Delta \Omega_{A,k} = -\frac{1}{2} \frac{(\mu_B - \mu_A)^2}{(s_{A,k} + s_{B,l})} s_{A,k} s_{B,l}^2 \quad (31)$$

$$\Delta\Omega_{B,l} = -\frac{1}{2} \frac{(\mu_B - \mu_A)^2}{(s_{A,k} + s_{B,l})} s_{B,l} s_{A,k}^2 \quad (32)$$

with

$$\Delta\Omega_{tot} = \Delta\Omega_{A,k} + \Delta\Omega_{B,l} \quad (33)$$

It should be noted that $\Delta\Omega_{tot} = \Delta E_{tot}$, indicating that the energy change governing reactivity equals the change in grand potential more suited to describe the evolution of the open system type "atoms in molecules". Minimization of $\Delta\Omega_{A,k}$ with respect to $s_{A,k}$ for fixed $\mu_B - \mu_A$ and $s_{B,l}$ yields the demand that

$$s_{A,k} = s_{B,l} \quad (34)$$

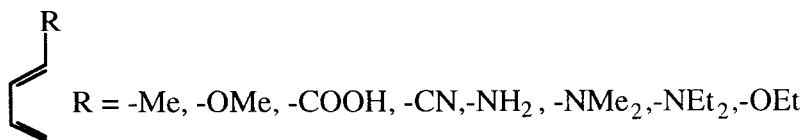
i.e. the softness values of the interacting centers should be as close as possible. In the final energy change,

$$\Delta E_{A,k} + \Delta E_{B,l} = -\frac{1}{2} (\mu_B - \mu_A)^2 \frac{s_{A,k} s_{B,l}}{s_{A,k} + s_{B,l}} \quad (35)$$

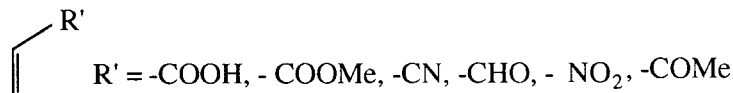
a proportionality with $s_{A,k}$ (or $s_{B,l}$) is noted indicating that the regioselectivity is governed by the closeness of the local softness values, the energy gain (cf. the sign in front of the total expression) by the actual softness value.

4.3.3. Results and Discussion

In order to test the above mentioned principle, we applied the theory to a series of 48 Diels Alder reactions. The following systems were considered :



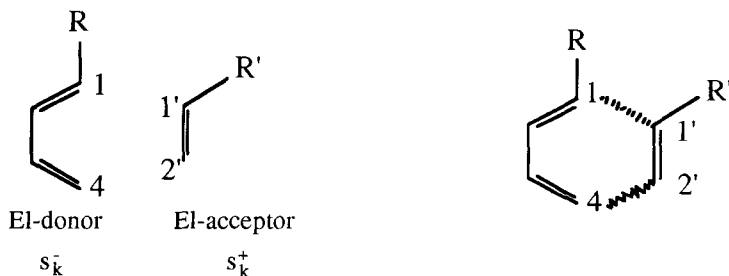
and



This gives rise to 48 cases, all of the NED (Normal Electron Demand) type (i.e. where the diene is the electron donor and the dienophile is the electron acceptor), which was checked by inspecting the HOMO and LUMO energies of the systems.

All geometries were optimized at the Hartree-Fock 3-21G level.

Suppose we have the following interaction between an electron acceptor and an electron donor :



Starting from the idea that the softness of the interacting atoms should be as close as possible, we considered the following expressions :

$$S_{ortho} = (s_1^- - s_{1'}^+)^2 + (s_4^- - s_{2'}^+)^2 \quad (36)$$

$$S_{meta} = (s_1^- - s_{2'}^+)^2 + (s_4^- - s_{1'}^+)^2 \quad (37)$$

and we looked for the smaller value of both expressions. The smaller the expression, the more likely the interaction they describe should occur. This procedure is in fact looking for a simultaneous fulfillment of local HSAB at both termini. It turned out that in the 48 cases considered, $S_{ortho} < S_{meta}$, except when the cyano group is present either in the diene and the dienophile. A first reason that could be invoked for this is the lack of correlation treatment in the calculations. The CN group is known to demand for a highly correlated treatment, as for example witnessed in our group properties study where the CN group was systematically an outlier. However, another aspect that should be mentioned is that the methodology is based on synchronicity : both couples of the reactive termini are attributed an identical role. Since concertedness is not a synonym for synchronicity, we looked for the smallest quadratic form of the four terms in (36) and (37). It appears that $(s_4^- - s_{2'}^+)^2$ is the smallest in the large majority of cases leading to the ortho products, which is at first sight not that unexpected in this sense that those carbon atoms are most remote from the substituents R and R'. They thus will be less influenced by their electronic effect, and as a result, be closer in local softness. This result may suggest an asynchronous mechanism, i.e. the bond forming between 2' and 4 may proceed faster than the bond formation between 1 and 1'. This point is strengthened by

the results of transition state calculations which invariably indicate that the C4-C2' bond distance is smaller than the C1-C1' distance, except for the parent reaction between ethene and 1,4-butadiene where both theory and experiment are conclusive for a concerted, synchronous mechanism. Combining the demand for the smallest of the quadratic forms with that of S_{ortho} and S_{meta} , one retrieves the correct regioselectivity for 47 cases., only one CN case remaining. In conclusion, it can be stated that ab initio calculated DFT concepts, together with the use of the local HSAB principle, permitted us to test the validity of a long pending hypothesis by Anh [91], stating that "it is likely that the first bond would link the softest centers". However, the hypothesis is only partially confirmed and should be modulated by the demand for local softness equalization between interacting centers.

5. CONCLUSIONS

We may state that DFT based concepts and techniques are of ever increasing importance in the study of electronic structure and charge distributions of molecular systems, both in inorganic, organic and biochemistry. Concepts can be used to rationalize chemical interactions both in their kinetic and thermodynamic aspects, whereas DFT techniques nowadays offer the possibility to carry out high quality (correlation included) quantum chemical studies starting from first principles for systems of ever increasing size, due to their more interesting quality cost ratio than wave function methods.

ACKNOWLEDGEMENTS

Besides his coauthors, PG wishes to acknowledge Dr. G. Van De Woude, and his Ph. D. student S. Damoun who contributed to the work described in Section 4.3. This contribution is however also an occasion to thank the other Ph. D. and graduate students (K. Choho, A. Baeten, G. Van Lier, B. Safi, F. Tielens, K. Demel, S. Amira, P. De Meester, N. Coussement, J. Peirs, S. Verhaeren and G. Boon) who contributed a lot to the development of the research activities around fundamental and applied aspects of DFT in recent years. Stimulating discussions and/or collaborations with Professor R. Schoonheydt, Professor W. Mortier (Catholic University of Leuven), Professor F. Méndez (University of Mexico City), Professor C. Van Alsenoy (University of Antwerp) are gratefully acknowledged. Professor Parr (University of North Carolina) is thanked for many years of intellectual support to the group. The Fund for Scientific Research - Flanders (Belgium) F.W.O and the Free University of Brussels are thanked for continuous financial support. FDP and WL are grateful to the Fund for Scientific Research - Flanders (Belgium) for positions as research assistant and postdoctoral fellow (FDP) and postdoctoral fellow (WL) respectively.

REFERENCES

1. R. G. Parr and W. Yang, *Density Functional Theory of Atoms and Molecules* (Oxford University Press, New York, 1989).
2. R. M. Dreizler and E. K. U. Gross, *Density Functional Theory* (Springer-Verlag, Berlin Heidelberg, New York, 1990).
3. *Density Functional Methods in Chemistry*, edited by J. Labanowski and J. Andzelm (Springer-Verlag, New York), 1991.
4. T. Ziegler, *Chem. Rev.* **91**, 651 (1991).
5. *Theoretical and Computational Chemistry, Vol. 2., Modern Density Functional Theory ; A Tool for Chemistry*, edited by P. Politzer and J. Seminario (Elsevier, Amsterdam, 1995).
6. R. G. Parr and W. Yang, *Ann. Rev. Phys. Chem.* **46**, 107 (1995).
7. W. Kohn, A. D. Becke and R. G. Parr, *J. Phys. Chem.* **100**, 12974 (1996).
8. C. C. Roothaan, *Rev. Mod. Phys.* **32**, 179 (1960).
9. J. C. Slater, *Phys. Rev.* **81**, 385 (1951).
10. Hohenberg, P. ; Kohn, W. *Phys. Rev. B* **136**, 864 (1964).
11. P. O. Löwdin, *Int. J. Quant. Chem. Symp.* **19**, 19 (1986).
12. W. Kohn and L. J. Sham *Phys. Rev. A* **140**, 1133 (1965).
13. R. Neumann, R. H. Nobes and N. C. Handy, *Mol. Phys.* **87**, 1 (1996).
14. A. D. Becke on American Chemical Society - DFT Symposium, San Francisco, USA, April, 1997.
15. J. Andzelm and E. Wimmer, *J. Chem. Phys.* **96**, 1280 (1991).
16. J. Baker, M. Muir and J. Andzelm, *J. Chem. Phys.* **102**, 2063 (1995).
17. F. De Proft, J. M. L. Martin and P. Geerlings, *Chem. Phys. Lett.* **250**, 393 (1996).
18. P. Geerlings, F. De Proft and J. M. L. Martin in *Theoretical and Computational Chemistry, Vol. 5. Recent Developments in Density Functional Theory*, edited by J. Seminario (Elsevier, 1996), p. 773-809.
19. F. De Proft, J. M. L. Martin and P. Geerlings, *Chem. Phys. Lett.* **256**, 400 (1996).
20. (a) B. G. Johnson, P. M. W. Gill and J. A. Pople, *J. Chem. Phys.* **98**, 5612 (1993).
(b) M. J. Frisch, G. W. Trucks and J. R. Cheeseman, in *Theoretical and Computational Chemistry, Vol. 5. Recent Developments in Density Functional Theory*, edited by J. Seminario (Elsevier, 1996), p. 679-707.
21. R. G. Parr, R. A. Donnelly, M. Levy and W. E. Palke, *J. Chem. Phys.* **69**, 3801 (1978).
22. L. Pauling, *The Nature of the Chemical Bond* (Cornell University Press, Ithaca, New York, 1960).
23. R. S. Mulliken, *J. Chem. Phys.* **2**, 782 (1934).
24. For a detailed review of the different electronegativity scales, see e.g. J. Mullay in *Electronegativity (Structure and Bonding, Vol. 66)*, edited by K. D. Sen and C. K. Jørgenson (Springer-Verlag, Berlin Heidelberg, 1987), p.1.
25. R. G. Parr and R. G. Pearson, *J. Am. Chem. Soc.* **105**, 1503 (1983).
26. W. Yang and R. G. Parr, *Proc. Natl. Acad. Sci. USA* **82**, 6723 (1985).
27. R. G. Parr and L. J. Bartolotti, *J. Phys. Chem.* **87**, 2810 (1983).
28. R. G. Parr and W. Yang, *J. Am. Chem. Soc.* **106**, 4049 (1984).

29. C. Lee, W. Yang and R. G. Parr., *J. Mol. Struct. (Theochem)* **163**, 305 (1987).
30. F. De Proft and P. Geerlings, *J. Phys. Chem.* **A101**, 5344 (1997).
31. B. G. Baekelandt, A. Cedillo and R. G. Parr, *J. Chem. Phys.* **103**, 8548 (1995).
32. E. Besalú, R. Carbó, J. Mestres and M. Solà in *Molecular Similarity I (Topics in Current Chemistry, Vol. 173)* (Springer-Verlag, Berlin Heidelberg, 1995), p.31.
33. G. Boon, F. De Proft, W. Langenaeker and P. Geerlings, in preparation.
34. W. Langenaeker, M. De Decker, P. Raeymaekers and P. Geerlings, *J. Mol. Struct. (Theochem)* **207**, 115 (1990).
35. W. Langenaeker, K. Demel and P. Geerlings, *J. Mol. Struct. (Theochem)* **234**, 329 (1991).
36. W. Langenaeker, K. Demel and P. Geerlings, *J. Mol. Struct. (Theochem)* **259**, 317 (1992).
37. M. Tielemans, V. Areschka, J. Colomer, R. Promel, W. Langenaeker and P. Geerlings, *Tetrahedron* **48**, 10575 (1992).
38. K. Choho, W. Langenaeker, G. Van de Woude and P. Geerlings, *J. Mol. Struct. (Theochem)* **338**, 293 (1995).
39. K. Choho, W. Langenaeker, G. Van de Woude and P. Geerlings, *J. Mol. Struct. (Theochem)* **362**, 305 (1996).
40. W. Langenaeker, F. De Proft and P. Geerlings, *J. Phys. Chem.* **99**, 6424 (1995).
41. F. De Proft, W. Langenaeker and P. Geerlings, *J. Phys. Chem.* **97**, 1826 (1993).
42. F. De Proft, W. Langenaeker and P. Geerlings, *J. Mol. Struct. (Theochem)* **339**, 45 (1995).
43. A. Baeten and P. Geerlings, *J. Mol. Struct. (Theochem)*, submitted.
44. W. Langenaeker, N. Coussement, F. De Proft and P. Geerlings, *J. Phys. Chem.* **98**, 3010 (1994).
45. F. De Proft, S. Amira, K. Choho and P. Geerlings, *J. Phys. Chem.* **98**, 5227 (1994).
46. F. De Proft, W. Langenaeker and P. Geerlings, *Tetrahedron* **51**, 4021 (1995).
47. S. Damoun, W. Langenaeker, G. Van de Woude and P. Geerlings, *J. Phys. Chem.* **99**, 12151 (1995).
48. F. De Proft, W. Langenaeker and P. Geerlings, *Int. J. Quant. Chem.* **55**, 459 (1995).
49. K. Choho, G. Van Lier, G. Van de Woude and P. Geerlings, *J. Chem. Soc., Perkin Trans. II*, 1723 (1996).
50. A. Baeten, F. De Proft, W. Langenaeker and P. Geerlings, *J. Mol. Struct. (Theochem)* **306**, 203 (1994).
51. A. Baeten, F. De Proft and P. Geerlings, *Chem. Phys. Lett.* **235**, 17 (1995).
52. A. Baeten, F. De Proft and P. Geerlings, *Int. J. Quant. Chem.* **60**, 931 (1996).
53. P. Geerlings, F. De Proft and P. Geerlings in *Density Functional Methods : Applications in Chemistry and Materials Science*, edited by M. Springborg (Wiley, New York, 1997), Chapter 2.

54. P. Geerlings, W. Langenaeker, F. De Proft and A. Baeten in *Theoretical and Computational Chemistry, Vol. 4. Molecular Electrostatic Potentials - Concepts and Applications*, edited by J. S. Murray and K. D. Sen (Elsevier, 1996), p. 587-617.
55. R. G. Pearson, *Science* **151**, 172 (1987).
56. R. G. Pearson, *Hard and Soft Acids and Bases* (Stroudsburg : Dowden, Hutchinson and Ross, 1973).
57. F. De Proft and P. Geerlings, *J. Chem. Phys.* **106**, 3270 (1997).
58. H. Toufar, K. Nulens, G. O. A. Janssens, W. J. Mortier, R. A. Schoonheydt, F. De Proft and P. Geerlings, *J. Phys. Chem.* **100**, 15383 (1996).
59. F. De Proft, C. Van Alsenoy and P. Geerlings, *J. Phys. Chem.* **100**, 7440 (1996).
60. S. Damoun, G. Van de Woude, F Méndez and P. Geerlings, *J. Phys. Chem.* **A101**, 886 (1997).
61. P. K. Chattaraj, A. Cedillo and R. G. Parr, *J. Chem. Phys.* **103**, 7645 (1995)
62. *Electronegativity (Structure and Bonding, Vol. 66)*, edited by K. D. Sen and C. K. Jørgenson (Springer-Verlag, Berlin Heidelberg, 1987).
63. *Chemical Hardness (Structure and Bonding, Vol. 80)*, edited by K. D. Sen (Springer-Verlag, Berlin Heidelberg, 1993).
64. A. D. Becke, *J. Chem. Phys.* **98**, 5648 (1993).
65. P. J. Stevens, F. J. Devlin, C. F. Chablowski and M. J. Frisch, *J. Phys. Chem.* **98**, 11623 (1994).
66. J. P. Perdew and Y. Wang, *Phys. Rev. B* **45**, 13244 (1992).
67. C. Lee, W. Yang and R. G. Parr, *Phys. Rev. B* **37**, 785 (1988).
68. T. H. Dunning, *J. Chem. Phys.* **90**, 1007 (1989).
69. R. A. Kendall, T. H. Dunning, R. J. Harrison, *J. Chem. Phys.* **96**, 6797 (1992).
70. L. A. Curtiss, K. Raghavachari, G. W. Trucks and J. A. Pople, *J. Chem. Phys.* **94**, 7221 (1991).
71. W. J. Hehre, L. Radom, P. v. R. Schleyer and J. A. Pople, *Ab Initio Molecular Orbital Theory*, (Wiley, New York, 1986).
72. K. Raghavachari, G. W. Trucks, J. A. Pople and M. Head-Gordon, *Chem. Phys. Lett.* **157**, 479 (1989).
73. R. T. Sanderson, *Chemical Bonds and Bond Energy* (Academic Press, New York, 1976).
74. R. T. Sanderson, *Polar Covalence* (Academic Press, New York, 1983).
75. P. Politzer and H. Weinstein, *J. Chem. Phys.* **71**, 4218 (1979).
76. W. J. Mortier, S. K. Ghosh and S. Shankar, *J. Am. Chem. Soc.* **108**, 4315 (1986).
77. W. J. Mortier in *Electronegativity, Electronegativity (Structure and Bonding, Vol. 66)*, edited by K. D. Sen and C. K. Jørgenson (Springer-Verlag, Berlin Heidelberg, 1987), p. 125.
78. K. A. Van Genechten, W. J. Mortier and P. Geerlings, *J. Chem. Phys.* **86**, 5063 (1987).
79. P. Geerlings, N. Tariel, A. Botrel, R. Lissilour and W. J. Mortier, *J. Phys. Chem.* **88**, 5752 (1984).

80. J. Datka, P. Geerlings, W. J. Mortier and P. A. Jacobs, *J. Phys. Chem.* **89**, 3483 (1985).
81. J. Datka, P. Geerlings, W. J. Mortier and P. A. Jacobs, *J. Phys. Chem.* **89**, 3488 (1985).
82. R. G. Pearson, *J. Am. Chem. Soc.* **85**, 3533 (1963).
83. P. K. Chattaraj, H. Lee and R. G. Parr, *J. Am. Chem. Soc.* **113**, 1855 (1991).
84. P. K. Chattaraj and R. G. Parr in *Chemical Hardness (Structure and Bonding, Vol. 80)*, edited by K. D. Sen (Springer-Verlag, Berlin Heidelberg, 1993), p. 12.
85. J. L. Gazqu  ez and F. M  endez, *J. Phys. Chem.* **98**, 459 (1994).
86. C. Van Alsenoy, *J. Comput. Chem.* **9**, 620 (1988).
87. C. Van Alsenoy and A. Peeters, *J. Mol. Struct. (Theochem)* **286**, 19 (1993).
88. (a) S. F. Boys and F. Bernardi, *Mol. Phys.* **19**, 553 (1970).
(b) F. B. Van Duijneveldt, J. G. C. M. Van Duijneveldt-Van De Rijdt and J. H. Van Lenthe, *Chem. Rev.* **94**, 1873 (1994).
89. J. Cioslowski and E. Fleischmann, *J. Chem. Phys.* **94**, 3730 (1991).
90. M. Berkowitz, S. K. Ghosh and R. G. Parr, *J. Am. Chem. Soc.* **107**, 6811 (1985).
91. O. Eisenstein, J. M. Lefour, N. T. Anh and R. F. Hudson, *Tetrahedron* **33**, 523 (1977).

Pure and Mixed Pb Clusters of Interest for Liquid Ionic Alloys

L. M. Molina, M. J. López, A. Rubio, L. C. Balbás,
and J. A. Alonso

*Departamento de Física Teórica. Universidad de Valladolid,
47011 Valladolid, Spain.*

Abstract

Ab initio Density Functional calculations for free Pb_n ($n = 3 - 14$), Na_nPb and Na_nPb_4 clusters are reported. In the case of pure lead clusters, stability maxima are found for Pb_7 , Pb_{10} and Pb_{13} , in agreement with the experimental abundance found in the mass spectra. A trend governed by icosahedral-like packing explains the ground state geometries. In the case of mixed sodium-lead clusters, high stability is predicted for Na_4Pb and Na_4Pb_4 , giving a hint for the presence of those units in the liquid alloys. A transition between a rhombus and a tetrahedral arrangement occurs in Pb_4 as a consequence of adding Na atoms to that unit.

1 Introduction

Some interesting effects associated to the presence of well-defined structural units appear on a broad class of binary alloys formed by mixing an alkali metal (Li, Na, K, Rb, Cs) with a tetravalent metal like Sn or Pb. Due to the large difference in electronegativities it is normally assumed that one electron is transferred from the alkali to the tetravalent atom. As the Sn^- or Pb^- anions are isoelectronic with the P and As atoms, which in the gas phase form tetrahedral molecules P_4 and As_4 , in the same way the anions group in the crystal compounds forming $(\text{Sn}_4)^{4-}$ and $(\text{Pb}_4)^{4-}$ tetrahedra, separated by the alkali cations. This building principle was developed by Zintl in the early thirties [1], and the presence of such tetrahedra has been detected in the equiatomic solid compounds of Pb and Sn with Na, K, Rb and Cs, but not with Li [2, 3, 4]. In this paper we focus on alkali-lead alloys.

Considerable evidence exists of the survival of Zintl ions in the liquid alloy. Neutron diffraction measurements [5], as well as molecular dynamics simulations [6, 7], give structure factors and radial distribution functions in agreement with the existence of a superstructure which has many features in common with a disordered network of tetrahedra. Resistivity plots against Pb concentration [8] show sharp maxima at 50% Pb in K-Pb, Rb-Pb and Cs-Pb. However, for Li-Pb and Na-Pb the maximum occurs at 20% Pb, and an additional shoulder appears at 50% Pb for Na-Pb. This means that Zintl ion formation is a well-established process in the K, Rb and Cs cases, whereas in the Li-Pb liquid alloy only Li_4Pb units (octet complex) seem to be formed. The Na-Pb alloy is then a transition case, showing coexistence of Na_4Pb clusters and $(\text{Pb}_4)^{4-}$ ions and the predominance of each one of them near the appropriate stoichiometric composition. Measurements of other physical properties like density, specific heat, and thermodynamic stability show similar features (peaks) as a function of composition, and support also the change of stoichiometry from the octet complex to the Zintl clusters between Li-Pb and K-Pb [8].

In this work we study a number of isolated clusters which may be relevant for understanding the clustering in the liquid alloys. Of course, the behaviour of those clusters in the alloy may be more complicated due to the interaction with the condensed medium, but by studying free clusters we expect to obtain useful information about the tendency of the atoms to cluster in the alloy. A preliminary calculation [9] using the Density Functional Formalism (DFT) [10, 11] and a simplified model for the cluster structure [12] has confirmed the high stability of the A_4Pb and A_4Pb_4 species (with $\text{A} = \text{Li}, \text{Na}, \text{K}, \text{Rb}, \text{Cs}$). However, the drastic simplification of the cluster structure used in that model calls for more accurate calculations. Consequently, in this work we report the results of *ab initio* molecular-dynamics DFT calculations.

The paper is divided in two parts. First (Sections 2 and 3), we have focussed our attention on the behaviour of pure lead clusters. Those clusters have been the subject of intense experimental research. Then, we consider that an *ab initio* study of small Pb_n clusters would be useful for understanding the Pb-Pb bonding. The second part of the paper (Sections 4 and 5) is dedicated to the study of mixed Na-Pb clusters.

2 Pb_n clusters: Computational details

We have performed calculations using *ab initio* total energy pseudopotential methods [13]. A Car-Parrinello-like scheme has been used for energy minimization [14]. Specifically, we made use of the fhi96md program, written by

Scheffler and coworkers [15, 16]. This code incorporates the LDA (Local Density Approximation) exchange-correlation functional, parametrized by Perdew and Zunger [17] from the electron gas results of Ceperley and Alder [18]. Hamann's generalized norm-conserving nonlocal pseudopotentials [19] with the Kleinman-Bylander decomposition [20] were constructed, attending to obtain good transferability and plane-wave convergence. The norm conserving pseudopotentials ensure that the integrals of the square amplitudes of the real and the pseudo wavefunctions inside the core regions are identical. The pseudopotentials are spin-averaged scalar relativistic potentials with d as local component. Then, spin polarization effects are omitted in the cluster calculations. This approximation induces some problems for small lead clusters, where spin-orbit effects are sometimes nonnegligible. These are specially important for Pb_2 , as reviewed by Balasubramanian [21] and by Bastug et al [22]. We have found that in order to obtain accurate cohesive energies a spin-polarized lead atom must be used as a reference energy. This procedure seems to work for Pb_n clusters with $n \geq 4$, although for Pb_2 (its ground state is a triplet) and Pb_3 the spin effects neglected here are essential to get accurate results. Scalar-relativistic calculations as the ones performed here give reasonable static structural results for the different structural phases of bulk lead; however, the spin-orbit interaction tends to change the total energy differences between structures without changing their relative ordering. Thus spin-orbit interactions are important to describe structural phase transitions [23] and less relevant for static geometrical optimization.

The calculations employed a supercell geometry with a simple cubic cell of lattice constant equal to 34 a.u., in order to minimize cluster-cluster interactions. This lattice constant appears to be large enough in most cases. However, for the largest Pb_n clusters ($n = 13, 14$) a bigger cubic cell with lattice constant of 38 a.u. was utilized. The calculations were performed using a plane wave basis set with a kinetic energy cutoff of 8 Rydbergs and a single Γ k -point. We have checked that energy differences converge much better than total energies. So, with a cutoff of 8 Rydbergs we can obtain accurate cohesive energies and evaporation energies. Comparison between calculated and experimental data, that confirms the good election of the computational parameters, is given in the next section.

3 Pb_n clusters: results

Several mass-spectrometry measurements for small Pb_n^+ clusters have shown high abundance peaks at $n = 7, 10, 13, 17$ and 19 [24, 25, 26, 27, 28]. This is due to the enhanced stability of the respective neutral species. However,

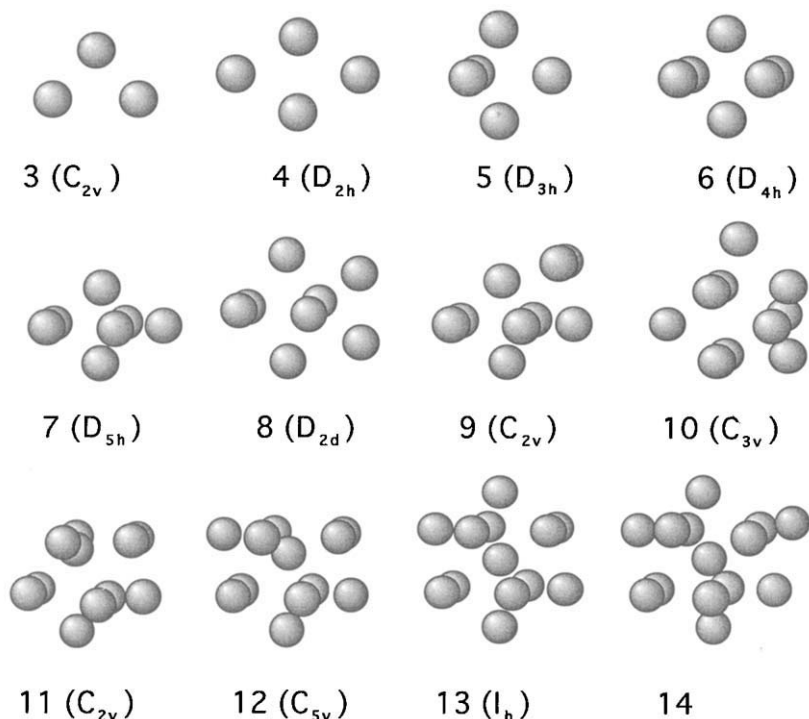


Figure 1: Calculated lowest energy structures of Pb_n ($n = 3 - 14$).

the origin of that stability is not yet completely established. Crystalline Pb is close-packed, and Phillips [29] has proposed that the stability for $n = 7, 13, 19$ could be explained by a packing effect (notice that $n = 13$ and 19 are magic numbers of inert gas clusters). On the other hand, an electronic shell filling effect has been proposed for $n = 10$ and 17 by the same author: Pb is a tetravalent atom, so that Pb_{10} and Pb_{17} have 40 and 68 valence electrons respectively, which are shell-closing numbers of the spherical jellium model. Then, the influence of electronic effects has to be considered in interpreting the stabilities of lead clusters, though the interplay between electronic and packing effects remains to be studied.

We have performed calculations for Pb_n clusters in the range $n = 3 - 14$. Apart from the interest in the relative stabilities, we are in particular interested in investigating the properties of Pb_4 , which is relevant for the study of Zintl complexes below. For each cluster size, several reasonable starting structures were selected, and each of those was relaxed following a damped molecular

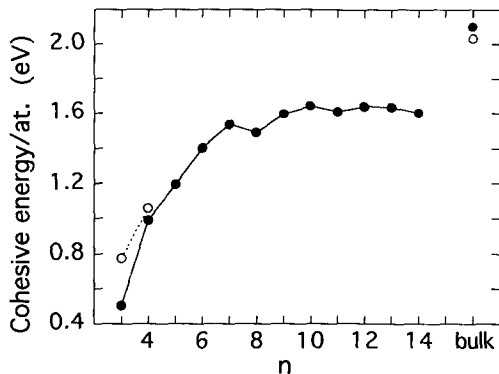


Figure 2: Cohesive energy (per atom) of Pb_n and bulk Pb. Filled circles: calculations. Empty circles: experiment.

dynamics scheme until equilibrium was achieved, that is, until the forces on all atoms are zero. Although it is not sure that we have explored all the low-lying isomers, we are confident of having obtained the lowest energy structure in each case. The minimum energy structures and their symmetries are shown in Fig. 1. Pb_4 has a planar (rhombus) structure and three dimensional structures begin at Pb_5 . Starting with Pb_7 , which is a pentagonal bipyramid, the Pb clusters follow a growth pattern based on icosahedral packing. The structures of Pb_n ($7 \leq n \leq 13$) are obtained by successively capping adjacent triangular faces on one side of the pentagonal bipyramid. Pb_{13} is a perfect icosahedron with a central atom and Pb_{14} is obtained by adding one atom to the surface of Pb_{13} . This distorts the icosahedron a little, by enlarging one of the Pb-Pb distances, which leaves some space for the extra atom to become close enough to form part of the surface layer. The geometries for Pb_7 and Pb_{13} proposed by Phillips [29] agree with the ones found here. The only two exceptions in the icosahedral growth sequence are Pb_8 and Pb_{10} . The geometry of Pb_8 has D_{2d} symmetry and can be viewed as formed by intersecting orthogonally two equal trapezia. Pb_{10} , on the other hand, is a triangular prism with one atom capping each of the lateral faces of the prism and the tenth atom capping one of the triangular bases. This structure can be viewed as a distortion of a C_{3v} structure corresponding to 10 atoms in the icosahedral growth sequence described above. It is worth noticing that the icosahedral growth pattern found here for lead clusters has also been found for other metallic (i.e., nickel [30, 31]) and non-metallic (Lennard-Jones) clusters [32]. What is more, for nickel clusters the only exception in the icosahedral type of growth is Ni_8 which has exactly the same geometry as the one found here for Pb_8 . The icosahedral packing seems

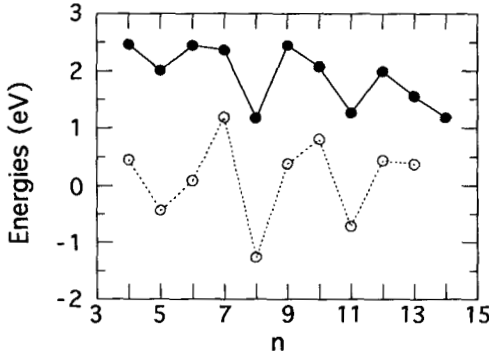


Figure 3: Evaporation energy (upper curve) and stability function (lower curve) for Pb_n clusters (see text).

to be a rather general feature of certain type of small (finite size) systems. In fact icosahedral packing has been described for much larger cluster sizes than the ones considered in this paper.

The cohesive energies per atom

$$E_c(\text{Pb}_n) = \frac{1}{n} [nE(\text{Pb}) - E(\text{Pb}_n)] \quad (1)$$

are given in Fig. 2. These are calculated with respect to the energy of a free Pb pseudoatom obtained by performing a spin-polarized calculation. We also report the calculated and experimental [33] cohesive energies of bulk lead. The calculated bulk cohesive energy is slightly higher than the experimental one, consistent with the known trend of an overestimation of cohesive energies by the LDA. The calculated cohesive energies of Pb_3 and Pb_4 are, nevertheless, smaller than the experimental values [34]. The discrepancy is specially important for the trimer. We ascribe this underestimation to the neglect of spin-polarization and spin-orbit effects in the clusters. Noticing, however, that the errors in the calculated cohesive energies for Pb_4 and for bulk Pb are not large (magnitude equal to 0.07 eV/atom) and of opposite sign, we speculate that the spin polarization and spin-orbit contributions are small except for very small clusters, although we clearly state that the use of nonmagnetic ground states is an assumption of our calculations.

The increase of the cohesive energy per atom with cluster size is fast up to $n = 7$ and then rather slow, and we observe that the value for Pb_{14} is still far from the bulk limit (about 20% lower). In Fig. 3 we plot the energies required

to evaporate a monomer from the Pb_n clusters. These are defined

$$E_v(Pb_n) = E(Pb_{n-1}) + E(Pb) - E(Pb_n), \quad (2)$$

in terms of the total energies of the Pb_n and Pb_{n-1} clusters and the energy of the free atom. E_v fluctuates about the value for the infinite cluster (2.10 eV, the

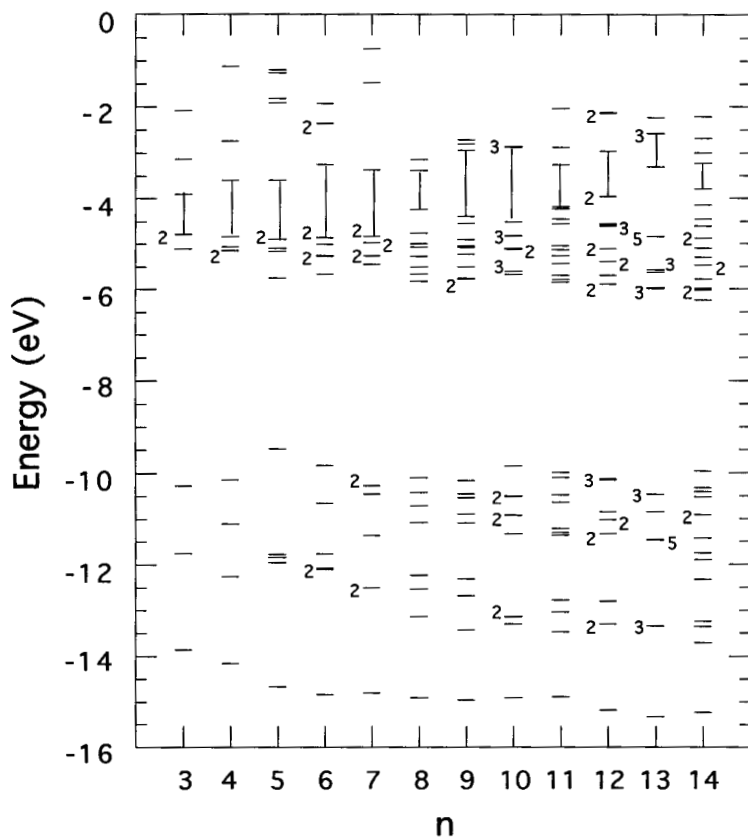


Figure 4: Electronic energy level diagram for Pb_n , $n = 3 - 14$. Degeneracies are indicated by a number attached to the level. A vertical bar indicates the HOMO-LUMO gap.

value of the bulk cohesive energy). Both the cohesive and evaporation energies provide information on the stability of the clusters. We find pronounced minima of E_v at Pb_8 and Pb_{11} . In fact, those two clusters together with Pb_{14} show the

lowest evaporation energies (all the rest have evaporation energies larger than 1.5 eV). This means that in the evaporative cooling stage of the process of cluster formation, the population of Pb₇, Pb₁₀ and Pb₁₃ is expected to become enhanced, as it is observed [24, 25, 26, 27, 28]. It is also traditional to plot the stability function measured by the second derivative of the energy with respect to the number of atoms

$$\Delta_2(n) = E(\text{Pb}_{n-1}) - 2E(\text{Pb}_n) + E(\text{Pb}_{n+1}). \quad (3)$$

This function is plotted as the lower curve in Fig. 3, and Pb₇ and Pb₁₀ are characterized by peaks that indicate their special stability.

A detailed electronic energy level diagram is given in Fig. 4. The main feature is the splitting of the occupied energy levels in two groups separated by a large gap (5.17 eV in Pb₃; 3.72 eV in Pb₁₄). This reflects the gap between the 6s and 6p levels in the free atom, which is 8.4 eV. This is referred in the literature as the relativistic inert-pair effect [21]: the relativistic mass-velocity contraction stabilizes the 6s orbital of the atoms Au to At. As a result the 6s² shell does not participate in the bonding. This effect is recovered in our calculations through the use of scalar relativistic pseudopotentials. The levels below the gap arise from the Pb valence electrons with atomic s-character (the number of doubly occupied levels below the gap is, indeed, equal to n). On the other hand, the levels above the gap correspond to the band formed mainly by the p-electrons of the Pb atom. This p-like band is only partially filled, and a gap (HOMO-LUMO gap) separates occupied from unoccupied states. The HOMO-LUMO gap is indicated in the figure by a vertical bar. The p-band is responsible for the bonding in these clusters. The variations in the magnitude of the HOMO-LUMO gap reflect the variations in stability of the clusters: there is a drastic reduction of the gap from Pb₇ to Pb₈, from Pb₁₀ to Pb₁₁ and to a lesser extent also from Pb₁₃ to Pb₁₄. We conclude that the abundance of Pb₇, Pb₁₀ and Pb₁₃ in the experimental mass spectra is due to an electronic effect: the combination of large HOMO-LUMO gaps for $n = 7, 10, 13$ and small gaps for $n = 8, 11, 14$. This behavior is reflected in the evaporation energies, and the abundance of Pb₇, Pb₁₀ and Pb₁₃ is enhanced by the easy evaporation from Pb₈, Pb₁₁ and Pb₁₄ respectively. Of course, the geometrical structure is intrinsically linked to the behavior of the HOMO-LUMO gaps. Connecting the energy level diagram with the simple electronic shell model is not possible in most cases. Only for Pb₁₃, which is the most spherical cluster, the level degeneracies suggest interpreting the calculated electronic structure as a jellium-like shell filling (1s)² (1p)⁶ (1d)¹⁰ (2s)² (2p)⁶ (1f)¹⁴ (2d)¹⁰ (3s)². But since this is an exceptional case we conclude that the electronic structure of Pb clusters cannot be directly interpreted by the jellium model.

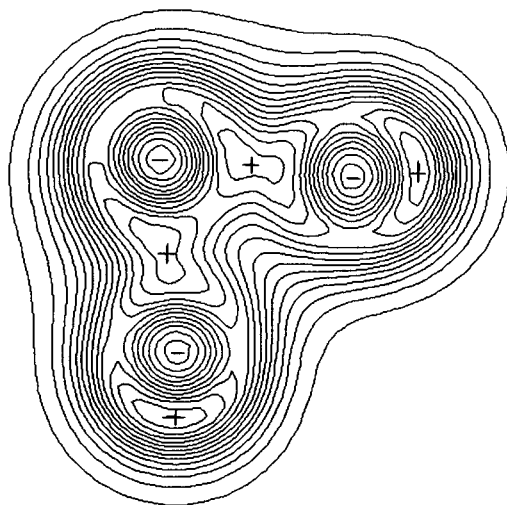


Figure 5: Electron density contours in the plane containing the three nuclei of Pb_3 . Plus (+) signs indicate maxima and those correspond roughly to 0.04 e/au^3 . Minus (-) signs indicate minima. The most external contour has a value 0.003 e/au^3 and the interval between contours is $\Delta n = 0.003 \text{ e/au}^3$.

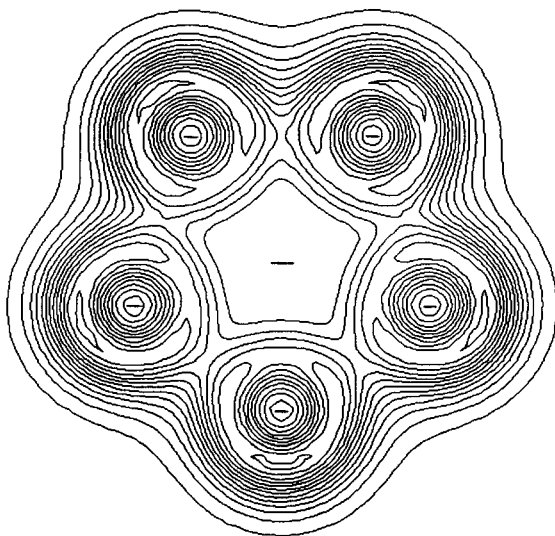


Figure 6: Electron density contours in the middle plane containing five atoms in Pb_7 . Other details are like in Fig. 5.

An interesting feature can be observed in the unoccupied part of the spectrum for Pb_5 and Pb_7 . In these two clusters the LUMO is a nondegenerate level and a substantial gap occurs between the LUMO and LUMO+1 levels. This fact suggests that Pb_5^{-2} and Pb_7^{-2} will be more stable than other doubly-charged anions. Experiments confirm the high stability of Pb_5^{-2} clusters in solution [35].

Table 1: Comparison between cohesive energies per atom of Pb_n clusters (in eV) calculated with kinetic energy cutoffs of 8 Ryd. and 16 Ryd.

n	8 Ryd.	16 Ryd.
3	0.452	0.500
4	0.987	0.996
5	1.191	1.187
6	1.398	1.406
7	1.534	1.546

Plots of the electron density help to elucidate the type of chemical bonding. Pb_3 and Pb_7 are fully representative cases. A plot for Pb_3 in the plane of the three atoms is given in Fig. 5. The closed contours around each atom are associated with the inert atomic s levels stabilized by the relativistic effects. Those closed contours can also be seen for Pb_7 , plotted in Fig. 6 (in the middle plane of the bipyramid containing the five atoms). A second set of contours appears in both figures. These correspond to the p -band and indicate a delocalized electronic distribution. This is a general feature, also found for other planes and common to all the clusters studied. Notice in particular the region of constant density in the middle of the pentagon in Pb_7 . The only cluster showing some signs of a “weak” covalent contribution to bonding is Pb_3 , for which we observe blobs of charge in the two regions between the atoms separated by short interatomic distances, with density maxima just halfway between the atoms. Those interatomic distances, equal to 5.16 a.u., are the shortest distances found in the set of clusters studied. For comparison, the separation between neighbor atoms in Pb_4 is already much larger, $d = 5.5$ a.u., and the distance between the two atoms forming the triangle basis of Pb_3 (see Fig. 3) is $d = 6.63$ a.u. In spite of the delocalized nature of the bonding charge for $n \geq 4$, we stress that the stability of the Pb clusters cannot be interpreted

by the shell model since the large level degeneracies of the shell model are drastically lifted (see Fig. 4) by the cluster field.

In order to check that our calculations are well converged with respect to the value of the plane-wave kinetic energy cutoff, we have recalculated the binding energies of the smallest Pb_n clusters ($n = 3 - 7$) increasing the cutoff from 8 Ryd. (the value used throughout this paper) to 16 Ryd. The results clearly show (see Table 1) that the cohesive energies of lead clusters are well converged already with a cutoff of 8 Ryd. So a cutoff of 8 Ryd. is sufficient for calculating the properties of these clusters.

4 Mixed Alkali-Pb clusters

The experimental information on liquid Na-Pb alloys suggests the presence of complexes with compositions Na_4Pb and Na_4Pb_4 , with maximum proportion of those complexes at alloy compositions consistent with the stoichiometry of the complexes. On the other hand, only one type of complexes appears to form for alloys of Pb with other alkali metals: Li_4Pb complexes in the case of lithium alloys and K_4Pb_4 , Rb_4Pb_4 , Cs_4Pb_4 in the case of alloys with heavy alkalis. The richness in complexes of the Na alloys is enhanced even more when one looks at the behavior of Na_nPb clusters produced in gas-phase experiments. The supersonic expansion of a lead-sodium vapor from a hot oven source has led to the observation of an exceptionally abundant Na_6Pb cluster [36] which dominates the mass spectrum under some conditions. For those reasons we concentrate here on clusters formed by Pb and Na atoms. We see below that the study of finite clusters gives useful results that help to interpret both the gas phase experiments and the alloy phenomenology.

4.1 Na_nPb clusters

These clusters, with particular emphasis on Na_6Pb , have been studied previously [37, 38] using the same ab initio method of this paper and other ab initio methods [39, 40, 41, 42] and we briefly review that work for completeness. The results are summarized in Fig. 7, where we plot the evaporation energy E_v of a sodium atom

$$E_v(\text{Na}_n\text{Pb}) = E(\text{Na}_{n-1}\text{Pb}) + E(\text{Na}) - E(\text{Na}_n\text{Pb}). \quad (4)$$

The largest value of E_v occurs for Na_4Pb and a local maximum occurs for Na_6Pb , followed by a deep minimum at Na_7Pb (its evaporation energy is only 0.76 eV). The following explanation has been proposed [37] for the high abundance of Na_6Pb in the mass spectrum. In the supersonic expansion of the

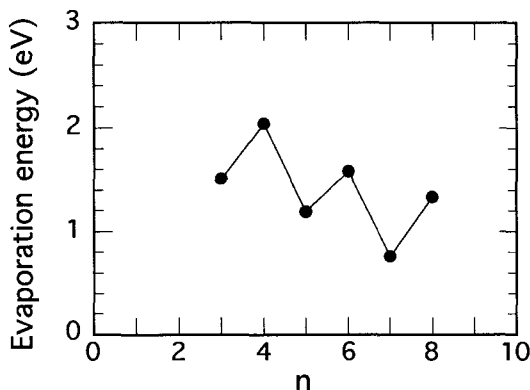


Figure 7: Calculated evaporation energy of a Na atom from Na_nPb clusters [37].

vapour [36] the clusters grow by aggregation of atoms following collisions. The conditions in the experiment of Yerezian *et al.* seem to be such that the Na_nPb clusters remain not much larger than Na_6Pb . This is because the concentration of Pb in the source is larger than 10% and the Pb atoms compete with one another to bind Na atoms, which prevents formation of clusters with many Na atoms. However, during growth the clusters become hot (growth is an exothermic process) and cool down by evaporating Na atoms. Since the evaporation energy is lowest for Na_7Pb and increases by a factor of 2 between Na_7Pb and Na_6Pb , it is reasonable to expect that the evaporation cascade practically stops at Na_6Pb , the population of this cluster thus becoming highly enriched in the beam.

We now focuss on the high stability of Na_4Pb revealed by its large evaporation energy. In the environment provided by the liquid alloy in equilibrium at a given temperature, all Na_nPb clusters of different n can compete with each other and we expect Na_4Pb to be more abundant because the energy to remove a Na atom from this cluster is the largest. This large abundance of Na_4Pb is indeed found in the liquid alloy.

4.2 Na_nPb_4 clusters

The presence of Na_4Pb_4 complexes in liquid Na-Pb alloys calls for *ab initio* calculations to study the reasons for the formation of those clusters. We have performed calculations for free Na_nPb_4 clusters, with n increasing from 1 to 5. Computational details are similar to those for the pure Pb_n clusters. However,

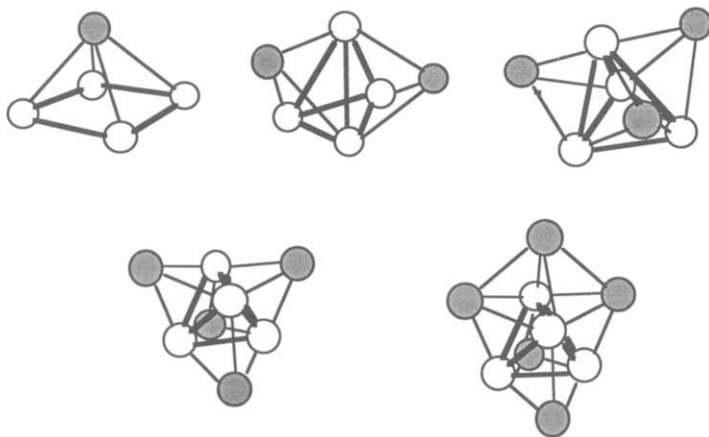


Figure 8: Calculated lowest energy structures of Na_nPb_4 ($n = 1 - 5$). Dark spheres represent the sodium atoms.

a partial core correction has been applied in generating the Na-pseudopotential [43]. The partial-core correction (also used in the calculations of Fig. 7 above) takes into account the nonlinearity of the exchange-correlation potential (with respect to the density) in the region where core and valence charge densities overlap, and includes some core-effects in the cluster calculations without explicitly including core wavefunctions. This is particularly important for sodium, where consideration of semi-core 2p electrons plays a small, but non negligible role in describing the correct lattice constant and bulk modulus of bcc-Na. This effect is in part included by the partial-core corrections.

The lowest energy arrangement for each cluster is shown in Fig. 8. Dark spheres represent the Na atoms. In section 3 we have shown that the most stable structure for pure Pb_4 is a planar rhombus. Now we observe that as the Na atoms are added to the Pb_4 unit, this one becomes progressively deformed until it reaches a tetrahedral structure. The Pb core is a deformed tetrahedron already in Na_2Pb_4 , but only becomes a perfect tetrahedron in Na_4Pb_4 . The Na atoms cap two faces, then three and finally four faces of the Pb-tetrahedron in Na_2Pb_4 , Na_3Pb_4 and Na_4Pb_4 respectively. A fifth Na atom does not affect the structure of Na_4Pb_4 and sits above one edge of the Pb tetrahedron.

The energy required to evaporate a Na monomer from those clusters is plotted on Fig. 9. This is defined

$$E_v(\text{Na}_n\text{Pb}_4) = E(\text{Na}_{n-1}\text{Pb}_4) + E(\text{Na}) - E(\text{Na}_n\text{Pb}_4). \quad (5)$$

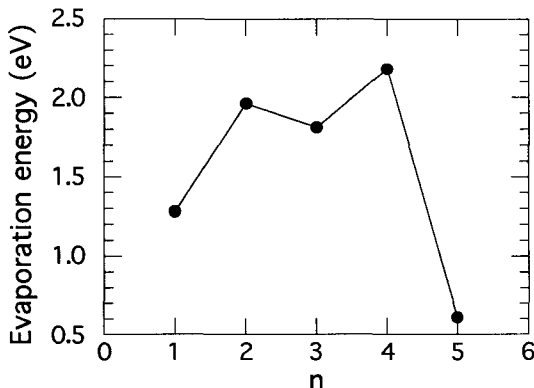


Figure 9: Evaporation energy of a Na atom from Na_nPb_4 clusters ($n = 1 - 5$).

The main features are: first a substantial increase of E_v between NaPb_4 and Na_2Pb_4 , an odd-even oscillatory behavior with a peak at Na_4Pb_4 and finally a drastic drop between Na_4Pb_4 and Na_5Pb_4 . The last two features indicate the high stability of Na_4Pb_4 , and this gives a hint to the presence of this compound in the liquid Na-Pb alloys, in particular at the equiatomic composition. We also notice the effect of the Na atoms in promoting the Pb_4 unit to adopt the tetrahedral arrangement: in the pure Pb_4 cluster the isomer with tetrahedral structure is 1.1 eV above the ground state (rhombus). The odd-even oscillation of E_v in Fig. 9 is simply related to the number of valence electrons. The clusters with two or four Na atoms have the HOMO level filled and a gap between this and the LUMO level; the gap is largest (2.0 eV) for Na_4Pb_4 (see Fig. 10). In contrast, the HOMO is only half-filled in NaPb_4 , Na_3Pb_4 and Na_5Pb_4 . The drastic difference between the electronic structures of Na_4Pb_4 and Na_5Pb_4 explains the difference of their stabilities.

Finally we propose some ideas to explain the fact that the properties of liquid Na-Pb alloys as a function of Pb concentration reveal a strong feature (a peak in the resistivity or in the thermodynamic stability function) at 20 atomic per cent Pb, and a smaller feature (a small peak or a shoulder) at 50 atomic per cent Pb. Those features can be interpreted as revealing the presence of Na_4Pb and Na_4Pb_4 clusters in the alloy, with predominance of the first type, at least for concentrations of Pb well below the equiatomic (50/50) one. In our view the prominent presence of Na_4Pb clusters can be explained by comparing the binding energies per Pb atom in Na_4Pb and Na_4Pb_4 . These are defined as

$$E_b^0(\text{per Pb}) = E(\text{Pb}) + 4E(\text{Na}) - E(\text{Na}_4\text{Pb}), \quad (6)$$

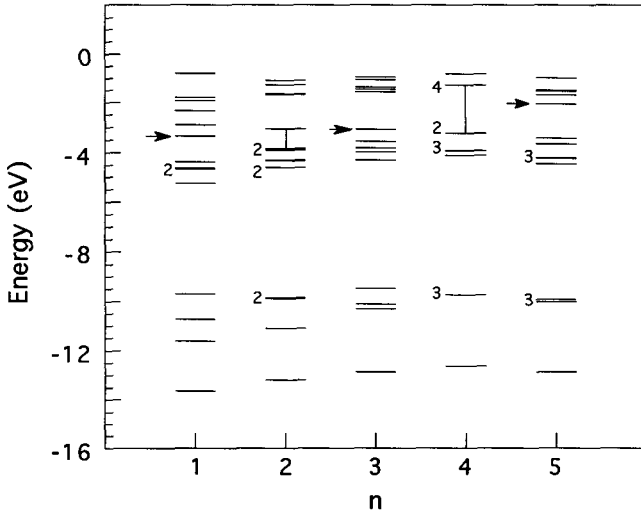


Figure 10: Electronic energy level diagram for Na_nPb_4 clusters. Degeneracies are indicated by a number attached to the level. A vertical bar indicates the HOMO-LUMO gap. The arrows indicate the position of the HOMO level when this is only partially filled.

and

$$E_b^z(\text{per Pb}) = \frac{1}{4} [4E(\text{Pb}) + 4E(\text{Na}) - E(\text{Na}_4\text{Pb}_4)], \quad (7)$$

the superscripts o and z indicating “octet” and “Zintl” respectively. We have obtained $E_b^o(\text{per Pb}) = 4.46$ eV and $E_b^z(\text{per Pb}) = 2.79$ eV, so $E_b^o - E_b^z = 1.67$ eV. Consequently, for alloys with a low Pb concentration the formation of Na_4Pb clusters is energetically favorable. As the concentration of Pb in the alloy increases there are restrictions to the formation of octet clusters just because (if we assume that clustering is very efficient) there is not enough Na atoms. In such a case formation of Na_4Pb_4 becomes competitive, especially in the alloys near the equiatomic (50/50) composition. Even in this case we can expect a sizable fraction of Na_4Pb clusters in the alloy, so the features in the alloy properties at equiatomic composition are expected to be less pronounced than at 20 atomic per cent Pb. This is, indeed, the behavior observed in the experiments [8].

If this argument is correct, one should obtain for the Li-Pb case a value $E_b^o - E_b^z$ substantially larger than 1.67 eV (this is because the Li-Pb alloys

present a single strong feature at 20 atomic per cent Pb). Preliminary results for the lithium case give a value of 2.87 eV in support of this argument.

5 Study of Na_6Pb using the GGA

Several workers [37, 38, 39, 40, 41, 42] have optimized the structure of the Na_6Pb cluster by *ab initio* methods. Car-Parrinello calculations using the LDA [37, 38] as well as the Configuration Interaction calculations of Marsden [39] predicted a centered octahedron (O_h symmetry). On the other hand Jinlong et al [42] have performed discrete variational LDA calculations under symmetry constraints. They reported a tricapped tetrahedron with C_{3v} symmetry as the ground state, and that the octahedral isomer was less stable. The difference in binding energy between the C_{3v} and O_h structures was surprisingly large: 1.1 eV. The DFT calculations of Albert et al [40] also employed symmetry constraints, and applied gradient corrections (GGA) to exchange and correlation in a “post hoc” way, that is, using the LDA densities. They found several isomers with a central Pb atom (between them the O_h and C_{3v} structures), with total binding energies differing by less than 0.09 eV (or by less than 0.04 eV including relativistic effects). Motivated by these conflicting results we have studied again this cluster with full consideration of the GGA of Perdew, Burke, and Ernzerhof [44]. Nonlocal norm conserving soft pseudopotentials were generated according to the procedure of Troullier and Martins [45], using also the

Table 2: Equilibrium bond lengths (in a.u.) and total binding energies (in eV) of the O_h and C_{3v} isomers of the Na_6Pb cluster. Distances r_1 , r_2 , r_3 , r_4 are indicated in Fig. 11. The asterisk in the C_{3v} structure indicates our unrelaxed calculation with the bond lengths taken from Jinlong [42].

Symmetry	r_1	r_2	r_3	r_4	E_b
$\text{O}_h(\text{LDA})$	7.84	7.84	7.84	5.54	9.66
$\text{C}_{3v}^*(\text{LDA})$	6.09	8.39	8.39	5.61	0.09
$\text{C}_{3v}(\text{LDA})$	7.60	7.65	8.05	5.54	9.67
$\text{O}_h(\text{GGA})$	8.03	8.03	8.03	5.69	8.53
$\text{C}_{3v}(\text{GGA})$	7.81	7.84	8.30	5.69	8.54

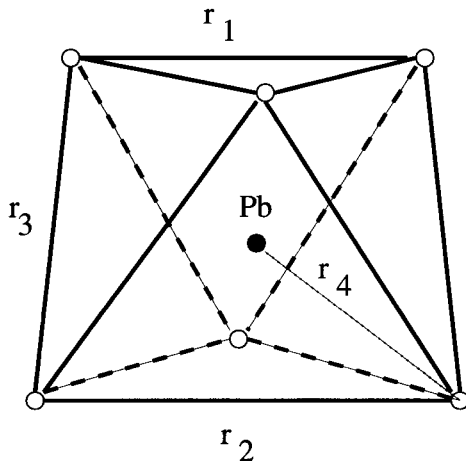


Figure 11: Na_6Pb cluster with the C_{3v} symmetry. The distances r_1 , r_2 , and r_3 become equal in the O_h structure.

GGA in the atomic calculations.

In our search for the lowest energy structure we have performed relaxations of a few selected initial structures using the conjugate-gradients method [13] without imposing any symmetry constraints. The results for a bcc supercell with lattice constant of 30 a.u. and a plane wave energy cutoff of 9 Ryd. are reported in Table 2, where we give interatomic distances (see Fig. 11) and binding energies. First we have performed LDA calculations again. Relaxations starting with an initial O_h structure maintain that structure and give a binding energy of 9.66 eV and a Na-Pb bond distance of 5.54 a.u., in agreement with our earlier work [38]. A calculation for the C_{3v} structure fixing the interatomic distances at the values reported by Jinlong et al leads to large forces on the atoms and to a very small binding energy (0.09 eV). When we allow for a full unconstrained relaxation of that structure, the interatomic distances change, although the symmetry remains C_{3v} . The Na-Na bond distances labelled r_1 , r_2 , and r_3 in Fig. 11 are now more similar than for the starting C_{3v} structure of Jinlong. This, in practice, means that the optimized C_{3v} structure is more similar to the O_h than the starting one. The C_{3v} and O_h isomers have almost identical binding energies.

In a second step fully self-consistent GGA calculations were performed starting with our LDA O_h and C_{3v} structures. After unconstrained relaxation the conclusions we obtained were similar to those of the LDA study. We find O_h and C_{3v} isomers with identical binding energies, 1.1 eV lower than the LDA

binding energies, and with bond distances 0.2 a.u. larger. These results are consistent with the known reduction of binding energies and increase of interatomic distances induced by the density gradient corrections as compared to LDA results. In summary we conclude that the O_h and C_{3v} isomers are degenerate both at the LDA and GGA levels. The agreement between LDA and GGA results for structural properties give us confidence on the LDA results we have obtained in this paper for pure and mixed Pb clusters.

6 Summary

The variations of abundance in the mass spectrum of small Pb_n clusters have been explained by ab initio density functional calculations. A study of free clusters formed by Pb and Na helps to explain the observation of an exceptionally abundant Na_6Pb cluster in gas phase experiments. It also gives strong support to the presence of Na_4Pb and Na_4Pb_4 clusters in the liquid alloys.

Acknowledgments

Work supported by DGES (Grants PB95-0720-C02-01 and PB95-0202), Junta de Castilla y León (Grant VA 25/95) and NATO (Grant CRG.961128). One of us (L.M.M) acknowledges a Postgraduate fellowship from MEC of Spain.

References

- [1] E. Zintl and G. Woltersdorf, *Z. Elektrochem.* **41**, 876 (1935)
- [2] R.E. Marsh and D.P. Shoemaker, *Acta Crystallogr.* **6**, 197 (1953).
- [3] I.F. Hewaidy, E. Busmann, and W. Klemm, *Z. Anorg. Allg. Chem.* **328**, 283 (1964).
- [4] W. Mueller and K. Volk, *Z. Naturforsch.* **B32**, 709 (1977).
- [5] B.P. Alblas, W. van der Lugt, J. Dijkstra, W. Geertsma, and C. van Dijk, *J. Phys. F* **13**, 2465 (1983).
- [6] M.T.J. Reijers, W. van der Lugt, and M.L. Saboungi, *Phys. Rev. B* **42**, 3395 (1990).
- [7] G.A. de Wijs, G. Pastore, A. Selloni, and W. van der Lugt, *J. Chem. Phys.* **103**, 5031 (1995).

- [8] W. van der Lugt, *Phys. Scripta T* **39**, 372 (1991).
- [9] L.M. Molina, M.J. López, J.A. Alonso, and M.J. Stott, *Ann. Physik* **6**, 35 (1997).
- [10] P. Hohenberg and W. Kohn, *Phys. Rev.* **136B**, 864 (1964).
- [11] W. Kohn and L.J. Sham, *Phys. Rev.* **140A**, 1133 (1965).
- [12] M.P. Iñiguez, M.J. López, J.A. Alonso, J.M. Soler, *Z. Phys. D* **11**, 163 (1989).
- [13] M.C. Payne, M.P. Teter, D.C. Allan, T.A. Arias, and J.D. Joannopoulos, *Rev. Mod. Phys.* **64**, 1045 (1992).
- [14] R. Car and M. Parrinello, *Phys. Rev. Lett.* **55**, 2571 (1985).
- [15] R. Stumpf and M. Scheffler, *Comp. Phys. Comm.* **79**, 447 (1994).
- [16] M. Bockstedte, A. Kley, and M. Scheffler, *Comp. Phys. Comm.* (to be published).
- [17] J.P. Perdew and A. Zunger, *Phys. Rev. B* **23**, 5048 (1981).
- [18] D.M. Ceperley and B.J. Alder, *Phys. Rev. Lett.* **45**, 566 (1980).
- [19] D.R. Hamann, *Phys. Rev. B* **40**, 2980 (1989).
- [20] L.K. Kleinman and D.M. Bylander, *Phys. Rev. Lett.* **48**, 1425 (1982).
- [21] K. Balasubramanian, *Chem. Rev.* **90**, 93 (1990).
- [22] T. Bastug, K. Rashid, W.D. Sepp, D. Kolb, and B. Fricke, *Phys. Rev. A* **55**, 1760 (1997).
- [23] A.Y. Liu, A. García, M.L. Cohen, B.K. Godwal, R. Jeanloz, *Phys. Rev. B* **43**, 1795 (1991).
- [24] J. Mühlbach, K. Sattler, P. Pfau, and E. Recknagel, *Phys. Lett.* **87A**, 415 (1982).
- [25] K. Sattler, *Surf. Sci.* **156**, 292 (1985).
- [26] K. Lai Hing, R.G. Wheeler, W.L. Wilson, and M. A. Duncan, *J. Chem. Phys.* **87**, 3041 (1987).
- [27] A. Hoareau, P. Mélinon, B. Cabaud, D. Rayane, B. Tribollet, and M. Broyer, *Chem. Phys. Lett.* **143**, 602 (1988).

- [28] I. Rabin, W. Schulze, and B. Winter, *Phys. Rev. B* **40**, 10282 (1989).
- [29] J.C. Phillips, *Chem. Rev.* **86**, 619 (1986).
- [30] M.J. López and J. Jellinek, *Phys. Rev. A* **50**, 1445 (1994).
- [31] M.S. Stave and A.E. DePristo, *J. Chem. Phys.* **97**, 3386 (1992).
- [32] C.L. Briant and J.J. Burton, *J. Chem. Phys.* **63** 2045 (1975).
- [33] C. Kittel, *Introduction to Solid State Physics*, 5th edition, John Wiley, New York (1976).
- [34] R.W. Farley, P. Ziemann, and A.W. Castleman Jr., *Z. Phys. D* **14**, 353 (1989).
- [35] J.D. Corbett, *Chem. Rev.* **85**, 383 (1985).
- [36] C. Yeretizian, U. Rothlisberger, and E. Schumacher, *Chem. Phys. Lett.* **237**, 334 (1995).
- [37] J. Chang, M.J. Stott and J.A. Alonso, *J. Chem. Phys.* **104**, 8403 (1996).
- [38] L.C. Balbás and J.L. Martins, *Phys. Rev. B* **54**, 2937 (1996).
- [39] C. Marsden, *Chem. Phys. Lett.* **245**, 475 (1995).
- [40] K. Albert, K.M. Neyman, V.A. Nasluzov, S.Ph. Ruzankin, Ch. Yeretizian, and N. Rösch, *Chem. Phys. Lett.* **245**, 671 (1995).
- [41] P.R. Schleyer and J. Kapp, *Chem. Phys. Lett.* **255**, 363 (1996).
- [42] Y. Jinlong, D. Kaiming, X. Chuanyun, and W. Kelin, *Phys. Rev. B* **55**, 13293 (1997).
- [43] S.G. Louie, S. Froyen, and M.L. Cohen, *Phys. Rev. B* **26**, 1738 (1982).
- [44] J.P. Perdew, K. Burke, and M. Ernzerhof, *Phys. Rev. Lett.* **77**, 3865 (1996).
- [45] N. Troullier and J.L. Martins, *Phys. Rev. B* **43**, 1993 (1991).

Density Functional Theory in Catalysis: Activation and Reactivity of a Hydrocarbon Molecule on a Metallic Active site.

Ewa Broclawik

Institute of Catalysis and Surface Chemistry,
Polish Academy of Sciences,
Cracow, Poland

ABSTRACT

Applications of density functional theory in the field of modelling catalytic reactions are discussed in terms of both methodological aspects of its usage as a tool for electronic structure evaluation and cluster modelling of the active center. Simple functional models are proposed for metal oxide/transition metal catalytic sites for gallium oxide in a zeolitic lattice and palladium or rhodium based supported catalysts. Reaction paths for C-H bond scission in methane interacting with such centers are analysed from the point of view of the interdependence between the electronic structure and reactivity of the bond. On this basis two mechanisms for the activation of the C-H bond are described: via electron withdrawal from bonding states (on oxide catalysts) and via electron insertion into antibonding orbitals (on metals).

1. INTRODUCTION

The understanding and modelling of heterogeneous catalysis and catalytic behaviour at the molecular level can benefit as well from accurate and significant quantum chemical calculations as from molecular statistics and dynamics simulations or all of these procedures. The following chapter will be devoted to applications of density functional theory in the field, its successes and problems. Although theory has had in the past a limited impact on the understanding and predicting of catalysis, the advent of more powerful computing facilities, which permit more complex calculations and simulations representing more realistically the system of interest, makes this area of research one of potential and rapid growth. Advanced computer systems, including large massively-parallel machines, and recent improvements in quantum chemical computer codes allow calculations on systems of considerable size, often involving more than 1000 basis functions and more than 100 atoms depending on the symmetry. Nevertheless, the

quantum chemical evaluation of potential energy surfaces for three-dimensional systems is highly complex. The enormous sizes of unit cells of such materials as zeolites, metal oxides or mixed catalysts make periodic *ab initio* calculations very demanding and only recently such calculations have become feasible for certain structures. Active sites, amorphous regions, or crystal perturbations introduce further limitations due to the broken translational and space symmetry, because these require larger pseudocell cells.

One approach to this problem involves finite clusters. Such clusters may consist of atoms or ions, real or hypothetical molecules. The standard "molecular" *ab initio* methods can be applied in calculations involving these models. This approach is particularly suited to tackle local phenomena, e.g. to describe active sites of catalysts or impurity centers in semiconductors, but it also helps to extend knowledge on structure and bonding of crystals and on their bulk properties. However, cutting the interior part out of large organic molecules, macromolecules and solids with covalent or partially covalent bonds, leaves dangling bonds. These have to be saturated with e.g. hydrogen atoms in order to create a realistic model for the quantum chemical description. Such an approach will be implemented in discussing the properties of active sites in metal-exchanged zeolites. In some problems it could prove very profitable to pursue properties of catalysts by assuming simple molecular models for the active site in the belief that the most important factors might be deduced from the properties of the constituent atoms bonded in a proper way. This approach could be fruitfully used for complex catalysts, especially when their structures are not defined or claimed to be amorphous. Such modelling schemes will be followed in studies on supported oxidized metal catalysts. Altogether, it must be strongly stressed that these studies are based on very small cluster models. The price paid, however, seems to be moderate in view of the possibility to access directly reaction pathways.

2. METHODOLOGICAL REMARKS

The other side of the problem of modelling catalysis is the choice of a suitable quantum chemical method. As the final target is one of chemical accuracy - fine energetical effects measured in units of a few kcal/mol - the most sophisticated quantum methodologies should be used. It is already well known that the treatment of highly open-shell systems is very difficult, if at all feasible, at the Hartree-Fock level. Moreover, the HF wavefunctions must be viewed, at best, as not always convenient starting points for more elaborate correlated calculations. On the other hand, there exists already rapidly growing evidence that the density functional theory (DFT) is capable of meeting such challenges and provide a unified theoretical framework for the study of electronic, geometric, and vibrational properties of solids, surfaces, interfaces, clusters, and molecular systems,^{1,2} encompassing metallic as well as covalent bonding.^{3,4,5} Density functional theory deals also with correlation where the use of fully correlated methods is generally limited. DFT is an example of an intrinsically many-body approach to the electronic structure of a system of interest, in principle avoiding the many-electron wave function. Nevertheless, in accord with the tendency to retain the features of the one-

particle picture of the electronic structure which cannot be overestimated in interpreting chemistry, one-particle equations have been delivered by Kohn and Sham.⁶ Even if the so called Kohn-Sham orbitals may be interpreted only in an approximate way, they are a great help in understanding the mechanisms of chemical processes. Thus in this work we will also refer to qualitative properties of Kohn-Sham orbitals to highlight e.g. spatial requirements of some interactions or directional bonding.

DFT methods appear to be especially attractive also for describing catalytic systems where weakly interacting subsystems still remain an area of major challenge for quantum chemistry⁷. The major gain of the DFT based methods is the explicitly included electron correlation, notwithstanding their computational modesty. There exist nowadays numerous implementations of the DFT methodology in a variety of software packages. We by no means intend to make any benchmark comparisons either with respect to their numerical efficiency or calculational accuracy. We would rather give the reader an impression of how the available software could be used as tools in formulating and testing hypotheses regarding intricate chemical processes. In this chapter we will describe the results of calculations obtained by means of the DMol software of BIOSYM Technologies, Inc.⁸ Numerical spin-polarized density functional calculations were performed at two levels of approximation to the exchange-correlation potential: the local density approximation (LDA) and the nonlocal gradient-corrected potential (NLDA). Among the variety of functionals offered in numerous implementations of DFT we have selected the local Janak-Moruzzi-Williams (JMW)⁹ and the nonlocal exchange of Becke combined with Lee-Yang-Parr correlation (BLYP)¹⁰ functionals as our numerical choice together with a set of double numerical plus polarization (DNP) basis functions of chemical quality. These constitute the recommended level of computation in the DMol software. Already the local density approximation, however, is known to yield excellent geometries and acceptable relative energies for metallic systems, and has achieved considerable success in studies of complex metal surfaces¹¹ while NLDA happens to worsen agreement with experiment,¹² let us recall palladium.¹³ Thus the basic flow of reasoning will rely here mainly on the results from the local density approximation. As the chapter is focused on physical properties of matter and the implementation of theory in materials science, practical tools for analysing electronic structure such as population analyses based on charges estimated by fitting the electrostatic potentials will be thoroughly investigated. Graphical part of the presentation is based on visualisation tools included in the recent version of the Biosym/MSI InsightII software.¹⁴

3. CATALYTIC ISSUES

Subjects such as the description of gas adsorption at the molecular level in terms of adsorption sites or type of bonding constitute nowadays a major field of research in surface science as well as in quantum chemistry.¹⁵ Experimentalists generally deal with techniques probing the global consequence of the interaction between an adsorbate and a surface. Quantum chemistry can play a complementary role in examining the detailed nature of the chemisorption interaction. For example, it can address such issues as charge

distribution and energy level changes within the adsorbed molecule. Such information from combined theory and experimental approaches is of primary importance to the understanding of the fundamental steps involved in catalytic processes. It may be also used to justify, or to improve, the quantum models used by theoreticians.

In particular, the breaking of C-H bonds in hydrocarbons has been pointed out as a key to many important catalytic processes, be it transforming resources of natural gas into useful products like hydrogen and petrochemicals,¹⁶ catalytic combustion¹⁷ or removing nitrogen oxides from exhaust gases for environmental protection by reducing with hydrocarbons.¹⁸ Methane takes a special position among hydrocarbons as it is the most common ingredient of petrochemical resources and natural gas. On the other hand the high stability of methane makes C-H bond activation a challenging technological problem. Thus methane activation on adsorption on catalytic media such as zeolites or precious metals and their oxides has long been an intriguing subject for both experiment and theory.^{19,5}

In the forthcoming paragraphs we are going to show how the interaction of a methane molecule with the active site influences properties of the C-H bond. One example is taken from a very important field of zeolite catalysis, with the metal site formed in metal-exchanged silicalites. Recently, much attention has been given to Ga-exchanged ZSM-5 which was found to promote the reduction of NO with methane.²⁰ The topic is very fashionable and attractive, nevertheless, the mechanism of this process is basically unknown. For example little is known about the mechanism of methane activation, of water poisoning, the specific role of the reductant and the catalyst in the reaction;²¹ also the identification of intermediates has not yet been accomplished. Thus, theoretical modelling of this reaction system would be of enormous value for both basic scientific understanding and practical applications.

The cluster model for quantum chemical calculations has been based upon the known crystal structure of ZSM-5 reported by X-ray diffraction study modified according to the equilibrium geometry given by molecular dynamics (MD) simulation.²² The physical and chemical state of the active metal species in H-ZSM-5 zeolites has not yet been unequivocally established. There exists, however, strong evidence that gallium is present in highly dispersed monomeric form, coordinated to basic oxygens within zeolite channels. In a reducing atmosphere it could be a reduced hydride moiety while in the presence of excess oxygen an oxidized $[\text{GaO}]^+$ unit may be proposed. Thus in our quantum chemical calculations, a single AlO_4 tetrahedron was considered as the representative of the active site, with adjacent silicons replaced by hydrogens and charge deficiency compensated by $[\text{GaO}]^+$ cationic species (see the cluster part in Figure 1a). We believe the cluster model specified above is adequate to reproduce the basic features of the local electronic structure of the zeolitic active site. At the same time, the modest size of the cluster allows one to meet more rigorous demands of quantum chemical methodology and testing various computational parameters.

The other example comes from transition metal chemistry. Theoretical modelling in modern materials science and catalysis cannot be accomplished without knowing the electronic properties of transition metals and their compounds as they are present in the

majority of systems of practical interest. In particular the accurate description of the bonding involving transition metal atoms is of fundamental importance for both theory and experiment. This is, however, a very difficult target for quantum chemistry because the electronic structure of such species is highly complicated and the computation requires explicit treatment of electron correlation. Even electronic properties of small systems such as transition metal oxide diatomic molecules and transition metal dimers is extremely intricate. The difficulties come from the many unpaired electrons, which produce a large number of electronic states, many with high spin multiplicity. On the other hand, such a variety of available close-lying energetic states, frequently with substantially different properties, may be the prerequisite factor for high activity and the extremely delicate and flexible nature of the interaction of these species with other molecules. The density functional theory has already been presented by us as a very promising tool for investigating such systems, in particular transition metal oxides.^{3,4,5,23}

The simplest system where the interaction of a hydrocarbon molecule with a metal oxide can be investigated is the metal oxide MeO diatomic molecule. Although it can be hardly taken as a realistic model of a bulk oxide or oxidized metal catalyst, it offers the possibility of deep studies on the electronic structure of the system composed of a cluster and a hydrocarbon molecule and its evolution along the adsorption and prospective dissociation processes, within high-level quantum chemical methodologies. Our studies on the electronic structure of palladium systems and the methane activation^{24,25,26} have clearly indicated that only detailed knowledge of the electronic state of the system, be it a simple diatomic cluster, may bring some insight into the intricate mechanism of hydrocarbon adsorption and the activation of a carbon - hydrogen bond. On this basis we have successfully drawn qualitative conclusions regarding some factors governing catalytic combustion of methane on an active site on a supported metal catalyst. In the same way the differences in behaviour of oxidized and metallic phases may be studied on the basis of the interaction of methane with a metallic dimer.^{25,26} One may attempt to extend this simple model by extending the cluster size which is the commonly adopted practice for metal surfaces (see e.g. recent work by van Santen *et al.*,⁷ Goursot *et al.*,²⁷ Kratzer *et al.*²⁸ or Rochefort *et al.*²⁹). The matter is much more complicated in the case of highly covalent oxides or complex supported transition metal based catalysts. For example the fine structure of the surface in supported metal/oxidized metal catalysts (where Me = Pd, Rh, Pt etc.), which are often used for the catalytic combustion of hydrocarbons, is still not well known and any model may be verified only by the validity of the predictions offered. Thus we strongly believe that high-level and high-accuracy description of the dimers aided occasionally with some extended systems modelling strictly selected features of the interaction between different phases could be of great importance for pursuing intrinsic factors which govern the catalysis. We will call such models functional models to distinguish them from direct modelling either the bulk, or the surface, or the active site in a supermolecule.

4. DFT DESCRIPTION OF THE INTERACTION OF A METHANE MOLECULE WITH ACTIVE SITES

Two factors may be responsible for specific routes of adsorption and transformation of a hydrocarbon molecule on the catalyst surface: a geometrical factor and an electronic factor. Certainly no ultimate conclusions with respect to adsorption geometry may be drawn on the basis of very small models of the site. We would rather show interrelations between the electronic structure of the "host" cluster or molecule and the preferable interaction geometry with the "guest" hydrocarbon molecule and point out the consequences regarding further reaction routes. The results discussed in this paragraph will be based on DFT geometry optimization within the LDA approximation

In the case of the $[\text{Al}(\text{OH})_4][\text{GaO}]$ cluster the "framework" $[\text{Al}(\text{OH})_4]$ part was kept fixed at the geometry derived from molecular dynamics simulations for a large model of the zeolite.²² The exact geometrical position of the GaO unit was determined by DFT total energy minimization and the gallium doubly coordinated to the framework in a bridging position between two oxygens was found as the best structure. This geometry rendered structurally unsaturated gallium forming a planar unit with the third bond to the extraframework oxygen.³⁰ Figure 1a shows the optimized geometry of methane adsorption on the $[\text{Al}(\text{OH})_4][\text{GaO}]$ cluster. The other stable structure was the one obtained after C-H bond scission with methyl bonded to gallium and hydrogen forming an OH group with the extraframework oxygen (Figure 1c).³¹

In a weakly bonded (by 4.5 kcal/mol) adsorption complex neither the geometry of the methane molecule nor the conformation of the center undergo any significant relaxation. Since the adsorption of methane has been found very weak the stability of the complex has been confirmed by independent semiempirical calculations. The adsorption distance

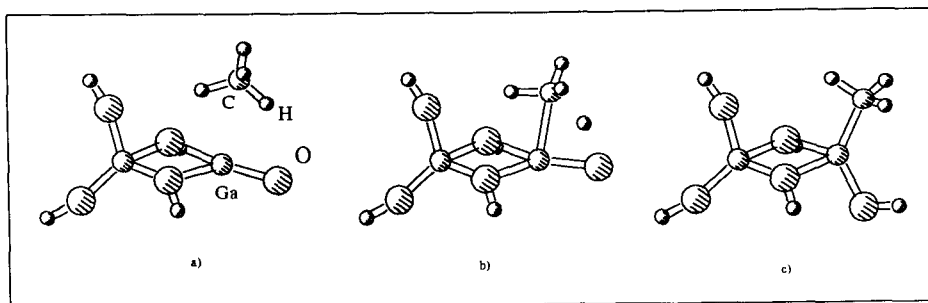


Figure 1. Geometry evolution along the dissociation pathway of methane on Ga-ZSM-5: a) adsorbed methane, b) transition state for C-H bond scission c) after dissociation

(carbon - gallium separation) is equal to 2.7 Å and slight elongation (1.10 Å→1.12 Å) of the bond between the carbon and the hydrogen closest to the extraframework oxygen may be noticed. This is accompanied by a small rearrangement of the charge distribution making this hydrogen (which we will call the dissociative hydrogen) more positive than other hydrocarbon hydrogens. The effect, however, is very delicate and its significance depends very much on the reliability of the charge distribution analysis. Thus we are going to show how various charge distribution analyses work in the software package.

Table 1 and Table 2 list charges in separate methane and for methane interacting with the $[\text{Al}(\text{OH})_4][\text{GaO}]$ system as obtained from three schemes available in a recent release of the DMol package³²: Hirschfeld partitioned charges, Mulliken population analysis and charges fitted to reproduce the electrostatic potential, compared to MOPAC PM3 calculations. We can see how dramatic differences in charge distribution follow from various population analyses. It is very well known that the populations depend strongly on the applied basis sets and on the partition scheme of the electron density. Hirshfeld populations seem to be rather underestimated whereas Mulliken and ESP-fitting schemes bring rather too large build-up of the charge, with the latter one carrying allegedly more physical meaning. It has been already pointed out that Mulliken approach fails to yield chemically meaningful atomic charges for CH_4 and that Hirshfeld is the most satisfactory method with regard to DFT computation of chemically meaningful and basis set independent atomic charges.³³ Nevertheless, they should not be regarded as an absolute quantity. Instead, it is more justified to consider trends in atomic charges along a series of molecular geometries. Table 2 lists the evolution of charge distribution along the reaction pathway for methane dissociation on Ga-ZSM-5 completed by the search for the transition state between the methane weakly adsorbed on $[\text{Al}(\text{OH})_4][\text{GaO}]$ and the system after C-H bond dissociation.³¹ The optimized transition state structure is shown on Figure 1b. The optimized transition state energy allowed the activation barrier for the C-H bond scission to be estimated at 13 kcal/mol at the LDA level and 30 kcal/mol at the NLDA level. As this makes a very substantial decrease in activation energy compared to methane adsorbed on an acidic Brönsted active site in non-exchanged zeolite (108 kcal/mol)⁷ the question could be raised what would be the reason for such a difference, imposed by such a weak interaction.

Table 1. Charge distribution in free methane as given by DFT (Hirschfeld partitioned charges, Mulliken population analysis, ESP fitted charges) and MOPAC calculations.

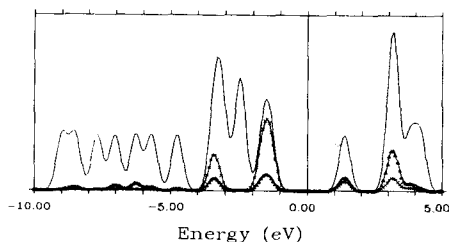
	Hirschfeld	Mulliken	ESP	MOPAC
C	-0.185	-1.287	-0.672	-0.361
H	0.046	0.323	0.168	0.090

Table 2. Evolution of charge distribution along C-H dissociation path in methane on Ga-ZSM-5 (columns as in Table 1): ads - adsorption complex, TS - transition state for C-H bond scission, dis - after C-H scission.

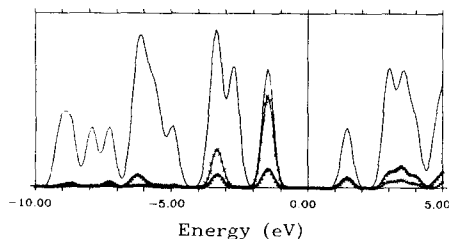
		Hirschfeld	Mulliken	ESP	MOPAC
Al	ads	0.450	0.819	1.378	1.025
	TS	0.450	0.823	1.347	1.108
	dis	0.439	0.811	1.373	1.002
Ga	ads	0.445	1.019	0.575	1.145
	TS	0.465	1.122	0.702	1.340
	dis	0.447	1.054	0.895	1.415
O _{fr}	ads	-0.237	-0.913	-0.623	-0.637
	TS	-0.239	-0.906	-0.642	-0.628
	dis	-0.258	-0.915	-0.675	-0.609
H _{fr}	ads	0.211	0.609	0.424	0.200
	TS	0.207	0.599	0.417	0.194
	dis	0.197	0.587	0.398	0.196
O _{Ga}	ads	-0.465	-0.739	-0.645	-0.463
	TS	-0.426	-0.748	-0.714	-0.579
	dis	-0.361	-0.923	-0.768	-0.724
C	ads	-0.168	-1.247	-0.463	-0.377
	TS	-0.212	-1.378	-0.695	-0.533
	dis	-0.232	-1.404	-0.818	-0.453
H _{met}	ads	0.061	0.399	0.123	0.071
	TS	0.052	0.424	0.159	0.096
	dis	0.042	0.398	0.175	0.061
H _{dis}	ads	0.039	0.350	0.165	0.064
	TS	0.049	0.233	0.307	0.294
	dis	0.130	0.545	0.356	0.135

Four types of framework atoms (Al, Ga, O_{fr} and H_{fr}), extraframework oxygen (O_{Ga}), carbon (C), methyl hydrogen (H_{met}) and dissociative hydrogen (H_{dis}) are listed in Table 2. The most profound changes may be clearly spotted for gallium, oxygen (we will refer to the extraframework oxygen within the GaO unit whenever oxygen is mentioned), carbon, and the dissociative hydrogen atom. On dissociation this hydrogen and the gallium loose electrons while the oxygen and carbon atoms acquire electrons. In the preadsorption step, however, the unsaturated gallium site withdraws electrons from the weakly bound methane molecule (on adsorption $\Delta Q_{\text{CH}_4} = +0.27$ according to ESP-fitted charges) decreasing C-H bond polarization and thus its

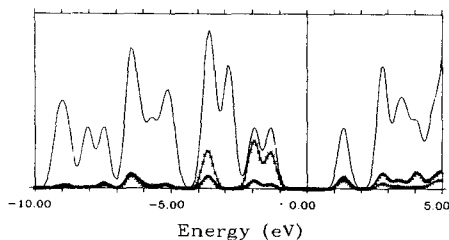
a) GaO cluster



b) adsorbed methane



c) transition state for C-H scission



d) dissociated C-H bond

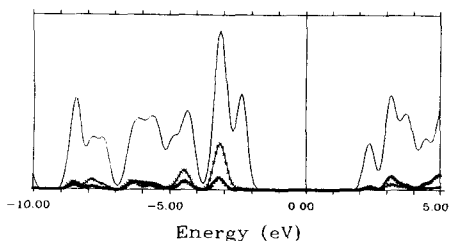
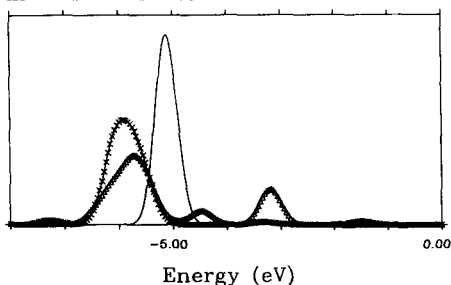


Figure 2. Evolution of DOS along methane dissociation pathway on GaO:—total DOS; Δ - Ga contribution; \times - O contribution.

strength. The dissociative hydrogen keeps its positive charge which is prerequisite to trigger the interaction with the oxygen furnished with additional negative charge. This makes the energetical cost of the C-H bond scission much smaller and the barrier lower. After crossing the saddle point the dissociative hydrogen makes a very strong, polarized OH bond while the methyl remains bonded to gallium already in the preferred tetrahedral coordination at 1.93 Å which makes a highly stabilized final system (the heat of dissociation has been estimated at 52 kcal/mol).

The analysis of the evolution of the density of states (DOS) graphs along the methane dissociation path given in Figure 2 provides further justification for the proposed mechanism. The graphs have been constructed relative to the Fermi level, with the total density of states depicted by solid line and partial contributions of the atoms forming the GaO unit marked with appropriate symbols. Apparently Ga and O atoms contribute fully to the top of the occupied part of the cluster DOS spectrum building exclusively the peak closest to the Fermi level (Figure 2a). Adsorption of methane is weak and the graph given in Figure 2b shows merely the same DOS shape with addition of a carbon contribution around 6 eV below the Fermi level, however, numerical data show that the GaO peak has been shifted

a) methane on Ga ZSM-5



b) methane on PdO

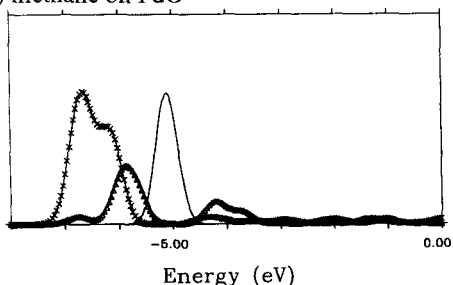


Figure 3. Evolution of carbon contribution to DOS along C-H dissociation pathway on gallium ZSM-5 and PdO clusters: — in free methane; x - adsorbed state; Δ - dissociated C-H bond.

imposes significant differences on the spectrum. One can analyse Figure 3 in a similar way as Figure 2 in terms of metal-carbon bond formation. In the case of Ga-ZSM-5 (Figure 3a) pre-adsorption of methane is apparently much weaker than that on PdO. The carbon peak in the adsorbed state is merely shifted down whereas for methane on PdO (Figure 3b) it is split and the shift is much more pronounced.

After the C-H bond dissociation, new carbon contribution appears around 3 eV below the Fermi level which can be ascribed to the formation of the bond between the carbon and gallium atoms. In the case of palladium oxide similar features may be spotted in the spectrum, the palladium-carbon bond, however, shows to be much weaker as the splitting of the carbon contribution is roughly two times smaller.

The stability of the adsorption of a hydrocarbon on the active site prior to C-H bond dissociation apparently strongly depends on the nature of the site and has not yet been unequivocally established. None of the studies on oxidative coupling of methane on non-transition metal oxides reported a stable methane preadsorption.³⁴ Transition metal oxides, however, may reveal different behaviour and there exists already theoretical evidence for stable methane adsorption on transition metal atoms and complexes.³⁵ Also the stability of the so-called encounter complexes has been qualitatively predicted to increase the reactivity of transition metal MO^+ species

upwards and the carbon peak downwards (see Figure 3a) which might be taken as an indication of the methane to GaO charge transfer. Already in the transition state the bond between the carbon and gallium atoms starts to form which manifests itself in the splitting of the highest GaO peak. In the dissociated system the higher energy GaO peak disappears on behalf of new bonds formed with methyl and hydrogen moieties. Figure 3 shows analyses of changes in carbon contribution to the valence part of the density of states for methane interacting with a gallium - zeolite cluster (a) and palladium oxide diatomic molecule (b). We are going to demonstrate in the next paragraphs that the type of interaction is basically similar as both "host" clusters comprise the metal - oxygen unit, palladium, however, being a transition metal,

toward hydrocarbons.³⁶ Thus comparing the interaction of a methane molecule with palladium and rhodium compounds and with GaO in zeolites is of considerable importance for answering general questions on the mechanism and preliminary steps in the oxidative coupling reaction.

In the following we shall analyse our results regarding methane adsorption and activation on diatomic molecules: PdO, Pd₂ and Rh₂. Figure 4 shows the stable structures of the system composed of methane and diatomic molecule in the case of the palladium dimer (left panel) and the palladium oxide (right panel). It may be easily noticed that the optimum geometries of interaction vary with the "host" cluster. In the case of PdO²⁴ no energy minimum was found for the approach toward oxygen whereas stable adsorption complexes emerged for collinear-to-palladium and bridging positions, with the first one lower by 13 kcal/mol. The bridging adsorption (not shown in the picture) was actually very weak (adsorption energy equal to 6.2 kcal/mol) and comparable to that on the GaO unit. The other very stable structure appeared to be the product of the C-H bond scission with the hydrogen forming OH group and the methyl carbon - palladium separation of 1.98 Å. The stability of the dissociated system with respect to the adsorbed state was 35.3 kcal/mol. From the similarity of the geometry of methane in the bridging position to that on Ga-ZSM-5 the prospective transition state for the C-H bond scission could be deduced. Indeed, stretching this bond (taken as the reaction coordinate) up to 1.4 Å required only 11

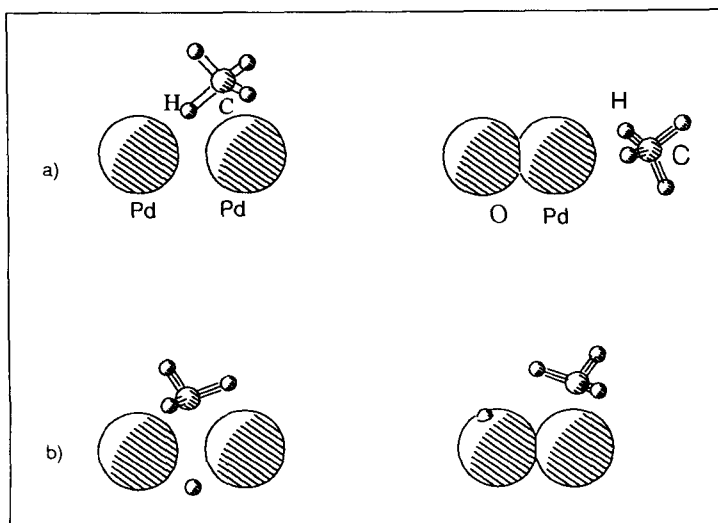


Figure 4. Geometry of methane interaction with palladium dimer (left panel) and PdO molecule (right panel): a) adsorbed methane and b) adsorbed methyl and hydrogen after C-H bond scission.

Table 3. Evolution of charge distribution along C-H dissociation pathway on PdO (DFT, Hirshfeld values).

	PdO	ads	TS	dis
Pd	0.294	0.274	0.364	0.376
O	-0.294	-0.278	-0.279	-0.364
C		-0.182	-0.205	-0.206
H _{met}		0.022	0.021	0.032
H _{dis}		0.062	0.024	0.096

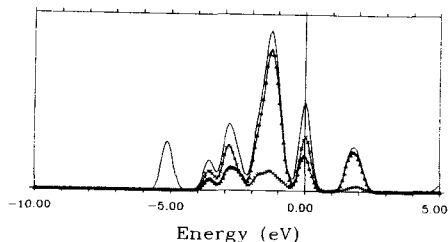
kcal/mol and then the structure was relaxed to the dissociated system. In the region of a saddle point close vicinity of the singlet (ground state for the dissociated system) and the triplet (ground state for PdO molecule and adsorption complexes) made rigorous calculation of the transition state in this case very difficult due to severe mixing and lack of convergence. Thus the overall activation barrier was estimated from simplified constrained reaction path calculations at about 25 kcal/mol (with respect to collinearly bound system), very much like the gallium site. One can wonder if the investigation of the transition state within the LDA approximation is justified. There exist, however, the studies showing that the underestimation of the bonding within nonlocal schemes may be so large that they are unable to locate any bound transition state at all where one would expect their existence.⁷ Thus we have decided to use the LDA for comparative description of transition state properties.

In the case of Pd₂²⁵ the adsorption properties of methane resemble neither the gallium site nor the PdO molecule (Figure 4, left panel). Detailed calculations revealed that the methane adsorbs strongly on Pd₂ in the bridging position with the Pd-C distance equal to 2.2 Å and the bonding energy equal to 25.7 kcal/mol.²⁵ It may be easily noticed that one hydrogen atom is actually within the coordination sphere of both metal atoms, whereas carbon is bonded by Pd₁. Already on adsorption the bonds between the carbon and active hydrogen atoms become substantially stretched up to 1.23 Å. Further stretching the bond is very cheap energetically, and for a C-H distance equal to 1.48 Å, the transition state is reached with an energy expense of only 2 kcal/mol. After crossing this point the hydrogen migrates almost freely around the palladium dimer. The shallow energy minimum has been spotted for the

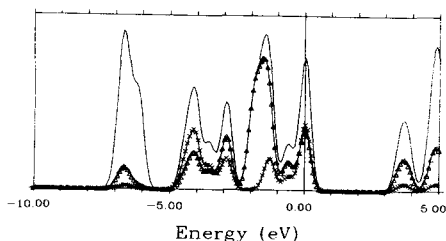
Table 4. Evolution of charge distribution along C-H dissociation pathway on Pd₂ (DFT, Hirshfeld values)

	ads	TS	dis
Pd ₁	0.007	0.005	0.193
Pd ₂	0.131	0.155	0.169
C	-0.199	-0.194	-0.250
H _{met}	0.029	0.027	0.013
H _{dis}	-0.056	-0.071	-0.143

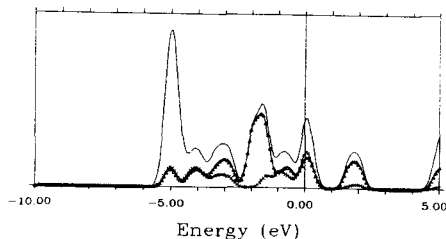
a) PdO and methane molecule



b) adsorbed methane



c) transition state for C-H scission



d) dissociated C-H

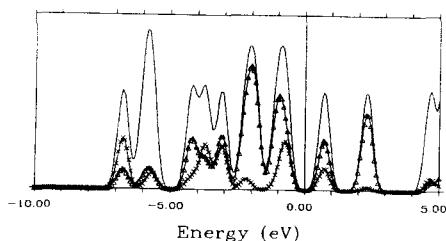
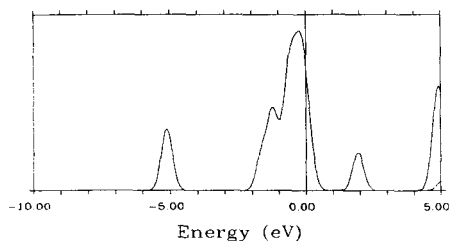


Figure 5. Evolution of DOS along methane dissociation pathway on PdO:—total DOS; Δ - Pd contribution; x - O contribution.

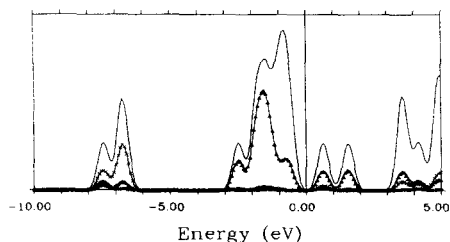
geometry where both the hydrogen and the methyl take bridging positions between the two palladiums, at opposite sides of the molecule. The stability of the system with respect to the adsorbed conformation, however, amounts only to 11 kcal/mol which indicates strong methane adsorption but weak bonds in the dissociated complex.

Table 3 and Table 4 show the Hirshfeld charge redistribution along the C-H bond scission reaction path on PdO and Pd₂ molecules, respectively. The most general difference in the charge redistribution is that while the PdO molecule withdraws electrons from methane molecule, the palladium dimer donates 0.1 e to the adsorbed molecule. The most influenced hydrogen becomes more positive in the first case while it bears a negative charge in the second case. The activation of the C-H bond is much more pronounced on Pd₂, where it undergoes 23% stretch compared to 2% on PdO. The reason for bond destabilization is different in both cases: on Pd₂ the donation of electrons to an antibonding orbital of methane with broken symmetry makes a very strong impact on the C-H bond strength; on PdO it is the withdrawal of bonding electrons from methane which weakens the bond. On the palladium dimer substantial decrease in bond polarization adds to the effect. On the contrary, the stabilization effect after C-H dissociation is much

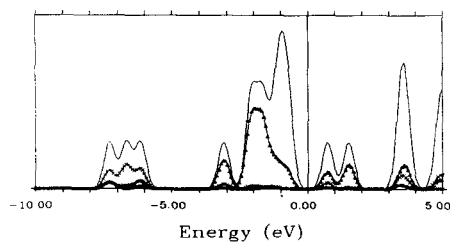
a) Pd dimer and methane molecule



b) adsorbed methane



c) transition state for C-H scission



d) dissociated C-H

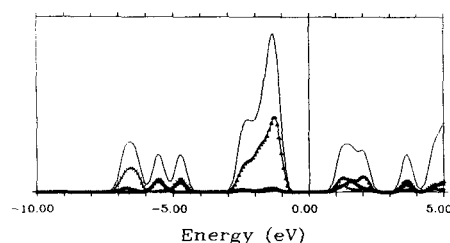


Figure 6. Evolution of DOS along methane dissociation pathway on Pd dimer: —total DOS; Δ - Pd₁ contribution; x - C contribution.

stronger on PdO where the hydrogen forms a very strong, polarized bond while the negatively charged hydrogen atom moves almost freely in the entire subspace of the palladium dimer and the recombination reaction is very probable. In both cases the adsorbed methyl moiety acquires overall negative charge, with much more negative carbon atom and highly polarized bonds.

Analyses of the evolution of the density of states graphs along the methane dissociation path on PdO and Pd₂ are given in Figure 5 and Figure 6, respectively. The graphs have been constructed relative to the Fermi level, with total density of states depicted by solid lines and partial contributions marked with appropriate symbols (these are Pd and O for PdO, and Pd and C for the palladium dimer). The main difference between the non-transition metal oxide in the zeolitic lattice and the transition metal oxide or dimer appears in the position of the Fermi level. Here the Fermi level lies within partially populated states, even if the singlet is low-lying, possibly the ground state of Pd₂, at least in the presence of the guest molecule.²⁵

Apart from the Fermi level position, palladium oxide shows behaviour similar to the GaO unit. Adsorption of the methane molecule is apparently weak, the overall shape of the spectrum does not change significantly while an additional feature due to carbon appears with similar shape and in a

similar position to the one shown in Figure 2b. In the transition state the bonding of methane is even weaker, the carbon peak shifts almost to its original position from the free molecule (see also Figure 3b), and only after final C-H bond scission does the Fermi level shift to the energy gap. Now the shape of the spectrum changes generally, new features appear in the lower part of the spectrum ascribed to the formation of strong bonds between carbon and palladium, and between hydrogen and oxygen.

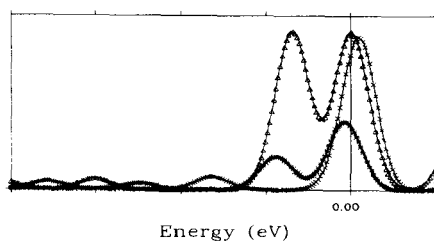
The case of the palladium dimer is completely different (see Figure 6), as was already underlined in the discussion of the interaction geometries and charge distributions. The dimer density of states (a) resembles very much that of large 135 palladium atom clusters.¹² Here already methane adsorption (b) is strong enough to shift the Fermi level to the energy gap. In addition, bonding states with large carbon contribution are split and shifted down by 2 eV. In the transition state (c) the system remains still strongly bonded and finally the dissociated system (d) furnishes the spectrum with a large energy gap and well developed shapes below 5 eV coming from methyl and hydrogen interacting with metal atoms.

Thus the DOS analyses add fully to the emerging picture of the methane interaction with various media. In order to widen the understanding of this phenomenon and to probe other transition metals, we include also a short discussion on rhodium compounds acting as the "host" cluster.²⁵ Open-shell rhodium oxide behaves very much like open shell palladium oxide showing comparable preliminary collinear adsorption and activation towards bridging adsorption and transition state. The rhodium dimer, however, does not provide any position for such strong adsorption of methane as does the palladium dimer, at least in the low-energy high-spin state. A methane molecule binds weakly (by 11 kcal/mol) in the collinear position, other positions are higher in energy, in addition no sizable, comparable to Pd₂, activation of the C-H bond is imposed here.

5. DISCUSSION AND CONCLUSIONS

At this point the question could be raised whether any common factor might be selected to discriminate between transition metal systems in view of their impact on the activation of the C-H bond in methane. We have already proposed a tentative interpretation of the source of the differences in the interaction of methane with the active site based on the interdependence between the electronic state and the reactivity in systems containing rhodium or palladium.²⁶ In the case of a palladium atom with closed-shell d¹⁰ electronic structure, no repulsive 5s electrons are present thus the adsorption complex is stable but the insertion product is not, due to the high energy of the d⁹s¹ state responsible for making bonds with scission products. On the contrary, the rhodium atom has the open-shell electronic d⁸s¹ configuration and repulsive 5s electrons make the adsorption complex unstable but the insertion product has substantial stability.³⁵ In the case of dimers, only Pd₂ has no 5s electrons in the ground state but the open shell configuration lies very close in energy. Thus

a) contribution of 5s functions



b) contribution of 4d functions

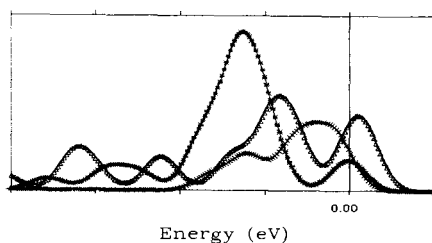


Figure 7. Contribution of metal s and d shells to total DOS of clusters: x - Pd₂, Δ - Rh₂, * - PdO.

both the adsorption complex and the dissociation product are stable. For rhodium dimer in its high-spin ground state the adsorption complex is less stable due to repulsive interaction with Rh 5s electrons while the dissociation complex lies on a low-spin surface and may be reached only via a prerequisite spin transition. The same is true for the palladium oxide molecule.²⁴ It is yet not clear at the present stage of the study if this tendency will be retained for larger clusters or the bulk.

The analysis of the DOS profile fully confirms this hypothesis. In Figure 7 contributions of metal s and d shells to the total density of states for the "host" Pd₂, Rh₂ and PdO clusters are given. The contribution of a 5s shell to the occupied part of the spectrum of the palladium dimer is much smaller than for other systems. In

the case of 4d shells (Figure 7b) it is the rhodium dimer molecule where the large part of the d spectrum lies above the Fermi level while for the palladium dimer spectrum the main d contribution keeps well below the Fermi level.

Finally Table 5 summarizes the most important global properties of the interacting systems. The charge transfer ΔQ is defined by the fraction of electrons transferred from the methane molecule to the "host" cluster on adsorption, calculated

Table 5. Properties of adsorption complexes of methane with studied systems: favored position, adsorption energy, methane-to-cluster charge transfer, activation barrier and stretching frequency of C-H bond.

	Adsorption position	Adsorption energy (kcal/mol)	ΔQ (methane \rightarrow cluster)	Activation energy (kcal/mol)	ν_{C-Hdis} (cm ⁻¹)
GaO	on top Ga	4.5	0.028	13	2884
PdO	collinear on Pd	19.2	0.004	spin trans.	2754
Rh ₂	collinear on Rh	11.0	0.047	spin trans.	2826
Pd ₂	bridging	25.7	-0.188	2	1903

with the use of Hirshfeld atomic charges in a free molecule and the adsorbed system (positive sign depicts withdrawal from and negative signs means donation of charge to the methane molecule). Barrier heights are given whenever rigorous calculations for the transition state was possible. Vibrational frequencies were obtained from the full vibrational analysis of the adsorbed systems.^{24-26,31} The palladium dimer appears to be the unique case among studied systems, with the strongest affinity to methane. It is the only closed-shell system, where electrons are donated to the hydrocarbon molecule on adsorption, which brings the most efficient activation of the C-H bond and the lowest barrier for its scission. At the same time the adsorption geometry is the bridging one where the bonding is mediated by hydrogens. Other systems withdraw electrons from the adsorbed hydrocarbon molecule. On PdO and Rh₂ collinear position on the metal is preferred with moderate strength of adsorption. On GaO methane interacts with the gallium but adsorption is very weak (one might speculate here that the favoured collinear to metal approach might be blocked by the zeolitic lattice). In accord with expectations emerging from the degree of preliminary elongation of the C-H bond, the activation energy required for final scission of the bond on Pd₂ is very small; breaking the C-H bond in methane interacting with the GaO site requires also moderate barrier height, while PdO and Rh₂ provide reaction routes with substantial barriers. In addition, for very strong interaction with Pd₂, already the adsorbed complex has the proper low-spin state whereas on PdO and Rh₂ weak adsorption leads to high spin and prerequisite spin transition to low spin (triplet-singlet for PdO or quintet-triplet for Rh₂) which adds to the reaction barrier. Gallium, being a non-transition metal, provides weak adsorption, the entire reaction pathway, however, lies on the low-spin surface. Finally, calculated frequencies for the carbon-dissociative hydrogen stretch in the adsorption complexes are given in the last column of Table 5. This property exactly reflects the trends discussed above: in each case weakening of the bond is visible (in free methane the DFT calculated frequency equals 2994 cm⁻¹³¹) but only on the palladium dimer the effect is remarkably large.

The examples presented in this work by no means cover the subject of the C-H bond activation on a spectrum of catalytic media. Interaction of methane with the small clusters discussed here obviously cannot pretend to fully mimic catalytic centers in reality. Nevertheless, they seem to justify drawing generalized conclusions regarding the mechanism of catalytic activation in terms of electron withdrawal or donation to the interacting hydrocarbon molecule. A variety of properties contribute consequently to the emerging scheme (electronic density redistribution, geometry evolution in critical points, energetical factors, vibrational analyses) which substantially increases credibility of the conclusions.

REFERENCES

1. D.R. Salahub and N. Russo (eds) *Metal-Ligand Interactions, from Atoms, to Clusters, to Surfaces*, NATO ASI Series, Series C, vol. 378 (Kluwer, Dordrecht, 1992); N. Russo and D.R. Salahub (eds) *Metal-Ligand Interactions, Structure and Reactivity*, NATO ASI Series, Series C, vol. 474 (Kluwer, Dordrecht, 1994).
2. J. Labanowski and J. Andzelm (eds) *Theory and Application of Density Functional Methods in Chemistry* (Springer Verlag, New York, 1991).
3. E. Broclawik and D.R. Salahub, *J. Mol. Catal* **82**, 117 (1993).
4. E. Broclawik, in: *Modern Density Functional Theory: A Tool for Chemistry*, J.M. Seminario and P. Politzer (eds) (Elsevier, Amsterdam, 1995) p. 349.
5. E. Broclawik, R. Vetrivel and A. Miyamoto in: *Recent Developments and Applications of Modern Density Functional Theory*, J.M. Seminario (ed) (Elsevier, Amsterdam, 1996) p. 621.
6. P. Hohenberg and W. Kohn, *Phys. Rev. B* **136**, 864, (1964); W.Kohn and L.J. Sham, *Phys. Rev. A* **140**, 1133 (1965).
7. H. Burghraef, A.P.J. Jansen and R.A. van Santen, *J. Chem. Phys.*, **101**, 11012; (1994) S.R. Blaszkowski, A.P.J. Jansen, M.A.C. Nascimento and R.A. van Santen, *J. Phys. Chem.*, **98**, 12938 (1994).
8. DMol Version 2.3.5, San Diego: Biosym Technologies, 1993.
9. V. L. Moruzzi, J. F. Janak and A. R. Williams, *Calculated Electronic Properties of Metals* (Pergamon, New York, 1978).
10. A. Becke, *J. Chem. Phys.* **88**, 2547 (1988); C. Lee, W. Yang and R. G. Parr, *Phys. Rev. B*, **37**, 786 (1988).
11. P.J. Feibelman, *Annu. Rev. Phys. Chem.* **40** 261 (1989).
12. D.R. Jennison, P.A. Schultz and M.P. Sears, *J. Chem. Phys.* **106**, 1856 (1997).
13. V. Ozolins and M. Korling, *Phys. Rev. B* **48**, 18304 (1993).
14. InsightII release 95.0, Biosym/MSI, San Diego, 1995.
15. R.D. Ramsier and J.T. Yates, Jr., *Dynamics of Gas - Surface Interactions*, C.T. Rettner and M.N.R. Ashford (eds), (The Royal Society of Chemistry: England 1991) p.257; R.C. Baetzold, *Theoretical Aspects of Heterogeneous Catalysis*, J.B. Moffat (ed), (Van Nostrand Reinhold, New York, 1990) p.458.
16. J.R. Rostrup-Nielsen, *Catalytic Steam Reforming*, Vol. 5 of CATALYSIS- Science and Technology, (Springer, Berlin, 1984).
17. H. Arai and M. Machida, *Catal. Today*, **10**, 81 (1991).
18. J.N. Armor, *Appl. Catal. B: Environmental* **1**, 221(1992); F. Jansen, R. Meijer, *Catal. Today* **16**, 157 (1993).
19. J.A. Davies, P.L. Watson, J.F. Liebman and A. Georg (eds), *Selective Hydrocarbon Activation*, (VCH Publishers, New York, 1990); A. Fontijn (ed), *Gas Phase Metal Reactions*, (Elsevier, Amsterdam, 1992).
20. E. Kikuchi and K. Yogo, *Catal. Today*, **22**, 73 (1994).

- 21 . R.A. Grinsted, H. -W. Jen, C.N. Montreuil, M.J. Rokosz and M. Shelef, *Zeolites*, **13**, 602 (1993).
- 22 . A. Miyamoto and M. Kubo, *J. Jpn. Petrol. Inst.*, **36**, 282 (1993); A. Miyamoto, H. Himei, Y. Oka E. Maruya, M. Katagiri, R. Vetrivel and M. Kubo, *Catal. Today*, **22**, 87 (1994); A. Miyamoto, M. Kubo, K. Matsuba and T. Inui, in: *Computer Aided Innovation of New Materials II*, M. Doyama *et al.* (eds), (Elsevier Science Publishers, Amsterdam, 1993), p. 1025.
- 23 . E. Broclawik, *Int. J. Quant. Chem.* **56**, 779 (1995).
- 24 . E. Broclawik, R. Yamauchi, A. Endou, M. Kubo and A. Miyamoto, *J. Chem. Phys.*, **104**, 4098 (1996).
- 25 . E. Broclawik, R. Yamauchi, A. Endou, M. Kubo and A. Miyamoto, *Int. J. Quant. Chem.* **61**, 673 (1997).
- 26 . E. Broclawik, J. Haber, A. Endou, A. Stirling, R. Yamauchi, M. Kubo and A. Miyamoto, *J. Molec. Catal. A.*, **119**, 35-44 (1997).
- 27 . A. Goursot, I. Papai and D.R. Salahub, *J. Am. Chem. Soc.* **114**, 7452 (1992); A. Goursot, I. Papai and C. Daul, *Int. J. Quant. Chem.* **52**, 799 (1994).
- 28 . P. Kratzer, B. Hammer and J.K. Nørskov, *J. Chem. Phys.* **105**, 5595 (1996).
- 29 . A. Rochefort, J. Andzelm, N. Russo and D.R. Salahub, *J. Am. Chem. Soc.* **112**, 8239 (1990).
- 30 . R. Vetrivel, M. Kubo, H. Himei, E. Maruya, M. Katagiri, E. Broclawik, and A. Miyamoto, in: *Science and Technology in Catalysis 1994*, Y. Izumi, H. Arai and M. Iwamoto (eds) *Studies in Surface Science and Catalysis* **92** (Kodansha, Tokyo, 1995), p. 233.
- 31 . E. Broclawik, H. Himei, M. Yamadaya, M. Kubo, R. Vetrivel and A. Miyamoto, *J. Chem. Phys.*, **103**, 2120 (1995); H. Himei, M. Yamadaya, M. Kubo, R. Vetrivel, E. Broclawik and A. Miyamoto, *J. Phys. Chem.*, **99**, 12461 (1995).
- 32 . Dmol Version 960, San Diego: Biosym/MSI, 1996.
- 33 . F. M. Bickelhaupt, N. J. R. van Eikemma Hommes, C. F. Guerra and E. J. Baerends, *Organometallics*, **15** (1996) 2923.
- 34 . K.J. Borve and L.G.M. Pettersson, *J. Phys. Chem.* **95**, 3214 (1991); Y. Aray, J. Rodriguez, J. Murgich and F. Ruetz, *J. Phys. Chem.* **97**, 8393 (1993); K. Borve, *J. Chem. Phys.* **95**, 4626 (1991).
- 35 . P.E.M. Siegbahn, M.R.A. Blomberg and M. Svensson, *J. Phys. Chem.* **98**, 2062 (1994); M.R.A. Blomberg, P.E.M. Siegbahn and M. Svensson, *J. Am. Chem. Soc.* **115**, 1952 (1993); L.A. Erickson, L.G.M. Pettersson, P.E.M. Siegbahn and U. Wahlgren, *J. Chem. Phys.* **102**, 872 (1995).
- 36 . A. Fiedler, D. Schroder, S. Shaik and H. Schwartz, *J. Am. Chem. Soc.* **116**, 10734 (1994); P.E.M. Siegbahn and M. Svensson, *J. Chem. Phys.* **100**, 423 (1994).

Recent Developments in High-precision Computational Methods for Simple Atomic and Molecular Systems

Frank C. Sanders

Department of Physics, Southern Illinois University at Carbondale
Carbondale, IL 62901, U.S.A.

Within the last few years, there has been a resurgence of interest in high-accuracy calculations of simple atomic and molecular systems. For helium, such calculations have reached an extraordinary degree of precision. These achievements are only partially based on the availability of increased computational power. We review the present state of developments for such accurate calculations, with an emphasis on variational methods. Because of the central place occupied by the helium atom and its ground state, much of the discussion centers on methods developed for helium. Some of these methods have also been applied to more complex systems, and calculations on such systems now approach or even surpass a level of precision once only associated with calculations on helium. Hence, other atoms and molecules amenable to high-precision methods are also discussed.

1. INTRODUCTION

In the implementation of density functional methods for atoms and molecules, accurate wave functions can be utilized to test or construct the energy density functional[1]. Except for one-electron systems, however, these wave functions are necessarily approximate. Beyond hydrogen, the most precise wave functions available are obtained by the use of variational methods. For the simplest, few-electron systems, such calculations are capable of producing energies and wave functions of very high accuracy, more than sufficient for the present requirements of density functional theory. In this article we review the development and present state of accurate, variational calculations on simple atomic and molecular systems. In order to facilitate comparison of various alternative

computational approaches, we discuss only “benchmark” calculations: non-relativistic calculations with infinite-mass nuclei for the ground states of the system. These are all based on correlated basis sets, as presently only such bases are capable of yielding this high level of precision.

Particular attention is given to calculations on two- and three-electron atoms. For helium, variational calculations have reached the extraordinary precision of roughly 16 significant figures[2]. Such precision, well beyond that required for comparison to experimental energies, is needed in order to generate very accurate wave functions. With these wave functions, expectation values and higher-order relativistic and QED corrections of sufficient accuracy for comparison to experiment can be obtained. In addition, with such high-precision results, fundamental theoretical characteristics of the helium system can be studied.

Recently calculations on lithium have also reached impressive levels of precision: on the order of 9 to 10 significant figures[3]. In the past, such accuracy would only have been associated with the most elaborate calculations on helium. Beyond lithium, this level of accuracy has not been achieved, as the use of correlated basis set methods becomes very cumbersome. At some point, large scale calculations based on simpler methods begin to surpass those produced with necessarily smaller, correlated basis sets. At present, this “crossover” occurs somewhere in the four to five electron range. Examples of such calculations on beryllium as well as some simple molecules will be presented.

All calculations discussed here have been chosen as representative of various computational methods and no attempt at encyclopedic coverage of calculations on simple atomic and molecular systems has been made. A somewhat more comprehensive discussion of computational methods for atoms and molecules can be found in Sanders[4] while Morgan[5] also reviews recent developments in high-precision computational methods.

2. VARIATIONAL METHODS

The non-relativistic Hamiltonian for an n -electron atom is (in atomic units),

$$H = \sum_i^n \left(-\frac{1}{2} \nabla_i^2 - \frac{Z}{r_i} + \sum_{j>i}^n \frac{1}{r_{ij}} \right). \quad (1)$$

Variational methods[6] for the solution of either the Schrödinger equation or its perturbation expansion can be used to obtain approximate eigenvalues and eigenfunctions of this Hamiltonian. The Ritz variational principle,

$$\langle \tilde{\Psi} | H - E | \tilde{\Psi} \rangle \geq 0. \quad (2)$$

permits optimization of a trial wave function $\tilde{\Psi}(\mathbf{r}_1, \dots, \mathbf{r}_N)$ satisfying appropriate boundary conditions. The trial function is almost always constructed from

a finite selection of terms obtained from a “basis set” ϕ_i which, in fact, need not be a basis in the strict mathematical sense,

$$\tilde{\Psi} = \sum_{i=1}^N c_i \mathcal{A} \phi_i(\alpha). \quad (3)$$

The projection operator \mathcal{A} produces an antisymmetrized wave function. Optimizing the linear coefficients c_i so as to minimize the energy yields a secular determinant whose eigenvalues are upper bounds to the energies of the N lowest states of the system and whose eigenvectors are approximations to the corresponding wave functions. The nonlinear parameters α_i are usually optimized by some search procedure.

As an alternative to the Ritz variational method, a variational perturbation method based on a perturbation expansion can be utilized. Here, the Hamiltonian is separated into an unperturbed Hamiltonian and a perturbing potential,

$$H = H_0 + \lambda H_1. \quad (4)$$

and the wave function and energy are expanded in the perturbation parameter,

$$\Psi = \sum_n \lambda^n \psi_n, \quad E = \sum_n \lambda^n \epsilon_n. \quad (5)$$

When introduced into the Schrödinger equation, these perturbation series yield the perturbation differential equations ,

$$\sum_{k=0}^n (H_k - \epsilon_k) \psi_{n-k} = 0, \quad (6)$$

where $H_k = 0$ for $k \geq 2$. The variational perturbation equations[7,8] are the Euler-Lagrange equations of these perturbation differential equations. For example, the variational perturbation equation for the first-order wave function is,

$$\langle \tilde{\psi}_1 | H_0 - \epsilon_0 | \tilde{\psi}_1 \rangle + 2 \langle \tilde{\psi}_1 | H_1 - \epsilon_1 | \psi_0 \rangle - \epsilon_2 \geq 0, \quad (7)$$

and yields an upper bound to the second-order energy. If the trial first-order wave function $\tilde{\psi}_1$ is expanded in some basis set, optimization of the linear coefficients yields a system of linear equations whose solution requires only a simple diagonalization of the $(H_0 - \epsilon_0)$ matrix. This can be accomplished by any direct diagonalization method, so that this procedure is intrinsically simpler than solving the secular determinant of the variational method[9].

Since high-accuracy variational calculations generally require correlated basis sets of one kind or another, much of the discussion that follows will focus on

the relative merits of these basis sets. If there were no restrictions on the size of a basis set, and if computing time were of no consideration, one basis set would serve as well as another. Even with significant improvements in computing power, however, this is not even remotely the case. Despite the fact that calculations with thousands of terms and elaborate basis sets have become the norm, the rate of convergence of a basis set remains of crucial importance for accurate calculations. Since the size of the basis set is necessarily limited by the computational resources available, there is a need for basis sets that can converge to the desired accuracy within these limits.

For larger systems (greater than four or five electrons) correlated basis sets must be restricted in order to limit the scale and complexity of the calculation. As the number of electrons increases, such restricted basis sets are no longer competitive with less elaborate methods. This raises questions as to whether correlated bases can be effectively utilized in more complex systems. Simpler alternatives to correlated basis sets exist for such systems, but suffer from slow convergence and correspondingly low accuracy. One of the most generally used of such methods is configuration interaction (CI). Despite its slow convergence, the CI method remains useful since its simplicity permits larger scale calculations than can presently be undertaken with correlated basis sets.

3. WAVE FUNCTIONS

Perhaps the simplest way of testing the accuracy of a trial wave function over the entire configuration space is through the local energy function,

$$E_{\text{loc}}(\mathbf{r}_1 \dots \mathbf{r}_n) = \frac{H\tilde{\Psi}(\mathbf{r}_1 \dots \mathbf{r}_n)}{\tilde{\Psi}(\mathbf{r}_1 \dots \mathbf{r}_n)}. \quad (8)$$

If the exact wave function were known, E_{loc} would be equal to the exact energy and constant everywhere. For variational wave functions, however, E_{loc} typically displays large deviations from the approximate eigenvalue obtained with the same wave function, even when the eigenvalue itself is very accurate. Of particular interest are those regions where the deviation in the local energy is greatest. Not surprisingly, these are found at just those points where the Hamiltonian is singular: at electron-nucleus and electron-electron collisions. This behavior of the local energy is related to the Kato "cusp" conditions[10] and suggests that satisfying the cusp conditions is critical if a trial wave function, and the variational energies obtained from it, are to yield accurate results. These conditions take the form of a cusp or discontinuity in the first derivative of the wave function at a two-particle coalescence:

$$\left\langle \frac{\partial \Psi}{\partial r} \Big|_{r=0} \right\rangle_{\text{Ave}} = C_r \Psi|_{r=0} \quad (9)$$

where $C_r = -Z$ for $r = (r_1, r_2)$ and $C_r = \frac{1}{2}$ for $r = r_{12}$ and the left hand side is an average over a small sphere about $r = 0$.

Fock[11] showed that a formal solution for the helium wave function could be obtained in terms of hyperspherical coordinates and that this would take the form of a power series in $R = (r_1^2 + r_2^2)^{1/2}$ and $\ln R$, multiplied by functions of the hyperspherical angles, α and θ_{12} . The lowest-order terms of Fock's expansion for the ground state wave function are,

$$\Psi = 1 - Z(r_1 + r_2) + \frac{1}{2}r_{12} - Z \frac{\pi - 2}{3\pi} r_1 r_2 \cos \theta_{12} \ln R. \quad (10)$$

The second and third terms handle two-body collisions while the fourth term is related to the three-body collision. The term second-order in R in the Fock expansion is also known, and Myers, *et al.*[12] have verified that this term eliminates the discontinuity in the local energy at the origin. This article also contains an analysis of the behavior of the wave function in the vicinity of these singular points.

A CI basis cannot describe the third term in the Fock expansion very easily while it can be included explicitly in a correlated basis, explaining the superior convergence of the latter over any one-electron basis. Studies of the partial wave expansion,

$$\phi_i = r_1^{a_i} r_2^{b_i} P_{l_i}(\cos \theta_{12}) e^{-(\alpha_1 r_1 + \alpha_2 r_2)}, \quad (11)$$

indicate that a trial function of this form reproduces the cusps only very slowly[13]. Since a configuration interaction wave function can be considered a particular variant of the partial wave expansion, all CI methods will suffer from the same slow convergence. The question of the convergence of atomic and molecular basis sets is a difficult one. In this case, however, it has been established that the contribution to the energy from each partial wave decreases as $(l + \frac{1}{2})^{-4}$ [14]. This slow rate of convergence guarantees that reaching the accuracy noted above for helium or lithium would be prohibitively expensive. Carroll, Silverstone and Metzger[15] estimate that the minimum l needed to reach an accuracy of a few parts in 10^9 would require a CI basis with partial waves up to at least $l = 256$, corresponding to roughly 42,000 terms.

4. HELIUM

A selection of calculations on the ground state of helium is presented in Table 1. From this Table we see that the choice of basis is more significant than the number of terms in determining the accuracy of a calculation.

The ground state of helium is itself a rather special case as the wave function is relatively compact. It is thus not difficult to get a reasonable representation of this wave function with a rather modest, correlated basis set. Hylleraas[16]

Table 1
Energy of the Ground State of Helium (in a.u.)

		Energy	Size/type of Basis
Hylleraas[16]	1929	-2.90324	6-term Hylleraas
Kinoshita[18]	1957	-2.9037237	80-term Kinoshita
Pekeris[19]	1959	-2.903724375	1078-term Pekeris
Schwartz[20]	1962	-2.90372437616	189-term $\frac{1}{2}$ -integer
Scherr & Knight(Z^{-1})[8]	1963	-2.90372433	100-term Kinoshita
Frankowski & Pekeris[22]	1966	-2.9037243770326	246-term Fock
Thakkar & Smith[25]	1977	-2.903724363	66-term EC
Freund, <i>et al.</i> [23]	1984	-2.9037243770340	230-term Fock
Kono & Hattori[26]	1986	-2.9037243766	196-term double
Baker, <i>et al.</i> (Z^{-1})[31]	1990	-2.9037243770341184	476term doubleFock
Drake & Yan[2]	1994	-2.903724377034119479	1262-term double

was able to obtain the energy of the ground state accurate to a few parts in 10^5 with only six terms in his trial wave function. Hence, chemical accuracy (1 kcal/mol or 1.6×10^{-3} atomic units) was already achieved by Hylleraas in this calculation, which represented an order of magnitude improvement in precision over results obtained with a CI basis[17]. In this work he introduced a correlated basis in Hylleraas variables,

$$s = r_1 + r_2, \quad t = r_2 - r_1, \quad u = r_{12}. \quad (12)$$

Improved experimental values for helium created renewed interest in such calculations in the late 1950's. In 1957, Kinoshita[18] utilized an 80-term trial function in Kinoshita variables,

$$s, \quad p = \frac{u}{s}, \quad q = \frac{t}{u}, \quad (13)$$

to obtain the non-relativistic energy accurate to 1 part in 10^7 , and, in 1959, Pekeris[19] used a 1078-term wave function in Pekeris, or perimetric coordinates,

$$u = \epsilon(r_2 + r_{12} - r_1), \quad v = \epsilon(r_1 + r_{12} - r_2), \quad w = 2\epsilon(r_1 + r_2 - r_{12}), \quad (14)$$

to obtain the energy accurate to 2 parts in 10^{10} . Pekeris' calculation was of such unprecedented size and accuracy that it stood as the standard for many years.

All these calculations can handle two-particle collisions, but none attempts to deal directly with the three-particle coalescence. Schwartz[20] recognized

the importance of including logarithmic terms in the wave function for this purpose, but found such a wave function cumbersome. Instead, he introduced half-integer powers[20] into his basis set:

$$\phi_i = s^{a_i/2} t^{b_i} u^{c_i} e^{-\alpha s}. \quad (15)$$

With only 89 terms in his trial function, Schwartz was able to surpass the 1078-term result of Pekeris. These results demonstrate how crucial a proper description of the wave function at small length scales is. Although logarithmic terms were utilized as early as 1958[21], it was not until 1966 that large-scale calculations were attempted. Frankowski and Pekeris[22] utilized such a 246-term, Fock basis to obtain an energy improved by three orders of magnitude over Pekeris' earlier 1078-term result. In fact, the 1078-term result was surpassed with a basis of just over 100 terms. More recently, Freund, Huxtable, and Morgan[23] constructed a 230-term wave function, paying special attention to the description of the low-order terms in the Fock expansion. With this smaller wave function, they were able to obtain an energy accurate to a few parts in 10^{14} , an order of magnitude improvement over the Frankowski-Pekeris result.

A natural extension of a Hylleraas-type basis might include correlation in the exponential function. Hylleraas[24] introduced this type of exponentially correlated (EC) wave function, using a single term of the form,

$$\phi_i = e^{-(\alpha_i r_1 + \beta_i r_2 + \gamma_i r_{12})}. \quad (16)$$

If we think of this correlated exponential as a very high-order but compact form of Hylleraas basis (think of its Taylor series expansion) we can see why this type of wave function can increase the rate of convergence significantly. A variant of this type of basis was utilized by Thakkar and Smith[25], who with only 66 terms, obtained a ground state energy in error by only 1 part in 10^8 . In their approach, Thakkar and Smith utilized three different nonlinear parameters for each term in the basis. It would have been very expensive to optimize every nonlinear parameter in the trial function independently. Instead, Thakkar and Smith imposed constraints on their nonlinear parameters, determining them through a set of relations involving only six parameters.

With the exception of the EC basis, the basis sets discussed to this point have utilized only one or two nonlinear parameters, relying on the flexibility available in large numbers of high- and low-order terms to simultaneously describe particle coalescences and the asymptotic behavior of the wave function. This same flexibility can be obtained with fewer terms by using multiple nonlinear parameters in the basis. Groups of terms with identical nonlinear parameters can be considered distinct basis sets, and the method can be described as a multiple basis set method. The first extensive use of such a "double-basis" set

was due to Kono and Hattori[26] in 1984. Kono and Hattori were interested in calculating accurate oscillator strengths for excited states of helium. In order to obtain consistently accurate wave functions for a number of very different excited states, they needed a very flexible basis. Table I lists their value of the ground state energy of helium obtained with a double basis containing a total of 196 terms:

$$\tilde{\Psi} = \sum_i b_i \mathcal{A} \phi_i(\alpha, \beta) + \sum_j c_j \mathcal{A} \phi_j(\gamma, \gamma), \quad (17)$$

with

$$\phi_i(\alpha, \beta) = r_1^{a_i} r_2^{b_i} r_{12}^{c_i} e^{-(\alpha r_1 + \beta r_2)}. \quad (18)$$

In this calculation, only γ was actually optimized while the other two nonlinear parameters were kept fixed. Despite this restriction, the method yields an energy for the ground state correct to 4 parts in 10^{10} . We can ascribe the accuracy of this result to the use of additional nonlinear parameters, permitting each basis to cover different parts of configuration space.

Drake[27] introduced several refinements to this multiple basis set approach: he developed a method to optimize all the nonlinear parameters in the wave function efficiently and he included a single, screened hydrogenic term in the basis. The latter was important in improving the convergence of the basis, particularly in calculations on excited states. In optimizing the nonlinear parameters, it was found that the parameters separated the two basis sets so that one described the wave function at small length scales while the second described large length scales. This also had the beneficial effect of reducing linear dependence between the two basis sets. In a more recent calculation utilizing a wave function with a total of 1262 terms, Drake and Yan[2] obtain a ground state energy apparently converged to a few parts in 10^{17} . The maximum metric (polynomial) order of any term in this wave function is $\omega = 18$, where $\omega = a_i + b_i + c_i$ (see Eq. 18). At this high metric order, machine precision can constrain the choice of terms included in the basis unless special efforts are made to contain the size of matrix elements.

A single basis set requires high metric order terms if it is to adequately describe both inner and outer regions of configuration space. Since the number of terms of a particular metric order is related to the number of partitions of the integer ω , this number increases very rapidly with ω and it becomes difficult to include all terms of some high metric order in a trial function. Multiple basis sets, however, can cover these regions of configuration space with a lower metric (and fewer terms) than would be required with a single basis set of the same form. Drake's calculations demonstrate that a sufficiently flexible (large) double-basis set can represent the particle coalescence region with sufficient accuracy that Fock-type terms can be avoided.

Table I also contains two examples of variational perturbation calculations for helium. These are both Z^{-1} expansions where, by the use of charge-scaled atomic units, Z^{-1} appears as a natural perturbation parameter[7]. The thirteenth-order calculation of Knight and Scherr[8] (sixth-order in the wave function) utilized a 100-term, Kinoshita-type basis in each order of the wave function. Since, for this calculation, the accuracy of the energy cannot be greater than the accuracy of ϵ_2 and this is obtained from the 100-term, first-order wave function, a comparison with Kinoshita's 80-term wave function is appropriate. It can be seen that, with 20 more terms in the basis, the Z^{-1} expansion improves the energy by an additional significant figure. Scherr and Knight[28] also showed that higher-order wave functions cover regions in configuration space at progressively larger length scales. Hence, in comparison to an equivalent 100-term, variational calculation, this calculation should provide an improved coverage of configuration space.

An interesting problem in the Z^{-1} expansion has to do with the radius of convergence of the series. Kato[29] showed that the perturbation series was indeed convergent, and obtained a lower bound for the radius of convergence of $Z^{-1} \approx 0.13$. An improved lower bound of $Z^{-1} \approx 0.505$ was subsequently obtained by Ahlrichs[30], but Knight and Scherr had found that their computed energy coefficients gave a radius of convergence close to $Z^{-1} \approx 1.25$, so that even the series for the H^- ion would converge. More recently, the Z^{-1} expansion was utilized by Baker, *et al.*[31] to calculate the perturbation energy coefficients through 401st order (corresponding to a 200th-order wave function). In their calculation, Baker, *et al.* employed a Fock-type basis of 476 terms with the terms divided into two basis sets. With this moderately-sized wave function, they were able to produce an energy in agreement with Drake and Yan's 1262-term result to 15 significant figures. From their energy coefficients they estimated the radius of convergence of the Z^{-1} expansion to be 1.09766. At precisely this value of Z , the energy of the ground state becomes degenerate with the first ionization threshold, confirming an earlier conjecture by Reinhardt[32] about the radius of convergence of the Z^{-1} expansion.

5. LITHIUM

In three-electron systems, the convergence of a basis set is complicated by the increasing number of terms required to reach a particular metric order. For three-electrons, a typical correlated Hylleraas (HY) basis might look like

$$\phi_i = r_1^{a_i} r_2^{b_i} r_3^{c_i} r_{12}^{d_i} r_{13}^{e_i} r_{23}^{f_i} e^{-(\alpha r_1 + \beta r_2 + \gamma r_3)}. \quad (19)$$

Because of the additional factors appearing in each term of this basis, the number of terms required to reach a particular metric order grows very rapidly. Where in a two-electron calculation, a relatively modest 84 terms suffice to

form a wave function complete through $\omega = 6$, the total number of terms needed to reach this metric in a three-electron problem is 811, a non-trivial number. Since the convergence of a trial function increases roughly as the metric order rather than as the number of terms in the basis, results obtained with an 84-term helium wave function should be roughly comparable to those obtained with a similar 811-term lithium wave function. The magnitude of this problem increases dramatically as the number of electrons increases. Since in practice, there is a limit on both the highest metric and total number of terms that can be incorporated in a wave function, basis sets that converge rapidly and can produce accurate results at lower metric and with fewer terms are of great interest.

Table 2 presents a number of calculations of increasing accuracy on the ground state of the lithium atom. Notable in this Table is the high precision recently achieved for this system. A CI calculation is also presented for comparison. The first calculation for lithium with a correlated basis set was made by James and Coolidge[33]. In this work they also developed methods for dealing with the three-electron integrals that appear in these calculations. Evaluating these integrals requires considerably more computation time than the equivalent two-electron integrals, and the efficient treatment of coupled three-electron integrals continues to be a problem.

Table 2
Energy of the Ground State of Lithium (in a.u.)

		Energy	Size/type of Basis set
James & Coolidge[33]	1936	-7.47607	17-term HY
Larsson[34]	1968	-7.478025	100-term HY
Sims & Hagstrom[39]	1975	-7.478023	150-term HY-CI
Ho[35]	1981	-7.478031	92-term HY
King & Shoup[36]	1986	-7.478058	352-term HY
King[37]	1988	-7.478059	602-term HY
Kleindienst & Beutner[40]	1989	-7.47805824	310-term HY-CI
King & Bergsbaken[38]	1990	-7.47805953	296-term HY
McKenzie & Drake[43]	1991	-7.478060312	1134-term HY
Pipin & Bishop[41]	1992	-7.4780601	1618-term HY-CI
Luchow & Kleindienst[42]	1992	-7.47806025	976-term HY-CI
Yan & Drake[3]	1995	-7.47806032156	1589-term HY
CI:			
Jitrik & Bunge[44]	1991	-7.477906662	3653-term CI

Progress in calculations on lithium developed slowly due to the complexity of the calculations and the limited computing power available. In 1968, however, Larsson[34] achieved five figure precision with a 100-term HY wave function. His basis contained terms with ω as high as 7 and included two terms with more than a single r_{ij} factor. The nonlinear parameters for the wave function were optimized on a small basis and fixed at that point. Given the limited number of terms that could be included in the trial function, higher-order terms had to be selected carefully. These were chosen by their effect on the energy. Selecting terms on the basis of their contribution to the energy is difficult. In a finite basis, the contribution any one term makes to the energy depends on all the other terms present in the basis. Removing an apparently insignificant term could have a negative impact on the contribution of other terms to the energy. Testing the importance of each term against all possible terms in a large basis is obviously not possible. On the other hand, for a system like lithium, it is also not possible to include all terms of a particular metric order, except for very low values of ω . Hence, some selection of terms for inclusion in a wave function is necessary. Thus, in constructing his 92-term wave function, Ho[35] included 60 of Larsson's terms, adding 32 other terms, including terms up to $\omega = 10$ and one additional term with a pair of r_{ij} factors. In this case, the effectiveness of these terms was tested by examining their contribution to the energy in groups instead of singly.

In 1986, calculations of considerably larger size were undertaken by King and Shoup[36] with a HY-basis of 352 terms. In this calculation, all 210 terms with $\omega \leq 4$ were included, while the other 142 terms included all remaining terms in Larsson's calculation. In this calculation, the nonlinear parameters of Larsson were used. Also terms up to metric order 11 were utilized, including a number of terms with multiple r_{ij} factors. These calculations were extended to a total of 602 terms by King[37], and then surpassed with a smaller wave function by King and Bergsbaken[38]. The latter wave function included some terms with all three r_{ij} factors and, in addition, an effort was made to optimize the nonlinear parameters carefully.

Note that, in all these calculations, very few terms containing more than a single r_{ij} factor were used. Inclusion of such terms improves the convergence of the basis, but these terms also introduce difficulties in the evaluation of the matrix elements. If the basis is constrained so that no more than a single r_{ij} factor appears in any term, these difficulties are minimized. This also dramatically reduces the number of terms required to reach a particular metric order. In more complex systems, such a basis produces integrals linking no more than four electrons, so that, despite its limitations, this basis can be very useful in calculations beyond lithium.

Sims and Hagstrom[39] utilized this approach in their HY-CI method, adding a single correlation factor to a CI basis. In this way, the HY-CI basis retains some of the advantages of a pure CI basis. From Table 2 we can see that their 150-term result matches the accuracy of Larsson's 100-term calculation. Other calculations of this type for lithium have extended the method to basis sets with over 1000 terms[41].

The multiple basis set method has also been applied to the lithium ground state by McKenzie and Drake[43]. With a 1134-term wave function which included terms up to $\omega = 7$, they obtained an energy converged to within one part in 10^9 . In this calculation, six different basis sets were utilized, each covering a different region of configuration space. In a subsequent calculation, Yan and Drake[3] utilized a 1589-term wave function which included terms up to $\omega = 8$, yielding an energy accurate to a few parts in 10^{11} . This wave function contained five basis sets, and differed from the McKenzie and Drake wave function in that these were constructed so as to describe different correlations among the electrons.

6. BERYLLIUM AND ONWARD

Table 3 lists results for the ground state of beryllium with a HY-CI basis[45]. This Table also contains CI and MCHF calculations for comparison.

Table 3
Energies of the Ground State of Beryllium (in a.u.)

		Energy	Size/type of Basis set
Sims & Hagstrom[45]	1975	-14.666547	107-term HY-CI
Komasa, <i>et al.</i> [47]	1995	-14.6673550217	1200-term ECG
CI:			
Chung, <i>et al.</i> [48]	1993	-14.66704376	1016-term CI
Fischer[49]	1993	-14.667113	3381-term MCHF

In this Table we also find a second form of exponentially correlated function[46]. Such functions have been referred to as explicitly correlated Gaussians (ECG). They take the form,

$$\phi_i = e^{-(\alpha_i r_1^2 + \beta_i r_2^2 + \gamma_i r_{12}^2)}. \quad (20)$$

This type of basis has been used in more complex atoms and, very effectively, in molecular systems where Gaussian exponentials simplify the calculation of

multi-center integrals. Morgan[5] has pointed out that sharply peaked ECG's can reproduce the cusps in the wave function very well, despite their formal inability to represent the two-particle coalescence. Komasa, *et al.*[47] used up to 1200 ECG's in applying this method to the ground state of beryllium, obtaining an energy of -14.6673550217, a significant improvement over any other variational calculation. Although this result is not as dramatic an improvement over CI calculations as those for helium or lithium, it should be noted that it represents over 99.1 % of the correlation energy of the atom. The only other calculations on this scale are all CI or MCHF calculations. From this it would seem that the ECG basis shows greater promise of being extensible to complex atomic systems than other methods relying on correlated basis sets.

Attempts at using correlated basis sets in systems much larger than beryllium have so far proved disappointing. As an example, we cite the 83-term HY-CI calculation of Clary and Handy[50] for the ground state of neon (see Table 4). This wave function was constructed using products of Slater-type orbitals (STO's) together with correlation factors r_{ij}^n representing every pair of electrons in the atom, but restricted to no more than one such factor per term. With this wave function, which does not cover all metric 2 terms, they were able to obtain only 73.5 % of the correlation energy of the ground state, failing to match the best CI results.

Table 4
Energies of the Ground State of Neon (in a.u.)

		Energy	Size/type of Basis set
Clary & Handy[50]	1976	-128.8298	83-term HY-CI
CI:			
Bunge & Peixoto[51]	1970	-128.8868	231-configuration CI
Sasaki & Yoshimine[52]	1974	-128.9168	1068-configuration CI

We see that, for atoms or molecules more complex than beryllium, the use of correlated basis sets of Hylleraas type rapidly becomes infeasible and the CI method and its variants become more attractive. For a correlated basis, the number of terms required to reach a particular metric order can become hopelessly large. In a 10-electron problem like neon, 1596 terms are needed to construct a wave function complete through $\omega = 2$. If instead the wave function is limited to a single r_{ij} factor per term, this number is reduced to 561 terms, still a sizeable number for such a low metric order. It must also be kept in mind that antisymmetrizing the wave function means that each term

in the basis can potentially generate a very large number of terms. If, loosely speaking, one needs to reach equal values of ω to achieve roughly the same degree of precision in a large system as in smaller systems, then correlated basis sets along the lines of those discussed here will not be able to compete with simpler methods. Nevertheless, the significantly more rapid convergence of a correlated basis would make it an attractive alternative to CI if the magnitude of the calculation could be controlled.

It is in this context that exponentially correlated basis sets (EC or ECG) become particularly interesting, since such bases behave as if they contained high metric terms, but in a very compact form. With multiple nonlinear parameters, a trial wave function may be able to represent the wave function at the cusps accurately while retaining sufficient flexibility to correctly reproduce its asymptotic behavior.

Following a different approach, Goldman[53] has proposed a modified configuration interaction (MCI) method that retains the simplicity of a CI calculation but with improved convergence. In its original form, Goldman proposed a basis consisting of products of one electron functions,

$$\phi_i = r_{<}^{a_i} r_{>}^{b_i} e^{-(\alpha r_{<} + \beta r_{>})} \Theta_{l_1 l_2}^{LM}(\hat{\mathbf{r}}_1, \hat{\mathbf{r}}_2). \quad (21)$$

Unlike the CI basis, however, the radial coordinates in these functions are $r_{<} = \min(r_1, r_2)$ and $r_{>} = \max(r_1, r_2)$. These functions yield improved radial convergence since the basis is better able to represent the electron-electron cusp. The angular functions,

$$\Theta_{l_1 l_2}^{LM}(\hat{\mathbf{r}}_1, \hat{\mathbf{r}}_2) = \sum_j^N c_j(\gamma) \Lambda_{l_1 l_2}^{LM} \quad (22)$$

are linear combinations of the usual coupled spherical harmonics,

$$\Lambda_{l_1 l_2}^{LM} = \sum_{m_1 m_2} \langle l_1 l_2 m_1 m_2 | LM \rangle \times Y_{l_1 m_1}(\hat{\mathbf{r}}_1) Y_{l_2 m_2}(\hat{\mathbf{r}}_2), \quad (23)$$

but include large numbers of these so that the basis is equivalent to a very high-order, partial wave expansion in compact form. The linear and nonlinear parameters, c_j and γ_k are to be optimized variationally.

More recently, Goldman has introduced two additional modifications to MCI. First, modified radial functions are introduced which are functions of $r_{>}$ and $r_{<}/r_{>}$ [54]. In these variables, all multidimensional integrals reduce to simple, one-electron integrals; a simplification even over CI, where coupled two-electron integrals always appear. Secondly, modified angular functions are introduced which implicitly contain an infinite number of coupled harmonics[55]. Several examples of such angular functions are given, one of which has an obvious connection to the ECG basis:

$$(\cos \theta_{12})^n e^{\gamma \cos \theta_{12}}. \quad (24)$$

The MCI basis has at present only been applied to two-electron systems, but Goldman has shown that it can be extended to multi-electron systems in a straightforward manner while still retaining all its computational advantages.

7. SIMPLE MOLECULES

This discussion would not be complete without some brief remarks about molecular systems. For the ground state of H_2 , James and Coolidge[56] constructed a correlated basis in confocal elliptic coordinates. This JC basis has the advantage of rapid convergence in comparison to other basis sets. However, it is not easily generalized to multi-electron or polyatomic molecules because of the complexity of correlated integrals over elliptic coordinates. In addition to the JC basis, other molecular, correlated basis sets are available, including the HY-CI basis with STO's, Gaussian-type orbitals (GTO's), or molecular orbitals (MO's) multiplied by a correlation factor. Explicitly correlated basis sets (ECG's) are also utilized, and for H_2 , have surpassed the JC-basis in accuracy[57]. Rychlewski[58] discusses a variety of these trial functions and compares recent calculations on simple molecules.

Table 5 presents results using these basis sets for the H_3^+ and H_3 molecule together with some CI calculations. Most notable here is the dramatic improvement recently achieved in H_3 with an ECG basis.

Application of HY-CI and other methods to simple atomic and molecular systems is also discussed in Clementi, *et al.*[68]. In particular, these authors give examples of computational times on a mainframe computer. They estimate that carrying out calculations on H_3 with a modest HY-CI basis would require from hundreds to thousands of hours to evaluate the integrals alone, while a larger calculation attempting to match spectroscopic accuracy would approach times more often associated with geological processes than with quantum chemistry.

One possible way of limiting the complexity of such calculations regardless of the size of the system, is through the use of perturbation theory, where the maximum number of correlated electrons and the maximum number of nuclear centers that appear in the calculation are determined by the perturbation order. If such a calculation yields the desired accuracy when carried to a particular order, that order determines the maximum complexity of the calculation. One example of such a perturbation theory[69], a variant of the Z^{-1} expansion method, has been applied to H_3^+ with promising results for such a low-order calculation.

Table 5
Energies for H_3^+ , and H_3 , (in a.u.)

H_3^+			
		Energy	Size/type of Basis set
Salmon & Poshusta[59]	1973	-1.34335	15-term ECG
Preiskorn & Woznicki[60]	1984	-1.343422	192-term HY-CI
Frye, <i>et al.</i> [61]	1988	-1.3438279	138-term HY-CI GTO
Alexander, <i>et al.</i> [62]	1989	-1.3438220	700-term ECG
CI:			
Meyer, <i>et al.</i> [63]	1986	-1.34340	104-term CI-GTO
Wenzel, <i>et al.</i> [64]		-1.343814	4974-term CI-GTO
H_3			
		Energy	Size/type of Basis set
Frye, Preiskorn, & Clementi[65]	1991	-1.636637	HY-CI (3s1p) GTO
Cencek & Rychlewski[66]	1993	-1.658965	200-term ECG
CI:			
Liu[67]	1984	-1.658755	CI (5s3p3d2f) STO

8. SUMMARY

Despite the variety and even disparity of computational methods in use for high-precision atomic and molecular calculations, it is possible to extract some general principles from the examples discussed here.

Clearly, computational resources are not yet to the point that "brute force" methods will suffice for high-precision calculations. Physical and chemical intuition play an important role in constructing appropriate trial wave functions and, despite the complexity and size of the basis sets used in these calculations, can improve the convergence of the basis significantly. It is important, therefore, to understand the nature of an atomic or molecular system in terms of its physical as well as its more formal mathematical properties.

Beyond this it is also clear that trial functions must satisfy the Kato cusp conditions explicitly or implicitly, or convergence will remain too slow for high-precision results. Morgan[5] has emphasized that satisfying these cusp conditions is of greater importance than building in the correct asymptotic

behavior for the wave function, and that requiring the correct behavior at the two-particle cusps takes precedence over three-body collisions. Looking beyond the lowest-order terms of the Fock expansion, Myers, *et al.*[12] have made an initial attempt at constructing a trial function which reproduces the $O(R^2)$ term in the Fock expansion.

At present, it is possible to achieve accuracy for two- and three-electron systems superior to that once obtained for two-electron atoms by Pekeris. This can be accomplished by dealing explicitly with the most difficult points of the wave function, as in the Fock basis, or implicitly by constructing sufficiently flexible trial functions through the use of multiple basis sets. In any case, such flexibility is required to deal with the differing character of the wave function at large and small length scales. Drake's[2,27] calculations on helium demonstrate how a double basis set can achieve this kind of flexibility, while Morgan and co-workers[23,31] have combined Fock and double basis sets in a relatively compact wave function to produce equally precise results.

The large number of terms needed to achieve high precision in complex systems suggests looking for alternative bases that can generate high-order, correlated terms in a compact form. Exponentially correlated basis sets can do this, and if implemented with large numbers of nonlinear parameters, can also achieve the kind of flexibility associated with larger basis sets. Given the possibility of achieving accuracy with smaller basis sets, this approach appears to have high potential for application to larger systems.

Though not yet applied to complex systems, Goldman's MCI method also shows promise for large systems because of its computational simplicity. This basis can also be considered "compact" in that it implicitly contains an infinite number of partial waves in each of its angular functions.

REFERENCES

1. C. J. Umrigar and X. Gonze, Phys. Rev. A **50**, 3827 (1994).
2. G. W. F. Drake and Z.-C. Yan, Chem. Phys. Lett. **229**, 486 (1994).
3. Z.-C. Yan and G. W. F. Drake, Phys. Rev. A **52**, 3711 (1995).
4. F. C. Sanders in *Recent Developments and Applications of Modern Density Functional Theory*, J. M. Seminario, ed. (Elsevier, Amsterdam, 1996).
5. J. D. Morgan III in *Numerical Determination of the Electronic Structure of Atoms, Diatomic and Polyatomic Molecules*, M. Defranchesi and J. Delhalle, eds. (Kulwer, Boston, 1989).
6. For a general review of variational methods, see M. A. Abdel-Raouf, Physics Repts. **84**, 163 (1982).
7. E. A. Hylleraas, Z. Physik **65**, 209 (1930).
8. R. E. Knight and C. W. Scherr, Rev. Mod. Phys. **35**, 431 (1963).

9. F. C. Sanders, Chem. Phys. Lett. **17**, 291 (1972).
10. T. Kato, Commun. Pure Appl. Math. **10**, 151 (1957).
11. V. Fock, Izv. Akad. Nauk. SSSR, Ser. Fiz. **18**, 161 (1954).
12. C. R. Myers, C. J. Umrigar, J. P. Sethna, and J. D. Morgan III, Phys. Rev. A **44**, 5537 (1991).
13. C. Schwartz, Phys. Rev. **126**, 1015 (1962); Methods Comp. Phys. **2**, 241 (1963).
14. R. N. Hill, J. Chem. Phys. **83**, 1173 (1985).
15. D. P. Carroll, H. J. Silverstone, and R. M. Metzger, J. Chem. Phys. **71**, 4142 (1979).
16. E. A. Hylleraas, Z. Physik **54**, 347 (1929).
17. E. A. Hylleraas, Z. Physik **48**, 469 (1928).
18. T. Kinoshita, Phys. Rev. **115**, 366 (1957).
19. C. L. Pekeris, Phys. Rev. **115**, 1216 (1959).
20. C. Schwartz, Phys. Rev. **128**, 1146 (1962).
21. E. A. Hylleraas and J. Midtdal, Phys. Rev. **109**, 1013 (1958).
22. K. Frankowski and C. L. Pekeris, Phys. Rev. **146**, 46 (1966); **150**, 366E (1966).
23. D. E. Freund, B. D. Huxtable, and J. D. Morgan III, Phys. Rev. A **29**, 980 (1984).
24. E. A. Hylleraas, Z. Physik **54**, 347 (1929).
25. A. J. Thakkar and V. H. Smith, Jr., Phys. Rev. A **15**, 1 (1977); **15**, 16 (1977).
26. A. Kono and S. Hattori, Phys. Rev. A **29**, 1984 (1984); **30**, 2093 (1984); **34**, 1727 (1986).
27. G. W. F. Drake, Phys. Rev. Lett. **59**, 1549 (1987); Nucl. Instrum. Methods B **31**, 7 (1988).
28. C. W. Scherr and R. E. Knight, J. Chem. Phys. **40**, 3034 (1964).
29. T. Kato, J. Faculty Sci. Univ. Tokyo, **6**, 145 (1951), and *Perturbation Theory for Linear Operators*, (Springer, Berlin, 1966)
30. R. Ahlrichs, Phys. Rev. A **5**, 605 (1972).
31. J. D. Baker, D. E. Freund, R. N. Hill, and J. D. Morgan III, Phys. Rev. A **41**, 1247 (1990).
32. W. P. Reinhardt, Phys. Rev. A **15**, 802 (1976).
33. H. M. James and A. S. Coolidge, Phys. Rev. **49**, 688 (1936); **55**, 873 (1939).
34. S. Larsson, Phys. Rev. **169**, 49 (1968).
35. Y. K. Ho, Int. J. Quantum Chem. **20**, 1077 (1981).
36. F. W. King and V. Shoup, Phys. Rev. A **33**, 2940 (1986).
37. F. W. King, Phys. Rev. A **38**, (1988) 6017; **40**, 1735 (1989); **43**, 3285 (1991).

38. F. W. King and M. P. Bergsbaken, *J. Chem. Phys.* **93**, 2570 (1990).
39. J. S. Sims and S. A. Hagstrom, *Phys. Rev.* **11**, 418 (1975).
40. H. Kleindienst and S. Beutner, *Chem. Phys. Lett.* **164**, 291 (1989).
41. J. Pipin and D. M. Bishop, *Phys. Rev. A* **45**, 2736 (1992).
42. A. Lüchow and H. Kleindienst, *Chem. Phys. Lett.* **197**, 105 (1992).
43. D. K. McKenzie and G. W. F. Drake, *Phys. Rev. A* **44**, R6973 (1991); **48**, 4809(E) (1993).
44. O. Jitrik and C. F. Bunge, *Phys. Rev. A* **43**, 5804 (1991).
45. J. S. Sims and S. A. Hagstrom, *Phys. Rev. A* **4**, 908 (1971); *Int. J. Quantum Chem.* **9**, 149 (1975).
46. S. F. Boys, *Proc. Royal Soc. (London) A* **258**, 402 (1960), K. Singer, *ibid.* **258**, 412 (1960).
47. J. Komasa, W. Cencek, and J. Rychlewski, *Phys. Rev. A* **52**, 4500 (1995).
48. K. T. Chung, X.-W. Zhu, and Z.-W. Wang, *Phys. Rev. A* **47**, 1740 (1993).
49. C. Froese Fischer, *J. Phys. B* **26**, 855 (1993).
50. D. C. Clary and N. C. Handy, *Phys. Rev. A* **14**, 1607 (1976).
51. C. F. Bunge and E. M. A. Peixoto, *Phys. Rev. A* **1**, 1277 (1970).
52. F. Sasaki and M. Yoshimine, *Phys. Rev. A* **9**, 17 (1974).
53. S. P. Goldman, *Phys. Rev. Lett.* **73**, 2547 (1994), *Phys. Rev. A* **52**, 3718 (1995).
54. S. P. Goldman, *Phys. Rev. Lett.* **78**, 2325 (1997).
55. S. P. Goldman, *Phys. Rev. A* **55**, 1772 (1997).
56. H. M. James and A. S. Coolidge, *J. Chem. Phys.* **1** **825**, (1933).
57. J. Rychlewski, W. Cencek, and J. Komasa, *Chem. Phys. Lett.* **229**, 657 (1994).
58. J. Rychlewski, *Intl. J. Quantum Chem.* **49**, 477 (1994).
59. L. Salmon and R. D. Poshusta, *J. Chem. Phys.* **59**, 3497 (1973).
60. A. Preiskorn and W. Woznicki, *Mol. Phys.* **52**, 1291 (1984).
61. D. Frye, G. C. Lie, and E. Clementi, *J. Chem. Phys.* **91**, 2369 (1989).
62. S. A. Alexander, H. J. Monkhorst, R. Roeland, and K. Szalewicz, *J. Chem. Phys.* **93**, 4230 (1990).
63. W. Meyer, P. Botschwina, and P. Burton, *J. Chem. Phys.* **84**, 891 (1986).
64. K. B. Wenzel, quoted in Ref.[61].
65. D. Frye, A. Preiskorn, and E. Clementi, *J. Comput. Chem.* **12**, 560 (1991).
66. W. Cencek and J. Rychlewski, *J. Chem. Phys.* **98**, 1252 (1993).
67. B. Liu, *J. Chem. Phys.* **80**, 581 (1984).
68. E. Clementi, G. Corongiu, D. Bhattacharya, B. Feuston, D. Frye, A. Preiskorn, A. Rizzo, and W. Xue, *Chem. Rev.* **91**, 679 (1991).
69. D. A. Galvan, M. Abu-Jafar, and F. C. Sanders. *J. Chem. Phys.* **102**, 4919 (1995).

Index

A

Ab initio calculations
 compatibility with DFT, 305
 Na_nPb clusters, 337–338
 Na_nPb₄ clusters, 338–342
 Pb_n clusters
 computational process, 328–329
 computational results, 329–337
Ab initio molecular dynamics
 application to chemical reactions, 168
 role of SCF calculations, 179–181
Absorption, gas at molecular level, 349–351
Active site–methane interaction, DFT,
 352–361
ADF codes, for molecular geometries,
 117–120
Adiabatic connection
 for cosine-wave jellium, 199–206
 for exchange–correlation energy, 191–194
AIMD, *see Ab initio* molecular dynamics
Alkali–lead clusters
 Na_nPb clusters, 337–338
 Na_nPb₄ clusters, 338–342
Anions, monoatomic, stabilization of
 endohedral complexes, 316–318
Asymptotic properties
 gradient-corrected exchange potential,
 113–115
 KLI potential, 45–47
 KS exchange energy functional and
 derivative, 264–266, 268
 OEP, 34–36
 theorem 1, 41
 theorem 2, 42–43
 in vacuum region, 250–257
Atoms
 collinear collisions, 178–181
 Dirac calculations, 154
 electronegativity and hardness, 308–311
 electronic structure, *n*-particle picture,
 88–94

 energy, KLI approximation, 153–157
 exchange energy in LS–DFT
 background, 50–51
 comparison to HKS–DFT, 53–60
 equations, 52
 halogen, photodissociation, 181–184
 kinetic energy in LS–DFT
 background, 50–51
 equations, 51–52
 in molecules, electronegativity and
 hardness, 311–315
 n-electron, non-relativistic Hamiltonian,
 368–370
3-Azidomethyl-3-methyloxetane,
 decomposition, 293–298

B

Band structure, Au and Pt, 215–220
Barium, BaTiO₃, IFC, 231–236
Basis sets
 double numerical plus polarization, in
 DFT, 349
 exponentially correlated, beryllium, 380
 Gaussian, in *ab initio* methods, 168–169
 Hylleras
 for helium, 372–373
 for lithium, 375–376
 multiple, for helium, 372–373
Becke–Lee–Yang–Parr correlation, in DFT,
 349
Beryllium
 CI calculations, 378–379
 MCHF calculations, 378–379
 MCI calculations, 380
3,3'-Bis(azidomethyl)oxetane,
 decomposition, 293–298
BLYP correlation, *see* Becke–Lee–Yang–
 Parr correlation
Bonds
 breaking in hydrocarbons, 350

Bonds (*continued*)

formation and fissure, configurational mixing, 169–171

Born–Oppenheimer potential energy, formalism, 226–231

C

C_{60} , stabilization energy, 316–318

Catalysis

modeling, 348–349

related issues, 349–351

Cations, monoatomic, stabilization of endohedral complexes, 316–318

Chemical energetics, definition, 1–3

Chemical hardness

absolute hardness, 282–283

atoms, 308–311

atoms-in-molecules, 311–315

definition, 274

orbital tensor, 275–279

profiles of reaction paths, 284–288

Chemical reactions

application of AIMD, 168

application of DFT, 168

application of GVB, 168

application of MCSCF, 168

energy and enthalpy, DFT calculations, 293

Chemical softness, role in local HSAB principle, 319–320

CI, *see* Configuration interaction

Cluster model

alkali–lead

Na_nPb clusters, 337–338

Na_nPb_4 clusters, 338–342

lead

Na_6Pb , GGA, 342–344

Pb_n

computational process, 328–329

computational results, 329–337

metal, $[\text{Al}(\text{OH})_4][\text{GaO}]$, 352–361

for quantum chemistry calculations, 350

Collisions

colinear

$(\text{NO})_{12}$, 178–181

ozone, 172–178

partners, potential energy, 180–181

Configurational mixing, in molecules, 169–171

Configuration interaction

for beryllium, 378–381

for lithium, 376

Configuration space, in wave functions, 370–371

Constants, exchange potential, lemma, 37–41

Correlation energy

approximations, 13

definition, 15

in DFT, 12

electronic

in LS–DFT

dynamical correlation, 60–62

nondynamical correlation, 60–62

nondynamical, in LS–DFT, 60–62

functional in LS–DFT, 62–65

HEG, 211–214

high-Z asymptotic expansion, 20–22

identification, 19–20

Kohn–Sham theory, physical

interpretation, 249–250

types, 17–18

Correlation–exchange energy

adiabatic connection, 191–194

in DFT, 304

GGA, 1–2

averages, 3

qualitative explanation of performance, 4

quantitative explanation of

performance, 6–7

HF approximation, 1

high-density expression, 16–17

KS theory, physical interpretation and derivative, 243–246

LS–DFT approximation, 1

averages, 3

qualitative explanation of performance, 4

quantitative explanation of function, 6–7

Correlation potential

Becke–Lee–Yang–Parr, in DFT, 349

bound-free, DFT, 79–80

contribution to Kohn–Sham exchange potential, 256

GGA treatment, 152

high-density limit relationships, 22–26

Janak–Moruzzi–Williams, in DFT, 349

LDA treatment, 152

structure in KS exchange potential,
257–259

Cosine-wave jellium
adiabatic connection, 199–206
QMC simulations, 196–197

Coulomb holes
and KS theory, 249–250
total charge, 257

Covalent solids, IFC, 231–236

Crystals
gradient corrections, 157–160
Pb, 330

Cyanohalides, photodissociation, 181–184

D

Decomposition, organic azide, 293–298

deMon codes, for molecular geometries,
117–120

Density functional theory
application
to many-body problem, 12
to ozone reaction, 172–178
atom electronegativity and hardness,
308–311
atoms-in-molecules electronegativity and
hardness, 311–315
with BLYP correlation, 349
bound-free correlation potential, 79–80
calculation of reaction energy and
enthalpy, 293
for catalysis modeling, 348–349
for chemical reactions, 168
compatibility with *ab initio* calculations,
305
conditions
classification, 106–108
fulfilled conditions, hierarchy, 109–113
correlation energy in, 12
with DNP, 349
exact exchange potential, 34–36
formalism, 226–231
free energy functional, in one dimension,
140–141
generalization, 98–99
history, 209–210
Hohenberg–Kohn theorem, 303–304
for IFC, 225–226
with JMW correlation, 349
Kohn–Sham approximation, 227

local response model, 77–79
for many-body effects, 190
many-electron system energy, 275
methane–active site interaction, 352–361
methodology, 308
numerical illustration, 99–102
reference-state DFT, 73–77
relativistic, review, 211–214
role in high-density limit of correlation
potential, 22–26

Density matrix, Dirac, equations, 245

Density parameters, averages, 3–6

Density of states, methane graphs,
evolution, 355–356

DFT, *see* Density functional theory

Diatomic molecules
metal oxide, 351
Pd₂, 357–358
PdO, 357–358
Rh₂, 357–358

Diels–Alder reactions, regioselectivity,
definition, 318–319

Differentiation, restricted, KS exchange
potential, 258

Dipole moments, and gradient-corrected
exchange potential, 120–122

Dirac calculations
atom, 154
eigenfunctions, 155

Dirac density matrix, equations, 245

DNP basis sets, *see* Double numerical plus
polarization basis sets

Double numerical plus polarization basis
sets, in DFT, 349

E

Eigenfunctions
in Dirac calculations, 155
Kohn–Sham, in Fock operators, 152

Eigenvalues
and gradient-corrected exchange potential,
120
Kohn–Sham, for chemical hardness, 277

Electron density
link to electron–electron interaction, 16
in local response model, 77–79
Pb clusters, 336–337

Electronegativity
atoms, 308–311

- Electronegativity (*continued*)
 - atoms-in-molecules, 311–315
- Electron–electron interaction, link to
 - electron density, 16
- Electron–electron repulsion operator,
 - definition, 14
- Electronic correlation
 - in LS–DFT
 - dynamical correlation, 60–62
 - nondynamical correlation, 60–62
 - nondynamical, in LS–DFT, 60–62
- Electronic energy, nonrelativistic fitted
 - energy, 169–171
- Electronic structure, n -particle picture,
 - 88–94
- Endohedral complex, stabilization energy,
 - 316–318
- Energy
 - atomic, KLI approximation, 153–157
 - Born–Oppenheimer potential, formalism,
 - 226–231
 - correlation, *see* Correlation energy
 - correlation–exchange, *see* Correlation–exchange energy
 - electronic, nonrelativistic fitted energy,
 - 169–171
 - exchange
 - atoms in LS–DFT
 - background, 50–51
 - comparison to HKS–DFT, 53–60
 - equations, 52
 - definition, 15
 - Kohn–Sham theory, physical
 - interpretation, 246–248
 - free
 - explicit functionals, 145–148
 - extended generating functionals,
 - 138–140
 - in one dimension, 140–141
 - semi-classical viewpoint, 142–144
 - functionals, definition, 1–3
 - gap between molecular orbitals, 276
 - ground state
 - application of KS approximation,
 - 191–194
 - equations, 14
 - kinetic, atoms in LS–DFT
 - background, 50–51
 - equations, 51–52
 - many-electron system, DFT, 275
 - potential
 - Born–Oppenheimer, formalism,
 - 226–231
 - for collision partners, 180–181
 - surface molecular geometry, 117–120
 - reaction, DFT calculations, 293
 - stabilization, endohedral complexes,
 - 316–318
- Enthalpy, reaction, DFT calculations, 293
- Equations
 - Euler–Lagrange, in variational methods,
 - 369
 - integral, OEP, derivation, 32–34,
 - 153–157
 - Schrödinger, in variational methods,
 - 368–370
- Equilibrium, thermal, simple fluid, 132–135
- Errors, exchange and correlation potentials,
 - 152
- Euler–Lagrange equations, in variational
 - methods, 369
- Exact exchange energy density functional,
 - from Fock operator, 152
- Exact exchange potential, DFT, 34–36
- Exchange–correlation energy
 - adiabatic connection, 191–194
 - in DFT, 304
 - GGA, 1–2
 - averages, 3
 - qualitative explanation of performance,
 - 4
 - quantitative explanation of
 - performance, 6–7
 - HF approximation, 1
 - high-density expression, 16–17
 - KS theory, physical interpretation and
 - derivative, 243–246
 - LS–DFT approximation, 1
 - averages, 3
 - qualitative explanation of performance,
 - 4
 - quantitative explanation of function,
 - 6–7
- Exchange energy
 - for atoms in LS–DFT
 - background, 50–51
 - comparison to HKS–DFT, 53–60
 - equations, 52
 - definition, 15
 - Kohn–Sham theory, physical
 - interpretation, 246–248
- Exchange potential

constant, lemma, 37–41
 contribution to Kohn–Sham exchange
 potential, 256
 exact, DFT, 34–36
 GGA treatment, 152
 gradient-corrected
 asymptotic behavior, 113–115
 calculations, 115
 dipole moments, 120–122
 eigenvalues, 120
 other properties, 122
 Kohn–Sham
 composition, 243
 Pauli and correlation–kinetic
 components, 257–259
 Pauli and correlation–kinetic
 contribution, 256
 LDA treatment, 152
 Exponentially correlated basis sets,
 beryllium, 380
 Extended generating functionals, free
 energy, 138–140

F

Fermi–Coulomb hole charge, distribution,
 244
 Fermi distribution, occupation numbers, 171
 Fermi holes
 dynamic, charge, 258–259
 and KS theory, 249–250
 total charge, equations, 246–247
 Fermions
 free, ground state, 135–138
 noninteracting, KS theory as model
 system, 242–243
 Fermi wavevector, in cosine-wave jellium,
 197
 Fixed-density variance minimization, QMC,
 194–196
 Fluid, simple, in thermal equilibrium,
 132–135
 Fock operator, KS eigenfunctions, 152
 FON methods, in ground-state calculations,
 169–171
 Forces, and fractional occupation numbers,
 169–171
 Free energy
 explicit functionals, 145–148
 extended generating functionals, 138–140

in one dimension, 140–141
 semi-classical viewpoint, 142–144

G

Gas
 absorption at molecular level,
 349–351
 homogeneous electron gas
 exchange contribution, 211–214
 LDA based on, 210
 Gaussian basis sets, in *ab initio* methods,
 168–169
 Gaussian-type orbitals, simple molecules,
 381
 Ge₆₀, stabilization energy, 316–318
 Generalized gradient approximation
 application to Na₈Pb, 342–344
 for exchange–correlation energy, 1–2
 qualitative explanation for performance,
 3
 quantitative explanation of function,
 6–7
 generalization, 210–211
 relativistic, for Au and Pt band structure,
 215–220
 Generalized valence bond method, for
 chemical reactions, 168
 Geometry, molecular
 Pb clusters, 331–332
 potential energy surface, 117–120
 GGA, *see* Generalized gradient
 approximation
 Gold
 application of LAPW, 214–215
 band structure, 215–220
 Gradient approximation
 corrections for crystals, 157–160
 generalized
 for exchange–correlation energy,
 1–2
 qualitative explanation for
 performance, 3
 quantitative explanation of function,
 6–7
 generalization, 210–211
 relativistic generalized, for Au and Pt,
 215–220
 Green function, and asymptotic structure,
 251–252

Ground state energy
 application of KS approximation,
 191–194
 beryllium, 378–381
 calculations with FON methods, 169–171
 equations, 14
 free fermions, 135–138
 helium, 371–375
N-electron system, 194–196
 GVB, *see* Generalized valence bond method

H

Halides, photodissociation, 181–184
 Halogens, photodissociation, 181–184
 Hamiltonian operator
 in adiabatic connection, 191–194
 definition, 14
 in DFT, 228
 N interacting particles, 88–94
 non-relativistic, in variational methods,
 368–370
 Hard and soft acids and bases
 definition, 274
 global principle, 316–318
 local level principle
 definition, 318–319
 role of reaction site softness, 319–320
 theory, 315–316
 Hartree–Fock calculations
 beryllium, 378–381
 for exchange–correlation energy, 1
 generalization, 94–96
 numerical illustration, 96–98
 and OEP, 31–32
 potential in Dirac atom calculations, 154
 HEG, *see* Homogeneous electron gas
 Helium
 correlated wave functions, 65–66
 ground state, 371–375
 HF, *see* Hartree–Fock calculations
 HKS–DFT, *see* Hohenberg–Kohn–Sham
 density functional theory
 Hohenberg–Kohn–Sham density functional
 theory, comparison to LS–DFT, 53–60
 Hohenberg–Kohn theory
 definition, 14
 in DFT, 303–304
 Hole charge, Fermi–Coulomb, distribution, 244
 Homogeneous electron gas

exchange contribution, 211–214
 LDA based on, 210
 HSAB, *see* Hard and soft acids and bases
 Hydrocarbons, C–H bond breaking, 350
 Hylleras basis sets
 for helium, 372–373
 for lithium, 375–376

I

IFC, *see* Interatomic force constants
 Integral equations, OEP, derivation, 32–34,
 153–157
 Interatomic force constants
 with DFT, 225–226
 formalism, 226–231
 in ionic and covalent solids, 231–236
 Ionic solids, IFC, 231–236

J

Janak–Moruzzi–Williams correlation, in
 DFT, 349
 Jellium, translational symmetry, 250
 Jellium slab metal, potential decay, 254
 JMW correlation, *see* Janak–Moruzzi–
 Williams correlation

K

Kinetic energy, for atoms in LS–DFT
 background, 50–51
 equations, 51–52
 Kinetic energy operator, definition, 14
 Kinetic potential, structure in KS exchange
 potential, 257–259
 KLI approximation, *see* Krieger–Li–Iafrate
 approximation
 Kohn–Sham approximation
 application, to ground state energy,
 191–194
 in DFT, 227
 Kohn–Sham density functional theory, orbital
 occupation numbers, 172
 Kohn–Sham eigenfunctions, in Fock
 operator, 152
 Kohn–Sham eigenvalues, for chemical
 hardness, 277

Kohn–Sham exchange energy, functional and derivative, 264–266, 268
 Kohn–Sham exchange potential
 composition, 243
 Pauli and correlation–kinetic components, 257–259
 Pauli and correlation–kinetic contribution, 256
 Kohn–Sham theory
 correlation energy functional and derivative, 249–250
 exchange–correlation energy functional, 243–246
 exchange energy functional and derivative, 246–248
 as model of noninteracting fermions, 242–243
 nonrelativistic fitted electronic energy, 169–171
 self-consistent, orbital structure, 250
 Kohn–Sham wavefunction, definition, 15
 Krieger–Li–Iafrate approximation
 asymptotic properties, 45–47
 atomic energies, 153–157
 derivation, 44
 for gradient corrections in crystals, 157–160
 and OEP method, 44
 KS eigenfunctions, *see* Kohn–Sham eigenfunctions
 KS theory, *see* Kohn–Sham theory

L

LAPW, *see* Linearized augmented plane wave
 LDA, *see* Local density approximation
 Lead clusters
 Na₆Pb, GGA, 342–344
 Pb_n
 computational process, 328–329
 computational results, 329–337
 Lee–Yang–Parr functional, role in high-density limit of correlation potential, 25–26
 Lemma, exchange potential constants, 37–41
 Linearized augmented plane wave, for solids, 214–215
 Lithium

 basis sets, 375–376
 CI calculations, 376
 Local density approximation
 in adiabatic connection, 203–206
 based on HEG, 210
 in DFT of methane–active site interaction, 352–361
 for gradient corrections in crystals, 157–160
 for IFC in ionic and covalent solids, 231–236
 for KS exchange energy, 266, 268
 Na₆Pb, 342–344
 nonrelativistic functional, 211–214
 Local response model, DFT, 77–79
 Local-scaling density functional theory
 atoms in
 exchange energy
 background, 50–51
 equations, 52
 kinetic energy
 background, 50–51
 comparison to HKS–DFT, 53–60
 equations, 51–52
 correlation energy functional, 62–65
 dynamical correlation, 60–62
 nondynamical correlation, 60–62
 Local-scaling transformations, for He
 correlated wave functions, 65–66
 Local spin density, for exchange–correlation energy
 qualitative explanation of function, 3
 quantitative explanation of function, 6–7
 LS–DFT, *see* Local–scaling density functional theory

M

Many-body problem
 application of DFT, 12, 190
 ground-state, application of QMC, 190–191
 Many-body wavefunctions
 in adiabatic connection, 199–206
 variational QMC, 198–199
 MCI, *see* Modified configuration interaction
 MCSCF, *see* Multiconfiguration self-consistent field theory
 MD, *see* Molecular dynamics
 Metal clusters, [Al(OH)₄][GaO], 352–361

- Metal oxide, MeO diatomic molecule, 351
 - Metal surface, jellium and pseudopotential models, 250
 - Methane—active site interaction, DFT, 352–361
 - Mixing, configurational, in molecules, 169–171
 - Models
 - catalysis, 348–349
 - cluster
 - alkali–lead
 - Na_nPb clusters, 337–338
 - Na_nPb_4 clusters, 338–342
 - lead
 - Na_6Pb , GGA, 342–344
 - Pb_n , 328–337
 - metal, $[\text{Al}(\text{OH})_4][\text{GaO}]$, 352–361
 - for quantum chemistry calculations, 350
 - explosive, nitric oxide system as, 179–181
 - local response, DFT, 77–79
 - noninteracting fermions, 242–243
 - pseudopotential, translational symmetry, 250
 - Modified configuration interaction, for beryllium, 380
 - Molecular dynamics
 - Pb clusters, 330–331
 - role in X-ray diffraction, 350
 - Molecular geometry
 - Pb clusters, 331–332
 - potential energy surface, 117–120
 - Molecular orbitals
 - reactivity indices, 283–284
 - simple molecules, 381
 - Molecules
 - atoms, electronegativity and hardness, 311–315
 - bond formation and fissure, configurational mixing, 169–171
 - diatomic, metal oxide, 351
 - electronic structure, n -particle picture, 88–94
 - gas absorption, 349–351
 - simple
 - GTO, 381
 - molecular orbitals, 381
 - Monte Carlo, and HEG, 211–214
 - Multiconfiguration self-consistent field theory, 168
 - Multiple basis sets, for helium, 372–373
- N**
- n -electron systems
 - with ground-state density, 194–196
 - non-relativistic Hamiltonian, 368–370
 - N interacting particles, basic notions, 88–94
 - Nitric oxide
 - as model explosive, 179–181
 - $(\text{NO})_{12}$, collinear collisions, 178–181
- O**
- Occupation numbers
 - Fermi distribution, 171
 - fractional, and forces, 169–171
 - orbital, in KS density functional theory, 172
 - OEP, *see* Optimized effective potential
 - Operators
 - electron–electron repulsion, definition, 14
 - Hamiltonian
 - in adiabatic connection, 191–194
 - definition, 14
 - in DFT, 228
 - N interacting particles, 88–94
 - non-relativistic, in variational methods, 368–370
 - kinetic energy, definition, 14
 - projection, in variational methods, 369
 - Optimized effective potential
 - asymptotic properties, 34–36
 - theorem 1, 41
 - theorem 2, 42–43
 - and HF expression, 31–32
 - integral equation, derivation, 32–34, 153–157
 - and KLI approximation, 44
 - Orbitals
 - hardness tensor, 275–279
 - reactivity indices, 279–281
 - self-consistent, Kohn–Sham, structure, 250
 - Organic azide, decomposition, 293–298
 - Oxygen, BaTiO_3 , IFC, 231–236
 - Ozone, collinear collisions, 172–178

P

- Particle density, simple fluid in thermal equilibrium, 132–135
- Pauli potential
 - contribution to Kohn–Sham exchange potential, 256
 - structure in KS exchange potential, 257–259
- Perdew–Burke–Ernzerhof functional, role in correlation potential, 25–26
- Perturbation theory
 - in DFT, 229
 - variational, for helium, 375
- Photodissociation, halides, 181–184
- Platinum
 - application of LAPW, 214–215
 - band structure, 215–220
- Potential energy
 - Born–Oppenheimer, formalism, 226–231
 - for collision partners, 180–181
 - surface molecular geometry, 117–120
- Potentials
 - correlation, *see* Correlation potential
 - exact exchange, DFT, 34–36
 - exchange, *see* Exchange potential
 - Hartree–Fock, in Dirac atom calculations, 154
 - kinetic, structure in KS exchange potential, 257–259
 - Kohn–Sham exchange
 - composition, 243
 - functional and derivative, construction, 264–266, 268
 - Pauli and correlation–kinetic components, 257–259
 - Pauli and correlation–kinetic contribution, 256
 - optimized effective
 - asymptotic properties, 34–36
 - theorem 1, 41
 - theorem 2, 42–43
 - and HF expression, 31–32
 - integral equation, derivation, 32–34, 153–157
 - and KLI approximation, 44
 - Pauli
 - contribution to Kohn–Sham exchange potential, 256
 - structure in KS exchange potential, 257–259

Slater

- asymptotic structure, 253
- KS exchange energy, 265
- Projection operator, in variational methods, 369

Q

- QMC, *see* Quantum Monte Carlo
- Quantum chemistry, cluster models, 350
- Quantum Monte Carlo
 - application to ground-state many-body problem, 190–191
 - cosine-wave jellium, 196–197
 - fixed-density variance minimization, 194–196
 - variational MC, 194, 198–199

R

- Reaction paths, hardness profiles, 284–288
- Reaction sites, softness, role in local HSAB principle, 319–320
- Reactivity index
 - molecular orbitals, 283–284
 - orbitals, 279–281
- Reference-state density functional theory, definition, 73–77
- Regioselectivity, Diels–Alder reactions, definition, 318–319
- Relativistic generalized gradient approximation, 215–220
- Ritz variational principle, in variational methods, 368–370

S

- SCF calculations, *see* Self-consistent field calculations
- Schrödinger equation, in variational methods, 368–370
- Self-consistent field calculations, role in AIMD, 179–181
- Semi-classical approximation, free energy functional, 142–144
- Silicon
 - IFC, 231–236
 - Si₆₀, stabilization energy, 316–318

Silicon dioxide, IFC, 231–236
 Silicon dioxide–stishovite, IFC, 231–236
 Slater potential
 asymptotic structure, 253
 KS exchange energy, 265
 Solids
 calculations with LAPW, 214–215
 electronic structure, *n*-particle picture,
 88–94
 ionic and covalent, IFC, 231–236
 Stishovite–silicon dioxide, IFC, 231–236

T

Tensor, orbital hardness, 275–279
 Thermal equilibrium, simple fluid, 132–135
 Titanium, BaTiO₃, IFC, 231–236

V

Vacuum, asymptotic structure, 250–257
 Variational methods
 Euler–Lagrange equations, 369
 non-relativistic Hamiltonian, 368

projection operator, 369
 Ritz variational principle, 368
 Schrödinger equation, 368
 Vosko–Wilk–Nusair parametrization,
 211–214

W

Wavefunctions
 accuracy testing, 370–371
 correlated, for He, 65–66
 many-body
 in adiabatic connection, 199–206
 in variational QMC, 198–199
 Wavevector, Fermi, in cosine-wave jellium,
 197
 Wilson–Levy functional, role in high-density
 limit of correlation potential,
 25–26

X

X-ray diffraction, role of MD simulation,
 350

ISBN 0-12-034832-2

